The importance of fast auditory processing for central learning mechanisms and related feedback adaptation processes to the auditory periphery

Dissertation

der Mathematisch-Naturwissenschaftlichen Fakultät
der Eberhard Karls Universität Tübingen
zur Erlangung des Grades eines
Doktors der Naturwissenschaften
(Dr. rer. nat.)

vorgelegt von
Philipp Eckert
aus Herrenberg

Tübingen
2020

Gedruckt mit Genehmigung der Mathematisch-Naturwissenschaftlichen Fakultät der Eberhard Karls Universität Tübingen.

Tag der mündlichen Qualifikation:	27.05.2020
Dekan:	Prof. Dr. Wolfgang Rosenstiel
1. Berichterstatter:	Prof. Dr. Marlies Knipper
2. Berichterstatter:	Prof. Dr. Peter Ruth

Index

Abbreviations

ABR	auditory brainstem response
AC	auditory cortex
ACTH	corticotropin
AMPA	α amino-3-hydroxy-5-methyl-4-isoxazolepropionic acid
Arc/Arg3.1	activity-regulated cytoskeletal protein
ASD	autism spectrum disorders
ASR	acoustic startle response
ASSR	auditory steady state response
AT	acoustic trauma
BC	basket cells
BDNF	brain-derived neurotrophic factor
BLEV	BDNF-Live-Exon-Visualization
BS	bistratified cells
CA	cornu ammonis
Ca2+	calcium
CaMKIIα	calcium/calmodulin dependent protein kinase II α
CaRF	Ca2+-response factor
CFP	cyan-fluorescent-protein
Cl-	chloride
CN	cochlear nucleus
CREB	cyclic AMP response element binding protein
CRH	corticotropin-releasing hormone
d	day
dB	decibel
DCN	dorsal cochlear nucleus
DG	dentate gyrus
DPOAE	distortion product of otoacoustic emission
EC	entorhinal cortex
fEPSP	field excitatory postsynaptic potentials
FH	fissura hippocampalis
GABA	γ-aminobutyric acid
GABA	γ-aminobutyric acid
GCL	granule cell layer
GFAP	glial fibrillary acidic protein
GR	glucocorticoid receptor
h	hour
kHz	kilohertz
high-SR	high spontaneous rate low threshold
HPA	hypothalamic-pituitary-adrenal
IBA-1	ionized calcium-binding adapter molecule 1
IC	inferior colliculus
IHC	inner hair cell
IR	immunoreactivity
K+	potassium
KCC2	potassium chloride cotransporter 2
Low-SR	low spontaneous rate high threshold
LTD	long-term depression
LTP	long-term potentiation
MET	mechano-electrical transducer
MGB	medial geniculate body
MNTB	medial nuclei of the trapezoid body
MR	mineralocorticoid receptor
MWM	Morris Water Maze
µV	microvolt
NKAα3	Na+, K+-ATPase subunit alpha3
OHC	outer hair cell
P	postnatal day
PV	parvalbumin
PV^+	parvalbumin-positive
PVN	hypothalamic paraventricular nucleus
SC	Schaffer collateral
S.E.M.	standard error of the mean
SL	sensation level
SGN	spiral ganglion neuron
SL	stratum lucidum
SOC	superior olivary complex
SP	stratum pyramidale
SPL	sound pressure level
SSC	somatosensory cortex
STG	superior temporal gyrus
Trk	tyrosine receptor kinase
USV	ultrasonic vocalization
VCN	ventral cochlear nucleus
VGluT1	vesicular glutamate transporter 1
VGluT3	vesicular glutamate transporter-3
WB	Western blot
WT	wild-type
YFP	yellow-fluorescent-protein

Zusammenfassung

Sprache ist die komplexeste Form der Kommunikation, ein Höhepunkt der Evolution, der den Menschen einzigartig macht. Um diese hohe Form der Kommunikation zu nutzen, bedarf es eines präzise entwickelten Hörsystems, welches in der Lage ist über Aufmerksamkeit akustische Information bewusst wahrzunehmen und über Lern-abhängige Prozesse zu speichern. Dies ist eine Voraussetzung für die Sprachentwicklung. Jüngste Studien zeigen, dass darüber hinaus Hörstörungen das dritthäufigste Risiko im mittleren Alter für mentale Erkrankungen, wie Demenz, darstellen. Wie Hören und Gedächtnisleistungen ebenso Hörstörungen und beeinträchtigte Gedächtnisleistungen zusammenhängen, ist bisher ungeklärt. Es ist bekannt, dass die bewusste Wahrnehmung auditorischer Stimuli Gedächtnisleistung benötigt. Zudem ist bekannt, dass Lern-abhängige Plastizitätsprozesse durch den Wachstumsfaktor BDNF und durch Stresshormone beeinflusst werden. Es wurde die Hypothese aufgestellt, dass BDNF und Stresshormone möglicherweise über schnelle auditorische Prozessierung an zentralen auditorischen Adaptationsprozessen und Gedächtnisleistungen beteiligt sein könnten. Tatsächlich konnte in der vorliegenden Studie gezeigt werden, dass Glukokortikoid-Rezeptor vermittelte Signalkaskaden einen negativen Einfluss auf zentrale auditorische Anpassungsprozesse nach akustischem Trauma haben. Darüber hinaus konnte gezeigt werden, dass sich explizit zentrale Stresshormon-Rezeptoren auf auditorische Anpassungsprozesse auswirken. Wurden Mineral- und Glukokortikoid-Rezeptoren in zentralen frontalen Hirnregionen der adulten Maus unter dem CaMKIIα Promotor, durch Tamoxifen-Induktion akut deletiert, veränderte sich die Hörnerv-Antwort ebenso wie die zentrale auditorische Antwort. Dies deutet darauf hin, dass zentrale hippocampale Mineral- und Glukokortikoid-Rezeptoren auf periphere auditorische Hörnerv-Antworten zurückwirken können. Schließlich konnte über die Analyse von Mausmutanten mit auditorisch-peripherer Deletion von *Bdnf* in distinkten Pax2-positiven Neuronen (***Bdnf*^{Pax2} KO**) neue Einblicke in die Funktion von BDNF in Cochlea- und Stammhirnregionen auf kognitive Prozesse gewonnen werden. Es zeigte sich, dass BDNF während der Entwicklung in Pax2 positiven Neuronen offenbar während erster sensorischer Erfahrung mit Hörfunktionsbeginn die Entwicklung schneller auditorischer Prozessierung initiiert und kontrolliert. Obwohl *Bdnf*^{Pax2} KO-Mausmutanten ein fast normales Hörvermögen erreichen, bleibt nicht

nur die Reifung schneller auditorischer Prozessierung, sondern ebenso die Reifung hippocampaler Langzeitpotenzierung eingeschränkt. Dies ging mit einer Reduktion der Lernfähigkeit, ebenso wie mit erhöhter Angst und eingeschränktem Sozialverhalten einher.

Mit Hilfe des in der Arbeitsgruppe Knipper generierten ***B***DNF-***L***ive-***E***xon-***V***isualization (**BLEV**)-Reportermaus-Modells, welches aktivitätsabhängig transkribierte *Bdnf* Exone (IV und VI) am Ort der Translation sichtbar macht, wurde schließlich geprüft, ob und in welchen Hirnregionen *Bdnf* Transkripte durch verschiedene Schallexpositionen aktiviert werden. Es zeigte sich das nach Schall-Stimulation und leichtem auditorischen Trauma, erhöhte *Bdnf* Transkript-Spiegel in der Hörbahn und im Hippocampus nachweisbar sind, die mit erhöhtem zentralen auditorischen Antwortverhalten und erhöhter hippocampaler Langzeitpotenzierung einhergehen. Umgekehrt konnte nach starkem auditorischen Trauma, weder aktivitätsabhängige *Bdnf* Transkripte noch hippocampale Langzeitpotenzierung rekrutiert werden. Dieser Verlust der Rekrutierung von aktivitätsabhängigen BDNF und hippocampaler Langzeitpotenzierung ging mit einem Verlust zentraler auditorischer Anpassung einher.

Zusammenfassend zeigte sich, dass schnelle auditorische Prozessierung aktivitätsabhängiges BDNF in der aufsteigenden Hörbahn und im Hippocampus rekrutiert, um Stresshormon-Rezeptor kontrollierte Gedächtnis-abhängige zentrale auditorische Anpassungsprozesse zu steuern.

Summary

Language is the most complex form of communication, a peak in evolution making humans unique. In order to use this high form of communication, a precisely developed auditory system is required, which is able to consciously perceive acoustic information through attention and to memorize it through learning dependent processes. This is a prerequisite for language development. Recent studies showed that hearing impairment is the third most common risk factor in middle age for mental diseases such as dementia. It is still unclear how hearing and memory performance, as well as hearing disorders and an increased risk of deficits in memory performance up to dementia are related. It is known that the conscious perception of auditory stimuli requires memory performance. Learning dependent plasticity processes are influenced by the brain-derived neurotrophic factor (**BDNF**) and stress hormone signaling. It was hypothesized that BDNF and stress hormones might be involved in central auditory adaptation processes and memory performance via fast auditory processing. Indeed, in the present study it could be shown that glucocorticoid receptor-mediated signaling cascades have a negative effect on central auditory adaptation processes after acoustic trauma. Furthermore, it was shown that altered stress hormone receptor expression also directly influence central auditory adaptation. When the mineralocorticoid and glucocorticoid receptors in central frontal brain regions of adult mice were acutely deleted under the CaMKIIα promoter by tamoxifen induction, both the auditory nerve response and the central auditory response were affected. This indicates that central hippocampal mineralocorticoid and glucocorticoid receptors may modulate peripheral auditory nerve responses. The analysis of mouse mutants with auditory-peripheral deletion of *Bdnf* in distinct Pax2-positive neurons (***Bdnf*^{Pax2} KO**) provided new insights into the function of BDNF in cochlear and brainstem regions on cognitive processes. It was shown that BDNF in Pax2 positive neurons apparently initiates and controls the development of fast auditory processing during first sensory experience with hearing onset. Although *Bdnf*^{Pax2} KO mice achieve almost normal hearing performance, not only the maturation of fast auditory processing but also the maturation of hippocampal long-term potentiation remains limited. This is accompanied by a reduction in learning ability as well as increased anxiety and social behavior. Finally, the ***B***DNF-***L***ive-***E***xon-***V***isualization (**BLEV**) reporter mouse model, which was newly generated in the Knipper research group and visualizes activity-dependent

transcribed *Bdnf* exons (IV and VI) at the site of translation, was used to prove whether and in which brain regions *Bdnf* transcripts are activated by different sound exposures. After enriching and mild traumatic sound exposure, elevated *Bdnf* transcript levels in the auditory pathway and hippocampus were found to be associated with increased central auditory response and increased hippocampal long-term potentiation. In contrast, after severe acoustic trauma, neither activity-dependent *Bdnf* transcripts nor hippocampal long-term potentiation could be recruited. This loss of recruitment of activity-dependent BDNF and hippocampal long-term potentiation was accompanied by a loss of central auditory adaptation.

In conclusion, fast auditory processing drives activity-dependent BDNF in the ascending auditory pathway and hippocampus to control stress hormone receptor-controlled memory-dependent central auditory adaptation processes.

List of publications

a) Accepted papers

Singer W*, Kasini K*, Manthey M*, **Eckert P***, Armbruster P*, Vogt MA, Jaumann M, Dotta M, Yamahara K, Harasztosi C, Zimmermann U, Knipper M, Rüttiger L. **"*The glucocorticoid antagonist mifepristone attenuates sound-induced long-term deficits in auditory nerve response and central auditory processing in female rats*".** FASEB J. 2018

Singer W*, Manthey M*, Panford-Walsh R, Matt L, Geisler HS, Passeri E, Baj G, Tongiorgi E, Leal G, Duarte CB, Salazar IL, **Eckert P**, Rohbock K, Hu J, Strotmann J, Ruth P, Zimmermann U, Rüttiger L, Ott T, Schimmang T, Knipper M. **"*BDNF-Live-Exon-Visualization (BLEV) allows differential detection of BDNF transcripts in vitro and in vivo*".** Front Mol Neurosci. 2018

Matt L*, **Eckert P***, Panford-Walsh R, Geisler HS, Bausch AE, Manthey M, Müller NIC, Harasztosi C, Rohbock K, Ruth P, Friauf E, Ott T, Zimmermann U, Rüttiger L, Schimmang T, Knipper M, Singer W. **"*Visualizing BDNF transcript usage during sound-Induced memory linked plasticity*".** Front Mol Neurosci. 2018

b) Manuscripts in preparation

Eckert P*, Marchetta P*, Manthey M*, Walter MH, Singer W, Jacob M, Rüttiger L, Schimmang T, Pilz PK, Knipper M. **"*Brain-derived neurotrophic factor in inhibitory hindbrain neurons controls central learning mechanisms*".**

Marchetta P*, **Eckert P***, Singer W, Rüttiger L, Knipper M.
"Stress receptors in frontal brain regions influence auditory nerve function and auditory brainstem responses".

*equal contribution

Personal contribution

Singer W*, Kasini K*, Manthey M*, **Eckert P***, Armbruster P*, Vogt MA, Jaumann M, Dotta M, Yamahara K, Harasztosi C, Zimmermann U, Knipper M, Rüttiger L. **"*The glucocorticoid antagonist mifepristone attenuates sound-induced long-term deficits in auditory nerve response and central auditory processing in female rats*"** FASEB J. 2018

Explicitly my part in this work: I calculated correlations of ABR threshold and endogenous stress hormone levels (Fig. 1B), ABR wave I amplitude and endogenous stress hormone levels (Fig. 2A), ribbons and endogenous stress hormone levels (Fig. 2B) and ABR wave I amplitude and ribbons (Fig. 2C). I performed part of the immunohistochemistry of inner hair cells (Figure 2D, E; Figure 3G, H), counting of ribbon synapses (Figure 8) and helped taking microscopic images of IHCs (Figure 2D, E; 3G, H). I also performed ABR wave fine structure analyses with corresponding dynamic range and maximum amplitude size (Figure 5A-C, F-H; Figure 6; Figure 7) in treated animals. I also calculated statistical analyses, created figures and wrote and edited the manuscript.

W. Singer was supervising injection of animals, helping with noise exposure and hearing measurements (Figure 4, 5, 6), analyzing cortisol levels, and was involved in editing figures and writing the manuscript. K. Kasini was establishing the drug application protocol, analyzing immunohistochemistry of ribbon synapses for correlation with hearing measurements (Figure 2, 3), editing figures, and writing the manuscript. M. Manthey performed part of the immunohistochemistry of inner hair cells (Figure 2D, E; Figure 3G, H), counting of ribbon synapses (Figure 8) and part of the analyses of auditory brainstem response (ABR) thresholds for click, noise-burst and pure-tone stimuli and the ABR wave fine structure with its reach, size and slope (Figure 5A-C, F-H; Figure 6; Figure 7) in treated animals. M. Manthey also performed statistical analyses, created figures and helped with the editing of the manuscript. P. Armbruster performed the drug application by injection of the rats, applied the noise exposure, ABR and the measurement of distortion product of otoacoustic emission (DPOAE) (Figure 4, 5, 6) and collected the urine for cortisol analyses. M. A. Vogt correlated IHC ribbon numbers and ABR wave amplitude with the cortisol level (Figure 1B; 2A, B; 3B, C). M. Jaumann was performing the ABR in the untreated animals (Figure 1, 2), analyzed it, collected urine from these rats and helped writing the manuscript. M. Dotta established and performed the cortisol analyses. K. Yamahara was injecting rats with mifepristone before and after trauma and analyzed the data (Supplement Figure 2). C. Harasztosi helped in hearing measurements in untreated and treated animals and helped analyzing data. U. Zimmermann was helping with the figures and writing the manuscript. M. Knipper was developing the concept of the study, involved in creating and writing the manuscript, helping with microscopic analyses, supervised the work. L. Rüttiger developed the concept of the study, was involved in analyzing the hearing measurements, and in all statistical analyses, writing, and editing of the manuscript.

Singer W*, Manthey M*, Panford-Walsh R, Matt L, Geisler HS, Passeri E, Baj G, Tongiorgi E, Leal G, Duarte CB, Salazar IL, **Eckert P**, Rohbock K, Hu J, Strotmann J, Ruth P, Zimmermann U, Rüttiger L, Ott T, Schimmang T, Knipper M. **"*BDNF-Live-Exon-Visualization (BLEV) allows differential detection of BDNF transcripts in vitro and in vivo*"** Front Mol Neurosci. 2018

Explicitly my part in this work: I performed the integrated density quantification of YFP and CFP, created and edited figures and helped writing and editing the manuscript.

W. Singer contributed to develop the experimental concept, supervised the experiments, weighed the transgenic mice (Figure 4B), analyzed the Southern Blot data (Figure 3), treated animals with kainic acid (Figure 7) and helped writing the manuscript. M. Manthey performed the RT-PCR, ABR for click and pure-tone stimuli, immunohistochemistry and analyses of RT-PCR, ABR thresholds and Western blots (Figure 4C-E, Figure 7). Additionally, M. Manthey performed statistical analyses, created the corresponding figures and helped writing the manuscript. R. Panford-Walsh developed the single and double construct (Figure 1A, B), was involved in conceptualization and writing and discussing the manuscript. L. Matt helped in writing and editing the manuscript. E. Tongiorgi helped in primary cell culture assays. H.S. Geisler was involved in study conceptualization, performing the cloning of the vector construct, established the detection of RNA and protein, performing the Western blot, Southern blot and genotyping of the mice, and assisted in their analyses. E. Passeri transfected SK-N-BE cells with the single and double construct (Figure 1C-F) and analyzed the protein expression. G. Baj helped in primary cell culture assays. G. Leal stimulated primary neuronal cultural cells with bicuculline (Figure 2B). C. B. Duarte and I.L. Salazar stimulated primary neuronal cultural cells with bicuculline (Figure 2B, Suppl. Figure 2). K. Rohbock was embedding and cutting all cochlea and brain tissues. J. Hu reviewed and edited the manuscript. J. Strotmann reviewed and edited the manuscript. P. Ruth supervised the study and edited and reviewed the manuscript. U. Zimmermann was helping creating figures, writing and editing the manuscript. T. Ott supervised the project, was involved in developing the concept and generated the transgenic mice by injecting embryonic stem cells into blastocysts. L. Rüttiger helped to analyze the hearing measurement, doing statistical analyses, writing and editing the manuscript, and supervised the project. T. Schimmang was involved in writing the manuscript. M. Knipper supervised the project, helped writing and editing the manuscript, helped to analyze microscopy data, and developed the study conceptualization.

Matt L*, **Eckert P***, Panford-Walsh R, Geisler HS, Bausch AE, Manthey M, Müller NIC, Harasztosi C, Rohbock K, Ruth P, Friauf E, Ott T, Zimmermann U, Rüttiger L, Schimmang T, Knipper M, Singer W. **"*Visualizing BDNF transcript usage during sound-Induced memory linked plasticity*"** Front Mol Neurosci. 2018

Explicitly my part in this work: I performed long-term potentiation recordings and their statistical analyses (Figure 3B, 6G) and performed analyses of immunohistochemistry on brain slices (Figure 2C, D; 4E, F; 5D; 6D,E). Additionally, I exposed mice to different sound stimuli and measured hearing function of mice which were used in the Morris Water Maze (Figure 3C), for histochemical stainings (Figure 2C, Suppl Figure 5) and for western blot (Figure 2C). Finally, I created and edited figures and participated in writing and editing the manuscript.

L. Matt contributed with conceptualization of the experimental design, performing the electrophysiological recordings (Figure 3B; 6G), the corresponding statistical analyses, writing, and editing the manuscript. R. Panford-Walsh contributed with conceptualization of the experimental design and discussing and writing the manuscript. H.-S. Geisler helped with conceptualization of experiments and performed protein isolation and Western blot assays (Figure 2A, 3A). A. Bausch performed the Morris Water Maze test and analyzed the corresponding data (Figure 3C). M. Manthey performed ABRs for click, noise-burst and pure-tone stimuli, and noise exposure to induce acoustic trauma. M. Manthey analyzed ABR thresholds, ABR wave amplitudes and correlation, and the anatomy of auditory input structures through immunohistochemically staining of IHC ribbon synapses (Figure 1). N. Müller assisted with electrophysiological recordings. C. Harasztosi helped with microscopy analyses (Figure 4D). K. Rohbock was embedding and cutting all cochlea and brain tissues. P. Ruth supervised the study, helped with interpretation and discussion of the data and editing the manuscript. E. Friauf was involved in analyses of electrophysiological recordings and supervision. T. Ott generated the transgenic mice, contributed in conceptualization and supervision of the study. U. Zimmermann helped by writing and editing the manuscript and creating the figures. L. Rüttiger was involved in statistical analyses, writing and editing the manuscript, and supervised the study. T. Schimmang was involved in discussing and writing the manuscript. M. Knipper contributed in developing the concept, taking all microscopic pictures, writing and editing the manuscript and supervised the experiments. W. Singer developed the experimental concepts, was involved in analyzing the Western blots, assisting with hearing measurements, immunohistochemistry and protein isolation, supervised the experiments, and helped writing and editing the manuscript.

Eckert P*, Marchetta P*, Manthey M*, Walter MH, Singer W, Jacob M, Rüttiger L, Schimmang T, Pilz PK, Knipper M. **"*Brain-derived neurotrophic factor in inhibitory hindbrain neurons controls central learning mechanisms*".**

In preparation

In this ongoing study explicitly my part is: I performed long-term potentiation recordings and their statistical analyses (Figure 3B, 6G) and performed analyses of immunohistochemistry and in-situ hybridization on brain slices with related integrated density quantification (Figure 2, 3, 4, Figure 3-figure supplement 1). Additionally, I created and edited figures and participated in writing and editing the manuscript.

P. Marchetta performed the Crawley's 3-chamber sociability test with related analyses of contact time in chambers (Figure 7b), latency to first entry (Figure 7c), number of entries (Figure 7d), stereotype and repetitive behavior (Figure 7e). Additionally, she recorded and analysed ultrasonic vocalization patterns in pups (Figure 7f,g,h) and measured the corticosterone level (Figure 7i). Finally, P. Marchetta was helping to perform immunohistochemical and in-situ hybridization stainings, creating and editing figures and writing and editing the manuscript. M. Manthey performed ABR measurements for click, noise-burst and pure-tone stimuli and auditory steady state response (ASSR) to amplitude modulated stimuli (Figure 1a,b,c,d,e,f). M.H. Walter performed and analyzed the multiple T-maze. W. Singer helped with conceptualization of the project, creating and editing figures and writing and editing the manuscript. M Jacob advised on the experiments and edited the manuscript. L. Rüttiger was involved in statistical analyses, writing and editing the manuscript, and supervised the study. T. Schimmang was involved in discussing and writing the manuscript. P.K. Pilz performed the acoustic startle response experiments (Figure 1g,h) and contributed in developing the concept and supportet writing and editing of the manuscript. M. Knipper contributed in developing the concept, taking microscopic pictures, writing and editing the manuscript and supervised the experiments.

Marchetta P*, **Eckert P***, Singer W, Rüttiger L, Knipper M.

"Stress receptors in frontal brain regions influence auditory nerve function and auditory brainstem responses".

In preparation

In this ongoing study explicitly my part is: I did the breeding of all four mouse strains and related Tamoxifen injection. I performed 35 % of the click-, noise-, pure tone evoked ABR as well as DPOAE recordings and analyses and helped with preparing immunohistochemical stainings (Figure 8-12). I also created and edited figures and helped writing the manuscript.
P. Marchetta performed Tamoxifen injection, and 65 % of the ABR and and DPOAE recordings and helped with preparing immunohistochemical stainings (Figure 8-12). Additionally, P. Marchetta performed ASSR, CAP and LTP measurements (data not shown) created and edited figures and helped writing the manuscript.. W. Singer helped with conceptualization of the project, creating and editing figures and writing and editing the manuscript. L. Rüttiger was involved in statistical analyses, writing and editing the manuscript, and supervised the study. M. Knipper contributed in developing the concept, taking microscopic pictures, writing and editing the manuscript and supervised the experiments.

1. Introduction

The auditory system is one of the crucial sensory system for human interactions such as rapid information exchange and social behavior. The successful evolutionary development of auditory skills in humans resulted in language which is the highest form of auditory interaction. Language, the ability to communicate with one another, is the basis of our modern human societies. It demands highest brain skills to understand language in all their components like the meaning of the spoken words, understanding the semantic and emotional content and to select information of spoken text. The processing of communication takes only milliseconds and is highly developed in humans, making them unique. (Fritzsch et al., 2015)

Fast auditory processing is also in lower vertebrates like rodents a characteristic feature of hearing, which requires fast and temporally precise auditory processing for sound localization, orientation and communication (Benasich et al., 2002b). How fast auditory processing develops and how it is related to general central auditory processes such as central adaptation processes and their deficits is less understood.

The world health organization analyzed that over 5 % of the world's population (466 million people) suffer from disabling hearing loss (40 dB in adults; 30 dB in children). Hearing impairments are considered to be a high risk of contributing to the development of cognitive impairments such as dementia (Golub et al., 2019; Lin et al., 2011; Livingston et al., 2017). It was hypothesized that adults who are isolated from society due to poor communication abilities will be affected by loneliness, frustration and depression resulting in a higher risk to develop dementia (Jayakody et al., 2018; Yanguas et al., 2018). Due to the demographic crisis and changes in leisure habits, it is expected that the number of people with hearing impairments will accelerate, which together with the increased risk of dementia will lead to a huge increase in health insurance costs with serious social and economic consequences (Livingston et al., 2017). Furthermore, stress related disorders are increasingly becoming a problem in our modern fast-paced society and various hearing disorders are associated with chronic stress (Dagnino-Subiabre, 2013). Even children, about 34 million estimated by the world health organization, are affected by hearing loss with increasing predicted number for 2050. The molecular and mechanistic associations between the hearing function and mental disorders are still unclear.

1.1 Inner ear function, development and central auditory processing

1.1.1 Basics of hearing

Hearing is the ability to perceive sounds by detecting fluctuations in the pressure of the surrounding medium. The outer ear bundles vibrations by the pinna, guide them along the ear canal and sets the tympanic membrane in motion. The middle ear is located medial to the tympanic membrane and transmits the vibrations of the tympanic membrane into the cochlea by the ossicles: malleus, incus, and stapes (Figure 1). The inner ear comprises the vestibular organ and the cochlea. The stapes is connected to the inner ear through the oval window membrane of the spiral-shaped cochlea, which is a fluid filled cavity. (Fettiplace, 2017; Fettiplace and Kim, 2014)

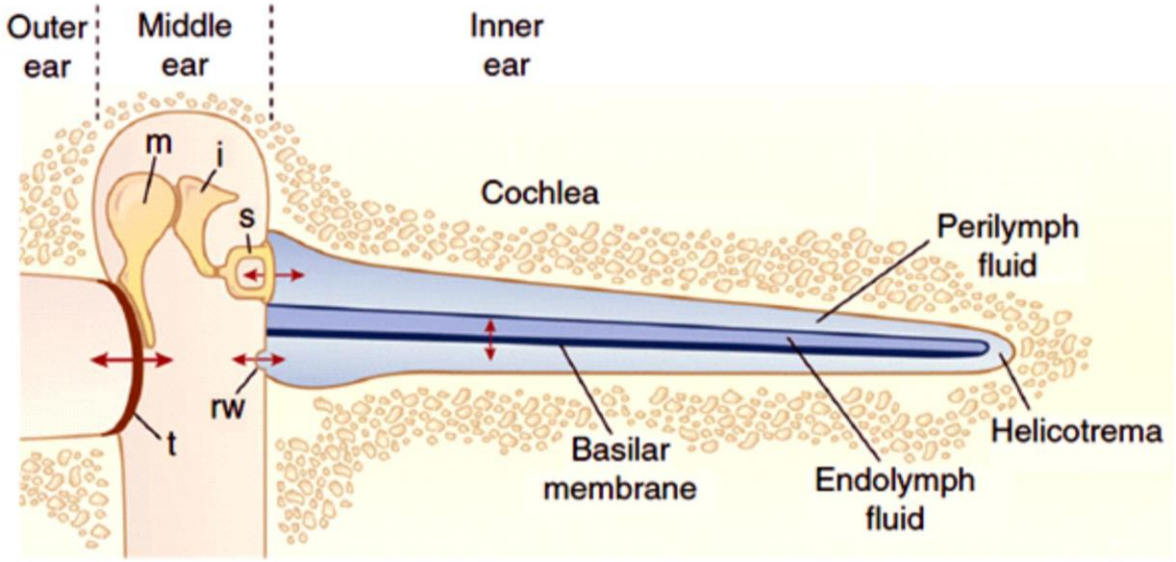

Figure 1: Schematic drawing of the sound transmission pathway from the tympanic membrane to the cochlea. The cochlea is depicted as straight, *in vivo* it is coiled like a snail shell and embedded in the temporal bone. Malleus (m), incus (i), stapes (s), tympanum (t), round window (rw; modified after Fettiplace, 2017).

The cochlea is composed of three compartments: the scala tympani, the scala vestibuli and the scala media which comprises the organ of Corti (Figure 2). The scala tympani and vestibuli are filled with low potassium (**K^+**)-containing perilymph whereas the scala media is filled with high K^+-containing endolymph, thus generates the endocochlear potential (Figure 1,2). When the stapes transduces vibrations to the oval window, the pressure wave deforms the basilar membrane specific to the frequency. The outer hair cells (**OHCs**) mechanically amplify the sound-driven

vibrations and the inner hair cells (**IHCs**) translate the vibrations into a neural code, which is processed in the central nervous system. (Fettiplace, 2017; Fettiplace and Kim, 2014)

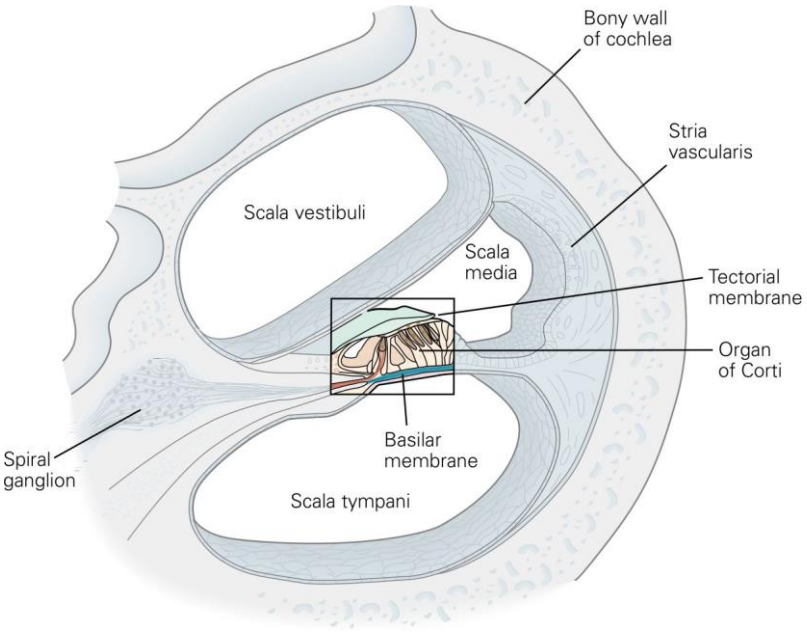

Figure 2: Cross section of the cochlea (modified after Kandel, 2013).

1.1.2 The organ of Corti

The organ of Corti is composed of two different sensory cell types which are surrounded by several types of supporting cells. The OHCs are arranged in three parallel rows while IHCs are in a single row but both contain V-patterned stereocilia at the apical end. The stereocilia of the OHCs are connected to the tectorial membrane which is crucial to induce receptor potentials by shearing movements between the basilar membrane and tectorial membrane (Figure 3). Each sound frequency generates a specific peak in traveling wave on the basilar membrane whose geometry and flexibility is frequency dependent in a tonotopical organization (Békésy and Wever, 1960). It is more flexible and wider at the apical end (low frequencies) and stiffer and narrower at the basal part (high frequencies) of the cochlea, which correlates with the length of OHCs which get shorter from the apical to the basal turn. (Malmierca and Ryugo, 2012)

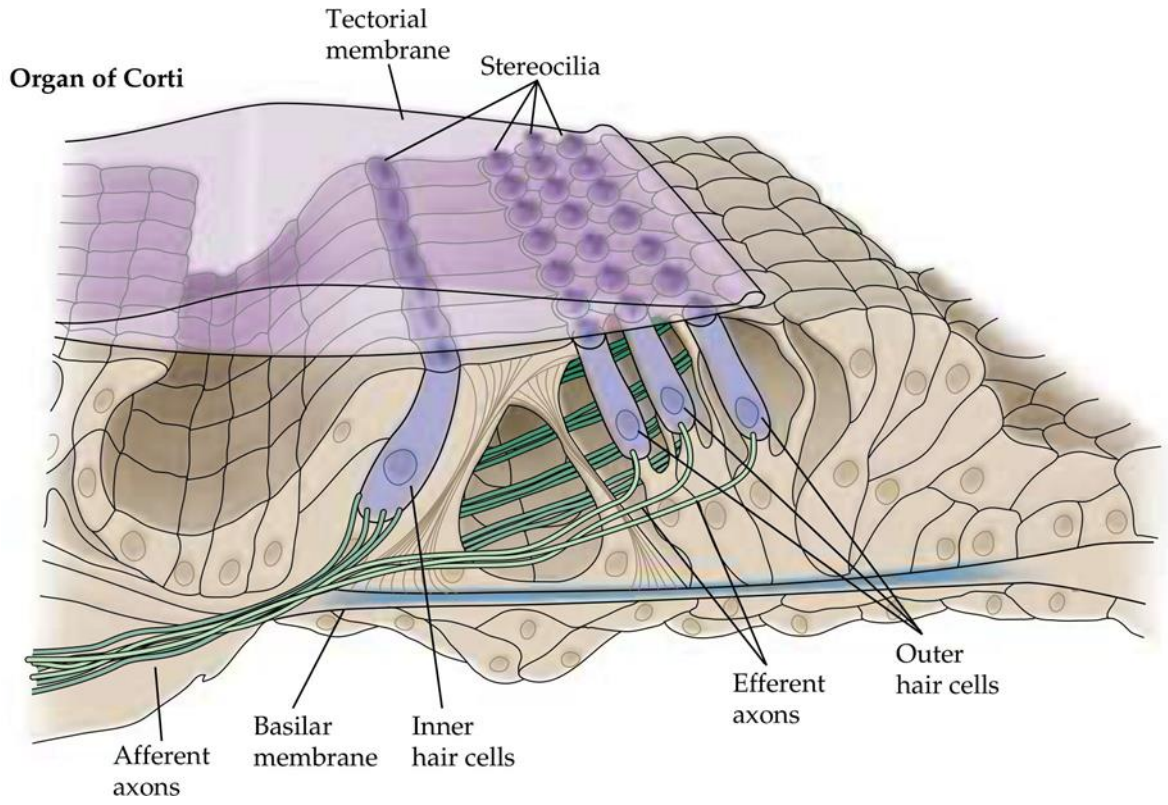

Figure 3: Schematic drawing of the organ of Corti (modified after Purves, 2004).

1.1.3 Peripheral signal transduction and hair cell innervation

The different K^+-concentrations in the fluids are important to maintain the endocochlear potential. The hair cells are surrounded by low K^+-containing perilymph while their stereocilia are bathed in high K^+-containing endolymph. This gradient in K^+-concentration is crucial for K^+-influx through mechano-electrical transducer (**MET**) channels in hair cells during stereocilia deflection which is called mechanotransduction. OHCs are responsible for cochlear amplification by voltage-dependent conformational changes of the protein prestin which is packed in the lateral membrane of OHCs. Chloride (**Cl^-**)-ions regulate the conformation of Prestin and thereby the stiffness of the membrane. This electromotility of OHCs enhances the cochlear sensitivity at threshold and frequency selectivity. (Fettiplace, 2017)
In IHCs K^+-influx causes depolarization and activates voltage-gated calcium (**Ca^{2+}**)-channels. The influx of Ca^{2+} induces transmitter release from the basal end of the cell and activates afferent fibers.
The molecular machinery of exocytosis of IHCs differs from conventional synapses causing the fast and non-fatigable release of neurotransmitter which is coped by phase-locking and fast vesicle release at the ribbon synapse (Johnson et al., 2019; Huet et al., 2019). Ribbons contribute as active IHC release sites connected to

postsynaptic terminals to control the precision of discharge rate of the auditory fibers (Buran et al., 2010; Safieddine et al., 2012). Ribbons are anchored by Bassoon, a large cytomatrix molecule, to the active zone to maintain ready releasable vesicle pools for proper afferent synaptic transmission (Nouvian et al., 2006). At lower sound frequencies (< 3 kHz) the receptor potential waveform of IHCs matches the sound stimulus and frequencies are encoded by alternating current membrane fluctuations of IHCs. But for higher sound frequencies (> 3 kHz) the time-coding ability decreases and the IHCs code the envelope of the sound stimulus only by direct current with a small alternating current component which decreases with increasing frequencies (Palmer and Russell, 1986; Purves, 2004). There are two types of afferent nerve fibers. Type I afferent fibers which are quite thick, myelinated (Spoendlin and Schrott, 1989) and extend radial from the spiral ganglion to the IHCs and represent 90-95%. Type II afferent fibers are thinner, mostly non-myelinated and reach only the OHCs. Each IHC has 10-20 synaptic connections (in mice) where each nerve terminal receives input from one ribbon (Johnson et al., 2019).

Signaling of sound intensities over a wide dynamic range is solved by two different type I synaptic fiber types: high spontaneous rate low threshold (**high-SR**) fibers located at the pillar side and low spontaneous rate high threshold (**low-SR**) fibers located at the modiolar side of IHCs (Safieddine et al., 2012).

The opening of MET channels in IHCs followed by K^+-influx leads to activation of L-type Ca^{2+}-channels ($Ca_V1.3$) and thereby activate transmitter vesicle membrane fusion and release at the basal pole of the IHCs. The ribbon specific protein RIBEYE and the Ca^{2+} binding proteins synaptotagmin and otoferlin are essential for fusion, release and replenishment of glutamate vesicles in the IHCs (Johnson et al., 2019; Marcotti, 2012).

1.1.4 Development of auditory function with hearing onset

The development of mouse hair cells takes approximately 3 weeks from their terminal mitosis at embryonic day 12-14 until hearing onset between postnatal day (**P**) 10-14. Hair cell maturation is initiated by spontaneous ATP driven Ca^{2+} dependent action potentials which also occur along the whole ascending auditory pathway. The combination of timely precise genetic expression of crucial developmental factors in combination with physiologically driven electrical activity are of highest importance for correct maturation of hair cells and SGN and their

synaptic connection. The refinement of the highly specialized ribbon synapse is one of the most important steps in maturation of hair cells. In the first postnatal week Ca^{2+} currents increase in IHCs reaching a peak at P7, when a high density of Ca^{2+} channels is expressed at the basolateral membrane. During the second postnatal week until hearing onset the Ca^{2+} current amplitude decreases and keeps on a constant value of 100 pA. This goes hand in hand with a decline of ribbon number as a consequence of the pruning of SGN type I fibers during hearing onset. Proper pruning of the ribbon synapse is crucial for encoding the full dynamic range of sound intensities and temporal sound processing. (Johnson et al., 2019; Marcotti, 2012)

1.1.5 Central auditory processing

Afferent nerve fibers from the hair cells innervate the cochlear nucleus (**CN**) in the brainstem, which represents an obligatory transmission relay and consists of a ventral (**VCN**; anterior and posterior) and a dorsal (**DCN**) part (Amunts et al., 2012). Each SGN bifurcates and reaches the anterior ventral and the posterior ventral CN, while the tonotopy is still maintained. The VCN is responsible for processing temporal and spectral structure information of sound stimuli. Bushy cells in the VCN receive input and reach bilaterally the superior olivary complex (**SOC**) to sharpen timing and spectral information (Figure 4; Kandel, 2013).

Stellate cells in the VCN receive input from the SGN and project neurons into the ipsilateral DCN and reach the contralateral inferior colliculus (**IC**). The IC receives further ipsilateral and contralateral input from the SOC and efferent input from the auditory cortex (**AC**; Malmierca and Ryugo, 2012). Beside the involvement of sound localization the IC is also connected to the motor system to induce alert reflexes (Figure 4; Purves, 2004).

The medial geniculate body (**MGB**) is a central relay for ascending and descending auditory processing. Predominant ascending inputs are received from the ipsilateral and contralateral IC. The MGB is selective for frequency combinations and above for time differences between different frequencies. The spectral and temporal identification and separation abilities are important for communication especially in human (Purves, 2004). The MGB, as part of the thalamus, is responsible for the processing of emotional meaning and response and is assumed to influence attention (Kraus and Canlon, 2012).

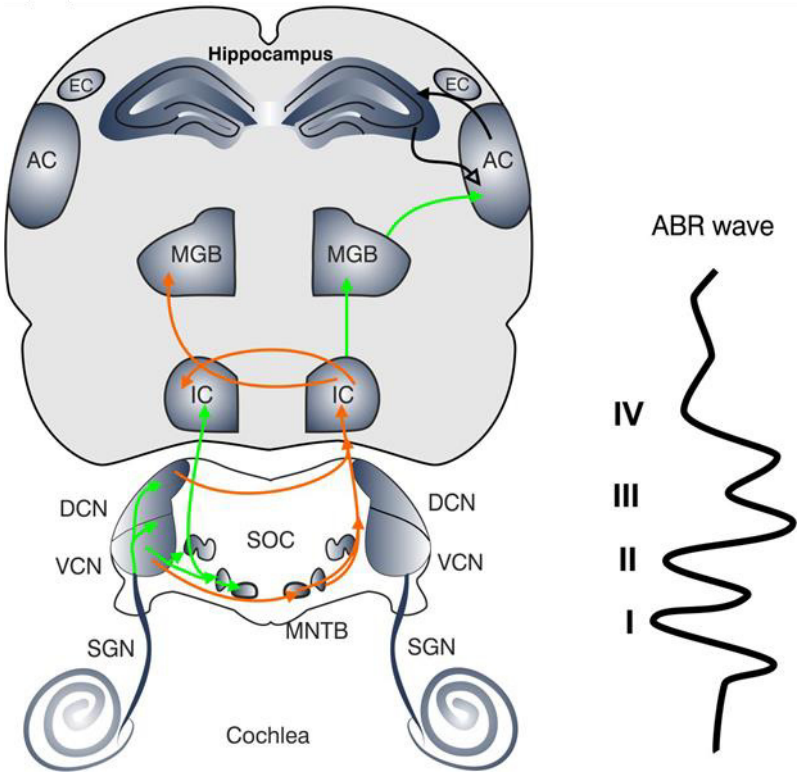

Figure 4: Schematic drawing of the ascending auditory pathway and corresponding auditory brainstem response (ABR) wave. Auditory cortex (AC), dorsal cochlear nucleus (DCN), entorhinal cortex (EC), inferior colliculus (IC), medial geniculate body (MGB), medial nuclei of the trapezoid body (MNTB), spiral ganglion neuron (SGN), superior olivary complex (SOC), ventral cochlear nucleus (VCN; modified after Knipper et al., 2013).

The superior target of auditory processing is the AC in the temporal lobe, which is built of several subdivisions (Malmierca and Ryugo, 2012). The primary AC is organized in a tonotopical map and receives direct input from the MGB. The secondary AC shows less frequency specificity and is responsible for perception of complex sounds such as frequency-modulated tones, harmonic complexes (Amunts et al., 2012; Binder et al., 2000; Hall et al., 2002), amplitude modulations (Giraud et al., 2000), spectrally dynamic sounds (Thivard et al., 2000), and sound sequences (Griffiths et al., 1999).

1.1.6 Efferent Feedback mechanisms of the auditory system

The descending auditory pathway from the AC over the MGB and IC reaches the CN where ipsilateral and contralateral projections from the medial SOC reach the OHCs and predominantly ipsilateral projections from the lateral SOC reach the IHCs (Amunts et al., 2012; Kandel, 2013). Efferent projections on OHCs hyperpolarize the membrane potential by activating a special class of nicotinic acetylcholine receptor-channels where Ca^{2+} enters the OHCs and activates K^{+}-influx (Malmierca

and Ryugo, 2012; Kandel, 2013). Neurons from lateral SOC innervate the region beneath the IHCs and release γ-aminobutyric acid (**GABA**), acetylcholine or dopamine (Malmierca and Ryugo, 2012). It is important in this context that the depolarizing inhibitory GABAergic switch appears in a region-specific pattern only after hearing onset (Friauf et al., 2011; Kandler and Friauf, 1995), possibly driven by sensory experience (Shibata et al., 2004; Vale and Sanes, 2002). This means that there is an initial stage of hyperexcitability at the onset of hearing when efferent GABAergic feedback is less developed because GABAergic neurons are initially still excitatory due to maturation shifts of the intracellular/extracellular chloride gradients (Ben-Ari, 2002; Marín and Rubenstein, 2001).

1.2 The hippocampus and its role in auditory learning and attention

1.2.1 Anatomy of the hippocampus and its role in memory

The hippocampus is a crucial component of mammalian brain for the consolidation from short-term memory to long-term memory and spatial navigation (Deshmukh and Knierim, 2012; Cappaert et al., 2015). The hippocampus has its origin in Greek terminology because of its vague analogy to the “seahorse” (*hippos* = horse; *kampos* = seamonster). It is shaped like a bent tube and located in the medial temporal lobe below the cerebral cortex of the brain. The hippocampus contains different cell types with distinct properties that are organized into layers. The importance of the hippocampus for the declarative memory (the memory of what, where, when) but not for procedural memory (the ability to learn new motor skills) was first confirmed with patient Henry Molaison who underwent a bilateral hippocampectomy as treatment for severe epilepsy (Bird and Burgess, 2008; Cappaert et al., 2015; Deshmukh and Knierim, 2012).

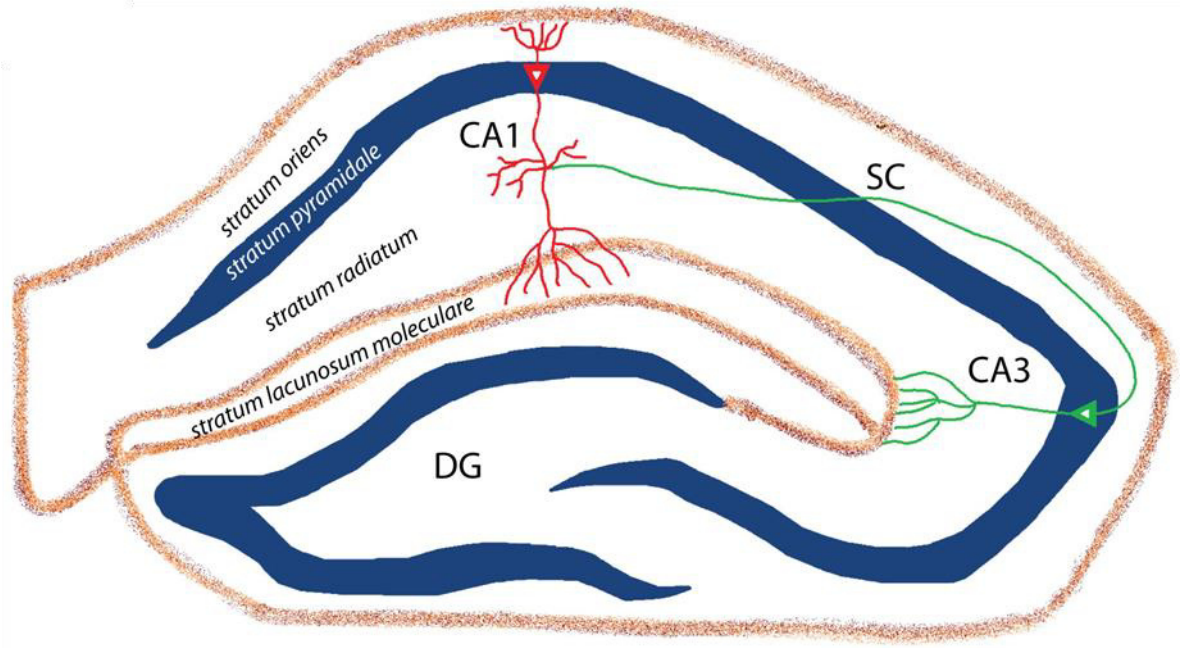

Figure 5: Cytoarchitecture of the hippocampus proper. Schematic transverse section of hippocampus. Cornu ammonis (CA), dentate gyrus (DG), Pyramidal cells of the CA1 are indicated in red, Schaffer collateral (SC) in green.

The hippocampus is characteristically composed of three distinct regions (Figure 5): the dentate gyrus, *cornu ammonis* (**CA**, horn of Amun) which is subdivided from CA1 to CA4 and the subiculum (Cheung and Cardinal, 2005). The hippocampus is connected to the neocortex by the entorhinal cortex (**EC**) which is located in the medial temporal lobe and constituted of 6 distinct layers. The EC is responsible for the cortical input into the hippocampus where fibers from layer II project to the dentate gyrus (**DG**) and CA3 while fibers from layer III project to CA1 and subiculum. Signals are processed in the perforant path including all hippocampal regions and CA1 axons projecting back to layer V and VI of the EC. The Schaffer collateral (**SC**) extends from CA3 to CA1 and is one of the best investigated models for synaptic plasticity and connected to memory and learning (Kullmann, 2011; Witter, 2012; Naber et al., 2001; Steward and Scoville, 1976). The specific serial organization of the hippocampus which is highly conserved in all mammals is the peak of successful evolution for memory formation, storage and retrieval. The DG is responsible for rapid encoding and pattern segregation (Aimone et al., 2011), while the primary function of the CA3 is the pattern completion through its autoassociative system of collateral projections (Lee et al., 2004; Jezek et al., 2011). CA1 and subiculum are probably involved in sequence coding and segregation over time (O'Mara et al., 2009; Hampson et al., 2000; O'Mara, 2005).

1.2.2 Role of the hippocampus in auditory information processing and auditory memory

The neurons in the amygdala, striatum, cingulate cortex (Chen et al., 2014; Vinogradova, 1976) and septum (Zhang et al., 2011; Vinogradova, 1976) which are directly connected with the hippocampus respond to sound stimuli, the amygdala and the striatum are even tonotopically organized (Bordi and LeDoux, 1992; Chen et al., 2012). There exists an amygdalar-auditory feedback loop in which the lateral amygdala receives direct neuronal input from MGB and AC (primarily association areas) while the basal amygdala projects back to inferior colliculus (Figure 6; Kraus and Canlon, 2012; Marsh et al., 2002). Therefore, acoustic stimuli impact the basolateral amygdala which in turn modulates the hippocampus including memory consolidation also by activating stress hormone release through the hypothalamic-pituitary-adrenal (**HPA**) axis (McGaugh, 2002; McIntyre et al., 2003; Paré, 2003). Further, direct afferent fibers project from the superior temporal gyrus (**STG**) to the EC and arise in the lateral parabelt areas of the AC (Amaral et al., 1983; Munoz-Lopez et al., 2010). Above, there is a direct connection from CA1 to the auditory association cortex and primary AC (Cenquizca and Swanson, 2007). Additionally, indirect connections project from the AC over the prefrontal cortex which could be found in rhesus (Romanski et al., 1999) and marmoset monkeys (Roberts et al., 2007). A non-cortical pathway is involved in auditory fear conditioning where neurons from the auditory brainstem activate the medial septum and thereby the hippocampus (Xiao et al., 2018). Hippocampal neurons respond to different sound stimuli for sound discrimination (Vinnik et al., 2012; Itskov et al., 2012), auditory recognition (O'Keefe and Nadel, 1978; Sakurai, 1990) and auditory fear conditioning (Moita et al., 2003; O'Keefe and Nadel, 1978).

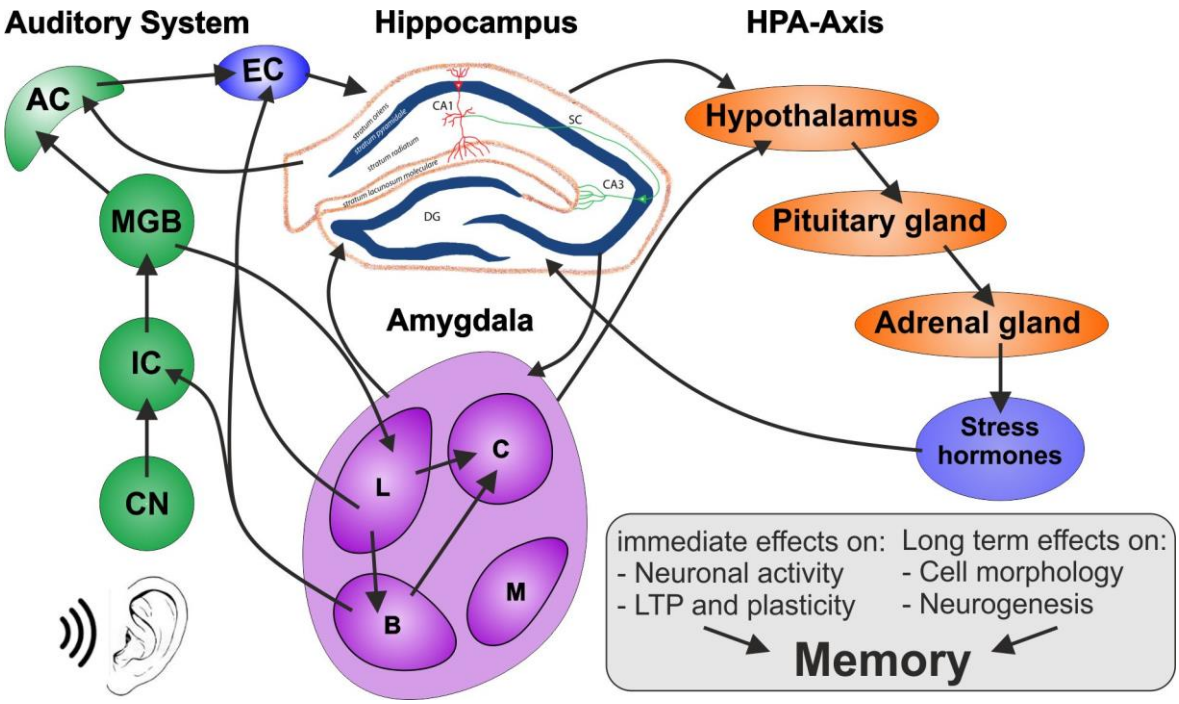

Figure 6: Connections between the auditory pathway and amygdala and hippocampus. Amygdala: basal (b), central (c), lateral (l), medial (m), auditory cortex (AC), cochlear nucleus (CN), Entorhinal cortex (EC), hypothalamic-pituitary-adrenal (HPA), inferior colliculus (IC), medial geniculate body (MGB; modified after Kraus and Canlon, 2012).

Thus, the formation of long-term auditory memories is the main function of the hippocampal-auditory system. In humans there are strong functional connectivities between the hippocampus and the AC during consolidation of auditory working memory (Kumar et al., 2016). Especially speech comprehension and music recognition are affecting hippocampal regions which could be shown in human functional magnetic resonance imaging studies (Pehrs et al., 2018; Davis and Johnsrude, 2003).

Attention is a crucial element of auditory processing concerning the hippocampus. Hippocampal neurons are involved in attention driven auditory gamma and theta rhythm phase locking which are associated with temporal processing of sensory (auditory) information (Nyhus and Curran, 2010). Phase-locking of theta waves is increasing during identification of novel sounds but decreasing with repetitive sound stimuli, suggesting an important role in attention and identification of novel sounds (Liberman et al., 2009) with a possible role of activity-dependent BDNF (Hill et al., 2016).

1.3 Brain derived neurotrophic factor

1.3.1 The role of BDNF in synaptic plasticity

Brain derived neurotrophic factor (**BDNF**) is involved in neuron proliferation, neurogenesis, differentiation and degeneration (Alderson et al., 1990; Barde, 1994; Barde et al., 1982) and therefore a crucial element for memory formation and cognitive function. It probably acts as major regulator of long-term potentiation (**LTP**), the strengthening of synapses, in the hippocampus and other brain regions (Bramham and Messaoudi, 2005; Messaoudi et al., 1998; Minichiello et al., 2002). On the other hand, the precursor of BDNF is assumed to regulate long-term depression (**LTD**) the weakening of synapses and a second key element of synaptic plasticity besides LTP (Yang et al., 2014). BDNF is part of the neurotrophin family and initially synthesized and released as precursor before it is cleaved by metalloproteinases (Chao and Bothwell, 2002). The active form of BDNF binds to the tyrosine receptor kinase (**Trk**) B receptor whilst the precursor pro-BDNF is activating the p75 neurotrophin receptor (Mowla et al., 2001). The activation of Trk receptors mediates differentiation and survival signaling pathways while p75 neurotrophin receptor activation affects apoptosis and growth inhibition (Chao, 2003).

1.3.2 Activity-dependent role of BDNF

BDNF mRNA levels are mainly regulated by neural activity, when Ca^{2+} influx triggers Ca^{2+} binding transcription factors like Ca^{2+}-response factor (**CaRF**) or cyclic AMP response element binding protein (**CREB**) and these then bind to the corresponding regulatory elements of *Bdnf* (Tao et al., 2002; Tao et al., 1998). In rodents 8 untranslated 5'-exons (I-VIII) which are spliced to the protein-encoding exon IX of *Bdnf* were described (Aid et al., 2007; Pruunsild et al., 2007). Among these exon IV and VI are highly responsive to neuronal activity (Hong et al., 2008; West et al., 2014; Tuvikene et al., 2016; Metsis et al., 1993). The transcription and translation of each exon is dependent on temporal and spatial location while the resulting BDNF protein is identical (Chiaruttini et al., 2008; Pattabiraman et al., 2005). The importance of activity-dependent transcription and translation of BDNF could be demonstrated in sensory systems where sensory experience induced BDNF expression was shown to be essential for the development of cortical inhibitory

circuits and thereby for the sharpening of receptive fields (Hong et al., 2008; Jiao et al., 2011; Itami et al., 2007; Heimel et al., 2011). In artificial conditions BDNF release is most pronounced after high frequency stimulation (≥ 100 Hz) or theta burst stimulation or by kainic acid infusion (Sathanoori et al., 2004; Singer et al., 2018; Haubensak et al., 1998; Balkowiec and Katz, 2000).

1.3.3 BDNF in the auditory system

BDNF is found in the cochlea from P4 onwards in SGN, phalangeal cells, and inner border cells that enclose the IHCs (Singer et al., 2014). In neonatal stage BDNF is only found in the apical cochlear turn in low concentrations while in the basal cochlear turn it is not detectable (Fritzsch et al., 2004). In mice BDNF disappears from the hair cells after birth and is gradually expressed in SGN until hearing onset between P10-14. BDNF is still expressed in SGN during the adult stage in a tonotopic gradient from low expression in the apical cochlear turn to high expression in the basal cochlear turn (Singer et al., 2014). During the first two postnatal weeks activity-dependent expression of *Bdnf* exon IV and VI is upregulated and maintains in adult stages (Singer et al., 2008; Panford-Walsh et al., 2008). For central auditory processing BDNF is crucial during the period of first auditory experience which induces long-lasting inhibitory potentiation of the thalamorecipient AC (Xu et al., 2010). The interplay of BDNF and Parvalbumin-positive (**PV**$^+$)-interneurons is essential for this sharpening of receptive fields (Hong et al., 2008; Jiao et al., 2011).

1.4 The role of Parvalbumin-positive interneurons

1.4.1 Features of fast-spiking parvalbumin-positive interneurons

PV$^+$-interneurons are GABAergic and possess unique features as short action potential duration and fast spiking action potential phenotype (Hu et al., 2014). PV$^+$-interneurons contain multiple dendritic connections across layers and receive input from different feed-forward and feed-back pathways what is different to glutamatergic principal neurons (Nörenberg et al., 2010; Tukker et al., 2013; Gulyás et al., 1999). Dendrites and somata of PV$^+$-interneurons are densely covered by synapses and receive 94 % excitatory and only 6 % inhibitory input (Gulyás et al., 1999; Tukker et al., 2013). PV$^+$-interneurons innervate perisomatic postsynaptic target cells like basket cells which form basket-like formations around principal

neuron somata and proximal dendrites. In axo-axonic cells like PV+-interneuron bistratified cells, the axon follows the axon of the principal neuron in a chandelier formation (Klausberger and Somogyi, 2008). These morphological characteristics of PV+-interneurons enable the inhibitory power for feed-forward and feed-back regulation and its significant role for several brain functions like memory and learning.

1.4.2 The role of parvalbumin-positive interneurons in microcircuits

PV+-interneurons are fundamental for feed-forward and feed-back circuits which is best investigated in the hippocampus. Following stimulation of hippocampal SC neurons feed-forward inhibition is mediated by perisomatic inhibitory interneurons, primarily by PV+-interneurons (Pouille and Scanziani, 2001; Pouille et al., 2009) while feed-back inhibition is best shown for reciprocal coupling of fast-spiking interneurons and principal neurons in the hippocampus and EC (Geiger et al., 1997; Pouille et al., 2009). Feed-forward and feed-back inhibition involving PV+-interneurons forms a complex 'winner-takes-all' process in which the principal neurons with the strongest input depolarize and fire while the remaining cells are inhibited (Almeida et al., 2009a, 2009b). Precise spatial and temporal information processing is therefore crucial for neuronal information processing (Lisman and Buzsáki, 2008) while different classes of network oscillations provide coordinated synchronous activity (Traub and Whittington, 2010). The 'winner-takes-all' mechanism is involved in these oscillations and the activity of PV+-interneurons is assumed to be responsible for γ-oscillations (Almeida et al., 2009a, 2009b).

1.5 Stress action in the brain

1.5.1 The stress (hypothalamic-pituitary-adrenal) axis

Threatening situations, also known as stressors, trigger the release of stress hormones in the brain to activate the fight-or-flight reaction of living organisms. These stressors can be of physical or psychological origin (Kloet et al., 2005). The stress response is necessary for surviving, coping with a threat, adapting to demand (Kloet and Joëls, 2016), and shaping the social behavior (Sandi and Haller, 2015). The hippocampus regulates the endocrine system by modulation of parvocellular neurons of the hypothalamic paraventricular nucleus (**PVN**) that release

corticotropin-releasing hormone (**CRH**) in response to a stressor. CRH activates the synthesis of pro-opiomelanocortin in the anterior pituitary which is processed to corticotropin (**ACTH**) and activates the adrenal gland to secrete corticosteroids, which are divided into gluco- and mineralocorticoids which bind to specific stress hormone receptors and thus have different functions in the body. In the brain, mineralocorticoid receptors (**MRs**) possess a 10-fold higher affinity to glucocorticoids than glucocorticoid receptors (**GRs**), corticosterone is the main regulating corticosteroid in the brain of rodents (Kloet et al., 2005). In a healthy system the secretion of stress hormones fluctuates following the circadian rhythm and adapts to different situations. But when there is no sufficient recovery from high stress hormone levels and the stress response becomes chronic, maladaptive changes such as impaired work performance, anxiety, depression and hearing disorders such as tinnitus, can be the consequences (Figure 7; Canlon et al., 2013).

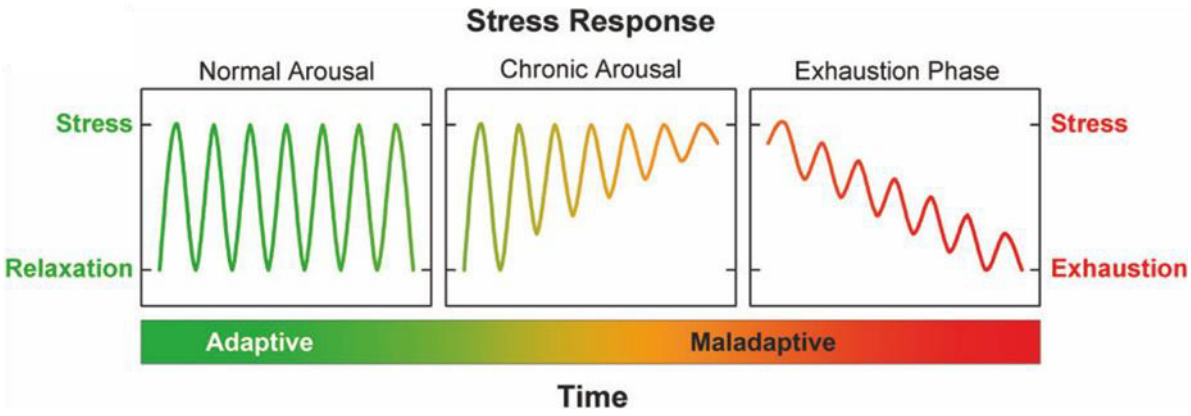

Figure 7: Schematic illustration of the stress response (modified after Canlon et al., 2013).

1.5.2 Mineralocorticoid and glucocorticoid receptors

MR and GR are nuclear receptors and belong to the family of steroid stress hormone receptors (Kloet et al., 1999; Canlon et al., 2007). The binding of corticosteroids to MR or GR initiate a multimeric protein complex dissociation leading to dimerization of MR or GR which act as homodimers or heterodimers on gene expression by binding at the glucocorticoid response element. This influence on gene expression and protein synthesis impact G-protein coupled receptors, ion channels, ionotropic receptors and ion pumps finally the whole homeostatic function of a nerve cell. Because of the higher affinity of MR to corticosteroids the fast stress response is assumed to be regulated by the MR while higher corticosterone levels activate the GR and the consequences of high chronic stress hormone levels are attributed to

the GR (Kloet et al., 2005). In brain regions which are highly involved in the stress response like the hippocampus and the hypothalamic PVN a high density of MR and GR can be observed (Kloet et al., 2005).

1.5.3 The influence of stress on the auditory function

Stress plays a major role in modulation of the hearing function (Canlon et al., 2007; Basappa et al., 2012). The effects of harmful mechanical stress like loud noise have been investigated in detail in animal (Canlon et al., 1988; Liberman and Gao, 1995) and human studies (Tambs et al., 2006; Job et al., 2009). Also the consequences of emotional chronic stress are well studied (Dagnino-Subiabre, 2013) even with associated neurological disorders (Pérez-Valenzuela et al., 2019). The effect of stress on the auditory function depends on the duration of the stress response which is fluctuating in a healthy system (Canlon et al., 2013). Acute stress can be protective during exposure of high sound pressure levels (Tahera et al., 2007; Wang and Liberman, 2002) and synthetic corticosteroids are a common remedy for different hearing disorders (El Sabbagh et al., 2017; Shim et al., 2017). On the other hand, high chronic stress hormone levels can operate as catalysator of tinnitus or sudden hearing loss (Mazurek et al., 2015; Schmitt et al., 2000). Additionally, chronic stress hormone release as well as excessive neuronal activity in the amygdala or auditory system during harmful noise exposure affects the hippocampus by reducing neuronal activity, altering LTP, modifying synaptic plasticity, changing memory properties and inducing long-term effects such as altered cell morphology and decrease of neurogenesis (Figure 6; Hirano et al., 2006; Kim and Haller, 2007; Lynch, 2004).

The stress response has a massive impact on hearing function, but the influence of the single stress hormone receptors, MR and GR, is still unclear.

2. Aim of this study

The main objective of this study was to investigate the connection between the auditory function and central cognitive response mechanisms. We focused on the relationship between BDNF and stress hormone signaling and its influence on auditory processing and central learning mechanisms. In addition, we wanted to understand how fast auditory processing affects central hippocampal memory and learning mechanisms and how feedback from central brain areas influences peripheral auditory processing.

First, we investigated the influence of endogenous stress hormone levels on auditory function in terms of both peripheral and central sound processing (auditory brainstem responses (**ABRs**), distortion product of otoacoustic emissions (**DPOAEs**)) and molecular properties (immunohistochemistry). Regarding the negative influence of increased stress hormone levels on auditory processing we investigated the influence of mineralocorticoid receptors (**MRs**) and glucocorticoid receptors (**GRs**) on peripheral and central sound processing after sham and traumatic sound exposure using specific MR and GR antagonists.
(Singer, Eckert et al.,"*The glucocorticoid antagonist mifepristone attenuates sound-induced long-term deficits in auditory nerve response and central auditory processing in female rats*", FASEB J. 2018)

Next, we investigated the top-down influence of central stress hormone receptors MR and GR by deletion under the CaMKIIα promoter. We analyzed the influence on peripheral auditory processing by DPOAE, ABR, and immunohistochemistry. (Marchetta, Eckert et al., *"Stress receptors in frontal brain regions influence auditory nerve function and auditory brainstem responses",* in preparation)

In addition, we studied the specific influence of BDNF in the auditory periphery in *Bdnf*^{Pax2} KO mice, which have deficits in temporal auditory processing. We investigated the impairment of fast auditory processing and thereby connected central learning mechanisms by ABR, acoustic startle, LTP, a behavioral memory task (multiple T-maze), a social behavior task (Crawley's 3-chamber sociability test) and molecular analyses (immunohistochemistry, in situ hybridization staining).
(Eckert et al., "*Brain-derived neurotrophic factor in inhibitory hindbrain neurons controls central learning mechanisms*", in preparation)

Finally, we proved the newly generated transgenic ***B***DNF-***L***ive-***E***xon-***V***isualization (**BLEV**) reporter mouse model by molecular and functional assays and analyzed the context specific role of activity-dependent BDNF. We investigated long-lasting adaptational changes driven by the activity-dependent expression of BDNF in response to different sound exposure paradigms using ABR, long-term potentiation (**LTP**), behavioral memory tasks and molecular analyses (immunohistochemistry, Western blot).

(Singer, Eckert et al., "*BDNF-Live-Exon-Visualization (BLEV) allows differential detection of BDNF transcripts in vitro and in vivo*" Front Mol Neurosci. 2018;

Matt, Eckert et al.,"*Visualizing BDNF transcript usage during sound-Induced memory linked plasticity*", Front Mol Neurosci. 2018)

3. Results

3.1 The influence of stress on auditory processing and the potential of pharmacological treatments

The results and figures described in the following section refer to Singer, Eckert et al., "*The glucocorticoid antagonist mifepristone attenuates sound-induced long-term deficits in auditory nerve response and central auditory processing in female rats*". FASEB J. 2018, which is attached in the appendix 7.1.

The hearing system is very sensitive to stress. Stress can be protective in acute situations or harmful after a long-term period of chronic stress. In clinical use, synthetic corticosteroids are the treatment of choice for various hearing disorders, illustrating the controversial different effects of stress on hearing function. How these contrary stress actions are connected with each other remains unclear. In the present study the question was raised if endogenous stress hormone levels may impact hearing function before and after acoustic trauma (**AT**).

It was hypothesized that the different stress hormone receptors, the glucocorticoid receptor (**GR**) and the mineralocorticoid receptor (**MR**) differentially effect hearing function. Moreover, the influence of endogenous corticosterone levels, determined in urine samples from rats, was investigated. Auditory brainstem responses (**ABRs**) were recorded and fine structure of supra-threshold ABR waves were analyzed and related to endogenous corticosterone levels. Further, distortion product of otoacoustic emissions (**DPOAEs**) were recorded to assess the electromotility of outer hair cells (**OHCs**). To evaluate the integrity of the inner hair cell (**IHC**) synapse distinct molecular markers were studied. To assess the effect of endogenous stress hormone levels and the antagonization of the GR or the MR during AT, rats were exposed to sound at a harmful sound pressure level (**SPL**).

3.1.1 Elevated corticosterone levels diminish high-frequency auditory nerve responses and promote inner hair cell damage after acoustic trauma

To investigate the influence of endogenous corticosterone levels on hearing function, we calculated a correlation of the sensitivity of auditory nerve responses to endogenous corticosterone levels. We could show that the wave I amplitude of supra-threshold ABRs to stimuli at 16 kHz and 65 dB SPL were significantly lower in animals with higher endogenous corticosterone level (Figure 2A; *Singer, Eckert et al., 2018, FASEB J, 7.1*). We also analyzed the number of IHC

ribbons, which was reduced only in the basal cochlea turns and this reduction correlated with increased corticosterone levels (Figure 2B,D,E; *Singer, Eckert et al., 2018, FASEB J, 7.1*). This was in line with the correlation to the reduced ABR wave I amplitude at high frequency (16 kHz). Additionally, supra-threshold ABR wave I amplitudes correlated with IHC ribbon number in the basal cochlear turn (Figure 2C; *Singer, Eckert et al., 2018, FASEB J, 7.1*) and thus revealed a direct influence of the stress-induced decrease in the number of ribbons on the decrease in the auditory nerve response.

Beside the presynaptic side also the postsynaptic side was affected by higher endogenous corticosterone levels shown by staining of the Na^+, K^+-ATPase subunit alpha3 (**NKAα3**). NKAα3 is a marker of afferent type I neurons and fibers (McLean et al., 2008). Less intense NKAα3-immunoreactivity (**IR**) in the bouton-like tip of the nerve terminals (Figure 2E, NKAα3, green, open arrows; *Singer, Eckert et al., 2018, FASEB J, 7.1*) in animals with elevated endogenous corticosterone levels correlated with a lower number of IHC ribbons at the presynaptic side in the basal cochlear turn (Figure 2E, CtBP2, red, closed arrows; *Singer, Eckert et al., 2018, FASEB J, 7.1*).

To evaluate the influence of high endogenous corticosterone levels on the vulnerability of hair cells under challenging conditions animals were exposed for 1 h to 10 kHz pure tone at 116 dB SPL (AT; Jaumann et al., 2012; Rüttiger et al., 2013). After 14 d of recovery, ABR measurements showed a permanent threshold shift at different frequencies in all animals (Figure 3A, red line; *Singer, Eckert et al., 2018, FASEB J, 7.1*) compared to unexposed animals (Figure 3A, black line; *Singer, Eckert et al., 2018, FASEB J, 7.1*). Among AT exposed animals, a difference in the ABR threshold at 32 kHz was observed, which could be correlated with endogenous stress hormone levels (Figure 3A, gray lines, encircled area; *Singer, Eckert et al., 2018, FASEB J, 7.1*). Indeed, higher ABR thresholds at 32 kHz stimuli correlated to higher corticosterone levels of individual animals (Figure 3B, red dots; *Singer, Eckert et al., 2018, FASEB J, 7.1*), which was not observed in unexposed animals (Figure 3B, black dots; *Singer, Eckert et al., 2018, FASEB J, 7.1*). A reduction of IHC ribbon number in all cochlear turns could be observed 14 d after AT, again predominantly at high-frequency representing basal cochlear turns when compared to unexposed animals. Emphasizing the effect of endogenous corticosterone levels on the vulnerability of IHCs the number of ribbons per IHC in

the basal cochlear turns of noise exposed animals was lower in animals with higher corticosterone levels (Figure 3C, AT, red dots; *Singer, Eckert et al., 2018, FASEB J, 7.1*). The IHC ribbon loss 14 d after AT in midbasal, medial (Figure 3D; *Singer, Eckert et al., 2018, FASEB J, 7.1*), or apical cochlear turns did not correlate to the corticosterone levels of the individual animals. The basal cochlear turns are responsible to conduct frequencies higher than 16 kHz (Müller and Robertson, 1991) and showed higher sensitivity to high endogenous corticosterone levels when supra-threshold ABR wave I amplitude evoked by 32 kHz pure tone stimuli was analyzed (Figure 3E, low stress: black line; high stress: grey line; *Singer, Eckert et al., 2018, FASEB J, 7.1*). Additionally, this reveals the sensitivity of IHC ribbons to chronic stress and was emphasized by the higher vulnerability after AT shown as dramatically decreased threshold and supra-threshold ABR wave I amplitude (Figure 3E, AT - low stress: blue line; AT - high stress: red line; *Singer, Eckert et al., 2018, FASEB J, 7.1*). Acoustically traumatized animals with increased endogenous stress hormone levels and increased ABR threshold could not be recorded >30 dB SPL above the threshold (Figure 3E, red crosses; *Singer, Eckert et al., 2018, FASEB J, 7.1*). The synaptic integrity of IHCs was shown to be influenced by high endogenous stress hormone levels confirming the negative impact of stress on IHCs when analyzing immunohistochemical staining of presynaptic CtBP2/RIBEYE (ribbons) and postsynaptic NKAα3. As shown for unexposed animals (Figure 2; *Singer, Eckert et al., 2018, FASEB J, 7.1*) both markers for synaptic integrity were distinctly decreased in animals with AT and high endogenous corticosterone levels (Figure 3H, CtBP2, red, closed arrow; NKAα3, green, open arrow; *Singer, Eckert et al., 2018, FASEB J, 7.1*) compared to acoustically traumatized animals with low endogenous corticosterone levels (Figure 3G; *Singer, Eckert et al., 2018, FASEB J, 7.1*).

In conclusion, high endogenous stress hormone levels do not only influence the hearing function in an unchallenging environment but also dramatically worsen the protection and recovery after AT.

3.1.2 Inhibition of MR and GR has no effect on OHC function before and after acoustic trauma

Because of the deep impact of endogenous corticosterone levels on the vulnerability of basal IHC synapses, we analyzed the potentially protective effect of MR and GR inhibitors. We treated rats intraperitoneally with either the GR antagonist

mifepristone (100 mg/kg), or the MR antagonist spironolactone (75 mg/kg) or a vehicle (polyethylene glycol and ethanol; 1:10, 2 ml/kg) 90 min before AT. Comparing the thresholds of sham exposed animals with pre measurements no differences for click stimuli (Figure 4A; *Singer, Eckert et al., 2018, FASEB J, 7.1*), noise burst stimuli (Figure 4B; *Singer, Eckert et al., 2018, FASEB J, 7.1*), or DPOAEs (Figure 4C; *Singer, Eckert et al., 2018, FASEB J, 7.1*) could be observed. 14 d after AT, slightly protected hearing thresholds could be seen in pharmacologically pretreated animals compared to vehicle-pretreated animals, but these differences were not statistically significant, neither for click stimuli (Figure 5A; *Singer, Eckert et al., 2018, FASEB J, 7.1*), nor for noise burst stimuli (Figure 5B; *Singer, Eckert et al., 2018, FASEB J, 7.1*), nor for tone bursts (Figure 5C; *Singer, Eckert et al., 2018, FASEB J, 7.1*). In addition, DPOAE response amplitudes (Figure 5D; *Singer, Eckert et al., 2018, FASEB J, 7.1*) and DPOAE thresholds were measured at different frequencies (Figure 5E; *Singer, Eckert et al., 2018, FASEB J, 7.1*), with a trend towards less, although not statistically significant damage in pharmacologically treated animals. The non-significant trend of mifepristone and spironolactone treated groups that appear to be mildly protected from hearing threshold loss became more distinct when ABR thresholds for single pure tone stimuli were specifically compared (Figure 5F-H; *Singer, Eckert et al., 2018, FASEB J, 7.1*).

In conclusion, the pharmacological inhibition of MR or GR prior to AT had only minor but not significant impact on hearing thresholds or OHC function 14 d after AT.

3.1.3 Inhibition of GR but not MR protects auditory acuity after acoustic trauma

Pharmacological inhibition of GR or MR prior to AT in rats did not significantly protect hearing thresholds but showed a protective trend especially at high frequencies. The protective effect was more pronounced for ABR thresholds in response to high frequency tone bursts of 16 kHz (Figure 5G; *Singer, Eckert et al., 2018, FASEB J, 7.1*) and 32 kHz (Figure 5H; *Singer, Eckert et al., 2018, FASEB J, 7.1*) compared to low frequency tone bursts of 4 kHz (Figure 5F; *Singer, Eckert et al., 2018, FASEB J, 7.1*) although it was not significant. For this reason, we analyzed supra-threshold ABR wave amplitudes to get further insights into auditory nerve processing. The amplitudes of evoked auditory nerve activity (ABR wave I) and evoked midbrain activity (ABR wave IV) in response to increasing

pure tones were recorded before and 14 d after AT and depicted as growth function (Figure 6A-C; *Singer, Eckert et al., 2018, FASEB J, 7.1*). Antagonization of GR led 14 d after AT to remarkably less affected supra-threshold ABR wave amplitudes of ABR wave I and wave IV, particularly in high frequencies (16 kHz, Figure 6B; 32 kHz, Figure 6C; *Singer, Eckert et al., 2018, FASEB J, 7.1*). The expanded dynamic range of mifepristone treated animals of ABR wave I and IV was striking, but also spironolactone treated animals showed a wider dynamic range than vehicle treated animals especially at higher frequencies. To specify the protective effect of mifepristone on supra-threshold ABR waves we further analyzed the dynamic range (Figure 7A, depicted as reach; *Singer, Eckert et al., 2018, FASEB J, 7.1*) and maximal amplitude size (Figure 7A, depicted as size; *Singer, Eckert et al., 2018, FASEB J, 7.1*). Inhibition of GR by mifepristone but not inhibition of MR by spironolactone had a strong effect on reach and size of auditory nerve and midbrain evoked amplitudes to 32 kHz tone burst (Figure 7D; *Singer, Eckert et al., 2018, FASEB J, 7.1*). At lower frequencies (Figure 7C, 16 kHz tone burst; Figure 7B, 11 kHz tone burst; *Singer, Eckert et al., 2018, FASEB J, 7.1*) the mifepristone treated group showed also a protective effect on dynamic range and maximal amplitude size even though not significant. The results clearly point out that an inhibition of GR but not MR, particularly at high frequencies, leads to a protective effect after AT on the dynamic range and emphasize the different effects of stress on hearing function. The range of auditory fiber responses may be related with the reliability of discharge rate and synchronously firing of auditory nerve fibers, that define ABR amplitude size (Johnson and Kiang, 1976).

We counted the number of IHC ribbons along the tonotopic axis of the cochlea of treated and untreated animals 14 d after AT and observed that the number of CtBP2-positive dots at the IHC synapse was significantly reduced in midbasal and basal cochlear turns of pharmacologically untreated animals after AT (Figure 8; *Singer, Eckert et al., 2018, FASEB J, 7.1*). Mifepristone but not spironolactone pretreatment partly prevented the IHC ribbon loss in midbasal and basal cochlear turns (Figure 8; *Singer, Eckert et al., 2018, FASEB J, 7.1*).

These findings strongly underline a negative effect of chronic stress on hearing function mainly mediated by GR, which additionally worsens hearing function during challenging situations like AT. In addition, we could show that elevated endogenous

corticosterone levels during AT are highly correlated with a decrease in auditory fiber responses predominantly in high-frequency cochlear regions.

3.2 Central stress hormone receptors modulate peripheral auditory processing

The results and figures described in the following section are depicted in the following pages and refer to Marchetta, Eckert et al., *"Stress receptors in frontal brain regions influence auditory nerve function and auditory brainstem responses"*, which is in preparation.

We hypothesized that long lasting adaptation processes of auditory stimuli are modulated by a central stress response. The primary aim was to investigate whether mouse mutants with a deletion of MRs or GRs or both receptors under the calcium/calmodulin dependent protein kinase II α (**CaMKIIα**) promoter by tamoxifen induction in the adult stage are suitable to study the influence of central stress hormone receptors on cochlear nerve fiber activity. We investigated the deletion profile of the stress hormone receptors and basal hearing function of all three mutant mouse strains to evaluate the influence of the single stress hormone receptors on peripheral and central auditory processing in the adult system.

3.2.1 Deletion of MR and GR in the mouse forebrain under the CaMKIIα promoter

To analyze the effect of the hormonal stress receptors MR and GR we used conditional knock-out mice where MR (**MRCaMKIIαCre KO**) or GR (**GRCaMKIIαCre KO**) or both (**MRGRCaMKIIαCre KO**) were deleted under the promoter of CaMKIIα by tamoxifen induction at the age of 8 weeks. To proof the expression pattern of CaMKIIα we used ROSA26 tdTomato mice crossed with CaMKIIαCre mice. We could observe a strong tdTomato staining in ROSA26 tdTomato CaMKIIαCre positive in the hippocampus (Figure 8A, left panel; *Marchetta, Eckert et al., in preparation*) but not in cochlear whole mount preparations (Figure 8B, left panel; *Marchetta, Eckert et al., in preparation*).
This expression profile of CaMKIIα visualized by ROSA26 tdTomato CaMKIIαCre mice serve a further proof to show that CaMKIIα is only expressed in the forebrain as previously described (Erdmann et al., 2007) and not in the cochlea.

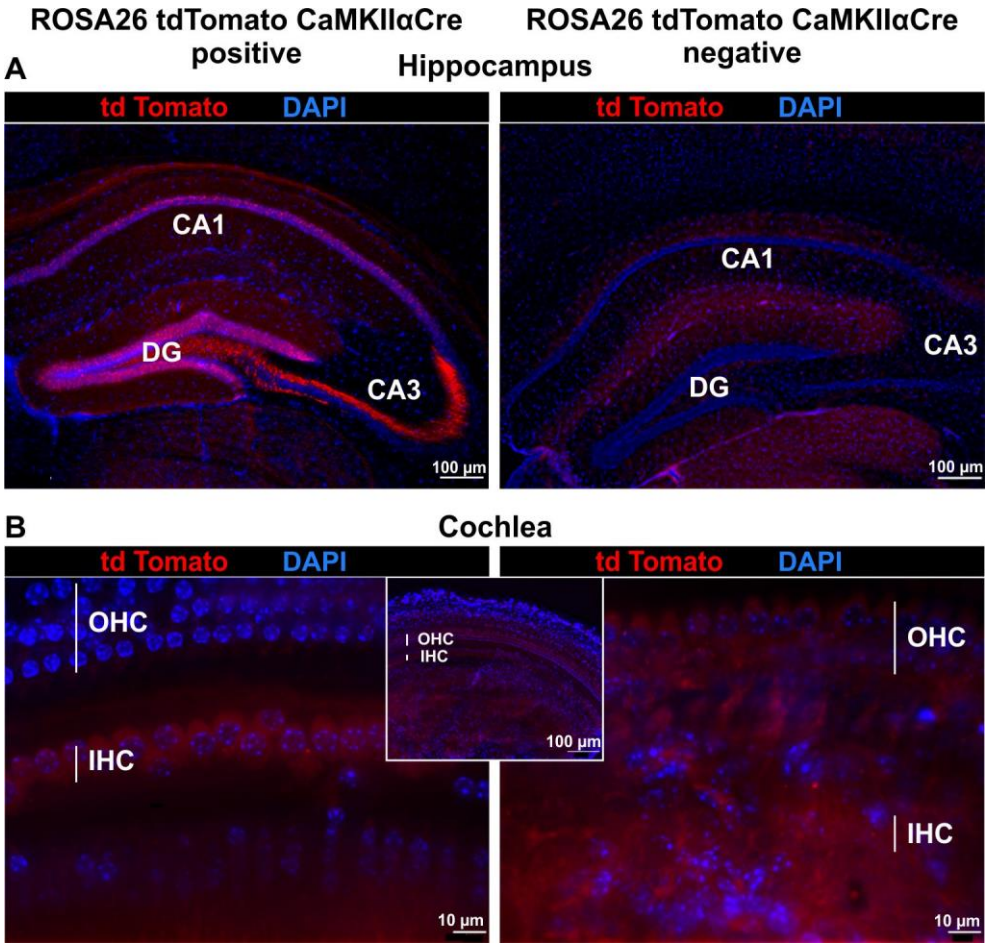

Figure 8: Expression profile of CaMKIIα revealed by cross-breeding of ROSA26 tdTomato mice with CaMKIIαCre mice. (**A**) Strong tdTomato staining in the hippocampus of ROSA26 tdTomato CaMKIIαCre positive mice while in (**B**) cochlear whole mount preparations no tdTomato staining could be observed. CA, cornu ammonis; DG, dentate gyrus; IHC, inner hair cells; OHC, outer hair cells. Scale bars: (a) 100 µm, (b) 10 µm. Nuclear staining DAPI (blue).

To visualize the expression of MR and GR to confirm the deletion of MR and GR under the promoter of CaMKIIα, immunohistochemical staining of MR and GR was performed in hippocampal brain slices and cochlear whole mount preparations.

We could show that the MR (Figure 9A, green; *Marchetta, Eckert et al., in preparation*) and GR (Figure 9C, green; *Marchetta, Eckert et al., in preparation*) deletion in the hippocampus was successful under the promoter of CaMKIIα. As shown in Figure 8B CaMKIIα was not expressed in the cochlea hence MR and GR staining (green) co-labeled with vesicular glutamate transporter-3 (**VGluT3**) could be detected in wild-type (**WT**) as well as in KO mice (Figure 9B,D; *Marchetta, Eckert et al., in preparation*). With this proofed deletion profile of MR and GR, all our observations and possible changes in hearing function can be attributed

to central stress hormone receptors because cochlear stress hormone receptors were still expressed.

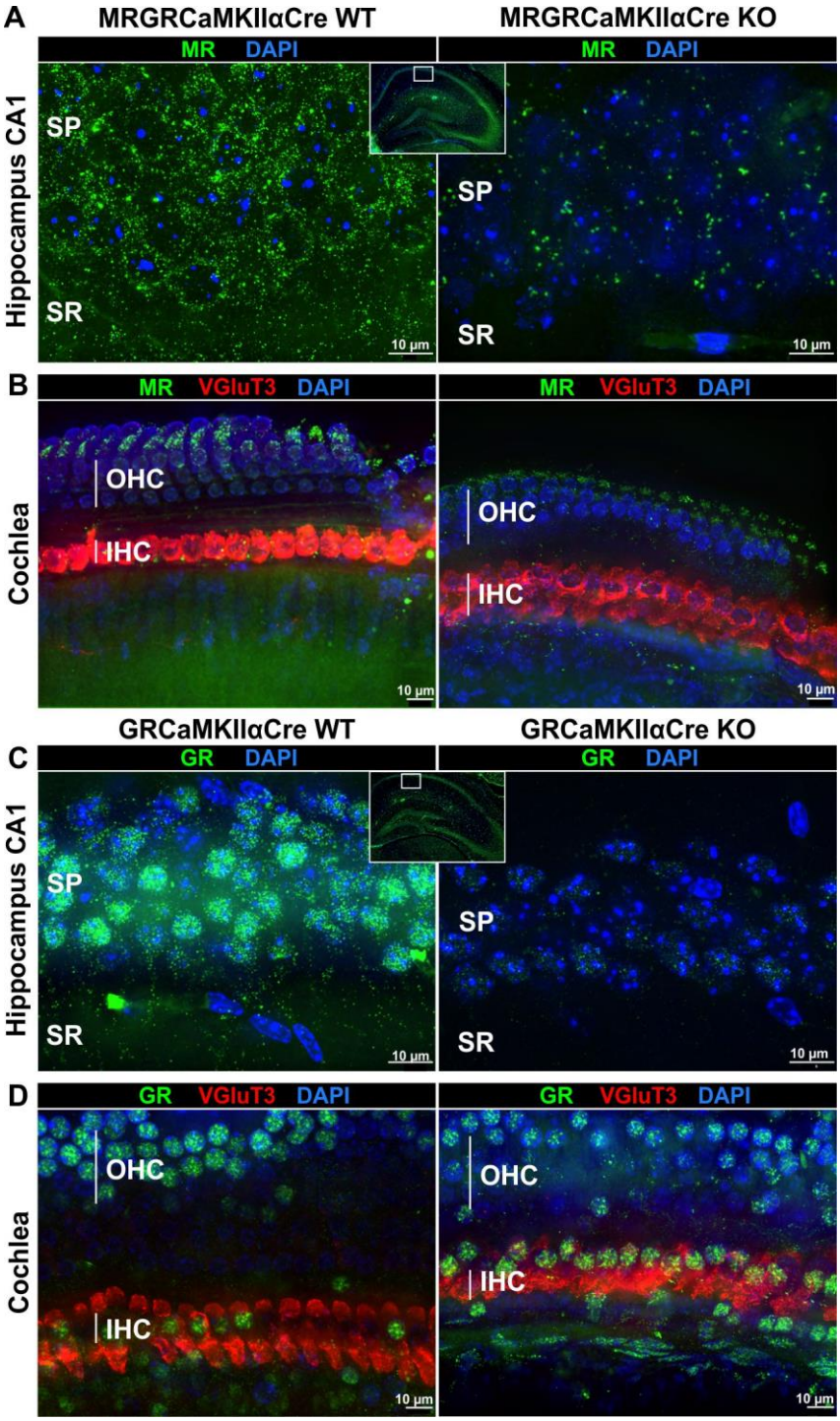

Figure 9: Expression profile of MR and GR in the hippocampus and cochlea of WT and KO mice. (**A**) MR-IR (green) in hippocampal mouse slices. (**B**) MR-IR (green) in cochlear whole mount preparations co-labeled by VGluT3 as IHC marker. (**C**) GR-IR (green) in hippocampal mouse slices from WT and KO mice. (**D**) GR-IR (green) in cochlear whole mounts co-labeled by VGluT3. SP, stratum pyramidale; SR, stratum radiatum; IHC, inner hair cells; OHC, outer hair cells. Scale bars: 10 µm. Nuclear staining DAPI (blue).

3.2.2 The central deletion of MR or/and GR has a differential impact on evoked auditory nerve and midbrain activity and latencies but not on auditory thresholds

The central deletion of MR and/or GR on hearing function was first assessed by ABR thresholds for click and pure tone stimuli as functional biomarker for destruction of OHCs in respective cochlear regions (Rüttiger et al., 2017).

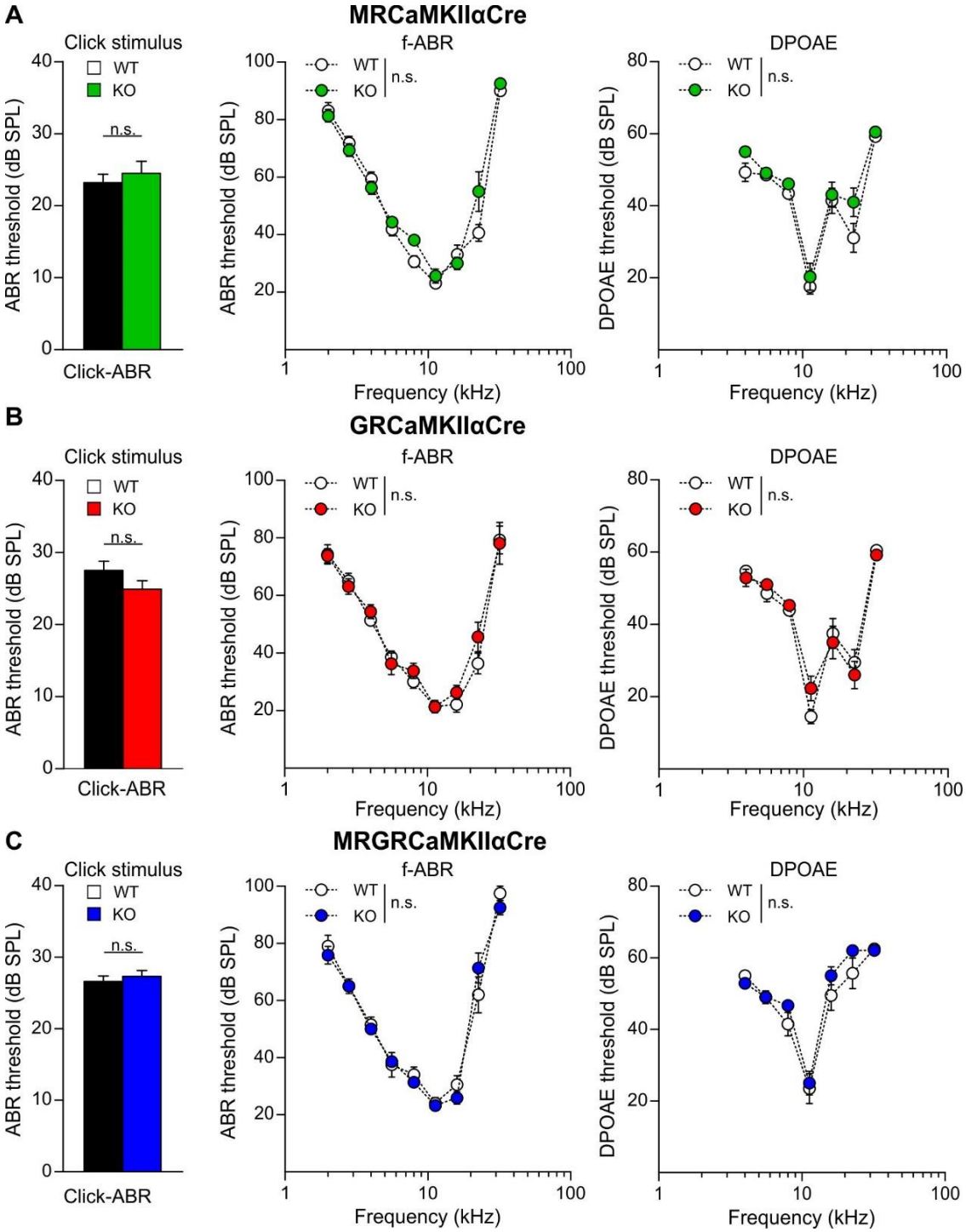

Figure 10: Click-, pure tone stimuli evoked ABR and DPOAE thresholds of (**A**; WT = black, KO = green) MRCaMKIIαCre (**B**; WT = black, KO = red) GRCaMKIIαCre mice and (**C**; WT = black, KO = blue) MRGRCaMKIIαCre mice. Error bars represent S.E.M.; n.s.: not significant.

MRCaMKIIαCre KO mice revealed no significant difference in click-evoked hearing thresholds (Figure 10A, MRCaMKIIαCre click stimuli: WT: $n = 16/32$ mice/ears, KO: $n = 16/32$ mice/ears; unpaired two-tailed students t-test, $t(30) = 0.646$, $P = 0.523$; *Marchetta, Eckert et al., in preparation*). ABR thresholds evoked by pure tone stimuli in a frequency range between 2 and 32 kHz (f-ABR) were also not affected by deleting MR (Figure 10A; MRCaMKIIαCre f-ABR: WT: $n = 8/16$ mice/ears; KO: $n = 8/16$ mice/ears; 2-way ANOVA, $F(1,122) = 2.725$, $P = 0.101$; *Marchetta, Eckert et al., in preparation*). Also, GRCaMKIIαCre KO mice and MRGRCaMKIIαCre KO mice did not differ for click- and pure tone stimuli evoked ABR thresholds from WT mice (Figure 10B,C; GRCaMKIIαCre click-stimuli: WT: $n = 14/28$ mice/ears, KO: $n = 16/32$ mice/ears; unpaired two-tailed students t-test, $t(28) = 1.521$, $P = 0.140$; f-ABR: WT: $n = 7/14$ mice/ears; KO: $n = 8/16$ mice/ears; 2-way ANOVA, $F(1,117) = 0.946$, $P = 0.333$; MRGRCaMKIIαCre click-stimuli: WT: $n = 24/48$ mice/ears, KO: $n = 28/56$ mice/ears; unpaired two-tailed students t-test, $t(50) = 0.620$, $P = 0.538$; MRGRCaMKIIαCre f-ABR: WT: $n = 10/20$ mice/ears; KO: $n = 11/22$ mice/ears; 2-way ANOVA, $F(1,154) = 0.191$, $P = 0.663$; *Marchetta, Eckert et al., in preparation*).

The electromotility of OHCs is specifically responsible for cochlear amplification and thereby mainly affects the threshold (Brownell et al., 1985; Ashmore, 2008). Our observations that ABR thresholds and by association OHCs are not affected by deleting central MR and/or GR could be proven by measuring DPOAE, where no effect could be observed (Figure 10A,B,C right panel; MRCaMKIIαCre DPOAE: WT: $n = 16/32$ mice/ears; KO: $n = 16/32$ mice/ears; 2-way ANOVA, $F(1,202) = 6.640$, $P = 0.011$; GRCaMKIIαCre DPOAE: WT: $n = 14/28$ mice/ears; KO: $n = 15/30$ mice/ears; 2-way ANOVA, $F(1,185) = 0.057$, $P = 0.810$; MRGRCaMKIIαCre DPOAE: WT: $n = 10/20$ mice/ears; KO: $n = 15/30$ mice/ears; 2-way ANOVA, $F(1,146) = 3.080$, $P = 0.081$; *Marchetta, Eckert et al., in preparation*).

We analyzed fine structure of supra-threshold click-evoked ABR waves which have amplitudes proportional to the discharge rate and number of synchronously firing auditory fibers (Rüttiger et al., 2017) to get specific insights into the influence of central MR and GR on IHC function. Indeed, MR and GR had a great impact on the IHC function disclosed by changed evoked auditory nerve activity (Figure 11 left panel; *Marchetta, Eckert et al., in preparation*) and response latency (Figure 12 left panel; *Marchetta, Eckert et al., in preparation*). Additionally, evoked midbrain activity (Figure 11 right panel; *Marchetta, Eckert et al., in preparation*) and response latency are affected (Figure 12 right panel; *Marchetta, Eckert et al., in preparation*).

The deletion of MR leads to a decreased ABR wave I amplitude but a normal ABR wave IV amplitude, which implies that MRCaMKIIαCre KO mice can compensate the reduced peripheral input in central regions (Figure 11A; MRCaMKIIαCre ABR wave I amplitude: WT: $n = 15/30$ mice/ears; KO: $n = 13/26$ mice/ears; 2-way ANOVA, $F(1,394) = 19.40$, $P < 0.0001$; MRCaMKIIαCre ABR wave IV amplitude: WT: $n = 15/30$ mice/ears; KO: $n = 13/26$ mice/ears; 2-way ANOVA, $F(1,409) = 6.991$, $P = 0.0085$; *Marchetta, Eckert et al., in preparation*). The deletion of GR leads to a distinct increase of ABR wave I and IV amplitude which could point out a missing inhibition component (Figure 11B; GRCaMKIIαCre ABR wave I amplitude: WT: $n = 13/26$ mice/ears; KO: $n = 15/30$ mice/ears; 2-way ANOVA, $F(1,397) = 45.83$, $P < 0.0001$; GRCaMKIIαCre ABR wave IV amplitude: WT: $n = 13/26$ mice/ears; KO: $n = 15/30$ mice/ears; 2-way ANOVA, $F(1,324) = 57.31$, $P < 0.0001$; *Marchetta, Eckert et al., in preparation*). Interestingly the central deletion of both nuclear stress hormone receptors MR and GR leads to slightly increased ABR wave I and IV amplitudes, indicating that the inhibiting effect of GR on ABR wave amplitudes dominates (Figure 11C; MRGRCaMKIIαCre ABR wave I amplitude: WT: $n = 20/40$ mice/ears; KO: $n = 25/50$ mice/ears; 2-way ANOVA, $F(1,672) = 10.80$, $P = 0.0011$; MRGRCaMKIIαCre ABR wave IV amplitude: WT: $n = 20/40$ mice/ears; KO: $n = 25/50$ mice/ears; 2-way ANOVA, $F(1,713) = 31.62$, $P < 0.0001$; *Marchetta, Eckert et al., in preparation*).

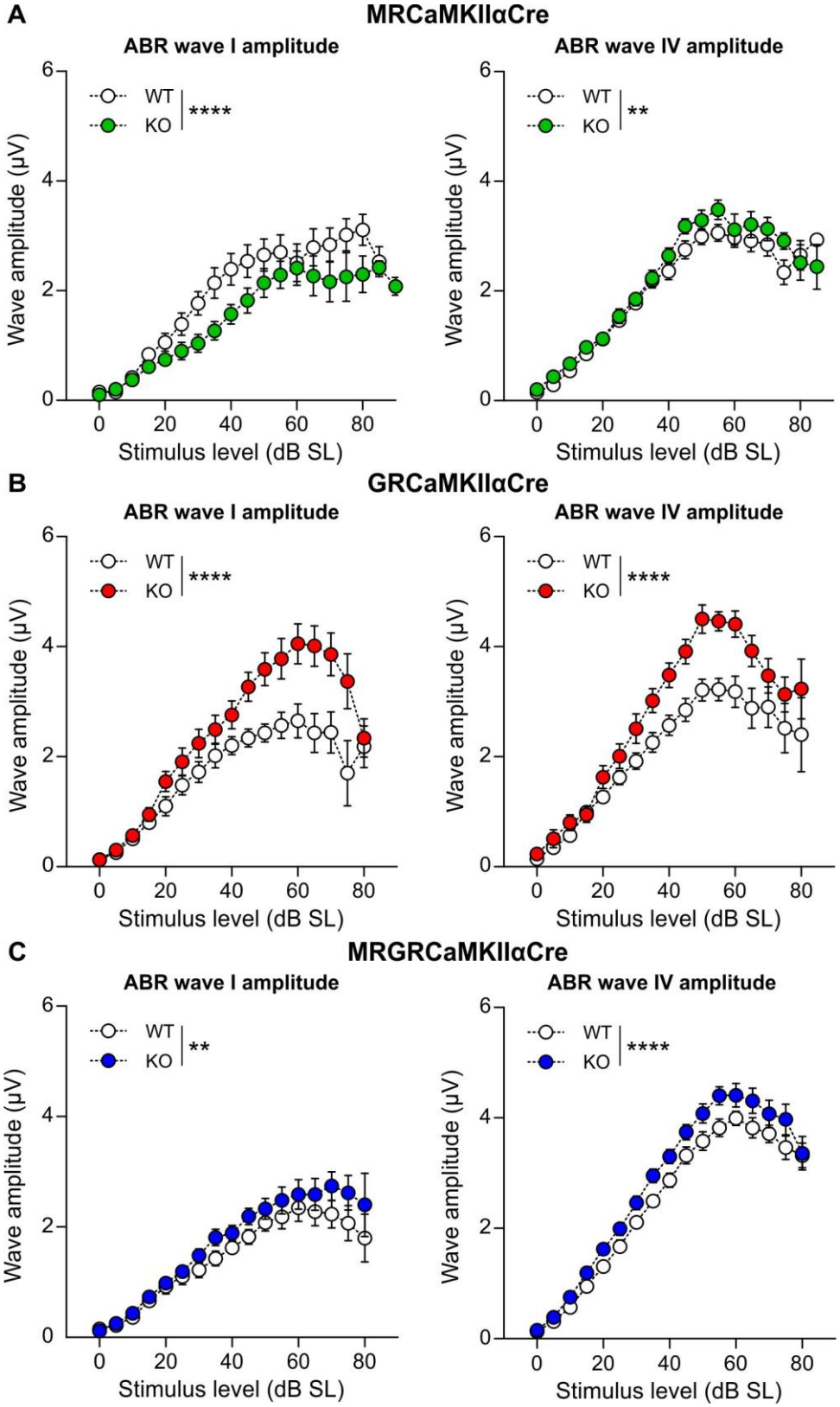

Figure 11: Click-evoked supra-threshold ABR wave I and IV amplitude of (**A**; WT = black, KO = green) MRCaMKIIαCre, (**B**; WT = black, KO = red) GRCaMKIIαCre mice and (**C**; WT = black, KO = blue) MRGRCaMKIIαCre mice. Error bars represent S.E.M.; ** $P < 0.01$, **** $P < 0.0001$

Regarding the ABR wave latency it became obvious that the single stress hormone receptors had an impact on specifically the evoked auditory nerve or midbrain latencies. A deletion of MR (Figure 12A; MRCaMKIIαCre ABR wave I latency: WT: n = 15/30 mice/ears; KO: n = 13/26 mice/ears; 2-way ANOVA, $F(1,414) = 3.75$, $P = 0.0534$; MRCaMKIIαCre ABR wave IV latency: WT: n = 15/30 mice/ears; KO: n = 13/26 mice/ears; 2-way ANOVA, $F(1,439) = 16.04$, $P < 0.0001$; *Marchetta, Eckert et al., in preparation*) results in a prolonged whereas a deletion of GR (Figure 12B; GRCaMKIIαCre ABR wave I latency: WT: n = 13/26 mice/ears; KO: n = 15/30 mice/ears; 2-way ANOVA, $F(1,430) = 30.08$, $P < 0.0001$; GRCaMKIIαCre ABR wave IV latency: WT: n = 13/26 mice/ears; KO: n = 15/30 mice/ears; 2-way ANOVA, $F(1,412) = 16.10$, $P < 0.0001$; *Marchetta, Eckert et al., in preparation*) results in shortened ABR wave I and IV latency. A deletion of MR and GR (Figure 12C; MRGRCaMKIIαCre ABR wave I latency: WT: n = 20/40 mice/ears; KO: n = 25/50 mice/ears; 2-way ANOVA, $F(1,827) = 0.89$, $P = 0.346$; MRGRCaMKIIαCre ABR wave IV latency: WT: n = 20/40 mice/ears; KO: n = 25/50 mice/ears; 2-way ANOVA, $F(1,760) = 11.20$, $P = 0.0009$; *Marchetta, Eckert et al., in preparation*) was balanced at least in ABR wave I latency while ABR wave IV latency was slightly prolonged.

In conclusion, central MR and GR influence distinctly peripheral auditory coding. These results manifest the hypothesis that the central stress response impact the peripheral auditory nerve function. The stress response is a complex interplay of stress hormones and their receptors and our results emphasized that the central MR and GR affect the hearing function in contrasting ways.

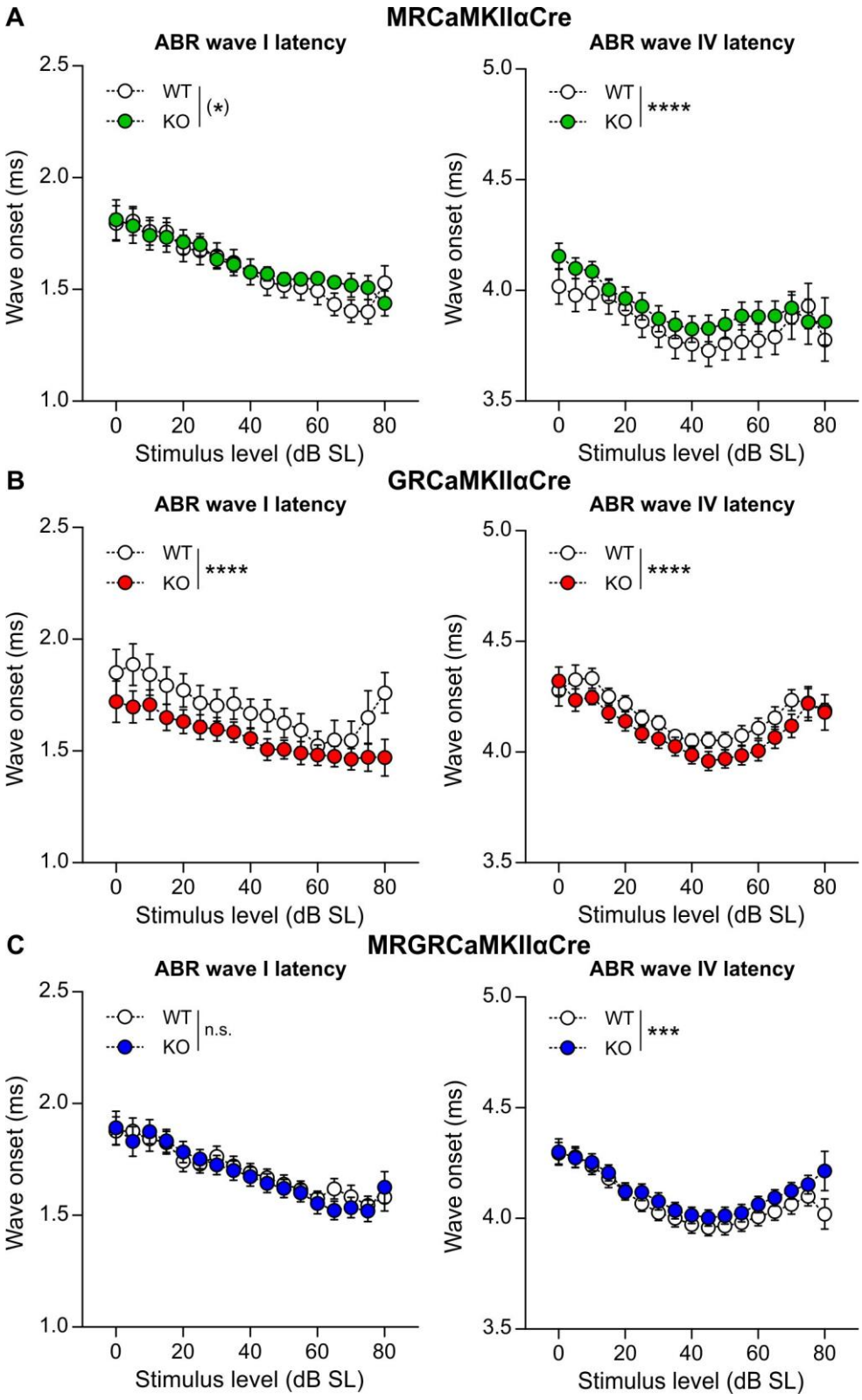

Figure 12: Click-evoked supra-threshold ABR wave I and IV latency of (**A**; WT = black, KO = green) MRCaMKIIαCre, (**B**; WT = black, KO = red) GRCaMKIIαCre mice and (**C**; WT = black, KO = blue) MRGRCaMKIIαCre mice. Error bars represent S.E.M.; n.s.: not significant, (∗) $P < 0.1$, ∗∗∗ $P < 0.001$, ∗∗∗∗ $P < 0.0001$

3.3 Fast auditory processing drives hippocampal maturation and social learning

The results and figures described in the following section refer to Eckert et al., *"Brain-derived neurotrophic factor in inhibitory hindbrain neurons controls central learning mechanisms"*, which is in preparation, and are depicted in the draft manuscript attached in the appendix 7.2.

Our individualized perception of the external world is established in early life, when task- and context-specific signals are first integrated by sensory memory-dependent circuits to adapt to a rapidly changing environment. During these adaptations local cortical Brain derived neurotrophic factor (**BDNF**) regulates the dendritic complexity of parvalbumin-positive (**PV$^+$**)-interneurons with sensory experience in all sensory systems (Griffen and Maffei, 2014; Hong et al., 2008; Itami et al., 2007; Jiao et al., 2011; Heimel et al., 2011) enabling thereby the integration of context and task-specific signals for improved performance and adaptation (Takesian et al., 2018). How auditory experience shapes auditory cortical receptive fields and task-specific learning is still not understood in detail. It is hypothesized that the perceptional learning ability is required for extraction of behaviorally relevant sound which is a prerequisite for speech understanding in humans (Irvine, 2018; David, 2018; Holdgraf et al., 2016). Perceptional learning depends on the reorganization of cortical circuits (Polley et al., 2006) and it is assumed that PV$^+$-interneurons mediate perceptual learning (Goel et al., 2019) and the control of attention in the prefrontal cortex (Goel et al., 2019; Kim et al., 2016). The ability of fast auditory processing during early life is crucial for language development in children (Benasich et al., 2002b; Merzenich et al., 1996) and deficits are associated with further cognitive disorders (Benasich, 2002a; Cantiani et al., 2016; Foss-Feig et al., 2017).

We addressed this question using a mouse model where *Bdnf* is deleted under the Pax2 promoter (***Bdnf^{Pax2}* KO**). The *Bdnf^{Pax2}* KO mice showed normal hearing thresholds but deficits in fast auditory processing (Chumak et al., 2016; Zuccotti et al., 2012). Therefore, we analyzed the deficits of fast auditory processing and the associated cognitive and behavioral deficits in this mouse model in more detail to obtain a deeper understanding of the relationship between fast auditory processing deficits during development and cognitive disorders.

3.3.1 *Bdnf*^{Pax2} KO mice exhibit deficits in fast auditory coding

The impairment of auditory acuity in *Bdnf*^{Pax2} KO mice in whom BDNF is deleted in the auditory periphery (Figure 1-figure supplement 1A,B; *Eckert et al., in preparation, 7.2*) was first shown in Zuccotti et al., 2012 and Chumak et al., 2016 and could be confirmed by slight but significant threshold elevations in response to click stimuli, noise-burst and pure tone stimuli (Figure 1a,b; *Eckert et al., in preparation, 7.2*). Fine structure analysis of supra-threshold ABR wave amplitudes in *Bdnf*^{Pax2} KO mice showed altered auditory nerve responses (ABR wave I) independent of OHC function, and impaired midbrain responses (ABR wave IV), compared to controls (Figure 1d; *Eckert et al., in preparation, 7.2*). ABR wave latencies exhibit significantly shortened ABR wave I latency and delayed ABR wave IV latency in comparison to controls, which indicates a less optimized temporal processing in auditory fibers (Figure 1e; *Eckert et al., in preparation, 7.2*). Temporal processing is critical for proper coding of auditory steady state responses (**ASSRs**). ASSR require low spontaneous rate high threshold (**low-SR**) auditory fibers with largest changes in average discharge rate in response to transient supra-threshold stimuli (Bharadwaj et al., 2014) and very likely additionally high spontaneous rate low threshold (**high-SR**) auditory fibers for coding of modulated sound stimuli in quiet environments (Paul et al., 2017). Responses to ASSR stimuli were analyzed dependent on modulation depth where a significant reduced response to modulation depth > 10 % was noted in *Bdnf*^{Pax2} KO mice compared to control mice (Figure 1f; *Eckert et al., in preparation, 7.2*). When these ASSRs were analyzed dependent on the stimulus level, responses in *Bdnf*^{Pax2} KO mice remained reduced particularly for low sound pressure levels close to threshold (Figure 1g; *Eckert et al., in preparation, 7.2*). This could indicate impaired ASSR coding and resolution close to threshold sound intensities due to possible coding deficits of high-SR auditory fibers. For further characterization of auditory processing, we performed acoustic startle responses (**ASR**) measurements with different leadtimes between prepulse and startle stimulus which provide insight into temporal resolution deficits. The ASR is one of the fastest reflexes found in mammals (Lauer et al., 2017) and a well-established method to behaviorally assess very fast auditory processing in awake animals (Steube et al., 2016). Prepulse inhibition (**PPI**) was induced by 50 ms leadtime, while prepulse facilitation (**PPF**) was induced by 6 ms leadtime prior to the startle stimulus. PPI and PPF are

independent processes that contribute to influence the startle response (Plappert et al., 2004). While *Bdnf*^{Pax2} KO mice showed a decreasing ASR change in PPI with increasing prepulse intensity similar to controls (Figure 1h; *Eckert et al., in preparation, 7.2*), PPF was nearly absent in *Bdnf*^{Pax2} KO (Figure 1i; *Eckert et al., in preparation, 7.2*).

In conclusion, *Bdnf*^{Pax2} KO mice exhibit severe deficits in central coding of fast auditory information.

3.3.2 Maturation deficits of the PV$^+$-interneuron network and elevated Arc/Arg3.1 levels in the auditory cortex, but not somatosensory cortex, in *Bdnf*^{Pax2} KO mice without changes in local BDNF levels

First hints of changed excitation/inhibition balance could be shown (Chumak et al., 2016) by reduced parvalbumin (**PV**)-IR in the inferior colliculus (**IC**) and changes of PV-IR in the auditory cortex (**AC**) of *Bdnf*^{Pax2} KO mice. Further analyses of correlated cortical excitability changes in *Bdnf*^{Pax2} KO mice could be demonstrated by co-detection of PV protein together with the excitability marker activity-regulated cytoskeletal protein (**Arc/Arg3.1**) which defines α-amino-3-hydroxy-5-methyl-4-isoxazolepropionic acid (**AMPA**) receptor mediated spine plasticity (Nikolaienko et al., 2018). Using the Geisler method to co-detect mRNA and protein (Singer et al., 2016), significantly reduced PV protein levels were found in *Bdnf*^{Pax2} KO mice together with significantly elevated Arc/Arg3.1 mRNA and protein, despite no difference in BDNF mRNA could be observed. The reduced PV protein levels were accompanied by significantly reduced PV$^+$-neurite arborizations, as shown for cortical layer III/IV of the AC (Figure 2a, high magnification; *Eckert et al., in preparation, 7.2*), the main termination field of thalamocortical axons from the ventral medial geniculate region (Malmierca and Ryugo, 2012). Further, we found less PV$^+$ perisomatic contacts exemplarily for layer III/IV of the AC (Figure 2c, arrow and inset; *Eckert et al., in preparation, 7.2*). The altered PV expression pattern in the AC for control and *Bdnf*^{Pax2} KO was detected from hearing onset onwards, shown in the AC at P14 (Figure 2d; *Eckert et al., in preparation, 7.2*). The specificity of the PV$^+$-interneuron changes in the auditory circuits was supported by the lack of change in the PV$^+$-interneuron network in the somatosensory cortex (**SSC**) where VGluT2 labeling confirms normal column formation (Figure 2e; *Eckert et al., in preparation, 7.2*) with no differences in PV$^+$-interneuron arborizations (Figure 2f; *Eckert et al., in preparation, 7.2*).

In conclusion, in *Bdnf*^{Pax2} KO mice diminished maturation of PV^{+}-interneuron networks occurs with hearing onset in the AC but not in the SSC. Despite unchanged BDNF mRNA levels, Arc/Arg3.1 mRNA and protein levels were enhanced in AC pyramidal neurons.

3.3.3 Maturation deficits of the PV^{+}-interneuron network and elevated Arc/Arg3.1 levels in the hippocampus in *Bdnf*^{Pax2} KO mice without changes in local BDNF levels

For behavioral relevant auditory perception (Kraus and White-Schwoch, 2015; Irvine, 2018) or for long-lasting adjustments to enriching or traumatic auditory input (Matt et al., 2018), memory-linked hippocampal synaptic circuit changes are essential. Questioning if the inhibitory/excitatory imbalance in the AC in *Bdnf*^{Pax2} KO mice might impact excitability in hippocampus regions PV protein was co-detected with Arc/Arg3.1 and BDNF in the dorsal hippocampus (Figure 3, Figure 3-figure supplement 1; *Eckert et al., in preparation, 7.2*). Elevated Arc/Arg3.1 mRNA (blue) in pyramidal neurons appeared together with a significant reduced PV protein level (red) at the somatic and dendritic level in all hippocampal regions in *Bdnf*^{Pax2} KO mice, shown for the CA1 (Figure 3a; *Eckert et al., in preparation, 7.2)* and CA3 (Figure 3-figure supplement 1a; *Eckert et al., in preparation, 7.2*). Arc/Arg3.1 protein was also elevated significantly as shown for the CA1 (Figure 3b; *Eckert et al., in preparation, 7.2*) and CA3 (Figure 3-figure supplement 1b; *Eckert et al., in preparation, 7.2*). The change in Arc/Arg3.1 protein was seen, despite no difference in BDNF mRNA levels was observed in same sections (Figure 3b, Figure 3-figure supplement 1b,c; *Eckert et al., in preparation, 7.2*). The decline of PV-IR was accompanied by significantly reduced PV^{+} neurite arborizations in CA1 shown for the stratum radiatum (**SR**) in the CA1 region (Figure 3c, and inset; *Eckert et al., in preparation, 7.2*) or at the mossy fiber level of the CA3 (Figure 3d and inset; *Eckert et al., in preparation, 7.2*). As another control for specificity, no difference in PV^{+}-interneuron-IR was seen in the cerebellum (Figure 3-figure supplement 1d; *Eckert et al., in preparation, 7.2*). To assess the onset of PV-IR changes in the hippocampus of *Bdnf*^{Pax2} KO mice, we analyzed the PV expression levels at three ages: prior to hearing onset (P6/P10), at the end of the critical developmental period of the auditory system at P14 (Villers-Sidani et al., 2007) and in adult mice (> 8 weeks). A significant elevation of PV-IR between P6-10 and P14 was observed in controls in the CA1 (Figure 4a; *Eckert et al.,*

in preparation, 7.2) and CA3 (Figure 4b; *Eckert et al., in preparation, 7.2*), while PV-IR levels were reduced at all three ages in *Bdnf*^{Pax2} KO mice.

In conclusion, the cause of diminished maturation of PV^{+}-interneuron networks in the hippocampus of *Bdnf*^{Pax2} KO mice arises the period of hearing onset, while PV levels in the cerebellum remain unchanged. Despite unaffected BDNF mRNA levels in pyramidal hippocampal neurons, Arc/Arg3.1 mRNA and protein levels are enhanced in *Bdnf*^{Pax2} KO mice.

3.3.4 *Bdnf*^{Pax2}KO mice exhibited elevated long-term potentiation similar to controls prior to hearing onset and failed to drive long-term potentiation during auditory adjustments

The reduced expression of PV^{+}-interneurons linked to elevated Arc/Arg3.1 mRNA and protein levels in the hippocampus in *Bdnf*^{Pax2} KO mice, might reveal an initial elevated stage of hyper-excitability of pyramidal neurons prior to maturation of PV^{+}-interneuron networks with hearing onset. We hypothesized that in this case *Bdnf*^{Pax2} KO mice might respond to stimuli with elevated potentiation through lower neuronal input resistance and that altered long-term potentiation (**LTP**) in *Bdnf*^{Pax2} KO mice might reflect LTP prior to hearing onset.

The field excitatory postsynaptic potentials (**fEPSP**) were recorded in the CA3 Schaffer collateral (**SC**) to CA1 synapses in the SR from acute forebrain slices of adult *Bdnf*^{Pax2} KO and control mice. Indeed, a significant higher fEPSP amplitude was observed after high-frequency LTP inducing stimulation (1s, 100 Hz) of SC in *Bdnf*^{Pax2} KO compared to control mice over the whole recording time of 60 min (Figure 5a, left panel; *Eckert et al., in preparation, 7.2*). Calculating the mean of the last 10 min of the recording showed that *Bdnf*^{Pax2} KO mice (175.5 % ± 5.7 %) exhibited significantly higher LTP than the controls (142.4 ± 8.2 %, Figure 5a, right panel; *Eckert et al., in preparation, 7.2*). When fEPSP slopes in acute brain slices were tested prior to hearing function at P6-P10 in comparison to adult controls, P6-P10 controls (171.6 % ± 6.5 %) revealed significantly higher LTP on the same level as adult *Bdnf*^{Pax2} KO mice (175.5 % ± 5.7 %; Figure 5a; *Eckert et al., in preparation, 7.2*). Representative traces before (black) and after (gray) induction of LTP of animals showed that all groups were able to induce LTP (Figure 5a left panel; *Eckert et al., in preparation, 7.2*).

Elevated LTP in adult *Bdnf*^{Pax2} KO mice might mirror an initially elevated LTP prior to hearing onset when it is not yet shaped by PV^{+}-network. In case PV^{+}-network

may adjust LTP with hearing onset to improve signal to noise ratio (Hu et al., 2014) and expand the dynamic range available for later adjustments (Turrigiano, 2012; Hu et al., 2014; Kimura and Itami, 2019), we would expect deficits in homeostatic facilitation after enrichment. To address this question, we exposed adult control and *Bdnf*^{Pax2} KO mice to enriching sound protocols (80-100 dB SPL) that lead 14 d after exposure to enhanced LTP linked to long lasting facilitated and adjusted central auditory responsiveness (Matt et al., 2018). As shown in (Figure 5b; *Eckert et al., in preparation, 7.2*) controls responded to sound enrichment with elevated LTP in CA1 region, while *Bdnf*^{Pax2} KO mice exhibit likewise elevated LTP levels prior and after sound enrichment. Neither *Bdnf*^{Pax2} KO mice nor adult, and P6-10 control mice nor sound exposed control and *Bdnf*^{Pax2} KO mice exhibited any alterations in basal synaptic transmission. Furthermore, all groups displayed similar fEPSP amplitudes in response to a range of input strengths, as well as similar levels of paired-pulse facilitation, indicating no changes in presynaptic function (Figure 5-figure supplement 1a,b; *Eckert et al., in preparation, 7.2*).

In conclusion, in *Bdnf*^{Pax2} KO mice initially elevated LTP seems to persist and prevent activity driven memory-linked homeostatic adjustment processes.

3.3.5 *Bdnf*^{Pax2}KO mice revealed diminished learning

To test if *Bdnf*^{Pax2} KO mice exhibit not only deficits in memory-linked long-term adjustments but also in fast adjustments like Arc/Arg3.1 dependent weakening of synapses, essential for detection and memorization of novelty response (Jakkamsetti et al., 2013) we used a learning paradigm in which mice were trained to have access to reward (their own mouse house) after finding their way through a multiple T-maze with 7 decision points (Figure 6a; *Eckert et al., in preparation, 7.2*; Lange-Asschenfeldt et al., 2007). Learning performance was measured after a successful run by counting errors at the decision points of the multiple T-maze in which the mice had been trained. The *Bdnf*^{Pax2} KO mice had a significantly higher median error rate in the four analyzed runs (Figure 6b; *Eckert et al., in preparation, 7.2*). The *Bdnf*^{Pax2} KO mice made 1-67 errors at the end of the learning phase (run 2), while the controls made only 0-1 errors (Figure 6b; *Eckert et al., in preparation, 7.2*). As most *Bdnf*^{Pax2} KO mice displayed circling behavior (Zuccotti et al., 2012), the correlation of circling behavior, motor activity and errors in the multiple T-maze was explicitly tested. Neither the number of errors

during the second run in the multiple T-maze (Figure 6-figure supplement 1a; *Eckert et al., in preparation, 7.2*) nor motor activity (Figure 6-figure supplement 1b; *Eckert et al., in preparation, 7.2*) showed significant correlation with the circling behavior. Although the *Bdnf*^{Pax2} KO mice exhibited significantly increased motor activity, measured on a ballistic platform during startle (Figure 6-figure supplement 1c; *Eckert et al., in preparation, 7.2*), learning errors were not correlated with altered motor activity. This suggests that neither the circling behavior nor the motor function contributed to the learning errors in *Bdnf*^{Pax2} KO mice.

In conclusion, significantly increased errors of *Bdnf*^{Pax2} KO mice in the multiple T-maze related to higher LTP are a remarkable paradox but considering the failed PV^{+}-interneuron network maturation with hearing onset may indicate that PV^{+}-interneuron network maturation during hearing onset is absolutely crucial to reduce the excitability and thereby improve the baseline for detection of memory-linked deviants and the capability for memory-linked adjustments (Figure 8; *Eckert et al., in preparation, 7.2*).

3.3.6 *Bdnf*^{Pax2} KO mice showed reduced exploratory activity and enhanced anxiety-related responses

Elevated learning errors may be linked to less explorative and social behavior or enhanced anxiety response. We used a Crawley's 3-chamber sociability test (Figure 7a; *Eckert et al., in preparation, 7.2*) that allowed to analyze social behavior by monitoring the time and number of sniffing contacts of control and mutant towards an empty cage or a cage with a stranger mouse normalized to the time they spent in the respective chamber. Control mice preferred to spend more time sniffling towards the stranger mouse chamber than the empty chamber, while *Bdnf*^{Pax2} KO mice did not show a preference between the two (Figure 7b; *Eckert et al., in preparation, 7.2*). Additionally control mice had in contrast to *Bdnf*^{Pax2} KO mice an increased contact time of sniffing to the cage with strangers (Figure 7b; *Eckert et al., in preparation, 7.2*) although the averaged latency for the first entry into the empty or stranger chamber was not different between control and *Bdnf*^{Pax2} KO mice (Figure 7c; *Eckert et al., in preparation, 7.2*). *Bdnf*^{Pax2}KO mice exhibited significantly decreased number of entries into both chambers in comparison to controls indicating a lower exploratory behavior (Figure 7d; *Eckert et al., in preparation, 7.2*). When analyzing freezing or self-grooming behavior, *Bdnf*^{Pax2} KO mice exhibit a significant increase in spontaneous freezing (Figure 7e; *Eckert et al.,*

in preparation, 7.2) and self-grooming behavior (Figure 7e; *Eckert et al., in preparation, 7.2*) and significant increased freezing when entering the chamber with strangers. Ultrasonic vocalization (**USV**) of nursing infants, tested at the age of P7, a time prior to hearing onset where the auditory processing differences between control and *Bdnf*^{Pax2}KO mice could not have an impact, revealed significant abnormalities in the vocalization patterns between control and *Bdnf*^{Pax2}KO pups (exemplarily depicted in Figure 7g,f; *Eckert et al., in preparation, 7.2*). USV with multiple frequency jumps were more frequent in *Bdnf*^{Pax2}KO pups (Figure 7f; *Eckert et al., in preparation, 7.2*). Additionally, isolated *Bdnf*^{Pax2}KO pups showed increased numbers of all USV calls during a 5 min period (Figure 7h; *Eckert et al., in preparation, 7.2*), which indicates a higher index of anxiety (Krömer et al., 2005; Groenink et al., 2008). Adult *Bdnf*^{Pax2}KO mice also were characterized by significantly elevated basal corticosterone levels in comparison to controls (Figure 7i; *Eckert et al., in preparation, 7.2*), suggesting *Bdnf*^{Pax2}KO mice to exhibit increased anxiety behavior pointing to distress.

In summary, significantly reduced explorative and social behavior and significantly increased freezing, self-grooming, USV and stress level in *Bdnf*^{Pax2}KO mice point to significantly increased anxiety behavior and imbalanced stress control in mutants. Moreover, *Bdnf* deletion in auditory periphery under the Pax2 promoter led to a persistence of a critical developmental step prior to hearing function when LTP was still elevated. An absence of BDNF in the auditory periphery, prevents the critical maturation of fast auditory processing parallel to the elevation of ABR wave amplitudes and shortening of ABR wave I latency, maturation of PV^{+}-interneuron network in the auditory and hippocampal paths. As a consequence, shaping of LTP and Arc/Arg3.1 levels in the hippocampus, linked to lowered spontaneous excitability through improved signal to noise ratio and facilitated learning and adjustment performance failed. In conclusion, fast auditory processing drives receptive field maturation and learning.

3.4 *B*DNF-*L*ive-*E*xon-*V*isualization allows differential detection of BDNF transcripts *in vitro* and *in vivo*

The results and figures described in the following section refer to Singer et al. Eckert et al., *"BDNF-Live-Exon-Visualization (BLEV) allows differential detection of BDNF transcripts in vitro and in vivo"*, Front Mol Neurosci. 2018, which is attached in the appendix 7.3.

BDNF is a key modulator of synaptic modifications during homeostatic readjustment processes and a master regulator of energy homeostasis (Bramham and Messaoudi, 2005; Turrigiano, 2012; Marosi and Mattson, 2013). It remains unclear how the different transcripts of the complex BDNF gene contribute to its multifaceted functions. The activity-dependent expressed *Bdnf* exons IV and VI are associated to various neurological pathologies related to sleep, fear or memory disorders (Hill et al., 2016), depression (Sakata et al., 2010) and cortical inhibition (Hong et al., 2008). The detection of BDNF is a challenging task, which is particularly complicated due to the very low endogenous BDNF expression levels in the mature central nervous system (Dieni et al., 2012). The functional analysis of BDNF *in vivo* is further complicated by the early death of *Bdnf*-null-mutant mice (Ernfors et al., 1994). Furthermore, the different levels of BDNF expression in platelets (Chacón-Fernández et al., 2016), capillary endothelial cells (Donovan et al., 2000), microglia and astrocytes (Ferrini and Koninck, 2013; Parkhurst et al., 2013) remain unclear.
To characterize cell type-specific, state-dependent usage of the BDNF promoters in response to altered activity patterns, we generated a transgenic reporter mouse model for ***B***DNF-***L***ive-***E***xon-***V***isualization (**BLEV**). This reporter mouse model visualizes the BDNF expression following promoter-specific usage of exon IV and exon VI by translating cyan-fluorescent-protein (**CFP**) and yellow-fluorescent-protein (**YFP**) additionally to BDNF protein in characteristic neuronal, glial, and vascular locations.

3.4.1 Generation of a mouse model to visualize activity-dependent BDNF transcripts at their site of translation

To monitor transcript-specific BDNF protein synthesis at the sites of translation ensuing to the activity-dependent activation of the exon IV or VI promoters, we generated a construct carrying exon IV and VI (including their promoter regions) and incorporated membrane and epitope tags in order to locate their differential expression (Figure 1A,B; *Singer, Eckert et al., 2018, Front Mol Neurosci, 7.3*). To

proof if this approach is feasible, the transfection of the neuroglioblastoma cell line SK-N-BE with either the exon IV-CFP (Figures 1A upper panel, C; *Singer, Eckert et al., 2018, Front Mol Neurosci, 7.3*) or the exon VI-YFP single construct (Figures 1A lower panel, D; *Singer, Eckert et al., 2018, Front Mol Neurosci, 7.3*) was tested. An ELISA assay revealed significantly higher levels of BDNF protein in SK-N-BE cells transfected with either of the *Bdnf* single constructs compared to untransfected cells, confirming successful BDNF translation from these transgenes (Figure 1C-F; *Singer, Eckert et al., 2018, Front Mol Neurosci, 7.3*).

3.4.2 Non-overlapping sites of *Bdnf* exons IV and VI translation co-localize with BDNF immunoreactivity in neuronal, glial, or vascular cells

To further proof the BLEV reporter mouse model hippocampal sections were co-stained with a specific antibody directed against the BDNF pro-domain (Figure 5; *Singer, Eckert et al., 2018, Front Mol Neurosci, 7.3*) to co-localize *Bdnf* exon IV-CFP and *Bdnf* exon VI-YFP fluorescence with BDNF protein expression *in vivo*. Additionally, excitatory, inhibitory, glial, or vascular cells which are described to correlate with BDNF expression (Edelmann et al., 2014) were co-stained.

BDNF-IR in the dentate gyrus (**DG**) was detected in the supra- and infra-pyramidal blades of the granule cell layer (**GCL**) (Figure 5A; *Singer, Eckert et al., 2018, Front Mol Neurosci, 7.3*) as previously observed (Dieni et al., 2012). No IR was detected when the primary BDNF antibody was omitted (Figure 5A, right upper panel; *Singer, Eckert et al., 2018, Front Mol Neurosci, 7.3*). High magnification images of the sections revealed that BDNF in the GCL was co-localized with few CFP-positive dots, while in this region no *Bdnf* exon VI-YFP could be detected (Figure 5A, lower panel, arrows; *Singer, Eckert et al., 2018, Front Mol Neurosci, 7.3*). In addition, BDNF-IR was detected in five different characteristic regions co-localized with either *Bdnf* exon IV-CFP (Figure 5B, No. 1; *Singer, Eckert et al., 2018, Front Mol Neurosci, 7.3*), with *Bdnf* exon VI-YFP (Figure 5B, No. 2-4; *Singer, Eckert et al., 2018, Front Mol Neurosci, 7.3*), or neither of the transcripts (Figure 5B, No. 5; *Singer, Eckert et al., 2018, Front Mol Neurosci, 7.3*). Moreover, a slight BDNF-IR was also detected in blood vessels co-labeled with *Bdnf* exon IV-CFP (Figure 5C; *Singer, Eckert et al., 2018, Front Mol Neurosci, 7.3*) not with *Bdnf* exon VI-YFP (Figure 5C, upper panel; *Singer, Eckert et al., 2018, Front Mol Neurosci, 7.3*). This BDNF-IR was not

detectable upon absence of the primary BDNF antibody (Figure 5C, lower panel; *Singer, Eckert et al., 2018, Front Mol Neurosci, 7.3*). BDNF expression was previously described in circulating blood in platelets (Chacón-Fernández et al., 2016). With the BLEV reporter mouse model we were able to detect CFP fluorescence in blood vessels of non-perfused animals (Figure 5D, upper panel; *Singer, Eckert et al., 2018, Front Mol Neurosci, 7.3*) in contrast to perfused animals (Figure 5D, lower panel; *Singer, Eckert et al., 2018, Front Mol Neurosci, 7.3*). In line with views that nerve and blood vessels sprout in parallel (Carmeliet and Tessier-Lavigne, 2005), we observed a dot-like pattern of BDNF-IR, which was co-labeled with *Bdnf* exon VI-YFP close to a *Bdnf* exon IV-CFP-positive capillary within the fissura hippocampalis (**FH**), exemplarily shown for an 80 dB SPL exposed BLEV mouse (Figure 5E, Figure 6A; *Singer, Eckert et al., 2018, Front Mol Neurosci, 7.3*). The characteristic dot-like pattern revealed as YFP-positive contacts on glutamatergic activity-regulated cytoskeletal protein (**Arc/Arg3.1**)-positive dendrites of CA1 neurons (Figure 5F; *Singer, Eckert et al., 2018, Front Mol Neurosci, 7.3*). These CA1 dendrites are often localized within the highly vascularized FH (Soriano and Frotscher, 1993). At higher magnification, it became clear that SC terminals are labeled by *Bdnf* exon VI-YFP and connected to Arc/Arg3.1-positive dendritic postsynaptic spines in the SR (Figure 5G; *Singer, Eckert et al., 2018, Front Mol Neurosci, 7.3*). Because only few Arc/Arg3.1-positive spines were contacted by *Bdnf* exon VI-YFP-positive dots (Figure 5G, compare closed and open arrow; *Singer, Eckert et al., 2018, Front Mol Neurosci, 7.3*), we assume that these are likely activated synapses. Co-localization of BDNF-positive dots with *Bdnf* exon VI-YFP were also detected in close proximity to an endothelial nucleus (Figure 5H, magnified from Figure 5B, No. 3; *Singer, Eckert et al., 2018, Front Mol Neurosci, 7.3*), as shown by co-staining with the $p75^{NGF}$ receptor, an endothelial marker (Figure 6B; *Singer, Eckert et al., 2018, Front Mol Neurosci, 7.3*; Catts et al., 2008). This characteristic pattern of *Bdnf* exon VI-YFP expression in proximity to endothelial nuclei was found repeatedly to either overlap with PV, a marker of fast-spiking inhibitory interneurons (Figure 5I; *Singer, Eckert et al., 2018, Front Mol Neurosci, 7.3*) or ionized calcium-binding adapter molecule 1 (**IBA-1**), a marker of microglia (Figure 5J; *Singer, Eckert et al., 2018, Front Mol Neurosci, 7.3*), an observation that needs to be considered in the context of BDNF release from

microglia to control plasticity through inhibitory PV circuits (Ferrini and Koninck, 2013; Parkhurst et al., 2013).

The BDNF-IR was typically observed close to blood vessels in the SR (Figure 5B, Figure 6C; *Singer, Eckert et al., 2018, Front Mol Neurosci, 7.3*) co-localized with *Bdnf* exon VI-YFP (Figure 6C, closed arrow; *Singer, Eckert et al., 2018, Front Mol Neurosci, 7.3*) and *Bdnf* exon IV-CFP (Figure 6C, arrowhead; *Singer, Eckert et al., 2018, Front Mol Neurosci, 7.3*), both clearly overlapping with IBA1-labeled microglia (Figure 6C, open arrow; *Singer, Eckert et al., 2018, Front Mol Neurosci, 7.3*). In addition to the *Bdnf* exon IV-CFP and *Bdnf* exon VI-YFP signals which could indicate that SC terminals contact microglia, the astrocyte specific marker glial fibrillary acidic protein (**GFAP**) also co-localizes with *Bdnf* exon VI-YFP close to blood vessels (Figure 6D; *Singer, Eckert et al., 2018, Front Mol Neurosci, 7.3*). Finally, we also detected BDNF-IR clusters within endothelial cells with BDNF-IR located in zones (Figure 5B, No. 5; *Singer, Eckert et al., 2018, Front Mol Neurosci, 7.3*), where pericyte processes variably surround the abluminal endothelial wall of a *Bdnf* exon IV-CFP-positive blood vessel surrounded by β1-guanylyl cyclase-positive smooth muscle cells (Figure 6E, red; *Singer, Eckert et al., 2018, Front Mol Neurosci, 7.3*), thus confirming previous observations (Donovan et al., 2000).

In conclusion, the BLEV mouse is a perfect tool to monitor activity-dependent exon specific translation of BDNF in different cell types during changes in synaptic plasticity. The findings indicate that wherever we detected *Bdnf* exon IV-CFP or *Bdnf* exon VI-YFP in the hippocampal path, we also observed BDNF-IR, supporting the notion that the CFP- and YFP-labeled transcripts indeed label the location of BDNF translation. *Bdnf* transcripts were detected at sites that correspond to previously described cell types that express BDNF. *Bdnf* exon IV-CFP and *Bdnf* exon VI-YFP transcripts exhibit differential, non-overlapping translation on the cellular and subcellular level. *Bdnf* exon IV-CFP is targeted to the somata of pyramidal, granule, or microglia cells, while *Bdnf* exon VI-YFP transcripts are located in the terminals of the tri-synaptic pathway, or in the end-feet of microglia or astrocytes. BDNF in circulating blood is translated by *Bdnf* exon IV, while BDNF in endothelial cells is probably translated neither by *Bdnf* exon IV nor by exon VI transcripts.

3.5 Visualizing BDNF transcript usage during sound-induced memory linked plasticity

The results and figures described in the following section refer to Matt, Eckert et al., *"Visualizing BDNF transcript usage during sound-Induced memory linked plasticity"*, Front Mol Neurosci. 2018, which is attached in the appendix 7.4.

We hypothesized that BDNF as key modulator of synaptic plasticity modulates long-lasting adaptations at the functional and molecular level along the ascending auditory pathway in response to different sound exposure paradigms (Singer et al., 2013) by activity-dependent expression of *Bdnf* exons IV and VI. We used the BLEV reporter mouse model to specifically analyze the usage of the *Bdnf* exon IV-CFP and *Bdnf* exon VI-YFP during long lasting adaptations along the ascending auditory pathway. For this purpose we exposed BLEV mice to enriching (80 dB SPL), mild (100 dB SPL) or severe traumatizing (120 dB SPL) sound and recorded ABRs and analyzed the usage of the *Bdnf* exon IV-CFP and *Bdnf* exon VI-YFP in defined hippocampal neurons, glial, and vascular cells after sound exposure. Further, resulting changes in the expression of fast-spiking PV^{+}-interneurons, changes in synaptic responsiveness and memory-related long-term activity changes were analyzed by LTP recordings and behavioral Morris Water Maze (**MWM**) task.

3.5.1 Acoustic enrichment and mild, but not severe acoustic trauma lead to increased sound responsiveness and LTP based plasticity of central synapses

With the BLEV reporter mouse model we challenged to monitor *Bdnf* exon IV-CFP and *Bdnf* exon VI-YFP promoter usage after inducing adaptive changes which were shown to be controlled by BDNF such as LTP, memory acquisition (Minichiello, 2009), and associated changes to inhibitory circuits (Hong et al., 2008; Huang and Reichardt, 2001). BLEV mice were exposed to different SPL causing acoustic enrichment (80 dB SPL), mild (100 dB SPL) or severe AT (120 dB SPL). 14 d after exposure we observed no (80 dB SPL), moderate (100 dB SPL) or severe (120 dB SPL) loss of hearing thresholds (Figure 1A-C; *Matt, Eckert et al., 2018, Front Mol Neurosci, 7.4*). These conditions have previously been shown to alter the expression of the immediate early activity-regulated protein Arc/Arg3.1 in hippocampal CA1 regions (Singer et al., 2013), Arc/Arg3.1 expression itself is altered during LTP consolidation (Messaoudi et al., 2007). As also observed in rats (Singer et al., 2013), the different sound exposure paradigms led to long-lasting

adaptations on functional and molecular level along the ascending auditory pathway (Figure 1D; *Matt, Eckert et al., 2018, Front Mol Neurosci, 7.4*). These adaptations include elevated (80 dB SPL, middle turn), moderately reduced (100 dB SPL, midbasal turn), or seriously reduced (120 dB SPL) numbers of CtBP2-positive active release sites in the IHC synapses (Figure 1E; *Matt, Eckert et al., 2018, Front Mol Neurosci, 7.4*). The amplitudes of the supra-threshold ABR wave I and IV were elevated after 80 dB SPL exposure, reduced but centrally compensated after 100 dB SPL exposure, and reduced after 120 dB SPL exposure (Figure 1G,H; *Matt, Eckert et al., 2018, Front Mol Neurosci, 7.4*). This indicates a persistently increased auditory nerve and central response (80 dB SPL), generation of compensating central gain (100 dB SPL), or a harmful damage (120 dB SPL) related to a failure to generate central gain. The correlation of the ABR wave fine structure before and 14 d after exposure confirmed the loss of ABR wave shape with intense exposure levels (Figure 1F; *Matt, Eckert et al., 2018, Front Mol Neurosci, 7.4*).

3.5.2 Transcript-specific changes in BDNF levels correlate along the ascending path with differences in sound response adjustment

It is shown for different brain regions that activity-dependent *Bdnf* transcription strengthens synapses via tyrosine receptor kinase (**Trk**) B receptor signaling (Kellner et al., 2014) and possibly alters sound responsiveness as well. Therefore, changes in sound sensitivity could correlate with activity-dependent BDNF expression and increased neuronal activity. Vesicular glutamate transporter-1 (**VGluT1**) is a marker for activity levels in sound-sensitive excitatory synapses in the auditory brainstem (Zhou et al., 2007). Western blot (**WB**) analysis of *Bdnf* exon IV-CFP and *Bdnf* exon VI-YFP expression levels in auditory brainstem tissue samples, following immunoprecipitation with HA and cMyc tags, respectively, revealed a qualitative increase of CFP and YFP levels after acoustic enrichment (80 dB SPL), but not after AT (120 dB SPL; Figure 2A, left panel; *Matt, Eckert et al., 2018, Front Mol Neurosci, 7.4*). In line with elevated CFP and YFP levels and elevated neuronal activity, VGluT1 levels were qualitatively increased 14 d after acoustic enrichment (80 dB SPL) but not after severe AT (120 dB SPL, Figure 2A, 2nd panel; *Matt, Eckert et al., 2018, Front Mol Neurosci, 7.4*) in the auditory brainstem. This suggests that harmful acoustic conditions (120 dB SPL) following reduction of relevant auditory input

prevents activity-dependent elevation of BDNF and VGluT1. This activity-dependent mobilization of *Bdnf* exon IV-CFP and *Bdnf* exon VI-YFP and VGluT1 was also observed in the IC although not statistically significant (Figure 2A, 3rd panel, Figure 2B; *Matt, Eckert et al., 2018, Front Mol Neurosci, 7.4*). To proof if these effects after enriching sound exposure are auditory specific, we analyzed *Bdnf* exon IV-CFP and *Bdnf* exon VI-YFP levels in the olfactory bulb and could show that enriching sound does not mobilize transcript-specific BDNF in the olfactory bulb (Figure 2A, right panel; *Matt, Eckert et al., 2018, Front Mol Neurosci, 7.4*). In addition, we quantitatively verified long-lasting changes of neuronal activity in the target cells of the auditory nerves, by analyzing VGluT1-IR in bushy cells of the cochlear nucleus (**CN**) in the auditory brainstem 14 d after acoustic enrichment (80 dB SPL; Figure 2C,D; *Matt, Eckert et al., 2018, Front Mol Neurosci, 7.4*). VGluT1-IR in bushy cells of the CN was significantly elevated in animals 14 d after 80 dB SPL exposure in comparison to sham exposed animals (exemplarily shown in Figure 2C and quantified in Figure 2D; *Matt, Eckert et al., 2018, Front Mol Neurosci, 7.4).* This indicates that 80 dB SPL exposure leads to larger numbers of active release sites or greater spike fidelity in auditory nerve synapses shown by increased VGluT1 levels as functional correlate following sound exposure (Ngodup et al., 2015).

Bdnf exon IV-CFP and *Bdnf* exon VI-YFP together with VGluT1 were only elevated in animals that were exposed to 80 dB SPL following elevated evoked auditory nerve and midbrain supra-threshold responses but not in animals that were exposed to traumatic sound (120 dB SPL). This was in line with the hypothesis that relevant auditory input drives *Bdnf* transcription in the brainstem and VGluT1 is regulated by activity-dependent BDNF expression and thereby strengthens synapses (Kellner et al., 2014). Elevated activity-dependent BDNF expression as a consequence of acoustic enrichment was not detected in other sensory regions such as the olfactory bulb, so that we can assume that this is an auditory specific process in which activity-dependent BDNF is responsible for the detection of relevant auditory information.

The applied sound-exposure conditions have previously been shown to alter the expression of the immediate early activity-regulated protein Arc/Arg3.1 in hippocampal CA1 regions (Singer et al., 2013). Arc/Arg3.1 expression itself is associated with altered hippocampal LTP (Messaoudi et al., 2007). Therefore, we recorded fEPSP of the CA3 to CA1 SC synapses in the SR from acute forebrain

slices of BLEV mice 14 d after exposure to 80, 100, or 120 dB SPL (Figure 3B; *Matt, Eckert et al., 2018, Front Mol Neurosci, 7.4*). None of the sound exposure paradigms led to changes in basal synaptic transmission. All groups displayed similar fEPSP amplitudes in response to a range of input strengths, as well as similar levels of paired-pulse facilitation, indicating no changes in presynaptic function relative to controls (Supplementary Figure 4A,B; *Matt, Eckert et al., 2018, Front Mol Neurosci, 7.4*). Significant LTP was observed in slices from mice in all four conditions in response to tetanic stimulation (1 s, 100 Hz). However, the potentiation was significantly stronger in animals that exhibited elevated or adaptive changes in sound response after 80 and 100 dB SPL (Figure 3B; *Matt, Eckert et al., 2018, Front Mol Neurosci, 7.4*). This indicates that the enriching and mild traumatic sound exposures caused altered peripheral sound responsiveness and induced adaptive changes in hippocampal plasticity. To further assure that the observed BDNF-dependent adaptations of hippocampal plasticity were behaviorally relevant (Soulé et al., 2006; Yamada and Nabeshima, 2003), we tested for differences in spatial learning (Richter-Levin et al., 1995) after 80 dB SPL sound exposure. Control mice and mice exposed to 80 dB SPL were subjected to a MWM learning paradigm starting 10 d after sound exposure. The experimental schedule with only two training trials per day was challenging for the mice. In comparison to the first training day control mice only slowly improved their performance over time. In contrast, mice exposed to the enriching 80 dB SPL were able to significantly improve their performance upon training. This was mirrored by shortened latencies to find the hidden platform in the water tank in comparison to the first training day (Figure 3C; *Matt, Eckert et al., 2018, Front Mol Neurosci, 7.4*).

In conclusion, specific sound exposure paradigms can lead to adaptive and non-adaptive changes in hippocampal plasticity including SC-LTP and spatial learning.

3.5.3 Transcript-specific changes in BDNF levels correlate with levels of PV mediated inhibition

BDNF signaling was shown to play a crucial role in the shaping of inhibitory circuits that might influence hippocampal LTP and hippocampus-dependent memory (Waterhouse et al., 2012; Minichiello, 2009; Yamada and Nabeshima, 2003). Therefore, we used antibodies against PV to label PV^{+}-interneurons predicted to target projecting neurons expressing BDNF (Dieni et al., 2012). Low-power examination of deconvoluted high-resolution fluorescence stacks revealed a striking

dynamic change of *Bdnf* exon VI-YFP, *Bdnf* exon IV-CFP, and PV in the CA1 regions (Figure 4A; *Matt, Eckert et al., 2018, Front Mol Neurosci, 7.4*), in the CA3 region (Figure 4B; *Matt, Eckert et al., 2018, Front Mol Neurosci, 7.4*) and in the DG (Figure 4C; *Matt, Eckert et al., 2018, Front Mol Neurosci, 7.4*) of the hippocampus. Compared to sham exposed animals (control), we observed a general upregulation of CFP, YFP, and PV in all regions of the hippocampus after acoustic enrichment and mild AT, the two conditions associated with increased hippocampal synaptic plasticity. In control animals, CFP fluorescence was mostly seen in capillary vessels of the highly vascularized FH (Figure 4A; *Matt, Eckert et al., 2018, Front Mol Neurosci, 7.4*). The CFP levels in the FH were significantly higher after acoustic enrichment and still higher after mild AT than after severe AT (Figure 4D; *Matt, Eckert et al., 2018, Front Mol Neurosci, 7.4*). In the CA1 region of animals exposed to enriching or mild traumatic sounds, we observed increased PV labeling in the pyramidal layer (Figure 4A, SP; *Matt, Eckert et al., 2018, Front Mol Neurosci, 7.4*) and an overall peak of *Bdnf* exon IV-CFP in capillaries most prominent at the level of the FH (Figure 4A,D; *Matt, Eckert et al., 2018, Front Mol Neurosci, 7.4*). In the CA3, we found both PV as well as *Bdnf* exon VI-YFP signals strongly amplified in the area where mossy fibers are predicted to target CA3 dendrites (Figure 4B,E; *Matt, Eckert et al., 2018, Front Mol Neurosci, 7.4*). PV labeling was also increased in the supra-pyramidal blade of the DG (Figure 4C; *Matt, Eckert et al., 2018, Front Mol Neurosci, 7.4*).

This generalized pattern of up-regulation was not detected in animals exposed to 120 dB SPL (Figure 4A-C, 120 dB SPL; *Matt, Eckert et al., 2018, Front Mol Neurosci, 7.4*). Particularly within the stratum lucidum (**SL**) of the CA3 region (Figure 4B,D; *Matt, Eckert et al., 2018, Front Mol Neurosci, 7.4*), the observed increase in *Bdnf* exon VI-YFP expression, aligned with PV, was either significant (80 dB SPL), moderate (100 dB SPL), or absent (120 dB SPL). The most intense areas of *Bdnf* exon VI-YFP staining in the SL were spatially separated from the areas of PV staining, which predominantly overlapped with *Bdnf* exon IV-CFP fluorescence, exemplarily shown in a line profile through the CA3 region of an 80 dB SPL exposed animal (Figure 4F; *Matt, Eckert et al., 2018, Front Mol Neurosci, 7.4*).

High-power sectional analysis revealed increased levels of PV-IR in 80 and 100 dB SPL-exposed animals in the CA3 region that could be localized to the SP

(Figure 5A; *Matt, Eckert et al., 2018, Front Mol Neurosci, 7.4*). The apparent peak in *Bdnf* exon VI-YFP was concentrated in the SL (Figure 5A lower panels; *Matt, Eckert et al., 2018, Front Mol Neurosci, 7.4*), where the BDNF expressing mossy fibers branch extensively to make contact with postsynaptic dendritic structures of pyramidal neurons or PV^+-interneurons (Figure 5E, schematic; *Matt, Eckert et al., 2018, Front Mol Neurosci, 7.4;* Dieni et al., 2012). Exemplary high-power images from Figure 5A (lower panels; *Matt, Eckert et al., 2018, Front Mol Neurosci, 7.4)* depict *Bdnf* exon VI-YFP-positive mossy fibers overlapping with PV-IR in the SL (Figure 5C; *Matt, Eckert et al., 2018, Front Mol Neurosci, 7.4*). Different from *Bdnf* exon VI-YFP, exon IV-CFP derived BDNF was increased in 80 and 100 dB SPL exposed animals in the SL in blood vessels (Figure 5A, lower panels, open arrow; *Matt, Eckert et al., 2018, Front Mol Neurosci, 7.4*) and in the SP in cytoplasmatic localization (Figure 5B, closed arrow; *Matt, Eckert et al., 2018, Front Mol Neurosci, 7.4*) of the CA3 pyramidal cells (**PCs**) relay. When averaging CFP, YFP, and PV fluorescence over the entire CA3 region (Figure 5D; at low-power magnification; *Matt, Eckert et al., 2018, Front Mol Neurosci, 7.4*), a significant (80 dB SPL), respectively not yet significant (100 dB SPL) increase in *Bdnf* exon IV-CFP or *Bdnf* exon VI-YFP became evident in comparison to sham-exposed animals or animals with repressed sound responsiveness and no LTP (120 dB SPL). The high correlation of elevated *Bdnf* exon VI-YFP in mossy fiber terminals (Figure 4B,E; *Matt, Eckert et al., 2018, Front Mol Neurosci, 7.4*), *Bdnf* exon IV-CFP in blood vessels (as in the FH, Figure 4A,D; Figure 5A lower panels; *Matt, Eckert et al., 2018, Front Mol Neurosci, 7.4*) or in the SP (Figure 5B,D; *Matt, Eckert et al., 2018, Front Mol Neurosci, 7.4*) with elevated PV levels in the SP regions (Figure 4A-E; Figure 5A lower panels; *Matt, Eckert et al., 2018, Front Mol Neurosci, 7.4*) in just those animals with elevated LTP and sound responsiveness (Figure 3B; *Matt, Eckert et al., 2018, Front Mol Neurosci, 7.4*) was remarkable. With the aim of further investigating this aspect, we reconsidered that in the classic hippocampal tri-synaptic pathway, SC from CA3-PC activate PV^+ basket cells (**BC**; Klausberger and Somogyi, 2008) conferring feed-forward inhibition of PC through perisomatic δ-γ-aminobutyric acid (**GABA**)$_A$ receptors (Glykys et al., 2008). Additionally, BC interneurons inhibit bistratified cells (**BS**) relaying to CA1-PC dendrites (Figure 6F; *Matt, Eckert et al., 2018,*

Front Mol Neurosci, 7.4;Waterhouse et al., 2012; Cutsuridis and Taxidis, 2013). We observed that elevated PV expression in CA1-SP region in animals with elevated LTP after 80 and 100 dB SPL-exposure (Figure 6A,D, SP; *Matt, Eckert et al., 2018, Front Mol Neurosci, 7.4*) correspond to an increase of perisomatic PV^+ puncta (shown in high-power magnification in Figure 6B**,** closed arrows; *Matt, Eckert et al., 2018, Front Mol Neurosci, 7.4*), while PV^+ puncta declined in the SR (Figure 6C,E; *Matt, Eckert et al., 2018, Front Mol Neurosci, 7.4*). At the level of the SP in CA1 a close relationship of δ$GABA_A$ receptor-IR and PV^+ boutons became evident (Supplementary Figure 5A; *Matt, Eckert et al., 2018, Front Mol Neurosci, 7.4*), with a trend of elevation in 80 and 100 dB SPL exposed animals (Supplementary Figure 5C closed arrows, Supplementary Figure 5E; *Matt, Eckert et al., 2018, Front Mol Neurosci, 7.4*). At the level of the CA1-SR, the decline of PV^+ puncta in 80 and 100 dB SPL exposed animals (Figure 6C,E; *Matt, Eckert et al., 2018, Front Mol Neurosci, 7.4*) was related to a maybe reduced α1$GABA_A$-receptor-IR in the SR of 80 and 100 dB SPL exposed animals (Supplementary Figure 5D closed arrows, Supplementary Figure 5F; *Matt, Eckert et al., 2018, Front Mol Neurosci, 7.4*). Important in this regard is that α1$GABA_A$-receptors are suggested to regulate the excitability and action potential thresholds of PC dendrites (Willadt et al., 2013).

These findings suggest that elevated *Bdnf* exon VI-YFP levels in mossy fiber terminals and *Bdnf* exon IV-CFP in capillaries and SP in animals with elevated LTP post 80 and 100 dB SPL correlate likewise with elevated perisomatic PV^+ contacts and with a reduction of dendritic PV^+ contacts on CA1 PCs (Figure 6F; *Matt, Eckert et al., 2018, Front Mol Neurosci, 7.4*). We functionally tested this disinhibition of CA1 dendrites in animals exposed to different SPLs. Wash-in of the $GABA_A$ receptor antagonist picrotoxin led to significantly less disinhibition in animals exposed to 80 or 100 dB SPL compared to controls and animals exposed to 120 dB SPL (Figure 6G; *Matt, Eckert et al., 2018, Front Mol Neurosci, 7.4*), suggesting that increased LTP in animals exposed to 80 and 100 dB SPL was due to a reduction in the number of picrotoxin-sensitive inhibitory inputs to CA1 dendrites. A relationship of elevated *Bdnf* exon IV-CFP and *Bdnf* exon VI-YFP levels with boosted perisomatic PV expression, reduced PV^+ puncta at CA1 dendrites and reduced picrotoxin-sensitive inhibitory input is suggested by the absence of these hallmarks in slices from animals exposed to 120 dB SPL.

In conclusion, long-lasting adaptations to sound along the ascending auditory pathway and in defined hippocampal neurons, glial, and vascular cells by a highly synchronized regulation of *Bdnf* exon IV and VI transcripts together with changes in the expression of fast-spiking PV^+-interneurons results in memory-related long-term activity changes. Central responses to enriching (80 dB SPL) or mild traumatic (100 dB SPL) sound exposure boost *Bdnf* exon VI-YFP-positive CA3 neurons representing SC. Additionally, this process leads to elevated PV^+ perisomatic contacts on *Bdnf* exon IV-CFP-positive PCs, possibly through BC interneuron activation (Figure 7B; *Matt, Eckert et al., 2018, Front Mol Neurosci, 7.4*), and to reduced PV^+ contacts and picrotoxin-sensitive inhibitory input at CA1 dendrites, possibly through BC mediated inhibition of BS cells (Figure 7C; *Matt, Eckert et al., 2018, Front Mol Neurosci, 7.4*). This chain of events, however, is not activated after severe AT, linking lacking compensation of hearing loss with a failure to recruit transcript-specific BDNF expression and LTP (Figure 7E,F; *Matt, Eckert et al., 2018, Front Mol Neurosci, 7.4*). The long lasting adaptation processes in the hippocampus after enriching or mild traumatic sound are possibly activated by the attentional/stress related pathway that acts through the basolateral amygdala, nucleus basalis and the prefrontal cortex to accentuate the perception by behaviorally important sounds by alteration of memory strength (Berlau and Weinberger, 2007; Jeanneteau and Chao, 2012). An attentional/stress related pathway was previously predicted to be impaired when stress and anxiety impairs hippocampal feed-forward inhibition and thereby cognition (Jeanneteau and Arango-Lievano, 2016; Kheirbek et al., 2012).

4. Discussion

In the present study we could show that BDNF and stress hormones might also be involved in central auditory adaptation processes and that deficits in fast auditory processing might influence memory performance via altered expression of BDNF and stress hormones.

(I) The study demonstrated that high endogenous stress hormone levels have a negative impact on the central auditory adaptation capacity, a process that may be realized by glucocorticoid receptor-mediated signaling cascades.

(*Singer, Eckert et al., 2018, FASEB J, 7.1*)

(II) Furthermore, it was shown that a deletion of mineralocorticoid receptors (**MRs**) and glucocorticoid receptors (**GRs**) in central regions, including the hippocampus, have impact on both the auditory nerve and the central auditory response. Central MR and GR could be important for attention processes by modulating auditory nerve activity through efferent feedback.

(*Marchetta, Eckert et al., in preparation*)

(III) The importance of processing and memorization of behaviorally relevant auditory stimuli came once more into focus when analyzing mouse mutants with auditory-peripheral deletion of *Bdnf* in distinct Pax2-positive neurons (***Bdnf*^{Pax2} KO**). Although *Bdnf*^{Pax2} KO mice achieve almost normal hearing, the maturation of fast auditory processing as well as the maturation of hippocampal long-term potentiation remains impaired. This has fundamental consequences for learning-dependent central auditory adaptations, anxiety and social behavior.

(*Eckert et al., in preparation, 7.2)*

(IV) Using the ***B***DNF-***L***ive-***E***xon-***V***isualization (**BLEV**) reporter mouse model, we could demonstrate that central auditory adaptation processes induce differentially activity-dependent BDNF expression along the ascending auditory pathway and in associated hippocampal brain regions depending on different sound exposures. In accordance with these observations, the altered auditory response could be directly associated with altered long-term hippocampal potentiation and learning. This could indicate that activity-dependent BDNF as an auditory-specific signal drives and thus consolidates memory-dependent central auditory adaptation processes via stress hormone receptor signaling.

(*Singer, Eckert et al., 2018, Front Mol Neurosci, 7.3;*

Matt, Eckert et al., 2018, Front Mol Neurosci, 7.4)

4.1 Inhibition of glucocorticoid receptor alleviates noise induced impairment of auditory processing

Singer, Eckert et al., "*The glucocorticoid antagonist mifepristone attenuates sound-induced long-term deficits in auditory nerve response and central auditory processing in female rats*". FASEB J. 2018, 7.1.

Stress related hearing disorders are an increasing problem of our modern society and related to many hearing disorders. We could show that GR-mediated stress responsiveness has a negative impact on auditory nerve function, noise-induced cochlear synaptopathy and auditory processing. Hearing thresholds were not significantly affected, whereby conventional audiometric assessment of threshold sensitivity would not reveal the negative effects of high endogenous stress hormone levels in humans. The results indicated severe impact of high endogenous stress hormone levels on auditory processing which should be considered in addition to the acute protective effects of stress on hearing.

4.1.1 Endogenous stress level differences do not permanently influence outer hair cells and hearing thresholds

We could show that elevated endogenous stress hormone levels in mature rats correlated with a distinct impairment in auditory nerve function particularly to high frequency stimuli. These stress induced changes in responsiveness to sound occur independent of outer hair cell (**OHC**) function as assessed by distortion products of the otoacoustic emissions (**DPOAE**; Shera and Guinan, 1999), the correlate of OHC electromotility, that defines hearing thresholds (El-Badry and McFadden, 2007; Marcon and Patuzzi, 2008; Rüttiger et al., 2017). Furthermore, we could not observe any significant influence of a pretreatment of the GR antagonist mifepristone or MR antagonist spironolactone on hearing threshold 2-3 weeks after sham or harmful acoustic exposure, although a trend of slightly protected thresholds was observed in pretreated groups (Figure 5A-E; *Singer, Eckert et al., 2018, FASEB J, 7.1*). This finding indicates that the elevation of hearing thresholds induced by acoustic trauma (**AT**) correlated with a damage to OHC electromotility after AT, is not exclusively determined by the stress component. However, previous studies have shown, that treatment with heat-shock (Yoshida et al., 1999), moderate level long-term sound (Yoshida and Liberman, 2000), or restraint stress (Canlon et al., 2007; Meltser and Canlon, 2011; Tahera et al., 2007; Tahera et al., 2006; Wang and

Liberman, 2002; Ma et al., 2015), can definitely trigger a protective effect on the injured cochlea. This protection is assumed to target primarily OHC function and cochlear mechanics especially in high frequency regions (Wang and Liberman, 2002).

4.1.2 GR-mediated stress response compromises ABR maximum amplitude size and dynamic range of the encodable hearing level of ABR waves in high frequency cochlear regions

A remarkable result of the present study is that the negative effect of increased endogenous stress hormone levels on auditory fiber responses in high-frequency cochlear regions is related to consequences for central auditory processing. Furthermore, the destructive role of elevated endogenous stress hormone levels on auditory nerve function after AT could be antagonized upon GR but not MR inhibition.

High-frequency stimulus-evoked supra-threshold auditory brainstem response (**ABR**) wave amplitudes corresponding to the auditory nerve (wave I) and lateral lemniscus plus inferior colliculus (**IC**; wave IV; Melcher and Kiang, 1996) were declined after AT in animals with increased stress hormone levels independent of hearing threshold, a trend that became significant for responses from higher frequency cochlear turns (Figure 5F-H; *Singer, Eckert et al., 2018, FASEB J, 7.1*). Additionally, inner hair cell (**IHC**) synapses that are responsible for the temporal precision in the auditory system (Buran et al., 2010), especially in higher frequency cochlear turns, are sensitive to increased endogenous stress hormone levels, shown by the loss of ribbons at the base of IHCs (Figure 3; *Singer, Eckert et al., 2018, FASEB J, 7.1*). This implicates that a detrimental influence of persistently increased stress hormone levels on the processing of the auditory nerve, especially in connection with a cochlear injury, would also negatively affect central auditory processing. There is further evidence for diminished central auditory processing in response to increased stress hormone levels, as described in tone perception (Felmingham et al., 2012), cortical responsiveness (Ma et al., 2017; Pérez et al., 2013; Ma et al., 2015), or dendritic structures in auditory nuclei (Dagnino-Subiabre et al., 2009). Thus, the increased endogenous stress hormone levels may in turn feed back to the auditory periphery and activate GR mediated decrease of auditory nerve activity. Since MRs have a higher affinity for cortisol or corticosterone than GRs, and MRs are already saturated when GRs can still

respond to pathologically increased stress hormone levels (Korte et al., 1995; Joëls and Kloet, 2017) the previously observed protective effects of acute restraint stress and pharmacological treatment with synthetic corticosteroids could be caused by the activation of MR. The selective effect of mifepristone (but not spironolactone) on auditory fiber amplitude and response range could indicate the effect of GR activation before auditory trauma (Figure 6; *Singer, Eckert et al., 2018, FASEB J, 7.1*). The maximal serum concentration of mifepristone is reached 1.5 h after application (Földesi et al., 1996; Tahera et al., 2006). It may therefore have counteracted basal glucocorticoid hypersecretion, which is a typical feature of hypothalamic-pituitary-adrenal (**HPA**) axis dysregulation (Oitzl et al., 2010; Howland, 2013) and that would explain the differences in urinary corticosterone levels measured in individual animals. Positive effects of antagonizing manifested basal glucocorticoid hypersecretion with mifepristone were also observed in stress-related elevated mild traumatic brain injury (Bay and Liberzon, 2009; Fox et al., 2016) or stress related cognitive decline (Golier et al., 2016). In this context it is also important to consider that a hypersecretion of glucocorticoids in response to HPA imbalance would reach GRs in the cochlea and the IHCs (Kil and Kalinec, 2013; Terakado et al., 2011; Yao and Rarey, 1996) via the blood (Le Prell et al., 2007). In analogy to the mechanisms already described in glutamatergic synapses in the hippocampus and basolateral amygdala (Boudaba and Tasker, 2006; Groeneweg et al., 2011; Karst et al., 2010), it could be assumed that increased stress hormone levels could influence the glutamatergic release properties of IHCs by genomic or non-genomic glucocorticoid activities in a similar way. It is also of interest that the mifepristone treatment prior to acoustic overexposure preserved in particular the integrity of the auditory nerve fiber responses to stimulation with high sound intensity high-frequency pure tones. This indicates that high endogenous stress hormone levels negatively influence IHCs and fibers more prominently in basal high frequency cochlear regions. The observation that mifepristone pretreatment prior to acoustic overexposure also partially counteracts IHC ribbon loss and the weaker Na^+, K^+-ATPase subunit alpha3 (**NKAα3**) immunoreactivity (**IR**) in basal cochlear turns could also point to a role of chronic stress on the auditory fibers (Figure 3G,H,8; *Singer, Eckert et al., 2018, FASEB J, 7.1*). Previous findings suggest that NKAα3 is particularly abundant in myelinated cochlear fiber types such as high spontaneous rate low threshold (**high-SR**) fibers (McLean et al., 2008). Increased stress hormone

levels have so far only been shown for a higher number of ribbon loss exceeding 40 %, and therefore the hypothesis was made that they also include high-SR fibers (Singer et al., 2013). The effects of chronic stress on certain auditory fibers need to be investigated in more detail in future studies. We thus assume that the long-term clinical use of corticosteroids as a therapy for hearing preservation (Trune and Canlon, 2012; Meltser and Canlon, 2011) is based on mechanisms related to acute stress effects, in which glucocorticoid levels may act as upstream protectors for AT-induced OHC damage.

In conclusion, the current findings reveal a significant impact of increased endogenous stress hormone levels on IHC synapse, auditory nerve fibers, and central auditory processing with and without AT. This GR-mediated detrimental chronic stress response probably coexists with the various protective functions of acute stress and synthetic corticoid therapies (Trune and Canlon, 2012; Meltser and Canlon, 2011).

4.2 Central stress hormone receptors modulate peripheral auditory processing

Marchetta, Eckert et al., *"Stress receptors in frontal brain regions influence auditory nerve function and auditory brainstem responses"*, in preparation.

Stress plays a fundamental role in the modulation of auditory processing (Basappa et al., 2012; Canlon et al., 2013; Canlon et al., 2007; Meltser and Canlon, 2011; Wang and Liberman, 2002) and memorizing behaviorally relevant information (Kloet et al., 2005; Sandi and Haller, 2015). Attention is essential for auditory information processing (Rhodes and Cowan, 2018) and associated with stress hormone receptors (Cornelisse et al., 2011; Otte et al., 2007; Diamond et al., 2007) and is relevant for auditory perception (Kraus and Canlon, 2012; Kraus and White-Schwoch, 2015). The deletion of central stress hormone receptors altered peripheral and central auditory processing in a remarkable way that we can suppose that central stress hormone receptors are crucial to modulate attention to behaviorally relevant auditory stimuli.

4.2.1 Successful deletion of central stress hormone receptors

MR and GR were both expressed in the hippocampus, while in the CA1 subregion, MR was mainly expressed in the cytoplasm and GR in the nuclei of pyramidal neurons, which is consistent with previous findings (Han et al., 2005). The expression profile of calcium/calmodulin dependent protein kinase II α (**CaMKIIα**) visualized by ROSA26 tdTomato CaMKIIαCre mice served as a further proof to show that CaMKIIα is only expressed in the forebrain and not in the cochlea (Figure 8, left panel; *Marchetta, Eckert et al., in preparation*). Hence, it was assumed that the deletion of MR and GR was successful throughout the forebrain, but MR and GR remained in the cochlea, where CaMKIIα is not expressed (Meese et al., 2017).

4.2.2 Central deletion of stress hormone receptors has no influence on OHCs but on IHC function

The deletion of central MR as well as GR and deletion of both MR and GR had no effect on the ABR thresholds, according to the findings of MR and GR antagonization with spironolactone and mifepristone (**3.1.2**; Figure 10; *Marchetta, Eckert et al., in preparation*). This indicates that central stress hormone receptors do not influence OHC function. However, the auditory function was altered in peripheral parts of the ascending auditory pathway although the stress hormone receptors were deleted only in the forebrain and not in the auditory periphery. MRCaMKIIα KO mice revealed a reduction in the summed auditory nerve response (ABR wave I), but this was centrally compensated (ABR wave IV), suggesting that the loss of MR did not affect the central gain adjustments. Central compensation as a consequence of altered processing acuity in the cochlea could be associated with a changed balance of excitation and inhibition leading to alterations in central auditory plasticity (Knipper et al., 2013). In addition, the central deletion of MR leads to prolonged auditory nerve and midbrain latencies, which results in reduced temporal auditory acuity (Figure 11A,12A; *Marchetta, Eckert et al., in preparation*). Pronounced disinhibition effects in the ascending auditory pathway could be observed in GRCaMKIIα KO mice where the evoked auditory nerve (ABR wave I) and midbrain activity (ABR wave IV) were increased together with a shortened latency in both ABR waves (Figure 11B,12B; *Marchetta, Eckert et al., in preparation*).

In MRGRCaMKIIα KO mice both ABR wave I and IV amplitude were increased but less distinct than in GRCaMKIIα KO mice while the latency was only slightly prolonged in ABR wave IV (Figure 11C,12C; *Marchetta, Eckert et al., in preparation*). The amplitude and latency of the ABR wave I is influenced, among other factors, by the synchronicity of auditory nerve firing and could possibly be affected by central stress hormone receptors. The strong disinhibition especially in GRCaMKIIα KO mice in combination with reduced latencies in ABR wave I and IV could be due to an increased synchronicity (Johnson and Kiang, 1976; Rüttiger et al., 2017). The latencies of evoked auditory nerve responses also provide information about the time of occurrence of the first spike (Johnson and Kiang, 1976). Disinhibition in GRCaMKIIα KO mice could recruit more fibers with high spontaneous firing rates to respond to the onset of low intensity sound stimuli. But the central deletion of both stress hormone receptors seems to balance the specific effect of each receptor on ABR wave amplitude and latency with a slightly higher impact of GR. Therefore, it appears to be an interaction between the two stress hormone receptors in the forebrain concerning the top-down feedback of auditory processing. Such top-down influences, which are processed by feedback loop signaling from forebrain regions to the cochlea, can occur through endocrine responses (McEwen, 2007). In previous studies it could be shown that the deletion of MR under the promoter of CaMKIIα does not influence the blood corticosterone levels (Berger et al., 2005) whereas the deletion of GR under the promoter of CaMKIIα increases blood corticosterone levels (Erdmann et al., 2007; Tronche et al., 1999). In section 3.1.1 we showed that high endogenous stress hormone levels have a negative impact on hearing function, but the changes were not as pronounced as the effects of central deletion of stress hormone receptors. Additionally, increased corticosterone worsens the hearing function, but we observed increased ABR wave amplitudes in GRCaMKIIα KO mice. Therefore we assume that a humoral response is not the reason for the distinct changes in ABR wave amplitudes and latencies. The final prove would require to use adrenalectomized mice and to substitute the daily dose of glucocorticoids (Dunn, 1988), what was beyond the purpose of our study.

We rather assume a neural, efferent feedback loop that controls peripheral auditory processing via MR and GR in the auditory associated areas of the forebrain. Central parts of the auditory pathway can modulate the auditory input through efferent

feedback projections (Terreros and Delano, 2015). Since OHC function was not altered by the deletion of central stress hormone receptors, the efferent innervation of IHCs came into our focus. Efferent fiber projections from the lateral olivary complex (**LOC**) innervate dendrites of auditory nerve fibers just beneath the IHCs (Guinan, 2017). Besides other neurotransmitters such as acetylcholine, dopamine plays a crucial role in the efferent modulation of auditory fibers (Ruel et al., 2001). Tonic inhibition of afferent auditory nerve fibers is modulated by dopamine release of efferent LOC fibers and thereby modulates the neuronal responses to sound (Wu et al., 2020; Ruel et al., 2001). Therefore, the disinhibition in GRCaMKIIα KO mice possibly resulted from a loss of dopamine mediated tonic inhibition and in MRCaMKIIα KO mice by an increased tonic inhibition. Due to the reduced ABR wave I amplitude in MRCaMKIIα KO mice, which is particularly pronounced near the threshold, efferent feedback may be impaired especially in fibers with high-SR, which are more sensitive to low SPLs and limited in their dynamic range (Furman et al., 2013). We conclude that central MR and GR are necessary for balance of inhibition and excitation in the auditory periphery. There is strong evidence that MR (Oliveira et al., 2014; Vogel et al., 2016) and GR (Butts and Phillips, 2013) modulates the expression of dopamine in the central nervous system, but to proof this hypothesis, tyrosine hydroxylase (Darrow et al., 2006) and dopamine receptor (Maison et al., 2012) staining in cochlear whole mount preparations should be performed to evaluate dopamine specific changes in efferent fibers as a result of central stress hormone receptor deletion.

4.3 Fast auditory processing drives hippocampal maturation and social learning

Eckert et al., *"Brain-derived neurotrophic factor in inhibitory hindbrain neurons controls central learning mechanisms"*, in preparation, 7.2.

How auditory processing deficits are linked to complex neurodevelopmental disorders with speech-related symptoms and memory deficits remains up to now unknown. We describe a domain-specific maturation deficit of the parvalbumin-positive (**PV⁺**)-interneuron dendritic network in *Bdnf*^{Pax2} KO mice in the frontal auditory pathway and the hippocampus that is associated with fast auditory processing deficits, reduced learning and increased anxiety behavior. It seems likely that Brain derived neurotrophic factor (**BDNF**) in Pax2 expressing neurons

promotes maturation of the parvalbumin (**PV**) dendritic network in frontal auditory circuits, driven by fast auditory processing. The maturation of PV-dendritic networks shapes hippocampal long-term potentiation (**LTP**) and Arc/Arg3.1 baseline levels and thereby provides a new mechanism of how sensory information guides plasticity and task-specific learning behavior with sensory experience via the auditory system.

4.3.1 Fast auditory processing deficits with hearing onset in *Bdnf*^{Pax2} KO mice

The deletion of *Bdnf* under the *Pax2* promoter leads to reduced supra-threshold ABR wave amplitudes and latency shifts, despite a rather normal hearing performance. This indicates that basic sound processing through low spontaneous rate high threshold (**low-SR**) auditory fibers that develop prior to hearing onset (Grant et al., 2010) is well established in *Bdnf*^{Pax2} KO mice. This is confirmed through normal coding of the envelope of auditory steady state responses (**ASSR**) at higher sound intensities in *Bdnf*^{Pax2}KO mice (Figure 1g; *Eckert et al., in preparation, 7.2*), a coding that requires intact, low-SR fiber function (Bharadwaj et al., 2014). In *Bdnf*^{Pax2}KO mice, however, the high-SR fiber characteristics appear to be less developed. These high-SR fibers, which promote the sharp rise times of EPSPs, can be recorded only after hearing onset (Grant et al., 2010). The high-SR fibers also participate in producing the shortest latencies of sound stimulus responses for all characteristic frequencies and define lowest-detection thresholds (Heil et al., 2008). Thus, the elevated ABR thresholds, reduced ABR wave amplitudes and prolonged late-ABR waves observed in *Bdnf*^{Pax2}KO mice (Figure 1a-e; *Eckert et al., in preparation, 7.2*)are best explained by the less developed high-SR fiber characteristics. Moreover, the shortened auditory fiber latencies of ABR wave I in *Bdnf*^{Pax2}KO mice may indicate less developed efferent tonic dopaminergic shaping of these high-SR auditory fibers. Accordingly, tonic dopaminergic shaping occurs particularly in high-SR fibers, and when functionally compromised, summed auditory nerve activity is reduced and spontaneous firing rates are elevated (Ruel et al., 2001), both consistent with reduced and shortened ABR wave I in *Bdnf*^{Pax2}KO mice (Figure 1e; *Eckert et al., in preparation, 7.2*). Deficits in the maturation of high-SR fiber response behavior in *Bdnf*^{Pax2}KO mice might also explain the reduced ASSR responses, particularly at low sound intensities (Figure 1g; *Eckert et al., in preparation, 7.2*), as high-SR fibers contribute to ASSR in quiet (Paul et al., 2017).

In addition to elevated thresholds, increased latencies and reduced response amplitudes in *Bdnf*^{Pax2}KO mice we also observed deficits in the prepulse facilitation (**PPF**), underlining characteristic fast auditory processing deficits in the *Bdnf*^{Pax2}KO mice. Thus, deficits in the processing of PPF with lead times of 6 ms are impaired in *Bdnf*^{Pax2}KO mice, while prepulse inhibition (**PPI**) with lead times of 50 ms were normal (Figure 1h,i; *Eckert et al., in preparation, 7.2*). These overall fast auditory processing deficits suggest that *Bdnf*^{Pax2}KO mice suffer from rapid auditory processing disorder often observed in children with autism spectrum disorders (**ASD**) or in children with early prenatal brain injuries, in particular in lower brain regions (Fitch et al., 2013).

4.3.2 BDNF in the auditory periphery drives fast auditory processing and hippocampal excitability with hearing onset

Deficits in PV-networks in frontal brain regions, such as the auditory cortex (**AC**) and hippocampus, as observed in *Bdnf*^{Pax2} KO mice, are unlikely to be directly linked to a role of BDNF in the migration or differentiation of inhibitory PV^{+}-interneurons in the frontal brain, as Pax2 has been shown to be confined to prospective GABA interneuron precursor cells that migrate posterior to midbrain regions within the first two postnatal weeks (Fotaki et al., 2008; Maricich and Herrup, 1999). Interneuron cells in the cortex or hippocampus instead migrate from progenitor zones in subpallidal regions expressing transcription factors different from Pax2, for example Nkx2.1, Pax6 or Gsh2 (Marín and Rubenstein, 2001). Accordingly, ROSA26 *Pax2*Cre does not express ß-Gal in frontal brain regions (Figure 1-figure supplement 1; *Eckert et al., in preparation, 7.2*), and no *Bdnf* deletion is found in these regions in *Bdnf*^{Pax2} KO mice (Figure 2,3; *Eckert et al., in preparation, 7.2*; Zuccotti et al., 2012).

Moreover, BDNF is upregulated in neurons of the cochlea and the ascending auditory pathway between P4 and the 2nd postnatal week (Singer et al., 2014), and Pax2 declines in regions posterior to the midbrain up to P15 (Fotaki et al., 2008; Maricich and Herrup, 1999). BDNF activities that define the *Bdnf*^{Pax2} KO mice phenotype occur around the 2nd postnatal week, the time of hearing onset (Villers-Sidani et al., 2007). This is the time when an initial hyperexcitability stage is described in the brain, caused by functional GABAergic contacts that are initially excitatory (Ben-Ari, 2002; Marín and Rubenstein, 2001). In the auditory system, GABAergic neurons switch in a region-specific way from depolarization to

hyperpolarization within the first two postnatal weeks (Koninck, 2007; Friauf et al., 2011; Owens and Kriegstein, 2002), a process likely driven by sensory experience (Shibata et al., 2004; Vale and Sanes, 2002) and influenced by BDNF (Owens and Kriegstein, 2002; Koninck, 2007). BDNF is assumed to facilitate the expression of potassium chloride cotransporter 2 (**KCC2**; Medina et al., 2014), which defines the membrane potential of GABA through a low intracellular Cl^- concentration (Koninck, 2007). It is challenging to consider that KCC2 membrane expression may need a critical fast auditory driving force with sensory experience that is not provided in *Bdnf*^{Pax2} KO mice, a feature that needs to be clarified in future studies.

Finally, BDNF levels in frontal regions are not changed in *Bdnf*^{Pax2} KO mice although dendritic complexity in the AC and hippocampus is reduced in mutants. We therefore predict that a fast auditory driving force, generated under the control of BDNF in Pax2-positive inhibitory precursor cells, is essential to facilitate local BDNF release from cortical neurons, which is shown to control the dendritic complexity of cortical PV^+-interneurons during auditory receptive field maturation (Hong et al., 2008; Jiao et al., 2011).

4.3.3 *Bdnf*^{Pax2} KO mice exhibit elevated hippocampal LTP, elevated Arc/Arg3.1, learning impairments, and altered explorative and anxiety behavior

In *Bdnf*^{Pax2} KO mice, the dendritic complexity of the PV^+-interneuron network between P10 and P14 is significantly diminished in the AC (shown for layer III and IV) and hippocampus (Figure 2,3; *Eckert et al., in preparation, 7.2*). This is the most critical time period of the auditory system, as between P10 and P14, cortical neural thresholds and responses to sound mature together with the improved shortening of latencies of cortical neuron responses at the end of the second postnatal week (Villers-Sidani et al., 2007) and the dendritic complexity of cortical PV^+-interneurons mature with sensory experience dependent on local BDNF release from projection neurons, as shown for the AC (Hong et al., 2008; Xu et al., 2010), SSC (Jiao et al., 2011; Itami et al., 2007) or visual cortex (Heimel et al., 2011). This is also the time when, under control of early auditory experience precise thalamic input terminating on layer IV neurons in the primary AC drive intracortical circuits of serotonergic (Takesian et al., 2018) and cholinergic inputs (Letzkus et al., 2011) in layer I interneurons. That induces disinhibition of layer IV pyramidal neurons through PV^+-interneuron suppression, enabling from that time onwards an integration of

contextual signals with specific auditory stimuli. The significant decrease of PV-IR on layer IV in primary AC pyramidal neurons (Figure 2; *Eckert et al., in preparation, 7.2*) and the inconspicuous PV-IR in the cerebellum and SSC, as observed in *Bdnf*^{Pax2} KO mice, underline the modality or domain specificity. This points to a possible domain specificity for BDNF in Pax2-positive cells, preferably for the auditory system, although visual processing deficits have not yet been analyzed. While further studies are essential to analyze auditory domain specificity in *Bdnf*^{Pax2} KO mice in more detail, we cannot exclude a preferential isolated auditory modality deficit. Thus, rapid auditory processing difficulties described in children with ASD, who have mostly temporal deficits isolated to the auditory modality, with normal tactile processing (Ganesan et al., 2016; Marco et al., 2012) and normal visual processing (Foss-Feig et al., 2017), separating ASD from disorders where both language and temporal processing are affected.

Indeed, deficits can be particularly profound when they occur in neural substrates on which a critical and distributed cognitive process such as temporal processing, e.g., the ability to process rapidly changing acoustic information, is built. The observed initially elevated excitability in the hippocampus of *Bdnf*^{Pax2} KO mice may particularly impair the processing of rapidly changing information. The diminished auditory processing in *Bdnf*^{Pax2} KO mice would reach the hippocampus through indirect connections from the associated AC projecting to the entorhinal cortex (Munoz-Lopez et al., 2010). *Bdnf*^{Pax2} KO mice appear to be arrested at a developmental stage prior to PV^{+}-interneuron maturation (Figure 5a; *Eckert et al., in preparation, 7.2*). Under these conditions, hippocampal CA1 neurons would be less shaped by the PV^{+}-interneuron network and thereby respond to stimuli with lower thresholds, explaining the elevated LTP in *Bdnf*^{Pax2}KO mice. In controls, CA1 neuron characteristics are shaped by PV^{+}-interneurons after hearing onset and are therefore expected to establish an improved signal to noise ratio and a widened dynamic range (Hu et al., 2014), a process that would also enhance the range to which activity can be further adjusted (Turrigiano, 2012; Kimura and Itami, 2019; Hu et al., 2014). This would explain the failure to further mobilize LTP in *Bdnf*^{Pax2}KO mice following sound enrichment, as observed in controls and previous studies (Matt et al., 2018). The immediate *Arc/Arg3.1* early gene is a regulator of synaptic plasticity during information processing expected to be influenced through neuron conductance (Shepherd and Bear, 2011), and the elevated expression levels in

Bdnf^{Pax2} KO mice could also explain the elevated LTP and incapability to adapt to enriching sound (Figure 5; *Eckert et al., in preparation, 7.2*; Matt et al., 2018). Typically, glutamate-induced stimulation of hippocampal projection neurons enables a remarkably fast (~15 s) Arc/Arg3.1 translation in postsynaptic excitatory synapses that leads to a rapid removal of postsynaptic α-amino-3-hydroxy-5-methyl-4-isoxazolepropionic acid (**AMPA**) receptor and a subsequent weakening of synapses (Waung, Pfeiffer, Nosyreva, Ronesi, & Huber, 2008). In *Bdnf*^{Pax2} KO mice, elevated LTP and overall enhanced excitability may maintain elevated basic Arc/Arg3.1 mRNA and protein levels, thereby hampering the stimulus-induced weakening of synapses, as stimuli would be unable to further enhance Arc/Arg.3.1 translation. This is expected to hamper the fast weakening of synapses and thus diminish the fast processing of novel experiences and contrast amplifications (Kimura and Itami, 2019). The described deficit in the learning of decision points in the multiple T-maze and the significantly reduced explorative behavior, as well as the increased stereotype self-grooming, USVs and corticosterone levels (Figure 6,7; *Eckert et al., in preparation, 7.2*), are thus likely the result of an inappropriate baseline for adjustments or attention-driven contrast amplification. Indeed, adjustment of activity levels relative to a 'set point' is essential for any learning-related change in synaptic input. Strengthening of synapses may then occur by unconstrained positive feedback cycles that drive neuronal activity to optimize output for that circuit (Turrigiano, 2012).

A failure to establish an appropriate baseline for adjustment or attention-driven contrast amplification has not yet been described in the context of cognitive disease phenotypes, such as ASD. Indeed, fast auditory processing deficits (Foss-Feig et al., 2017), reduced PV^{+}-interneuron levels (Goel et al., 2019; Korb and Finkbeiner, 2011; Mohn et al., 2014; Pirone et al., 2017), correlated gamma and beta oscillation differences (Wenhart et al., 2019), elevated Arc/Arg3.1 levels and learning deficits (Goel et al., 2019; Korb and Finkbeiner, 2011; Mohn et al., 2014; Pirone et al., 2017), as well as elevated corticosterone levels (Das et al., 2019), deficits in explorative behavior, increased self-grooming or increased levels to emit USVs or enhanced motor activity (Schmeisser et al., 2012) all these characteristics of *Bdnf*^{Pax2} KO mice have been previously linked with an autism-like phenotype. The finding provides also crucial new insight into the complex function of BDNF predicted for neurodevelopmental (Ohja et al., 2018; Saghazadeh et al., 2017) and

neuropsychiatric disorders (Autry and Monteggia, 2012). Here BDNF in lower hindbrain regions may be reconsidered as prerequisite to enable the engaging of contextual (auditory) signals paired with training to enhance plasticity from early development onwards.

In conclusion, a novel role of BDNF in the inhibitory neurons of lower auditory brain regions that shapes, along with sensory experience, the baseline for learning dependent adjustments and improved auditory skills by driving PV^{+}-interneuron networks has to be considered. This finding provides new insights into the relationship between sensory processing deficits in the auditory system and impaired perceptional learning.

4.4 *B*DNF-*L*ive-*E*xon-*V*isualization enables differential detection of activity-dependent BDNF transcripts usage *in vitro* and *in vivo*

Singer et al. Eckert et al., "*BDNF-Live-Exon-Visualization (BLEV) allows differential detection of BDNF transcripts in vitro and in vivo*", Front Mol Neurosci. 2018, 7.3;
Matt, Eckert et al., "*Visualizing BDNF transcript usage during sound-Induced memory linked plasticity*", Front Mol Neurosci. 2018, 7.4

Activity-dependent synaptic modification in a neural circuit in response to external stimuli can lead to long-lasting activity changes of connected circuit activity. How synaptic modifications store their information within the connected circuit is currently difficult to identify *in vivo*. We generated the BLEV reporter mouse model which visualizes BDNF expression following promoter-specific usage of exon IV or exon VI by translating CFP or YFP additionally to BDNF protein in characteristic neuronal, glial, and vascular locations. Animals exposed to enriching and mild traumatic sound showed increased Schaffer collateral (**SC**)-LTP together with improved acquisition in the Morris Water Maze (**MWM**). In parallel, usage of *Bdnf* promoters IV and VI was altered together with the expression of PV in the hippocampus and along the auditory axis. Altered BDNF promoter usage and increased hippocampal synaptic plasticity were not observed following AT. Enriched sensory experience may thus synchronize BDNF promotor usage in different cell types linked to improved stimulus coding through associated learning, a feature that fails upon traumatic acoustic events.

4.4.1 BLEV Mice enables visualization of differential expression of activity-dependent BDNF in various cell types

BLEV mice are a perfect tool to visualize the localization of translation of *Bdnf* transcripts generated by *Bdnf* exons IV and VI promoters *in vivo*. BDNF is a key master regulator of energy homeostasis and long-term memory (Marosi and Mattson, 2013; Park and Poo, 2013). Using BLEV mice, we observed that translation of *Bdnf* exons IV-CFP and VI-YFP mRNA in the hippocampal tri-synaptic path correlates well with LTP, memory acquisition, and PV expression changes. All of these processes have been shown to be BDNF dependent (Park and Poo, 2013; Leal et al., 2017; Minichiello, 2009; Leal et al., 2015).

We demonstrated that it is possible to label BDNF translation during sensory processing without intervening with normal BDNF expression and function. We confirmed differential targeting of *Bdnf* exons IV and VI between the somata (exon IV) of neurons and their dendrites (exon VI), as described before in primary cultures (Figure 2,5; *Singer, Eckert et al., 2018, Front Mol Neurosci, 7.3*; Baj et al., 2013). In contrast, the targeting of *Bdnf* exon IV in the mature brain was confined to the soma of projecting neurons and microglia, while *Bdnf* exon VI localized to presynaptic terminals of projecting neurons and glial extensions. Thus, our results support previous proposals of anterograde presynaptic BDNF transport in the mature organ in regulated neural circuits *in vivo* (Dieni et al., 2012). However, we cannot completely exclude the possibility that *Bdnf* transcripts may be differentially compartmentalized depending on the type of stimuli and time course as shown previously (Chiaruttini et al., 2008). Importantly, the differential distribution of *Bdnf* exon IV-CFP and *Bdnf* exon VI-YFP in BLEV mice also suggests that the GAP43 membrane-tag seems not to interfere with the visualization of the fluorescence tags as observed previously (Liu et al., 1994).

We could show that an anti-BDNF antibody co-localizes with either *Bdnf* exon IV-CFP or *Bdnf* exon VI-YFP signals in neuronal, glial, or vascular compartments within the hippocampal circuit (Figure 5,6; *Singer, Eckert et al., 2018, Front Mol Neurosci, 7.3*). Our data indicate that BDNF expression in principle hippocampal neurons and their terminals may be driven by *Bdnf* exon IV (pyramidal cells (**PCs**) soma) and exon VI (tri-synaptic terminals) promoters, respectively. Similarly, BDNF expression in astrocytes or microglia (Parkhurst et al., 2013), which is thought to influence the recruitment of

vascularization during complex homeostatic changes in plasticity (Edelmann et al., 2014), seems to be generated by somatic translation of *Bdnf* exon IV, whereas *Bdnf* exon VI seems to be translated more in their end-feet structures. This observation is of crucial interest since the dendritic trafficking deficit of *Bdnf* exon VI caused by the Val66Met polymorphism in the *Bdnf* gene is suggested to lead to cognitive brain deficits (Baj et al., 2013; Mallei et al., 2015). Moreover, our studies in BLEV mice revealed that the predicted BDNF expression in circulating blood is derived from *Bdnf* exon IV, which was previously proposed as the *Bdnf* transcript present in platelets of humans and rats (Chacón-Fernández et al., 2016). How exon IV derived BDNF from capillaries can communicate at sites where the blood brain barrier is maintained by endothelia tight junctions, pericytes, or astrocyte end-feet (Marosi and Mattson, 2013) should be part of future studies in BLEV mice. Finally, BDNF expression in endothelial cells, here defined through $p75^{NGFR}$ expression, appear to be neither generated by exon IV nor by exon VI promoters.

From these observations, a role of synchronized BDNF transcript usage in the adjustment of metabolic supply to sustain alterations of neuronal network may be hypothesized but remains speculative. The coincident changes in BDNF transcript in the ascending pathway that vary dependent on enriching or traumatic sound exposure may, however, suggest that ascending activity changes act as the driving force for transcript changes. Accordingly, the long-lasting changes in VGluT1 labeled auditory nerve terminals (Ngodup et al., 2015; Zhou et al., 2007) and GluA2 in the hippocampus after boosting sound exposures, indicate elevated presynaptic (Ngodup et al., 2015) and postsynaptic (Tanaka et al., 2000) activity in the ascending pathway. Correlated excitability changes would lead to elevated levels of neuronal calcium, shown to act on *Bdnf* exon IV promoter (West et al., 2014). Since neuronal activity closely regulates blood flow (Hillman, 2014) *Bdnf* exon IV, which has been shown to be activated in platelets by calcium channels (Chacón-Fernández et al., 2016), could be mobilized by the same event. As *Bdnf* exon IV promoter is activated by neuronal activity only to a small extent (Aid et al., 2007; Timmusk et al., 1993) it is possible that BDNF-positive feedback loops (Bambah-Mukku et al., 2014) following the same stimulus, activate *Bdnf* exon VI indirectly via binding of the AP-1 family of the transcription factor site (Tuvikene et al., 2016).

In conclusion, the comparison of *Bdnf* transcript and protein localization in BLEV mice visualized a previously elusive cell- and transcript-specific BDNF expression

pattern in hippocampal pathways that may be activated in an orchestrated manner in response to ascending excitability changes.

4.4.2 Differential localization of *Bdnf* exon IV-CFP and *Bdnf* exon VI-YFP transcripts after enriching and traumatic sound exposure

Enriching sound or mild AT, different from severe AT, mobilized *Bdnf* exon VI-YFP fluorescence most prominently in the hippocampal CA3 region, coincident to *Bdnf* exon IV-CFP in capillaries or in soma of PCs in animals with elevated LTP response (Figure 4,5; *Matt, Eckert et al., 2018, Front Mol Neurosci, 7.4*). Mossy fiber activation is known to drive rapid generation and contextualization of episodic memories for example in response to environmental enrichment in conjunction with elevated neurogenesis and feed-forward inhibition, a feature that can fail post traumatic events (Donato et al., 2013; Kheirbek et al., 2012). Therefore, it is tempting to consider that enriching sound and mild AT, different from severe AT, may drive a synchronized activation of *Bdnf* promoter usage in different cells such as neurons, capillaries and likely glial cells as part of the predicted role of BDNF in LTP and memory (Leal et al., 2017; Minichiello, 2009; van Lu et al., 2012). Particularly, the observed improvement in memory acquisition after an enriching sound exposure together with elevated LTP and sound responsiveness(Figure 3; *Matt, Eckert et al., 2018, Front Mol Neurosci, 7.4*), which coincides with elevated transcript-specific BDNF and VGluT1 expression in the brainstem and IC (Figure 2; *Matt, Eckert et al., 2018, Front Mol Neurosci, 7.4*), and GluA2 expression in the hippocampus may support the idea that sound exposure can act as a cognitive stimulant in the hippocampus (Meng et al., 2009; Angelucci et al., 2007). During this process enriching or mild traumatic sound may reach the hippocampus through the attentional/stress related pathway that acts through the basolateral amygdala, nucleus basalis and the prefrontal cortex to accentuate behaviorally important sound upon alteration of memory strength (Berlau and Weinberger, 2007). An attentional related pathway was previously predicted to be impaired when stress and anxiety impairs hippocampal feed-forward inhibition and thereby cognition (Kheirbek et al., 2012).

Bdnf exon IV-CFP and *Bdnf* exon VI-YFP expression correlates with PV expression during adaptive and non-adaptive network changes (Figure 4,5,6; *Matt, Eckert et al., 2018, Front Mol Neurosci, 7.4*). A close correlation of altered transcript-specific BDNF expression with PV expression was observed. We refer to

previous findings that BDNF expressing SCs contact PV+-interneurons (Dieni et al., 2012) and BDNF influences feed-forward inhibition and LTP. We observed a correlation of elevated *Bdnf* exon VI-YFP level in the CA3 region with up-regulation of perisomatic PV-IR in CA1 neurons and *Bdnf* exon IV-CFP in their soma in animals with elevated LTP and temporally improved memory. PV+-basket cells (**BCs**) contacts, shown to target the perisomatic region of neighboring PCs through δ-γ-aminobutyric acid (**GABA**)$_A$ receptors (Figure 6, Supplementary Figure 5; *Matt, Eckert et al., 2018, Front Mol Neurosci, 7.4*) Glykys et al., 2008; Klausberger et al., 2003), have been shown to be activated through BDNF in SCs (Danzer et al., 2008). Future studies should investigate a link of elevated *Bdnf* exon IV-CFP in soma of PCs to recruit perisynaptic and extrasynaptic δ-subunit-containing GABA$_A$-R (Duguid et al., 2012).

We also observed reduced PV-IR and α1GABA$_A$-R puncta in the stratum radiatum (**SR**) in animals with elevated LTP, *Bdnf* exon IV in capillaries and *Bdnf* exon VI in mossy fiber terminals of animals with boosted or compensated sound responses (80, 100 dB SPL; Supplementary Figure 5; *Matt, Eckert et al., 2018, Front Mol Neurosci, 7.4*). This observation may be regarded in the context of mossy fiber activation that acts through SCs on BCs to inhibit PV+-bistratified (**BS**) interneurons that target CA1 dendrites through α1GABA$_A$-R expressing synapses (Klausberger and Somogyi, 2008; Willadt et al., 2013). Additionally, blocking the dendritically localized *Bdnf* mRNA *in vivo* reduced BDNF protein levels in the dendrites and led to a selective impairment of LTP in the dendrites (An et al., 2008). Taken together, these results indicate a critical role of dendritically synthesized BDNF for synaptic plasticity.

Bdnf exon VI-YFP boutons on microglial somata expressing both *Bdnf* transcripts within the SR and the observed overlap of microglial IBA-1-IR with PV-IR in the SR close to micro-vessels could indicate an involvement of microglia-induced changes in chloride (**Cl$^-$**) homeostasis of inhibitory inputs during the process of disinhibition of CA1 dendrites (Ferrini and Koninck, 2013). A link of elevated transcript-specific BDNF expression and PV levels in animals with improved LTP needs thus to be regarded in the context of the predicted role of PV-mediated feed-forward inhibition for improvement of signal to noise ratio and pattern segregation (Kheirbek et al., 2012; Hu et al., 2014; Pouille and Scanziani, 2001) and to its predicted BDNF dependency (Waterhouse et al., 2012; Kuipers et al., 2016). Interestingly feed-

forward inhibition is assumed to be accelerated after acute stress events (Korz and Frey, 2005) or it can fail in stress-related disorders like post-traumatic stress syndrome (Kheirbek et al., 2012).

The failure of a sychnronized activation of BDNF transcripts in the hippocampus coincident to a unaltered LTP and PV expression following traumatic sound (120 dB SPL) may point to an impairment of memory related improvement of sound responsiveness. The relation of hearing loss and cognitive impairment, such as dementia as currently discussed (Livingston et al., 2017), may be reconsidered in this context.

We conclude that there is a link between the differential expression of the non-coding *Bdnf* exons in response to differential activity changes and the multifaceted BDNF function in neurons, platelets, capillary endothelial cells, microglia, and astrocytes. The use of different promoters and cell type specific expression of multiple *Bdnf* transcripts may offer the chance to selectively synchronize differential neuronal and vascular BDNF activities in response to differential activity changes.

Future studies should use BLEV mice to investigate different transcriptional activities related to the function of BDNF in energy homeostasis and neurovascular coupling during these processes.

4.5 Overall Conclusion

We could demonstrate that the hearing function influences central learning mechanisms including the hippocampus in a not negligible way. Here we have proposed a model how auditory processing and perception is connected to central hippocampal memory processes.

Fast auditory processing acts as a driving force for the initiation of activity-dependent BDNF expression, which regulates central memory processes that are strongly influenced by stress hormone levels and stress hormone receptors. With the onset of hearing and sensory experience, fast auditory processing matures simultaneously with the development of high-SR fiber characteristics. This induces the implementation of sharply increasing inhibitory PV^+-interneuron networks into auditory circuits and the integration of stress hormone-regulated attentional control circuits on auditory stimuli. It is essential to activate this system to percept, process and memorize behaviorally relevant auditory stimuli and to suppress and ignore irrelevant and interfering stimuli. Attention is crucial for perceptional learning of relevant auditory stimuli (Polley et al., 2006; Weinberger et al., 2013) and stress hormone receptors are associated with attention (Cornelisse et al., 2011; Otte et al., 2007; Diamond et al., 2007) and memorizing relevant information (Kloet et al., 2005; Sandi and Haller, 2015) but chronic stress impairs perceptual learning (Dinse et al., 2017) and contextual discrimination (Kheirbek et al., 2012). We therefore assume that the interplay of the central stress hormone receptors is crucial to focus attention on relevant sound information and to promote perceptual learning by manipulating peripheral auditory activity. The importance of fast auditory processing of central learning mechanisms and their preservation should also be considered in the context of mental disorders with increasing age, where hearing loss is the highest midlife risk factor for dementia (Livingston et al., 2017).

It is a multifaceted interaction between the hearing system and central learning mechanisms whereby it has been shown that both systems can influence each other and react interdependently to positive and negative stimuli.

5. Acknowledgements

An erster Stelle möchte ich mich bei Frau Prof. Dr. Marlies Knipper sehr herzlich bedanken die Möglichkeit gehabt zu haben in ihrer Arbeitsgruppe an vielen spannenden Themen zu arbeiten, bei den Veröffentlichungen beizutragen und meine Doktorarbeit anzufertigen.

Herrn Prof. Dr. Dr. Peter Ruth möchte ich für die hervorragende und erfolgreiche Kooperation und die Unterstützung und Betreuung während meiner Promotion danken.

Herrn Prof. Dr. Peter Pilz möchte ich für die hervorragende und erfolgreiche Kooperation und die Unterstützung bei gemeinsamen Projekten und Veröffentlichungen bedanken und dafür, dass er als Prüfer bei meiner Verteidigung fungiert.

Bei Herrn Prof. Dr. Robert Lukowski möchte ich mich bedanken, dass er als Prüfer bei meiner Verteidigung fungiert.

Herzlich danken möchte ich auch Prof. Dr. Lukas Rüttiger und Dr. Wibke Singer für die ausgezeichnete Betreuung, das große Engagement und die Unterstützung bei Experimenten, Analysen, Veröffentlichungen, Präsentationen und schließlich meiner Doktorarbeit.

Mein ganz besonderer Dank gilt Karin, Iris und Hyun-Soon ohne eure großartige Unterstützung wären die Projekte in dieser Form nicht möglich gewesen.

Vielen Dank auch an Kerstin und Monika für Eure Hilfe bei allen administrativen Fragen.

Auch möchte ich mich bei meinen großartigen Kollegen Dr. Dorit Möhrle, Dr. Marie Manthey und Dr. Steffen Wolter für die Hilfe und Zusammenarbeit bei den Projekten und den Spaß bedanken.

Bei Benedikt (Dr. B) und Philine (Dr. Φ) möchte ich mich quasizusagen ganz besonders bedanken für die unvergessliche Zeit und die Perlen, welche zumindest teilweise an der „Wall of Fame“ festgehalten sind.

Ganz herzlich möchte ich auch meinen Eltern, Familie, Freunden und meiner Frau Caro danken, die mich zu jedem Zeitpunkt meiner Promotion unterstützt haben.

6. References

Aid T, Kazantseva A, Piirsoo M, Palm K, Timmusk T (2007) Mouse and rat BDNF gene structure and expression revisited. Journal of neuroscience research 85:525–535.

Aimone JB, Deng W, Gage FH (2011) Resolving new memories: a critical look at the dentate gyrus, adult neurogenesis, and pattern separation. Neuron 70:589–596.

Alderson RF, Alterman AL, Barde Y-A, Lindsay RM (1990) Brain-derived neurotrophic factor increases survival and differentiated functions of rat septal cholinergic neurons in culture. Neuron 5:297–306.

Almeida L de, Idiart M, Lisman JE (2009a) A second function of gamma frequency oscillations: an E%-max winner-take-all mechanism selects which cells fire. The Journal of neuroscience : the official journal of the Society for Neuroscience 29:7497–7503.

Almeida L de, Idiart M, Lisman JE (2009b) The input-output transformation of the hippocampal granule cells: from grid cells to place fields. The Journal of neuroscience : the official journal of the Society for Neuroscience 29:7504–7512.

Amaral DG, Insausti R, Cowan WM (1983) Evidence for a direct projection from the superior temporal gyrus to the entorhinal cortex in the monkey. Brain Research 275:263–277.

Amunts K, Morosan P, Hilbig H, Zilles K (2012) Auditory System. In: The Human Nervous System, pp 1270–1300: Elsevier.

An JJ, Gharami K, Liao G-Y, Woo NH, Lau AG, Vanevski F, Torre ER, Jones KR, Feng Y, Lu B, Xu B (2008) Distinct role of long 3' UTR BDNF mRNA in spine morphology and synaptic plasticity in hippocampal neurons. Cell 134:175–187.

Angelucci F, Fiore M, Ricci E, Padua L, Sabino A, Tonali PA (2007) Investigating the neurobiology of music: brain-derived neurotrophic factor modulation in the hippocampus of young adult mice. Behavioural pharmacology 18:491–496.

Ashmore J (2008) Cochlear outer hair cell motility. Physiological reviews 88:173–210.

Autry AE, Monteggia LM (2012) Brain-derived neurotrophic factor and neuropsychiatric disorders. Pharmacological reviews 64:238–258.

Baj G, Carlino D, Gardossi L, Tongiorgi E (2013) Toward a unified biological hypothesis for the BDNF Val66Met-associated memory deficits in humans: a model of impaired dendritic mRNA trafficking. Frontiers in Neuroscience 7.

Balkowiec A, Katz DM (2000) Activity-Dependent Release of Endogenous Brain-Derived Neurotrophic Factor from Primary Sensory Neurons Detected by ELISAIn Situ. J. Neurosci. 20:7417–7423.

Bambah-Mukku D, Travaglia A, Chen DY, Pollonini G, Alberini CM (2014) A Positive Autoregulatory BDNF Feedback Loop via C/EBPβ Mediates Hippocampal Memory Consolidation. J. Neurosci. 34:12547–12559.

Barde YA (1994) Neurotrophins: a family of proteins supporting the survival of neurons. Progress in clinical and biological research 390:45–56.

Barde YA, Edgar D, Thoenen H (1982) Purification of a new neurotrophic factor from mammalian brain. The EMBO journal 1:549–553.

Basappa J, Graham CE, Turcan S, Vetter DE (2012) The cochlea as an independent neuroendocrine organ: expression and possible roles of a local hypothalamic-pituitary-adrenal axis-equivalent signaling system. Hearing Research 288:3–18.

Bay EH, Liberzon I (2009) Early stress response: a vulnerability framework for functional impairment following mild traumatic brain injury. Research and theory for nursing practice 23:42–61.

Békésy G, Wever EG (1960) Experiments in hearing. New York: MacGraw-Hill.

Ben-Ari Y (2002) Excitatory actions of gaba during development: the nature of the nurture. Nature reviews. Neuroscience 3:728–739.

Benasich AA (2002) Impaired processing of brief, rapidly presented auditory cues in infants with a family history of autoimmune disorder. Developmental neuropsychology 22:351–372.

Benasich AA, Thomas JJ, Choudhury N, Leppänen PHT (2002) The importance of rapid auditory processing abilities to early language development: evidence from converging methodologies. Developmental psychobiology 40:278–292.

Berger S, Wolfer DP, Selbach O, Alter H, Erdmann G, Reichardt HM, Chepkova AN, Welzl H, Haas HL, Lipp H-P, Schütz G (2005) Loss of the limbic mineralocorticoid receptor impairs behavioral plasticity. Proceedings of the National Academy of Sciences of the United States of America 103:195–200.

Berlau KM, Weinberger NM (2007) Learning strategy determines auditory cortical plasticity. Neurobiology of learning and memory 89:153–166.

Bharadwaj HM, Verhulst S, Shaheen L, Liberman MC, Shinn-Cunningham BG (2014) Cochlear neuropathy and the coding of supra-threshold sound. Frontiers in systems neuroscience 8:26.

Binder JR, Frost JA, Hammeke TA, Bellgowan PS, Springer JA, Kaufman JN, Possing ET (2000) Human temporal lobe activation by speech and nonspeech sounds. Cerebral cortex (New York, N.Y. : 1991) 10:512–528.

Bird CM, Burgess N (2008) The hippocampus and memory: insights from spatial processing. Nature reviews. Neuroscience 9:182–194.

Bordi F, LeDoux J (1992) Sensory tuning beyond the sensory system: an initial analysis of auditory response properties of neurons in the lateral amygdaloid nucleus and overlying areas of the striatum. J. Neurosci. 12:2493–2503.

Boudaba C, Tasker JG (2006) Intranuclear coupling of hypothalamic magnocellular nuclei by glutamate synaptic circuits. American journal of physiology. Regulatory, integrative and comparative physiology 291:R102-11.

Bramham CR, Messaoudi E (2005) BDNF function in adult synaptic plasticity: the synaptic consolidation hypothesis. Progress in neurobiology 76:99–125.

Brownell WE, Bader CR, Bertrand D, Ribaupierre Y de (1985) Evoked mechanical responses of isolated cochlear outer hair cells. Science (New York, N.Y.) 227:194–196.

Buran BN, Strenzke N, Neef A, Gundelfinger ED, Moser T, Liberman MC (2010) Onset coding is degraded in auditory nerve fibers from mutant mice lacking synaptic ribbons. The Journal of neuroscience : the official journal of the Society for Neuroscience 30:7587–7597.

Butts KA, Phillips AG (2013) Glucocorticoid receptors in the prefrontal cortex regulate dopamine efflux to stress via descending glutamatergic feedback to the ventral tegmental area. International Journal of Neuropsychopharmacology 16:1799–1807.

Canlon B, Borg E, Flock Å (1988) Protection against noise trauma by pre-exposure to a low level acoustic stimulus. Hearing Research 34:197–200.

Canlon B, Meltser I, Johansson P, Tahera Y (2007) Glucocorticoid receptors modulate auditory sensitivity to acoustic trauma. Hearing Research 226:61–69.

Canlon B, Theorell T, Hasson D (2013) Associations between stress and hearing problems in humans. Hearing Research 295:9–15.

Cantiani C, Choudhury NA, Yu YH, Shafer VL, Schwartz RG, Benasich AA (2016) From Sensory Perception to Lexical-Semantic Processing: An ERP Study in Non-Verbal Children with Autism. PloS one 11.

Cappaert NLM, van Strien NM, Witter MP (2015) Hippocampal Formation. In: The Rat Nervous System, pp 511–573: Elsevier.

Carmeliet P, Tessier-Lavigne M (2005) Common mechanisms of nerve and blood vessel wiring. Nature 436:193–200.

Catts VS, Al-Menhali N, Burne THJ, Colditz MJ, Coulson EJ (2008) The p75 neurotrophin receptor regulates hippocampal neurogenesis and related behaviours. The European journal of neuroscience 28:883–892.

Cenquizca LA, Swanson LW (2007) Spatial organization of direct hippocampal field CA1 axonal projections to the rest of the cerebral cortex. Brain research reviews 56:1–26.

Chacón-Fernández P, Säuberli K, Colzani M, Moreau T, Ghevaert C, Barde Y-A (2016) Brain-derived Neurotrophic Factor in Megakaryocytes. The Journal of biological chemistry 291:9872–9881.

Chao MV (2003) Neurotrophins and their receptors: a convergence point for many signalling pathways. Nature reviews. Neuroscience 4:299–309.

Chao MV, Bothwell M (2002) Neurotrophins. Neuron 33:9–12.

Chen G-D, Manohar S, Salvi R (2012) Amygdala hyperactivity and tonotopic shift after salicylate exposure. Brain Research 1485:63–76.

Chen G-D, Radziwon KE, Kashanian N, Manohar S, Salvi R (2014) Salicylate-induced auditory perceptual disorders and plastic changes in nonclassical auditory centers in rats. Neural plasticity 2014:658741.

Cheung THC, Cardinal RN (2005) Hippocampal lesions facilitate instrumental learning with delayed reinforcement but induce impulsive choice in rats. BMC neuroscience 6:36.

Chiaruttini C, Sonego M, Baj G, Simonato M, Tongiorgi E (2008) BDNF mRNA splice variants display activity-dependent targeting to distinct hippocampal laminae. Molecular and cellular neurosciences 37:11–19.

Chumak T, Rüttiger L, Lee SC, Campanelli D, Zuccotti A, Singer W, Popelář J, Gutsche K, Geisler H-S, Schraven SP, Jaumann M, Panford-Walsh R, Hu J, Schimmang T, Zimmermann U, Syka J, Knipper M (2016) BDNF in Lower Brain Parts Modifies Auditory Fiber Activity to Gain Fidelity but Increases the Risk for Generation of Central Noise After Injury. Molecular neurobiology 53:5607–5627.

Cornelisse S, Joëls M, Smeets T (2011) A Randomized Trial on Mineralocorticoid Receptor Blockade in Men: Effects on Stress Responses, Selective Attention, and Memory. Neuropsychopharmacology 36:2720–2728.

Cutsuridis V, Taxidis J (2013) Deciphering the role of CA1 inhibitory circuits in sharp wave-ripple complexes. Frontiers in systems neuroscience 7:13.

Dagnino-Subiabre A (2013) Effects of chronic stress on the auditory system and fear learning: an evolutionary approach. Reviews in the neurosciences 24:227–237.

Dagnino-Subiabre A, Muñoz-Llancao P, Terreros G, Wyneken U, Díaz-Véliz G, Porter B, Kilgard MP, Atzori M, Aboitiz F (2009) Chronic stress induces dendritic atrophy in the rat medial geniculate nucleus: effects on auditory conditioning. Behavioural Brain Research 203:88–96.

Danzer SC, Kotloski RJ, Walter C, Hughes M, McNamara JO (2008) Altered Morphology of Hippocampal Dentate Granule Cell Presynaptic and Postsynaptic Terminals Following Conditional Deletion of TrkB. Hippocampus 18:668–678.

DARROW KN, SIMONS EJ, DODDS L, Liberman MC (2006) Dopaminergic Innervation of the Mouse Inner Ear: Evidence for a Separate Cytochemical Group of Cochlear Efferent Fibers. J. Comp. Neurol. 498:403–414.

Das I, Estevez MA, Sarkar AA, Banerjee-Basu S (2019) A multifaceted approach for analyzing complex phenotypic data in rodent models of autism. Molecular autism 10:11.

David SV (2018) Incorporating behavioral and sensory context into spectro-temporal models of auditory encoding. Hearing Research 360:107–123.

Davis MH, Johnsrude IS (2003) Hierarchical Processing in Spoken Language Comprehension. J. Neurosci. 23:3423–3431.

Deshmukh SS, Knierim JJ (2012) Hippocampus. Wiley interdisciplinary reviews. Cognitive science 3:231–251.

Diamond DM, Campbell AM, Park CR, Halonen J, Zoladz PR (2007) The temporal dynamics model of emotional memory processing: a synthesis on the neurobiological basis of stress-induced amnesia, flashbulb and traumatic memories, and the Yerkes-Dodson law. Neural plasticity 2007:60803.

Dieni S, Matsumoto T, Dekkers M, Rauskolb S, Ionescu MS, Deogracias R, Gundelfinger ED, Kojima M, Nestel S, Frotscher M, Barde Y-A (2012) BDNF and its pro-peptide are stored in presynaptic dense core vesicles in brain neurons. The Journal of cell biology 196:775–788.

Dinse HR, Kattenstroth JC, Lenz M, Tegenthoff M, Wolf OT (2017) The stress hormone cortisol blocks perceptual learning in humans. Psychoneuroendocrinology 77:63–67.

Donato F, Rompani SB, Caroni P (2013) Parvalbumin-expressing basket-cell network plasticity induced by experience regulates adult learning. Nature 504:272–276.

Donovan MJ, Lin MI, Wiegn P, Ringstedt T, Kraemer R, Hahn R, Wang S, Ibañez CF, Rafii S, Hempstead BL (2000) Brain derived neurotrophic factor is an endothelial cell survival factor required for intramyocardial vessel stabilization. Development (Cambridge, England) 127:4531–4540.

Duguid I, Branco T, London M, Chadderton P, Häusser M (2012) Tonic Inhibition Enhances Fidelity of Sensory Information Transmission in the Cerebellar Cortex. J. Neurosci. 32:11132–11143.

Dunn AJ (1988) Stress-related changes in cerebral catecholamine and indoleamine metabolism: lack of effect of adrenalectomy and corticosterone. Journal of neurochemistry 51:406–412.

Edelmann E, Lessmann V, Brigadski T (2014) Pre- and postsynaptic twists in BDNF secretion and action in synaptic plasticity. Neuropharmacology 76 Pt C:610–627.

El Sabbagh NG, Sewitch MJ, Bezdjian A, Daniel SJ (2017) Intratympanic dexamethasone in sudden sensorineural hearing loss: A systematic review and meta-analysis. The Laryngoscope 127:1897–1908.

El-Badry MM, McFadden SL (2007) Electrophysiological Correlates of Progressive Sensorineural Pathology in Carboplatin-Treated Chinchillas. Brain Research 1134:122–130.

Erdmann G, Schütz G, Berger S (2007) Inducible gene inactivation in neurons of the adult mouse forebrain. BMC neuroscience 8:63.

Ernfors P, Lee KF, Jaenisch R (1994) Mice lacking brain-derived neurotrophic factor develop with sensory deficits. Nature 368:147–150.

Felmingham KL, Rennie C, Gordon E, Bryant RA (2012) Autonomic and cortical reactivity in acute and chronic posttraumatic stress. Biological psychology 90:224–227.

Ferrini F, Koninck Y de (2013) Microglia control neuronal network excitability via BDNF signalling. Neural plasticity 2013:429815.

Fettiplace R (2017) Hair Cell Transduction, Tuning, and Synaptic Transmission in the Mammalian Cochlea. Comprehensive Physiology 7:1197–1227.

Fettiplace R, Kim KX (2014) The physiology of mechanoelectrical transduction channels in hearing. Physiological reviews 94:951–986.

Fitch RH, Alexander ML, Threlkeld SW (2013) Early neural disruption and auditory processing outcomes in rodent models: implications for developmental language disability. Frontiers in systems neuroscience 7.

Földesi I, Falkay G, Kovács L (1996) Determination of RU486 (mifepristone) in blood by radioreceptorassay; A pharmacokinetic study. Contraception 54:27–32.

Foss-Feig JH, Schauder KB, Key AP, Wallace MT, Stone WL (2017) Audition-Specific Temporal Processing Deficits Associated with Language Function in Children with Autism Spectrum Disorder. Autism research : official journal of the International Society for Autism Research 10:1845–1856.

Fotaki V, Price DJ, Mason JO (2008) Newly identified patterns of Pax2 expression in the developing mouse forebrain. BMC developmental biology 8:79.

Fox LC, Davies DR, Scholl JL, Watt MJ, Forster GL (2016) Differential effects of glucocorticoid and mineralocorticoid antagonism on anxiety behavior in mild traumatic brain injury. Behavioural Brain Research 312:362–365.

Friauf E, Rust MB, Schulenborg T, Hirtz JJ (2011) Chloride cotransporters, chloride homeostasis, and synaptic inhibition in the developing auditory system. Hearing Research 279:96–110.

Fritzsch B, Knipper M, Friauf E (2015) Auditory system: development, genetics, function, aging, and diseases. Cell and tissue research 361:1–6.

Fritzsch B, Tessarollo L, Coppola E, Reichardt LF (2004) Neurotrophins in the ear: their roles in sensory neuron survival and fiber guidance. In: NGF and related molecules in health and disease. 7th International Conference on NGF and related Molecules held in Modena, Italy from 15 to 19 May, 2002 (Aloe L, Calzà L, eds), pp 265–278. Amsterdam: Elsevier.

Furman AC, Kujawa SG, Liberman MC (2013) Noise-induced cochlear neuropathy is selective for fibers with low spontaneous rates. Journal of neurophysiology 110:577–586.

Ganesan S, Khan S, Garel K-LA, Hämäläinen MS, Kenet T (2016) Normal Evoked Response to Rapid Sequences of Tactile Pulses in Autism Spectrum Disorders. Frontiers in human neuroscience 10:433.

Geiger JRP, Lübke J, Roth A, Frotscher M, Jonas P (1997) Submillisecond AMPA Receptor-Mediated Signaling at a Principal Neuron–Interneuron Synapse. Neuron 18:1009–1023.

Giraud AL, Lorenzi C, Ashburner J, Wable J, Johnsrude I, Frackowiak R, Kleinschmidt A (2000) Representation of the temporal envelope of sounds in the human brain. Journal of neurophysiology 84:1588–1598.

Glykys J, Mann EO, Mody I (2008) Which GABA(A) receptor subunits are necessary for tonic inhibition in the hippocampus? The Journal of neuroscience : the official journal of the Society for Neuroscience 28:1421–1426.

Goel A, Cantu DA, Guilfoyle J, Chaudhari GR, Newadkar A, Todisco B, Alba D de, Kourdougli N, Schmitt LM, Pedapati E, Erickson CA, Portera-Cailliau C (2019) Author Correction: Impaired perceptual learning in a mouse model of Fragile X syndrome is mediated by parvalbumin neuron dysfunction and is reversible. Nature neuroscience 22:143.

Golier JA, Caramanica K, Michaelides AC, Makotkine I, Schmeidler J, Harvey PD, Yehuda R (2016) A randomized, double-blind, placebo-controlled, crossover trial of mifepristone in Gulf War veterans with chronic multisymptom illness. Psychoneuroendocrinology 64:22–30.

Golub JS, Brickman AM, Ciarleglio AJ, Schupf N, Luchsinger JA (2019) Association of Subclinical Hearing Loss With Cognitive Performance. JAMA otolaryngology-- head & neck surgery.

Grant L, Yi E, Glowatzki E (2010) Two modes of release shape the postsynaptic response at the inner hair cell ribbon synapse. J. Neurosci. 30:4210–4220.

Griffen TC, Maffei A (2014) GABAergic synapses: their plasticity and role in sensory cortex. Frontiers in cellular neuroscience 8.

Griffiths TD, Johnsrude I, Dean JL, Green GG (1999) A common neural substrate for the analysis of pitch and duration pattern in segmented sound? Neuroreport 10:3825–3830.

Groeneweg FL, Karst H, Kloet ER de, Joëls M (2011) Rapid non-genomic effects of corticosteroids and their role in the central stress response. The Journal of endocrinology 209:153–167.

Groenink L, Verdouw PM, van Oorschot R, Olivier B (2008) Models of anxiety: ultrasonic vocalizations of isolated rat pups. Current protocols in pharmacology Chapter 5:Unit 5.18.

Guinan JJ (2017) Olivocochlear Efferents: Their action, effects, measurement and uses, and the impact of the new conception of cochlear mechanical responses. Hearing Research 362:38–47.

Gulyás AI, Megías M, Emri Z, Freund TF (1999) Total Number and Ratio of Excitatory and Inhibitory Synapses Converging onto Single Interneurons of Different Types in the CA1 Area of the Rat Hippocampus. J. Neurosci. 19:10082–10097.

Hall DA, Johnsrude IS, Haggard MP, Palmer AR, Akeroyd MA, Summerfield AQ (2002) Spectral and temporal processing in human auditory cortex. Cerebral cortex (New York, N.Y. : 1991) 12:140–149.

Hampson RE, Hedberg T, Deadwyler SA (2000) Differential information processing by hippocampal and subicular neurons. Annals of the New York Academy of Sciences 911:151–165.

Han F, Ozawa H, Matsuda K-i, Nishi M, Kawata M (2005) Colocalization of mineralocorticoid receptor and glucocorticoid receptor in the hippocampus and hypothalamus. Neuroscience research 51:371–381.

Haubensak W, Narz F, Heumann R, Lessmann V (1998) BDNF-GFP containing secretory granules are localized in the vicinity of synaptic junctions of cultured cortical neurons. Journal of cell science 111 (Pt 11):1483–1493.

Heil P, Neubauer H, Brown M, Irvine DRF (2008) Towards a unifying basis of auditory thresholds: distributions of the first-spike latencies of auditory-nerve fibers. Hearing Research 238:25–38.

Heimel JA, van Versendaal D, Levelt CN (2011) The role of GABAergic inhibition in ocular dominance plasticity. Neural plasticity 2011:391763.

Hill JL, Hardy NF, Jimenez DV, Maynard KR, Kardian AS, Pollock CJ, Schloesser RJ, Martinowich K (2016) Loss of promoter IV-driven BDNF expression impacts oscillatory activity during sleep, sensory information processing and fear regulation. Translational Psychiatry 6:e873-.

Hillman EMC (2014) Coupling Mechanism and Significance of the BOLD Signal: A Status Report. Annual review of neuroscience 37:161–181.

Hirano Y, Fujita M, Watanabe K, Niwa M, Takahashi T, Kanematsu M, Ido Y, Tomida M, Onozuka M (2006) Effect of unpleasant loud noise on hippocampal activities during picture encoding: an fMRI study. Brain and cognition 61:280–285.

Holdgraf CR, Heer W de, Pasley B, Rieger J, Crone N, Lin JJ, Knight RT, Theunissen FE (2016) Rapid tuning shifts in human auditory cortex enhance speech intelligibility. Nature communications 7:13654.

Hong EJ, McCord AE, Greenberg ME (2008) A biological function for the neuronal activity-dependent component of Bdnf transcription in the development of cortical inhibition. Neuron 60:610–624.

Howland RH (2013) Mifepristone as a therapeutic agent in psychiatry. Journal of psychosocial nursing and mental health services 51:11–14.

Hu H, Gan J, Jonas P (2014) Interneurons. Fast-spiking, parvalbumin^{+} GABAergic interneurons: from cellular design to microcircuit function. Science (New York, N.Y.) 345:1255263.

Huang EJ, Reichardt LF (2001) Neurotrophins: roles in neuronal development and function. Annual review of neuroscience 24:677–736.

Huet A, Batrel C, Wang J, Desmadryl G, Nouvian R, Puel JL, Bourien J (2019) Sound Coding in the Auditory Nerve: From Single Fiber Activity to Cochlear Mass Potentials in Gerbils. Neuroscience 407:83–92.

Irvine DRF (2018) Auditory perceptual learning and changes in the conceptualization of auditory cortex. Hearing Research 366:3–16.

Itami C, Kimura F, Nakamura S (2007) Brain-derived neurotrophic factor regulates the maturation of layer 4 fast-spiking cells after the second postnatal week in the developing barrel cortex. The Journal of neuroscience : the official journal of the Society for Neuroscience 27:2241–2252.

Itskov PM, Vinnik E, Honey C, Schnupp J, Diamond ME (2012) Sound sensitivity of neurons in rat hippocampus during performance of a sound-guided task. Journal of neurophysiology 107:1822–1834.

Jakkamsetti V, Tsai N-P, Gross C, Molinaro G, Collins KA, Nicoletti F, Wang KH, Osten P, Bassell GJ, Gibson JR, Huber KM (2013) Experience-induced Arc/Arg3.1 primes CA1 pyramidal neurons for metabotropic glutamate receptor-dependent long-term synaptic depression. Neuron 80:72–79.

Jaumann M et al. (2012) cGMP-Prkg1 signaling and Pde5 inhibition shelter cochlear hair cells and hearing function. Nature medicine 18:252–259.

Jeanneteau F, Arango-Lievano M (2016) Linking Mitochondria to Synapses: New Insights for Stress-Related Neuropsychiatric Disorders. Neural plasticity 2016.

Jeanneteau F, Chao MV (2012) Are BDNF and glucocorticoid activities calibrated? Neuroscience 239:173–195.

Jezek K, Henriksen EJ, Treves A, Moser EI, Moser M-B (2011) Theta-paced flickering between place-cell maps in the hippocampus. Nature 478:246–249.

Jiao Y, Zhang Z, Zhang C, Wang X, Sakata K, Lu B, Sun Q-Q (2011) A key mechanism underlying sensory experience-dependent maturation of neocortical GABAergic circuits in vivo. Proceedings of the National Academy of Sciences of the United States of America 108:12131–12136.

Job A, Raynal M, Kossowski M, Studler M, Ghernaouti C, Baffioni-Venturi A, Roux A, Darolles C, Guelorget A (2009) Otoacoustic detection of risk of early hearing loss in ears with normal audiograms: a 3-year follow-up study. Hearing Research 251:10–16.

Joëls M, Kloet ER de (2017) 30 YEARS OF THE MINERALOCORTICOID RECEPTOR: The brain mineralocorticoid receptor: a saga in three episodes. The Journal of endocrinology 234:T49-T66.

Johnson DH, Kiang NY (1976) Analysis of discharges recorded simultaneously from pairs of auditory nerve fibers. Biophysical Journal 16:719–734.

Johnson SL, Safieddine S, Mustapha M, Marcotti W (2019) Hair Cell Afferent Synapses: Function and Dysfunction. Cold Spring Harbor perspectives in medicine.

Kandel ER (2013) Principles of neural science. New York, Toronto: McGraw-Hill Medical.

Karst H, Berger S, Erdmann G, Schütz G, Joëls M (2010) Metaplasticity of amygdalar responses to the stress hormone corticosterone. Proceedings of the National Academy of Sciences of the United States of America 107:14449–14454.

Kellner Y, Gödecke N, Dierkes T, Thieme N, Zagrebelsky M, Korte M (2014) The BDNF effects on dendritic spines of mature hippocampal neurons depend on neuronal activity. Frontiers in synaptic neuroscience 6:5.

Kheirbek MA, Klemenhagen KC, Sahay A, Hen R (2012) Neurogenesis and generalization: a new approach to stratify and treat anxiety disorders. Nature neuroscience 15:1613–1620.

Kil S-H, Kalinec F (2013) Expression and Dexamethasone-induced Nuclear Translocation of Glucocorticoid and Mineralocorticoid Receptors in Guinea Pig Cochlear Cells. Hearing Research 299:63–78.

Kim H, Ährlund-Richter S, Wang X, Deisseroth K, Carlén M (2016) Prefrontal Parvalbumin Neurons in Control of Attention. Cell 164:208–218.

Kim JJ, Haller J (2007) Glucocorticoid hyper- and hypofunction: stress effects on cognition and aggression. Annals of the New York Academy of Sciences 1113:291–303.

Kimura F, Itami C (2019) A Hypothetical Model Concerning How Spike-Timing-Dependent Plasticity Contributes to Neural Circuit Formation and Initiation of the Critical Period in Barrel Cortex. J. Neurosci. 39:3784–3791.

Klausberger T, Magill PJ, Márton LF, Roberts JDB, Cobden PM, Buzsáki G, Somogyi P (2003) Brain-state- and cell-type-specific firing of hippocampal interneurons in vivo. Nature 421:844–848.

Klausberger T, Somogyi P (2008) Neuronal diversity and temporal dynamics: the unity of hippocampal circuit operations. Science (New York, N.Y.) 321:53–57.

Kloet ER de, Joëls M (2016) Stress Research: Past, Present, and Future. In: Neuroscience in the 21st century. From basic to clinical (Pfaff DW, Volkow ND, eds), pp 2381–2410. New York, NY: Springer.

Kloet ER de, Joëls M, Holsboer F (2005) Stress and the brain: from adaptation to disease. Nature reviews. Neuroscience 6:463–475.

Kloet ER de, Oitzl MS, Joëls M (1999) Stress and cognition: are corticosteroids good or bad guys? Trends in Neurosciences 22:422–426.

Knipper M, van Dijk P, Nunes I, Rüttiger L, Zimmermann U (2013) Advances in the neurobiology of hearing disorders: recent developments regarding the basis of tinnitus and hyperacusis. Progress in neurobiology 111:17–33.

Koninck Y de (2007) Altered chloride homeostasis in neurological disorders: a new target. Current opinion in pharmacology 7:93–99.

Korb E, Finkbeiner S (2011) Arc in synaptic plasticity: from gene to behavior. Trends in Neurosciences 34:591–598.

Korte SM, Boer SF de, Kloet ER de, Bohus B (1995) Anxiolytic-like effects of selective mineralocorticoid and glucocorticoid antagonists on fear-enhanced behavior in the elevated plus-maze. Psychoneuroendocrinology 20:385–394.

Korver AMH, Smith RJH, van Camp G, Schleiss MR, Bitner-Glindzicz MAK, Lustig LR, Usami S-i, Boudewyns AN (2017) Congenital hearing loss. Nature reviews. Disease primers 3:16094.

Korz V, Frey JU (2005) Bidirectional Modulation of Hippocampal Long-Term Potentiation under Stress and No-Stress Conditions in Basolateral Amygdala-Lesioned and Intact Rats. J. Neurosci. 25:7393–7400.

Kraus KS, Canlon B (2012) Neuronal connectivity and interactions between the auditory and limbic systems. Effects of noise and tinnitus. Hearing Research 288:34–46.

Kraus N, White-Schwoch T (2015) Unraveling the Biology of Auditory Learning: A Cognitive-Sensorimotor-Reward Framework. Trends in cognitive sciences 19:642–654.

Krömer SA, Kessler MS, Milfay D, Birg IN, Bunck M, Czibere L, Panhuysen M, Pütz B, Deussing JM, Holsboer F, Landgraf R, Turck CW (2005) Identification of glyoxalase-I as a protein marker in a mouse model of extremes in trait anxiety. J. Neurosci. 25:4375–4384.

Kuipers SD, Trentani A, Tiron A, Mao X, Kuhl D, Bramham CR (2016) BDNF-induced LTP is associated with rapid Arc/Arg3.1-dependent enhancement in adult hippocampal neurogenesis. Scientific reports 6.

Kullmann DM (2011) Interneuron networks in the hippocampus. Current opinion in neurobiology 21:709–716.

Kumar S, Joseph S, Gander PE, Barascud N, Halpern AR, Griffiths TD (2016) A Brain System for Auditory Working Memory. J. Neurosci. 36:4492–4505.

Lange-Asschenfeldt C, Lohmann P, Riepe MW (2007) Spatial performance in a complex maze is associated with persistent long-term potentiation enhancement in mouse hippocampal slices at early training stages. Neuroscience 147:318–324.

Leal G, Afonso PM, Salazar IL, Duarte CB (2015) Regulation of hippocampal synaptic plasticity by BDNF. Brain Research 1621:82–101.

Leal G, Bramham CR, Duarte CB (2017) BDNF and Hippocampal Synaptic Plasticity. Vitamins and hormones 104:153–195.

Lee I, Yoganarasimha D, Rao G, Knierim JJ (2004) Comparison of population coherence of place cells in hippocampal subfields CA1 and CA3. Nature 430:456–459.

Letzkus JJ, Wolff SBE, Meyer EMM, Tovote P, Courtin J, Herry C, Lüthi A (2011) A disinhibitory microcircuit for associative fear learning in the auditory cortex. Nature 480:331–335.

Liberman MC, Gao W-Y (1995) Chronic cochlear de-efferentation and susceptibility to permanent acoustic injury. Hearing Research 90:158–168.

Liberman T, Velluti RA, Pedemonte M (2009) Temporal correlation between auditory neurons and the hippocampal theta rhythm induced by novel stimulations in awake guinea pigs. Brain Research 1298:70–77.

Lin FR, Metter EJ, O'Brien RJ, Resnick SM, Zonderman AB, Ferrucci L (2011) Hearing Loss and Incident Dementia. Archives of Neurology 68:214–220.

Lisman J, Buzsáki G (2008) A Neural Coding Scheme Formed by the Combined Function of Gamma and Theta Oscillations. Schizophrenia Bulletin 34:974–980.

Liu Y, Fisher DA, Storm (1994) Intracellular sorting of neuromodulin (GAP-43) mutants modified in the membrane targeting domain. J. Neurosci. 14:5807–5817.

Livingston G et al. (2017) Dementia prevention, intervention, and care. The Lancet 390:2673–2734.

Lynch MA (2004) Long-term potentiation and memory. Physiological reviews 84:87–136.

Ma L, Li W, Li S, Wang X, Qin L (2017) Effect of chronic restraint stress on inhibitory gating in the auditory cortex of rats. Stress (Amsterdam, Netherlands) 20:312–319.

Ma L, Zhang J, Yang P, Wang E, Qin L (2015) Acute restraint stress alters sound-evoked neural responses in the rat auditory cortex. Neuroscience 290:608–620.

Maison SF, Liu X-P, Eatock RA, Sibley DR, Grandy DK, Liberman MC (2012) Dopaminergic Signaling in the Cochlea: Receptor Expression Patterns and Deletion Phenotypes. J. Neurosci. 32:344–355.

Mallei A, Baj G, Ieraci A, Corna S, Musazzi L, Lee FS, Tongiorgi E, Popoli M (2015) Expression and Dendritic Trafficking of BDNF-6 Splice Variant are Impaired in Knock-In Mice Carrying Human BDNF Val66Met Polymorphism. International Journal of Neuropsychopharmacology 18.

Malmierca MS, Ryugo DK (2012) Auditory System. In: The Mouse Nervous System, pp 607–645: Elsevier.

Marco EJ, Khatibi K, Hill SS, Siegel B, Arroyo MS, Dowling AF, Neuhaus JM, Sherr EH, Hinkley LNB, Nagarajan SS (2012) Children with autism show reduced somatosensory response: an MEG study. Autism research : official journal of the International Society for Autism Research 5:340–351.

Marcon S, Patuzzi R (2008) Changes in cochlear responses in guinea pig with changes in perilymphatic K+. Part I: summating potentials, compound action potentials and DPOAEs. Hearing Research 237:76–89.

Marcotti W (2012) Functional assembly of mammalian cochlear hair cells. Experimental physiology 97:438–451.

Maricich SM, Herrup K (1999) Pax-2 expression defines a subset of GABAergic interneurons and their precursors in the developing murine cerebellum. J. Neurobiol. 41:281–294.

Marín O, Rubenstein JL (2001) A long, remarkable journey: tangential migration in the telencephalon. Nature reviews. Neuroscience 2:780–790.

Marosi K, Mattson MP (2013) BDNF Mediates Adaptive Brain and Body Responses to Energetic Challenges. Trends in endocrinology and metabolism: TEM 25:89–98.

Marsh RA, Fuzessery ZM, Grose CD, Wenstrup JJ (2002) Projection to the Inferior Colliculus from the Basal Nucleus of the Amygdala. J. Neurosci. 22:10449–10460.

Matt L, Eckert P, Panford-Walsh R, Geisler H-S, Bausch AE, Manthey M, Müller NIC, Harasztosi C, Rohbock K, Ruth P, Friauf E, Ott T, Zimmermann U, Rüttiger L, Schimmang T, Knipper M, Singer W (2018) Visualizing BDNF Transcript Usage During Sound-Induced Memory Linked Plasticity. Frontiers in molecular neuroscience 11:260.

Mazurek B, Szczepek AJ, Hebert S (2015) Stress and tinnitus. HNO 63:258–265.

McEwen BS (2007) Physiology and neurobiology of stress and adaptation: central role of the brain. Physiological reviews 87:873–904.

McGaugh JL (2002) Memory consolidation and the amygdala: a systems perspective. Trends in Neurosciences 25:456–461.

McIntyre CK, Power AE, Roozendaal B, McGaugh JL (2003) Role of the basolateral amygdala in memory consolidation. Annals of the New York Academy of Sciences 985:273–293.

McLean WJ, Smith KA, Glowatzki E, Pyott SJ (2008) Distribution of the Na,K-ATPase α Subunit in the Rat Spiral Ganglion and Organ of Corti. JARO: Journal of the Association for Research in Otolaryngology 10:37–49.

Meese S, Cepeda AP, Gahlen F, Adams CM, Ficner R, Ricci AJ, Heller S, Reisinger E, Herget M (2017) Activity-Dependent Phosphorylation by CaMKIIδ Alters the Ca2+ Affinity of the Multi-C2-Domain Protein Otoferlin. Frontiers in synaptic neuroscience 9:13.

Melcher JR, Kiang NYS (1996) Generators of the brainstem auditory evoked potential in cat III: identified cell populations. Hearing Research 93:52–71.

Meltser I, Canlon B (2011) Protecting the auditory system with glucocorticoids. Hearing Research 281:47–55.

Meng B, Zhu S, Li S, Zeng Q, Mei B (2009) Global view of the mechanisms of improved learning and memory capability in mice with music-exposure by microarray. Brain research bulletin 80:36–44.

Merzenich MM, Jenkins WM, Johnston P, Schreiner C, Miller SL, Tallal P (1996) Temporal processing deficits of language-learning impaired children ameliorated by training. Science (New York, N.Y.) 271:77–81.

Messaoudi E, Bårdsen K, Srebro B, Bramham CR (1998) Acute intrahippocampal infusion of BDNF induces lasting potentiation of synaptic transmission in the rat dentate gyrus. Journal of neurophysiology 79:496–499.

Messaoudi E, Kanhema T, Soulé J, Tiron A, Dagyte G, da Silva B, Bramham CR (2007) Sustained Arc/Arg3.1 synthesis controls long-term potentiation consolidation through regulation of local actin polymerization in the dentate gyrus in vivo. The Journal of neuroscience : the official journal of the Society for Neuroscience 27:10445–10455.

Metsis M, Timmusk T, Arenas E, Persson H (1993) Differential usage of multiple brain-derived neurotrophic factor promoters in the rat brain following neuronal activation. Proceedings of the National Academy of Sciences of the United States of America 90:8802–8806.

Minichiello L (2009) TrkB signalling pathways in LTP and learning. Nature reviews. Neuroscience 10:850–860.

Minichiello L, Calella AM, Medina DL, Bonhoeffer T, Klein R, Korte M (2002) Mechanism of TrkB-Mediated Hippocampal Long-Term Potentiation. Neuron 36:121–137.

Mohn JL, Alexander J, Pirone A, Palka CD, Lee S-Y, Mebane L, Haydon PG, Jacob MH (2014) Adenomatous polyposis coli protein deletion leads to cognitive and autism-like disabilities. Molecular psychiatry 19:1133–1142.

Moita MAP, Rosis S, Zhou Y, LeDoux JE, Blair HT (2003) Hippocampal Place Cells Acquire Location-Specific Responses to the Conditioned Stimulus during Auditory Fear Conditioning. Neuron 37:485–497.

Moore DR (2015) Sources of pathology underlying listening disorders in children. International journal of psychophysiology : official journal of the International Organization of Psychophysiology 95:125–134.

Mowla SJ, Farhadi HF, Pareek S, Atwal JK, Morris SJ, Seidah NG, Murphy RA (2001) Biosynthesis and post-translational processing of the precursor to brain-derived neurotrophic factor. The Journal of biological chemistry 276:12660–12666.

Müller M, Robertson D (1991) Relationship between tone burst discharge pattern and spontaneous firing rate of auditory nerve fibres in the guinea pig. Hearing Research 57:63–70.

Munoz-Lopez MM, Mohedano-Moriano A, Insausti R (2010) Anatomical pathways for auditory memory in primates. Frontiers in neuroanatomy 4:129.

Naber PA, Lopes da Silva FH, Witter MP (2001) Reciprocal connections between the entorhinal cortex and hippocampal fields CA1 and the subiculum are in register with the projections from CA1 to the subiculum. Hippocampus 11:99–104.

Ngodup T, Goetz JA, McGuire BC, Sun W, Lauer AM, Xu-Friedman MA (2015) Activity-dependent, homeostatic regulation of neurotransmitter release from auditory nerve fibers. Proceedings of the National Academy of Sciences of the United States of America 112:6479–6484.

Nikolaienko O, Patil S, Eriksen MS, Bramham CR (2018) Arc protein: a flexible hub for synaptic plasticity and cognition. Seminars in cell & developmental biology 77:33–42.

Nörenberg A, Hu H, Vida I, Bartos M, Jonas P (2010) Distinct nonuniform cable properties optimize rapid and efficient activation of fast-spiking GABAergic interneurons. Proceedings of the National Academy of Sciences of the United States of America 107:894–899.

Nouvian R, Beutner D, Parsons TD, Moser T (2006) Structure and function of the hair cell ribbon synapse. The Journal of membrane biology 209:153–165.

Nyhus E, Curran T (2010) Functional role of gamma and theta oscillations in episodic memory. Neuroscience and biobehavioral reviews 34:1023–1035.

Ohja K, Gozal E, Fahnestock M, Cai L, Cai J, Freedman JH, Switala A, El-Baz A, Barnes GN (2018) Neuroimmunologic and Neurotrophic Interactions in Autism Spectrum Disorders: Relationship to Neuroinflammation. Neuromolecular medicine 20:161–173.

Oitzl MS, Champagne DL, van der Veen R, Kloet ER de (2010) Brain development under stress: hypotheses of glucocorticoid actions revisited. Neuroscience and biobehavioral reviews 34:853–866.

O'Keefe J, Nadel L (1978) The hippocampus as a cognitive map. Oxford: Clarendon.

Oliveira AR de, Reimer AE, Brandão ML (2014) Mineralocorticoid receptors in the ventral tegmental area regulate dopamine efflux in the basolateral amygdala during the expression of conditioned fear. Psychoneuroendocrinology 43:114–125.

O'Mara S (2005) The subiculum: what it does, what it might do, and what neuroanatomy has yet to tell us. Journal of anatomy 207:271–282.

O'Mara SM, Sanchez-Vives MV, Brotons-Mas JR, O'Hare E (2009) Roles for the subiculum in spatial information processing, memory, motivation and the temporal control of behaviour. Progress in neuro-psychopharmacology & biological psychiatry 33:782–790.

Otte C, Moritz S, Yassouridis A, Koop M, Madrischewski AM, Wiedemann K, Kellner M (2007) Blockade of the mineralocorticoid receptor in healthy men: effects on experimentally induced panic symptoms, stress hormones, and cognition. Neuropsychopharmacology 32:232–238.

Owens DF, Kriegstein AR (2002) Is there more to GABA than synaptic inhibition? Nature reviews. Neuroscience 3:715–727.

Palmer AR, Russell IJ (1986) Phase-locking in the cochlear nerve of the guinea-pig and its relation to the receptor potential of inner hair-cells. Hearing Research 24:1–15.

Panford-Walsh R, Singer W, Rüttiger L, Hadjab S, Tan J, Geisler H-S, Zimmermann U, Köpschall I, Rohbock K, Vieljans A, Oestreicher E, Knipper M (2008) Midazolam reverses salicylate-induced changes in brain-derived neurotrophic factor and arg3.1 expression: implications for tinnitus perception and auditory plasticity. Molecular pharmacology 74:595–604.

Paré D (2003) Role of the basolateral amygdala in memory consolidation. Progress in neurobiology 70:409–420.

Park H, Poo M-m (2013) Neurotrophin regulation of neural circuit development and function. Nature reviews. Neuroscience 14:7–23.

Parkhurst CN, Yang G, Ninan I, Savas JN, Yates JR, Lafaille JJ, Hempstead BL, Littman DR, Gan W-B (2013) Microglia promote learning-dependent synapse formation through brain-derived neurotrophic factor. Cell 155:1596–1609.

Paul BT, Bruce IC, Roberts LE (2017) Evidence that hidden hearing loss underlies amplitude modulation encoding deficits in individuals with and without tinnitus. Hearing Research 344:170–182.

Pehrs C, Zaki J, Taruffi L, Kuchinke L, Koelsch S (2018) Hippocampal-Temporopolar Connectivity Contributes to Episodic Simulation During Social Cognition. Scientific reports 8:9409.

Pérez MÁ, Pérez-Valenzuela C, Rojas-Thomas F, Ahumada J, Fuenzalida M, Dagnino-Subiabre A (2013) Repeated restraint stress impairs auditory attention and GABAergic synaptic efficacy in the rat auditory cortex. Neuroscience 246:94–107.

Pérez-Valenzuela C, Terreros G, Dagnino-Subiabre A (2019) Effects of stress on the auditory system: an approach to study a common origin for mood disorders and dementia. Reviews in the neurosciences 30:317–324.

Pirone A, Alexander J, Lau LA, Hampton D, Zayachkivsky A, Yee A, Yee A, Jacob MH, Dulla CG (2017) APC conditional knock-out mouse is a model of infantile spasms with elevated neuronal β-catenin levels, neonatal spasms, and chronic seizures. Neurobiology of disease 98:149–157.

Polley DB, Steinberg EE, Merzenich MM (2006) Perceptual learning directs auditory cortical map reorganization through top-down influences. The Journal of neuroscience : the official journal of the Society for Neuroscience 26:4970–4982.

Pouille F, Marin-Burgin A, Adesnik H, Atallah BV, Scanziani M (2009) Input normalization by global feedforward inhibition expands cortical dynamic range. Nature neuroscience 12:1577–1585.

Pouille F, Scanziani M (2001) Enforcement of temporal fidelity in pyramidal cells by somatic feed-forward inhibition. Science (New York, N.Y.) 293:1159–1163.

Pruunsild P, Kazantseva A, Aid T, Palm K, Timmusk T (2007) Dissecting the human BDNF locus: bidirectional transcription, complex splicing, and multiple promoters. Genomics 90:397–406.

Purves D (2004) NEUROSCIENCE. Sunderland Mass.: Sinauer Associates Publishers.

Reciprocal connections between the entorhinal cortex and hippocampal fields CA1 and the subiculum are in register with the projections from CA1 to the subiculum.

Rhodes S, Cowan N (2018) Attention in working memory: attention is needed but it yearns to be free. Annals of the New York Academy of Sciences 1424:52–63.

Richter-Levin G, Canevari L, Bliss TVP (1995) Long-term potentiation and glutamate release in the dentate gyrus: links to spatial learning. Behavioural Brain Research 66:37–40.

Roberts AC, Tomic DL, Parkinson CH, Roeling TA, Cutter DJ, Robbins TW, Everitt BJ (2007) Forebrain connectivity of the prefrontal cortex in the marmoset monkey (Callithrix jacchus): an anterograde and retrograde tract-tracing study. J. Comp. Neurol. 502:86–112.

Romanski LM, Bates JF, Goldman-Rakic PS (1999) Auditory belt and parabelt projections to the prefrontal cortex in the Rhesus monkey. J. Comp. Neurol. 403:141–157.

Ruel J, Nouvian R, Gervais d'Aldin C, Pujol R, Eybalin M, Puel JL (2001) Dopamine inhibition of auditory nerve activity in the adult mammalian cochlea. The European journal of neuroscience 14:977–986.

Rüttiger L, Singer W, Panford-Walsh R, Matsumoto M, Lee SC, Zuccotti A, Zimmermann U, Jaumann M, Rohbock K, Xiong H, Knipper M (2013) The reduced cochlear output and the failure to adapt the central auditory response causes tinnitus in noise exposed rats. PloS one 8:e57247.

Rüttiger L, Zimmermann U, Knipper M (2017) Biomarkers for Hearing Dysfunction: Facts and Outlook. ORL; journal for oto-rhino-laryngology and its related specialties 79:93–111.

Safieddine S, El-Amraoui A, Petit C (2012) The auditory hair cell ribbon synapse: from assembly to function. Annual review of neuroscience 35:509–528.

Saghazadeh A, Mahmoudi M, Dehghani Ashkezari A, Oliaie Rezaie N, Rezaei N (2017) Systematic review and meta-analysis shows a specific micronutrient profile in people with Down Syndrome: Lower blood calcium, selenium and zinc, higher red blood cell copper and zinc, and higher salivary calcium and sodium. PloS one 12:e0175437.

Sakata K, Jin L, Jha S (2010) Lack of promoter IV-driven BDNF transcription results in depression-like behavior. Genes, brain, and behavior 9:712–721.

Sakurai Y (1990) Hippocampal cells have behavioral correlates during the performance of an auditory working memory task in the rat. Behavioral Neuroscience 104:253–263.

Sandi C, Haller J (2015) Stress and the social brain: behavioural effects and neurobiological mechanisms. Nature reviews. Neuroscience 16:290–304.

Sathanoori M, Dias BG, Nair AR, Banerjee SB, Tole S, Vaidya VA (2004) Differential regulation of multiple brain-derived neurotrophic factor transcripts in the postnatal and adult rat hippocampus during development, and in response to kainate administration. Brain research. Molecular brain research 130:170–177.

Schmeisser MJ et al. (2012) Autistic-like behaviours and hyperactivity in mice lacking ProSAP1/Shank2. Nature 486:256–260.

Schmitt C, Patak M, Kröner-Herwig B (2000) Stress and the onset of sudden hearing loss and tinnitus. The international tinnitus journal 6:41–49.

Shepherd JD, Bear MF (2011) New views of Arc, a master regulator of synaptic plasticity. Nature neuroscience 14:279–284.

Shera CA, Guinan JJ (1999) Evoked otoacoustic emissions arise by two fundamentally different mechanisms: a taxonomy for mammalian OAEs. The Journal of the Acoustical Society of America 105:782–798.

Shibata S, Kakazu Y, Okabe A, Fukuda A, Nabekura J (2004) Experience-dependent changes in intracellular Cl- regulation in developing auditory neurons. Neuroscience research 48:211–220.

Shim HJ, Lee ES, An YH, Kim DH (2017) Comparison of Long-Term Outcome of Intratympanic Dexamethasone Therapy between Acute Noise-Induced Tinnitus and Acute Idiopathic Tinnitus. The journal of international advanced otology 13:53–60.

Singer W et al. (2018) BDNF-Live-Exon-Visualization (BLEV) Allows Differential Detection of BDNF Transcripts in vitro and in vivo. Frontiers in molecular neuroscience 11:325.

Singer W, Geisler H-S, Panford-Walsh R, Knipper M (2016) Detection of Excitatory and Inhibitory Synapses in the Auditory System Using Fluorescence Immunohistochemistry and High-Resolution Fluorescence Microscopy. Methods in molecular biology (Clifton, N.J.) 1427:263–276.

Singer W, Panford-Walsh R, Knipper M (2014) The function of BDNF in the adult auditory system. Neuropharmacology 76 Pt C:719–728.

Singer W, Panford-Walsh R, Watermann D, Hendrich O, Zimmermann U, Köpschall I, Rohbock K, Knipper M (2008) Salicylate alters the expression of calcium response transcription factor 1 in the cochlea: implications for brain-derived neurotrophic factor transcriptional regulation. Molecular pharmacology 73:1085–1091.

Singer W, Zuccotti A, Jaumann M, Lee SC, Panford-Walsh R, Xiong H, Zimmermann U, Franz C, Geisler H-S, Köpschall I, Rohbock K, Varakina K, Verpoorten S, Reinbothe T, Schimmang T, Rüttiger L, Knipper M (2013) Noise-induced inner hair cell ribbon loss disturbs central arc mobilization: a novel molecular paradigm for understanding tinnitus. Molecular neurobiology 47:261–279.

Soriano E, Frotscher M (1993) GABAergic innervation of the rat fascia dentata: a novel type of interneuron in the granule cell layer with extensive axonal arborization in the molecular layer. J. Comp. Neurol. 334:385–396.

Soulé J, Messaoudi E, Bramham CR (2006) Brain-derived neurotrophic factor and control of synaptic consolidation in the adult brain. Biochemical Society transactions 34:600–604.

Spoendlin H, Schrott A (1989) Analysis of the human auditory nerve. Hearing Research 43:25–38.

Steward O, Scoville SA (1976) Cells of origin of entorhinal cortical afferents to the hippocampus and fascia dentata of the rat. The Journal of comparative neurology 169:347–370.

Tahera Y, Meltser I, Johansson P, Hansson AC, Canlon B (2006) Glucocorticoid receptor and nuclear factor-kappa B interactions in restraint stress-mediated protection against acoustic trauma. Endocrinology 147:4430–4437.

Tahera Y, Meltser I, Johansson P, Salman H, Canlon B (2007) Sound conditioning protects hearing by activating the hypothalamic-pituitary-adrenal axis. Neurobiology of disease 25:189–197.

Takesian AE, Bogart LJ, Lichtman JW, Hensch TK (2018) Inhibitory circuit gating of auditory critical-period plasticity. Nature neuroscience 21:218–227.

Tambs K, Hoffman HJ, Borchgrevink HM, Holmen J, Engdahl B (2006) Hearing loss induced by occupational and impulse noise: results on threshold shifts by frequencies, age and gender from the Nord-Trøndelag Hearing Loss Study. International journal of audiology 45:309–317.

Tanaka H, Grooms SY, Bennett MVL, Zukin RS (2000) The AMPAR subunit GluR2: still front and center-stage11Published on the World Wide Web on 30 October 2000. Brain Research 886:190–207.

Tao X, Finkbeiner S, Arnold DB, Shaywitz AJ, Greenberg ME (1998) Ca2+ Influx Regulates BDNF Transcription by a CREB Family Transcription Factor-Dependent Mechanism. Neuron 20:709–726.

Tao X, West AE, Chen WG, Corfas G, Greenberg ME (2002) A Calcium-Responsive Transcription Factor, CaRF, that Regulates Neuronal Activity-Dependent Expression of BDNF. Neuron 33:383–395.

Terakado M, Kumagami H, Takahashi H (2011) Distribution of glucocorticoid receptors and 11 beta-hydroxysteroid dehydrogenase isoforms in the rat inner ear. Hearing Research 280:148–156.

Terreros G, Delano PH (2015) Corticofugal modulation of peripheral auditory responses. Frontiers in systems neuroscience 9:134.

Thivard L, Belin P, Zilbovicius M, Poline JB, Samson Y (2000) A cortical region sensitive to auditory spectral motion. Neuroreport 11:2969–2972.

Timmusk T, Palm K, Metsis M, Reintam T, Paalme V, Saarma M, Persson H (1993) Multiple promoters direct tissue-specific expression of the rat BDNF gene. Neuron 10:475–489.

Traub RD, Whittington MA (2010) Cortical oscillations in health and disease. Oxford: Oxford University Press.

Tronche F, Kellendonk C, Kretz O, Gass P, Anlag K, Orban PC, Bock R, Klein R, Schütz G (1999) Disruption of the glucocorticoid receptor gene in the nervous system results in reduced anxiety. Nature genetics 23:99–103.

Trune DR, Canlon B (2012) Corticosteroid therapy for hearing and balance disorders. Anatomical record (Hoboken, N.J. : 2007) 295:1928–1943.

Tukker JJ, Lasztóczi B, Katona L, Roberts JDB, Pissadaki EK, Dalezios Y, Márton L, Zhang L, Klausberger T, Somogyi P (2013) Distinct dendritic arborization and in vivo firing patterns of parvalbumin-expressing basket cells in the hippocampal area CA3. The Journal of neuroscience : the official journal of the Society for Neuroscience 33:6809–6825.

Turrigiano G (2012) Homeostatic synaptic plasticity: local and global mechanisms for stabilizing neuronal function. Cold Spring Harbor perspectives in biology 4:a005736.

Tuvikene J, Pruunsild P, Orav E, Esvald E-E, Timmusk T (2016) AP-1 Transcription Factors Mediate BDNF-Positive Feedback Loop in Cortical Neurons. J. Neurosci. 36:1290–1305.

Vale C, Sanes DH (2002) The effect of bilateral deafness on excitatory and inhibitory synaptic strength in the inferior colliculus. The European journal of neuroscience 16:2394–2404.

van Lu B, Colmers WF, Smith PA (2012) Long-term actions of BDNF on inhibitory synaptic transmission in identified neurons of the rat substantia gelatinosa. Journal of neurophysiology 108:441–452.

Villers-Sidani E de, Chang EF, Bao S, Merzenich MM (2007) Critical period window for spectral tuning defined in the primary auditory cortex (A1) in the rat. J. Neurosci. 27:180–189.

Vinnik E, Antopolskiy S, Itskov PM, Diamond ME (2012) Auditory stimuli elicit hippocampal neuronal responses during sleep. Frontiers in systems neuroscience 6:49.

Vinogradova OS (1976) Functional Organization of the Limbic System in the Process of Registration of Information: Facts and Hypotheses. In: The Hippocampus (Isaacson RL, Pribram KH, eds), pp 3–69. Boston, MA: Springer US.

Vogel S, Fernández G, Joëls M, Schwabe L (2016) Cognitive Adaptation under Stress: A Case for the Mineralocorticoid Receptor. Trends in cognitive sciences 20:192–203.

Wang Y, Liberman MC (2002) Restraint stress and protection from acoustic injury in mice. Hearing Research 165:96–102.

Waterhouse EG, An JJ, Orefice LL, Baydyuk M, Liao G-Y, Zheng K, Lu B, Xu B (2012) BDNF promotes differentiation and maturation of adult-born neurons through GABAergic transmission. The Journal of neuroscience : the official journal of the Society for Neuroscience 32:14318–14330.

Weinberger NM, Miasnikov AA, Bieszczad KM, Chen JC (2013) GAMMA BAND PLASTICITY IN SENSORY CORTEX IS A SIGNATURE OF THE STRONGEST MEMORY RATHER THAN MEMORY OF THE TRAINING STIMULUS. Neurobiology of learning and memory 104:49–63.

Wenhart T, Bethlehem RAI, Baron-Cohen S, Altenmüller E (2019) Autistic traits, resting-state connectivity, and absolute pitch in professional musicians: shared and distinct neural features. Molecular autism 10:20.

West AE, Pruunsild P, Timmusk T (2014) Neurotrophins: transcription and translation. Handbook of experimental pharmacology 220:67–100.

Willadt S, Nenniger M, Vogt KE (2013) Hippocampal feedforward inhibition focuses excitatory synaptic signals into distinct dendritic compartments. PloS one 8:e80984.

Witter M (2012) Hippocampus. In: The Mouse Nervous System, pp 112–139: Elsevier.

Wu JS, Yi E, Manca M, Javaid H, Lauer AM, Glowatzki E (2020) Sound exposure dynamically induces dopamine synthesis in cholinergic LOC efferents for feedback to auditory nerve fibers. eLife 9.

Xiao C, Liu Y, Xu J, Gan X, Xiao Z (2018) Septal and Hippocampal Neurons Contribute to Auditory Relay and Fear Conditioning. Frontiers in cellular neuroscience 12:102.

Xu H, Kotak VC, Sanes DH (2010) Normal hearing is required for the emergence of long-lasting inhibitory potentiation in cortex. The Journal of neuroscience : the official journal of the Society for Neuroscience 30:331–341.

Xu J, Yu L, Cai R, Zhang J, Sun X (2009) Early auditory enrichment with music enhances auditory discrimination learning and alters NR2B protein expression in rat auditory cortex. Behavioural Brain Research 196:49–54.

Yamada K, Nabeshima T (2003) Brain-derived neurotrophic factor/TrkB signaling in memory processes. Journal of pharmacological sciences 91:267–270.

Yang J, Harte-Hargrove LC, Siao C-J, Marinic T, Clarke R, Ma Q, Jing D, Lafrancois JJ, Bath KG, Mark W, Ballon D, Lee FS, Scharfman HE, Hempstead BL (2014) proBDNF negatively regulates neuronal remodeling, synaptic transmission, and synaptic plasticity in hippocampus. Cell reports 7:796–806.

Yang J, Siao C-J, Nagappan G, Marinic T, Jing D, McGrath K, Chen Z-Y, Mark W, Tessarollo L, Lee FS, Lu B, Hempstead BL (2009) Neuronal release of proBDNF. Nature neuroscience 12:113–115.

Yao X, Rarey KE (1996) Localization of the mineralocorticoid receptor in rat cochlear tissue. Acta oto-laryngologica 116:493–496.

Yoshida N, Kristiansen A, Liberman MC (1999) Heat Stress and Protection from Permanent Acoustic Injury in Mice. J. Neurosci. 19:10116–10124.

Yoshida N, Liberman MC (2000) Sound conditioning reduces noise-induced permanent threshold shift in mice. Hearing Research 148:213–219.

Yoshinaga-Itano C (2003) Early intervention after universal neonatal hearing screening: impact on outcomes. Mental retardation and developmental disabilities research reviews 9:252–266.

Zhang H, Lin S-C, Nicolelis MAL (2011) A distinctive subpopulation of medial septal slow-firing neurons promote hippocampal activation and theta oscillations. Journal of neurophysiology 106:2749–2763.

Zhou J, Nannapaneni N, Shore S (2007) Vessicular glutamate transporters 1 and 2 are differentially associated with auditory nerve and spinal trigeminal inputs to the cochlear nucleus. J. Comp. Neurol. 500:777–787.

Zuccotti A, Kuhn S, Johnson SL, Franz C, Singer W, Hecker D, Geisler H-S, Köpschall I, Rohbock K, Gutsche K, Dlugaiczyk J, Schick B, Marcotti W, Rüttiger L, Schimmang T, Knipper M (2012) Lack of brain-derived neurotrophic factor hampers inner hair cell synapse physiology, but protects against noise-induced hearing loss. J. Neurosci. 32:8545–8553.

7. Appendix

7.1

Singer W*, Kasini K*, Manthey M*, **Eckert P***, Armbruster P*, Vogt MA, Jaumann M, Dotta M, Yamahara K, Harasztosi C, Zimmermann U, Knipper M, Rüttiger L. **"*The glucocorticoid antagonist mifepristone attenuates sound-induced long-term deficits in auditory nerve response and central auditory processing in female rats*"**, FASEB J. 2018

7.2

Eckert P*, Marchetta P*, Manthey M*, Walter MH, Singer W, Jacob M, Rüttiger L, Schimmang T, Pilz PK, Knipper M. **"*Brain-derived neurotrophic factor in inhibitory hindbrain neurons controls central learning mechanisms*",**
in preparation

7.3

Singer W*, Manthey M*, Panford-Walsh R, Matt L, Geisler HS, Passeri E, Baj G, Tongiorgi E, Leal G, Duarte CB, Salazar IL, **Eckert P**, Rohbock K, Hu J, Strotmann J, Ruth P, Zimmermann U, Rüttiger L, Ott T, Schimmang T, Knipper M. **"*BDNF-Live-Exon-Visualization (BLEV) allows differential detection of BDNF transcripts in vitro and in vivo*",** Front Mol Neurosci. 2018

7.4

Matt L*, **Eckert P***, Panford-Walsh R, Geisler HS, Bausch AE, Manthey M, Müller NIC, Harasztosi C, Rohbock K, Ruth P, Friauf E, Ott T, Zimmermann U, Rüttiger L, Schimmang T, Knipper M, Singer W. **"*Visualizing BDNF transcript usage during sound-Induced memory linked plasticity*"**, Front Mol Neurosci. 2018

*equal contribution

THE FASEB JOURNAL • RESEARCH • www.fasebj.org

The glucocorticoid antagonist mifepristone attenuates sound-induced long-term deficits in auditory nerve response and central auditory processing in female rats

Wibke Singer,[*,1] Kamyar Kasini,[*,1] Marie Manthey,[*,1] Philipp Eckert,[*,1] Philipp Armbruster,[*,1] Miriam Annika Vogt,[*] Mirko Jaumann,[*] Michela Dotta,[*] Kohei Yamahara,[*,†] Csaba Harasztosi,[‡] Ulrike Zimmermann,[*] Marlies Knipper,[*,2] and Lukas Rüttiger[*]

[*]Molecular Physiology of Hearing and [‡]Section of Physiological Acoustics and Communication, Department of Otolaryngology, Tübingen Hearing Research Centre, University of Tübingen, Tübingen, Germany; and [†]Department of Otolaryngology, Head and Neck Surgery, Graduate School of Medicine, Kyoto University, Kyoto, Japan

ABSTRACT: Systemic corticosteroids have been the mainstay of treatment for various hearing disorders for more than 30 yr. Accordingly, numerous studies have described glucocorticoids (GCs) and stressors to be protective in the auditory organ against damage associated with a variety of health conditions, including noise exposure. Conversely, stressors are also predictive risk factors for hearing disorders. How both of these contrasting stress actions are linked has remained elusive. Here, we demonstrate that higher corticosterone levels during acoustic trauma in female rats is highly correlated with a decline of auditory fiber responses in high-frequency cochlear regions, and that hearing thresholds and the outer hair cell functions (distortion products of otoacoustic emissions) are left unaffected. Moreover, when GC receptor (GR) or mineralocorticoid receptor (MR) activation was antagonized by mifepristone or spironolactone, respectively, GR, but not MR, inhibition significantly and permanently attenuated trauma-induced effects on auditory fiber responses, including inner hair cell ribbon loss and related reductions of early and late auditory brainstem responses. These findings strongly imply that higher corticosterone stress levels profoundly impair auditory nerve processing, which may influence central auditory acuity. These changes are likely GR mediated as they are prevented by mifepristone.—Singer, W., Kasini, K., Manthey, M., Eckert, P., Armbruster, P., Vogt, M. A., Jaumann, M., Dotta, M., Yamahara, K., Harasztosi, C., Zimmermann, U., Knipper, M., Rüttiger, L. The glucocorticoid antagonist mifepristone attenuates sound-induced long-term deficits in auditory nerve response and central auditory processing in female rats. FASEB J. 32, 000–000 (2018). www.fasebj.org

KEY WORDS: glucocorticoid receptors · mineralocorticoid receptors · hidden hearing loss · synaptic ribbon · auditory trauma

Subsequent to the activation of the hypothalamic-pituitary-adrenal axis, glucocorticoids (GCs) are secreted from the adrenal glands in hourly pulses as well as after physically or mentally demanding, stirring, or even frightening experiences, with the goal of maintaining resilience and health. GCs act as stress hormones and display an impressive diversity of actions. At physiologic concentrations, they activate 2 types of steroid receptors, mineralocorticoid receptors (MRs) and GC receptors (GRs) (1–3). GCs belong to the most widely used and effective therapies for many chronic inflammatory diseases (4) and are increasingly used to treat various hearing disorders, such as sudden hearing loss and cochlear fibrosis, or for hearing preservation during cochlear implantation (3, 5–9). In the auditory system, different treatments with stressors, such as heat shock (10), moderate-level long-term sound exposure (11), or restraint stress (12, 13), exhibit protective effects against trauma-induced inner ear function. Because GRs and MRs are not only expressed in the central auditory system (14) but also in the peripheral cochlea (15–18), the protective stressor effect is discussed as a direct effect of GCs on the cochlea compartments in addition to its anti-inflammatory action (12, 13); however, stressors are also known to negatively influence auditory functions, as demonstrated by the chronic post-traumatic stress–induced reduction of tone perception acuity (19), the repeated restraint

ABBREVIATIONS: ABR, auditory brainstem response; AT, acoustic trauma; c/c, corticosterone/creatinine; DPOAE, distortion product of otoacoustic emissions; GC, glucocorticoid; GR, glucocorticoid receptor; IHC, inner hair cell; MR, mineralocorticoid receptor; NKAα3, Na,K-ATPase subunit α3; OHC, outer hair cell; SPL, sound pressure level; SR, spontaneous rate

[1] These authors contributed equally to this work.

[2] Correspondence: Tübingen Hearing Research Centre, Department der Otolaryngologie, Universität Tübingen, Elfriede-Aulhorn-Straße 5, 72076 Tübingen, Germany. E-mail: marlies.knipper@uni-tuebingen.de

doi: 10.1096/fj.201701041RRR
This article includes supplemental data. Please visit *http://www.fasebj.org* to obtain this information.

stress–induced reduction in cortical synaptic plasticity responses (20), or the chronic stress–related dendritic structure abnormality in the auditory nuclei (21). How these contrasting activities of stressors in auditory processes are linked remains elusive. Previous preliminary studies have revealed divergent protective and harmful effects on auditory function that are dependent on the corticosterone level at the time of the auditory damage (22). Here, we hypothesized that there is an influence of corticosterone level variations on auditory functions, and we investigated this aspect in female Wistar rats. We used 1) distortion products of otoacoustic emissions (DPOAEs), as outer hair cell (OHC) function contributes to the thresholds for sound-evoked neural potentials and because DPOAEs are objective indicators of OHC electromotility (23); 2) the number of CtBP2/RIBEYE$^+$ ribbon synapses of the inner hair cell (IHC) as a measure for the number of auditory nerve fiber contacts and to indicate the degree of altered cochlear input (24); 3) auditory brainstem response (ABR) thresholds and the amplitudes of the first ABR wave, which reflects the summed activity of the auditory nerve (25) or amplitude of the ABR wave IV, generated in the lateral lemniscus and inferior colliculus (26); and 4) mifepristone and spironolactone treatments to antagonize GRs and MRs, respectively, on noise-induced hearing loss (27–29).

Our findings suggest a long-lasting destructive influence of elevated GR-mediated corticosterone action on acoustic trauma–induced IHC synapse integrity and auditory nerve response in high-frequency regions. This striking finding expands the current view of GCs as protectors of cochlear OHC function and suggests that corticosterone levels act in a contrasting manner to the acute protective activities of stressors. Corticosterone levels might exhibit the potential to severely compromise sound responses at the level of the first IHC synapse, with significant impairment of central auditory processing.

MATERIALS AND METHODS

Animals

In this study, we used 3- to 5-mo-old female Wistar rats, purchased from Charles River Laboratories (Research Models and Services Germany, Sulzfeld, Germany). Rats were housed for the time of the experiments in the animal care facility of the institute under a 12-h light/dark cycle, where noise levels did not exceed a 50- to 60-dB sound pressure level (SPL). Food and water were given *ad libitum*. Care and use of rats and the experimental protocol were reviewed and approved by the University of Tübingen, Veterinary Care Unit, and the Animal Care and Ethics Committee of the regional board of the Federal State Government of Baden-Württemberg, Germany, and followed the guidelines of the European Union Directive 2010/63/EU for animal experiments.

Drug application

For ABR recordings and noise exposure, we anesthetized animals with an intraperitoneal injection of a mixture of ketamine-hydrochloride (75 mg/kg body weight; Ketavet; Pharmacia, Erlangen, Germany) and xylazine hydrochloride (5 mg/kg body weight; Rompun; Bayer, Leverkusen, Germany). Additional doses of anesthetics were administered as needed.

Mifepristone (also known as RU-486, a GR antagonist; Sigma-Aldrich, St. Louis, MO, USA) and spironolactone (an MR antagonist; Sigma-Aldrich), solved in polyethylene glycol (Sigma-Aldrich) and ethanol (1:10 dilution), were used at concentrations of 100 and 75 mg/kg bodyweight, respectively, as previously described (30). Rats received a single injection of either vehicle (polyethylene glycol and ethanol; 1:10, 2 ml/kg, i.p.), spironolactone, or mifepristone 90 min before sham or noise exposure (30).

Noise exposure

Adult female Wistar rats weighing 200–300 g were binaurally exposed in anesthesia to a sinusoidal-free field tone in a reverberating chamber (10 kHz, 116 dB SPL root mean square for 1 or 2 h), or sham exposed with loud speaker switched off and sacrificed 15 d after exposure (Supplemental Fig. 1). Urine was collected during the time period (1–2 h) of sound or sham exposure while rats were in anesthesia—for details, see previous works (22, 31, 32).

ABRs

ABRs, evoked by short-duration sound stimuli, represent the summed activity of neurons in distinct anatomic structures or nuclei along the ascending auditory pathway (33), and are measured by averaging the evoked electrical response recorded *via* s.c. electrodes. In brief, ABRs were evoked by click (100 μs), noise burst (1-ms random phase), or pure tone stimuli (3-ms duration, 1-ms rise/fall times, 4- to 32-kHz frequencies) of gradually increasing sound pressure in 5-dB steps. The response threshold was determined at each frequency as the minimal sound pressure that evoked a noticeable potential peak in the expected time window of the recorded signal. For details, see a previous work (32).

DPOAEs

We assessed OHC function by using the growth function and the maximum response in the distortion product audiogram of the cubic DPOAE as previously described (34). Frequency pairs of tones were between $f2 = 4$ kHz and 32 kHz.

ABR waveform analysis

ABR waveforms were analyzed for consecutive amplitude deflections (waves), with each wave consisting of a starting negative (n) peak and the following positive (p) peak. Peak amplitudes of ABR waves I and IV were extracted in the present study and defined as follows: wave I: $I_n - I_p$ (0.9–2 ms); and wave IV: $IV_n - IV_p$ (3.4–5.9 ms). A customized program was used to extract ABR peaks on the basis of these definitions. ABR peak-to-peak (wave amplitude) growth functions were constructed for individual ears on the basis of the extracted peaks. ABR wave amplitude growth functions were calculated for increasing stimulus levels with reference to the ABR thresholds (from −20 to a maximum of 85 dB above the threshold before noise exposure, and from −20 to a maximum of 55 dB above threshold after noise exposure). ABR waveforms, shown in Fig. 1*C*, were smoothed by a moving 0-phase gaussian filter with a window length of 5 data points (0.5 ms).

Corticosterone analysis

Urine was collected during the noise exposure (Supplemental Fig. 1) and analyzed by using Idexx (Vet Med Labor,

Ludwigsburg, Germany) as previously described (22). In brief, we used the chemiluminescence immunoassay, IMMULITE 2000 Cortisol (Siemens Healthcare Diagnostics, Tarrytown, NY, USA). Data are provided for cortisol in micrograms per liter and for creatinine in milligrams per deciliter. Their ratio is calculated from SI units (cortisol: nM/L; creatinine: μN/L). Raw cortisol data are multiplied by a factor of 2.76 and for creatinine by a factor of 88.4 (data provided in Supplemental Table 1). According to the manufacturer in this immunoassay, there exists a cross-reactivity with corticosterone, the primary glucocorticoid in rats, of 1.2%. In this study, we used the cortisol/creatinine ratio to determine the corticosterone levels in female Wistar rats. To rule out major influences resulting from the circadian rhythm, all experiments were conducted in the morning (8–12 AM), and experimental groups were distributed equally in terms of the daytime of the trauma induction.

Tissue preparation

Animals were deeply anesthetized in CO_2. After decapitation, cochleae were isolated from the bulla, fixed in 2% paraformaldehyde, decalcified using rapid decalcifier (RDO; Apex Engineering Product Corp., Aurora, IL, USA), embedded in Tissue Tek (optimum cutting temperature compound; Thermo Fisher Scientific, Waltham, MA, USA), and stored at −80°C. Cochleae are cut in 10-μm sections using a Cryostat (Leica Cryostat 1720 Digital Leica; Leica, Wetzlar, Germany) and transferred to microscope slides (Superfrost Plus; Thermo Fisher Scientific, Waltham, MA, USA). Store slides at −20°C until use. For additional details, see a previous work (35).

Immunohistochemistry and ribbon counting

Cochleae were stained using primary Abs against CtBP2/RIBEYE (Cell Applications, San Diego, CA, USA) and Na,K-ATPase subunit α3 (NKAα3) (36). Image acquisition and CtBP2/RIBEYE-immunopositive spot counting were carried out as previously described (35). In brief, sections were viewed by using an Olympus BX61 microscope equipped with an X-Cite Lamp (Olympus, Tokyo, Japan). Cryosectioned cochleae were imaged over a distance of 8 μm, covering the entire IHC nucleus and areas beyond it in an image stack along the *z* axis (*z* stack). One z-stack consisted of 30 layers with az-increment of 0.28 μm. For each layer, 1 image per fluorochrome was acquired. To display spatial protein distribution, *z* stacks were 3-dimensionally deconvoluted. Images were acquired by using an Olympus XM10 CCD monochrome camera and analyzed with cellSens Dimension software (OSIS; Olympus, Hamburg, Germany).

Statistical analyses

For correlations, the Pearson product-moment correlation coefficient (R^2), Student's *t* tests, and slope comparison were calculated. Statistical data are indicated in the figures.

For the frequency-dependent ABR and DPOAE data and the waveform analysis, we used 2-way ANOVA and *post hoc* Holm-Sidak's multiple comparison test (Prism; GraphPad Software, La Jolla, CA, USA). For the click, noise, and frequency-dependent ABR and DPOAE max threshold analysis and growth function analysis of ABR waves I and IV amplitude, we used 1-way ANOVA and *post hoc* Holm-Sidak's multiple comparison test and 2-sided Student's *t* test with Holm-Sidak's *post hoc* test. Counts for CtBP2 immunopositive ribbons were compared by using 1-way ANOVA with Holm-Sidak's multiple comparison test. Detailed information about the statistical analyses is given in **Table 1**.

RESULTS

Elevated corticosterone levels diminish high-frequency suprathreshold auditory nerve response pre– and postaccoustic trauma independent of hearing thresholds

To investigate the role of elevated corticosterone levels on cochlear function, we first examined the influence of corticosterone variations of GC levels on hearing. The urinary corticosterone/creatinine ratio (c/c) in the analyzed animal groups of female Wistar rats (3–5 mo old) varied between 0.3 and 19.6, with an average of 6.69 ± 1.74 (Supplemental Fig. 2 and Supplemental Table 1). The hearing function was measured *via* click, noise, and frequency specific tone–induced ABR, which represented the summed, synchronous activity of neurons in the ascending auditory pathway. The individual hearing thresholds of 13 rats are shown (gray lines) as well as their averages (**Fig. 1*A***, black line). None of the tested sound frequencies revealed that ABR thresholds correlated with different corticosterone levels. A representative data set for high-frequency stimuli (at 32 kHz) is shown in Fig. 1*B*. This indicated that the basic OHC function that defines ABR thresholds (37, 38) does not differ significantly according to different corticosterone levels; however, the growth of the summed auditory nerve responses (ABR wave I amplitude) across increasing sound intensities (Fig. 1*C*) revealed that auditory nerve responses to stimuli ≥16 kHz were decreased with higher stress hormone levels compared with lower stress hormone levels (Fig. 1*D*). Thus, the ABR wave I amplitudes generated upon a 16-kHz stimulus of animals with lower corticosterone levels (Fig. 1*D*, blue line) grew significantly steeper than the amplitudes of those animals with higher corticosterone levels (Fig. 1*D*, red line).

A sensitivity of auditory nerve responses to higher corticosterone levels was confirmed when suprathreshold ABR wave I amplitudes with stimuli at 16 kHz and 65 dB SPL were plotted against corticosterone levels (**Fig. 2*A***). ABR wave I amplitudes were significantly lower with higher corticosterone concentrations (Fig. 2*A*). Ribbons of IHCs contribute as active IHC release sites to the precision of the discharge rate of auditory fibers (39) and, thus, to the ABR response amplitude size (25). Likewise, ABR wave I amplitudes also IHC ribbon number was declined in the basal cochlear turns when corticosterone levels are elevated (Fig. 2*B*). This correlation was only found for IHC ribbon number in the basal cochlear region, and was not significant for the midbasal, medial, and apical cochlear turns (data not shown). It is important to note that suprathreshold ABR wave I amplitude to high-frequency stimuli (16 kHz at 65 dB SPL), when plotted against IHC ribbons in the basal cochlear turn, were observed to decline in correlation with lesser ribbons in basal cochlear turns (Fig. 2*C*), which emphasized a reasonable correlation of ribbon number and auditory nerve response. In addition, an influence of the animals' stress hormone levels on IHC synapse integrity was observed at the morphologic level, when animals

TABLE 1. *Statistical analysis*

Figure	Parameter	Rats/ears (*n*)	*P*	Statistics
Figure 1*D*	Wave I amplitude	Low stress: 7/14 High stress: 4/8	<0.0001	2-way ANOVA followed by *post hoc* test Holm-Sidak's multiple comparison test
Figure 3*A*	f-ABR	8/8	<0.0001	2-way ANOVA followed by *post hoc* Holm-Sidak's multiple comparison test
Figure 4*A*	Click stimulus	Pre: 8/16 14 d: 4/8	Pre: 0.102 14 d: 0.947	1-way ANOVA followed by *post hoc*
Figure 4*B*	Noise-burst stimulus	Pre: 8/16 14 d: 4/8	Pre: 0.011 14 d: 0.189	Holm-Sidak's multiple comparison test
Figure 4*C*	DPOAE max	Pre: 8/16 14 d: 4/8	Pre: 0.463 14 d: 0.735	
Figure 5*A*	Click stimulus	3–4/6–8	0.41	1-way ANOVA followed by
Figure 5*B*	Noise-burst stimulus	3–4/6–8	0.126	*post hoc* test Holm-Sidak's multiple comparison test
Figure 5*C*	Tone burst	3–4/4	0.09	2-way ANOVA followed by *post hoc* test Holm-Sidak's multiple comparison test
Figure 5*D*	DPOAE max	3–4/6–8	0.454	1-way ANOVA followed by *post hoc* test Holm-Sidak's multiple comparison test
Figure 5*E*	DPOAE threshold: vehicle-AT 14 d *vs.* Mif-AT 14 d *vs.* Spir-AT 14 d	3–4/6–8	0.0009	2-way ANOVA followed by *post hoc* test Holm-Sidak's multiple comparison test
Figure 5*F*	4-kHz tone burst			
	Vehicle-sham 14 d *vs.* Vehicle-AT 14 d	3–4/6–8	0.457; $t = 0.761$	Unpaired 2-sided Student's
	Mif-sham 14 d *vs.* Mif-AT 14 d	3–4/6–8	0.998; $t = 1.741$	*t* test
	Spir-sham 14 d *vs.* Spir-AT 14 d	4/8	0.830; $t = 0.218$	
	Vehicle-AT 14 d *vs.* Mif-AT 14 d *vs.* Spir-AT 14 d	4/8	0.307	1-way ANOVA followed by *post hoc* test Holm-Sidak's multiple comparison test
Figure 5*G*	16-kHz tone burst			
	Vehicle-sham 14 d *vs.* Vehicle-AT 14 d	3–4/6–8	0.018; $t = 2.617$	Unpaired 2-sided Student's
	Mif-sham 14d *vs.* Mif-AT 14 d	3–4/6–8	0.217; $t = 1.281$	*t* test
	Spir-sham 14 d *vs.* Spir-AT 14 d	4/8	0.073; $t = 1.909$	
	Vehicle-AT 14 d *vs.* Mif-AT 14 d *vs.* Spir-AT 14 d	4/8	0.587	1-way ANOVA followed by *post hoc* test Holm-Sidak's multiple comparison test
Figure 5*H*	32-kHz tone burst			
	Vehicle-sham 14 d *vs.* Vehicle-AT 14 d	3–4/6–8	0.004; $t = 3.342$	Unpaired 2-sided Student
	Mif-sham 14 d *vs.* Mif-AT 14 d	3–4/6–8	0.031; $t = 2.36$	*t* test
	Spir-sham 14 d *vs.* Spir-AT 14 d	4/8	0.018; $t = 2.622$	
	Vehicle-AT 14 d *vs.* Mif-AT 14 d *vs.* Spir-AT 14 d	4/8	0.799	1-way ANOVA followed by *post hoc* test Holm-Sidak's multiple comparison test
Figure 7*B*	11-kHz tone burst			
	Wave I reach	3–4		1-way ANOVA followed by
	AT effect		0.046	*post hoc* test
	Pharm effect		0.244	Holm-Sidak's multiple comparison test
	Wave I size			
	AT effect		0.021	
	Pharm effect		0.203	

(*continued on next page*)

TABLE 1. (*continued*)

Figure	Parameter	Rats/ears (*n*)	*P*	Statistics
	Wave IV reach	4		
	AT effect		0.099	
	Pharm effect		0.330	
	Wave IV size			
	AT effect		0.147	
	Pharm effect		0.264	
Figure 7*C*	16-kHz tone burst			
	Wave I reach	1–4		1-way ANOVA followed by
	AT effect		ND	*post hoc* test
	Pharm effect		0.135	Holm-Sidak's multiple
	Wave I size			comparison test
	AT effect		ND	
	Pharm effect		0.071	
	Wave IV reach	3–4		
	AT effect		0.032	
	Pharm effect		0.097	
	Wave IV size			
	AT effect		0.005	
	Pharm effect		0.015	
Figure 7*D*	32-kHz tone burst			
	Wave I reach	3–4		1-way ANOVA followed by
	AT effect		0.001	*post hoc* test
	Pharm effect		0.033	Holm-Sidak's multiple
	Wave I size			comparison test
	AT effect		0.0006	
	Pharm effect		0.041	
	Wave IV reach			
	AT effect	2–4	<0.001	
	Pharm effect		0.057	
	Wave IV size			
	AT effect		<0.001	
	Pharm effect		0.052	
Figure 8	IHC ribbon number			
	Apical	3–4	0.626	1-way ANOVA followed by
	Medial		0.021	*post hoc* test
	Midbasal		0.001	Holm-Sidak's multiple
	Basal		0.004	comparison test
Supplemental Fig. 3A	Noise-burst stimulus	Pre: 9/18 Vehicle-AT: 6/12 Mif-AT: 3/6	<0.0001	1-way ANOVA followed by *post hoc* test Holm-Sidak's multiple comparison test
Supplemental Fig. 3B	Wave I amplitude		<0.0001	2-way ANOVA followed by *post hoc* test Holm-Sidak's multiple comparison test
Supplemental Fig. 3C	Noise-burst stimulus	Pre: 6/12 Vehicle-AT: 3/6 Mif-AT: 3/6	0.025	1-way ANOVA followed by *post hoc* test Holm-Sidak's multiple comparison test
Supplemental Fig. 3D	Wave I amplitude		<0.0001	2-way ANOVA followed by *post hoc* test Holm-Sidak's multiple comparison test

Mif, mifepristone; ND, not determined; Spir, spironolactone.

with extreme variations in corticosterone levels were costained for CtBP2/RIBEYE and NKAα3, a marker of afferent type I neurons and fibers (36). A lower number of $CtBP2^{+}$ dots in IHC presynapses of the basal cochlear turn (Fig. 2*E*, CtBP2, closed arrows) was observed with less intense NKAα3 immunoreactivity in the bouton-like tip of the nerve terminal (Fig. 2*E*, NKAα3, open arrows) in animals with elevated corticosterone levels (c/c ratio = 11.9) compared with animals with lower corticosterone levels (c/c ratio = 4.7; Fig. 2*D*).

To further specify the effect of corticosterone level variations on acoustic trauma (AT)–induced auditory nerve responses, animals were exposed for 1 h to a 10-kHz tone at 116 dB SPL (see Materials and Methods) (31, 32). After 2 wk of recovery, a permanent elevation of ABR thresholds over

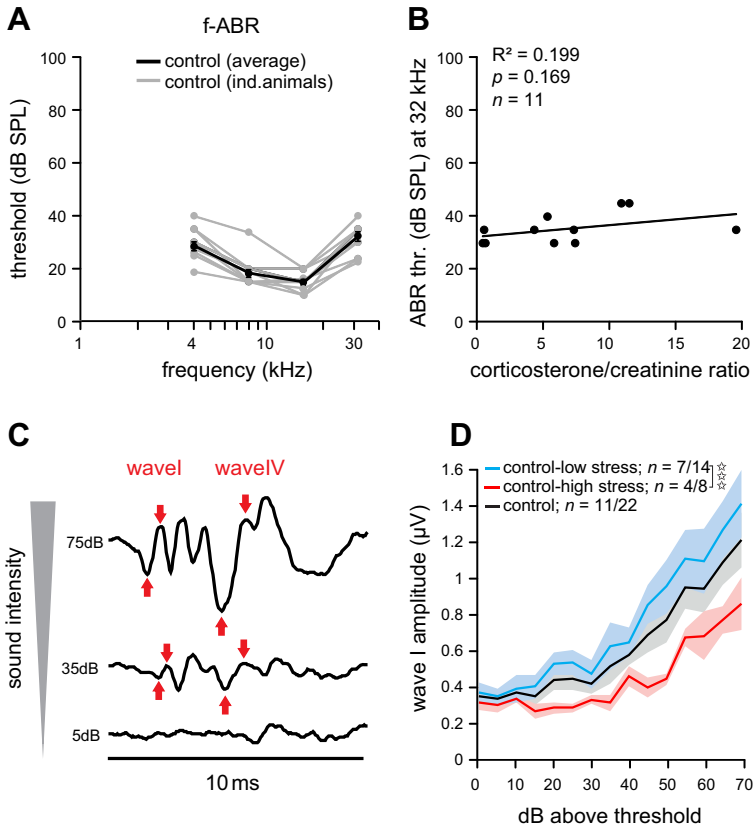

Figure 1. Auditory thresholds do not vary with corticosterone level, but suprathreshold wave I amplitudes do. *A*) Frequency-specific ABR thresholds, with the individual thresholds in gray and the average in black. *B*) Urinary corticosterone levels and thresholds at 32 kHz were independent ($n = 11$ animals). *C*) Schematics of an ABR wave for 16 kHz and increasing sound intensity (5, 35, and 75 dB SPL). Red arrows indicate low and high points of waves I and IV. *D*) Corticosterone influenced suprathreshold ABR wave I amplitude growth upon a 16 kHz stimulus. Amplitudes of ABR wave I were consistently higher in animals with low corticosterone level (c/c ratio = 3.46 ± 1.1; blue, low stress) compared with animals with high corticosterone level (c/c ratio = 12.35 ± 2.6; red, high stress); 2-way ANOVA with Holm-Sidak's post-test, $P < 0.001$. ABR wave I amplitudes grew steeper with lower levels of stress hormone (blue, $n = 7$ animals/14 ears analyzed) compared with higher levels (red, $n = 4$ animals/8 ears analyzed). For reference, the average of all animals is replotted as a black line ($n = 11$ animals/22 ears analyzed). Error bars and shaded areas represent SEM. For details of statistical analyses (see Table 1). $*P < 0.0001$ (ANOVA).

different frequencies was observed (**Fig. 3*A***) for all exposed animals (Fig. 3*A*, red line) compared with unexposed animals (Fig. 3*A*, black line). Individual variations of ABR threshold at 32 kHz were observed when thresholds were depicted for individual animals (Fig. 3*A*, gray lines, encircled area). When ABR thresholds at 32-kHz stimuli were correlated with corticosterone levels of the individual animals, elevated hearing thresholds after acoustic overexposure were observed to correlate significantly with high corticosterone levels (Fig. 3*B*, AT, red dots), a feature that was not observed in unexposed animals (Fig. 3*B*, control, black dots; see also Fig. 2*A*). The corticosterone level itself was not significantly affected by the sound exposure. Nevertheless, the c/c ratio produces effects on the physiologic changes that occur after acoustic overexposure.

IHC ribbon loss in basal cochlear turns exhibited a sensitivity for corticosterone levels (Fig. 3*C*). Two weeks after trauma induction (AT), a reduction of IHC ribbon number for all cochlear turns was significant in high-frequency representing cochlear turns compared with unexposed animals. The number of ribbons per IHC in the basal cochlear turns was lower for noise-exposed animals with elevated corticosterone levels (Fig. 3*C*, AT, red dots) compared with unexposed animals (Fig. 3*C*, control, black dots). IHC ribbon loss 14 d after AT in medial (Fig. 3*D*, red), midbasal, or apical cochlear turns (data not shown) were not correlated with the corticosterone levels of individual animals. Sound-induced ABR responses to frequencies >16 kHz are predicted to preferentially cover potentials generated in the basal cochlear turns (40); therefore, not surprisingly, IHC ribbon sensitivity to increasing corticosterone levels in basal cochlear turns was also reflected in the sensitivity of suprathreshold ABR wave I amplitude to sound stimuli >16 kHz after AT (Fig. 3*E*, blue and red lines), as previously observed in sham-treated control animals (Fig. 3*E*, black and gray lines). Accordingly, the suprathreshold summed auditory nerve response (ABR wave I) of acoustically overexposed animals in response to 32 kHz could be recorded up to higher sound intensities in animals with low corticosterone levels (Fig. 3*E*, AT-low stress, blue line), while no reliable sound response at >30 dB above threshold could be recorded in acoustically traumatized animals with elevated corticosterone levels (Fig. 3*E*, red crosses). The impaired sound response pattern in animals with elevated corticosterone levels was also observed 2 wk after AT as a morphologic correlate of IHC synapse integrity (Fig. 3).

In summary, these data demonstrate that higher corticosterone levels lowered high-frequency auditory fiber responses before and 2 wk after acoustic overexposure independent of hearing thresholds.

Inhibition of MRs and GRs does not affect hearing threshold loss and OHC function before or after acoustic trauma

To specify the effect of corticosterone levels on auditory fiber responses and trace the function back to distinct GRs, we blocked GRs and MRs types before AT with either mifepristone (GR antagonist) or spironolactone (MR antagonist) (27–29).

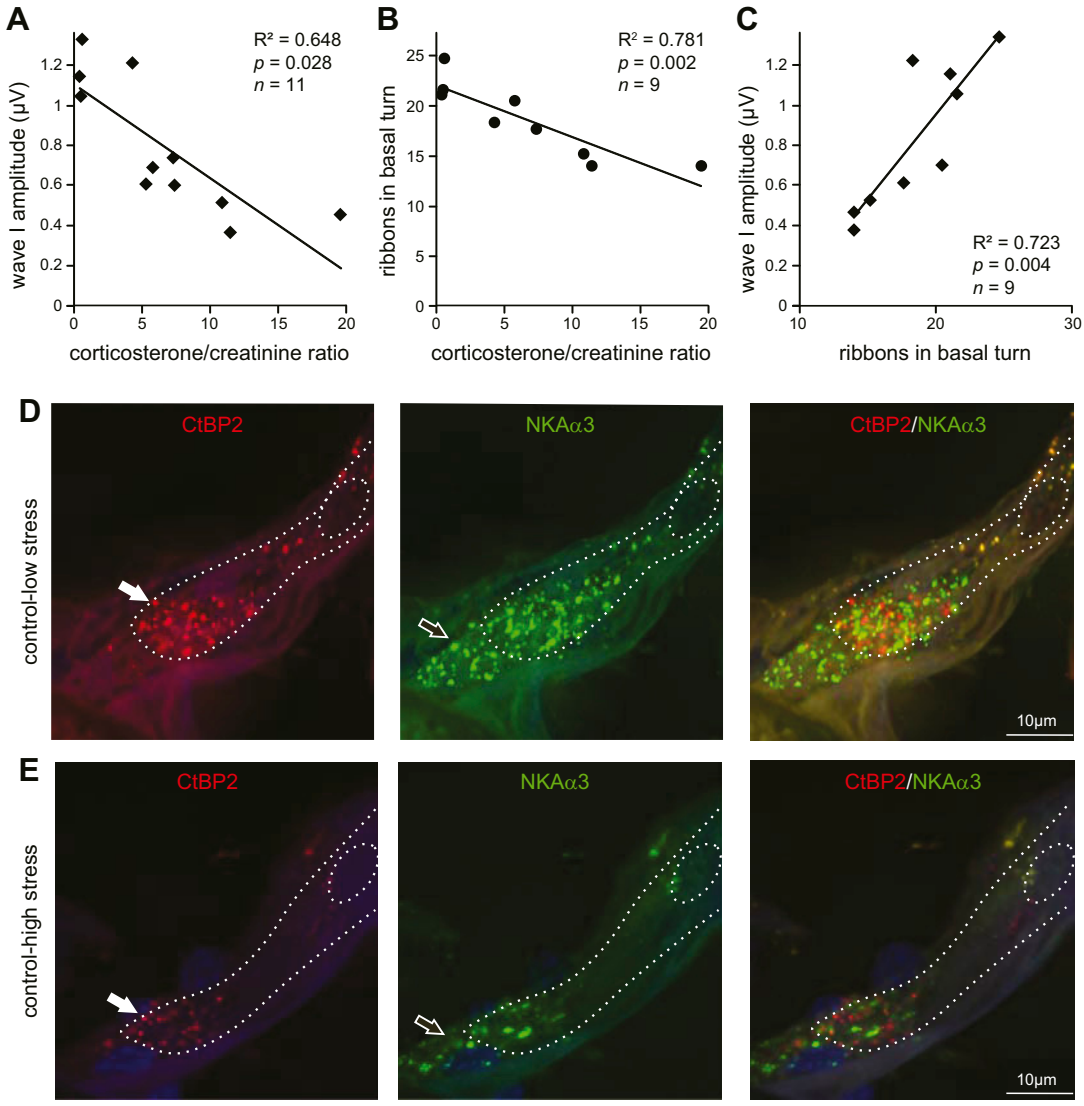

Figure 2. High levels of stress hormone negatively influence ABR wave I amplitude and IHC ribbons. *A*) ABR wave I amplitude at 16 kHz and 65 dB SPL correlates negatively with high corticosterone levels ($n = 11$ animals). *B*) Average ribbon number per IHC in the basal cochlear turn is negatively correlated with corticosterone level ($n = 9$ animals). *C*) ABR Wave I amplitude for 16 kHz and 65 dB SPL stimulation correlates with a higher number of IHC ribbons ($n = 9$ animals). *D*, *E*) Immunostaining of IHC synaptic ribbons by CtBP2/RIBEYE (arrows, red dots), NKAα3 (open arrows, green), and cell nuclei (blue, DAPI) of IHCs (white dashed line) in an animal with low levels stress hormone (c/c ratio = 4.7; $n = 3$ animals/6 ears) (*D*) and high levels of stress hormone (c/c ratio = 11.9; exemplarily done in $n = 1$ animal/2 ears) (*E*). A lower number of IHC ribbons and weaker NKAα3 immunoreactivity could be observed in animals with high levels of stress hormone compared with animals with low levels of stress hormone. Scale bars, 10 µm.

Rats received a single i.p. injection of either vehicle (polyethylene glycol and ethanol; 1:10, 2 ml/kg), the MR antagonist spironolactone (75 mg/kg), or the GR antagonist mifepristone (100 mg/kg) (28, 29) 90 min before sham or noise exposure. As shown in **Fig. 4*A*, *B***, neither mifepristone, nor spironolactone alone influenced the threshold of sound-induced ABR response of sham-exposed animals for click stimuli (Fig. 4*A*) or noise burst stimuli (Fig. 4*B*). In addition, DPOAE maximal response amplitudes (Fig. 4*C*) were not affected by the application of mifepristone or spironolactone in sham-exposed rats, which suggests that the inhibition of stress receptors did not affect OHC electromechanical properties and its contribution to hearing thresholds.

Two weeks after exposure (AT 14 d), no significant differences in hearing thresholds between pharmacologically pretreated or vehicle-pretreated animals were observed (**Fig. 5*A*–*C***). In addition, when DPOAE amplitudes (Fig. 5*D*) or distortion product thresholds at different frequencies (Fig. 5*E*) were measured, the difference between the pharmacologically treated animals and controls did not reach statistical significance. When ABR responses were explicitly compared for specific pure tone stimuli (Fig. 5*F*–*H*), a clear gradual elevation of threshold was observed for ABR responses to higher-frequency tones between 4 kHz (Fig. 5*F*), 16 kHz (Fig. 5*G*), and 32 kHz (Fig. 5*H*) 2 wk after noise exposure (AT 14 d), with nonsignificant differences

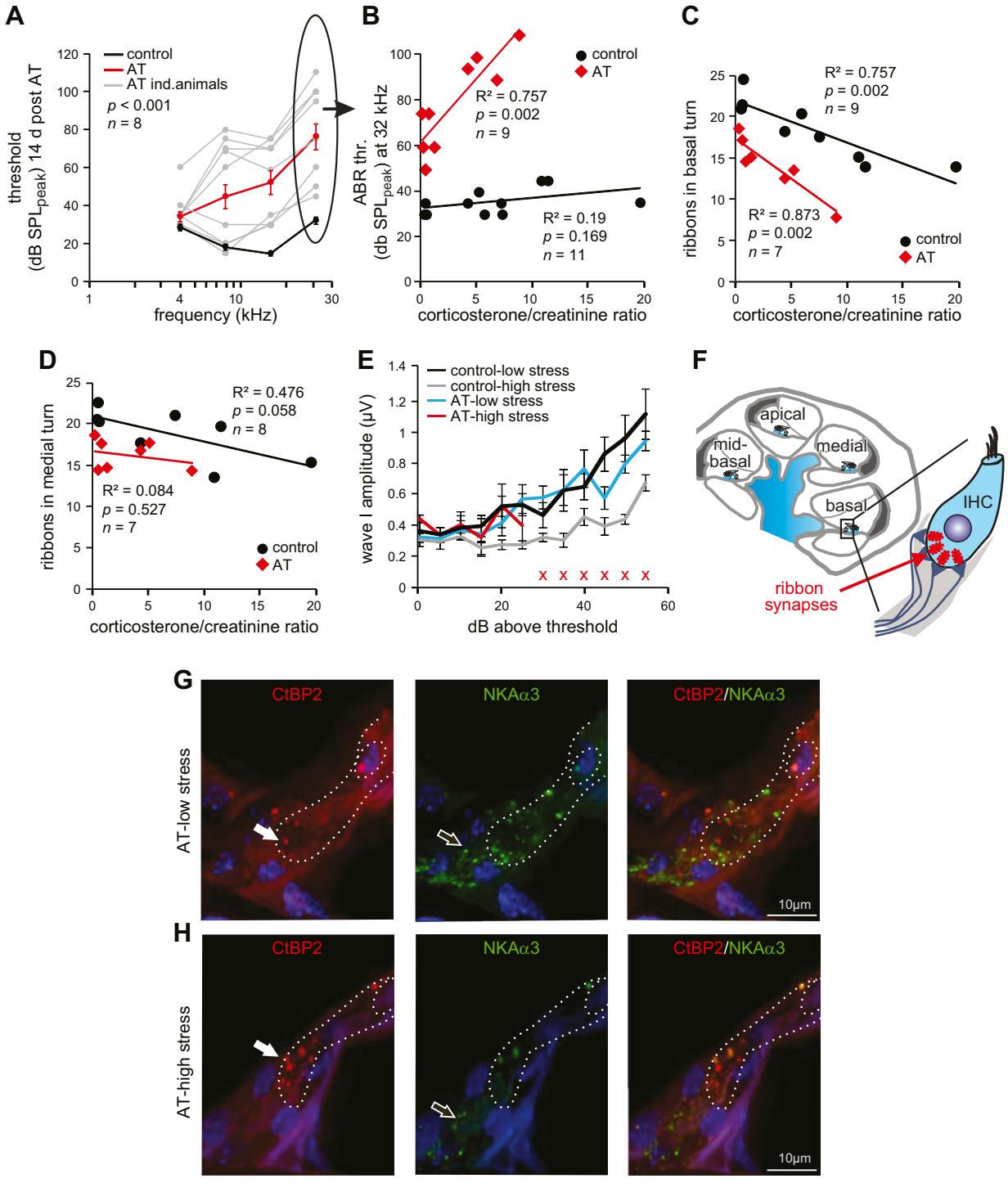

Figure 3. IHC vulnerability after AT is enhanced with elevated stress hormone levels. *A*) Frequency-specific ABR thresholds (average as red line, individuals as gray lines) of noise-exposed (116 dB SPL at 10 kHz for 1 h) and sham-exposed (average as black line) animals 2 wk after AT. Noise exposure resulted in a significant increase of threshold. Thresholds at 32 kHz are circled and replotted in panel *B* (n = 8 animals). *B*) Increased ABR thresholds at 32 kHz of noise-exposed animals correlated with increasing corticosterone level (comparison of 2 slopes: P = 0.002; control: n = 11 animals; AT: n = 9 animals). *C*) With increasing corticosterone levels, the number of ribbons in the basal cochlear turn of noise-exposed animals decreased (red; comparison of 2 slopes: P = 0.028; control: n = 9 animals; AT: n = 7 animals). *D*) The number of ribbons in the medial turn was barely influenced by corticosterone in both control (black line) and noise-exposed animals (red line; comparison of 2 slopes: P = 0.596; control: n = 8 animals; AT: n = 7 animals). *E*) Threshold-adapted growth functions of ABR wave I amplitudes of control and noise-exposed animals grouped by corticosterone level. The growth in noise-exposed animals with low corticosterone level (blue line) was similar to control sham-exposed animals with low corticosterone (black line). Noise-exposed animals with high corticosterone level (red line) demonstrated a decreased response range (reached levels) compared with all other groups (red crosses). Error bars represent SEM; control: low stress, n = 7 animals/14 ears, high stress, n = 4 animals/8 ears; AT: low stress, n = 7 animals/14

(*continued on next page*)

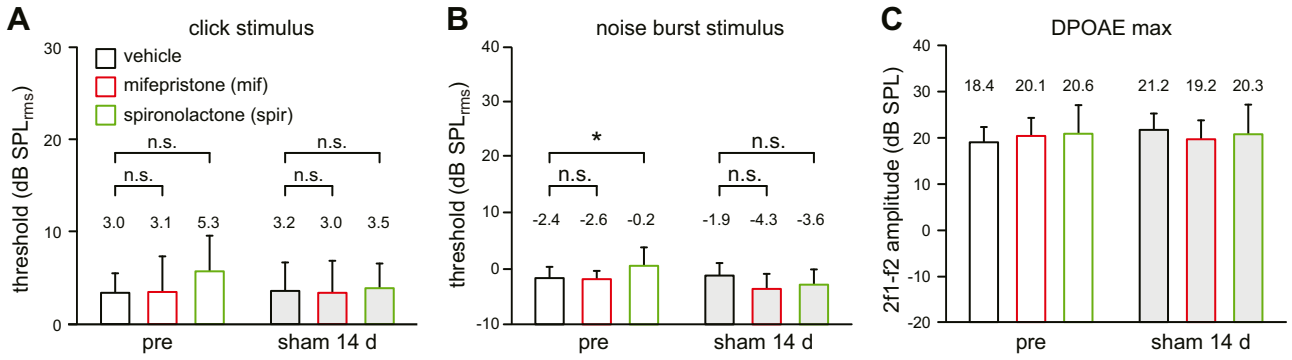

Figure 4. Treatment with either mifepristone (mif; GR antagonist) or spironolactone (spir; MR antagonist) has no influence on ABR thresholds and DPOAE amplitude. *A*) We observed no significant difference in ABR thresholds for click ABR of animals that were treated with vehicle (gray bars), mifepristone (red bars), or spironolactone (green bars) before and 2 wk after sham exposure. *B*) Thresholds for noise-evoked ABR of vehicle- and spironolactone-treated animals were not different (a randomly observed statistical significance appeared at pretreatment). *C*) DPOAE maximum response amplitudes were not significantly different. Error bars represent SD. For details of statistical analyses, see Table 1. Pretreatment: $n = 8$ animals/16 ears; 14 d: $n = 4$ animals/8 ears were measured; n.s., not significant. $^*P < 0.05$ (pairwise comparison).

between pharmacologically treated and untreated groups.

In summary, in accordance with our observation that elevated corticosterone levels pre- or post-AT did not influence basic hearing thresholds or OHC cochlear mechanics (Figs. 2 and 3), the inhibition of GR (with mifepristone) or MR (with spironolactone) before AT also did not significantly affect hearing thresholds or OHC cochlear mechanics 2 wk post-AT.

Inhibition of GR, but not MR, restored the stress-dependent diminution of auditory responses

Because high-frequency suprathreshold auditory nerve responses were sensitive for elevated corticosterone levels (Figs. 2 and 3), we next analyzed the effect of the inhibition of stress hormone receptors on auditory nerve processing. The growth of suprathreshold early ABR (wave I) and late ABR (wave IV) amplitude to increasing intensities of pure tones was analyzed 2 wk after AT in mifepristone- and spironolactone-pretreated specimens (**Fig. 6*A*–*E***). Strikingly, the suprathreshold ABR wave I and ABR wave IV responses particular to 32-kHz tone bursts, as well as for 16-kHz bursts, were less restricted in their sound response range in mifepristone-pretreated groups (Fig. 6*B, C*). Here, in mifepristone-treated groups, but not in spironolactone-treated groups, the auditory nerve responses (wave I) and midbrain responses (wave IV) were maintained 2 wk after AT over a more expanded dynamic range (reach) of stimulus level in response to higher-frequency tones compared with vehicle-treated groups (Fig. 6*A, B*), whereas vehicle- or spironolactone-treated animals could not be measured anymore at these highest sound levels (Fig. 6*B, C*). To specify this effect, the early and late ABR wave response was plotted for the ABR amplitude size (**Fig. 7*A***, size) and dynamic response range (Fig. 7*A*, reach). Strikingly, mifepristone-treated animals, but not spironolactone-treated animals, maintained their response size and reach over coded sound intensities for early and late ABR waves to 32-kHz tones after AT significantly better (Fig. 7*D*). The response was also better to 16-kHz, but not 11-kHz tones (Fig. 7*B, C*, compare wave I with wave IV at different stimuli frequencies for the amplitude size). This clearly suggests that the suppression of GRs, but not MRs, before AT can maintain the size and reach of sound-induced auditory response patterns, which indicates the diverging impact of elevated corticosterone levels on auditory processing.

The amplitude size of auditory fiber responses is defined by the reliability of the discharge rate and synchronicity of firing rates of auditory nerve fibers (25). The reliability of the discharge rates of auditory nerve responses critically depends of the number of IHC ribbons (41) that maintain a readily releasable vesicle pool and define the reliability of spikes as shown in the Bassoon mouse mutants (39). We counted the numbers of IHC ribbons along the tonotopic axis of the cochlea of treated and untreated animals 2 wk after AT by using cryosections that were stained with CtBP2/RIBEYE. As shown for the basal cochlear turn of 3–4 animals, with counting performed on both ears (6–8 ears), the number of CtBP2$^+$ dots below the IHCs is significantly reduced in midbasal and basal cochlear turns after AT (**Fig. 8**). Mifepristone, but not

ears, high stress, $n = 3$ animals/6 ears). For details of statistical analyses, see Table 1. *F*) Schematic drawing of cochlear turns and magnified IHC with ribbon synapses are depicted in red. *G, H*) Immunostaining of IHC synaptic ribbons by CtBP2/RIBEYE (arrows, red dots), NKAα3 (open arrows, green), and cell nuclei (blue, DAPI) in IHCs (white dashed line) in animals with low stress hormone level (c/c ratio = 4.7; $n = 2$ animals/4 ears) (*G*) and high stress hormone level (c/c ratio = 16.5; exemplarily done in $n = 1$ animal/2 ears) (*H*) 14 d after noise exposure (AT). As described for unexposed animals in Fig. 2, in animals with a high stress hormone level, a lower number of ribbons and less staining of NKAα3 could be observed compared with animals with low stress hormone level. Scale bars, 10 μm.

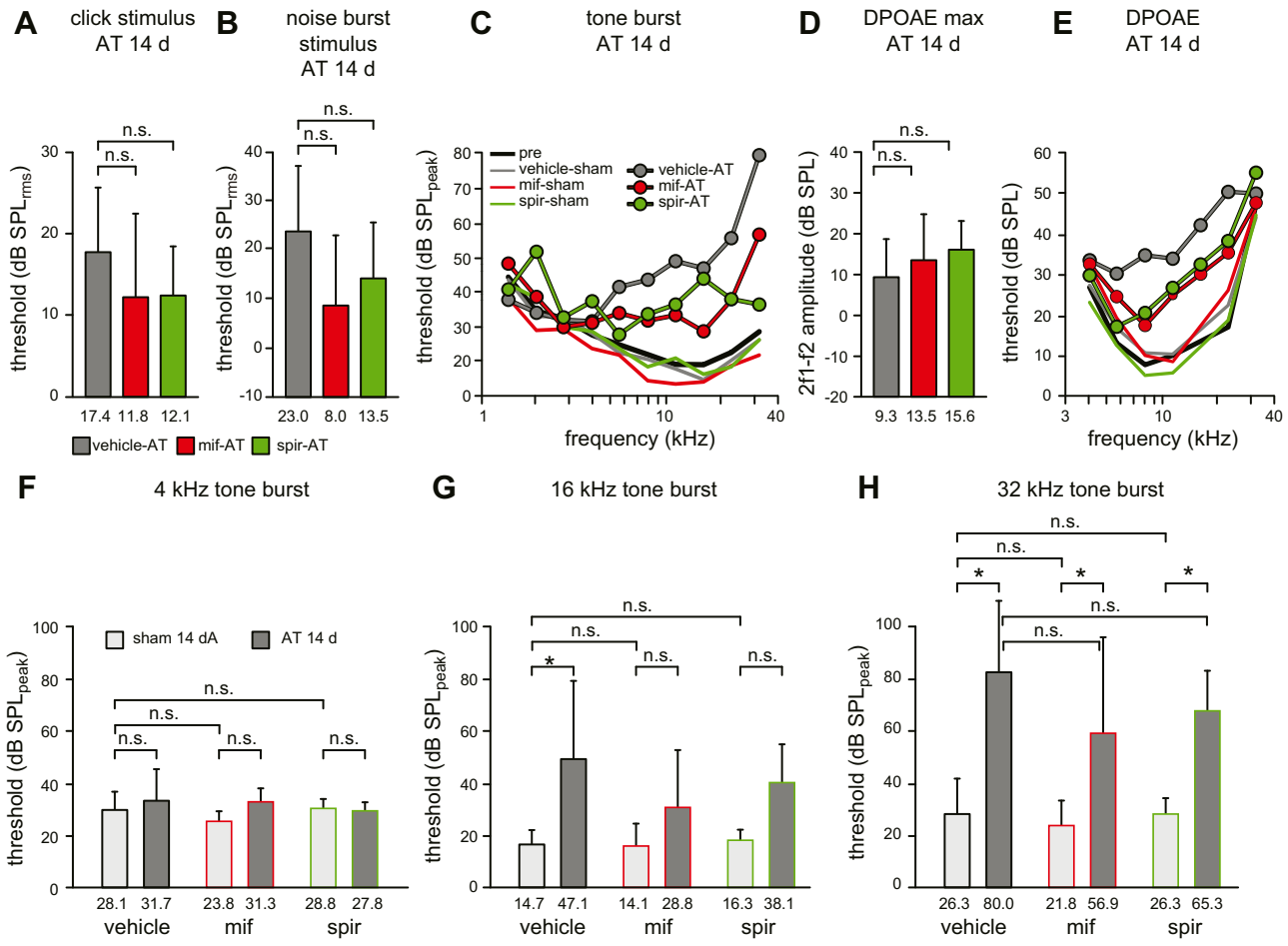

Figure 5. Mifepristone (mif) and spironolactone (spir) do not influence hearing thresholds 14 d after sham or traumatic sound exposure. *A*, *B*) Treatment with mifepristone (GR antagonist; red bars) and spironolactone (MR antagonist; green bars) exhibit no significant improvement in noise-induced threshold loss, either on click or noise-burst stimulus-evoked ABRs compared with vehicle (gray bars). *C*) ABR thresholds for frequency-specific tones of vehicle-, mifepristone-, or spironolactone-treated animals at different frequencies before (pre) and 14 d after noise exposure (AT 14 d) and sham exposure (sham 14 d). Thresholds of sound-exposed animals increased for higher frequencies. *D*) Neither mifepristone, nor spironolactone influenced DPOAE amplitude 14 d after AT. *E*) DPOAE thresholds before and 14 d after noise exposure (AT 14 d). DPOAE threshold 14 d after AT (lines with dots) was elevated at higher stimulus frequencies compared with pretreatment measurements (pre; black line) or sham exposure (colored lines without dots). *F*, *G*) Thresholds upon treatment with mifepristone (GR antagonist; red-framed bars) and spironolactone (MR antagonist; green-framed bars) are not significantly altered 14 d after noise exposure at 4 and 16 kHz compared with vehicle treatment (black-framed bars). *H*) A significant threshold loss for 32 kHz stimuli after exposure but no significant protective impact of mifepristone or spironolactone was observed. Animals at 14 d after sham exposure are depicted in light gray and at 14 d after sound exposure in dark gray. Error bars represent SD (n = 3–4 animals/6–8 ears); n.s., not significant. For details of statistical analyses, see Table 1. *$P < 0.05$ (pairwise comparison).

spironolactone, pretreatment prevented, in part, IHC ribbon loss in midbasal and basal cochlear turns (Fig. 8).

This finding suggests that the prevention of GR activation by mifepristone before AT can prevent, in part, the auditory trauma–induced decline of auditory nerve fiber responses and IHC ribbon loss in high-frequency cochlear turns.

This finding contradicts previous observations of a deteriorating effect of mifepristone treatment on hearing threshold when administered before AT and measured 24 h post-AT (30, 42). Strikingly, when ABR response patterns of mifepristone-treated and vehicle-treated animals were measured directly after AT (20 min), mifepristone did significantly worsen hearing thresholds compared with vehicle-treated animals (Supplemental Fig. 3*A*), whereas in the same experiment, hearing thresholds in mifepristone-treated groups 2 wk after AT demonstrated a trend of attenuation of AT-induced threshold elevation (not yet significant; Supplemental Fig. 3*C*). Of interest, despite the destructive effect of mifepristone on hearing thresholds directly after AT, the auditory nerve response (ABR wave I) was not different between mifepristone- and vehicle-treated groups (Supplemental Fig. 3*B*). Again, 2 wk later, as observed previously (Fig. 6), mifepristone pretreatment significantly preserved ABR wave I (Supplemental Fig. 3*D*). This essential finding suggests that mifepristone pretreatment acutely worsened hearing threshold, perhaps *via* the prevention of acute protective effects on OHCs vulnerability, as previously observed (12, 30, 42).

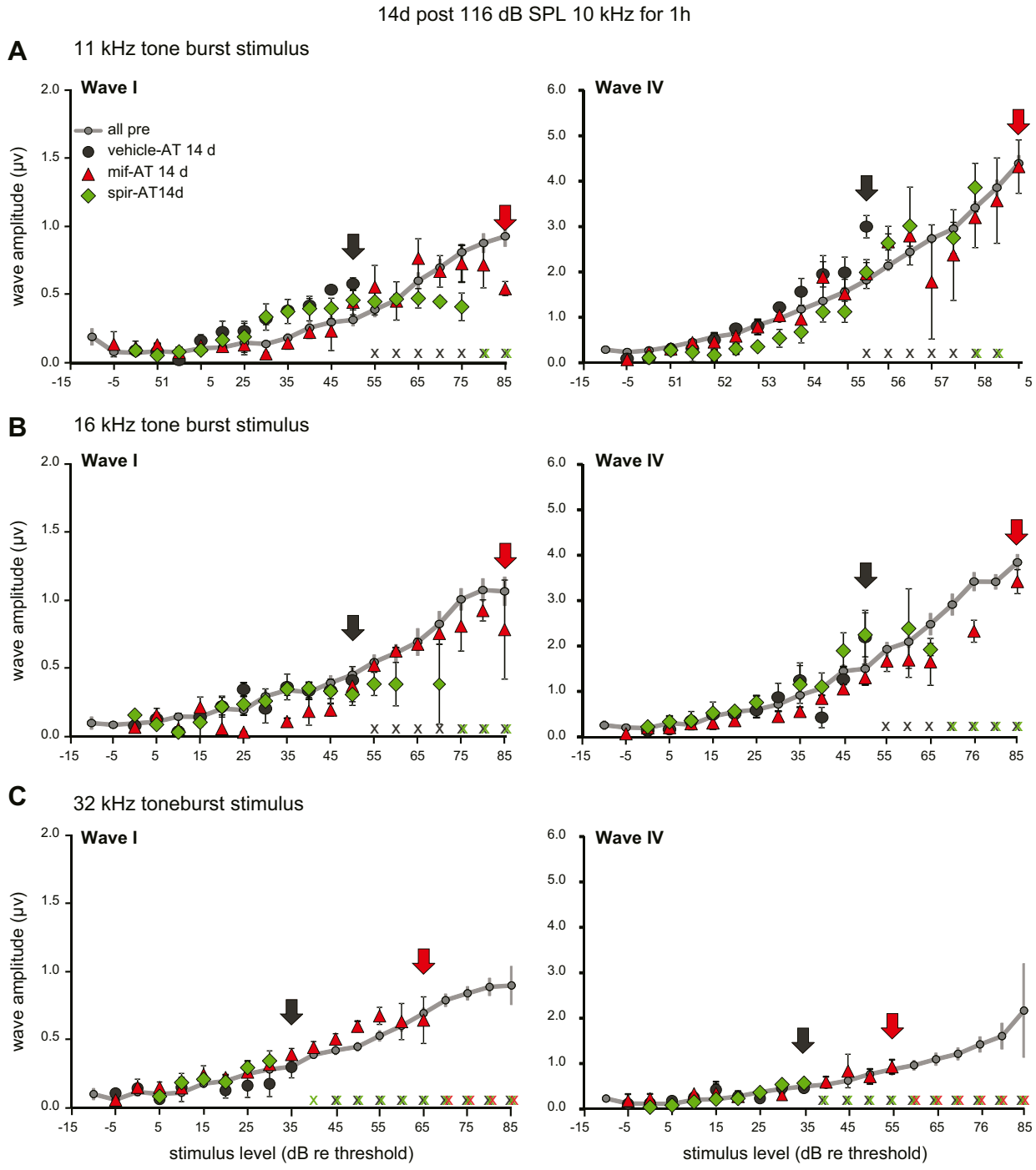

Figure 6. Treatment with mifepristone (mif; GR antagonist), but not spironolactone (spir; MR antagonist), maintains early (wave I) and late (wave IV) ABRs to a wider range particularly at high-frequency pure-tone stimuli. *A–C*) Shown is the effect of mifepristone and spironolactone application before AT on early and late suprathreshold ABR wave responses to frequency-specific tone burst stimuli. Suprathreshold ABR amplitudes at the level of the auditory nerve (wave I) and of the inferior colliculus (IC; wave IV) in response to 11 kHz (*A*), 16 kHz (*B*), and 32 kHz (*C*) pure-tone burst stimuli 2 wk after noise exposure. Animals were pretreated with vehicle (black dots), mifepristone (red triangles), or spironolactone (green diamonds). Baseline responses before exposure are shown as gray dots and lines. Arrows in the respective colors indicate the highest stimulus level above threshold for which responses could still be determined. Small crosses above the *x*-axis mark stimulus levels that surpass the limits of stimulation levels (usually 110 dB SPL). Error bars indicate SEM (n = 1–4 animals/group).

In summary, we found a long-lasting destructive role of elevated corticosterone levels on IHC synapses and auditory fiber processing after noise exposure. The destructive effects were prevented by blocking GR with its antagonist, mifepristone. This finding strongly supports the notion that, in addition to the acute protective effects of GCs for cochlear OHCs, GR-mediated stress pathways must be considered to impair sound-response amplitudes and to reduce the encodable range of sound processing.

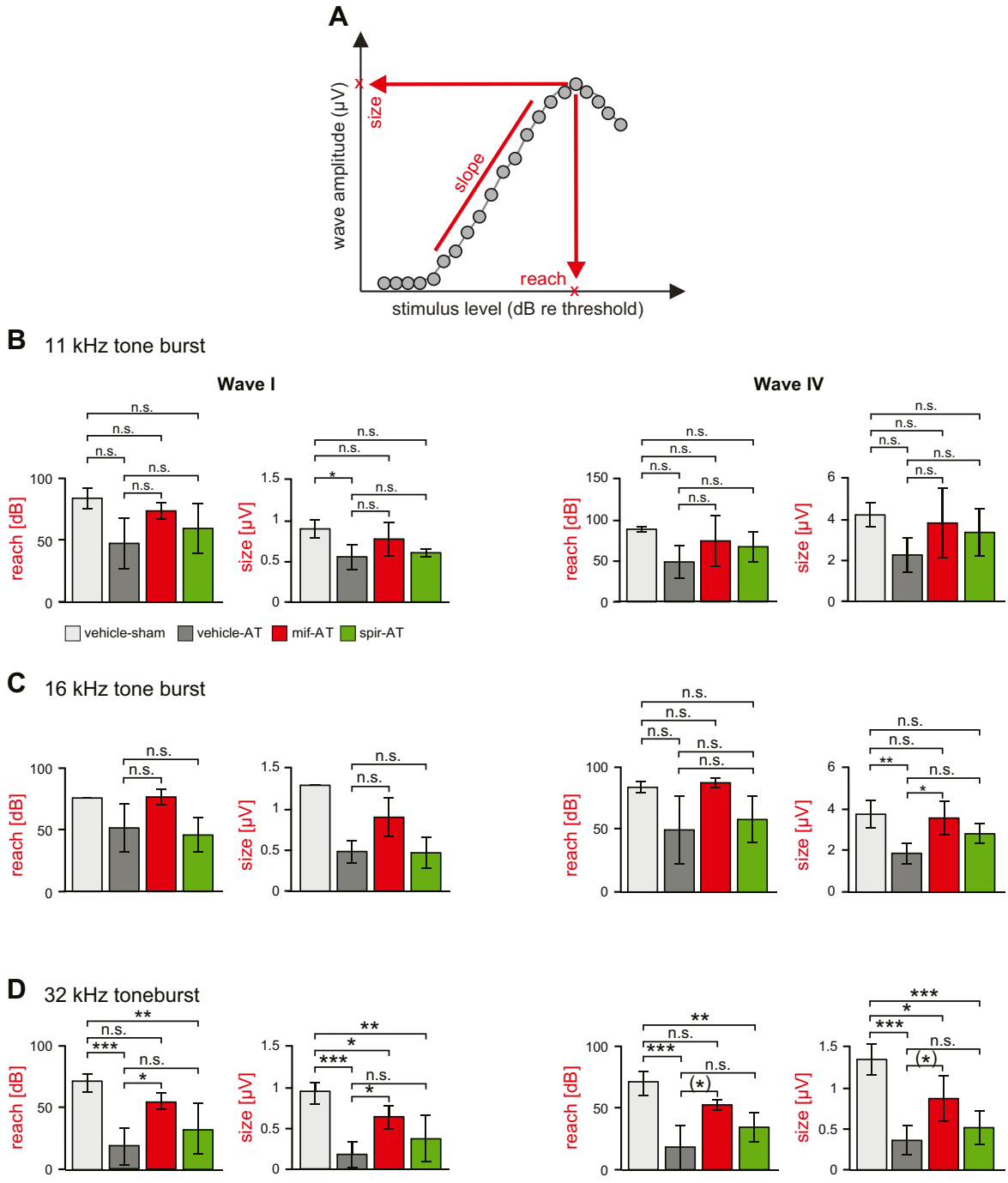

Figure 7. Pretreatment with mifepristone (GR antagonist), but not spironolactone (MR antagonist), maintains the reach for coding high stimulus levels and response size of ABRs to 32 kHz of sound stimuli after AT. *A*) Schematic of ABR amplitude growth function. The reach of the response range that can be coded is defined as the stimulus level at the maximum response of the wave amplitude. The maximum size of response is defined as the maximal wave amplitude. *B–D*) ABR wave I reach and size for 11 kHz (*B*), 16 kHz (*C*), and 32 kHz (*D*) stimuli at 14 d after sham or noise exposure. Animals were pretreated with vehicle (gray bars), mifepristone (red bars), or spironolactone (green bars). Error bars represent SD (n = 1–4 animals/group); n.s., not significant. For details of statistical analyses, see Table 1. *$P < 0.05$, **$P < 0.01$, ***$P < 0.001$ (pairwise comparison).

DISCUSSION

Here, we demonstrate for the rat animal model, that GR-mediated stress hormone signaling can negatively interfere with auditory nerve responses, noise-induced cochlear synaptopathic injury, and central auditory processing, while leaving hearing thresholds mostly unaffected. Thus, the negative influences of elevated corticosterone levels on hearing would likely hide in a conventional audiometric assessment of threshold sensitivity. These negative detrimental effects of elevated corticosterone levels on auditory nerve responses may coexist with various accepted protective activities of acute stress responses on hearing function.

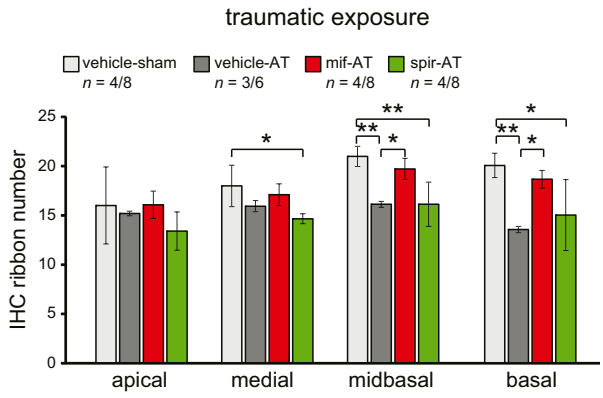

Figure 8. Mifepristone (mif), but not spironolactone (spir), pretreatment prevents, in part, IHC ribbon loss in high-frequency cochlear turns. *A*) Pretreatment with mifepristone (GR antagonist; red bars), but not spironolactone (MR antagonist; green bars), has a protective effect on IHC ribbon loss in midbasal and basal cochlear turns. Error bars represent SD (n = 3–4 animals/6–8 ears per group). For details of statistical analyses, see Table 1. $*P < 0.05$, $**P < 0.01$ (pairwise comparison).

Corticosterone level differences do not permanently influence OHCs and hearing thresholds

Here, we observed that the variation of stress hormone levels in mature female rats correlated with a prominent variation in auditory nerve function for processing especially high-frequency stimuli. These variations in responsiveness to sound occur independently of OHC function as assessed from DPOAEs (43) that define hearing thresholds *via* OHC electromotile response properties (23, 44, 45). We also did not observe any significant influence from pretreatment with the GC antagonist, mifepristone, or the mineralocorticoid antagonist, spironolactone, on hearing threshold 2–3 wk after nontraumatic (sham) or traumatic sound exposure (AT). This finding suggests that the AT-induced increase in hearing threshold correlates with the impairment of OHC electromotility after trauma and is not significantly influenced by corticosterone levels; however, previous studies have shown that treatment with heat shock (10), moderate-level long-term sound (11), or restraint stress (13, 18, 42, 46–48), among other stressors, can trigger a protective effect on the injured cochlea. This protection is believed to primarily target OHC function and cochlear mechanics in the tonotopically most damaged frequency regions (18). Our own preliminary finding—that mifepristone pretreatment exhibits no significant difference in hearing threshold 2 wk after AT, but significantly worsens hearing thresholds directly after AT—may unravel a short-lasting protective effect of acute stress responses on hearing thresholds and OHCs as previously observed (18, 30). This protective effect may wear off during the physiologic recovery period. We therefore assume that the clinical use of corticosteroids as therapy for hearing preservation (5, 6, 13) may be based on mechanisms that are related to acute effects. It remains to be explained whether GC levels act as upstream protectors of AT-induced OHC damage, by, for example, reducing oxidative cell stress as one of the major parts of AT-induced cochlear and OHC damage (49–51).

GR-mediated differences in stress hormone signaling result in long-lasting destruction of encodable hearing level of early and late ABR responses in high-frequency cochlear regions

To our knowledge, this study provides the first evidence of a clearly negative effect of elevated corticosterone levels on auditory fiber responses in high-frequency cochlear regions, with consequences for central auditory processes. The destructive role of elevated corticosterone levels on auditory nerve function after AT could be antagonized upon GR, but not MR, inhibition.

Here, high-frequency stimulus-evoked ABR wave form amplitudes, when compared before and after noise exposure for responses that correspond to the auditory nerve (wave I) and lateral lemniscus and inferior colliculus (wave IV) (26), were reduced in animals with higher levels of stress hormone independently of hearing threshold, a trend that became significant for responses from higher-frequency cochlear turns. Furthermore, the loss of ribbon structures in IHC synapses, which are required to guarantee spike temporal precision in the auditory system (39), contains a stress-sensitive component in high-frequency cochlear turns. This implies that a detrimental influence of increased corticosterone levels on auditory nerve processing, particularly when coinciding with cochlear injury, would also negatively influence central auditory processing. This is a crucial finding with regard to various evidences for diminished central auditory capacity—for example, tone perception (19), cortical responsiveness (20, 52), or plasticity of dendritic structures in auditory nuclei (21) in response to elevated stressors. The present finding challenges the hypothesis that the previously observed reduction of central auditory acuity in response to chronic stress (19–21, 52) may be a result of elevated stress levels that act first at the level of the IHC synapse *via* MRs. This may be the case, because MRs have a higher affinity for cortisol and corticosterone than GRs, and are already saturated when GRs can still respond to pathologic elevated stress hormone levels (53, 54). The elevation of corticosterone levels, observed here to profoundly influence auditory processing, might result from basal GC hypersecretion typical of hypothalamic-pituitary-adrenal axis dysregulation and chronic stress (55–57). Future studies should address whether the observed differences in urinary corticosterone levels as measured in individual animals in the present study target GRs in the cochlea and IHC (15–17) *via* the blood (58). Considering this scenario, elevated stress hormone levels may influence the glutamatergic release properties of IHCs *via* genomic or nongenomic GC activities in a similar way to that described for glutamatergic synapses in the hippocampus and basolateral amygdala (59–61). It is interesting to note that mifepristone treatment before acoustic overexposure particularly preserved the capacity of auditory nerve fiber responses for higher sound intensities. This may indicate the preservation of low spontaneous rate (SR), high-threshold auditory fibers that add up to ~40% of auditory fibers and increase the firing rate in response to moderate-to-higher sound intensities. This fiber type plays a special role for speech understanding (62) and exhibits a profound vulnerability to noise-induced trauma (63) or aging (64, 65). The present finding may thus reveal a sensitivity

of low-SR, high-threshold auditory fibers for changes in corticosterone levels. The observation that mifepristone treatment before auditory overexposure partially counteracts AT-induced IHC ribbon loss, together with a weaker NKAα3 immunoreactivity in basal cochlear turns, may also point to a role for corticosterone levels for auditory fibers with sustained high firing rates, such as high-SR, low-threshold auditory nerve fibers (36). However, a limitation for the specific interpretation of the urine corticosterone levels reported here was the low cortisol/corticosterone cross-reactivity of the chemiluminescence immunoassay used in the current study (Immulite 2000). Therefore, urinary corticosterone levels should be considered with caution when interpreting elevated stress levels. The specification of the effects of corticosterone levels on distinct auditory fibers needs additional evaluation in future studies.

In summary, the current findings demonstrate a significant influence of elevated corticosterone levels—mediated *via* elevated GC activities—on the vulnerability of the IHC synapse, the auditory nerve fiber, and central auditory processing. This destructive effect of GR-mediated stress hormone signaling likely coexists with the various acute protective functions of stressors on hearing that are suggested to positively influence the vulnerability of OHCs (13, 66) that form the basis of hearing preservation (7, 67–70). Amazingly, the present study evidenced that negative effects observed for hearing can be prevented by blocking GRs before noise-induced damage of the ear. FJ

ACKNOWLEDGMENTS

This work was supported by the Deutsche Forschungsgemeinschaft (Grants DFG-Kni-316-10-1, SPP 1608 RU 316/12-1, and KN 316/12-1). The authors thank Michael Paolillo (Interfaculty Institute of Biochemistry, University of Tübingen) for reading the manuscript. The authors declare no conflicts of interest.

AUTHOR CONTRIBUTIONS

M. Knipper and L. Rüttiger conceived of the study; W. Singer, K. Kasini, M. Manthey, P. Eckert, P. Armbruster, M. A. Vogt, M. Jaumann, M. Dotta, K. Yamahara, C. Harasztosi, M. Knipper, and L. Rüttiger analyzed the data; W. Singer, K. Kasini, M. Manthey, P. Eckert, P. Armbruster, M. A. Vogt, M. Jaumann, D. Z., M. Dotta, K. Yamahara, C. Harasztosi, M. Knipper, and L. Rüttiger performed experiments; W. Singer, M. Manthey, P. Eckert, M. Jaumann, U. Zimmermann, M. Knipper, and L. Rüttiger wrote the manuscript; M. Knipper and L. Rüttiger supervised the work; and W. Singer, M. Manthey, P. Eckert, U. Zimmermann, M. Knipper, and L. Rüttiger reviewed and edited the manuscript.

REFERENCES

1. De Kloet, E. R. (2013) Functional profile of the binary brain corticosteroid receptor system: mediating, multitasking, coordinating, integrating. *Eur. J. Pharmacol.* **719**, 53–62
2. De Kloet, E. R. (2014) From receptor balance to rational glucocorticoid therapy. *Endocrinology* **155**, 2754–2769
3. Hobson, C. E., Alexander, T. H., and Harris, J. P. (2016) Primary treatment of idiopathic sudden sensorineural hearing loss with intratympanic dexamethasone. *Curr. Opin. Otolaryngol. Head Neck Surg.* **24**, 407–412
4. O'Byrne, P. M., and Pedersen, S. (1998) Measuring efficacy and safety of different inhaled corticosteroid preparations. *J. Allergy Clin. Immunol.* **102**, 879–886
5. O'Leary, S. J., Monksfield, P., Kel, G., Connolly, T., Souter, M. A., Chang, A., Marovic, P., O'Leary, J. S., Richardson, R., and Eastwood, H. (2013) Relations between cochlear histopathology and hearing loss in experimental cochlear implantation. *Hear. Res.* **298**, 27–35
6. Niedermeier, K., Braun, S., Fauser, C., Kiefer, J., Straubinger, R. K., and Stark, T. (2012) A safety evaluation of dexamethasone-releasing cochlear implants: comparative study on the risk of otogenic meningitis after implantation. *Acta Otolaryngol.* **132**, 1252–1260
7. El Sabbagh, N. G., Sewitch, M. J., Bezdjian, A., and Daniel, S. J. (2017) Intratympanic dexamethasone in sudden sensorineural hearing loss: a systematic review and meta-analysis. *Laryngoscope* **127**, 1897–1908
8. Plontke, S. K., Glien, A., Rahne, T., Mäder, K., and Salt, A. N. (2014) Controlled release dexamethasone implants in the round window niche for salvage treatment of idiopathic sudden sensorineural hearing loss. *Otol. Neurotol.* **35**, 1168–1171
9. Jia, H., François, F., Bourien, J., Eybalin, M., Lloyd, R. V., Van De Water, T. R., Puel, J. L., and Venail, F. (2016) Prevention of trauma-induced cochlear fibrosis using intracochlear application of anti-inflammatory and antiproliferative drugs. *Neuroscience* **316**, 261–278
10. Yoshida, N., and Liberman, M. C. (1999) Stereociliary anomaly in the guinea pig: effects of hair bundle rotation on cochlear sensitivity. *Hear. Res.* **131**, 29–38
11. Yoshida, N., and Liberman, M. C. (2000) Sound conditioning reduces noise-induced permanent threshold shift in mice. *Hear. Res.* **148**, 213–219
12. Wang, Y., Hirose, K., and Liberman, M. C. (2002) Dynamics of noise-induced cellular injury and repair in the mouse cochlea. *J. Assoc. Res. Otolaryngol.* **3**, 248–268
13. Meltser, I., and Canlon, B. (2011) Protecting the auditory system with glucocorticoids. *Hear. Res.* **281**, 47–55
14. Trune, D. R., Kempton, J. B., and Gross, N. D. (2006) Mineralocorticoid receptor mediates glucocorticoid treatment effects in the autoimmune mouse ear. *Hear. Res.* **212**, 22–32
15. Yao, X., and Rarey, K. E. (1996) Localization of the mineralocorticoid receptor in rat cochlear tissue. *Acta Otolaryngol.* **116**, 493–496
16. Terakado, M., Kumagami, H., and Takahashi, H. (2011) Distribution of glucocorticoid receptors and 11 beta-hydroxysteroid dehydrogenase isoforms in the rat inner ear. *Hear. Res.* **280**, 148–156
17. Kil, S. H., and Kalinec, F. (2013) Expression and dexamethasone-induced nuclear translocation of glucocorticoid and mineralocorticoid receptors in guinea pig cochlear cells. *Hear. Res.* **299**, 63–78
18. Wang, Y., and Liberman, M. C. (2002) Restraint stress and protection from acoustic injury in mice. *Hear. Res.* **165**, 96–102
19. Felmingham, K. L., Rennie, C., Gordon, E., and Bryant, R. A. (2012) Autonomic and cortical reactivity in acute and chronic posttraumatic stress. *Biol. Psychol.* **90**, 224–227
20. Pérez, M. A., Pérez-Valenzuela, C., Rojas-Thomas, F., Ahumada, J., Fuenzalida, M., and Dagnino-Subiabre, A. (2013) Repeated restraint stress impairs auditory attention and GABAergic synaptic efficacy in the rat auditory cortex. *Neuroscience* **246**, 94–107
21. Dagnino-Subiabre, A., Muñoz-Llancao, P., Terreros, G., Wyneken, U., Díaz-Véliz, G., Porter, B., Kilgard, M. P., Atzori, M., and Aboitiz, F. (2009) Chronic stress induces dendritic atrophy in the rat medial geniculate nucleus: effects on auditory conditioning. *Behav. Brain Res.* **203**, 88–96
22. Singer, W., Zuccotti, A., Jaumann, M., Lee, S. C., Panford-Walsh, R., Xiong, H., Zimmermann, U., Franz, C., Geisler, H. S., Köpschall, I., Rohbock, K., Varakina, K., Verpoorten, S., Reinbothe, T., Schimmang, T., Rüttiger, L., and Knipper, M. (2013) Noise-induced inner hair cell ribbon loss disturbs central arc mobilization: a novel molecular paradigm for understanding tinnitus. *Mol. Neurobiol.* **47**, 261–279
23. El-Badry, M. M., and McFadden, S. L. (2007) Electrophysiological correlates of progressive sensorineural pathology in carboplatin-treated chinchillas. *Brain Res.* **1134**, 122–130
24. Kujawa, S. G., and Liberman, M. C. (2009) Adding insult to injury: cochlear nerve degeneration after "temporary" noise-induced hearing loss. *J. Neurosci.* **29**, 14077–14085
25. Johnson, D. H., and Kiang, N. Y. (1976) Analysis of discharges recorded simultaneously from pairs of auditory nerve fibers. *Biophys. J.* **16**, 719–734
26. Melcher, J. R., and Kiang, N. Y. (1996) Generators of the brainstem auditory evoked potential in cat. III: identified cell populations. *Hear. Res.* **93**, 52–71

27. Griesbach, G. S., Vincelli, J., Tio, D. L., and Hovda, D. A. (2012) Effects of acute restraint-induced stress on glucocorticoid receptors and brain-derived neurotrophic factor after mild traumatic brain injury. *Neuroscience* **210**, 393–402
28. Adamec, R., Muir, C., Grimes, M., and Pearcey, K. (2007) Involvement of noradrenergic and corticoid receptors in the consolidation of the lasting anxiogenic effects of predator stress. *Behav. Brain Res.* **179**, 192–207
29. Fox, L. C., Davies, D. R., Scholl, J. L., Watt, M. J., and Forster, G. L. (2016) Differential effects of glucocorticoid and mineralocorticoid antagonism on anxiety behavior in mild traumatic brain injury. *Behav. Brain Res.* **312**, 362–365
30. Tahera, Y., Meltser, I., Johansson, P., Bian, Z., Stierna, P., Hansson, A. C., and Canlon, B. (2006) NF-kappaB mediated glucocorticoid response in the inner ear after acoustic trauma. *J. Neurosci. Res.* **83**, 1066–1076
31. Jaumann, M., Dettling, J., Gubelt, M., Zimmermann, U., Gerling, A., Paquet-Durand, F., Feil, S., Wolpert, S., Franz, C., Varakina, K., Xiong, H., Brandt, N., Kuhn, S., Geisler, H. S., Rohbock, K., Ruth, P., Schlossmann, J., Hütter, J., Sandner, P., Feil, R., Engel, J., Knipper, M., and Rüttiger, L. (2012) cGMP-Prkg1 signaling and Pde5 inhibition shelter cochlear hair cells and hearing function. *Nat. Med.* **18**, 252–259
32. Rüttiger, L., Singer, W., Panford-Walsh, R., Matsumoto, M., Lee, S. C., Zuccotti, A., Zimmermann, U., Jaumann, M., Rohbock, K., Xiong, H., and Knipper, M. (2013) The reduced cochlear output and the failure to adapt the central auditory response causes tinnitus in noise exposed rats. *PLoS One* **8**, e57247
33. Burkard, R. F., and Don, M. (2007) The auditory brainstem response. In Auditory Evoked Potentials: Basic Principles and Clinical Application (Burkard, R. F., Eggermont, J. J., and Don, M., eds.), pp. 229–250, Lippincott Williams and Wilkins, Philadelphia
34. Engel, J., Braig, C., Rüttiger, L., Kuhn, S., Zimmermann, U., Blin, N., Sausbier, M., Kalbacher, H., Münkner, S., Rohbock, K., Ruth, P., Winter, H., and Knipper, M. (2006) Two classes of outer hair cells along the tonotopic axis of the cochlea. *Neuroscience* **143**, 837–849
35. Singer, W., Geisler, H. S., Panford-Walsh, R., and Knipper, M. (2016) Detection of excitatory and inhibitory synapses in the auditory system using fluorescence immunohistochemistry and high-resolution fluorescence microscopy. *Methods Mol. Biol.* **1427**, 263–276
36. McLean, W. J., Smith, K. A., Glowatzki, E., and Pyott, S. J. (2009) Distribution of the Na,K-ATPase alpha subunit in the rat spiral ganglion and organ of corti. *J. Assoc. Res. Otolaryngol.* **10**, 37–49
37. Dallos, P., and Harris, D. (1978) Properties of auditory nerve responses in absence of outer hair cells. *J. Neurophysiol.* **41**, 365–383
38. Ashmore, J. (2008) Cochlear outer hair cell motility. *Physiol. Rev.* **88**, 173–210
39. Buran, B. N., Strenzke, N., Neef, A., Gundelfinger, E. D., Moser, T., and Liberman, M. C. (2010) Onset coding is degraded in auditory nerve fibers from mutant mice lacking synaptic ribbons. *J. Neurosci.* **30**, 7587–7597
40. Müller, M., and Robertson, D. (1991) Relationship between tone burst discharge pattern and spontaneous firing rate of auditory nerve fibres in the guinea pig. *Hear. Res.* **57**, 63–70
41. Safieddine, S., El-Amraoui, A., and Petit, C. (2012) The auditory hair cell ribbon synapse: from assembly to function. *Annu. Rev. Neurosci.* **35**, 509–528
42. Tahera, Y., Meltser, I., Johansson, P., Hansson, A. C., and Canlon, B. (2006) Glucocorticoid receptor and nuclear factor-kappa B interactions in restraint stress-mediated protection against acoustic trauma. *Endocrinology* **147**, 4430–4437
43. Shera, C. A., and Guinan, J. J., Jr. (1999) Evoked otoacoustic emissions arise by two fundamentally different mechanisms: a taxonomy for mammalian OAEs. *J. Acoust. Soc. Am.* **105**, 782–798
44. Marcon, S., and Patuzzi, R. (2008) Changes in cochlear responses in guinea pig with changes in perilymphatic K^+. Part I: summating potentials, compound action potentials and DPOAEs. *Hear. Res.* **237**, 76–89
45. Rüttiger, L., Zimmermann, U., and Knipper, M. (2017) Biomarkers for hearing dysfunction: facts and outlook. *ORL J. Otorhinolaryngol. Relat. Spec.* **79**, 93–111
46. Rarey, K. E., Gerhardt, K. J., Curtis, L. M., and ten Cate, W. J. (1995) Effect of stress on cochlear glucocorticoid protein: acoustic stress. *Hear. Res.* **82**, 135–138
47. Tahera, Y., Meltser, I., Johansson, P., Salman, H., and Canlon, B. (2007) Sound conditioning protects hearing by activating the hypothalamic-pituitary-adrenal axis. *Neurobiol. Dis.* **25**, 189–197
48. Canlon, B., Meltser, I., Johansson, P., and Tahera, Y. (2007) Glucocorticoid receptors modulate auditory sensitivity to acoustic trauma. *Hear. Res.* **226**, 61–69
49. Sha, S. H., and Schacht, J. (2017) Emerging therapeutic interventions against noise-induced hearing loss. *Expert Opin. Investig. Drugs* **26**, 85–96
50. Fetoni, A. R., Rolesi, R., Paciello, F., Eramo, S. L. M., Grassi, C., Troiani, D., and Paludetti, G. (2016) Styrene enhances the noise induced oxidative stress in the cochlea and affects differently mechanosensory and supporting cells. *Free Radic. Biol. Med.* **101**, 211–225
51. Kurabi, A., Keithley, E. M., Housley, G. D., Ryan, A. F., and Wong, A. C. (2017) Cellular mechanisms of noise-induced hearing loss. *Hear. Res.* **349**, 129–137
52. Ma, L., Li, W., Li, S., Wang, X., and Qin, L. (2017) Effect of chronic restraint stress on inhibitory gating in the auditory cortex of rats. *Stress* **20**, 312–319
53. Korte, S. M., de Boer, S. F., de Kloet, E. R., and Bohus, B. (1995) Anxiolytic-like effects of selective mineralocorticoid and glucocorticoid antagonists on fear-enhanced behavior in the elevated plus-maze. *Psychoneuroendocrinology* **20**, 385–394
54. Joëls, M., and de Kloet, E. R. (2017) 30 years of the mineralocorticoid receptor: the brain mineralocorticoid receptor: a saga in three episodes. *J. Endocrinol.* **234**, T49–T66
55. Howland, R. H. (2013) Mifepristone as a therapeutic agent in psychiatry. *J. Psychosoc. Nurs. Ment. Health Serv.* **51**, 11–14
56. Tsigos, C., Kyrou, I., Kassi, E., and Chrousos, G. P. (2000) Stress, endocrine physiology and pathophysiology. In Endotext (De Groot, L. J., Chrousos, G., Dungan, K., Feingold, K. R., Grossman, A., Hershman, J. M., Koch, C., Korbonits, M., McLachlan, R., New, M., Purnell, J., Rebar, R., Singer, F., and Vinik, A., eds.), MDText.com, South Dartmouth, MA, USA
57. Oitzl, M. S., Champagne, D. L., van der Veen, R., and de Kloet, E. R. (2010) Brain development under stress: hypotheses of glucocorticoid actions revisited. *Neurosci. Biobehav. Rev.* **34**, 853–866
58. Chavez, C. M., McGaugh, J. L., and Weinberger, N. M. (2009) The basolateral amygdala modulates specific sensory memory representations in the cerebral cortex. *Neurobiol. Learn. Mem.* **91**, 382–392
59. Karst, H., Berger, S., Erdmann, G., Schütz, G., and Joëls, M. (2010) Metaplasticity of amygdalar responses to the stress hormone corticosterone. *Proc. Natl. Acad. Sci. USA* **107**, 14449–14454
60. Boudaba, C., and Tasker, J. G. (2006) Intranuclear coupling of hypothalamic magnocellular nuclei by glutamate synaptic circuits. *Am. J. Physiol. Regul. Integr. Comp. Physiol.* **291**, R102–R111
61. Groeneweg, F. L., Karst, H., de Kloet, E. R., and Joëls, M. (2011) Rapid non-genomic effects of corticosteroids and their role in the central stress response. *J. Endocrinol.* **209**, 153–167
62. Bharadwaj, H. M., Masud, S., Mehraei, G., Verhulst, S., and Shinn-Cunningham, B. G. (2015) Individual differences reveal correlates of hidden hearing deficits. *J. Neurosci.* **35**, 2161–2172
63. Furman, A. C., Kujawa, S. G., and Liberman, M. C. (2013) Noise-induced cochlear neuropathy is selective for fibers with low spontaneous rates. *J. Neurophysiol.* **110**, 577–586
64. Schmiedt, R. A., Mills, J. H., and Boettcher, F. A. (1996) Age-related loss of activity of auditory-nerve fibers. *J. Neurophysiol.* **76**, 2799–2803
65. Sergeyenko, Y., Lall, K., Liberman, M. C., and Kujawa, S. G. (2013) Age-related cochlear synaptopathy: an early-onset contributor to auditory functional decline. *J. Neurosci.* **33**, 13686–13694
66. Trune, D. R., and Canlon, B. (2012) Corticosteroid therapy for hearing and balance disorders. *Anat. Rec. (Hoboken)* **295**, 1928–1943
67. Hickox, A. E., Larsen, E., Heinz, M. G., Shinobu, L., and Whitton, J. P. (2017) Translational issues in cochlear synaptopathy. *Hear. Res.* **349**, 164–171
68. Kobel, M., Le Prell, C. G., Liu, J., Hawks, J. W., and Bao, J. (2017) Noise-induced cochlear synaptopathy: past findings and future studies. *Hear. Res.* **349**, 148–154
69. Lee, H. Y., Kim, D. K., Park, Y. H., Cha, W. W., Kim, G. J., and Lee, S. H. (2017) Prognostic factors for profound sudden idiopathic sensorineural hearing loss: a multicenter retrospective study. *Eur. Arch. Otorhinolaryngol.* **274**, 143–149
70. Müller, M., Tisch, M., Maier, H., and Löwenheim, H. (2017) Reduction of permanent hearing loss by local glucocorticoid application: guinea pigs with acute acoustic trauma. *HNO* **65** (Suppl 1), 59–67

Received for publication September 27, 2017.
Accepted for publication December 26, 2017.

Brain-derived neurotrophic factor in inhibitory hindbrain neurons controls central learning mechanisms

Philipp Eckert**[1], Philine Marchetta**[1], Marie Manthey**[1,2], Michael H. Walter[3], Wibke Singer[1], Michele H. Jacob[2], Lukas Rüttiger[1], Thomas Schimmang[4], Peter K. Pilz[3], Marlies Knipper*[1]

[1] University of Tübingen, Department of Otolaryngology, Head and Neck Surgery, Tübingen Hearing Research Centre, Molecular Physiology of Hearing, Elfriede-Aulhorn-Str. 5, 72076 Tübingen, Germany

[2] Tufts University School of Medicine, Department of Neuroscience, Sackler School of Biomedical Sciences, Boston, MA, United States.

[3] University of Tübingen, Department of Animal Physiology, Institute of Neurobiology, Auf der Morgenstelle 28, 72076 Tübingen, Germany

[4] Instituto de Biologíay Genética Molecular, Universidad de Valladolid, Consejo Superior de Investigaciones Científicas (CSIC), Valladolid, Spain

*Correspondence: marlies.knipper@uni-tuebingen.de

**These authors contributed equally to this work

ABSTRACT

Brain-derived neurotrophic factor (**BDNF**), a key modulator of synaptic plasticity, is predicted to locally control cortical receptive field maturation and memory with sensory experience. Here, we demonstrate that the deletion of *Bdnf* in the cochlea and brainstem under the *Pax2* promoter (***Bdnf*^{Pax2}KO**) leads to memory deficits, reduced explorative behavior and increased anxiety. These profound executive dysfunctions in *Bdnf*^{Pax2}KOs could be traced back to deficits in rapid auditory processing and diminished maturation of the fast-spiking parvalbumin (**PV**)-dendritic network in the auditory cortex (**AC**) and hippocampus from hearing onset onwards, despite normal BDNF levels in these forebrain regions. A diminished hippocampal PV-dendritic network in *Bdnf*^{Pax2}KOs is associated with a persistent premature state of elevated hippocampal long-term potentiation (**LTP**) and increased activity-regulated cytoskeleton-associated protein (**Arc**/**Arg3.1**) levels. Functional maturation of the hippocampus with onset of fast sensory processing is thus dependent on BDNF in lower brain regions, with relevance to the etiology of neurodevelopmental disorders.

Key words: BDNF, Pax2, Arc/Arg3.1, rapid auditory processing (RAP), parvalbumin-interneuron, Autism spectrum disorders (ASD), memory & learning

INTRODUCTION

Our individualized perception of the external world is established during windows of early life when task- or context specific signals are first integrated through sensory memory-dependent circuits to improve or adapt to fast changing surrounding environment. How auditory experience sculpts auditory receptive fields and task-specific learning is still not understood in detail. It is known that local cortical BDNF, identified in 1982 (Barde, Edgar, & Thoenen, 1982) as key modulator of synaptic plasticity, memory and homeostatic readjustment processes (for reviews, see: (Bramham & Messaoudi, 2005; Leal, Bramham, & Duarte, 2017; Minichiello, 2009; Monteggia et al., 2004; Park & Poo, 2013; Rauskolb et al., 2010; Zagrebelsky & Korte, 2014)), regulate the dendritic complexity of cortical parvalbumin (**PV**)-interneurons (**INs**) with sensory experience in all sensory systems (Griffen & Maffei, 2014; Hong, McCord, & Greenberg, 2008; Xu, Kotak, & Sanes, 2010), enabling thereby the integration of contextual with task-specific signals for improved performance and adjustment (Takesian, Bogart, Lichtman, & Hensch, 2018). The perforant path of the hippocampus receives sensory auditory input from auditory association cortices (Munoz-Lopez, Mohedano-Moriano, & Insausti, 2010) that are activated during auditory perception and accentuation of behaviorally relevant sound (Kilgard, Pandya, Engineer, & Moucha, 2002; Kraus & White-Schwoch, 2015; Weinberger, 2015) as well as during auditory adjustments (Matt et al., 2018), enabling learning-dependent adjustments with remarkable temporal precision in response to ethologically-relevant stimuli from first sensory experience onwards (Froemke, Merzenich, & Schreiner, 2007).

What drives cortical local BDNF during this critical period of first sensory experience is elusive. As constitutive BDNF knockout (**KO**) mice die too prematurely (Ernfors, Lee, & Jaenisch, 1994), our understanding of BDNF's role after hearing onset, including

memory-linked auditory processing, which is essential for normal speech and language development (Truong et al., 2014), is still limited.

To overcome the lethality of constitutive BDNF KO mutants, BDNF was conditionally deleted in lower brain-level regions under the promoter of the paired-box transcription factor *Pax2* (Chumak et al., 2016; Zuccotti et al., 2012) that is expressed neonatally in the otic placode (Fritzsch, Jahan, Pan, & Elliott, 2015; Ohyama & Groves, 2004). The neonatal role of BDNF in the cochlea prior to hearing onset is confined to survival and outgrowth of afferent fibers in lower frequency regions before P4 via its expression in hair cells (Fritzsch et al., 2015; Fritzsch, Tessarollo, Coppola, & Reichardt, 2004). Surprisingly, constitutive *Bdnf*^{Pax2}KOs developed no afferent fiber or ganglion loss but rather normal basal hearing function (Chumak et al., 2016). *Bdnf*^{Pax2}KOs instead exhibited auditory acuity deficits that suggests BDNF function in Pax2-positive neurons after hearing onset. Therefore, the phenotype of *Bdnf*^{Pax2}KOs must be linked to gradually upregulated BDNF in cochlear neurons and the ascending auditory pathway during the time of hearing onset until the second postnatal week (Singer, Panford-Walsh, & Knipper, 2014). Between embryonal day (**E**) 13 and the second postnatal week, Pax2 is confined to prospective γ-aminobutyric acid (**GABA**)-IN precursor cells migrating from ventricular zones to lower level brain regions mostly posterior to the midbrain around the 2nd postnatal week in rodents (Fotaki, Price, & Mason, 2008; Maricich & Herrup, 1999). Therefore, Pax2-positive GABA-IN precursors are distinguished from Pax2-negative IN precursor subtypes that migrate parallel from defined subpallidal regions to either the cortical plate, including the hippocampus, or the olfactory bulb (Marin & Rubenstein, 2001).

As GABAergic INs in the mature brain do not express BDNF but rather its receptor tropomyosin receptor kinase (**Trk**) B (Marty, Berzaghi Mda, & Berninger, 1997), we challenged the roles of BDNF in Pax2 inhibitory precursor cells beyond auditory acuity.

Here, we identified BDNF in Pax2 cells in lower brain regions to be essential for the maturation of PV-IN networks in frontal brain regions with hearing onset when PV-IN network appear to shape hippocampal field excitatory postsynaptic potentials (**fEPSPs**) and activity-regulated cytoskeleton-associated protein (**Arc**/**Arg3.1**) levels. A failure of this shaping process as observed in *Bdnf*^{Pax2}KOs led to learning and adjustment deficits, including reduced social and explorative and greater anxiety behaviors.

RESULTS

BDNF loss in lower brain regions prior to hearing onset in *Bdnf*^{Pax} KOs

To validate the selective *Bdnf* deletion profile in *Bdnf*^{Pax2}KOs, which show deficits in auditory acuity (Chumak et al., 2016), the *Pax2*Cre driver line (Figure 1-figure supplement 1a, in red) was compared to the *TrkC*Cre driver line, using ROSA26 reporter mice (Figure 1-figure supplement 1d, in red, (Funfschilling et al., 2004)), with the knowledge that *Bdnf*^{TrkC}KOs exhibit normal hearing quality (Chumak et al., 2016). In ROSA26 *Pax2*Cre animals, ß-galactosidase (**ß-gal**) staining was observed at the levels of the organ of Corti, the spiral ganglion neurons, and the inferior colliculus (**IC**), but not in the hippocampus and auditory cortex (**AC**) (Figure 1-figure supplement 1b). In ROSA26 *TrkC*Cre animals, no ß-gal-positive neurons were detected at the level of the organ of Corti, while they were observed in spiral ganglion neurons, the IC, the AC and the hippocampus (Figure 1-figure supplement 1c).

In conclusion, auditory acuity deficits in *Bdnf*^{Pax2}KOs are linked to BDNF depletion in Pax2-positive neurons of the cochlea, hind and midbrain regions but not in frontal brain regions.

Deficits in fast auditory coding in *Bdnf*^{Pax2}KOs

The diminished auditory acuity in *Bdnf*^{Pax2}KOs (Chumak et al., 2016; Zuccotti et al., 2012) was confirmed by the demonstration of mild but significant threshold elevations in response to click stimuli, noise bursts and pure tone stimuli (Figure 1a,b; click, noise-ABR, control $n = 26/52$ mice/ears; *Bdnf*^{Pax2}KO $n = 23/46$ mice/ears; $P = 0.002$, $P = 0.026$; f-ABR, control $n = 16/32$ mice/ears; *Bdnf*^{Pax2}KO $n = 16/32$ mice/ears; $P < 0.0001$). Analysis of suprathreshold peak-to-peak ABR waveform amplitudes in *Bdnf*^{Pax2}KOs (Figure 1c) indicated altered summed auditory nerve (**AN**) responses independent of outer hair cell function, with significant declines in summed AN activity

(ABR wave I) and its spreading midbrain response (ABR wave IV), compared to controls (Figure 1d; wave I/IV: control $n = 14/28$ mice/ears, *Bdnf*^{Pax2}KO $n = 14/28$ mice/ears, $P < 0.0001$, $P < 0.0001$). Reduced early and late sound-induced response amplitudes in *Bdnf*^{Pax2}KOs were linked with significantly shortened ABR wave I latencies and delayed ABR wave IV latencies in comparison to controls (Figure 1e, wave I/IV: control $n = 14/28$ mice/ears, *Bdnf*^{Pax2}KO $n = 12/24$ mice/ears, $P < 0.0001$, $P < 0.0001$), indicating less optimized temporal processing in auditory fibers.

Temporal processing is critical for proper coding of amplitude-modulated (**AM**) tones. When responses to AM stimuli were analyzed dependent on modulation depth in *Bdnf*^{Pax2}KOs, a significantly reduced auditory steady state response (**ASSR**) > 10 % was noted in comparison to controls (Figure 1f; control $n = 10/10$ mice/ears each, $P = 0.001$). When these ASSR were analyzed dependent on the stimulus level in a phase-locked manner, responses in *Bdnf*^{Pax2}KO mice remained reduced, particularly for low sound pressure levels close to threshold (Figure 1g; $n = 10/10$ mice/ears, $P < 0.0001$, significant Bonferroni *post hoc* test from 15 to 40 dB SL). This indicated impaired AM coding and resolution, particularly at close to threshold sound intensities. To further characterize auditory processing, we elicited acoustic startle responses (**ASR**) that, through different lead times between prepulse and startle stimuli, can provide insight into central temporal resolution deficits. Prepulse inhibition (**PPI)** was induced with a 50 ms lead time, while prepulse facilitation (**PPF)** was induced with a 6 ms lead time prior to the startle stimulus. While *Bdnf*^{Pax2}KOs showed a decreasing ASR change in PPI with increasing prepulse intensity similar to that of the controls (Figure 1h, control $n = 7$, *Bdnf*^{Pax2}KO $n = 9$, $P = 0.869$), PPF was nearly absent in *Bdnf*^{Pax2}KOs (Figure 1i, control $n = 7$, *Bdnf*^{Pax2}KO $n = 9$, $P = 0.029$).

In conclusion, *Bdnf*^{Pax2}KOs show severe deficits in central coding of fast auditory information.

Maturation deficits of the PV-IN network and elevated Arc/Arg3.1 levels in the AC, but not somatosensory cortex, in *Bdnf*^{Pax2}KOs without changes in local BDNF levels

Reduced PV levels in the IC and preliminary observations on changes in PV levels in the AC of *Bdnf*^{Pax2}KOs (Chumak et al., 2016) motivated us to codetect PV protein together with the excitability marker Arc/Arg3.1, which defines α-amino-3-hydroxy-5-methyl-4-isoxazolepropionic acid receptor (**AMPAR**)-mediated spine plasticity. Using the Geisler method to codetect mRNA and protein, significantly reduced PV protein levels were found in the AC of *Bdnf*^{Pax2}KOs together with significantly elevated Arc/Arg3.1 mRNA (blue) (Figure 2a; Arc/Arg3.1 mRNA: $n = 5$ each, $P = 0.028$, PV protein: $n = 5$ each, $P < 0.0001$) and Arc/Arg3.1 protein (Figure 2b; $n = 4$ each, $P = 0.045$), despite constant levels of BDNF mRNA (Figure 2b; $n = 5$ each, $P = 0.243$). The reduced PV immunostaining was accompanied by significantly reduced PV-positive neurite arborizations, as shown in cortical layer III/IV of the AC, the main termination field of thalamocortical axons from the ventral medial geniculate (Malmierca & Merchan, 2004) (Figure 2a; high magnification). Furthermore, we found decreased PV-positive perisomatic contacts, exemplarily shown for layer III/IV of the AC (Figure 2c; arrow and inset, $n = 5$ each, $P < 0.001$). The altered PV expression pattern in the AC between controls and *Bdnf*^{Pax2}KOs was detected from hearing onset onwards, shown here for the AC at P14 (Figure 2d; $n = 5$ each, $P < 0.001$). The specificity of the PV-IN changes in the auditory circuits was supported by a lack of change in the PV-IN network in the somatosensory cortex (**SSC**), where vesicular

glutamate receptor (**vGluT**) 2 labeling confirmed normal column formation (Figure 2e) with no differences in PV-IN arborizations (Figure 2f; $n = 5$ each, $P = 0.303$).

In conclusion, in *Bdnf*^{Pax2}KOs, diminished maturation of PV-IN networks occurs with hearing onset in the AC but not in the SSC. Furthermore, Arc/Arg3.1 mRNA and protein levels were enhanced in AC pyramidal neurons in *Bdnf*^{Pax2}KOs, whereas BDNF mRNA levels were normal.

Maturation deficits of the PV-IN network and elevated Arc/Arg3.1 levels in the hippocampus in *Bdnf*^{Pax2}KOs without changes in local BDNF levels

During behaviorally relevant auditory perception (Irvine, 2018) or during long-lasting adjustments to enriched or traumatic auditory input (Matt et al., 2018), the perforant path of the hippocampus is activated from auditory associated cortices during memory-linked hippocampal synaptic circuit changes. PV protein was therefore codetected with Arc/Arg3.1 and BDNF in the hippocampus (Figure 3, Figure 3-figure supplement 1). Elevated Arc/Arg3.1 mRNA (blue) in pyramidal neurons appeared together with a significantly reduced PV protein (red) level at the somatic and dendritic levels in all hippocampal regions in *Bdnf*^{Pax2}KOs, shown for CA1 (Figure 3a; Arc/Arg3.1 mRNA: $n = 4$ each, $P = 0.042$; PV protein: $n = 4$ each, $P < 0.001$) and CA3 (Figure 3-figure supplement 1a; Arc/Arg3.1 mRNA $n = 4$ each, $P = 0.013$, PV Protein: $n = 5$ each, $P = 0.026$). Arc/Arg3.1 protein levels were also significantly elevated, as shown for CA1 (Figure 3b; $n = 4$ each, $P < 0.001$) and CA3 (Figure 3-figure supplement 1b; $n = 5$ each, $P = 0.006$). However, no differences in BDNF mRNA levels were observed in the same sections (Figure 3b, Figure 3-figure supplement 1b,c; CA1: $n = 4$ each, $P = 0.979$; CA3: $n = 5$ each, $P = 0.802$). The decline of PV immunostaining was accompanied by significantly reduced PV-positive neurite arborizations in the stratum radiatum in the CA1 region (Figure 3c and inset; $n = 5$ each, $P = 0.004$) and at the

mossy fibers level of the CA3 (Figure 3d and inset; $n = 6$ each, $P < 0.0001$), but not the cerebellum (Figure 3-figure supplement 1d; $n = 3$ each, $P = 0.331$).

To assess the onset of PV-IN changes in the *Bdnf*^{Pax2}KO hippocampus, we analyzed the PV expression levels at three ages: prior to hearing onset (P6-10), at the end of the critical developmental period of the auditory system at P14 (de Villers-Sidani, Chang, Bao, & Merzenich, 2007) and in adults. Controls showed a significant elevation of PV-immunoreactivity (**IR**) between P6-10 and P14 in the CA1 (Figure 4a; Genotype: $P < 0.0001$; Age: $P < 0.0001$) and CA3 (Figure 4b; $n = 4$-7, Genotype: $P < 0.0001$; Age: $P < 0.05$; interaction: $P < 0.001$). In contrast, PV-IR levels were reduced at all 3 ages in *Bdnf*^{Pax2}KOs.

In conclusion, in *Bdnf*^{Pax2}KOs, diminished maturation of PV-IN networks in the hippocampus occurred with hearing onset, while PV levels in the cerebellum remained unchanged. A reduced PV-IN network in *Bdnf*^{Pax2}KOs co-occurred with enhanced Arc/Arg3.1 mRNA and protein levels and unchanged BDNF mRNA in pyramidal hippocampal neurons.

Elevated LTP and failed LTP facilitation during sound adjustments in *Bdnf*^{Pax2}KOs, resembling elevated LTP prior to hearing onset in controls

The reduced PV-IN levels linked to elevated Arc/Arg3.1 mRNA and protein levels in the hippocampus in *Bdnf*^{Pax2}KOs might indicate an initial elevated stage of hyperexcitability of pyramidal neurons prior to maturation of PV-IN networks with hearing onset. To test this hypothesis, we recorded fEPSPs at the CA3 to CA1 Schaffer collateral in the stratum radiatum from acute forebrain slices of adult *Bdnf*^{Pax2}KOs and controls. Indeed, a significantly higher fEPSP amplitude was observed after stimulation (1 s, 100 Hz) of the Schaffer collateral in *Bdnf*^{Pax2}KOs (175.5 ± 5.7 %, $n = 9/13$ animals/slices) compared to controls (142.4 ± 8.2 %, $n = 9/14$ animals/slices) over the

entire recording time of 60 min (Figure 5a left panel). Calculation of the mean of the last 10 min showed that *Bdnf*^{Pax2}KOs exhibited significantly higher LTP (Figure 5a right panel; $P < 0.001$). When fEPSP slopes in acute brain slices were tested prior to hearing function, we found significantly elevated LTP in the P6-10 controls (171.6 ± 6.5 %, $n = 6/7$ animals/slices) relative to the adult controls but similar to that of *Bdnf*^{Pax2}KOs. This suggests that elevated LTP in adult *Bdnf*^{Pax2}KOs mirrors the initially elevated LTP prior to hearing onset, which are not shaped by the PV-network. As the PV-IN network has been suggested to mature in parallel with improved Hebbian plasticity in the first two postnatal weeks (Hu, Gan, & Jonas, 2014; Kimura & Itami, 2019; Turrigiano, 2012), we tested *Bdnf*^{Pax2}KOs for normal homeostatic facilitation responses as previously observed following an enriching sound (80-100 dB SPL), which had been shown to lead to enhanced LTP in parallel to improved or adjusted central auditory responsiveness (Matt et al., 2018). As shown in Figure 5b, controls responded to sound enrichment with elevated LTP in the CA1 region (142.4 ± 8.2 %, $n = 9/14$ animals/slices, $P < 0.05$), while *Bdnf*^{Pax2}KOs exhibited similarly elevated LTP levels with and without sound enrichment (172.9 ± 12.9 %, $n = 3/5$ animals/slices, $P > 0.05$). Under all conditions, neither controls, *Bdnf*^{Pax2}KOs, P6-10 controls nor sound-exposed animals exhibited changes in basal synaptic transmission. Furthermore, all groups displayed similar fEPSP amplitudes in response to a range of input strengths, as well as similar levels of paired-pulse facilitation, indicating that no changes in presynaptic function relative to controls might have caused the observed differences (Figure 5-figure supplement 1a,b; fEPSP input-output relation: $n = 3/5$-$9/14$ animals/slices each, $P = 0.54$; paired pulse facilitation: $n = 3/5$-$9/14$ animals/slices each, $P = 0.75$).

In conclusion, this suggests that in *Bdnf*^{Pax2}KOs, an initial elevated LTP persists and prevents dynamic activity changes during memory-linked homeostatic adjustment processing.

Diminished learning in *Bdnf*^{Pax2}KOs

Initially, enhanced LTP and altered sound–induced adjustments in *Bdnf*^{Pax2}KO may point to deficits in normal learning behavior. A learning paradigm was used in which adult mice, trained over 7 trials to have access to a reward (their own mouse house), learned to find their way to the reward by memorizing 7 decision points in a multiple T-maze (Figure 6a). The learning performance was measured after completion of a successful run by counting errors at the decision points of the maze in which the mice had been trained (see methods). As shown in Figure 6b, the *Bdnf*^{Pax2}KOs had a significantly higher median error rate in the four analyzed runs. The *Bdnf*^{Pax2}KOs made 1-67 errors at the end of the learning phase (run 7), while the controls made only 0-1 errors (Figure 6b $n = 8/9$ each, Run 2: $P < 0.001$; Run 7: $P < 0.001$; 3 d post: $P = 0.001$; 18 d post: $P = 0.002$). As most *Bdnf*^{Pax2}KOs displayed circling behaviors (Ernfors et al., 1994), the correlation of circling behaviors, motor activity and errors in the T-maze was explicitly tested. The circling behavior had neither an effect on the number of errors during run 2 and 7 in the T-maze (Figure 6-figure supplement 1a, $n = 8$, $R^2 = 0.039$) nor on the motor activity (Figure 6-figure supplement 1b, $n = 8$, $R^2 = 0.053$) which was significantly increased in *Bdnf*^{Pax2}KOs, measured on a ballistic platform in the startle apparatus (Figure 6-figure supplement 1c, $n = 7\text{-}9$ each, $P = 0.007$).

In conclusion, significant increases in learning errors in *Bdnf*^{Pax2}KOs together with enhanced LTP are a noticeable paradox that may be explained when considering that failed PV-network maturation with hearing onset may have prevented a typically

occurring diminution of LTP that improves the baseline for detection of memory-linked deviants and adjustments (Figure 8).

Reduced exploratory activity and enhanced anxiety-related responses in *Bdnf*^{Pax2}KOs

Increased learning errors may be linked to less explorative or social behavior. We used Crawley's sociability 3-chamber test (Figure 7a) to analyze social and explorative behaviors of controls and *Bdnf*^{Pax2}KOs through monitoring the time of sniffing contacts towards an empty cage or a cage with a stranger mouse normalized to the time they spent in the respective chamber. Controls spent more time sniffling towards the stranger mouse chamber than the empty chamber, while *Bdnf*^{Pax2}KOs did not show a preference between the two (Figure 7b, control: $n = 20$, $P = 0.027$; *Bdnf*^{Pax2}KO: $n = 20$, $P = 0.916$). Furthermore, *Bdnf*^{Pax2}KOs differed from controls in significantly reduced sniffing contacts towards both cages (Figure 7b, $n = 20$ each, stranger: $P < 0.0001$; empty: $P = 0.028$), although the averaged latency for the first entry into the empty or stranger chamber was not different between controls and *Bdnf*^{Pax2}KOs (Figure 7c, $n = 14$-19 each, stranger: $P = 0.486$; empty: $P = 0.104$). *Bdnf*^{Pax2}KOs exhibited significantly decreased numbers of entries into both chambers in comparison to controls (Figure 7d, $n = 14$-19 each, stranger: $P = 0.014$; empty: $P = 0.046$). Reduced explorative behavior is often linked to an enhanced anxiety response that can be indexed through, e.g., altered grooming, ultrasonic vocalizations **(USVs)** or corticosterone levels (Kromer et al., 2005). When analyzing freezing or self-grooming behaviors, *Bdnf*^{Pax2}KOs revealed a significant increase in spontaneous freezing (Figure 7e, $n = 20$ each, $P < 0.0001$) and self-grooming behaviors (Figure 7e, $n = 20$ each, $P < 0.0001$). The USV of nursing infants was tested next at P7, prior to hearing onset and thus a timepoint when auditory processing differences between control and

Bdnf^{Pax2}KOs should not be substantial. Our findings revealed significant abnormalities in the vocalization patterns between control and *Bdnf*^{Pax2}KO pups, as exemplarily depicted in Figure 7g,f. USV with multiple frequency jumps were more frequent in *Bdnf*^{Pax2}KO pups (Figure 7f, $n = 8$ each, Genotype: $P = 0.004$). Additionally, isolated *Bdnf*^{Pax2}KO pups showed increased numbers of all USV calls during a 5 min period (Figure 7 h, $n = 8$ each; $P < 0.001$), which indicated a higher index of anxiety (Groenink, Verdouw, van Oorschot, & Olivier, 2008; Kromer et al., 2005). Adult *Bdnf*^{Pax2}KOs were also characterized by significantly elevated basal corticosterone levels in comparison to controls (Figure 7i, $n = 13$ each, $P = 0.048$), suggesting that *Bdnf*^{Pax2}KOs exhibited increased anxiety behavior indicative of distress.

In conclusion, significant reductions in explorative behaviors and increases in freezing, self-grooming, juvenile USVs and stress levels in *Bdnf*^{Pax2}KOs point to enhanced anxiety behaviors and imbalanced stress control.

Overall, BDNF deletion in the cochlea, hindbrain, and midbrain under the *Pax2* promoter in *Bdnf*^{Pax2}KOs (Figure 8, left panel) led to developmental arrest at a critical step prior to hearing function when LTP was still elevated (Figure 8, left panel). As shown in the *Bdnf*^{Pax2}KOs, this prevents the critical maturation of fast auditory processing, an elevation of amplitudes of ABR waves, a shortening of ABR wave I, and maturation of the PV-IN network in the auditory and hippocampal paths (Figure 8, right panel). Therefore, baseline LTP and Arc/Arg3.1 levels fail to be set towards improved homeostatic adjustments, facilitated learning and fast novelty discrimination (Figure 8, right panel).

DISCUSSION

Here, we describe a domain-specific maturation deficit of the PV-IN dendritic network in *Bdnf*^{Pax2}KOs in the frontal auditory pathway and the hippocampus that is associated with fast auditory processing deficits, reduced learning and enhanced anxiety behavior. As BDNF in Pax2-IN precursor cells migrates from ventricular progenitor zones to lower level brain regions posterior to the midbrain, different from IN precursors that migrate to frontal brain regions, *Bdnf* in Pax2-expressing neurons drive PV-dendritic network maturation in frontal auditory-related circuits indirectly, likely through fast auditory processing that, through PV-dendritic network maturation, shapes hippocampal LTP and Arc/Arg3.1 baseline levels, thereby providing a new mechanism of how sensory information guides task-specific learning behavior and plasticity across auditory modalities with sensory experience.

Rapid auditory processing (RAP) deficits with hearing onset in *Bdnf*^{Pax2}KOs

Here, we report that the deletion of BDNF under the *Pax2* promoter leads to reduced suprathreshold ABR waves and latency shifts, despite a normal basal hearing performance. This indicates that basic sound processing through low-spontaneous rate (**SR**)**,** high-threshold auditory fibers that develop prior to hearing onset (Grant, Yi, & Glowatzki, 2010) is well established in *Bdnf*^{Pax2}KOs. This is confirmed through normal coding of the envelope of sound stimuli (ASSR) at higher intensity sound pressure levels in *Bdnf*^{Pax2}KOs (Figure 1g), a coding performance that requires intact, low-SR, high threshold fiber function (Bharadwaj, Verhulst, Shaheen, Liberman, & Shinn-Cunningham, 2014). In *Bdnf*^{Pax2}KOs, however, the high-SR, low-threshold auditory fiber characteristics appear to be less developed. These high-SR fibers, which promote the sharp rise times of EPSPs, can be recorded only after hearing onset (Grant et al., 2010). The high-SR fibers also participate in producing the shortest latencies of sound stimulus responses for all characteristic frequencies and define

lowest-detection thresholds (Heil, Neubauer, Brown, & Irvine, 2008). Thus, the elevated ABR thresholds, reduced ABR wave amplitudes and prolonged late-ABR waves observed in *Bdnf*^{Pax2}KOs (Figure 1a-e) are best explained by the less developed high-SR fiber characteristics. Moreover, the shortened auditory fiber latencies of ABR wave I in *Bdnf*^{Pax2}KOs may indicate less developed efferent tonic dopaminergic shaping of these high-SR auditory fibers. Accordingly, tonic dopaminergic shaping occurs particularly in high-SR fibers, and when functionally compromised, summed AN activity is reduced and spontaneous firing rates are elevated (Ruel et al., 2001), both consistent with reduced and shortened ABR wave I in *Bdnf*^{Pax2}KOs (Figure 1e). Deficits in the maturation of high-SR fiber response behaviors in *Bdnf*^{Pax2}KOs might also explain the reduced ASSR responses, particularly at low sound intensities (Figure 1g), as high-SR fibers contribute to ASSR in quiet (Paul, Bruce, & Roberts, 2017).

Last, in addition to elevated thresholds, increased latencies and reduced response amplitudes in *Bdnf*^{Pax2}KOs (present study, (Chumak et al., 2016)), we also observed deficits in the processing outcome of short gaps through impaired PPF, underlining characteristic RAP deficits in the *Bdnf*^{Pax2}KOs. Thus, deficits in the processing outcome of particular short gaps during PPF with lead times of 6 ms are impaired in *Bdnf*^{Pax2}KOs, while PPI with lead times of 50 ms were normal (Figure 1h,i). These overall auditory processing deficits suggest that *Bdnf*^{Pax2}KOs suffer from RAP disorder often observed, e.g., in children with autism spectrum disorders (**ASD**) or in children with early prenatal brain injuries, in particular in lower brain regions (Fitch, Alexander, & Threlkeld, 2013).

Deletion of BDNF in Pax2 inhibitory precursor cells in lower brain regions drives maturation of inhibitory PV-IN networks in frontal brain regions in *Bdnf*^{Pax2}KOs

Deficits in PV-networks in frontal brain regions, such as the AC and hippocampus, as observed in *Bdnf*^{Pax2}KOs, are unlikely to be directly linked to a role of BDNF in the migration or differentiation of PV-inhibitory neurons in the frontal brain, as Pax2 has been shown to be confined to prospective GABA-IN precursor cells that migrate posterior to midbrain regions within the first 2 postnatal weeks (Fotaki et al., 2008; Maricich & Herrup, 1999). IN cells in the cortex or hippocampus instead migrate from progenitor zones in subpallidal regions expressing transcription factors different from Pax2, e.g., Nkx2.1, Pa6 or Gsh2 (Marin & Rubenstein, 2001). Accordingly, ROSA26 *Pax2*Cre does not express ß-Gal in frontal brain regions (Figure 1-figure supplement 1), and no BDNF deletion is found in *Bdnf*^{Pax2}KOs (Zuccotti et al., 2012) (Figure 2,3, Figure 3-figure supplement 1).

Moreover, BDNF is upregulated in neurons of the cochlea and the ascending auditory pathway between P4 and the 2nd postnatal week (Singer et al. 2014), and Pax2 declines in regions posterior to the midbrain up to P15 (Fotaki et al., 2008; Maricich & Herrup, 1999). BDNF activities that define the *Bdnf*^{Pax2}KO phenotype occur around the 2nd postnatal week, the time of hearing onset (de Villers-Sidani et al., 2007). This is the time when an initial hyperexcitability stage is described in the brain, caused by functional GABAergic contacts that are initially excitatory (Ben-Ari, 2002; Marin & Rubenstein, 2001). In the auditory system, GABAergic neurons switch in a region-specific way from depolarization to hyperpolarization within the first two postnatal weeks (De Koninck, 2007; Friauf, Rust, Schulenborg, & Hirtz, 2011; Owens & Kriegstein, 2002), a process likely driven by sensory experience (Shibata, Kakazu, Okabe, Fukuda, & Nabekura, 2004; Vale & Sanes, 2002) and influenced by BDNF (De Koninck, 2007; Owens & Kriegstein, 2002). BDNF is assumed to facilitate the expression of potassium chloride cotransporter 2 (**KCC2**), which defines the membrane potential of GABA through a low intracellular chloride concentration (De

Koninck, 2007). It is challenging to consider that KCC2 membrane expression may need a critical fast auditory driving force with sensory experience that is **not** provided in *Bdnf*^{Pax2}KOs, a feature that needs to be clarified in future studies.

Finally, BDNF levels in frontal regions are not changed in *Bdnf*^{Pax2}KOs although dendritic complexity in the AC and hippocampus is reduced in the mutants. We therefore predict that a fast auditory driving force, generated under the control of BDNF in Pax2-positive inhibitory precursor cells, is essential to facilitate local BDNF release from cortical neurons, which is shown to control the dendritic complexity of cortical PV-INs during auditory receptive field maturation (Xu et al., 2010).

***BDNF*^{Pax2}KOs exhibit elevated hippocampal LTP, elevated Arc/Arg3.1, learning impairments, and altered explorative and anxiety behaviors**

In *Bdnf*^{Pax2}KOs, the maturation and elevation of the dendritic complexity of the PV-IN network between P10 and P14 is significantly diminished in the AC (shown for layer III and IV) and hippocampus (Figure 2,3, Figure 3-figure supplement 1). This is the most critical time period of the auditory system, as between P10 and P14, cortical neural thresholds and responses to sound mature together with the improved shortening of latencies of cortical neurons at the end of the second postnatal week (de Villers-Sidani et al., 2007; Froemke et al., 2007) and the dendritic complexity of cortical PV-INs matures with sensory experience dependent on local BDNF release from projection neurons, as shown for the AC (Hong et al., 2008; Xu et al., 2010), SSC (Jiao et al., 2011) or visual cortex (Itami, Kimura, & Nakamura, 2007; Xu et al., 2010).

This is also the time when under control of early auditory experience precise thalamic (MGB) input terminating on layer IV neurons in primary AC drive an intracortical circuit of serotonergic (Takesian et al., 2018) and cholinergic inputs (Letzkus et al., 2011) in

layer I IN that induces disinhibition of layer IV pyramidal neurons through PV IN suppression, enabling from that time onwards an integration of contextual signals with specific auditory stimuli. The significant decline of PV staining on layer IV in primary AC pyramidal neurons (Figure 2) and the inconspicuous PV staining levels in the cerebellum and SSC, as observed in *Bdnf*^{Pax2}KOs, underscore the modality or domain specificity may indicate a possible domain specificity for BDNF in Pax2-positive cells preferential for the auditory system, although visual processing deficits have not yet been analyzed. While further studies are essential to analyze auditory domain specificity in *Bdnf*^{Pax2}KOs in more detail, we cannot exclude a preferential isolated auditory modality deficit. Thus, RAP difficulties described in children with ASD, who have mostly temporal deficits isolated to the auditory modality, with normal tactile processing (Ganesan, Khan, Garel, Hamalainen, & Kenet, 2016; Marco et al., 2012) and normal visual processing (Foss-Feig, Schauder, Key, Wallace, & Stone, 2017), separating ASD from disorders where both language and temporal processing are affected.

Indeed, deficits may be particularly profound when they occur in neural substrates upon which a critical and distributed cognitive process such as temporal processing, e.g., the ability to process rapidly changing acoustic information, is built.

Within this view, the observed initial elevated excitability in the hippocampus of *Bdnf*^{Pax2}KOs may particularly impair the processing of rapidly changing information. The diminished auditory processing in *Bdnf*^{Pax2}KOs would reach the hippocampus through indirect connections from the associated AC projecting to the entorhinal cortex (Amaral, Scharfman, & Lavenex, 2007). *Bdnf*^{Pax2}KOs appear to be arrested at a developmental stage prior to PV-IN maturation (Figure 5a). Under these conditions, hippocampal CA1 neurons would be less shaped by the PV-IN network and thereby respond to stimuli with lower thresholds, explaining the elevated LTP in *Bdnf*^{Pax2}KOs

(Figure 5a). In controls, CA1 neurons are shaped by PV-IN after hearing onset and are therefore expected to establish an improved signal-to-noise ratio and a widened dynamic range (Hu et al., 2014), a process that would also enhance the range to which activity can be further adjusted (Hu et al., 2014; Kimura & Itami, 2019; Turrigiano, 2012).

This would explain the failure to further mobilize LTP in *Bdnf*^{Pax2}KOs following sound enrichment (Figure 5b), as observed in controls (Figure 5b) and previous studies (Matt et al., 2018). This would also explain the elevated immediate *Arc/Arg3.1* early gene expression levels in *Bdnf*^{Pax2}KOs (Figure 3, Supplementary 2) - the 'master regulator' of synaptic plasticity during information processing (Shepherd & Bear, 2011) - which are expected to be influenced through neuron conductance. Typically, glutamate-induced stimulation of hippocampal projection neurons enables a remarkably fast (~15 s) Arc/Arg3.1 translation in postsynaptic excitatory synapses that leads to a rapid removal of postsynaptic AMPAR and a subsequent weakening of synapses (Waung, Pfeiffer, Nosyreva, Ronesi, & Huber, 2008). In *Bdnf*^{Pax2}KOs, elevated LTP and overall enhanced excitability may maintain elevated basic Arc/Arg3.1 mRNA and protein levels (Figure 2,3, Supplementary 2), thereby hampering the stimulus-induced weakening of synapses, as stimuli would be unable to further enhance Arc/Arg.3.1 translation. This is expected to hamper the fast weakening of synapses and thus diminish the fast processing of novel experiences and contrast amplifications (Kimura & Itami, 2019). The described deficit in the learning of decision points in the multiple T-maze (Figure 6) and the significantly reduced explorative behavior (Figure 7a-c), as well as the increased stereotype self-grooming, USVs and corticosterone levels (Figure 7d-f), are thus likely the result of an inappropriate baseline for adjustments or attention-driven contrast amplification. Indeed, adjustment of activity levels relative to a 'setpoint' is essential for any learning-related change in synaptic input where

strengthening of synapses occurs through unconstrained positive feedback cycles that drive neuronal activity to optimize output for that circuit (for a review see (Turrigiano, 2012)).

A failure to establish an appropriate baseline for adjustment or attention-driven contrast amplification has not yet been described in the context of cognitive disease phenotypes, such as ASD. Indeed, RAP deficits (Foss-Feig et al., 2017), reduced PV-IN levels (Goel et al., 2019; Korb & Finkbeiner, 2011; Mohn et al., 2014; Pirone et al., 2017) and correlated gamma and beta oscillation differences(Wenhart, Bethlehem, Baron-Cohen, & Altenmuller, 2019), elevated Arc/Arg3.1 levels and learning deficits (Goel et al., 2019; Korb & Finkbeiner, 2011; Mohn et al., 2014; Pirone et al., 2017), as well as elevated corticosterone levels (Das, Estevez, Sarkar, & Banerjee-Basu, 2019), deficits in explorative behavior, increased self-grooming or enhanced levels to emit USVs or enhanced motor activity (Schmeisser et al., 2012) all characteristics of *Bdnf*^{Pax2}KOs have been previously linked with an autism-like phenotype. The finding provides also crucial new insight in the complex function of BDNF predicted to play for neurodevelopmental (Ohja et al., 2018; Saghazadeh, Mahmoudi, Dehghani Ashkezari, Oliaie Rezaie, & Rezaei, 2017) and neuropsychiatric disorders (Autry & Monteggia, 2012). Here BDNF in lower hindbrain regions may be reconsidered as prerequisite to enable the engaging of contextual (auditory) signals paired with training that are needed to enhance plasticity from early development onwards.

Conclusion

A novel role of BDNF in the inhibitory neurons of lower auditory brain regions that shapes, along with sensory experience, the baseline for learning dependent adjustments and improved auditory skills by driving PV-IN networks has to be considered. This finding provides new insights into the relationship between sensory processing deficits in the auditory system and impaired perceptional learning.

METHODS

Care and use of mice and the experimental protocol were reviewed and approved by the University of Tübingen, Veterinary Care Unit, and the Animal Care and Ethics Committee of the regional board of the Federal State Government of Baden-Württemberg, Germany, and followed the guidelines of the European Union Directive 2010/63/EU for animal experiments.

Animals. *Bdnf*^{Pax2}KO and control mice were obtained by crossing a Cre line, in which Cre is expressed under the promoter of the *Pax2* gene and a mouse line in which the protein coding *Bdnf-exon IX* is flanked by *lox P* sites. Both lines were obtained by the Mutant Mouse Regional Research Center, MMRRC. (Ohyama & Groves, 2004; Rios et al., 2001; Zuccotti et al., 2012). *Bdnf*^{TrkC} KO mice were generated by crossing a *TrkC*Cre line (Funfschilling et al., 2004) with the same *Bdnf* lox/lox line as above. To verify the deletion pattern of *Bdnf*, *TrkC*Cre mice and *Pax2*Cre mice were crossed with ROSA26 (Reverse Oriented Splice Acceptor, Clone 26) reporter mice as previously described (Chumak et al., 2016; Zuccotti et al., 2012). β-Galactosidase activity was analyzed in adult ROSA26 *Pax2*Cre and ROSA26 *TrkC*Cre mice through immunohistochemistry with an anti-β-galactosidase antibody as described in methods part “immunohistochemistry”. Deletion of the *Bdnf* gene in distinct brain areas of *Bdnf*^{Pax2}KO and *Bdnf*^{TrkC} KO was verified by Northern and Western blots. Genotyping of the mouse lines were performed as described (Rios et al., 2001). For all experiments mice of either sex were used. Sample size were chosen with the experience of previous publications, recommendations in literature and on the basis of the expected effect size n calculated with G power.

Hearing measurements and sound exposure. The hearing function of 1-6 months old *Bdnf*^{Pax2}KO and controls of both sexes was studied by measuring auditory

brainstem responses (ABR) and auditory steady state responses (ASSR), as previously described (Rüttiger et al., 2013; Zuccotti et al., 2012). In short, ABR thresholds were determined with click (100 µs), noise burst (1 ms), or pure tone stimuli (3 ms, including 1 ms cosine squared rise and fall envelope, 2 – 32 kHz). Auditory steady state responses were measured with amplitude-modulated sinusoidal stimuli using a 11.3 kHz carrier and modulation frequencies between 64 – 2048 Hz with one step per octave. At a fixed modulation frequency of 512 Hz at 40 dB above threshold (Decibel sensation level, dB SL), responses to 552 modulation depths between 0 % (unmodulated), and 0.78 % to 100 % modulation indices (in half-553 octave steps) were recorded. For I-O functions the carrier level ranged from -10 to 60 dB SL. During hearing measurements, animals were anesthetized with an intraperitoneal injection of a mixture of opioid agonist fentanyl (0.05 mg/kg bodyweight, Fentadon®; Albrecht GmbH, Aulendorf, Germany), benzodiazepine midazolam (2.5 mg/kg body weight, Midazolam-hameln®; Hameln Pharma plus GmbH, Hameln, Germany), 2-adrenoceptoragonist medetomidin (0.5 mg/kg bodyweight, Sedator®; Albrecht GmbH, Aulendorf, Germany) and atropinesulfate (0.2 mg/kg body weight, B. Braun, Melsungen, Germany). Additional doses of anesthetics were administered if needed. For enriching sound exposure, animals were exposed to 10 kHz for 40 min at 80-100 dB SPL while under anesthesia.

Acoustic startle response and prepulse inhibition. Apparatus: Startle response was measured with a piezoelectric force transducer situated inside a sound-attenuated chamber lit by a 5-W cold light bulb. The apparatus consisted of a measuring platform on which the test cage was fastened. The test cage was a 5 x 9 x 5 cm wire mesh cage with a metal floor plate. The output of the transducer was amplified and filtered from 2 to 150 Hz (University of Tuebingen, Piezo-Amp-System, Tuebingen, Germany). The

resulting voltage was sampled (1 kHz) by an analog-to-digital converter located within a computer (Microstar DAP 1200, Washington, DC), results are given in mN (milli-Newton). Acoustic stimuli and steady white background noise were generated by a computer with a digital signal processor board (Medav, SigGen, Uttenreuth, Germany) and delivered through a loudspeaker (Visaton HTM 5.6, Haan, Germany) placed at a distance of 35 cm from the test cage inside the sound-attenuated chamber. The SPL within the cage was measured with a 0.5-in. (1.3 cm) condenser microphone (Brüel and Kjaer, Model 4113, Naerum, Denmark) with a measuring amplifier (Brüel and Kjaer, Model 2606). The level of the startle stimuli was 105 dB SPL PEAK, the level of the background noise was 32 dB SPL root mean square (RMS) relative to 0.02 mPa. Startle stimuli were presented with an interval of 15 sec.

Procedure: Mice were tested in one of four identical chambers. During the experiment, the mice were observed via a video camera. On two days the mice were given 5 min to adapt to the experimental environment inside the sound-attenuated chamber, then 20 startle stimuli were given which were not included in evaluation. On the day preceding testing mice were put back into their home cages, on the testing day a series of testing stimuli immediately followed the adaption period. PPI prepulses had a lead time of 50 ms and a duration of 20 ms. PPF prepulses had a lead time of 6 ms and a duration of 6 ms. Prepulses had a SPL of 35, 45, 55 or 65 dB RMS. Each prepulse condition was presented 20 times, control stimuli without prepulse were presented 60 times in pseudorandom order.

Measurement: The force of the mouse movement was measured in 3 time windows: first, 50 ms before any stimulation; second, 50 ms after the first time window during a period where sometimes prepulses were given; third, 50 ms after startle stimulus onset or in case of no stimulation (first 5 min of the experiment) at the same point of time

(15 s after previous trigger). In each time window the peak-to-peak force was calculated. Motor activity was measured in the first time window. Startle amplitude was calculated as the difference of the peak-to-peak force after stimulus onset diminished by the measure of the spontaneous motor activity in the respective time window 100 ms earlier. For each mouse and each stimulus condition the startle responses were averaged. If the control startle amplitude was below 25 mN, the respective mouse was discarded from PPI and PPF evaluation; this was the case in three *control* mice. Prepulse facilitation was calculated as difference between startle amplitudes to stimuli with PPF prepulses and control stimuli without prepulses. This was done for each mouse and stimulus condition and then averaged over mice. PPI was calculated as relative difference, i.e. for each mouse the respective difference was divided by its control response.

Multiple T-maze. The maze consisted of nine equally sized T-elements (Lange-Asschenfeldt, Lohmann, & Riepe, 2007) made of 0.4 cm thick grey PVC. Each arm of a T-element measured 8 cm in length and 4.5 cm in width. The maze also included a start element (14 x 4.5 cm) and a target platform (19 x 12.6 cm). Each element was mounted on a foot stand; total element height was 23 cm and the maze was set up on a 75 cm high table. The maze was arranged as shown in Figure 2. The number of decision points on the path from the start to the target platform was seven, including four left and three right turns (order: LRRLLRL). Elements were placed next to each other and taped together on the underside. The mouse house (Tecniplast, Italy) from the home cage of each mouse was placed on the target platform before each trial. Mice were trained on the maze for three consecutive days. On the first and second day, each mouse had three runs. The sequence in which the mice were placed on the maze was pseudorandomized and then maintained throughout the experiment. If a

mouse reached the target platform within the time limit of ten minutes, it was scored as a successful run; if not, the trial was terminated. Mice were returned to their home cage after each run. On the third training day, each mouse had to perform as many runs as necessary until it reached the criterion of seven successful training runs. Mice were re-tested twice after a break of 3 and 18 days after their last training run, respectively. Experiments were performed during the light phase between 10 am and 6 pm. After each run, the maze was cleaned with 70% ethanol. The average light intensity on the maze was 75 lux.

Field excitatory postsynaptic potential (fEPSP) recordings in hippocampal slices. Extracellular fEPSP recordings were performed according to standard methods as previously described (Chenaux et al., 2016; Matt et al., 2011).

In brief: 400 µm thick brain slices were cut on a vibratome (Leica VT 1000S) while submerged in ice-cold dissection buffer (composition in mM) 127 NaCl, 1.9 KCl, 1.2 KH_2PO_4, 26 $NaHCO_3$, 10 D-glucose, 23 $MgSO_4$, and 1.1 $CaCl_2$, saturated with 5% CO_2 and 95% O_2 (pH 7.4). Slices were incubated in oxygenated artificial cerebrospinal fluid (ACSF, in mM: 127 NaCl, 26 $NaHCO_3$, 1.2 KH_2PO_4, 1.9 KCl, 2.2$CaCl_2$, 1 $MgSO_4$ and 10 D-glucose; pH 7.4) for 1 h at 30°C and then stored at room temperature. Recordings were performed in a submerged-type recording chamber (Warner Instruments). Stimulation (ACSF-filled glass pipettes, 2-3 MΩ) and recording electrodes (TM53CCINS, WPI) were positioned in the stratum radiatum to record Schaffer collateral fEPSPs. Signals were amplified with an Axopatch 200B (Molecular Devices), digitized at 5 kHz with an ITC-16 (HEKA) and recorded using WinWCP from the Strathclyde Electrophysiology Suite. Stimuli (100 µs) were delivered through a stimulus isolator (WPI). The same stimulus intensity was used during baseline recording (0.067 Hz) and induction of long-term potentiation (LTP) using 100 stimuli

given at 100 Hz (1 sec). The baseline was determined by the average of fEPSP initial slopes from the period before the tetanus. The level of LTP was determined by the average of fEPSP initial slopes from the period between 50 and 60 min after the tetanus. Before tetanic stimulation or wash-in, each slice was used to record input-output relation (IOR) and paired-pulse facilitation (PPF) at the same stimulation strength as LTP recordings. Four traces were averaged for each data point.

Social interaction test. The apparatus for Crawley's sociability (Silverman, Yang, Lord, & Crawley, 2010) test consisted of a rectangular three-chamber box made of PVC in which each compartment had a ground area of 19 x 45 cm in size. In the outer chambers two identical wire cup-like containers were placed. In one of these containers a “stranger” (mouse of the same background, age and gender but without prior contact to the subject mouse) was placed randomly. In the other chamber, an empty wire cup-like container worked as a novel object without housing a mouse. The experimental mouse was placed at the center of the middle compartment for 5 minutes to adapt, while the lateral compartments were isolated by dividing walls. The walls were removed and the experimental mouse was allowed to discover all three chambers for 10 minutes. The behavioral testing was performed between 9:00 am and 5:00 pm. After each trial, the chambers were cleaned and disinfected with ethanol.

Ultrasonic vocalization. Ultrasonic vocalizations (USV) of P7 pups were recorded to analyze the reaction of short (5 min) separation from the parental cage as described in (Groenink et al., 2008; Kromer et al., 2005). The pups were randomly selected, the body weight was measured and the single animal was placed on a fresh paper towel in the middle of a plastic box (13 x 13 cm) in a soundproofed chamber with constant temperature of 23 ± 1°C. An ultrasonic microphone (Neutrix), connected with a preamplifier (Avisoft UltraSoundGate416) was fixed with a distance of 12 cm from the

middle of the experimental box. For recording, Avisoft (Avisoft Bioacoustic RECORDER Version 4.2.29) was used with a sampling rate of 250 kHz which allows a frequency range from 0 to 125 kHz. With SASlab (Avisoft-SASLabPro Version 5.2.13) a spectrogram of the recordings was calculated and manually the number of calls was counted.

Blood corticosterone level analysis. Blood was collected from the tail vein of anesthetized mice, centrifuged and stored at -80°C. The corticosterone concentration in the blood was measured by using a Corticosterone ELISA Kit (Enzo Life Sciences, Farmingdale, NY, USA). The optical density of the samples finally was read at 405 nm in the FLUOstar Optima (BMG LABTECH GmbH, Ortenberg, Version 2.20). To rule out major influences of the circadian rhythm, all blood was taken in the afternoon (3:00 and 5:00 pm) and the experimental groups were equally distributed in terms of daytime.

Tissue preparation. For immunohistochemistry, cochleae were isolated, prepared, cryosectioned at 10 µm, and mounted on SuperFrost*/plus microscope slides at –20 °C as previously described (Knipper et al., 2000). Brain tissue for immunohistochemistry was prepared and sectioned with a vibratome at 60 µm and stored free floating at -20°C as previously described (Singer, Geisler, Panford-Walsh, & Knipper, 2016). For RNA and protein isolation, different brain regions were dissected with small forceps, immediately frozen in liquid nitrogen, and stored at -80°C before use.

Colocalization of mRNA and Protein in Brain Sections. mRNA and protein were colocalized on free-floating brain sections as previously described (Singer et al., 2014). In brief, following prehybridization for 1 h at 37 °C, sections were incubated overnight with BDNF or Arc/Arg3.1 riboprobes at 56 °C, incubated with antidigoxigenin antibody

conjugated to alkaline phosphatase (anti-Dig-AP, Roche, Germany, 11093274910), and developed as previously described (Singer, Geisler, & Knipper, 2013). For protein detection, streptavidin–biotin was blocked according to the manufacturer's instructions (Streptavidin–Biotin Blocking Kit, Vector Laboratories, USA) after blocking endogenous peroxidase. Sections were incubated overnight at 4 °C with the primary antibodies against Arc/Arg3.1 (Synaptic Systems, Germany, anti-rabbit, 1:200, 156003) (Nikolaienko, Patil, Eriksen, & Bramham, 2018) or Parvalbumin (Abcam, United Kingdom, anti-rabbit, 1:500, ab11427), followed by incubation with the secondary antibody (biotinylated goat anti-rabbit, Vector Laboratories, BA-1000) and chromogenic detection (AEC, 3-amino-9-ethylcarbazole, Vector Laboratories, SK-4200). Sections were coverslipped with gelatin, and analyzed using a BX61 microscope (Olympus, Japan).

Immunohistochemistry. For fluorescence-immunohistochemistry, mouse cochlea and brain sections were stained as described (Singer et al., 2016; Tan et al., 2007). Antibodies directed against BDNF (Santa Cruz, United States, anti-rabbit, 1:200, SC20981), β-galactosidase (Promega, Germany, anti-mouse, 1:100, Z3781), GFAP (Agilent Dako, United States, anti-rabbit, 1:2000, Z0334), Neurofilament 200 (Sigma-Aldrich, United States, anti-mouse, 1:8000, N0142), Parvalbumin (Abcam, United Kingdom, anti-rabbit, 1:2000, ab11427) and vGluT2 (Synaptic Systems, Germany, anti-mouse, 1:500, 135421) and were used and detected using appropriate Alexa 488 (Molecular Probes, Germany, 1:500, A11001) and Cy3 (Jackson Immuno Research Europe, United Kingdom, 1:500, 711-166-152) conjugated secondary antibodies. Sections were viewed by a BX61 microscope (Olympus, Japan) as previously described (Zampini et al., 2010).

Data analyses

Statistics and Numbers. All statistical information and n numbers can be found in the results part and in Supplementary Tables 2, 3. In figures, significance is indicated by asterisks (∗ $P < 0.05$, ∗∗ $P < 0.01$, ∗∗∗ $P < 0.001$, **** $P < 0.0001$). n.s. denotes non-significant results ($P > 0.05$).

Colocalization of mRNA and Protein in Brain Sections. Brain sections were quantified by integrating density values of color pixels for each single specimen using ImageJ software. The density values of all specimens stained within the same experiment were then normalized to the group mean (i.e. all hippocampal brain sections stained in the same experiment gave an average value of 1.0). This correction allowed to compensate for the high inter-trial variation of staining intensity. Within every single experiment, the same number of control and *Bdnf*^{Pax2}KO sections were stained by the same experimenter. These sections were in parallel exposed to the identical solutions, antibody concentration, temperature, and environmental variations. All sections from one mouse were then averaged and entered the statistical evaluation as n = 1.

Immunohistochemistry. Brain sections were quantified by integrating density values of color pixels for each single specimen using ImageJ software. The density values of all specimens stained within the same experiment were then normalized to the group mean (i.e. all hippocampal brain sections stained in the same experiment gave an average value of 1.0) or in case of development studies they were normalized to all animals in the age of P6-10. This correction allowed to compensate for the high inter-trial variation of staining intensity. Within every single experiment, the same number of control and *Bdnf*^{Pax2}KO sections were stained by the same experimenter. These sections were in parallel exposed to the identical solutions, antibody concentration,

temperature, and environmental variations. All sections from one mouse were then averaged and entered the statistical evaluation as n = 1.

Hearing measurements. Click- and noise-ABR thresholds were analyzed by two-sided Student's t-test. F-ABR measurements were group analyzed by 2-way ANOVA with $\alpha = 0.05$, post-test: Bonferroni (GraphPad Prism). Auditory steady state response were analyzed by 2-way ANOVA with $\alpha = 0.05$, post-test: Uncorrected Fisher's LSD test (GraphPad Prism). Data are shown as mean ± SEM.

ABR wave form analysis. ABR waveforms were analyzed for consecutive amplitude deflections (waves), with each wave consisting of a starting negative (n) peak and the following positive (p) peak. Wave latencies were defined by the onset timing (negative peak) of each corresponding wave. Peak amplitudes and latencies of ABR waves I and IV were extracted and defined as wave I: $I_n - I_p$ (0.85-1.9 ms); wave IV: $IV_n - IV_p$ (3.15-6.05 ms). A customized computer program (Peak, University of Tübingen) was used to extract ABR peak amplitudes and latencies based on these definitions. From the extracted peaks, ABR peak-to-peak (wave) amplitude and latency growth functions (Burkard & Don, 2007) were calculated for individual ears for increasing stimulus levels. All ABR wave amplitude and latency growth functions were normalized with reference to the ABR thresholds (from -10 dB to a maximum of 90 dB above threshold for wave amplitudes and from 0 dB to a maximum of 90 dB above threshold for wave latencies).

Electrophysiology. Data were analyzed and processed using Clampfit 10 (Molecular Devices) and Microsoft Excel. Statistics and visualization were performed with GraphPad Prism. Results between genotypes were statistically compared using 1-way ANOVA and Bonferroni's Multiple Comparison Test to compare baseline vs. LTP for

both genotypes and sound exposed animals as well as LTP between genotypes and sound exposed animals.

Multiple T-maze. Each trial was video-recorded with a webcam (Logitech c920). If a mouse fell from the maze, it was immediately placed back on the spot where it had fallen down. Errors were counted offline using the software BORIS (Friard & Gamba, 2016). An error was counted when a mouse deviated from the correct path to the target with all four feet at any of the seven decision points. Consecutive errors made at the same decision point were counted as one error until the mouse moved on to an adjacent decision point. The number of errors between control and KO mice was compared using the nonparametric Wilcoxon/Man-Whitney-U rank sum test performed with JMP 14 (SAS Institute Inc., USA). Additionally, the amount of circling behaviour was measured by counting the number of full 360° rotations around each mice' own axis during the time on the maze. Two mice failed to find the target platform in any of their first five training runs. The data from these two mice (1 control, 1 *Bdnf*^{Pax2}KO) were excluded from further analysis.

Time measurement was started after the mouse was placed on the start element and was stopped when a mouse had all four feet inside or on top of the mouse house on the target platform.

Social interaction test. The duration of sniffing contact of the mouse at the stranger and empty container normalized to the time spent in the respective compartment, the number of entries the mouse did in each of the compartments, the latency to first entry into each chamber as well as the time the experimental mouse spent with freezing or grooming during the 10 min period was analyzed.

Data availability

The data that support the findings of this study are available from the corresponding author upon request.

Code availability

The custom-written software supporting the findings of this study is available from the corresponding author upon request.

Acknowledgements

We thank Hyun-Soon Geisler, Karin Rohbock and Iris Köpschall for excellent technical assistance.

Author contributions

Conceptualization: P.E. and M.K.;

Analysis: P.E., P.M., M.M., M.H.W., W.S., L.R. and P.K.P.

Investigation: P.E., P.M., M.M., M.H.W. and P.K.P.

Writing: P.E., M.H.J., T.S. and M.K.;

Supervision: W.S., L.R., and M.K.;

Review and Editing: T.S., L.R., P.K.P. and M.K.

Conflict of interest

The authors declare that they have no conflict of interest.

There is no competing financial interest.

Funding disclosure

This work was supported by the Deutsche Forschungsgemeinschaft FOR 2060 project RU 713/3-2 (W.S., L.R.); GRK 2381 (P.M.); SPP 1608 RU 316/12-1 (P.E., L.R.) and KN 316/12-1 (M.M, M.K.); BFU2013-40944 (T.S); NIH NIMH 1R01MH106623 (M.H.J.).

References

Amaral, D. G., Scharfman, H. E., & Lavenex, P. (2007). The dentate gyrus: fundamental neuroanatomical organization (dentate gyrus for dummies). *Prog. Brain Res., 163*, 3-22. doi:10.1016/S0079-6123(07)63001-5

Autry, A. E., & Monteggia, L. M. (2012). Brain-derived neurotrophic factor and neuropsychiatric disorders. *Pharmacol Rev, 64*(2), 238-258. doi:10.1124/pr.111.005108

Barde, Y. A., Edgar, D., & Thoenen, H. (1982). Purification of a new neurotrophic factor from mammalian brain. *Embo J., 1*(5), 549-553.

Ben-Ari, Y. (2002). Excitatory actions of gaba during development: the nature of the nurture. *Nat Rev Neurosci, 3*(9), 728-739. doi:10.1038/nrn920

Bharadwaj, H. M., Verhulst, S., Shaheen, L., Liberman, M. C., & Shinn-Cunningham, B. G. (2014). Cochlear neuropathy and the coding of supra-threshold sound. *Front Syst Neurosci, 8*, 26. doi:10.3389/fnsys.2014.00026

Bramham, C. R., & Messaoudi, E. (2005). BDNF function in adult synaptic plasticity: the synaptic consolidation hypothesis. *Prog. Neurobiol., 76*(2), 99-125.

Burkard, R. F., & Don, M. (2007). The Auditory Brainstem Response. In R. F. Burkard, J. J. Eggermont, & M. Don (Eds.), *Auditory evoked potentials: Basic principles and clinical application.* Philadelphia: Lippincott Williams and Wilkins.

Chenaux, G., Matt, L., Hill, T. C., Kaur, I., Liu, X.-B., Kirk, L. M., . . . Díaz, E. (2016). Loss of SynDIG1 reduces excitatory synapse maturation but not formation *in vivo*. SynDIG1 regulates excitatory synapse maturation. *eNeuro, DOI: 10.1523/ENEURO.0130-16.2016*. doi:10.1523/ENEURO.0130-16.2016

Chumak, T., Rüttiger, L., Lee, S. C., Campanelli, D., Zuccotti, A., Singer, W., . . . Knipper, M. (2016). BDNF in Lower Brain Parts Modifies Auditory Fiber Activity to Gain Fidelity but Increases the Risk for Generation of Central Noise After Injury. *Mol. Neurobiol., 53*(8), 5607-5627. doi:10.1007/s12035-015-9474-x

Das, I., Estevez, M. A., Sarkar, A. A., & Banerjee-Basu, S. (2019). A multifaceted approach for analyzing complex phenotypic data in rodent models of autism. *Mol Autism, 10*, 11. doi:10.1186/s13229-019-0263-7

De Koninck, Y. (2007). Altered chloride homeostasis in neurological disorders: a new target. *Curr Opin Pharmacol, 7*(1), 93-99. doi:10.1016/j.coph.2006.11.005

de Villers-Sidani, E., Chang, E. F., Bao, S., & Merzenich, M. M. (2007). Critical period window for spectral tuning defined in the primary auditory cortex (A1) in the rat. *J Neurosci, 27*(1), 180-189. doi:10.1523/JNEUROSCI.3227-06.2007

Ernfors, P., Lee, K. F., & Jaenisch, R. (1994). Mice lacking brain-derived neurotrophic factor develop with sensory deficits. *Nature, 368*(6467), 147-150. doi:10.1038/368147a0

Fitch, R. H., Alexander, M. L., & Threlkeld, S. W. (2013). Early neural disruption and auditory processing outcomes in rodent models: implications for developmental language disability. *Front Syst Neurosci, 7*, 58. doi:10.3389/fnsys.2013.00058

Foss-Feig, J. H., Schauder, K. B., Key, A. P., Wallace, M. T., & Stone, W. L. (2017). Audition-specific temporal processing deficits associated with language function in children with autism spectrum disorder. *Autism Res, 10*(11), 1845-1856. doi:10.1002/aur.1820

Fotaki, V., Price, D. J., & Mason, J. O. (2008). Newly identified patterns of Pax2 expression in the developing mouse forebrain. *BMC Dev Biol, 8*, 79. doi:10.1186/1471-213X-8-79

Friard, O., & Gamba, M. (2016). BORIS: a free, versatile open-source event-logging software for video/audio coding and live observations. *Methods in Ecology and Evolution, 7*(11), 1325-1330. doi: https://doi.org/10.1111/2041-210X.12584

Friauf, E., Rust, M. B., Schulenborg, T., & Hirtz, J. J. (2011). Chloride cotransporters, chloride homeostasis, and synaptic inhibition in the developing auditory system. *Hear Res, 279*(1-2), 96-110. doi:10.1016/j.heares.2011.05.012

Fritzsch, B., Jahan, I., Pan, N., & Elliott, K. L. (2015). Evolving gene regulatory networks into cellular networks guiding adaptive behavior: an outline how single cells could have evolved into a centralized neurosensory system. *Cell Tissue Res, 359*(1), 295-313. doi:10.1007/s00441-014-2043-1

Fritzsch, B., Tessarollo, L., Coppola, E., & Reichardt, L. F. (2004). Neurotrophins in the ear: their roles in sensory neuron survival and fiber guidance. *Prog Brain Res, 146*, 265-278.

Froemke, R. C., Merzenich, M. M., & Schreiner, C. E. (2007). A synaptic memory trace for cortical receptive field plasticity. *Nature, 450*(7168), 425-429. doi:10.1038/nature06289

Funfschilling, U., Ng, Y. G., Zang, K., Miyazaki, J., Reichardt, L. F., & Rice, F. L. (2004). TrkC kinase expression in distinct subsets of cutaneous trigeminal innervation and nonneuronal cells. *J Comp Neurol, 480*(4), 392-414. doi:10.1002/cne.20359

Ganesan, S., Khan, S., Garel, K. A., Hamalainen, M. S., & Kenet, T. (2016). Normal Evoked Response to Rapid Sequences of Tactile Pulses in Autism Spectrum Disorders. *Front Hum Neurosci, 10*, 433. doi:10.3389/fnhum.2016.00433

Goel, A., Cantu, D. A., Guilfoyle, J., Chaudhari, G. R., Newadkar, A., Todisco, B., . . . Portera-Cailliau, C. (2019). Author Correction: Impaired perceptual learning in a mouse model of Fragile X syndrome is mediated by parvalbumin neuron dysfunction and is reversible. *Nat Neurosci, 22*(1), 143. doi:10.1038/s41593-018-0273-3

Grant, L., Yi, E., & Glowatzki, E. (2010). Two modes of release shape the postsynaptic response at the inner hair cell ribbon synapse. *J Neurosci, 30*(12), 4210-4220. doi:10.1523/JNEUROSCI.4439-09.2010

Griffen, T. C., & Maffei, A. (2014). GABAergic synapses: their plasticity and role in sensory cortex. *Front Cell Neurosci, 8*, 91. doi:10.3389/fncel.2014.00091

Groenink, L., Verdouw, P. M., van Oorschot, R., & Olivier, B. (2008). Models of anxiety: ultrasonic vocalizations of isolated rat pups. *Curr Protoc Pharmacol, Chapter 5*, Unit 5 18. doi:10.1002/0471141755.ph0518s43

Heil, P., Neubauer, H., Brown, M., & Irvine, D. R. (2008). Towards a unifying basis of auditory thresholds: distributions of the first-spike latencies of auditory-nerve fibers. *Hear Res, 238*(1-2), 25-38. doi:10.1016/j.heares.2007.09.014

Hong, E. J., McCord, A. E., & Greenberg, M. E. (2008). A biological function for the neuronal activity-dependent component of Bdnf transcription in the development of cortical inhibition. *Neuron, 60*(4), 610-624. doi:S0896-6273(08)00802-7 [pii] 10.1016/j.neuron.2008.09.024

Hu, H., Gan, J., & Jonas, P. (2014). Interneurons. Fast-spiking, parvalbumin^{+} GABAergic interneurons: from cellular design to microcircuit function. *Science, 345*(6196), 1255263. doi:10.1126/science.1255263

Irvine, D. R. F. (2018). Auditory perceptual learning and changes in the conceptualization of auditory cortex. *Hear Res, 366*, 3-16. doi:10.1016/j.heares.2018.03.011

Itami, C., Kimura, F., & Nakamura, S. (2007). Brain-derived neurotrophic factor regulates the maturation of layer 4 fast-spiking cells after the second postnatal

week in the developing barrel cortex. *J Neurosci, 27*(9), 2241-2252. doi:10.1523/JNEUROSCI.3345-06.2007
Jiao, Y., Zhang, Z., Zhang, C., Wang, X., Sakata, K., Lu, B., & Sun, Q. Q. (2011). A key mechanism underlying sensory experience-dependent maturation of neocortical GABAergic circuits in vivo. *Proc Natl Acad Sci U S A, 108*(29), 12131-12136. doi:10.1073/pnas.1105296108
Kilgard, M. P., Pandya, P. K., Engineer, N. D., & Moucha, R. (2002). Cortical network reorganization guided by sensory input features. *Biol Cybern, 87*(5-6), 333-343. doi:10.1007/s00422-002-0352-z
Kimura, F., & Itami, C. (2019). A hypothetical model concerning how spike-timing-dependent plasticity contributes to neural circuit formation and initiation of the critical period in barrel cortex. *J Neurosci*. doi:10.1523/JNEUROSCI.1684-18.2019
Knipper, M., Zinn, C., Maier, H., Praetorius, M., Rohbock, K., Kopschall, I., & Zimmermann, U. (2000). Thyroid hormone deficiency before the onset of hearing causes irreversible damage to peripheral and central auditory systems. *J Neurophysiol, 83*(5), 3101-3112. doi:10.1152/jn.2000.83.5.3101
Korb, E., & Finkbeiner, S. (2011). Arc in synaptic plasticity: from gene to behavior. *Trends Neurosci., 34*(11), 591-598. doi:10.1016/j.tins.2011.08.007
Kraus, N., & White-Schwoch, T. (2015). Unraveling the Biology of Auditory Learning: A Cognitive-Sensorimotor-Reward Framework. *Trends Cogn Sci, 19*(11), 642-654. doi:10.1016/j.tics.2015.08.017
Kromer, S. A., Kessler, M. S., Milfay, D., Birg, I. N., Bunck, M., Czibere, L., . . . Turck, C. W. (2005). Identification of glyoxalase-I as a protein marker in a mouse model of extremes in trait anxiety. *J Neurosci, 25*(17), 4375-4384. doi:10.1523/JNEUROSCI.0115-05.2005
Lange-Asschenfeldt, C., Lohmann, P., & Riepe, M. W. (2007). Spatial performance in a complex maze is associated with persistent long-term potentiation enhancement in mouse hippocampal slices at early training stages. *Neuroscience, 147*(2), 318-324. doi:10.1016/j.neuroscience.2007.04.020
Leal, G., Bramham, C. R., & Duarte, C. B. (2017). BDNF and Hippocampal Synaptic Plasticity. *Vitam Horm, 104*, 153-195. doi:10.1016/bs.vh.2016.10.004
Letzkus, J. J., Wolff, S. B., Meyer, E. M., Tovote, P., Courtin, J., Herry, C., & Luthi, A. (2011). A disinhibitory microcircuit for associative fear learning in the auditory cortex. *Nature, 480*(7377), 331-335. doi:10.1038/nature10674
Malmierca, M., & Merchan, M. (2004). The Auditory System. In G. Paxinos (Ed.), *The Rat Nervous System* (pp. 997-1082). San Diego: Academic Press.
Marco, E. J., Khatibi, K., Hill, S. S., Siegel, B., Arroyo, M. S., Dowling, A. F., . . . Nagarajan, S. S. (2012). Children with autism show reduced somatosensory response: an MEG study. *Autism Res, 5*(5), 340-351. doi:10.1002/aur.1247
Maricich, S. M., & Herrup, K. (1999). Pax-2 expression defines a subset of GABAergic interneurons and their precursors in the developing murine cerebellum. *J Neurobiol, 41*(2), 281-294.
Marin, O., & Rubenstein, J. L. (2001). A long, remarkable journey: tangential migration in the telencephalon. *Nat Rev Neurosci, 2*(11), 780-790. doi:10.1038/35097509
Marty, S., Berzaghi Mda, P., & Berninger, B. (1997). Neurotrophins and activity-dependent plasticity of cortical interneurons. *Trends Neurosci, 20*(5), 198-202.
Matt, L., Eckert, P., Panford-Walsh, R., Geisler, H. S., Bausch, A. E., Manthey, M., . . . Singer, W. (2018). Visualizing BDNF Transcript Usage During Sound-Induced Memory Linked Plasticity. *Front Mol Neurosci, 11*, 260. doi:10.3389/fnmol.2018.00260

Matt, L., Michalakis, S., Hofmann, F., Hammelmann, V., Ludwig, A., Biel, M., & Kleppisch, T. (2011). HCN2 channels in local inhibitory interneurons constrain LTP in the hippocampal direct perforant path. *Cell. Mol. Life Sci., 68*(1), 125-137. doi:10.1007/s00018-010-0446-z

Minichiello, L. (2009). TrkB signalling pathways in LTP and learning. *Nat Rev Neurosci, 10*(12), 850-860. doi:nrn2738 [pii] 10.1038/nrn2738

Mohn, J. L., Alexander, J., Pirone, A., Palka, C. D., Lee, S. Y., Mebane, L., . . . Jacob, M. H. (2014). Adenomatous polyposis coli protein deletion leads to cognitive and autism-like disabilities. *Mol Psychiatry, 19*(10), 1133-1142. doi:10.1038/mp.2014.61

Monteggia, L. M., Barrot, M., Powell, C. M., Berton, O., Galanis, V., Gemelli, T., . . . Nestler, E. J. (2004). Essential role of brain-derived neurotrophic factor in adult hippocampal function. *Proc Natl Acad Sci U S A, 101*(29), 10827-10832. doi:10.1073/pnas.0402141101

Munoz-Lopez, M. M., Mohedano-Moriano, A., & Insausti, R. (2010). Anatomical pathways for auditory memory in primates. *Front. Neuroanat., 4*, 129. doi:10.3389/fnana.2010.00129

Nikolaienko, O., Patil, S., Eriksen, M. S., & Bramham, C. R. (2018). Arc protein: a flexible hub for synaptic plasticity and cognition. *Semin Cell Dev Biol, 77*, 33-42. doi:10.1016/j.semcdb.2017.09.006

Ohja, K., Gozal, E., Fahnestock, M., Cai, L., Cai, J., Freedman, J. H., . . . Barnes, G. N. (2018). Neuroimmunologic and Neurotrophic Interactions in Autism Spectrum Disorders: Relationship to Neuroinflammation. *Neuromolecular Med, 20*(2), 161-173. doi:10.1007/s12017-018-8488-8

Ohyama, T., & Groves, A. K. (2004). Generation of Pax2-Cre mice by modification of a Pax2 bacterial artificial chromosome. *Genesis, 38*(4), 195-199. doi:10.1002/gene.20017

Owens, D. F., & Kriegstein, A. R. (2002). Is there more to GABA than synaptic inhibition? *Nat Rev Neurosci, 3*(9), 715-727. doi:10.1038/nrn919

Park, H., & Poo, M. M. (2013). Neurotrophin regulation of neural circuit development and function. *Nat. Rev. Neurosci., 14*(1), 7-23. doi:10.1038/nrn3379

Paul, B. T., Bruce, I. C., & Roberts, L. E. (2017). Evidence that hidden hearing loss underlies amplitude modulation encoding deficits in individuals with and without tinnitus. *Hear Res, 344*, 170-182. doi:10.1016/j.heares.2016.11.010

Pirone, A., Alexander, J., Lau, L. A., Hampton, D., Zayachkivsky, A., Yee, A., . . . Dulla, C. G. (2017). APC conditional knock-out mouse is a model of infantile spasms with elevated neuronal beta-catenin levels, neonatal spasms, and chronic seizures. *Neurobiol Dis, 98*, 149-157. doi:10.1016/j.nbd.2016.11.002

Rauskolb, S., Zagrebelsky, M., Dreznjak, A., Deogracias, R., Matsumoto, T., Wiese, S., . . . Barde, Y. A. (2010). Global deprivation of brain-derived neurotrophic factor in the CNS reveals an area-specific requirement for dendritic growth. *J. Neurosci., 30*(5), 1739-1749. doi:30/5/1739 [pii] 10.1523/JNEUROSCI.5100-09.2010

Rios, M., Fan, G., Fekete, C., Kelly, J., Bates, B., Kuehn, R., . . . Jaenisch, R. (2001). Conditional deletion of brain-derived neurotrophic factor in the postnatal brain leads to obesity and hyperactivity. *Molecular Endocrinology, 15*(10), 1748-1757.

Ruel, J., Nouvian, R., Gervais d'Aldin, C., Pujol, R., Eybalin, M., & Puel, J. L. (2001). Dopamine inhibition of auditory nerve activity in the adult mammalian cochlea. *Eur J Neurosci, 14*(6), 977-986.

Rüttiger, L., Singer, W., Panford-Walsh, R., Matsumoto, M., Lee, S. C., Zuccotti, A., . . . Knipper, M. (2013). The reduced cochlear output and the failure to adapt the

central auditory response causes tinnitus in noise exposed rats. *PLoS One, 8*(3), e57247. doi:10.1371/journal.pone.0057247

Saghazadeh, A., Mahmoudi, M., Dehghani Ashkezari, A., Oliaie Rezaie, N., & Rezaei, N. (2017). Systematic review and meta-analysis shows a specific micronutrient profile in people with Down Syndrome: Lower blood calcium, selenium and zinc, higher red blood cell copper and zinc, and higher salivary calcium and sodium. *PLoS One, 12*(4), e0175437. doi:10.1371/journal.pone.0175437

Schmeisser, M. J., Ey, E., Wegener, S., Bockmann, J., Stempel, A. V., Kuebler, A., . . . Boeckers, T. M. (2012). Autistic-like behaviours and hyperactivity in mice lacking ProSAP1/Shank2. *Nature, 486*(7402), 256-260. doi:10.1038/nature11015

Shepherd, J. D., & Bear, M. F. (2011). New views of Arc, a master regulator of synaptic plasticity. *Nat Neurosci, 14*(3), 279-284. doi:10.1038/nn.2708

Shibata, S., Kakazu, Y., Okabe, A., Fukuda, A., & Nabekura, J. (2004). Experience-dependent changes in intracellular Cl- regulation in developing auditory neurons. *Neurosci Res, 48*(2), 211-220.

Silverman, J. L., Yang, M., Lord, C., & Crawley, J. N. (2010). Behavioural phenotyping assays for mouse models of autism. *Nat Rev Neurosci, 11*(7), 490-502. doi:10.1038/nrn2851

Singer, W., Geisler, H. S., & Knipper, M. (2013). The Geisler method: tracing activity-dependent cGMP plasticity changes upon double detection of mRNA and protein on brain slices. *Methods Mol Biol, 1020*, 223-233. doi:10.1007/978-1-62703-459-3_15

Singer, W., Geisler, H. S., Panford-Walsh, R., & Knipper, M. (2016). Detection of Excitatory and Inhibitory Synapses in the Auditory System Using Fluorescence Immunohistochemistry and High-Resolution Fluorescence Microscopy. *Methods Mol Biol, 1427*, 263-276. doi:10.1007/978-1-4939-3615-1_15

Singer, W., Panford-Walsh, R., & Knipper, M. (2014). The function of BDNF in the adult auditory system. *Neuropharmacology, 76 Pt C*, 719-728. doi:10.1016/j.neuropharm.2013.05.008

Takesian, A. E., Bogart, L. J., Lichtman, J. W., & Hensch, T. K. (2018). Inhibitory circuit gating of auditory critical-period plasticity. *Nat Neurosci, 21*(2), 218-227. doi:10.1038/s41593-017-0064-2

Tan, J., Rüttiger, L., Panford-Walsh, R., Singer, W., Schulze, H., Kilian, S. B., . . . Knipper, M. (2007). Tinnitus behavior and hearing function correlate with the reciprocal expression patterns of BDNF and Arg3.1/arc in auditory neurons following acoustic trauma. *Neuroscience, 145*(2), 715-726.

Truong, D. T., Che, A., Rendall, A. R., Szalkowski, C. E., LoTurco, J. J., Galaburda, A. M., & Holly Fitch, R. (2014). Mutation of Dcdc2 in mice leads to impairments in auditory processing and memory ability. *Genes Brain Behav, 13*(8), 802-811. doi:10.1111/gbb.12170

Turrigiano, G. (2012). Homeostatic synaptic plasticity: local and global mechanisms for stabilizing neuronal function. *Cold Spring Harb Perspect Biol, 4*(1), a005736. doi:10.1101/cshperspect.a005736

Vale, C., & Sanes, D. H. (2002). The effect of bilateral deafness on excitatory and inhibitory synaptic strength in the inferior colliculus. *Eur J Neurosci, 16*(12), 2394-2404.

Waung, M. W., Pfeiffer, B. E., Nosyreva, E. D., Ronesi, J. A., & Huber, K. M. (2008). Rapid translation of Arc/Arg3.1 selectively mediates mGluR-dependent LTD through persistent increases in AMPAR endocytosis rate. *Neuron, 59*(1), 84-97. doi:10.1016/j.neuron.2008.05.014

Weinberger, N. M. (2015). New perspectives on the auditory cortex: learning and memory. *Handb Clin Neurol, 129*, 117-147. doi:10.1016/B978-0-444-62630-1.00007-X

Wenhart, T., Bethlehem, R. A. I., Baron-Cohen, S., & Altenmuller, E. (2019). Autistic traits, resting-state connectivity, and absolute pitch in professional musicians: shared and distinct neural features. *Mol Autism, 10*, 20. doi:10.1186/s13229-019-0272-6

Xu, H., Kotak, V. C., & Sanes, D. H. (2010). Normal hearing is required for the emergence of long-lasting inhibitory potentiation in cortex. *J Neurosci, 30*(1), 331-341. doi:10.1523/JNEUROSCI.4554-09.2010

Zagrebelsky, M., & Korte, M. (2014). Form follows function: BDNF and its involvement in sculpting the function and structure of synapses. *Neuropharmacology, 76 Pt C*, 628-638. doi:10.1016/j.neuropharm.2013.05.029

Zampini, V., Johnson, S. L., Franz, C., Lawrence, N. D., Munkner, S., Engel, J., . . . Marcotti, W. (2010). Elementary properties of CaV1.3 Ca(2+) channels expressed in mouse cochlear inner hair cells. *J Physiol, 588*(Pt 1), 187-199. doi:10.1113/jphysiol.2009.181917

Zuccotti, A., Kuhn, S., Johnson, S. L., Franz, C., Singer, W., Hecker, D., . . . Knipper, M. (2012). Lack of brain-derived neurotrophic factor hampers inner hair cell synapse physiology, but protects against noise-induced hearing loss. *J. Neurosci., 32*(25), 8545-8553. doi:10.1523/JNEUROSCI.1247-12.2012

Figure 1-figure supplement 1

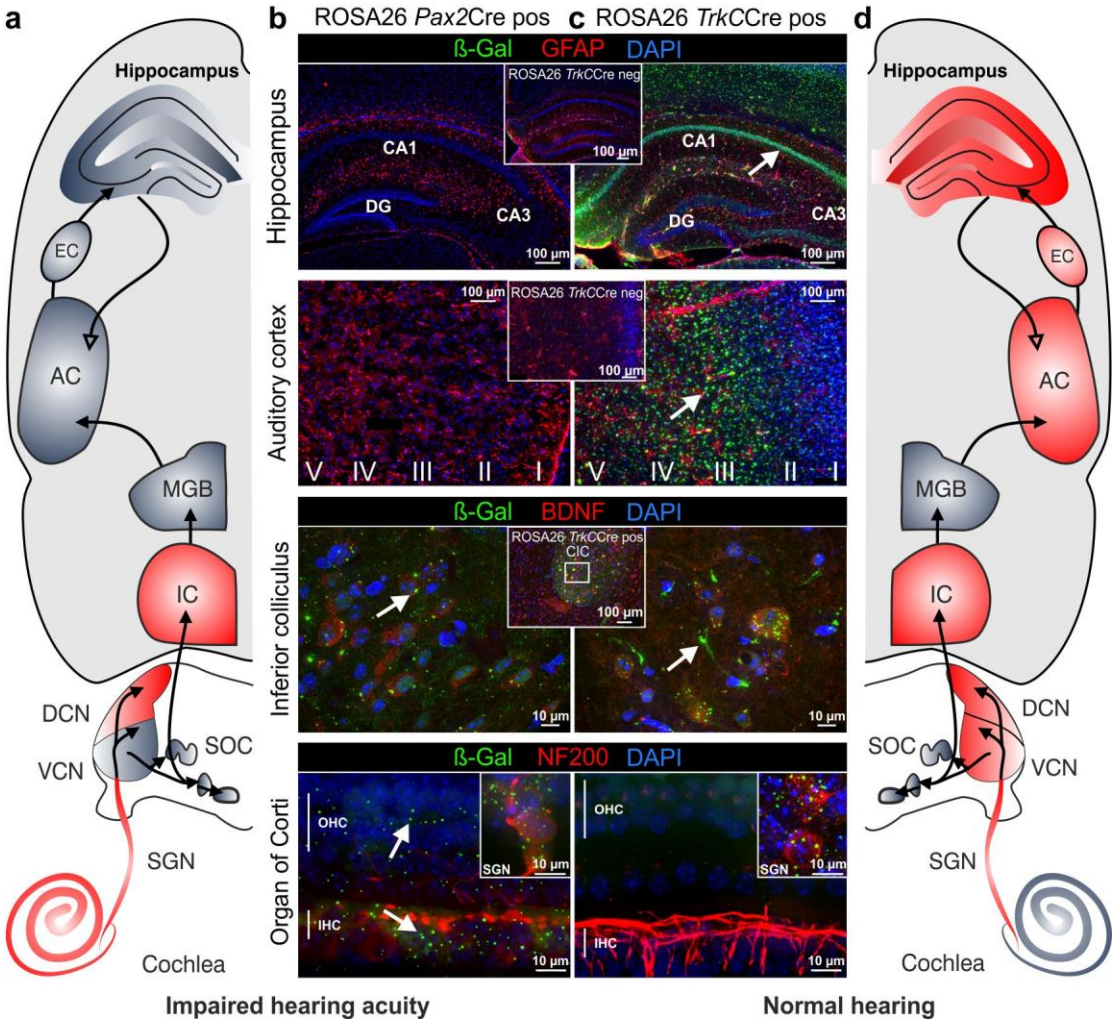

Figure 1-figure supplement 1 | ROSA26 *Pax2*Cre positive mice did not show any β-gal immunolabeling in frontal brain regions.

(**a**/**d**) Schematic diagrams of the ascending auditory pathway. Red areas showed the regions of Cre expression in the *Pax2*Cre line **a** and the *TrkC*Cre line **d**, respectively.

(**b**) No β-gal immunolabeling (green), counterstained with GFAP (red), could be observed in ROSA26 *Pax2*Cre mice in comparison to

(**c**) ROSA26 *TrkC*Cre mice in the hippocampus or the AC. In the IC (inset: overview of the central IC) both mouse lines showed β-gal expression (green). In the cochlea only ROSA26 *Pax2*Cre showed ß-gal immunoreactivity (Inset: in SGN both show ß-gal staining). Counterstaining with BDNF in the IC and NF200 in the cochlea. Insets: Negative controls exemplarily shown for ROSA26 *TrkC*Cre negative mice. Scale bars: **b**: 100µm, 10µm. Nuclear staining DAPI (blue).

Figure 1

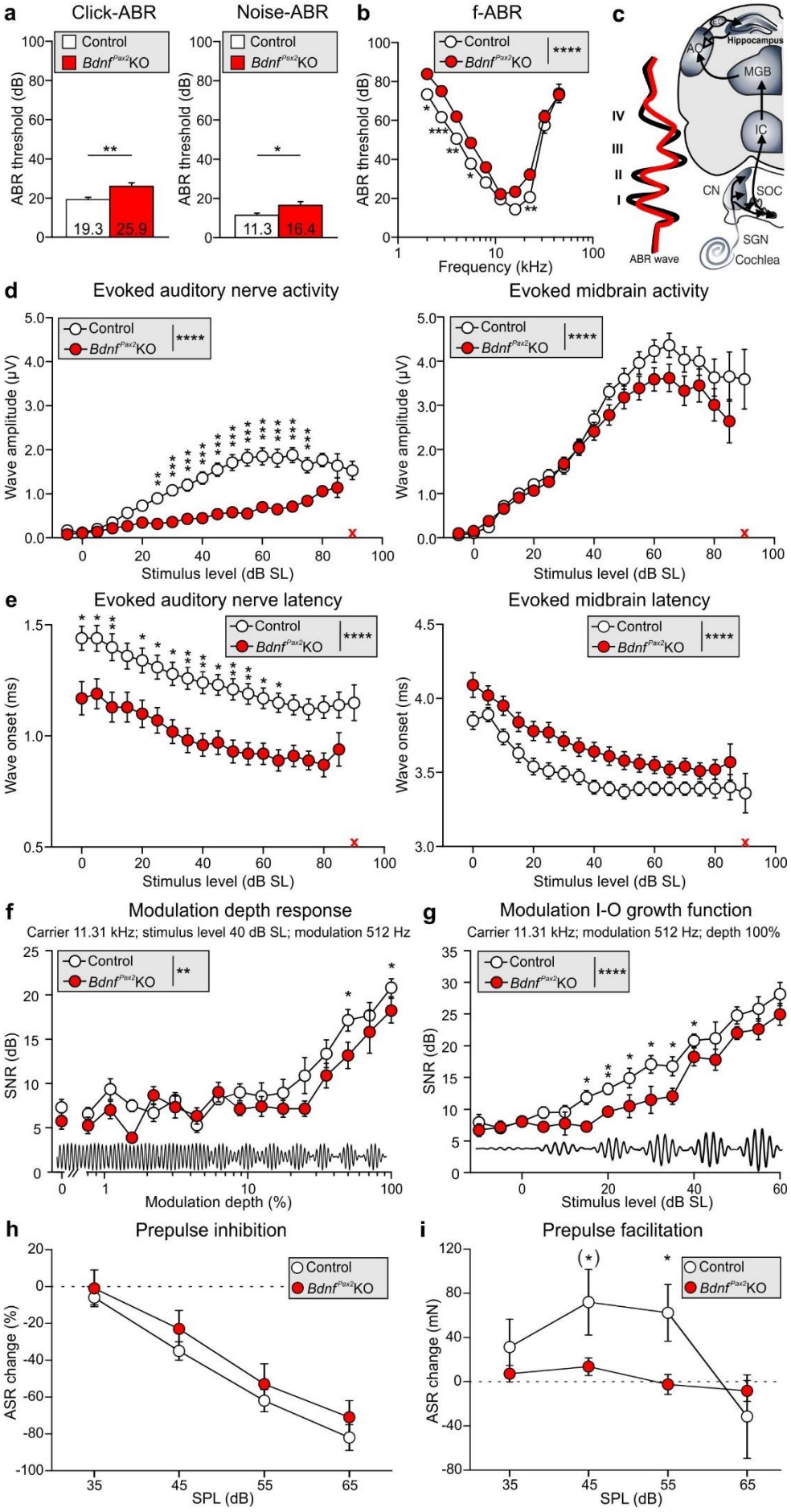
a
Click-ABR
Noise-ABR
Control
Bdnf Pax2 KO
ABR threshold (dB)
19.3
25.9
11.3
16.4
b
f-ABR
****
Frequency (kHz)
c
Hippocampus
AC
MGB
IC
SOC
CN
SGN
Cochlea
ABR wave
IV
III
II
I
d
Evoked auditory nerve activity
Evoked midbrain activity
Wave amplitude (µV)
Stimulus level (dB SL)
e
Evoked auditory nerve latency
Evoked midbrain latency
Wave onset (ms)
f
Modulation depth response
Carrier 11.31 kHz; stimulus level 40 dB SL; modulation 512 Hz
SNR (dB)
Modulation depth (%)
g
Modulation I-O growth function
Carrier 11.31 kHz; modulation 512 Hz; depth 100%
h
Prepulse inhibition
ASR change (%)
SPL (dB)
i
Prepulse facilitation
ASR change (mN)

Figure 1 | *Bdnf*^{Pax2}KOs demonstrated a decreased hearing acuity compared to controls.
(**a**) Mean click evoked ABR (controls $n = 26/52$ mice/ears; *Bdnf*^{Pax2}KOs $n = 23/46$ mice/ears; unpaired two-tailed students t-test, $t(47) = 3.22$, $P = 0.002$) and noise burst ABR (controls $n = 26/52$ mice/ears; *Bdnf*^{Pax2}KOs $n = 23/46$ mice/ears; unpaired two-tailed students t-test, $t(47) = 2.31$, $P = 0.026$) and
(**b**) frequency-specific ABR thresholds (f-ABR, controls $n = 16/32$ mice/ears; *Bdnf*^{Pax2}KOs $n = 16/32$ mice/ears; 2-way ANOVA, $F(1,9) = 59.72$, $P < 0.0001$).
(**c**), Schematic drawing of an ABR waveform of controls (black) and *Bdnf*^{Pax2}KOs (red) in relation to the corresponding auditory nuclei in the ascending auditory pathway (black arrows) hippocampal projections to cortical areas (open arrow). AN: auditory nerve, CN: cochlear nucleus, SOC: superior olivary complex, IC: inferior colliculus, MGB: medial geniculate body, AC: auditory cortex, EC: entorhinal cortex.
(**d**) ABR wave I (left) and IV (right) amplitude (wave I: controls $n = 14/28$ mice/ears, *Bdnf*^{Pax2}KOs $n = 14/28$ mice/ears; 2-way ANOVA, $F(1,18) = 199.0$, $P < 0.0001$, interaction $P < 0.0001$; wave IV: controls $n = 14/28$ mice/ears, *Bdnf*^{Pax2}KOs $n = 12/24$ mice/ears; 2-way ANOVA with Bonferroni's post-hoc test, Genotype: $F(1,18) = 15.76$, $P < 0.0001$).
(**e**) Noise ABR wave I (left) and IV (right) latency (wave I: controls $n = 14/28$ mice/ears, *Bdnf*^{Pax2}KOs $n = 12/24$ mice/ears; 2-way ANOVA, Genotype: $F(1,17) = 187.50$, $P < 0.0001$; wave IV: controls $n = 14/28$ mice/ears, *Bdnf*^{Pax2}KOs $n = 12/24$ mice/ears; 2-way ANOVA with Bonferroni's post-hoc test, Genotype: $F(1,17) = 78.96$, $P < 0.0001$).
(**f**) The signal-to-noise ratio (SNR) of modulation depth response (carrier frequency: 11.3 kHz; modulation frequency: 512 Hz; 40 dB above threshold; controls $n = 10/10$ mice/ears; *Bdnf*^{Pax2}KOs $n = 10/10$ mice/ears, 2-way ANOVA with Bonferroni's post-hoc test, Genotype: $F(1,15) = 10.92$, $P = 0.001$) and
(**g**), SNR modulation I-O function of an amplitude-modulated tone (carrier frequency: 11.3 kHz; modulation frequency: 512 Hz; 100 % modulation depth; controls $n = 10/10$ mice/ears; *Bdnf*^{Pax2}KOs $n = 10/10$ mice/ears 2-way ANOVA, $F(1,14) = 28.15$, $P < 0.0001$) was reduced in *Bdnf*^{Pax2}KOs.
(**h**) Prepulse inhibition (controls $n = 7$, *Bdnf*^{Pax2}KOs $n = 9$; Repeated measures ANOVA, Genotype: $F(2,28) = 0.14$, $P = 0.869$).
(**i**) Prepulse facilitation (controls $n = 7$, *Bdnf*^{Pax2}KOs $n = 9$; Repeated measures ANOVA, Interaction: $F(2,26) = 4.19$, $P = 0.029$; Bonferroni's post-hoc controls vs. *Bdnf*^{Pax2}KOs: * $P < 0.05$, (*) $0.05 < P < 0.1$). Mean ± S.E.M.

Figure 2

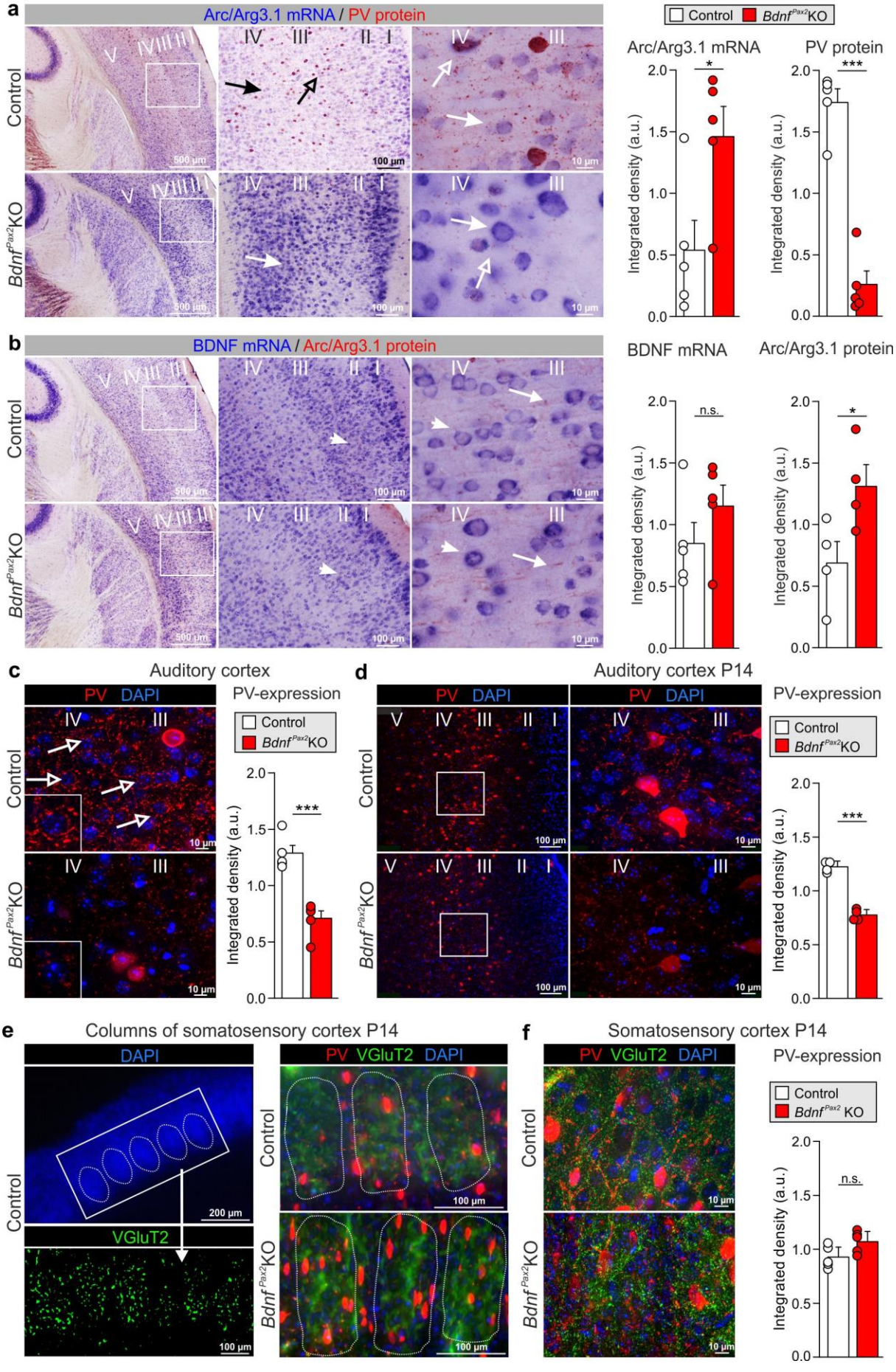
a
Arc/Arg3.1 mRNA / PV protein
Control
Bdnf Pax2 KO
Control
Bdnf Pax2 KO
Arc/Arg3.1 mRNA
PV protein
Integrated density (a.u.)
b
BDNF mRNA / Arc/Arg3.1 protein
BDNF mRNA
Arc/Arg3.1 protein
n.s.
c
Auditory cortex
PV DAPI
PV-expression
d
Auditory cortex P14
e
Columns of somatosensory cortex P14
DAPI
VGluT2
PV VGluT2 DAPI
f
Somatosensory cortex P14

Figure 2 | Alterations of Arc/Arg3.1 and PV expression in the AC but not in SSC of *Bdnf*^{Pax2}KO mice.
(**a**) *Bdnf*^{Pax2}KOs showed increased Arc/Arg3.1 mRNA (blue; unpaired two-tailed student's t-test; $n = 5$ each, $t(8) = 2.69$, $P = 0.028$) and decreased PV protein (red; unpaired two-tailed student's t-test; $n = 5$ each, $t(8) = 9.48$, $P < 0.0001$) levels in the AC in comparison to controls.
(**b**) *Bdnf*^{Pax2}KOs reavealed similar levels of BDNF mRNA in the AC (blue; unpaired two-tailed student's t-test; $n = 5$ each, $t(8) = 1.26$, $P = 0.243$) but increased Arc Protein (red; unpaired two-tailed student's t-test; $n = 4$ each, $t(6) = 2.52$, $P = 0.0453$) compared to controls.
(**c**/**d**) Decreased expression of PV in the AC of adult *Bdnf*^{Pax2}KOs (**c**: unpaired two-tailed student's t-test: $n = 5$ each, $t(8) = 6.165$, $P < 0.001$) and P14 *Bdnf*^{Pax2}KOs (**d**: unpaired two-tailed student's t-test; $n = 5$ each, $t(8) = 6.165$, $P < 0.001$) in comparison to controls.
(**e**) Left panel, exemplary picture for SSC columns. Right panel: Normal development of columns in the SSC of P14 *Bdnf*^{Pax2}KOs (red: PV; green: vGluT2) and
(**f**) similar PV expression in SSC of P14 *Bdnf*^{Pax2}KOs (unpaired two-tailed student's t-test: $n = 5$ each, $t(8) = 1.10$, $P = 0.303$) compared to controls. Nuclear staining DAPI (blue). Mean ± S.E.M.

Figure 3

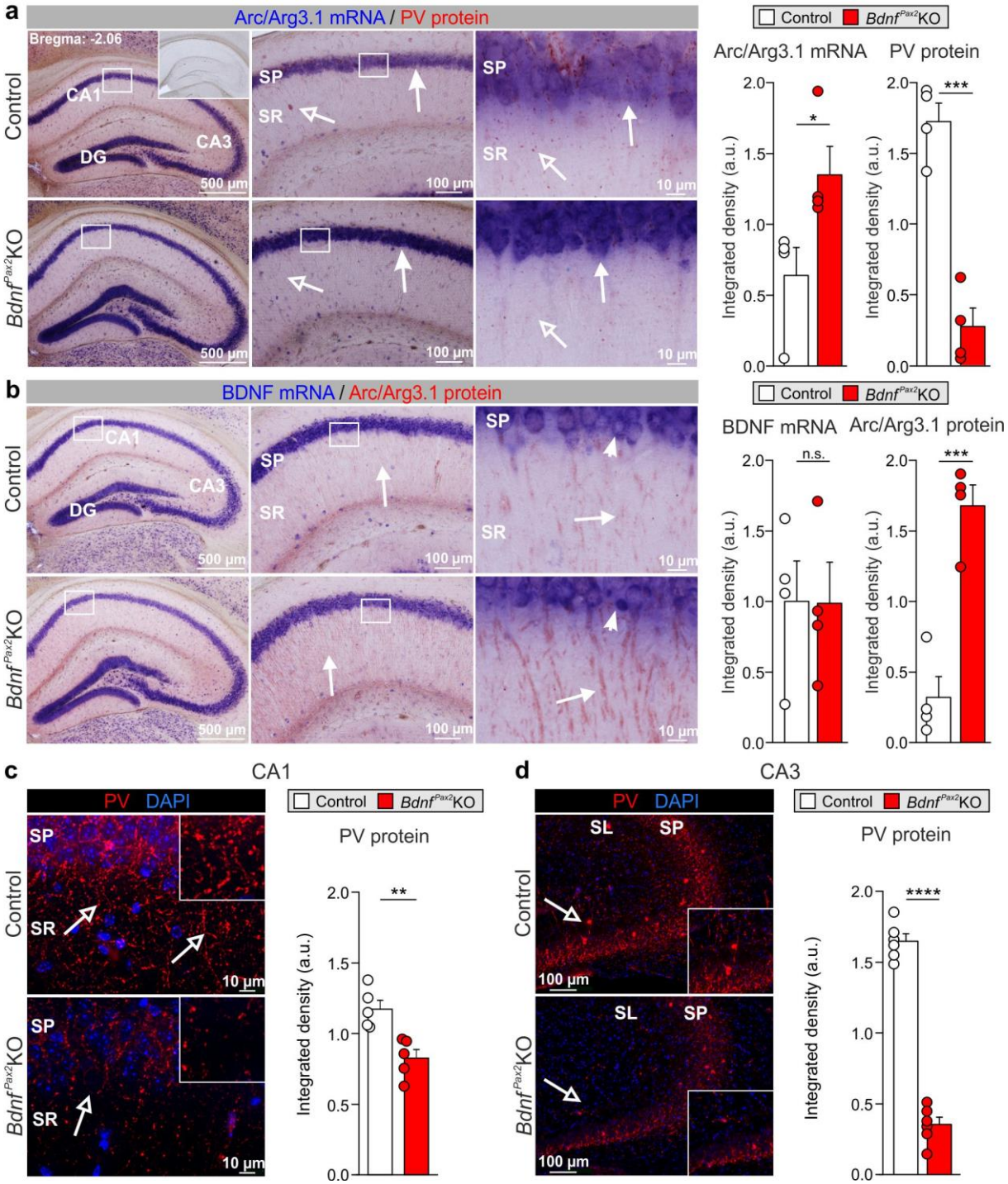
a
Arc/Arg3.1 mRNA / PV protein
Bregma: -2.06
Control
BdnfPax2KO
CA1
CA3
DG
SP
SR
500 µm
100 µm
10 µm
Control BdnfPax2KO
Arc/Arg3.1 mRNA
PV protein
Integrated density (a.u.)
*
***
b
BDNF mRNA / Arc/Arg3.1 protein
n.s.
***
c
CA1
PV DAPI
PV protein
**
d
CA3
SL
****

Figure 3 | Imbalance of Arc/Arg3.1 and PV expression in the hippocampus of *Bdnf*^{Pax2}KOs.
(**a**) *Bdnf*^{Pax2}KOs showed increased Arc/Arg3.1 mRNA (blue; unpaired two-tailed student's t-test; CA1: $n = 4$ each, $t(6) = 2.59$, $P = 0.042$) and decreased PV protein (red; unpaired two-tailed student's t-test; CA1: $n = 4$ each, $t(6) = 7.82$, $P < 0.001$) levels in hippocampal CA1 region in comparison to controls.
(**b**) BDNF mRNA (blue; unpaired two-tailed student's t-test; CA1: $n = 4$ each, $t(6) = 0.28$, $P = 0.979$) remained unaltered in *Bdnf*^{Pax2}KOs while Arc/Arg3.1 protein (red; unpaired two-tailed student's t-test; CA1: $n = 4$ each, $t(6) = 6.53$, $P < 0.001$) was increased in hippocampal CA1 regions in comparison to controls.
(**c**) Decreased expression of PV in hippocampal CA1 and
(**d**) CA3 regions in *Bdnf*^{Pax2}KOs in comparison to controls (unpaired two-tailed student's t-test; CA1: $n = 5$ each, $t(8) = 3.94$, $P = 0.004$; CA3: $n = 6$ each, $t(10) = 7.26$, $P < 0.0001$).
SL: stratum lucidum, SP: stratum pyramidale; SR: stratum radiatum. Scale bar **a**,**b**: left panels: 500 µm; middle panels: 100 µm; right panels: 10 µm; →: Arc/Arg3.1 mRNA + Protein; ⇾: PV Protein; ►: BDNF mRNA. (**c,d**)**:** CA1: 10 µm; CA3: 100 µ. Mean ± S.E.M.

Figure 3-figure supplement 1

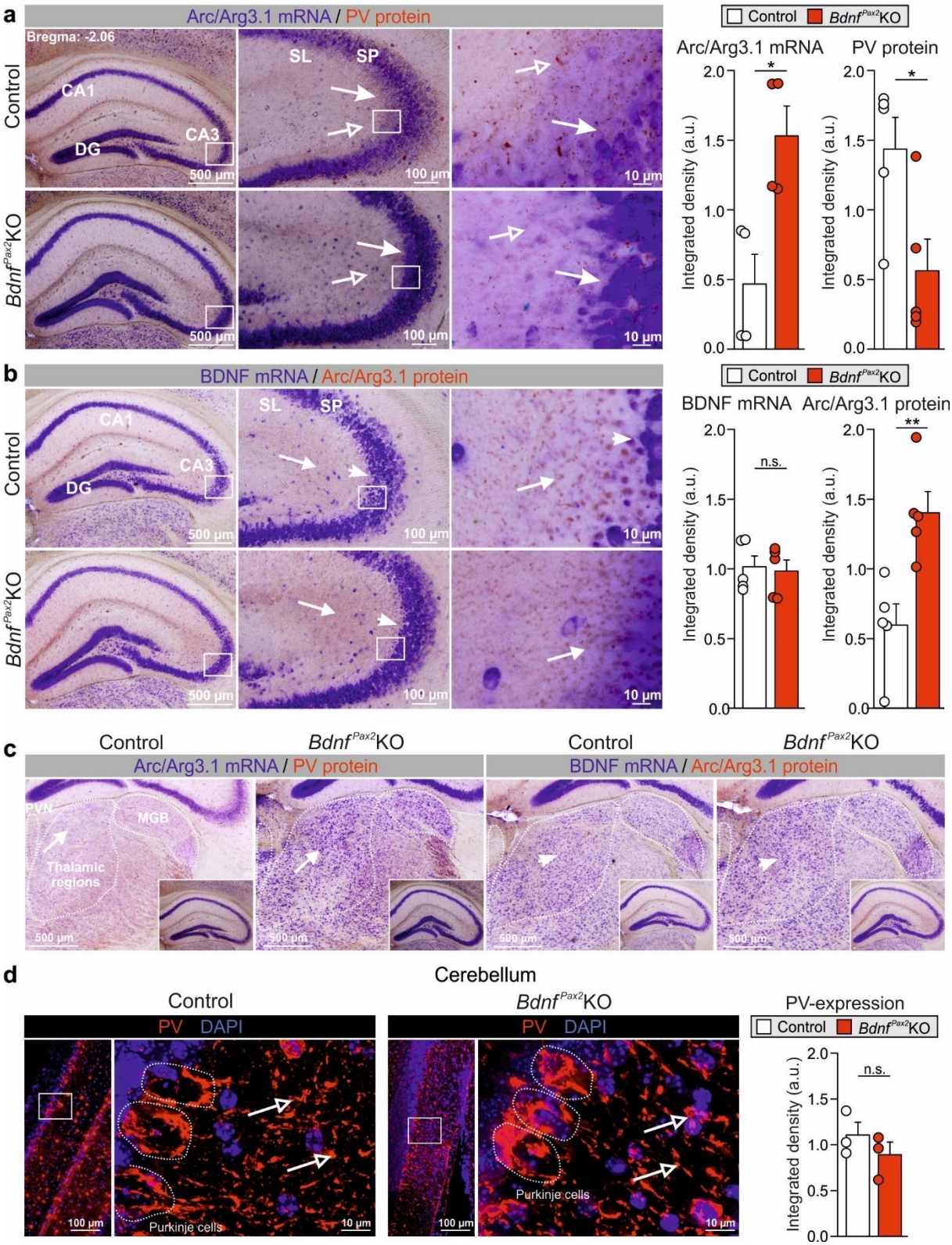

Figure 3-figure supplement 1 | Altered Arc/Arg3.1 and PV expression in the forebrain but not in the cerebellum of *Bdnf*^{Pax2}KOs.

(**a**) *Bdnf*^{Pax2}KOs showed increased Arc/Arg3.1 mRNA (blue; unpaired two-tailed student's t-test; CA3: $n = 4$ each, $t(6) = 3.50$, $P = 0.013$) and decreased PV protein (red; unpaired two-tailed student's t-test; CA3: $n = 5$ each, $t(8) = 2.72$, $P = 0.026$) levels in hippocampal CA3 region in comparison to controls.

(**b**) BDNF mRNA (blue; unpaired two-tailed student's t-test; CA3: $n = 5$ each, $t(8) = 0.26$, $P = 0.802$) remained unaltered in *Bdnf*^{Pax2}KOs while Arc/Arg3.1 protein (red; unpaired two-tailed student's t-test; CA3: $n = 5$ each, $t(8) = 3.76$, $P = 0.006$) was increased in hippocampal CA3 regions in comparison to controls.

(**c**) left panel, *Bdnf*^{Pax2}KOs showed increased Arc/Arg3.1 mRNA (blue) and (right panel) unchanged BDNF mRNA (blue) expression in the paraventricular nucleus (PVN), medial geniculate nucleus (MGN) and thalamic regions. Scale bars = 500 µM.

(**d**) Normal PV expression in cerebellum in *Bdnf*^{Pax2}KOs (unpaired two-tailed student's t-test; $n = 3$ each, $t(4) = 1.10$, $P = 0.331$).

Scale bars: **a**,**b**: left panels: 500 µm; middle panels: 100 µm; right panels: 10 µm; **c**: 500 µm **d**: left panels: 100 µm; right panels: 10 µm; ➞: Arc/Arg3.1 mRNA + Protein; ➪: PV Protein; ►: BDNF mRNA. **c:** left panel = 10µm; right panel = 100 µm. Nuclear staining DAPI (blue). Mean ± S.E.M.

Figure 4

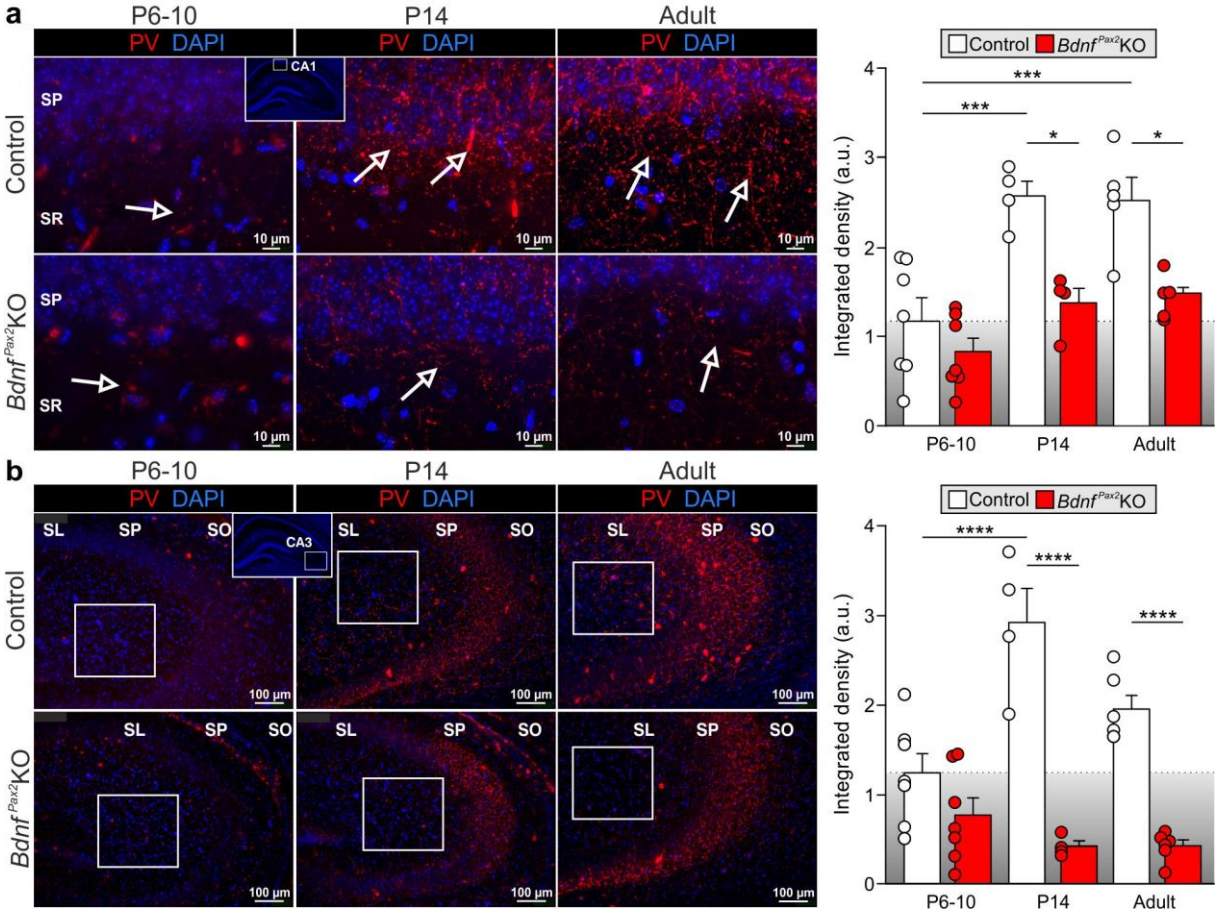

Figure 4 | Only mature controls showed increased PV arborization during development in the hippocampus.

(**a**) Immunostaining of PV (red) the CA1 region over development. Scale bar = 10 µm. Right panel: Quantification of PV fluorescence intensity in the CA1 region over development (2-way ANOVA; P6-10: $n = 7$ each; P14: $n = 4$ each; adult: $n = 5$ each, Genotype: $F(1,26) = 27.10$, $P < 0.0001$; Age: $F(2,26) = 17.30$, $P < 0.0001$; Bonferroni post-hoc test: P6-10 controls vs. P14 controls $P < 0.001$, P6-10 controls vs. adult controls $P < 0.001$, P14 controls vs. adult controls $P > 0.05$, P6-10 *Bdnf*^{Pax2}KOs vs. P14 *Bdnf*^{Pax2}KOs $P > 0.05$, P14 *Bdnf*^{Pax2}KOs vs. adult *Bdnf*^{Pax2}KOs $P > 0.05$, P6-10 controls vs. P6-10 *Bdnf*^{Pax2}KOs $P > 0.05$, P14 controls vs. P14 *Bdnf*^{Pax2}KOs $P < 0.05$, adult controls vs. adult *Bdnf*^{Pax2}KOs $P < 0.05$).

(**b**) Immunostaining of PV (red) in the CA3 of adult *Bdnf*^{Pax2}KOs and controls. Scale bars = 100µm. Right panel: Quantification of the PV expression in the CA3 region (see white squares; 2-way ANOVA; P6-10: $n = 7$ each; P14: $n = 4$ each; adult: $n = 6$ each, Genotype: $F(1,28) = 80.16$, $P < 0.0001$; Age: $F(2,24) = 5.05$, $P < 0.05$; interaction: $P < 0.001$; Bonferroni post-hoc test: P6-10 controls vs. P14 controls $P < 0.0001$, P6-10 controls vs. adult controls $P > 0.05$, P14 controls vs. adult controls $P > 0.05$, P6-10 *Bdnf*^{Pax2}KOs vs. P14 *Bdnf*^{Pax2}KOs $P < 0.01$, P6-10 *Bdnf*^{Pax2}KOs vs. adult *Bdnf*^{Pax2}KOs $P > 0.05$, P14 *Bdnf*^{Pax2}KOs vs. adult *Bdnf*^{Pax2}KOs $P > 0.05$, P6-10 controls vs. P6-10 *Bdnf*^{Pax2}KOs $P > 0.05$, P14 controls vs. P14 *Bdnf*^{Pax2}KOs $P < 0.0001$, adult controls vs. adult *Bdnf*^{Pax2}KOs $P < 0.0001$). Nuclear staining DAPI (blue). Mean ± S.E.M.

Figure 5

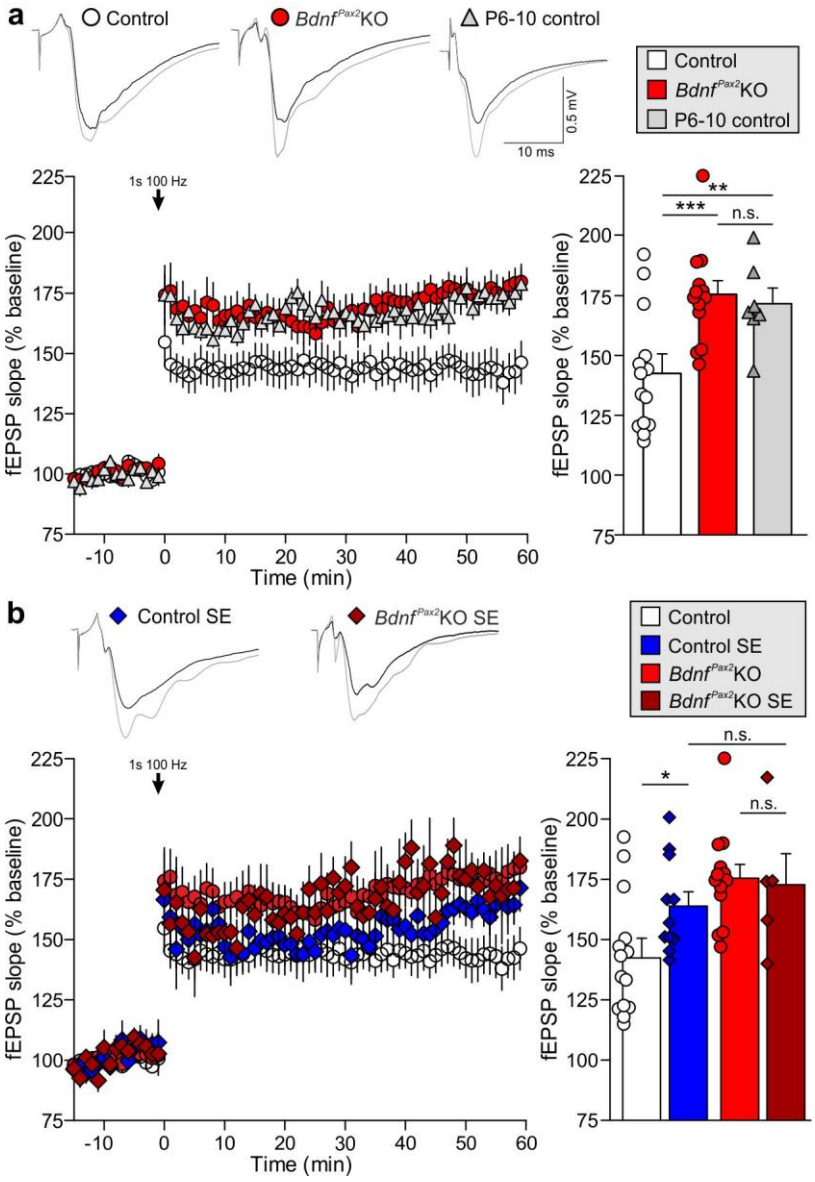
a
Control
Bdnf^Pax2KO
P6-10 control
0.5 mV
10 ms
1s 100 Hz
fEPSP slope (% baseline)
Time (min)
**
***
n.s.
b
Control SE
Bdnf^Pax2KO SE
*

Figure 5 | *Bdnf*^{Pax2}KOs showed elevated LTP and failed LTP facilitation during sound adjustments.

(**a**,**b**) Left Panel, Averaged time courses of fEPSP slopes in acute brain slices from controls, *Bdnf*^{Pax2}KOs, P6-10 controls and sound exposed controls and *Bdnf*^{Pax2}KOs. Representative traces before (black) and after (gray) induction of LTP are shown on top. Animals from all conditions readily showed significant LTP.

(**a**) Right panel: Significantly increased LTP was observed for *Bdnf*^{Pax2}KOs (n = 9/13 animals/slices; 175.5 ± 5.7 %) and P6-10 controls (n = 6/7 animals/slices; 171.6 ± 6.5 %) compared to adult controls (n = 9/14 animals/slices; 142.4 ± 8.2 %; 1-way ANOVA, $F(5,62) = 42.81$, $P < 0.0001$, Bonferroni's post-hoc test tetanized/tetanized (t/t): controls vs. *Bdnf*^{Pax2}KOs $P < 0.001$; controls vs P6-10 controls $P < 0.01$; P6-10 controls vs *Bdnf*^{Pax2}KOs $P > 0.05$).

(**b**) Right panel: Significantly increased LTP was observed for enriching sound exposed (80-100 dB; SE) controls (n = 4/11 animals/slices, 164.9 ± 5.9 %) compared to unexposed controls (n = 9/14 animals/slices; 142.4 ± 8.2 %) but not in enriching sound exposed *Bdnf*^{Pax2}KOs (n = 3/5 animals/slices; 172.9 ± 12.9 %) compared to unexposed *Bdnf*^{Pax2}KOs (n = 9/14 animals/slices; 175.5 ± 5.7 %; 1-way ANOVA, $F(7,78) = 37.24$, $P < 0.0001$, Bonferroni's post-hoc test tetanized/tetanized (t/t): controls vs. controls exposed $P < 0.05$; *Bdnf*^{Pax2}KOs vs *Bdnf*^{Pax2}KOs exposed $P > 0.05$; control exposed vs. *Bdnf*^{Pax2}KOs exposed $P > 0.05$). Mean ± S.E.M.

Figure 5-figure supplement 1

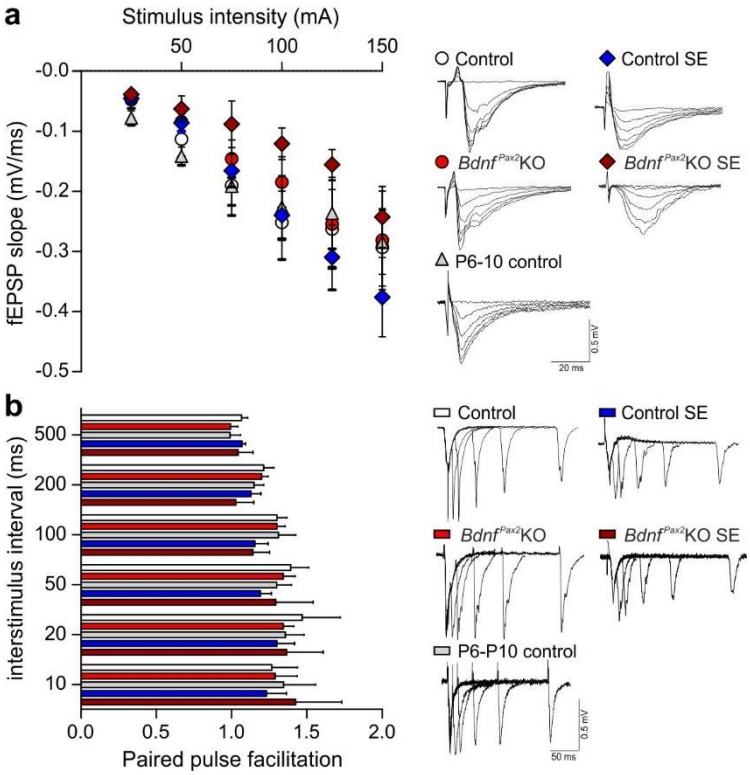

Figure 5-figure supplement 1 | All groups showed normal basal synaptic transmission and presynaptic function.

(**a**) Averaged fEPSP slope was plotted against stimulus intensity. No difference was observed between slices from controls, *Bdnf*^{Pax2}KOs, P6-10 controls and enriching sound exposed (SE) controls and *Bdnf*^{Pax2}KOs. Traces from representative recordings are shown on the right (control: $n = 9/14$ animals/slices, *Bdnf*^{Pax2}KOs: $n = 9/10$ animals/slices, P6-10 controls $n = 6/7$ animals/slices, controls exposed $n = 4/11$ animals/slices, *Bdnf*^{Pax2}KOs exposed $n = 3/5$ animals/slices; 1-way ANOVA, $F(4,25) = 0.80$, $P = 0.54$).

(**b**) Paired pulse facilitation was not different between slices from controls, *Bdnf*^{Pax2}KOs, P6-10 controls and sound exposed controls and *Bdnf*^{Pax2}KOs for all inter-stimulus intervals. Traces from representative recordings are shown on the right. (controls: $n = 9/14$ animals/slices, *Bdnf*^{Pax2}KOs: $n = 9/10$ animals/slices, P6-10 controls $n = 6/7$ animals/slices, controls exposed $n = 4/11$ animals/slices, *Bdnf*^{Pax2}KOs exposed $n = 3/5$ animals/slices; 1-way ANOVA, $F(4,25) = 0.49$, $P = 0.75$). Mean ± S.E.M.

Figure 6

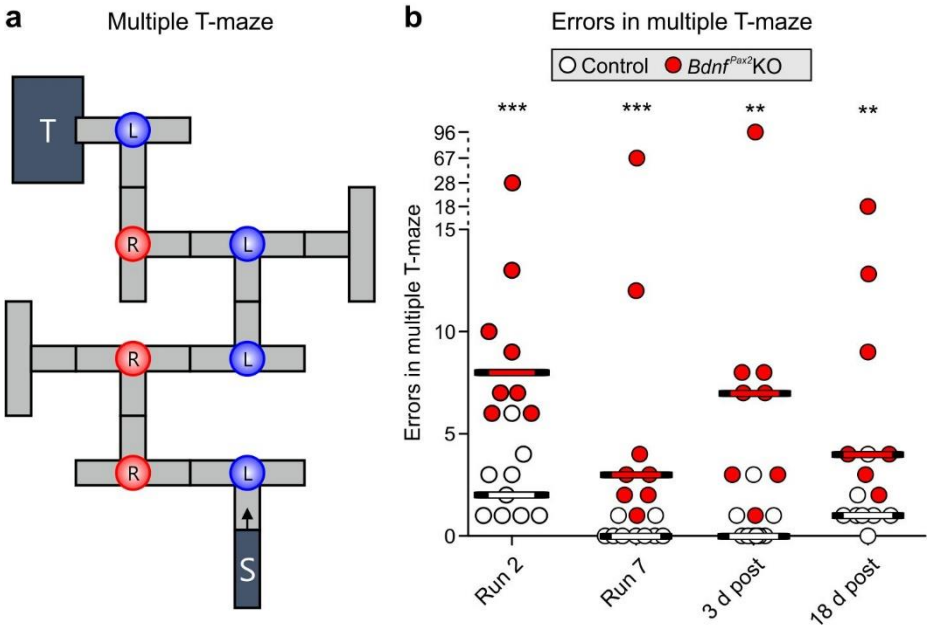

Figure 6 | *Bdnf*^{Pax2}KOs showed deficits in learning and memory.

(**a**) The learning experiment was conducted in a multiple T-maze with 7 decision points (L: left turn correct; R: right turn correct).

(**b**) *Bdnf*^{Pax2}KOs had a significantly higher median error rate in all evaluated runs (Wilcoxon/Kruskal-Wallis-Tests: Run 2: $X^2(1, n = 8/9) = 11.6$, $P < 0.001$; Run 7: $X^2(1, n = 8/9) = 12.3$, $P < 0.001$; 3 d post: $X^2 = (1, n = 8/9) = 10.7$, $P = 0.001$; 18 d post: $X^2 = (1, n = 8/9) = 9.2$, $P = 0.002$), but showed successful learning from run 2 to run 7. However, long-term memory 3 d and 18 d after the last training run was impaired in *Bdnf*^{Pax2}KOs compared with controls.

Figure 6-figure supplement 1

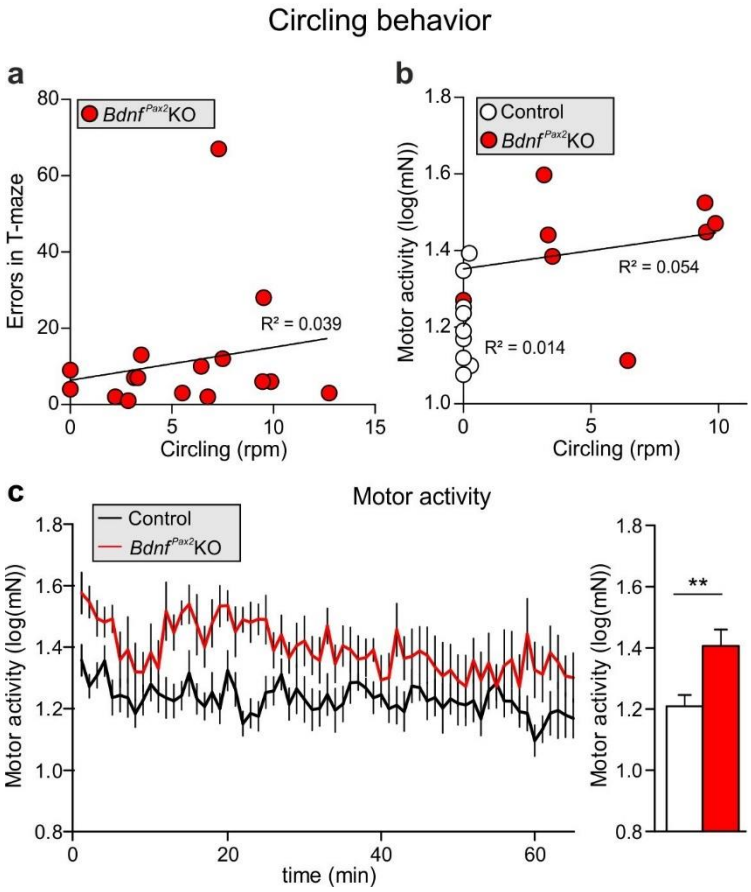

Figure 6-figure supplement 1 | Circling behavior did not influence memory performance and hyperactivity.

(**a**) Most *Bdnf*^{Pax2}KOs displayed circling behavior; this circling behavior was not significantly correlated with learning errors (*Bdnf*^{Pax2}KOs: $n = 8$; data shown for run 2 and 7; linear regression: $R^2 = 0.039$).

(**b**) While *Bdnf*^{Pax2}KOs displayed more circling as well as more motor activity than controls, there was no significant correlation between these two measures inside the two genotypic groups (linear regression: controls: $R^2 = 0.014$; *Bdnf*^{Pax2}KOs: $R^2 = 0.054$).

(**c**) Motor activity was increased in *Bdnf*^{Pax2}KOs, measured on a ballistic platform during a startle measurement (unpaired two-tailed student's t-test: controls $n = 7$, *Bdnf*^{Pax2}KOs $n = 9$; $t(17) = 3.08$, $P = 0.007$).

Figure 7

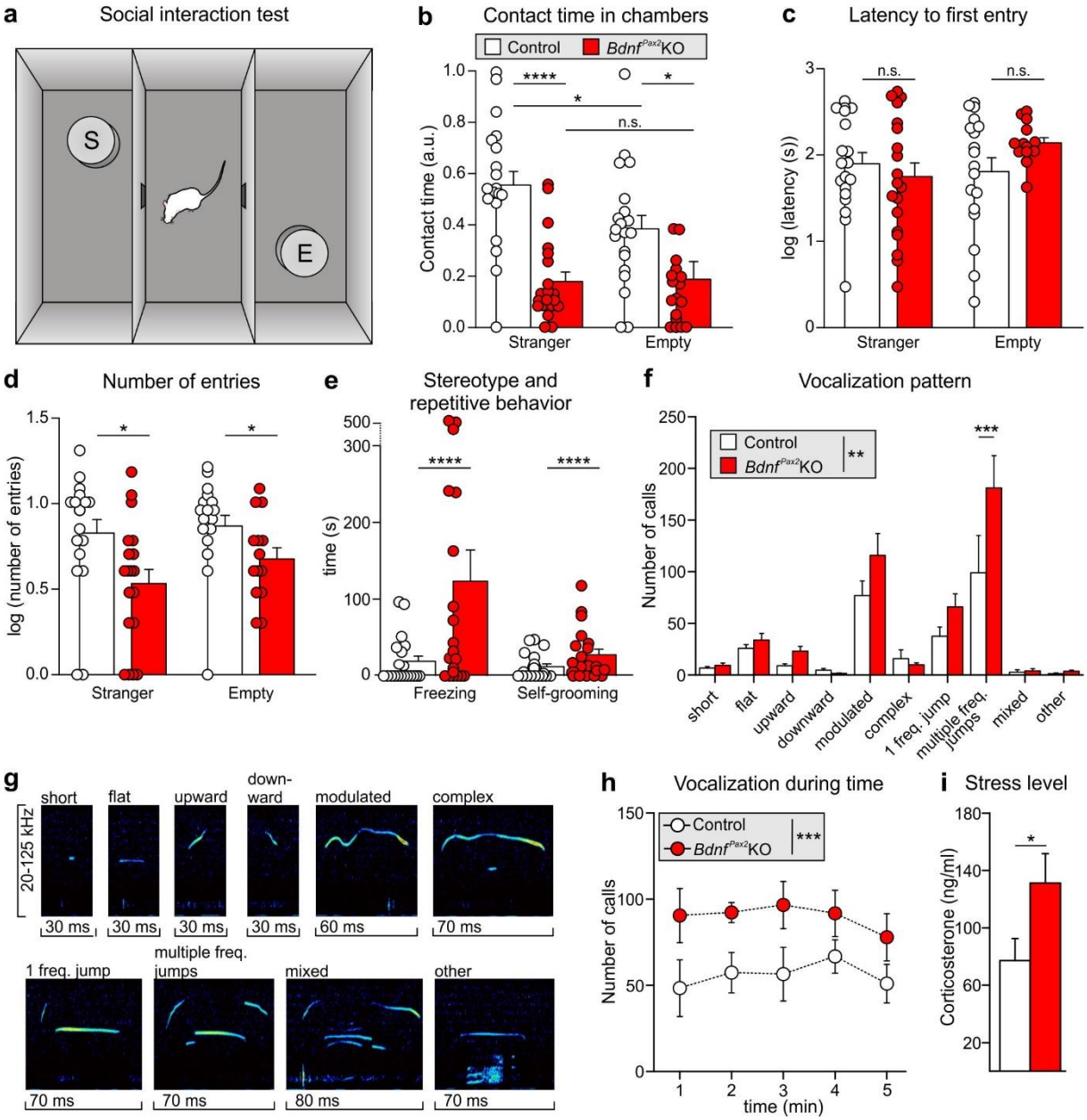
a
Social interaction test
S
E
b
Contact time in chambers
Control
Bdnf Pax2 KO
Contact time (a.u.)
Stranger
Empty
c
Latency to first entry
log (latency (s))
n.s.
d
Number of entries
log (number of entries)
e
Stereotype and repetitive behavior
time (s)
Freezing
Self-grooming
f
Vocalization pattern
Number of calls
short
flat
upward
downward
modulated
complex
1 freq. jump
multiple freq. jumps
mixed
other
g
20-125 kHz
30 ms
60 ms
70 ms
80 ms
h
Vocalization during time
time (min)
i
Stress level
Corticosterone (ng/ml)

Figure 7 | *Bdnf*^{Pax2}KOs exhibited less explorative behavior.

(**a**) Schematic drawing of the Crawley's sociability apparatus with three chambers. In one of the outer chambers a stranger mouse (S) was placed below the container while the other chamber was equipped with an empty (E) container.

(**b**) *Bdnf*^{Pax2}KOs spent less time with sniffing contacts towards the stranger and empty container (unpaired two-tailed student's t-test; $n = 20$ each, stranger: $t(38) = 5.84$, $P < 0.0001$; empty $t(18) = 2.29$, $P = 0.0278$). Controls exhibit a preference for sniffing contact with stranger container compared to *Bdnf*^{Pax2}KOs (unpaired two-tailed student's t-test; control: $n = 20$, $t(38) = 2.29$, $P = 0.027$; *Bdnf*^{Pax2}KOs: $n = 20$, $t(18) = 0.11$, $P = 0.916$)

(**c**) The latency to the first entry of either outer compartment was similar in both genotypes (unpaired two-tailed student's t-tests: $n = 14$-19 each, stranger: $t(36) = 0.70$, $P = 0.486$; empty: $t(30) = 1.68$, $P = 0.104$) but

(**d**) the number of entries to both chambers was decreased in *Bdnf*^{Pax2}KOs (unpaired two-tailed student's t-tests: $n = 14$-19 each, stranger: $t(36) = 2.59$, $P = 0.0138$; empty: $t(30) = 2.08$, $P = 0.0462$).

(**e**) *Bdnf*^{Pax2}KOs revealed an increased stereotype and repetitive behavior shown by freezing (Chi-square test for trend; $X^2(1, n = 20 \text{ each}) = 199.8$, $P < 0.0001$) and self-grooming (Chi-square test for trend; $X^2(1, n = 20 \text{ each}) = 24.5$, $P < 0.0001$).

(**f**) Differences in the vocalization pattern (shown in **g**) between *Bdnf*^{Pax2}KO and control pups with increased multiple frequency jumps in *Bdnf*^{Pax2}KOs (2-way ANOVA; $n = 8$ each, Genotype: $F(1,9) = 8.57$, $P = 0.004$; Pattern: $F(1,9) = 26.32$ $P < 0.0001$ Interaction: $F(1,9) = 2.18$ $P = 0.027$).

(**g**) Typical examples of vocalization pattern in mouse pups.

(**h**) Ultrasonic call rate recorded in short-term isolated pups was increased in *Bdnf*^{Pax2}KOs (2-way ANOVA; $n = 8$ each; $F(1,4) = 16.76$, $P < 0.001$).

(**i**) Blood corticosterone level was increased in *Bdnf*^{Pax2}KOs (unpaired two-tailed student's t-tests: $n = 13$ each, $t(24) = 2.08$, $P = 0.048$). Mean ± S.E.M.

Figure 8

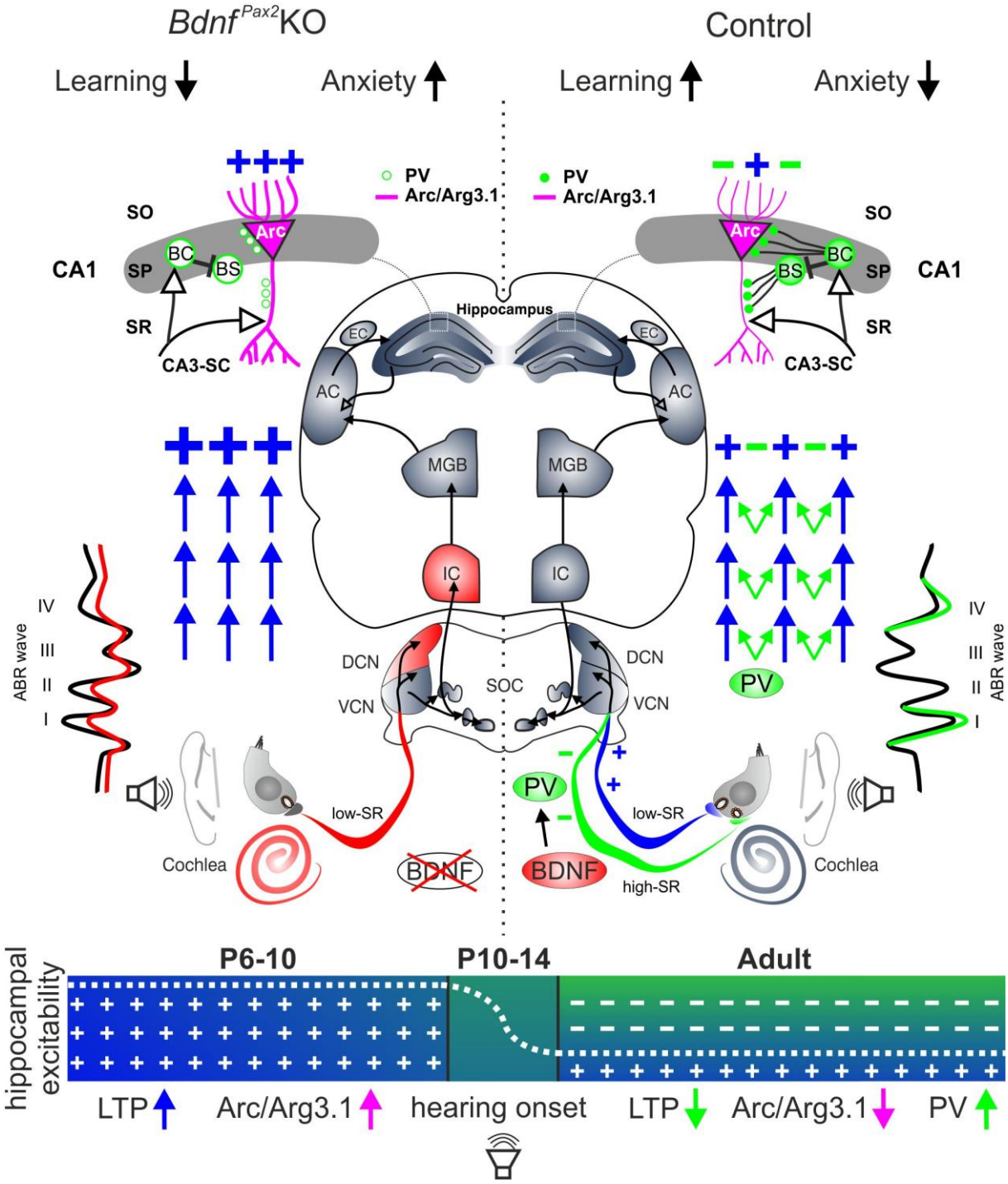

Figure 8 | Summary of the shaping of PV-IN network in the auditory pathway in controls and *Bdnf*^{Pax2}KOs. The deletion of *Bdnf* in cochlea, DCN and IC in *Bdnf*^{Pax2}KOs diminishes coding of rapid auditory processing. This leads to incomplete maturation of fast-spiking PV-network in the AC and hippocampus from hearing onset onwards, although BDNF levels are not changed in these forebrain regions. The incomplete maturation of fast-spiking PV-network in *Bdnf*^{Pax2}KOs leads to elevated LTP in CA1 dendrites as observed prior to hearing. This causes elevated Arc/Arg3.1 levels, impaired adjustment of LTP to enrichment, impaired memory, decreased explorative and increased anxiety behavior.

frontiers in Molecular Neuroscience

ORIGINAL RESEARCH
published: 27 September 2018
doi: 10.3389/fnmol.2018.00325

BDNF-Live-Exon-Visualization (BLEV) Allows Differential Detection of BDNF Transcripts *in vitro* and *in vivo*

*Wibke Singer[1†], Marie Manthey[1†], Rama Panford-Walsh[1], Lucas Matt[2], Hyun-Soon Geisler[1], Eleonora Passeri[1], Gabriele Baj[3], Enrico Tongiorgi[3], Graciano Leal[4], Carlos B. Duarte[4], Ivan L. Salazar[4], Philipp Eckert[1], Karin Rohbock[1], Jing Hu[5], Jörg Strotmann[6], Peter Ruth[2], Ulrike Zimmermann[1], Lukas Rüttiger[1], Thomas Ott[7], Thomas Schimmang[8] and Marlies Knipper[1]**

[1] Department of Otolaryngology, Tübingen Hearing Research Centre (THRC), Molecular Physiology of Hearing, University of Tübingen, Tübingen, Germany, [2] Department of Pharmacology, Institute of Pharmacy, Toxicology and Clinical Pharmacy, University of Tübingen, Tübingen, Germany, [3] B.R.A.I.N. Centre for Neuroscience, Department of Life Sciences, University of Trieste, Trieste, Italy, [4] Centre for Neuroscience and Cell Biology (CNC), Department of Life Sciences, University of Coimbra, Coimbra, Portugal, [5] Centre for Integrative Neuroscience (CIN), University of Tübingen, Tübingen, Germany, [6] Department of Physiology, Institute of Physiology, University of Hohenheim, Stuttgart, Germany, [7] Transgenic Facility Tübingen, University of Tübingen, Tübingen, Germany, [8] Instituto de Biologíay Genética Molecular, Universidad de Valladolid y Consejo Superior de Investigaciones Científicas, Valladolid, Spain

OPEN ACCESS

Edited by:
Isabel Varela-Nieto, Consejo Superior de Investigaciones Científicas (CSIC), Spain

Reviewed by:
Jean-Philippe Guilloux, Université Paris-Sud, France
Lucas Pozzo-Miller, University of Alabama at Birmingham, United States

***Correspondence:**
Marlies Knipper
marlies.knipper@uni-tuebingen.de

† These authors have contributed equally to this work

Received: *20 June 2018*
Accepted: *22 August 2018*
Published: *27 September 2018*

Citation:
Singer W, Manthey M, Panford-Walsh R, Matt L, Geisler H-S, Passeri E, Baj G, Tongiorgi E, Leal G, Duarte CB, Salazar IL, Eckert P, Rohbock K, Hu J, Strotmann J, Ruth P, Zimmermann U, Rüttiger L, Ott T, Schimmang T and Knipper M (2018) BDNF-Live-Exon-Visualization (BLEV) Allows Differential Detection of BDNF Transcripts in vitro and in vivo. Front. Mol. Neurosci. 11:325. doi: 10.3389/fnmol.2018.00325

Bdnf exon-IV and exon-VI transcripts are driven by neuronal activity and are involved in pathologies related to sleep, fear or memory disorders. However, how their differential transcription translates activity changes into long-lasting network changes is elusive. Aiming to trace specifically the network controlled by exon-IV and -VI derived BDNF during activity-dependent plasticity changes, we generated a transgenic reporter mouse for ***B****DNF-****l****ive-****e****xon-****v****isualization (BLEV)*, in which expression of *Bdnf* exon-IV and -VI can be visualized by co-expression of CFP and YFP. CFP and YFP expression was differentially activated and targeted in cell lines, primary cultures and BLEV reporter mice without interfering with BDNF protein synthesis. CFP and YFP expression, moreover, overlapped with BDNF protein expression in defined hippocampal neuronal, glial and vascular locations *in vivo*. So far, activity-dependent BDNF cannot be explicitly monitored independent of basal BDNF levels. The BLEV reporter mouse therefore provides a new model, which can be used to test whether stimulus-induced activity-dependent changes in BDNF expression are instrumental for long-lasting plasticity modifications.

Keywords: BDNF detection, *Bdnf* exon-IV and -VI, transgenic BDNF reporter mice, activity-dependent BDNF expression, long-lasting plasticity changes

INTRODUCTION

Brain derived neurotrophic factor (BDNF), identified and purified in 1982 (Barde et al., 1982), is a key modulator of synaptic function during homeostatic readjustment processes and a master regulator of energy homeostasis (for review see: Bramham and Messaoudi, 2005; Rauskolb et al., 2010). Despite its importance, the influence of BDNF on circuit stabilization in the adult system, or its complex role in numerous brain and cardio-vascular diseases (Kuipers and Bramham, 2006; Marosi and Mattson, 2014; Leal et al., 2017), is still not completely understood (Nahmani and Turrigiano, 2014). Several factors impede detailed analysis. On the one hand, expression of BDNF in the mature CNS is extremely low and not

restricted to neurons (Danzer and McNamara, 2004; Dieni et al., 2012), but also found in platelets (Chacón-Fernández et al., 2016), capillary endothelial cells (Donovan et al., 2000), microglia, and astrocytes (Ferrini and De Koninck, 2013; Parkhurst et al., 2013). Most enigmatic, however, is the complex structure of the BDNF gene, which consists of eight non-coding exons (I-VIII), which are alternatively spliced to the protein-encoding exon-IX. Transcription of each of the resulting mRNAs is regulated differently in terms of temporal and spatial location, additionally some transcripts show stimulus- and activity-dependence (Pattabiraman et al., 2005; Chiaruttini et al., 2008). The resulting transcripts in turn display different stability, targeting, and translatability (Timmusk et al., 1993; West et al., 2014). Ultimately, each transcript is translated into an identical BDNF peptide, cleaved and released as mature BDNF (Yang et al., 2009). BDNF transcripts containing *Bdnf* exon-IV and -VI are particularly interesting as their translation is directly or indirectly regulated by changes in neuronal activity (Hong et al., 2008; West et al., 2014; Tuvikene et al., 2016) and their dysregulation is linked to various brain pathologies related to sleep, loss of fear memory (Hill et al., 2016), and depression (Marosi and Mattson, 2014). BDNF-TrkB receptor signaling is crucial for activity-dependent regulation of synaptic strength in various brain regions (Kellner et al., 2014). Moreover, activity-dependent regulation of synaptic strength was previously suggested to play a role during long-lasting adaptation of brain responses to external demand. Accordingly, only the coincidence of for example glucocorticoid function acting on mitochondria and dendritic spines together with context-specific activity (e.g., motor learning), lead to long-lasting spine formation, memory consolidation and behavioral performance (see for a review: Jeanneteau and Arango-Lievano, 2016). In this context the potential function of activity-dependent BDNF to provide context information cannot be tested due to difficulties in its detection in the adult organ (Dieni et al., 2012), and unfeasibility to extract activity-dependent BDNF from background BDNF levels.

To investigate whether activity-dependent *Bdnf* exon-IV or -VI promoter usage provides context-specific information during task-specific learning, we generated a knock-in reporter mouse line for ***B**DNF-**l**ive-**e**xon-**v**isualization* (BLEV). In contrast to previous studies analyzing the distinct functions of *Bdnf* transcripts through deletion of promoter function (Hong et al., 2008; Sakata et al., 2010; Parkhurst et al., 2013; Mallei et al., 2015), we generated a BDNF knock-in reporter mouse. In the BLEV reporter mouse line, the marker proteins CFP and YFP (cyan- and yellow-fluorescent protein) tag the sites, where mRNA containing the activity-dependent *Bdnf* exon-IV or exon-VI is translated. This allows monitoring of exon-IV and exon-VI promoter usage *in vitro* and *in vivo* above the background of basal BDNF levels. We verify that the knock-in does not interfere with the normal BDNF transcription, translation or protein function and approve the specific detection of activity-driven BDNF transcript changes in the brain.

The BLEV reporter mouse thus constitutes the first model to allow selective and sensitive tracing of activity-dependent *Bdnf* transcripts in functional neuronal networks *in vitro* and *in vivo*, without impairing normal BDNF protein functions.

MATERIALS AND METHODS

Animals

Animal care and use and experimental protocols correspond to national and institutional guidelines and were reviewed and approved by the animal welfare commissioner and the regional board for animal experimentation. All experiments were performed according to the European Union Directive 2010/63/EU for the protection of animals used for experimental and other scientific purposes.

Vector Construct for a Transgenic BDNF Mouse

The *Bdnf* exon-IV sequence is extended by CFP and the *Bdnf* exon-VI sequence by YFP, both containing a stop codon. The translation of *Bdnf* exon-IX is enabled by an IRES sequence, which keeps the mRNA at the ribosome, despite the presence of a stop codon. Additionally, the growth-associated protein 43 (GAP43), is added to anchor the fluorescent proteins at the site of translation. This allows differential monitoring of the non-coding *Bdnf* exon-IV and *Bdnf* exon-VI by the fluorescent proteins CFP and YFP without interfering with *Bdnf* exon-IX.

In detail, to generate a mouse line in which different *Bdnf* exons are labeled by different fluorescent markers (**Figure 1A**), *Bdnf* exon-IV and -VI were amplified from genomic DNA. Primers were designed to amplify *Bdnf* exon-IV (5′-TAGAA CCTTGGGGACCATGCTGTGCTGTATGAG-3′, 5′-CAGCA CAGCATGGTCCCCAAGGTTCTAGACTC-3′; 5′-GAGAA AGCGCAGGGACCATGCTGTGCTGTGCTGTATGAG-3′; 5′-CAGCACAGCATGGTCCGTGCGCTTTCTCTGCTGC C-3′) or *Bdnf* exon-VI (5′-GTGGGGCAAAGCGAACTGTG A-3′, 5′-CGCAACCCCCATAACGACCAG-3′) including their promoter regions. The PCR product was digested with the enzymes XhoI, SbfI, and MluI for exon-IV and XhoI, AccIII, and MluI for exon-VI to separate the two exons. In a next step, oligonucleotides specific for the membrane anchoring sequence of GAP43, the hemagglutinin (HA) epitope tag, and cMyc (cellular myelocytomatosis oncogene) epitope tag were designed. GAP43 was cloned into the 5′-multiple cloning site (MCS) of the CFP and the YFP vectors (Takara Bio Europe/Clontech; https://www.takarabio.com/assets/documents/Vector%20Documents/pAmCyan%20Vector%20Information.pdf, https://www.takarabio.com/assets/documents/Vector%20Documents/PT3481-5_080612.pdf). The HA tag was inserted into the 3′-MCS of the CFP vector, and the cMyc tag was inserted into the 3′-MCS of the YFP vector. A chimera of *Bdnf* exon-IV and the CFP vector containing GAP43 and HA was amplified. The same was done for *Bdnf* exon-VI and the YFP vector containing GAP43 and cMyc. To make use of an internal ribosomal entry site (IRES), the two PCR products were cloned into a pIRES vector (Takara Bio Europe/Clontech, http://www.takara.co.kr/file/manual/pdf/PT3266-5.pdf). The PCR product containing *Bdnf* exon-IV, GAP43, CFP, and HA was inserted into the MCS A of the pIRES vector. The same was done for the PCR product containing *Bdnf* exon-VI, GAP43, YFP, and cMyc. To design a construct containing *Bdnf* exon-IV and -VI in one vector, *Bdnf* exon-VI, GAP43, YFP, cMyc, and pIRES were cut out

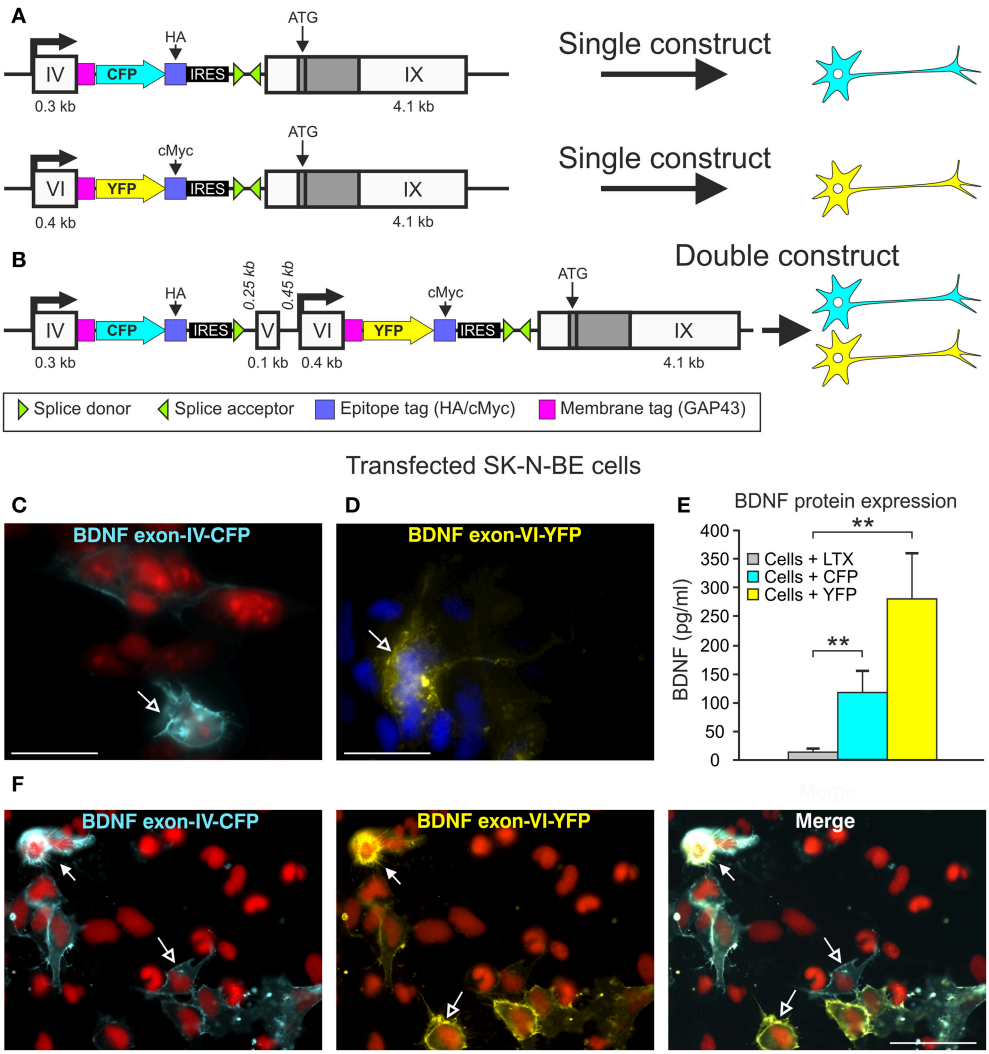

FIGURE 1 | BLEV construct and verification of the in *vitro*. **(A)** Schematic drawing of the *Bdnf* exon-IV-CFP and *Bdnf* exon-VI-YFP single constructs used in cell culture. **(B)** Schematic drawing of the *Bdnf* exon-IV-CFP and exon-VI-YFP double construct used in cell culture. **(C,D)** CFP expression of the *Bdnf* exon-IV-CFP single construct (blue, left panel, nuclear staining: propidium iodide, in red) and YFP expression of the *Bdnf* exon-VI-YFP single construct (yellow, right panel, nuclear staining: DAPI, in blue). **(E)** ELISA of BDNF protein in SK-N-BE cells transfected with either the *Bdnf* exon-IV-CFP single construct or the *Bdnf* exon-VI-YFP single construct. BDNF is not expressed in cells treated with Lipofectamine (LTX, gray bar) only. BDNF is expressed in SK-N-BE cells transfected with either of the two single constructs (blue bar: *Bdnf* exon-IV-CFP; yellow bar: *Bdnf* exon-VI-YFP). Data are shown as mean BDNF concentration (pg/ml) ± SEM [1-way ANOVA: $F_{(3,36)} = 8.35$ $p = 0.0002$; post-test 2-sided Student's *t*-test: CFP $p = 0.008$; YFP $p = 0.003$; done in duplicate for 4 independent experiments]. **(F)** SK-N-BE cells transfected with the *Bdnf* exon-IV-CFP exon-VI-YFP double construct. The left panel shows the CFP expression (blue), the middle panel shows the YFP expression (yellow), and the right panel shows a merged image of *Bdnf* exon-IV-CFP and *Bdnf* exon-VI-YFP expression. Open arrows show cells expressing either CFP or YFP, filled arrows show cells expressing CFP and YFP. Nuclear staining in red (propidium iodide). **(C,D)** scale bars = 20 μm; **(F)** scale bar = 50 μm.

of one pIRES vector and cloned into the MCS B of the pIRES vector, which already contained *Bdnf* exon-IV, GAP43, CFP, and HA. From this pIRES vector, the part containing *Bdnf* exon-IV, GAP43, CFP, HA, pIRES and *Bdnf* exon-VI, GAP43, YFP, cMyc, pIRES were inserted together with the loxP sites of the pMCS 5 vector (http://www.mobitec.com/cms/products/bio/04_vector_sys/multiple_cloning_site_pmcs5.html, kindly provided by Prof. Dusan Bartsch; Central Institute of Mental Health, Department of Molecular Biology, Mannheim, Germany), into the pEasyFloxII/SK62 vector between the neomycin cassette and the HSV-TK cassette. The 5′-homologous sequence was also inserted into the pEasyFloxII/SK62 vector in front of the neomycin cassette. This vector construct was used to generate the transgenic mouse line.

Generation of the Transgenic BDNF Mouse

The construct was linearized with NotI and electroporated into HM1 embryonic stem (ES) cells (Magin et al., 1992). ES cell clones were selected with neomycin. Recombinant ES cell clones were verified by PCR using oligonucleotides for the 5′-end (for: 5′-GAGTTGGGAGAATATTAGGC-3′; rev: AGGTAGCCGGATCAAGCGTATGCAGC-3′) and the 3′-end

(for: 5′-GTCCTGCTGGATATATACATGGGGCAG-3′; rev: 5′-GTCAACTTATAATTACCGGTTCC-3′) resulting in PCR products of either 2.5 or 6.7 kb, respectively. Positive clones were screened additionally by Southern blot. In brief, isolated DNA was digested using EcoRV and SalI (Roche). DNA fragments were separated on a 0.8% agarose gel. The DNA was blotted onto a nylon membrane and fixed. Different DNA probes were hybridized to the membrane at 68°C overnight. On the next day, bands were visualized using the detection starter Kit II (Roche). The probes were specific either for the 5′-end, the 3′-end and two internal sequences, covering either parts of the transgenic exon-IV or -VI. Due to the restriction sites, the WT and the transgenic allele could be differentiated. For the 5′-end probe, the WT band was 9.8 kb, the band of the transgenic allele was 3 kb; for the 3′-end, the WT and the transgenic band was 12.7 kb. For the probe covering exon-IV, a WT band of 9.8 and 5.3 kb band for the transgenic allele were obtained. The probe covering exon-VI resulted in a 9.8 kb band for the WT and a 6.3 kb band for the transgenic allele (**Figure 3C**, **Supplementary Figure 1**). A selected ES cell clone was used for injection into blastocysts. Chimeras were carried out by foster mothers. Deletion of the Neo cassette was achieved by breeding the offspring with Pgk-*Cre* mice (Lallemand et al., 1998). Genotyping of these mice was performed using oligonucleotides for *Cre* (for: 5′-ACGACCAAGTGACAGCAATA-3′, rev: 5′-CCATGCCTCGACCAGTTTAG-3′). For genotyping the transgenic BDNF mouse, two primer sets were used. The insert PCR of CFP (for: 5′-GAACAGGAGTACATATCGGCC-3′, rev: 5′-TTCATATGACATTCCGTCAGG-3′) resulted in a 437 bp PCR product for the transgenic mouse and no PCR product for the WT. To verify the different genotypes, additional PCRs were performed using the forward primer 5′-GAACAGGAGTACATATCGGCC-3′ and either the reverse primer 5′-GAACACACAATGAAACTACACAGAG-3′ for the WT resulting in a 428 bp product, or 5′-TTCATATGACA TTCCGTCAGG-3′ for the transgene (437 bp). The BLEV mouse line (B6;129-Bdnftm1(ex4CFPex6YFP)MknixB6;HM1-Pgktm1(Cre)Lni/Mkni) was maintained by breeding heterozygotes.

CELL CULTURE

Vector Construct for Cell Culture

For the constructs used in cell culture, *Bdnf* exon-IX was inserted in the MCS B of the pIRES vectors containing either *Bdnf* exon-IV, GAP43, CFP, and HA, or *Bdnf* exon-VI, GAP43, YFP, and cMyc (single constructs, **Figure 1A**). To receive the double construct, *Bdnf* exon-IX was cut out of the pIRES vector containing *Bdnf* exon-IV, GAP43, CFP, and HA. Instead, the vector part *Bdnf* exon-VI, GAP43, YFP, cMyc, and *Bdnf* exon-IX from the single construct was inserted into the MCS B (**Figure 1B**).

Cell Culture and Transfection

SK-N-BE cells, kindly provided by PD Dr. Ulrike Naumann (Hertie Institute, Tübingen, Germany), were grown on 75 cm^2 flasks in 11 ml Dulbecco's Modified Eagle's Medium (DMEM) (Gibco/Life Technologies) containing 10% fetal calf serum (Gibco/Life Technologies) and 1% penicillin and streptomycin (Gibco/Life Technologies). Cells were sub-cultured for 2 days at 3×10^4 cells/well (BD Bioscience), ensuring cells would be in the log phase of differentiation. The cells were transfected with two different BDNF single constructs or the double construct (**Figures 1A–D**) when they were 50–80% confluent using the lipid-based transfection reagent LTX (Lipofectamine, Life Technologies) according to manufacturer's guidelines. For each DNA construct, 3.5 μg of DNA was gently diluted in 700 μl of DMEM together with 3.5 μl of plus reagent and 7 μl of LTX and incubated for 25-30 min at room temperature. DNA/LTX solution (about 700 μl) and 1,300 μl of serum-free medium were added to each well and mixed by gently rocking the plate for 5 h. The culture medium was changed to standard medium and the cells were incubated at 37°C, 5% CO_2 for 24 h.

ELISA (Enzyme-Linked Immunosorbent Assay) for BDNF

For SK-N-BE cells transfected with 1.5 μg of either single construct (**Figure 1A**) or treated with Lipofectamine only, ELISA for BDNF protein was performed using the ELISA kit from Chemicon. BDNF content was determined from A_{450} readings of human BDNF standards.

Primary Neuronal Culture

Primary mixed neuronal cultures of cortical neurons (mice postnatal day P1-7) or hippocampus (rat, embryonic day E17-18) were prepared following the procedure described by Goslin et al. (1998) and Salazar et al. (2017).

For transfection, primary cortical neurons were plated 7–11 days and transfected with 1–2 μg of the double construct *Bdnf* exon-IV-(HA)-CFP/*Bdnf* exon-VI-(cMyc)-YFP-exon-IX and 1–2 μl Lipofectamine 2000 (Life Technologies) solution (1 mg/ml) diluted in 50–80 μl MEM without serum and antibiotics. The Lipofectamine 2000 and DNA mix was removed 1 h after transfection. The cells were returned to the initial conditioned medium and were incubated in a 5% CO_2-humidified incubator at 37°C for 7 d to allow the expression of transfected constructs.

Stimulation of Hippocampal Primary Culture With Bicuculline

Hippocampal neurons transfected at 7 DIV were stimulated at 15 DIV with 50 μM bicuculline, 2.5 mM 4-Aminopyridine and 10 μM glycine for 3 h as previously described (Costa et al., 2016). They were fixed for 15 min at RT in 4% paraformaldehyde in PBS and mounted in fluorescence mounting medium (DAKO). Fluorescence was analyzed with a Nikon C1Si confocal microscope (Nikon Instruments Europe BV, Amsterdam, Netherlands). A series of optical images at 0.2 μm increments along the "z" axis of the cells stained was acquired. Images were processed for z-projection and for illustration purposes by using ImageJ (NIH, Bethesda, USA) and Adobe Photoshop CS4 (Adobe Systems, San Jose, CA). For immunohistochemistry (**Supplementary Figure 2**) hippocampal neurons were fixed as described above. They were permeabilized with 0.3% Triton X-100 in PBS and incubated with 10% BSA in PBS, for 30 min

at 37°C, to block non-specific staining. Afterwards they were incubated for 2 h at 37°C with the primary antibodies against HA (-CFP) and cMyc (-YFP) diluted in 3% BSA in PBS, for antibody information see **Supplementary Table 1**. The cells were washed 6 times with PBS for 2 min and incubated with the secondary antibodies (see **Supplementary Table 1),** for 45 min at 37°C. Afterwards the coverslips were mounted with a fluorescence mounting medium (DAKO). Here fluorescence images were acquired using a Carl Zeiss LSM 710 confocal microscope with a Plan-Apochromat 63×/1.4 objective using identical settings, with the following excitation lasers/wavelengths: DPSS 561-10/561nm [Red; to visualize *Bdnf* exon-IV-(HA)-CFP], and HeNe633/633nm [Far-Red; to visualize *Bdnf* exon-VI-(cMyc)-YFP].

Kainic Acid Injection

Two to three-month-old homozygous BLEV mice of either sex were injected intraperitoneally with 12 mg/kg kainic acid (Tocris) (KA). This concentration has been previously shown to induce an activity-dependent expression of *Bdnf* exon-IV and -VI in the hippocampus (Chiaruttini et al., 2008). Control animals received the same amount of 0.9% NaCl solution (Fresenius) (vehicle-treated animals). Two hours after injection animals were sacrificed. Animals developed hardly any seizures as they were generated on a C57BL/6N background, which was shown to be resistant to KA-induced insults (Mclin and Steward, 2006).

Hearing Measurements

The hearing function of 2–3 months old homozygous BLEV mice of both sexes was studied by measuring auditory brainstem responses (ABRs), as described previously (Zuccotti et al., 2012; Rüttiger et al., 2013).

Tissue Preparation

For RNA and protein isolation, brains were dissected with small forceps and immediately frozen in liquid nitrogen and stored at −80°C before use. Brain and cochlear tissue for immunohistochemistry was prepared as previously described (Singer et al., 2016).

RNA Isolation

RNA was extracted from brain tissues with a ready-to-use kit according to the manufacturer's protocol (Macherey-Nagel).

Semi-quantitative Reverse Transcription and Polymerase Chain Reaction (RT-PCR)

Transcription of RNA to cDNA was carried out as previously described (Tan et al., 2007). Transcribed cDNA was amplified using PuReTaq Ready-To-Go PCR beads (Amersham Biosciences). Specific forward- and reverse primers for *Bdnf* exon-IX (for: 5′-GAAGCAAACGTCCACGGACAA-3′, rev: 5′-CTGGATGAGGACCAGAAGGTT-3′, 171 bp) were used. Glyceraldehyde 3-phosphate dehydrogenase (GAPDH, for: 5'-TCTACTGGTGTCTTCACCACCA-3′, rev: 5′-ACTGAGGACCAGGTTGTCTCCT-3′, 600 bp) was used as housekeeping gene. Primers for *Bdnf* exons I, II, III, IV, V, VI, VII, VIII and XIA were used according to (Aid et al., 2007). A probe containing the same reagents except the cDNA was used as a negative control. The resulting PCR products were separated on 1.5% agarose gels by electrophoresis and stained with ethidium bromide.

Protein Isolation and Western Blot

For isolation of cMyc-tagged proteins and HA-tagged proteins, the Mild Purification kit and the HA-tagged Protein Purification kit were used, respectively (BiozolDiagnostica). In brief, tissues were dissolved in a lysis buffer (CelLytic M, Sigma-Aldrich) and incubated for 1 h with anti-cMyc or anti-HA tag beads suspension. The suspension was then centrifuged and washed; cMyc- and HA-tagged proteins were eluted with Elution Peptide Solution from the kit.

For BDNF Western blot, co-immunoprecipitation was performed using the Catch and Release v2.0 (Merck Millipore). In brief, tissues were dissolved in lysis buffer (CelLytic M). After preparing the columns with Catch and Release wash buffer, tissue lysate, antibody (anti-BDNF, Genaxxon Bioscience), antibody capture affinity ligand and wash buffer were added to the column. Loaded columns were incubated overnight at a mixer at room temperature. On the next day, the column was centrifuged and washed followed by the elution of the proteins.

Proteins were separated by electrophoresis and placed on a transfer membrane; non-specific epitopes of the membrane were blocked with 5% milk powder solution and incubated overnight at 4°C with the primary antibody (see **Supplementary Table 1**). On the second day, the membrane was washed three times with Tris buffer/0.1% Tween 20; the secondary antibody (HRP-linked ECL anti-rabbit IgG or HRP-linked ECL anti-mouse IgG; GE Healthcare) was incubated for 1 h at room temperature in a sealed envelope. The membrane was washed again three times with Tris buffer/0.1% Tween 20. Finally, the protein bands were visualized with ECL Prime WB Detection Reagent (GE Healthcare) using the Proxima 2700 (Isogen Life Science).

Immunohistochemistry

Brain tissue were isolated, fixed, sectioned, and stained as previously described (Tan et al., 2007; Singer et al., 2016). For antibody information see **Supplementary Table 1**.

DATA ANALYSES

Statistics

All Statistical results and information can be found in the figure legends and in **Supplementary Table 2**. In figures, significance is indicated by asterisks ($^*p < 0.05$, $^{**}p < 0.01$). For animal experiments Power analyses is performed a priori for the applications for animal experiments. A sample size of 4-5 animals per group is sufficient to evaluate a difference in hearing threshold of 10 – 15 dB SPL (alpha 0.05, Power 0.8). For molecular analyses a sample size of 3 – 4 is sufficient to evaluate a difference in gene/protein expression of 15% (alpha 0.05, Power 0.8). For analyses of hearing thresholds no data were excluded, in all mice a hearing threshold could be measured. Molecular samples were excluded when the standard curves were not fitting (ELISA), bands were missing or the housekeeping genes in PCR or Western Blot were irregularly expressed.

ELISA

Data are shown as mean BDNF protein concentration in (pg/ml) (± SEM). Data were statistically analyzed by Student's *t*-test with $\alpha = 0.05$.

PCR

The intensity of the bands was analyzed using the TotalLab Quant software (TotalLab Ltd.). Band intensities of BDNF were normalized to housekeeping gene GAPDH. Results are depicted in relation to *Bdnf* exon-IX expression of WT mice, which was set to 1 (dotted line) as mean ± % SEM. Data were analyzed by 1-way ANOVA with $\alpha = 0.05$, post-test: Bonferroni-Holms (GraphPad Prism). For the untranslated *Bdnf* exons I, II, III, IV, VI, and XIA mean expression values ± SEM are shown for WT and homozygous mice. Data were analyzed for each exon by 2-sided Student's *t*-test with $\alpha = 0.05$ (GraphPad Prism). For original picture see **Supplementary Figure 6D.**

Western Blot

The intensity of the bands was analyzed using the TotalLab Quant software. Band intensities of the genes of interest were normalized to housekeeping gene GAPDH. For BDNF results are depicted in relation to BDNF expression of WT mice, which was set to 1 (dotted line) as mean ± % SEM. Data were analyzed by 1-way ANOVA with $\alpha = 0.05$, post-test: Bonferroni-Holms. For tissue from kainic acid-treated mice, results are shown as % of vehicle-treated mice as mean ± % SEM. Data were analyzed by a 1-sided Student's *t*-test with $\alpha = 0.05$ (GraphPad Prism). For original Blots see **Supplementary Figures 6B,C.**

Hearing Measurements

Click-ABR measurements were analyzed by 1-way ANOVA with $\alpha = 0.05$, post-test: Bonferroni-Holms. Frequency-ABR measurements were group analyzed by multiple *t*-test with $\alpha = 0.05$, corrected for multiple comparison using the Holm-Sidak method (GraphPad Prism). Data are shown as mean ± SD.

Fluorescence Analysis of Brain Immunohistochemistry

Sections shown here were viewed using an Olympus BX61 microscope (Olympus, Center Valley, PA, USA) equipped with an X-Cite Lamp (Olympus). Images were acquired using an Olympus XM10 CCD monochrome camera and analyzed with cellSens Dimension software (OSIS).

To increase spatial resolution, slices were imaged over a distance of 13–15 µm in steps of 0.49 µm within an image-stack along the *z*-axis (*z*-stack) followed by 3-dimensional deconvolution, using a cellSens Dimension built-in algorithm. Typically *z*-stacks consisted of 27–30 layers, for each layer one image was acquired per fluorochrome.

Picture acquired from brain section stained for parvalbumin (PV), were analyzed using the free software ImageJ. (NIH, Bethesda, MD, USA). For each section, three pictures for each single channel (YFP, CFP, PV) were saved and analyzed independently.

For integrated density analysis following vehicle and kainic acid treatment, images from equivalent CA3 regions between treatments were analyzed with ImageJ software to quantify integrated density of CFP and YFP staining within each image for each replicate. Threshold adjustments were set to ensure quantification of only positive immunostaining.

Data Availability

The datasets generated during and/or analyzed during the current study are available from the corresponding author upon request.

RESULTS

Generation of a Transgene to Monitor Transcript IV- and Transcript VI-Specific BDNF Synthesis

In order to generate a system to monitor the sites of transcript-specific BDNF synthesis subsequent to activity-dependent activation of exon-IV or exon-VI promoters *in vivo*, we generated constructs, which allow ***B**DNF-**l**ive-**e**xon-**v**isualization* (BLEV) (**Figure 1**). In the BLEV constructs *Bdnf* exons-IV and -VI are labeled by two different fluorescence proteins: the *Bdnf* exon-IV sequence is extended by CFP and the *Bdnf* exon-VI sequence by YFP, both containing a stop codon. To retain translation of the coding *Bdnf* exon-IX, we introduced an IRES (internal ribosome entry site) sequence, which keeps the mRNA at the ribosome, despite the presence of a stop codon within CFP or YFP. Additionally, the fluorescent proteins were fused to the membrane tag GAP43, in order to anchor them at the site of translation. This design allows localization of when and where *Bdnf* exon-IV and -VI mRNA is used by CFP and YFP fluorescence without interrupting post-translational processing of BDNF (**Figures 1A,B**). Two different epitope tags (HA, cMyc) were incorporated into the construct to facilitate the quantification of CFP or YFP expression by e.g., Western blot (**Figures 1A,B**). Thus, the design of these constructs allows for the quantification of the amount of transcript specific mRNA used for protein translation.

The feasibility of this approach was first tested by transfecting the neuroglioblastoma cell line SK-N-BE, with either the exon-IV-CFP (**Figures 1A** upper panel, **C**) or the exon-VI-YFP single construct (**Figures 1A** lower panel, **D**). Distinct SK-N-BE cells exhibited either CFP or YFP expression (**Figures 1C,D**). To confirm whether BDNF protein is synthetized from these constructs, we performed ELISA assays to compare BDNF protein levels between untransfected and transfected cells (**Figure 1E**). Both single constructs clearly led to elevated levels of BDNF protein expression (blue column: *Bdnf* exon-IV-CFP (HA)-IX; yellow column: *Bdnf* exon-VI-YFP (cMyc)-IX) in comparison to untransfected cells treated with Lipofectamine (LTX) only (**Figure 1E,** gray column). The differences in BDNF protein expression between the two single constructs might be due to the different activation potential of the promoter regions of *Bdnf* exon-IV and -VI (Baj and Tongiorgi, 2009). Furthermore, a different transfection rate of the exon-IV-CFP and the exon-VI-YFP single constructs cannot be excluded as the cells are not stably transfected. Next, we tested the capacity of the double construct to visualize differential expression of *Bdnf* exon-IV-CFP and *Bdnf* exon-VI-YFP in

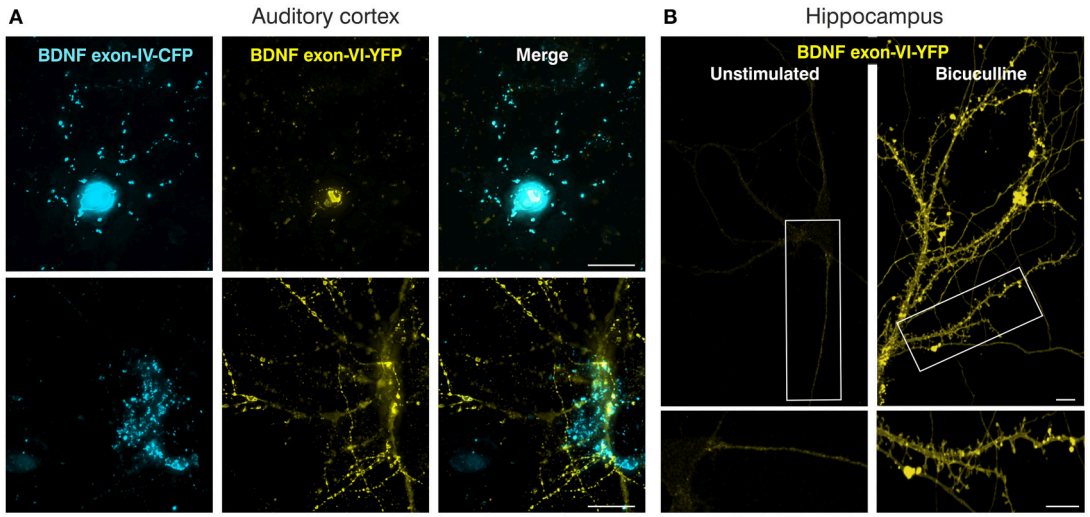

FIGURE 2 | Verification of the BLEV double construct in primary neuronal cultures. **(A)** Mouse primary cortical cell culture (postnatal day 2) transfected with the BDNF double construct. Left panels: *Bdnf* exon-IV-CFP expression; middle panels: *Bdnf* exon-VI-YFP expression; right panels: merged images. Top and bottom panels represent two different neurons. Scale bar: 20 μm. **(B)** Transfected rat primary hippocampal neurons (embryonic day E18) without (left) or with bicuculline (right) stimulation showing *Bdnf* exon-VI-YFP expression. *Bdnf* exon-IV-CFP expression showed an increase preferentially in the cell body (**Supplementary Figure 2A**, arrows), while exon-VI-YFP was predominantly detected in proximal and distal regions of the neurites (**Supplementary Figure 2B**, lower panels). Scale bars: 10 μm.

distinct cells (**Figure 1F**). Transfection of the SK-N-BE cells lead either to the expression of CFP (**Figure 1F,** left panel, open arrows), YFP (**Figure 1F**, middle panel, open arrows), or both fluorescence proteins (**Figure 1F**, closed arrows) confirming that parallel observation of the two non-coding exons expressed from the double construct is feasible. When the double construct (**Figure 1B**) was transfected into primary neuronal cultures of the auditory cortex (AC) (**Figure 2A**), exon-IV-CFP preferentially localized to somata, with comparably limited targeting to dendrites (**Figure 2A,** upper and left panels). Exon-VI-YFP, in contrast, was predominantly found in dendrites, and only rarely in the soma (**Figure 2A**, compare upper and lower panel). This differential distribution of exon-IV-CFP and exon-VI-YFP suggests that the GAP43 membrane-tag does not interfere with the visualization of the fluorescence proteins as observed previously (Liu et al., 1994). Next, transfected primary cultures of hippocampal neurons were treated with the $GABA_A$ receptor antagonist bicuculline (50 μM), 4-aminopyridine (2.5 mM), and glycine (10 μM) (**Figure 2B**), to elevate spontaneous activity which upregulates BDNF expression (Kim et al., 2012). This led to a clear increase in localization of exon-VI-YFP in dendrites and dendritic spines (**Figure 2B**). Distinct results were obtained for exon-VI-YFP and exon-IV-CFP, with the latter construct showing following bicuculline treatment an increased expression preferentially in the cell body (**Supplementary Figure 2A**, arrows), while exon-VI-YFP was predominantly detected in proximal and distal regions of the neurites (**Supplementary Figure 2B**, lower panels). These results confirm that in primary cultures of hippocampal neurons BDNF derived from both exons is differentially targeted to distinct subcellular compartments (Vaghi et al., 2014).

In summary, we introduce a new gene construct, BLEV, allowing observation of changes in exon-IV and exon-VI *Bdnf* promoter usage in response to defined stimuli *in vitro*.

Generation of a Reporter Mouse Model to Monitor Exon-IV-CFP and Exon-VI-YFP

The BLEV construct was inserted into the genomic locus of *Bdnf* via homologous recombination in mouse embryonic stem cells to replace the region harboring exon-IV, -V, -VI, and -VII (between bp 21,000 and 30,485 GenBank ID AY057907) (**Figures 3A,B**). Fidelity of the targeting event was validated by Southern blots using internal as well as 5' or 3' external probes (**Figure 3C**). The genomic DNA was cut by EcoRV [**Figure 3C**, arrows indicate EcoRV restriction sites (RS)] for Southern blotting. The results confirmed the correct insertion within the genomic BDNF sequence using specific probes for the 5'-end (Probe 1, wildtype (WT) band 9.8 kb, transgenic allele 3 kb), the exon-IV transgene (Probe 2, WT band 9.8 kb, transgenic allele 5.3 kb), the exon-VI transgene (Probe 3, WT band 9.8 kb, transgenic allele 6.3 kb) and the 3'-end (Probe 4: WT and transgenic allele 12.7 kb), respectively (**Figure 3C**).

Chimeras were carried by foster mothers and bred over two generations to obtain homozygous BLEV reporter mice. All three genotypes (WT, heterozygous and homozygous animals) were obtained at the expected Mendelian ratio (**Figure 4A**), were fertile, and had a normal life span. Also, no differences in body weight, known to occur upon BDNF deficits (for reviews see: (Rios, 2013, 2014) were observed between WT, heterozygous, and homozygous mice (**Figure 4B**). Furthermore, using RT-PCR (**Figure 4C**) and Western blot (**Figure 4D**), no differences in the hippocampal levels of mRNA containing *Bdnf* exon-IX, the only protein-encoding region of BDNF, or

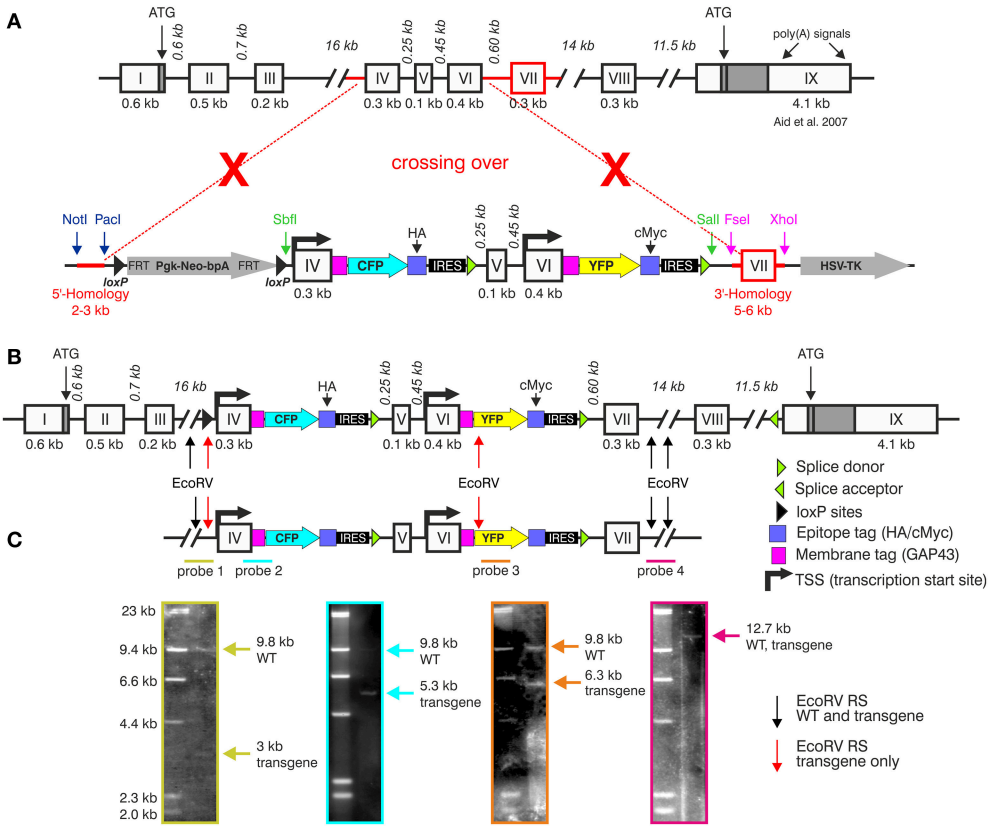

FIGURE 3 | Generation of the BLEV reporter mouse. **(A)** Schematic drawing of the *Bdnf* gene (Aid et al., 2007) and the BDNF vector construct used for homologous recombination. Crossing-over events are indicated by red dotted lines and crosses. The 5' and 3' parts for homologous recombination are marked in red. **(B)** *Bdnf* gene construct depicting insertion sites of the BLEV construct. Arrows indicate the EcoRV restriction sites (RS) used for Southern blot. Black arrows indicate EcoRV RS cutting the WT and the transgenic sequence, red arrows cut only the transgenic sequence. **(C)** Southern blot of a positively transfected ES cell clone. The positions of the four Southern blot probes (colored lines: green, blue, orange, and pink) are shown under the schematic drawing of the BDNF construct. Probe 1, specific for the 5′-end: WT band 9.8 kb, transgenic allele 3 kb; probe 2, covering parts of exon-IV transgene: WT band 9.8 kb, transgenic allele 5.3 kb; probe 3, covering parts of the exon-VI transgene: WT band 9.8 kb, transgenic allele 6.3 kb; probe 4, specific for the 3′-end: WT and transgenic allele 12.7 kb. Note that the size of the drawn construct and probes does not reflect the real size of the DNA fragments obtained by Southern blot. For original Blots see **Supplementary Figure 1**.

BDNF protein between adult WT, heterozygous and homozygous BLEV mice were detected (**Figures 4C,D**). No changes in the expression of untranslated *Bdnf* exons (I, II, III, IV, VI, IXA) were observed using RT-PCR (**Supplementary Figure 3**). The untranslated exons V, VII, and VIII were below the detection level of RT-PCR in the hippocampus.

Previous findings demonstrated mild but significant hearing loss in mice with BDNF deletion in the cochlea (Zuccotti et al., 2012). We compared threshold of ABRs of heterozygous and homozygous BLEV mice to WT controls for click-stimuli (**Figure 4E**, click-ABR) and frequency-dependent ABRs (**Figure 4E**, frequency-ABR). No apparent differences between the genotypes were observed. Additionally, BLEV mice did also not show any circling behavior indicating impaired BDNF expression in the vestibular system (Kaiser et al., 2001; Zuccotti et al., 2012).

Taken together, normal BDNF levels in the CNS and the lack of BDNF-specific phenotypes suggest that BLEV reporter mice retain physiological BDNF expression and functionality.

Exon-IV-CFP and Exon-VI-YFP Expression in BLEV Reporter Mice Co-localize With Endogenous BDNF in Neuronal, Glial, and Vascular Cells

To further validate the BLEV reporter mouse line we next compared exon-IV-CFP and exon-VI-YFP fluorescence signals with BDNF protein expression *in vivo*. These experiments were performed in hippocampal brain slices of homozygous BLEV reporter mice (**Figures 5**, **6**). Hippocampal sections were stained with an antibody specific for the BDNF pro-domain (Dieni et al., 2012; **Figures 5**, **6,** BDNF, see **Supplementary Table 1**). BDNF staining was compared to exon-IV-CFP and exon-VI-YFP signals in sections co-stained with markers for excitatory and inhibitory neurons, glial cells or vascular cells and correlated to previously described sites of BDNF expression (**Figures 5**, **6,** see **Supplementary Table 1**) (for review see: Edelmann et al., 2014). In particular those described in distinct hippocampal cells (Danzer and McNamara, 2004; Danzer et al., 2008).

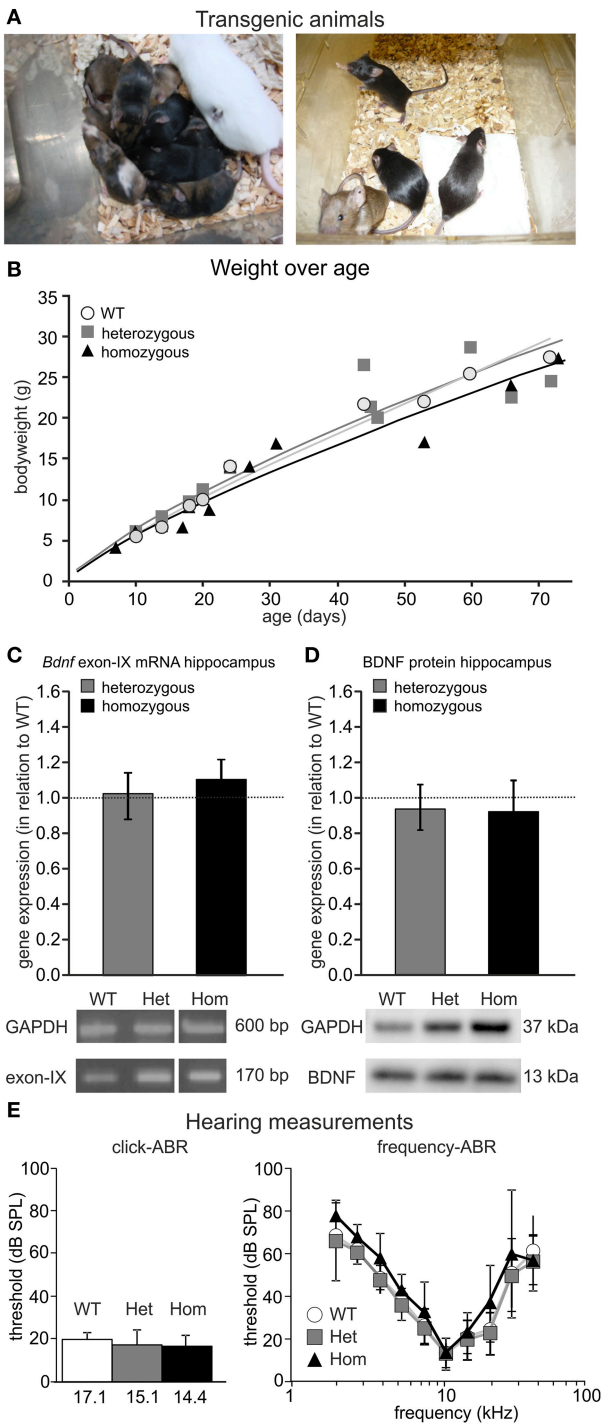

FIGURE 4 | Phenotype of the BLEV mouse line. **(A)** Heterozygous BLEV mouse (white; left panel) and adult homozygous animals (right panel). **(B)** Comparison of the weight of the different genotypes (WT; het; hom). Individual symbols represent individual animals (WT $n = 9$, Het $n = 11$, Hom $n = 11$ animals). **(C)** Analysis of *Bdnf* exon-IX mRNA expression by RT-PCR in the hippocampus of BLEV mice for WT, heterozygous and homozygous animals. BDNF expression was normalized to the WT expression level (dotted line). No changes in the expression of untranslated *Bdnf* exons (I, II, III, IV, VI, IXA) were observed using RT-PCR (**Supplementary Figure 3**). Housekeeping gene: GAPDH. Data represented as mean ± SEM [1-way ANOVA: $F_{(2,9)} = 0.15$ $p = 0.86$; $n = 3$ animals/genotype]. For original picture see **Supplementary Figure 6A**. **(D)** Analysis of BDNF protein expression by Western Blot in the hippocampus of BLEV mice for WT, heterozygous and homozygous animals. BDNF expression was normalized to the WT expression level. Housekeeping gene: GAPDH. Data represented as mean ± SEM [1-way ANOVA: $F_{(2,12)} = 0.20$ $p = 0.82$; $n = 4$ animals/genotype]. For original blot see **Supplementary Figure 6B**. **(E)** Basic hearing function of BLEV mice for WT, heterozygous and homozygous animals. Thresholds for auditory brainstem responses (ABR) to click-stimuli (left panel) and varying pure tone frequencies (right panel). Data represented as mean ± SD [click-ABR: 1-way ANOVA: $F_{(2,26)} = 1.988$ $p = 0.16$; f-ABR: 2-way ANOVA: $F_{(18,2665)} = 0.50$ $p = 0.96$; WT $n = 10$; het $n = 15$; hom $n = 5$ animals].

Examination of BDNF signals in the dentate gyrus (DG) at low-magnification revealed immunoreactivity (IR) in the supra- and infra-pyramidal blades of the granule cell layer (GCL, **Figure 5A**), as previously observed (Dieni et al., 2012). No labeling was detected when the BDNF antibody was omitted (**Figure 5A**, right upper panel). Under high magnification, we detected co-localization of BDNF with a few exon-IV-CFP positive dots in the GCL, but not with exon-VI-YFP (**Figure 5A**, lower panel, arrows). Moreover, BDNF-IR was observed in at least five different characteristic regions, as here shown for the SR at the level of the CA1, that were either co-labeled with exon-IV-CFP (**Figure 5B,** No. 1, **Supplementary Figure 4**), exon-VI-YFP (**Figure 5B,** No. 2–4), or neither of the fluorochromes (**Figure 5B,** No. 5; **Supplementary Video 1**, **Supplementary Figure 4**). Additionally, faint BDNF-IR was observed in blood vessels (**Figure 5C**) where it co-localized with exon-IV-CFP, but not exon-VI-YFP (**Figure 5C,** upper panel). No BDNF labeling was detected upon omission of the primary antibody (**Figure 5C,** lower panel). Related to previous observations of BDNF in circulating platelets (Chacón-Fernández et al., 2016), we also detected CFP fluorescence in vessels of non-perfused animals (**Figure 5D,** upper panel; **Supplementary Video 1**) in contrast to perfused animals, where platelets are expected to be washed out (**Figure 5D,** lower panel).

Common wiring of nerve and blood vessels has been suggested (Carmeliet and Tessier-Lavigne, 2005) but its monitoring has so far been elusive. Our analysis revealed a dot-like BDNF-IR, co-localized with exon-VI-YFP close to an exon-IV-CFP positive capillary embedded in the fissura hippocampalis (FH) (**Figure 5E**; **Supplementary Video 2**). YFP dots represent glutamatergic terminals contacting Arc-positive dendrites of CA1 neurons (**Figures 5F, 6A**; **Supplementary Video 1**). These dendrites of CA1 neurons are often embedded within the highly vascularized FH (Soriano and Frotscher, 1993). At higher magnification, it became evident that exon-VI-YFP labeled presumptive Schaffer collateral (SC) terminals contacted postsynaptic spines of Arc-positive dendrites in the stratum radiatum (SR) (**Figure 5G**; **Supplementary Video 1**). As only a few Arc-positive spines were contacted by exon-VI-YFP positive dots (**Figure 5G**, compare closed and open arrow), we surmise that these may correspond to activated synapses. Presynaptic expression of

YFP could be further confirmed by co-localization of YFP with the presynaptic marker proteins VGLUT1, VGLUT2 and VGLUT3 (**Supplementary Figure 5**; Somogyi et al., 2004; Herzog et al., 2006). VGLUT1 and VGLUT3, described in mossy fiber terminals (Somogyi et al., 2004; Herzog et al., 2006), were found to be co-localized with YFP in the CA3 region (**Supplementary Figures 5A,B).** VGLUT2, described in perforant path terminals contacting dentate gyrus granular cells (Herzog et al., 2006), was found to be co-localized with YFP in the stratum moleculare (**Supplementary Figure 5C).** Interestingly, YFP also co-localized with VGLUT3 in the glomerular layer of the olfactory bulb, suggesting exon-VI-YFP to co-localize in glomerular layer-projecting cholinergic terminals (Case et al., 2017).

BDNF-positive dots co-localizing with exon-VI-YFP were also observed close to a nucleus of an endothelial cell (**Figure 5H**, magnified from **Figure 5B**, No. 3), as shown by co-staining with the $p75^{NGF}$ receptor, an endothelial marker (Xu et al., 2008; **Figure 6B**). The characteristic exon-VI-YFP pattern close to endothelial nuclei was repeatedly found to either overlap with parvalbumin (PV), a marker of inhibitory neurons (**Figure 5I**; **Supplementary Video 1**), or IBA-1 (ionized calcium-binding adapter molecule 1), a marker of microglia (Frick et al., 2013; **Figure 5J; Supplementary Video 1**).

The BDNF-IR pattern typically seen close to blood vessels in the SR (**Figures 5B**, **6C**) co-localized with exon-VI-YFP (**Figure 6C,** closed arrow) and exon-IV-CFP expressing presynaptic boutons (**Figure 6C,** arrowhead), both clearly overlapping with IBA1-labelled microglia (**Figure 6C,** open arrow; **Supplementary Video 2**). The exon-IV-CFP and exon-VI-YFP signals may represent SC terminals contacting microglia. In addition to microglia, the astrocyte specific marker GFAP (glial fibrillary acidic protein) also co-localized with exon-VI-YFP in close proximity to blood vessels (**Figure 6D; Supplementary Video 2**).

Finally, we observed BDNF-IR in capillary vessels, possibly within endothelial cells (**Figure 5B,** No. 5; **Figure 6E**), confirming previous observations (Donovan et al., 2000). Here, clusters of BDNF-IR were seen in zones (**Figure 6E**) where desmin positive pericyte processes variably surrounded the abluminal endothelial wall of an exon-IV-CFP positive blood vessel encircled by β 1-guanylyl cyclase (GC)-positive smooth muscle cells (**Figure 6E,** red; **Supplementary Video 2**).

These findings demonstrated several key points. First, wherever we detect exon-IV-CFP or exon-VI-YFP in the hippocampal path we also detect BDNF. Second, sites where BDNF is detected correspond to cell types previously shown to express BDNF. Third exon-IV-CFP and exon-VI-YFP containing splice variants are translated in non-overlapping locations on the cellular and subcellular level. Exon-IV-CFP is targeted to the somata of pyramidal, granule, or microglial cells, while exon-VI-YFP is detected in terminals of the tri-synaptic pathway as well as in the end-feet of microglia or astrocytes. Finally, BDNF in circulating blood is translated from exon-IV containing transcripts while BDNF in endothelial cells is probably translated neither from exon-IV nor from exon-VI containing transcripts.

In conclusion, the BLEV reporter mouse line allows observation of differences in exon-IV and -VI specific BDNF expression in distinct neuronal, glial, and vascular cells using high-resolution fluorescence microscopy.

Activity-Dependent Up-Regulation of Exon-IV-CFP and Exon-VI-YFP Expression in BLEV Reporter Mice After Injection With Kainic Acid

To investigate whether the BLEV reporter mouse line is suitable to study activity-dependent alterations of *Bdnf* exon-IV and *Bdnf* exon-VI usage *in vivo*, we validated CFP and YFP expression following the injection of kainic acid (KA) into homozygous BLEV reporter mice. KA has been shown to increase BDNF expression in the hippocampus by agonizing glutamate receptors (Zafra et al., 1990; Sathanoori et al., 2004; Chiaruttini et al., 2008) and to activate translation of exon-IV and -VI containing *Bdnf* mRNA (Metsis et al., 1993; Tao et al., 1998; Pattabiraman et al., 2005; Aid et al., 2007; Chiaruttini et al., 2008). Two hours following intra-peritoneal injection of KA (12 mg/kg), significant up-regulation of CFP and YFP protein was observed in the hippocampus in comparison to vehicle-treated animals using Western blot (**Figure 7A**).

We next focused on dentate mossy fiber boutons contacting hippocampal CA3 pyramidal neurons (**Figure 7B**), where activity-dependent expression of BDNF was previously described (Danzer and McNamara, 2004; Danzer et al., 2008; Dieni et al., 2012). Brain slices of vehicle- and KA-treated homozygous BLEV mice were co-labeled with antibodies against the cytoskeletal activity-regulated gene Arc, a protein essential for BDNF-dependent consolidation of LTP (Soulé et al., 2006; Messaoudi et al., 2007; Nair et al., 2017). Low power examination of deconvoluted high-resolution fluorescence stacks revealed a strong up-regulation of *Bdnf* exon-VI (YFP) fluorescence in KA-treated animals in mossy fiber projection fields of CA3 pyramidal neurons (**Figure 7C**), suggesting a KA-induced recruitment of *Bdnf* exon-VI derived BDNF in perforant path dendrites. We also co-stained sections with parvalbumin (PV) antibodies, a marker for fast inhibitory circuits suggested to be shaped by BDNF (Yamada and Nabeshima, 2003; Messaoudi et al., 2007; Minichiello, 2009; Waterhouse et al., 2012). Low power examination of deconvoluted high-resolution fluorescence stacks revealed an upregulation of *Bdnf* exon-IV (CFP) at the level of CA3 pyramidal neurons which correlated with elevated PV levels in dendritic pre-synaptic terminals surrounding pyramidal neurons in a perisomatic distribution (Klausberger et al., 2003; Somogyi et al., 2014; **Figure 7E,** CFP: closed arrow, PV: open arrows). Quantification of the integrated density of YFP and CFP in the CA3 region approved a significant increase after KA injection (**Figures 7D,F**). The quantitative change of YFP and CFP expression in the hippocampus shown by Western blot (**Figure 7A**, right panel), together with the parallel qualitative and quantitative change in YFP and CFP expression in the CA3 regions (**Figures 7C–F**), suggest that BLEV reporter mice are suitable to detect activity-dependent exon-specific changes under healthy and pathological conditions.

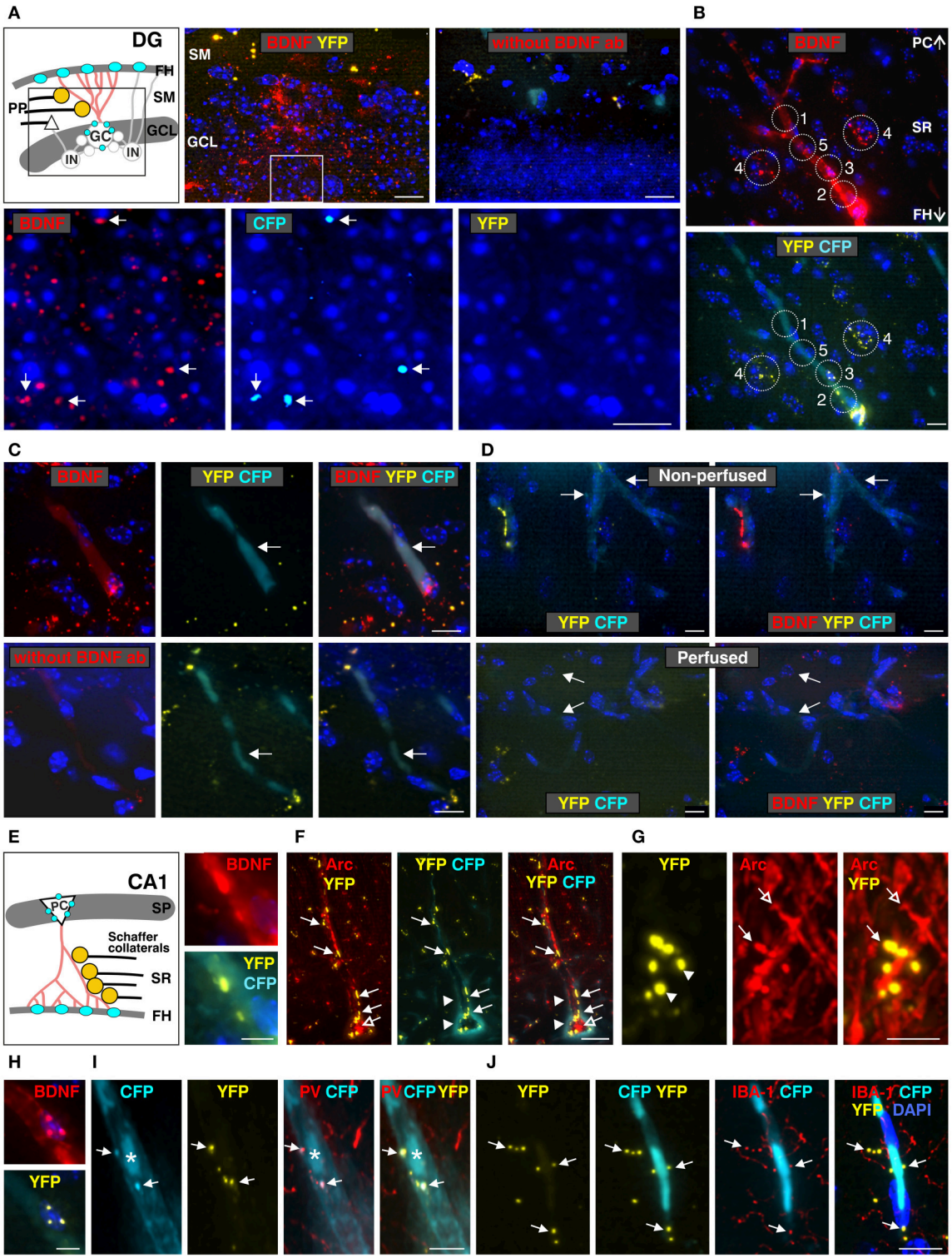

FIGURE 5 | Co-localization of anti-BDNF antibody with *Bdnf* exon-IV-CFP and *Bdnf* exon-VI-YFP in the dentate gyrus (DG, **A**) and the CA1 region **(B–J)** (see **Supplementary Video 1**). **(A)** Top panel: schematic view of the granule cell layer (GCL) and the stratum moleculare (SM) of the DG. Low-power examination depicts BDNF-IR within the GCL of the DG (boxed area in sketch). No labeling was seen when anti-BDNF was omitted. Bottom panel: high-power examination from boxed area shows BDNF to co-localize with a few CFP-positive dots (arrows) but not with YFP-positive dots. Scale bars: 100 μm. **(B)** BDNF-IR in 5 different characteristic regions at the level of the stratum radiatum (SR) co-localized with *Bdnf* exon-VI-YFP and *Bdnf* exon-IV-CFP, see also **Supplementary Figure 4**. Scale bars: 100 μm. **(C)** BDNF-IR in blood vessel (arrows) co-localized with *Bdnf* exon-IV-CFP but not with *Bdnf* exon-VI-YFP. No BDNF-IR is observed when BDNF antibody is omitted

(Continued)

FIGURE 5 | (lower panel). Corresponds to area 1 and 5 in **(B)**. Scale bars: 20 μm. **(D)** *Bdnf* exon-IV-CFP labeling in blood vessels (arrows) of non-perfused BLEV mice (upper panel) was lost when animals were perfused (lower panel). Scale bars: 20 μm. **(E)** Schematic overview of the SR in the CA1 region. BDNF-IR co-localized with *Bdnf* exon-VI-YFP close to a *Bdnf* exon-IV-CFP positive capillary in the fissura hippocampalis (FH). Corresponds to 3 and 4 in **(B)**. Scale bar: 10 μm. **(F)** YFP-positive contacts (closed arrows, see also **Supplementary Figure 5**) on glutamatergic, Arc-positive dendrites (open arrows) of CA1 neurons embedded within the highly vascularized FH (arrowheads). Scale bar: 20 μm. **(G)** High-power examination of potential Schaffer collateral (SC) terminals labeled with *Bdnf* exon-VI-YFP and contacting postsynaptic Arc-positive spines in the SR (compare open and closed arrows). Scale bar: 5 μm. **(H)** BDNF-IR co-localized with *Bdnf* exon-VI-YFP-positive puncta on *Bdnf* exon-IV-CFP-positive capillaries (CFP not shown). Corresponds to 2 in **(B)**. Scale bar: 10 μm. **(I)** *Bdnf* exon-VI-YFP-positive puncta close to an endothelial nucleus (asterisk) overlapping with parvalbumin (PV)-positive interneuron dendrites (arrows). Corresponds to 2 in **(B)**. Scale bar: 10 μm. **(J)** *Bdnf* exon-VI-YFP-positive puncta close to an endothelial nucleus overlapping with the microglia marker IBA-1 (arrows). Corresponds to 3 and 4 in **(B)**. Scale bar: 20 μm. GC, granular cell; IN, inhibitory interneuron; PC, pyramidal cell; PP, perforant path; SP, stratum pyramidale.

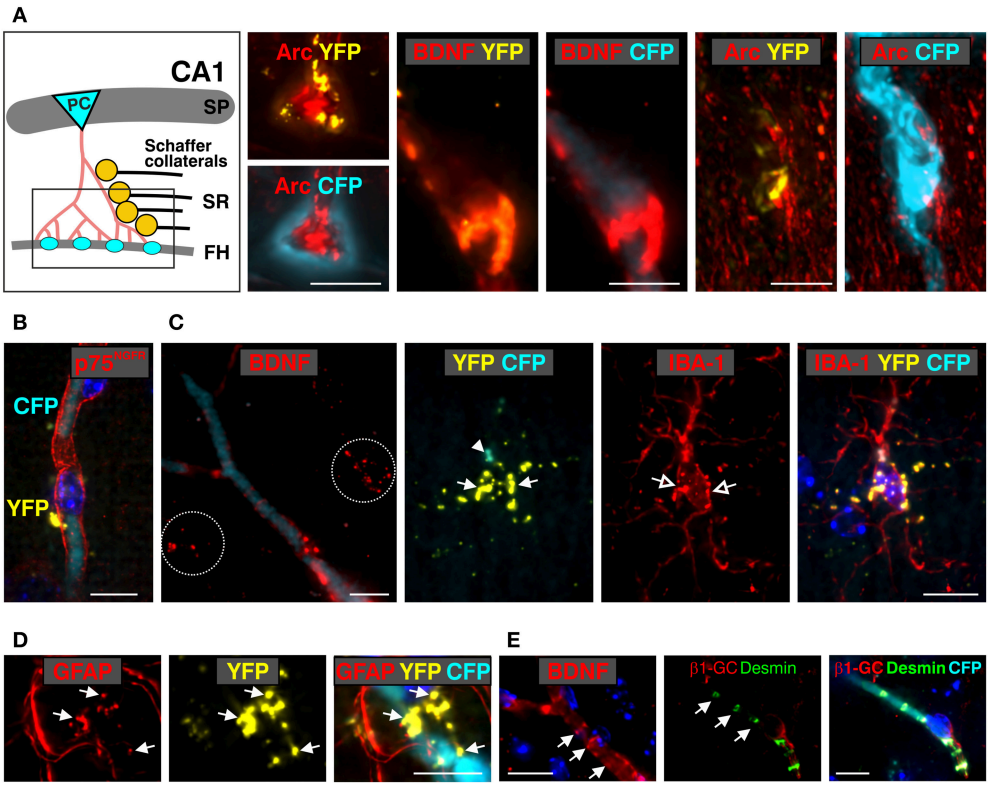

FIGURE 6 | Co-localization of anti-BDNF with *Bdnf* exon-IV-CFP and *Bdnf* exon-VI-YFP in the stratum radiatum (SR) and the vasculature of the fissura hippocampalis (FH) (see **Supplementary Video 2**). **(A)** Schematic overview of the stratum radiatum (SR) region of the hippocampal formation. Arc-positive (red) pyramidal cell (PC) dendrites contact the vascularized fissura hippocampalis (FH) embedded within a *Bdnf* exon-IV-CFP-positive capillary bed (left). BDNF immunoreactivity (red) co-localizes with *Bdnf* exon-VI-YFP puncta within this region covering a *Bdnf* exon-IV-CFP-positive blood vessel (middle). In another view of the FH region, the *Bdnf* exon-VI-YFP puncta contacting Arc-positive dendrites deeply entering the basal membrane of a *Bdnf* exon-IV-CFP-positive blood vessel is shown (right). Scale bars: 10 μm. SP, stratum pyramidale. **(B)** *Bdnf* exon-VI-YFP contacting $p75^{NGF}$ receptor-positive (red) endothelia cells of a *Bdnf* exon-IV-CFP-positive blood vessel. Nuclei are stained in dark blue with DAPI. Scale bars: 10 μm. **(C)** The characteristic BDNF immunoreactivity pattern (red, dotted circles) seen in the SR region close to blood vessels outlined with *Bdnf* exon-IV-CFP. *Bdnf* exon-VI-YFP-positive labeling (closed arrows) is observed close to an IBA-1-positive (red) microglia soma (open arrows) that itself targets *Bdnf* exon-IV-CFP at the microglia pole (closed arrowhead). Scale bars: 10 μm. **(D)** *Bdnf* exon-VI-YFP-positive pattern (closed arrow) observed in overlap with glial fibrillary acidic protein (GFAP)-labeled astrocyte endfeets close to a *Bdnf* exon-IV-CFP-positive blood vessel. Scale bars: 10 μm. **(E)** BDNF-IR (red, arrows) in endothelial cells in a pattern resembling localization of desmin (green, arrows), a marker of pericytes. Pericyte processes embrace the abluminal endothelium wall of an exon-IV-CFP-positive blood vessel encircled by β1-guanylyl cyclase (GC)-positive (red) smooth muscle cells. Scale bars: 10 μm.

DISCUSSION

The present study proposes the BLEV system as a novel tool for monitoring BDNF expression based on the localization of mRNA containing the activity-dependent exons-IV and -VI of cellular and sub-cellular levels *in vitro* and *in vivo* through cyan fluorescent protein (CFP) and yellow fluorescent protein (YFP).

We introduce the BLEV construct and mouse line as a tool to (i) analyze promoter activation or targeting characteristics of *Bdnf* exon-IV and -VI splice-variants *in vitro*; (ii) analyze cell specific differences in *Bdnf* exon-IV and -VI transcript usage in neuronal and non-neuronal cells; and (iii) detect activity-dependent and cell-specific BDNF splice-variant usage under healthy and pathological conditions *in vivo*.

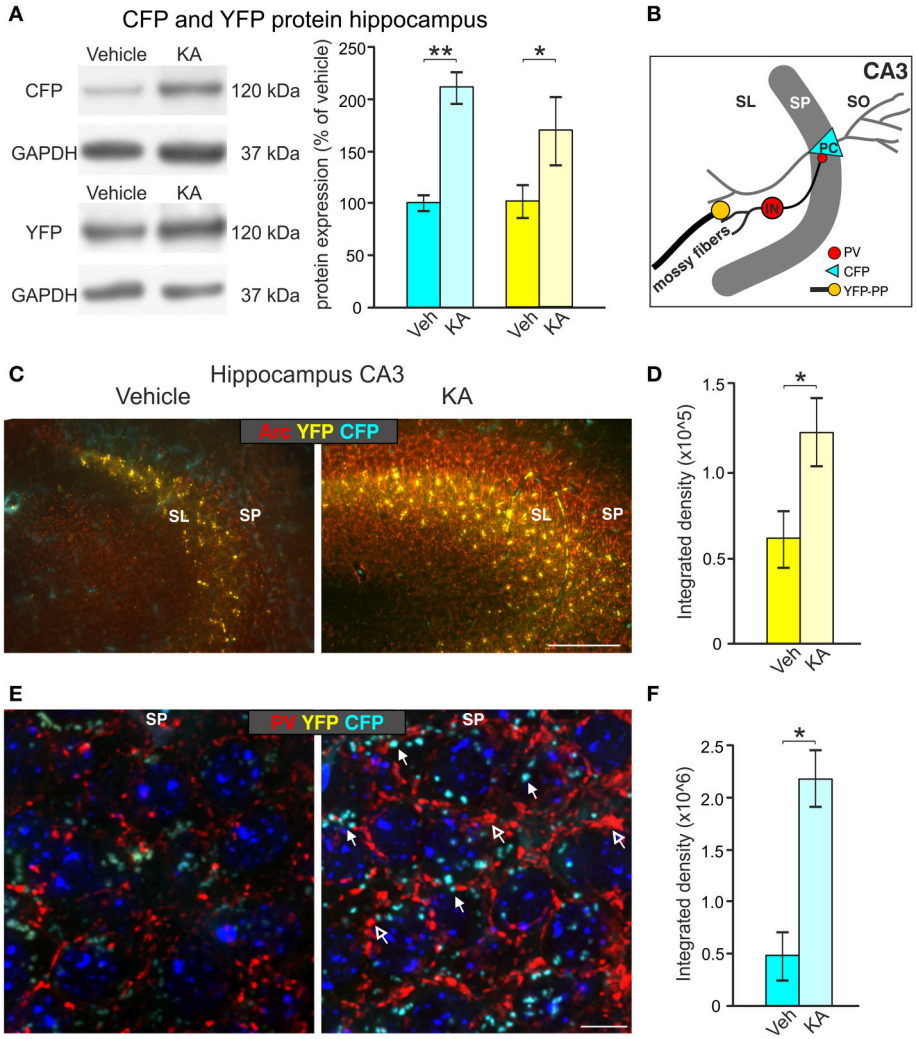

FIGURE 7 | Induction of CFP and YFP expression by kainic acid treatment (KA). **(A)** Western blot analysis of hippocampal tissue lysates from animals injected with vehicle or KA. Left panel: representative Western blot against CFP (top) and YFP (bottom). Right panel: densitometric quantification shows significant up-regulation of CFP and YFP expression after KA treatment. Data represented as mean ± SEM normalized to vehicle treated controls, $n = 3$–4 animals/group (CFP: 1-sided Student's t-test: $t = 6.25$ DF $= 4$ $p = 0.002$; $n = 3$ animals/group; YFP: 1-sided Student's t-test: $t = 1.99$ DF $= 6$ $p = 0.04$; $n = 4$ animals/group). For original blot see **Supplementary Figure 6C**. **(B)** Schematic overview of the hippocampal CA3 region depicting the assumed locations of altered CFP, YFP and Parvalbumin (PV) expression. **(C)** CFP and YFP fluorescence in brain slices of vehicle- and KA-treated animals co-labeled with the cytoskeletal activity-regulated gene Arc. Clear upregulation of Arc (red) mainly in the SP and YFP mainly in the SL can be seen in the hippocampal CA3 region of KA-treated animals in comparison to vehicle-treated mice. Scale bars: 100 μm. **(D)** Quantification of the integrated density of YFP which is increased after KA injection (YFP: 1-sided Student's t-test: $t = 4.14$ DF $= 3$ $p = 0.0128$; $n = 3$ animals/group). **(E)** An increase in perisomatic CFP (closed arrows) and PV (red, open arrows) signals can be seen in the SP of the hippocampal CA3 region in KA-treated animals in contrast to vehicle-treated mice. Scale bars = 10 μm. **(F)** Quantification of the integrated density of CFP which is increased after KA injection (CFP: 1-sided Student's t-test: $t = 2.32$ DF $= 4$ $p = 0.0405$; $n = 2$–3 animals/group). SL, stratum lucidium; SP, stratum pyramidale; SO, stratum oriens; PC, pyramidal cell; PP, perforant path; IN, interneuron.

BLEV Mice as a Tool to Investigate Promoter Activation Patterns of BDNF

Analysis of the gene-structure of BDNF reveals the presence of nine exons where the eight upstream exons (I-VIII) are alternatively spliced to the ninth exon (IX), corresponding to the only exon encoding the BDNF protein (Timmusk et al., 1993; Aid et al., 2007; **Figure 3A**). The functions of the eight untranslated *Bdnf* exons (I-VIII) each containing a different promoter region is still unclear (Aid et al., 2007). Several studies investigated the different *Bdnf* exons and their activity-dependent activation (Timmusk et al., 1993; Lauterborn et al., 1996; Shieh et al., 1998; Takeuchi et al., 2000, 2002; Zha et al., 2001; Fang et al., 2003; Sathanoori et al., 2004; Sakata et al., 2009). Based on these studies, it was suggested that these promoters show a spatially distinct expression pattern and are regulated in a stimulus- and activity-dependent manner (Timmusk et al., 1993; Aid et al., 2007).

To our knowledge, however, BDNF expression initiated from the untranslated *Bdnf* exons-IV and -VI containing transcripts has never been addressed in parallel *in vivo*. Therefore, cell-specific differences in exon-IV and -VI promoter activation in the mature system in response to external stimuli have so far never been detected under physiological conditions. The observed transcript specific expression corresponding to either of the distinct splice-variants or both, detected in a neuroglioblastoma cell line suggests that the BLEV construct may be useful to identify subtle and complex promoter activation patterns (**Figure 1**). While it is well established that activation from exon-IV promoter occurs following elevated levels of calcium (Ca^{2+}) (West et al., 2014), the details under which conditions this occurs, e.g., through glutamate-induced NMDA receptors, voltage gated Ca^{2+} channels (VGCCs) or intracellular Ca^{2+} stores is still elusive. It is also not understood if neuronal, glial or vascular cells exhibit differences in second messenger cascades acting on specific promoter sites (e.g., CaMKII or CaMKIV, MAP kinase) (West et al., 2001; Takeuchi et al., 2002; Tao et al., 2002; Chen et al., 2003). While e.g., *Bdnf* exon-IV in platelets is suggested to be activated through store-operated Ca^{2+} channels (Chacón-Fernández et al., 2016), the mechanism associated with promoter activation remains elusive. An even greater complexity is observed regarding the *Bdnf* exon-VI promoter that is activated only modestly by neuronal activity (Timmusk et al., 1993; Aid et al., 2007), but is indirectly activated by neuronal activity through binding to the AP-1 family transcription factor site (Tuvikene et al., 2016). Here, BDNF-autoregulatory loops, acting via its promoters (Bambah-Mukku et al., 2014; Harward et al., 2016) may also be involved. The BLEV reporter system now allows investigation of this hypothesis *in vitro* or *in vivo*.

Kainic acid (KA), shown to activate glutamate receptors in hippocampal neurons (Zafra et al., 1992; Sathanoori et al., 2004; Chiaruttini et al., 2008), not only elevates exon-IV- and exon-VI- derived BDNF expression in hippocampal tissue but does so in a cell-specific manner (**Figure 7**), indicating that the activity-driven activation of BDNF promoters-IV and -VI is not impaired by the BLEV construct. This experiment also anticipates the usage of the BLEV construct to investigate not only cell specific differences in promoter usage but also the predicted complex interplay between transmitter-induced changes in BDNF expression and its reciprocal effects on its receptor TrkB (Flavell and Greenberg, 2008; Sakata et al., 2009; Lu et al., 2010). Here the perspective that the BLEV construct can be viewed using two-photon microscopy (Thaler and Vogel, 2006) following manipulations of promoter activation under different conditions is most promising.

In this context, the demonstration of differences in intraneuronal targeting of BDNF transcripts between *in vitro* and *in vivo* conditions observed in the present study is particularly interesting. Accordingly, *Bdnf* exon-IV and -VI were found in primary neuronal cultures to be targeted mainly to the soma and dendrites, respectively, as described previously (Chiaruttini et al., 2008; Baj et al., 2011; Vaghi et al., 2014). In the mature BLEV mouse model a differential intraneuronal targeting of BDNF transcripts derived from exon-IV-CFP to the soma and exon-VI-YFP to terminals (Chiaruttini et al., 2008; Baj et al., 2011; Vaghi et al., 2014) could not only be demonstrated for projecting neurons but interestingly also for microglia (**Figures 5J**, **6C**). Importantly, however, and different from previous suggestions, we did not observe exon-VI-YFP signals in dendrites of e.g., the CA1 region (**Figures 5F,G**). Whether these observations support the previously suggested elusive anterograde transport of BDNF transcripts and its restricted presynaptic BDNF release (Dieni et al., 2012) needs further investigation. Indeed, we cannot entirely exclude that *Bdnf* transcripts may be differentially compartmentalized depending on the type of stimulus and time course, as shown previously (Chiaruttini et al., 2008).

This observation is of crucial interest since trafficking of exon-VI derived BDNF to nerve terminals is thought to be disturbed in animals or humans carrying the $BDNF^{Val66Met}$ allele, causing a mutation linked to cognitive deficits (Baj et al., 2013; Mallei et al., 2015).

BLEV Mice as a Tool to Investigate Cell-Specific and Transcript-Specific Differences of BDNF Expression

The low abundance of BDNF in the mature CNS currently hampers investigation of cell-specific BDNF expression differences in the healthy or diseased mature brain (Dieni et al., 2012). We have shown that the localization of BDNF via specific antibodies overlaps with either exon-IV-CFP or exon-VI-YFP signals in neuronal, glial, or vascular compartments within the hippocampus (**Figure 5**). Importantly, the identified BDNF patterns correspond to previously observed regions of BDNF expression in neuronal or non-neuronal cells (Dieni et al., 2012; Chacón-Fernández et al., 2016). Thus our data imply that for example BDNF translation in the soma of hippocampal pyramidal cells (Danzer et al., 2008) results from *Bdnf* exon-IV splice variants, while BDNF translation in tri-synaptic hippocampal terminals (Danzer et al., 2008; Dieni et al., 2012) is generated by *Bdnf* exon-VI splice variants (**Figures 5B**, **6**; **Supplementary Video 1**). In addition, expression of BDNF in astrocytes or microglia (Snapyan et al., 2009; Parkhurst et al., 2013), predicted to participate in the recruitment of blood vessels during complex homeostatic changes in plasticity (Edelmann et al., 2014, 2017), may be driven by exon-IV in the glial soma or by exon-VI when released from glial end-feet structures (**Figures 6C,D**; **Supplementary Video 1**). The BLEV reporter mice may thus provide a new resource to investigate to what extent the $BDNF^{Val66Met}$ polymorphism, linked to cognitive deficits, may not only affect trafficking in neuronal (Baj et al., 2013; Mallei et al., 2015) but possibly also in microglial cells. Moreover, our results in BLEV mice indicate for the first time that BDNF is also present in mouse platelets, as previously described in humans and rats (Chacón-Fernández et al., 2016). How exon-IV derived BDNF in platelets can communicate through the blood-brain barrier that is maintained by endothelial tight junctions, pericytes, or astrocytic end-feet (Marosi and Mattson, 2014) could be part of future studies in BLEV mice. Finally, BDNF in endothelial cells, identified through co-localization of BDNF with $p75^{NGFR}$ (for review see: Donovan et al., 2000;

Marosi and Mattson, 2014), appears to be neither generated by exon-IV nor by exon-VI promoters (**Figures 5B**, **6B**).

Conclusively, BLEV mice may thus be the first animal model enabling the parallel monitoring of BDNF expression differences in neurons, glial cells, and capillaries, including subcellular targeting in neurons and glial cells.

BLEV Mice as a Tool to Investigate Stimulus-Driven Cell-Specific and Transcript-Specific Differences of BDNF in Healthy and Pathological Conditions *in vivo*

The analysis of the role that BDNF plays for the nervous system has until now mainly focused on *in vitro* studies or BDNF knock-out mouse models. BDNF knock-out mice die postnatally (Ernfors et al., 1995) and therefore escape investigations of BDNF's roles in the mature system, particularly of those in response to changes in neuronal activity. However, the presently existing mouse models have indicated important phenotypic differences in the absence of BDNF signaling in the mature system. Accordingly, heterozygous BDNF knock-out animals show anxiety-like behavior (Chourbaji et al., 2008) or signs of obesity (Rios et al., 2001; Vanevski and Xu, 2013). Mice with a point mutation in the BDNF receptor TrkB gene exhibit progressive hearing loss (Postigo et al., 2002), while mice with a conditional deletion of BDNF from cortical neurons show a severe reduction of dendritic contacts (Rauskolb et al., 2010). A first hint for a crucial role of distinct BDNF transcripts in control of cortical inhibition, aggressive behavior (Lyons and West, 2011; Hill et al., 2016; Maynard et al., 2016), or e.g., in the induction of depression was obtained in BDNF mouse models in which one of its promoters had been impaired (Hong et al., 2008; Sakata et al., 2009). A further indication that intracellular targeting of BDNF transcript defines e.g., cognitive competence has been observed in $BDNF^{Val66Met}$ mutants (Mallei et al., 2015). So far, however, none of these studies can explain why different activity-dependent BDNF promoters may provide advantages over usage of a single promoter.

Various studies have confirmed the requirement of glucocorticoid signaling in selected networks to support morphological changes at synapses (Cheng et al., 2012; Liston et al., 2013; Arango-Lievano et al., 2015) and an activity-dependent process to provide information about the appropriate context (De Kloet et al., 2014; Jeanneteau and Arango-Lievano, 2016). Indeed, previous hypotheses considered that activity-dependent BDNF expression provides context-dependent information for GR-mediated task-evoked plasticity changes to be associated with memory formation (Jeanneteau and Arango-Lievano, 2016). Up to now, however, it was not possible to directly observe activity-driven BDNF transcription. With the BLEV mouse, we now provide a suitable new tool for this purpose. In contrast to existing BDNF-GFP reporter mice (Guillemot et al., 2007), the BLEV model provides the advantage to allow visualization of different BDNF transcripts following activity and thereby to specifically monitor stimulus-driven activation patterns in networks. As a prerequisite to detect stimulus-driven BDNF transcript changes, we had to assure that gene replacement within the *Bdnf* locus did not interfere with the normal expression of the BDNF protein. BLEV mice were confirmed to express unchanged levels of BDNF and showed normal weight, lifespan, fertility, and function of the audio-vestibular sensory system. This is particularly important with regard to the crucial role BDNF plays for normal cognitive function (reviews: Minichiello, 2009; Lu et al., 2014; Leal et al., 2015), neurogenesis (Kheirbek et al., 2012; Waterhouse et al., 2012), energy homeostasis and pattern segregation (for review see: Bramham and Messaoudi, 2005; Rauskolb et al., 2010; Park and Poo, 2013; Marosi and Mattson, 2014; Turrigiano, 2014; Bothwell, 2016; Mitre et al., 2017). The lack of a changed phenotype thus qualifies BLEV reporter mice as new tool to investigate how expression of exon-IV and -VI derived BDNF changes after altered input activity in the different neuronal, glial or vascular cells during modulation of the aforementioned processes. This includes the use of BLEV mice for examining potential therapies in various disease models, where dysregulation of BDNF expression is predicted to contribute to the pathology, such as depression, epilepsy, or Alzheimer's, Huntington's, and Parkinson's disease (Bibel and Barde, 2000; Ginsberg et al., 2017).

As a first attempt to test if BLEV mice enable identification of activity-dependent adaptations in central networks under healthy or pathological conditions we shall focus on known plasticity paradigms in the hippocampus. The hippocampus is the region with highest levels of BDNF expression (Nawa et al., 1995; Conner et al., 1997), where it is predicted to play crucial roles for accentuating behaviorally important sound signals (Kilgard and Merzenich, 1998; Sadaghiani et al., 2009; Kraus and White-Schwoch, 2015; Weinberger, 2015). The precise organization of the peripheral and central auditory system together with functionally and molecularly established protocols (Rüttiger et al., 2017) to induce long-lasting plasticity changes related to memory (for review see: Knipper et al., 2013; Singer et al., 2013), provides an excellent model to investigate sound-induced activation patterns of *Bdnf* transcripts with the help of BLEV mice.

CONCLUSION

In the present study, a transgenic system for ***B**DNF-**l**ive-**e**xon-**v**isualization* (BLEV) has been generated enabling the detection of activity-dependent BDNF translation from *Bdnf* exon-IV and -VI containing transcripts through CFP and YFP fluorescent proteins, respectively. The present study confirms (i) that transfection of different cell lines with the BLEV construct enables the tracking of intraneuronal targeting differences of the BDNF splice variants; (ii) that insertion of the BLEV construct into the genomic locus of *Bdnf* via homologous recombination resulted in healthy homozygous BLEV reporter mice without any apparent phenotypic changes and with normal levels of BDNF expression; (iii) that CFP and YFP fluorescence in BLEV mice overlaps with BDNF protein expression in neuronal, glial, and vascular locations; and (iv) that the BLEV construct allows identification of elevated *Bdnf* exon-IV-CFP and exon-VI-YFP

expression levels following glutamate receptor activation *in vivo*. BLEV reporter mice can now be used to trace the potential role of activity-dependent BDNF promoter usage for providing context-specific information during task-specific memory formation.

AUTHOR CONTRIBUTIONS

WS, RP-W, H-SG, TO, and MK conceptualization. WS, H-SG, MM, LR, and MK analysis. WS, H-SG, MM, GL, CBD, ILS, GB, EP, ET, KR, and TO investigation. WS, RP-W, MM, LM, PE, UZ, LR, TS, and MK writing. PR, TO, LR, and MK supervision. JH, LM, JS, PR, UZ, LR, and MK review and editing.

FUNDING

This work was supported by the Deutsche Forschungs gemeinschaft DFG-Kni-316-10-1 (RP-W; WS; H-SG; EP; MK; TO); FOR 2060 project RU 713/3-2 (LR); SPP 1608 RU 316/12-1 (PE; KR; H-SG); KN 316/12-1 (MM; UZ; MK); the Brain and Behavior Research Foundation NARSAD Young Investigator Grant 20748 (LM), BFU2013-40944 (TS); DFG-STR 619/5-1 (JS); CIN-EXC 307 (JH); DFG KFO134 (PR); PRIN2010-11 2010N8PBAA (GB; ET); Pest-C/SAU/LA0001/2013-2014, CENTRO-01-0145-FEDER-000008 (CENTRO2020), POCI-01-0145-FEDER-007440 and POCI-01-0145-FEDER-028656 (COMPETE2020 and FCT), UID/NEU/04539/2013, and UID/BIM/4501/2013 (GL; ILS; CBD). We acknowledge support by Deutsche Forschungsgemeinschaft and Open Access Publishing Fund of University of Tübingen.

ACKNOWLEDGMENTS

The authors thank PD. Dr. Ulrike Naumann (Hertie Institute, Tübingen, Germany) who kindly provided the SK-N-BE cells and Prof. Dr. Dusan Bartsch (Central Institute of Mental Health, Department of Molecular Biology, Mannheim, Germany) who kindly provided the pMCS 5 vector. Thank you to Michael Paolillo for reading the manuscript. The authors wish to thank the MICC Imaging facility of CNC.

SUPPLEMENTARY MATERIAL

The Supplementary Material for this article can be found online at: https://www.frontiersin.org/articles/10.3389/fnmol.2018.00325/full#supplementary-material

REFERENCES

Aid, T., Kazantseva, A., Piirsoo, M., Palm, K., and Timmusk, T. (2007). Mouse and rat BDNF gene structure and expression revisited. *J. Neurosci. Res.* 85, 525–535. doi: 10.1002/jnr.21139

Arango-Lievano, M., Lambert, W. M., Bath, K. G., Garabedian, M. J., Chao, M. V., and Jeanneteau, F. (2015). Neurotrophic-priming of glucocorticoid receptor signaling is essential for neuronal plasticity to stress and antidepressant treatment. *Proc. Natl. Acad. Sci. U.S.A.* 112, 15737–15742. doi: 10.1073/pnas.1509045112

Baj, G., Carlino, D., Gardossi, L., and Tongiorgi, E. (2013). Toward a unified biological hypothesis for the BDNF Val66Met-associated memory deficits in humans: a model of impaired dendritic mRNA trafficking. *Front. Neurosci.* 7:188. doi: 10.3389/fnins.2013.00188

Baj, G., Leone, E., Chao, M. V., and Tongiorgi, E. (2011). Spatial segregation of BDNF transcripts enables BDNF to differentially shape distinct dendritic compartments. *Proc. Natl. Acad. Sci. U.S.A.* 108, 16813–16818. doi: 10.1073/pnas.1014168108

Baj, G., and Tongiorgi, E. (2009). BDNF splice variants from the second promoter cluster support cell survival of differentiated neuroblastoma upon cytotoxic stress. *J. Cell Sci.* 122, 36–43. doi: 10.1242/jcs.03506

Bambah-Mukku, D., Travaglia, A., Chen, D. Y., Pollonini, G., and Alberini, C.M. (2014). A positive autoregulatory BDNF feedback loop via C/EBPb mediates hippocampal memory consolidation. *J. Neurosci.* 34, 12547–12559. doi: 10.1523/JNEUROSCI.0324-14.2014

Barde, Y. A., Edgar, D., and Thoenen, H. (1982). Purification of a new neurotrophic factor from mammalian brain. *EMBO J.* 1, 549–553.

Bibel, M., and Barde, Y. A. (2000). Neurotrophins: key regulators of cell fate and cell shape in the vertebrate nervous system. *Genes Dev.* 14, 2919–2937. doi: 10.1101/gad.841400

Bothwell, M. (2016). Recent advances in understanding neurotrophin signaling. *F1000Res* 5:F1000. doi: 10.12688/f1000research.8434.1

Bramham, C. R., and Messaoudi, E. (2005). BDNF function in adult synaptic plasticity: the synaptic consolidation hypothesis. *Prog. Neurobiol.* 76, 99–125. doi: 10.1016/j.pneurobio.2005.06.003

Carmeliet, P., and Tessier-Lavigne, M. (2005). Common mechanisms of nerve and blood vessel wiring. *Nature* 436, 193–200. doi: 10.1038/nature03875

Case, D. T., Burton, S. D., Gedeon, J. Y., Williams, S. G., Urban, N. N., and Seal, R. P. (2017). Layer- and cell type-selective co-transmission by a basal forebrain cholinergic projection to the olfactory bulb. *Nat. Commun.* 8:652. doi: 10.1038/s41467-017-00765-4

Chacón-Fernández, P., Säuberli, K., Colzani, M., Moreau, T., Ghevaert, C., and Barde, Y. A. (2016). Brain-derived Neurotrophic factor in Megakaryocytes. *J. Biol. Chem.* 291, 9872–9881. doi: 10.1074/jbc.M116.720029

Chen, W. G., West, A. E., Tao, X., Corfas, G., Szentirmay, M. N., Sawadogo, M., et al. (2003). Upstream stimulatory factors are mediators of Ca^{2+}-responsive transcription in neurons. *J. Neurosci.* 23, 2572–2581. doi: 10.1523/JNEUROSCI.23-07-02572.2003

Cheng, A., Wan, R., Yang, J. L., Kamimura, N., Son, T. G., Ouyang, X., et al. (2012). Involvement of PGC-1α in the formation and maintenance of neuronal dendritic spines. *Nat. Commun.* 3:1250. doi: 10.1038/ncomms2238

Chiaruttini, C., Sonego, M., Baj, G., Simonato, M., and Tongiorgi, E. (2008). BDNF mRNA splice variants display activity-dependent targeting to distinct hippocampal laminae. *Mol. Cell. Neurosci.* 37, 11–19. doi: 10.1016/j.mcn.2007.08.011

Chourbaji, S., Brandwein, C., Vogt, M. A., Dormann, C., Hellweg, R., and Gass, P. (2008). Nature vs. nurture: can enrichment rescue the behavioural phenotype of BDNF heterozygous mice? *Behav. Brain Res.* 192, 254–258. doi: 10.1016/j.bbr.2008.04.015

Conner, J. M., Lauterborn, J. C., Yan, Q., Gall, C. M., and Varon, S. (1997). Distribution of brain-derived neurotrophic factor (BDNF) protein and mRNA in the normal adult rat CNS: evidence for anterograde axonal transport. *J. Neurosci.* 17, 2295–2313. doi: 10.1523/JNEUROSCI.17-07-02295.1997

Costa, J. T., Mele, M., Baptista, M. S., Gomes, J. R., Ruscher, K., Nobre, R.J., et al. (2016). Gephyrin cleavage in *in vitro* brain Ischemia decreases GABAA receptor clustering and contributes to neuronal death. *Mol. Neurobiol.* 53, 3513–3527. doi: 10.1007/s12035-015-9283-2

Danzer, S. C., Kotloski, R. J., Walter, C., Hughes, M., and Mcnamara, J. O. (2008). Altered morphology of hippocampal dentate granule cell presynaptic and postsynaptic terminals following conditional deletion of TrkB. *Hippocampus* 18, 668–678. doi: 10.1002/hipo.20426

Danzer, S. C., and McNamara, J.O. (2004). Localization of brain-derived neurotrophic factor to distinct terminals of mossy fiber axons implies

regulation of both excitation and feedforward inhibition of CA3 pyramidal cells. *J. Neurosci.* 24, 11346–11355. doi: 10.1523/JNEUROSCI.3846-04.2004

De Kloet, E. R., Claessens, S. E., and Kentrop, J. (2014). Context modulates outcome of perinatal glucocorticoid action in the brain. *Front. Endocrinol.* 5:100. doi: 10.3389/fendo.2014.00100

Dieni, S., Matsumoto, T., Dekkers, M., Rauskolb, S., Ionescu, M. S., Deogracias, R., et al. (2012). BDNF and its pro-peptide are stored in presynaptic dense core vesicles in brain neurons. *J. Cell Biol.* 196, 775–788. doi: 10.1083/jcb.201201038

Donovan, M. J., Lin, M. I., Wiegn, P., Ringstedt, T., Kraemer, R., Hahn, R., et al. (2000). Brain derived neurotrophic factor is an endothelial cell survival factor required for intramyocardial vessel stabilization. *Development* 127, 4531–4540.

Edelmann, E., Cepeda-Prado, E., and Leßmann, V. (2017). Coexistence of multiple types of synaptic plasticity in individual hippocampal CA1 pyramidal neurons. *Front. Synaptic Neurosci.* 9:7. doi: 10.3389/fnsyn.2017.00007

Edelmann, E., Lessmann, V., and Brigadski, T. (2014). Pre- and postsynaptic twists in BDNF secretion and action in synaptic plasticity. *Neuropharmacology* 76(Pt C), 610–627. doi: 10.1016/j.neuropharm.2013.05.043

Ernfors, P., Van De Water, T., Loring, J., and Jaenisch, R. (1995). Complementary roles of BDNF and NT-3 in vestibular and auditory development. *Neuron* 14, 1153–1164. doi: 10.1016/0896-6273(95)90263-5

Fang, H., Chartier, J., Sodja, C., Desbois, A., Ribecco-Lutkiewicz, M., Walker, P. R., et al. (2003). Transcriptional activation of the human brain-derived neurotrophic factor gene promoter III by dopamine signaling in NT2/N neurons. *J. Biol. Chem.* 278, 26401–26409. doi: 10.1074/jbc.M211539200

Ferrini, F., and De Koninck, Y. (2013). Microglia control neuronal network excitability via BDNF signalling. *Neural Plast.* 2013:429815. doi: 10.1155/2013/429815

Flavell, S. W., and Greenberg, M. E. (2008). Signaling mechanisms linking neuronal activity to gene expression and plasticity of the nervous system. *Annu. Rev. Neurosci.* 31, 563–590. doi: 10.1146/annurev.neuro.31.060407.125631

Frick, L. R., Williams, K., and Pittenger, C. (2013). Microglial dysregulation in psychiatric disease. *Clin. Dev. Immunol.* 2013:608654. doi: 10.1155/2013/608654

Ginsberg, S. D., Malek-Ahmadi, M. H., Alldred, M. J., Che, S., Elarova, I., Chen, Y., et al. (2017). Selective decline of neurotrophin and neurotrophin receptor genes within CA1 pyramidal neurons and hippocampus proper: correlation with cognitive performance and neuropathology in mild cognitive impairment and Alzheimer's disease. *Hippocampus*. doi: 10.1002/hipo.22802. [Epub ahead of print].

Goslin, K., Asmussen, H., and Banker, G. (1998). "Rat hippocampal neurons in low-density cultures," in *Culturing Nerve Cells,* eds G. Banker and K. Goslin (Cambridge, MA: The MIT Press), 339–370.

Guillemot, F., Cerutti, I., Auffray, C., and Devignes, M. D. (2007). A transgenic mouse model engineered to investigate human brain-derived neurotrophic factor *in vivo*. *Transgenic Res.* 16, 223–237. doi: 10.1007/s11248-006-9060-0

Harward, S. C., Hedrick, N. G., Hall, C. E., Parra-Bueno, P., Milner, T. A., Pan, E., et al. (2016). Autocrine BDNF-TrkB signalling within a single dendritic spine. *Nature* 538, 99–103. doi: 10.1038/nature19766

Herzog, E., Takamori, S., Jahn, R., Brose, N., and Wojcik, S. M. (2006). Synaptic and vesicular co-localization of the glutamate transporters VGLUT1 and VGLUT2 in the mouse hippocampus. *J. Neurochem.* 99, 1011–1018. doi: 10.1111/j.1471-4159.2006.04144.x

Hill, J. L., Hardy, N. F., Jimenez, D. V., Maynard, K. R., Kardian, A. S., Pollock, C. J., et al. (2016). Loss of promoter IV-driven BDNF expression impacts oscillatory activity during sleep, sensory information processing and fear regulation. *Transl. Psychiatry* 6:e873. doi: 10.1038/tp.2016.153

Hong, E. J., Mccord, A. E., and Greenberg, M. E. (2008). A biological function for the neuronal activity-dependent component of Bdnf transcription in the development of cortical inhibition. *Neuron* 60, 610–624. doi: 10.1016/j.neuron.2008.09.024

Jeanneteau, F., and Arango-Lievano, M. (2016). Linking mitochondria to synapses: new insights for stress-related neuropsychiatric disorders. *Neural Plast.* 2016:3985063. doi: 10.1155/2016/3985063

Kaiser, A., Fedrowitz, M., Ebert, U., Zimmermann, E., Hedrich, H. J., Wedekind, D., et al. (2001). Auditory and vestibular defects in the circling (ci2) rat mutant. *Eur. J. Neurosci.* 14, 1129–1142. doi: 10.1046/j.0953-816x.2001.01726.x

Kellner, Y., Gödecke, N., Dierkes, T., Thieme, N., Zagrebelsky, M., and Korte, M. (2014). The BDNF effects on dendritic spines of mature hippocampal neurons depend on neuronal activity. *Front. Synaptic Neurosci.* 6:5. doi: 10.3389/fnsyn.2014.00005

Kheirbek, M. A., Klemenhagen, K. C., Sahay, A., and Hen, R. (2012). Neurogenesis and generalization: a new approach to stratify and treat anxiety disorders. *Nat. Neurosci.* 15, 1613–1620. doi: 10.1038/nn.3262

Kilgard, M. P., and Merzenich, M. M. (1998). Cortical map reorganization enabled by nucleus basalis activity. *Science* 279, 1714–1718. doi: 10.1126/science.279.5357.1714

Kim, D. H., Kim, J. M., Park, S. J., Cai, M., Liu, X., Lee, S., et al. (2012). $GABA_A$ receptor blockade enhances memory consolidation by increasing hippocampal BDNF levels. *Neuropsychopharmacology* 37, 422–433. doi: 10.1038/npp.2011.189

Klausberger, T., Magill, P. J., Márton, L. F., Roberts, J. D., Cobden, P. M., Buzsáki, G., et al. (2003). Brain-state- and cell-type-specific firing of hippocampal interneurons *in vivo*. *Nature* 421, 844–848. doi: 10.1038/nature01374

Knipper, M., Van Dijk, P., Nunes, I., Rüttiger, L., and Zimmermann, U. (2013). Advances in the neurobiology of hearing disorders: recent developments regarding the basis of tinnitus and hyperacusis. *Prog. Neurobiol.* 111, 17–33. doi: 10.1016/j.pneurobio.2013.08.002

Kraus, N., and White-Schwoch, T. (2015). Unraveling the biology of auditory learning: a cognitive-sensorimotor-reward framework. *Trends Cogn. Sci.* 19, 642–654. doi: 10.1016/j.tics.2015.08.017

Kuipers, S. D., and Bramham, C. R. (2006). Brain-derived neurotrophic factor mechanisms and function in adult synaptic plasticity: new insights and implications for therapy. *Curr. Opin. Drug Discov. Devel.* 9, 580–586.

Lallemand, Y., Luria, V., Haffner-Krausz, R., and Lonai, P. (1998). Maternally expressed PGK-Cre transgene as a tool for early and uniform activation of the Cre site-specific recombinase. *Transgenic Res.* 7, 105–112. doi: 10.1023/A:1008868325009

Lauterborn, J. C., Rivera, S., Stinis, C. T., Hayes, V. Y., Isackson, P. J., and Gall, C. M. (1996). Differential effects of protein synthesis inhibition on the activity-dependent expression of BDNF transcripts: evidence for immediate-early gene responses from specific promoters. *J. Neurosci.* 16, 7428–7436. doi: 10.1523/JNEUROSCI.16-23-07428.1996

Leal, G., Afonso, P. M., Salazar, I. L., and Duarte, C. B. (2015). Regulation of hippocampal synaptic plasticity by BDNF. *Brain Res.* 1621, 82–101. doi: 10.1016/j.brainres.2014.10.019

Leal, G., Bramham, C. R., and Duarte, C. B. (2017). BDNF and hippocampal synaptic plasticity. *Vitam. Horm.* 104, 153–195. doi: 10.1016/bs.vh.2016.10.004

Liston, C., Cichon, J. M., Jeanneteau, F., Jia, Z., Chao, M. V., and Gan, W. B. (2013). Circadian glucocorticoid oscillations promote learning-dependent synapse formation and maintenance. *Nat. Neurosci.* 16, 698–705. doi: 10.1038/nn.3387

Liu, Y., Fisher, D. A., and Storm, D. R. (1994). Intracellular sorting of neuromodulin (GAP-43) mutants modified in the membrane targeting domain. *J. Neurosci.* 14, 5807–5817. doi: 10.1523/JNEUROSCI.14-10-05807.1994

Lu, B., Nagappan, G., and Lu, Y. (2014). BDNF and synaptic plasticity, cognitive function, and dysfunction. *Handb. Exp. Pharmacol.* 220, 223–250. doi: 10.1007/978-3-642-45106-5_9

Lu, H., Cheng, P. L., Lim, B. K., Khoshnevisrad, N., and Poo, M. M. (2010). Elevated BDNF after cocaine withdrawal facilitates LTP in medial prefrontal cortex by suppressing GABA inhibition. *Neuron* 67, 821–833. doi: 10.1016/j.neuron.2010.08.012

Lyons, M. R., and West, A. E. (2011). Mechanisms of specificity in neuronal activity-regulated gene transcription. *Prog. Neurobiol.* 94, 259–295. doi: 10.1016/j.pneurobio.2011.05.003

Magin, T. M., Mcwhir, J., and Melton, D. W. (1992). A new mouse embryonic stem cell line with good germ line contribution and gene targeting frequency. *Nucleic Acids Res.* 20, 3795–3796. doi: 10.1093/nar/20.14.3795

Mallei, A., Baj, G., Ieraci, A., Corna, S., Musazzi, L., Lee, F. S., et al. (2015). Expression and dendritic trafficking of BDNF-6 splice variant are impaired in knock-in mice carrying human BDNF Val66Met Polymorphism. *Int. J. Neuropsychopharmacol.* 18:pyv069. doi: 10.1093/ijnp/pyv069

Marosi, K., and Mattson, M. P. (2014). BDNF mediates adaptive brain and body responses to energetic challenges. *Trends Endocrinol. Metab.* 25, 89–98. doi: 10.1016/j.tem.2013.10.006

Maynard, K. R., Hill, J. L., Calcaterra, N. E., Palko, M. E., Kardian, A., Paredes, D., et al. (2016). Functional role of BDNF production from unique promoters in

aggression and serotonin signaling. *Neuropsychopharmacology* 41, 1943–1955. doi: 10.1038/npp.2015.349

Mclin, J. P., and Steward, O. (2006). Comparison of seizure phenotype and neurodegeneration induced by systemic kainic acid in inbred, outbred, and hybrid mouse strains. *Eur. J. Neurosci.* 24, 2191–2202. doi: 10.1111/j.1460-9568.2006.05111.x

Messaoudi, E., Kanhema, T., Soulé, J., Tiron, A., Dagyte, G., Da Silva, B., et al. (2007). Sustained Arc/Arg3.1 synthesis controls long-term potentiation consolidation through regulation of local actin polymerization in the dentate gyrus *in vivo*. *J. Neurosci.* 27, 10445–10455. doi: 10.1523/JNEUROSCI.2883-07.2007

Metsis, M., Timmusk, T., Arenas, E., and Persson, H. (1993). Differential usage of multiple brain-derived neurotrophic factor promoters in the rat brain following neuronal activation. *Proc. Natl. Acad. Sci. U.S.A.* 90, 8802–8806. doi: 10.1073/pnas.90.19.8802

Minichiello, L. (2009). TrkB signalling pathways in LTP and learning. *Nat. Rev. Neurosci.* 10, 850–860. doi: 10.1038/nrn2738

Mitre, M., Mariga, A., and Chao, M. V. (2017). Neurotrophin signalling: novel insights into mechanisms and pathophysiology. *Clin. Sci.* 131, 13–23. doi: 10.1042/CS20160044

Nahmani, M., and Turrigiano, G. G. (2014). Adult cortical plasticity following injury: recapitulation of critical period mechanisms? *Neuroscience* 283, 4–16. doi: 10.1016/j.neuroscience.2014.04.029

Nair, R. R., Patil, S., Tiron, A., Kanhema, T., Panja, D., Schiro, L., et al. (2017). Dynamic Arc SUMOylation and selective interaction with F-Actin-Binding protein Drebrin A in LTP consolidation *in vivo*. *Front. Synaptic Neurosci.* 9:8. doi: 10.3389/fnsyn.2017.00008

Nawa, H., Carnahan, J., and Gall, C. (1995). BDNF protein measured by a novel enzyme immunoassay in normal brain and after seizure: partial disagreement with mRNA levels. *Eur. J. Neurosci.* 7, 1527–1535. doi: 10.1111/j.1460-9568.1995.tb01148.x

Park, H., and Poo, M. M. (2013). Neurotrophin regulation of neural circuit development and function. *Nat. Rev. Neurosci.* 14, 7–23. doi: 10.1038/nrn3379

Parkhurst, C. N., Yang, G., Ninan, I., Savas, J. N., Yates, J. R. III., Lafaille, J. J., et al. (2013). Microglia promote learning-dependent synapse formation through brain-derived neurotrophic factor. *Cell* 155, 1596–1609. doi: 10.1016/j.cell.2013.11.030

Pattabiraman, P. P., Tropea, D., Chiaruttini, C., Tongiorgi, E., Cattaneo, A., and Domenici, L. (2005). Neuronal activity regulates the developmental expression and subcellular localization of cortical BDNF mRNA isoforms *in vivo*. *Mol. Cell. Neurosci.* 28, 556–570. doi: 10.1016/j.mcn.2004.11.010

Postigo, A., Calella, A. M., Fritzsch, B., Knipper, M., Katz, D., Eilers, A., et al. (2002). Distinct requirements for TrkB and TrkC signaling in target innervation by sensory neurons. *Genes Dev.* 16, 633–645. doi: 10.1101/gad.217902

Rauskolb, S., Zagrebelsky, M., Dreznjak, A., Deogracias, R., Matsumoto, T., Wiese, S., et al. (2010). Global deprivation of brain-derived neurotrophic factor in the CNS reveals an area-specific requirement for dendritic growth. *J. Neurosci.* 30, 1739–1749. doi: 10.1523/JNEUROSCI.5100-09.2010

Rios, M. (2013). BDNF and the central control of feeding: accidental bystander or essential player? *Trends Neurosci.* 36, 83–90. doi: 10.1016/j.tins.2012.12.009

Rios, M. (2014). Neurotrophins and the regulation of energy balance and body weight. *Handb. Exp. Pharmacol.* 220, 283–307. doi: 10.1007/978-3-642-45106-5_11

Rios, M., Fan, G., Fekete, C., Kelly, J., Bates, B., Kuehn, R., et al. (2001). Conditional deletion of brain-derived neurotrophic factor in the postnatal brain leads to obesity and hyperactivity. *Mol. Endocrinol.* 15, 1748–1757. doi: 10.1210/mend.15.10.0706

Rüttiger, L., Singer, W., Panford-Walsh, R., Matsumoto, M., Lee, S. C., Zuccotti, A., et al. (2013). The reduced cochlear output and the failure to adapt the central auditory response causes tinnitus in noise exposed rats. *PLoS ONE* 8:e57247. doi: 10.1371/journal.pone.0057247

Rüttiger, L., Zimmermann, U., and Knipper, M. (2017). Biomarkers for hearing dysfunction: facts and outlook. *ORL J. Otorhinolaryngol. Relat. Spec.* 79, 93–111. doi: 10.1159/000455705

Sadaghiani, S., Hesselmann, G., and Kleinschmidt, A. (2009). Distributed and antagonistic contributions of ongoing activity fluctuations to auditory stimulus detection. *J. Neurosci.* 29, 13410–13417. doi: 10.1523/JNEUROSCI.2592-09.2009

Sakata, K., Jin, L., and Jha, S. (2010). Lack of promoter IV-driven BDNF transcription results in depression-like behavior. *Genes Brain Behav.* 9, 712–721. doi: 10.1111/j.1601-183X.2010.00605.x

Sakata, K., Woo, N. H., Martinowich, K., Greene, J. S., Schloesser, R. J., Shen, L., et al. (2009). Critical role of promoter IV-driven BDNF transcription in GABAergic transmission and synaptic plasticity in the prefrontal cortex. *Proc. Natl. Acad. Sci. U.S.A.* 106, 5942–5947. doi: 10.1073/pnas.0811431106

Salazar, I. L., Mele, M., Caldeira, M., Costa, R. O., Correia, B., Frisari, S., et al. (2017). Preparation of primary cultures of embryonic rat hippocampal and cerebrocortical neurons. *Bio-protocol* 7:e2551. doi: 10.21769/BioProtoc.2551

Sathanoori, M., Dias, B. G., Nair, A. R., Banerjee, S. B., Tole, S., and Vaidya, V. A. (2004). Differential regulation of multiple brain-derived neurotrophic factor transcripts in the postnatal and adult rat hippocampus during development, and in response to kainate administration. *Brain Res. Mol. Brain Res.* 130, 170–177. doi: 10.1016/j.molbrainres.2004.08.002

Shieh, P. B., Hu, S. C., Bobb, K., Timmusk, T., and Ghosh, A. (1998). Identification of a signaling pathway involved in calcium regulation of BDNF expression. *Neuron* 20, 727–740. doi: 10.1016/S0896-6273(00)81011-9

Singer, W., Geisler, H. S., Panford-Walsh, R., and Knipper, M. (2016). Detection of excitatory and inhibitory synapses in the auditory system using fluorescence immunohistochemistry and high-resolution fluorescence microscopy. *Methods Mol. Biol.* 1427, 263–276. doi: 10.1007/978-1-4939-3615-1_15

Singer, W., Zuccotti, A., Jaumann, M., Lee, S. C., Panford-Walsh, R., Xiong, H., et al. (2013). Noise-induced inner hair cell ribbon loss disturbs central arc mobilization: a novel molecular paradigm for understanding tinnitus. *Mol. Neurobiol.* 47, 261–279. doi: 10.1007/s12035-012-8372-8

Snapyan, M., Lemasson, M., Brill, M. S., Blais, M., Massouh, M., Ninkovic, J., et al. (2009). Vasculature guides migrating neuronal precursors in the adult mammalian forebrain via brain-derived neurotrophic factor signaling. *J. Neurosci.* 29, 4172–4188. doi: 10.1523/JNEUROSCI.4956-08.2009

Somogyi, J., Baude, A., Omori, Y., Shimizu, H., El Mestikawy, S., Fukaya, M., et al. (2004). GABAergic basket cells expressing cholecystokinin contain vesicular glutamate transporter type 3 (VGLUT3) in their synaptic terminals in hippocampus and isocortex of the rat. *Eur. J. Neurosci.* 19, 552–569. doi: 10.1111/j.0953-816X.2003.03091.x

Somogyi, P., Katona, L., Klausberger, T., Lasztóczi, B., and Viney, T. J. (2014). Temporal redistribution of inhibition over neuronal subcellular domains underlies state-dependent rhythmic change of excitability in the hippocampus. *Philos. Trans. R. Soc. Lond. B Biol. Sci.* 369:20120518. doi: 10.1098/rstb.2012.0518

Soriano, E., and Frotscher, M. (1993). GABAergic innervation of the rat fascia dentata: a novel type of interneuron in the granule cell layer with extensive axonal arborization in the molecular layer. *J. Comp. Neurol.* 334, 385–396. doi: 10.1002/cne.903340305

Soulé, J., Messaoudi, E., and Bramham, C. R. (2006). Brain-derived neurotrophic factor and control of synaptic consolidation in the adult brain. *Biochem. Soc. Trans.* 34, 600–604. doi: 10.1042/BST0340600

Takeuchi, Y., Miyamoto, E., and Fukunaga, K. (2002). Analysis on the promoter region of exon IV brain-derived neurotrophic factor in NG108-15 cells. *J. Neurochem.* 83, 67–79. doi: 10.1046/j.1471-4159.2002.01096.x

Takeuchi, Y., Yamamoto, H., Miyakawa, T., and Miyamoto, E. (2000). Increase of brain-derived neurotrophic factor gene expression in NG108-15 cells by the nuclear isoforms of Ca^{2+}/calmodulin-dependent protein kinase II. *J. Neurochem.* 74, 1913–1922. doi: 10.1046/j.1471-4159.2000.0741913.x

Tan, J., Rüttiger, L., Panford-Walsh, R., Singer, W., Schulze, H., Kilian, S. B., et al. (2007). Tinnitus behavior and hearing function correlate with the reciprocal expression patterns of BDNF and Arg3.1/arc in auditory neurons following acoustic trauma. *Neuroscience* 145, 715–726. doi: 10.1016/j.neuroscience.2006.11.067

Tao, X., Finkbeiner, S., Arnold, D. B., Shaywitz, A. J., and Greenberg, M.E. (1998). Ca^{2+} influx regulates BDNF transcription by a CREB family transcription factor-dependent mechanism. *Neuron* 20, 709–726. doi: 10.1016/S0896-6273(00)81010-7

Tao, X., West, A. E., Chen, W. G., Corfas, G., and Greenberg, M. E. (2002). A calcium-responsive transcription factor, CaRF, that regulates

neuronal activity-dependent expression of BDNF. *Neuron* 33, 383–395. doi: 10.1016/S0896-6273(01)00561-X

Thaler, C., and Vogel, S. S. (2006). Quantitative linear unmixing of CFP and YFP from spectral images acquired with two-photon excitation. *Cytometry A* 69, 904–911. doi: 10.1002/cyto.a.20267

Timmusk, T., Palm, K., Metsis, M., Reintam, T., Paalme, V., Saarma, M., et al. (1993). Multiple promoters direct tissue-specific expression of the rat BDNF gene. *Neuron* 10, 475–489. doi: 10.1016/0896-6273(93)90335-O

Turrigiano, G. (2014). Neurobiology: keeping a lid on it. *Nature* 511, 297–298. doi: 10.1038/nature13641

Tuvikene, J., Pruunsild, P., Orav, E., Esvald, E. E., and Timmusk, T. (2016). AP-1 transcription factors mediate BDNF-positive feedback loop in cortical neurons. *J. Neurosci.* 36, 1290–1305. doi: 10.1523/JNEUROSCI.3360-15.2016

Vaghi, V., Polacchini, A., Baj, G., Pinheiro, V. L., Vicario, A., and Tongiorgi, E. (2014). Pharmacological profile of brain-derived neurotrophic factor (BDNF) splice variant translation using a novel drug screening assay: a "quantitative code". *J. Biol. Chem.* 289, 27702–27713. doi: 10.1074/jbc.M114.586719

Vanevski, F., and Xu, B. (2013). Molecular and neural bases underlying roles of BDNF in the control of body weight. *Front. Neurosci.* 7:37. doi: 10.3389/fnins.2013.00037

Waterhouse, E. G., An, J. J., Orefice, L. L., Baydyuk, M., Liao, G. Y., Zheng, K., et al. (2012). BDNF promotes differentiation and maturation of adult-born neurons through GABAergic transmission. *J. Neurosci.* 32, 14318–14330. doi: 10.1523/JNEUROSCI.0709-12.2012

Weinberger, N. M. (2015). New perspectives on the auditory cortex: learning and memory. *Handb. Clin. Neurol.* 129, 117–147. doi: 10.1016/B978-0-444-62630-1.00007-X

West, A. E., Chen, W. G., Dalva, M. B., Dolmetsch, R. E., Kornhauser, J. M., Shaywitz, A. J., et al. (2001). Calcium regulation of neuronal gene expression. *Proc. Natl. Acad. Sci. U.S.A.* 98, 11024–11031. doi: 10.1073/pnas.191352298

West, A. E., Pruunsild, P., and Timmusk, T. (2014). Neurotrophins: transcription and translation. *Handb. Exp. Pharmacol.* 220, 67–100. doi: 10.1007/978-3-642-45106-5_4

Xu, M., Remillard, C. V., Sachs, B. D., Makino, A., Platoshyn, O., Yao, W., et al. (2008). p75 neurotrophin receptor regulates agonist-induced pulmonary vasoconstriction. *Am. J. Physiol. Heart Circ. Physiol.* 295, H1529–H1538. doi: 10.1152/ajpheart.00115.2008

Yamada, K., and Nabeshima, T. (2003). Brain-derived neurotrophic factor/TrkB signaling in memory processes. *J. Pharmacol. Sci.* 91, 267–270. doi: 10.1254/jphs.91.267

Yang, J., Siao, C. J., Nagappan, G., Marinic, T., Jing, D., Mcgrath, K., et al. (2009). Neuronal release of proBDNF. *Nat. Neurosci.* 12, 113–115. doi: 10.1038/nn.2244

Zafra, F., Hengerer, B., Leibrock, J., Thoenen, H., and Lindholm, D. (1990). Activity dependent regulation of BDNF and NGF mRNAs in the rat hippocampus is mediated by non-NMDA glutamate receptors. *Embo. J.* 9, 3545–3550.

Zafra, F., Lindholm, D., Castrén, E., Hartikka, J., and Thoenen, H. (1992). Regulation of brain-derived neurotrophic factor and nerve growth factor mRNA in primary cultures of hippocampal neurons and astrocytes. *J. Neurosci.* 12, 4793–4799. doi: 10.1523/JNEUROSCI.12-12-04793.1992

Zha, X. M., Bishop, J. F., Hansen, M. R., Victoria, L., Abbas, P. J., Mouradian, M. M., et al. (2001). BDNF synthesis in spiral ganglion neurons is constitutive and CREB-dependent. *Hear. Res.* 156, 53–68. doi: 10.1016/S0378-5955(01)00267-2

Zuccotti, A., Kuhn, S., Johnson, S. L., Franz, C., Singer, W., Hecker, D., et al. (2012). Lack of brain-derived neurotrophic factor hampers inner hair cell synapse physiology, but protects against noise-induced hearing loss. *J. Neurosci.* 32, 8545–8553. doi: 10.1523/JNEUROSCI.1247-12.2012

Conflict of Interest Statement: The authors declare that the research was conducted in the absence of any commercial or financial relationships that could be construed as a potential conflict of interest.

Supplementary Figure 1

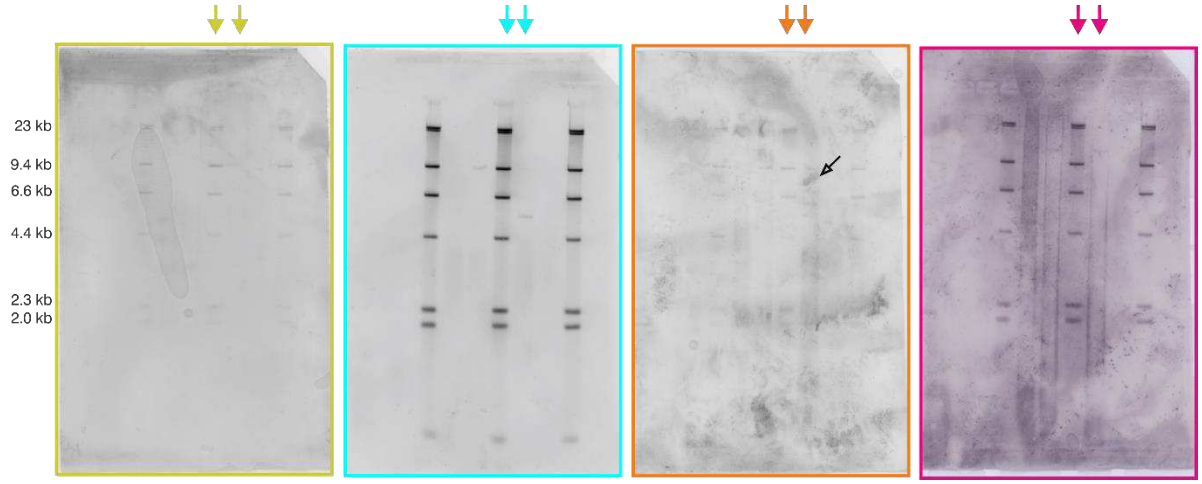

Supplementary Figure 1 Original Southern Blots used for Figure 3 C. Four different probes were used for Southern Blot analyses. Probe 1 (green), specific for the 5´-end: WT band 9.8 kb, transgenic allele 3 kb; probe 2 (blue), covering parts of exon-IV transgene: WT band 9.8 kb, transgenic allele 5.3 kb; probe 3 (orange), covering parts of the exon-VI transgene: WT band 9.8 kb, transgenic allele 6.3 kb; probe 4 (pink), specific for the 3´-end: WT and transgenic allele 12.7 kb. Colored arrows indicate lanes used in Figure 3C. All lanes used for Figure 3C are derived from the same ES cell clone. Southern Blots were inverted and the contrast was increased for all pixels similarly to increase visibility of the band. For probe 3 an unspecific spot was darkened between the 9.8 and 6.3 kb bands, otherwise the bands would not have been clearly visible (black open arrow).

Supplementary Figure 2

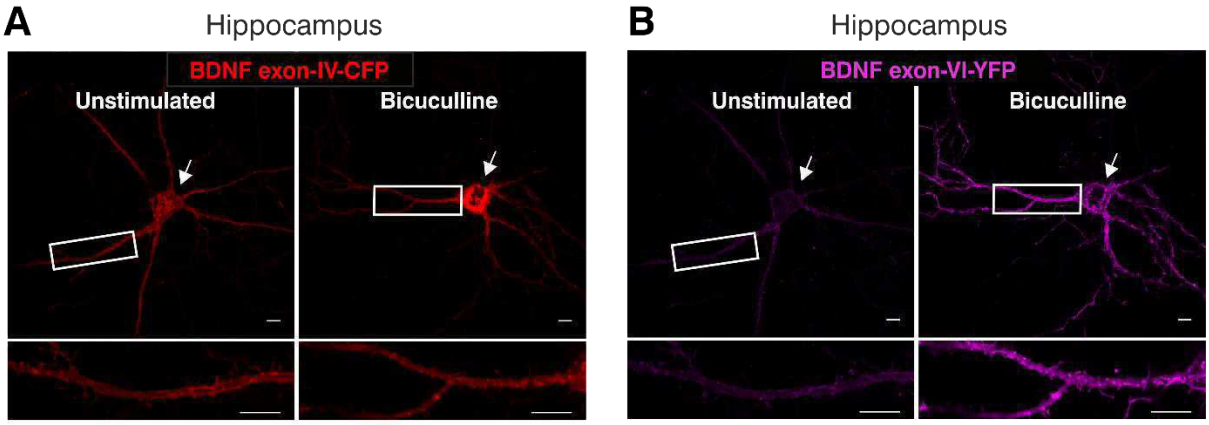

Supplementary Figure 2 Transfected rat primary hippocampal neurons (embryonic day E18) without (left panel) and with bicuculline (right panel) stimulation. Staining against HA (coupled to *Bdnf* exon-IV-CFP) (**A**) and cMyc (coupled to *Bdnf* exon-VI-YFP) (**B**) was performed with specific antibodies against the HA and c-Myc tags, respectively. Lower panels show higher magnification of area in solid frame. (**A**) Increased expression of *Bdnf* exon-IV-CFP detected preferentially in cell bodies after stimulation with bicuculline (right panel, arrow). (**B**) Increased expression of *Bdnf* exon-VI-YFP after treatment with bicuculline predominantly detected in proximal and distal regions of the neurites (right panel, solid frame). Scale bars: 10 µm**.**

Supplementary Figure 3

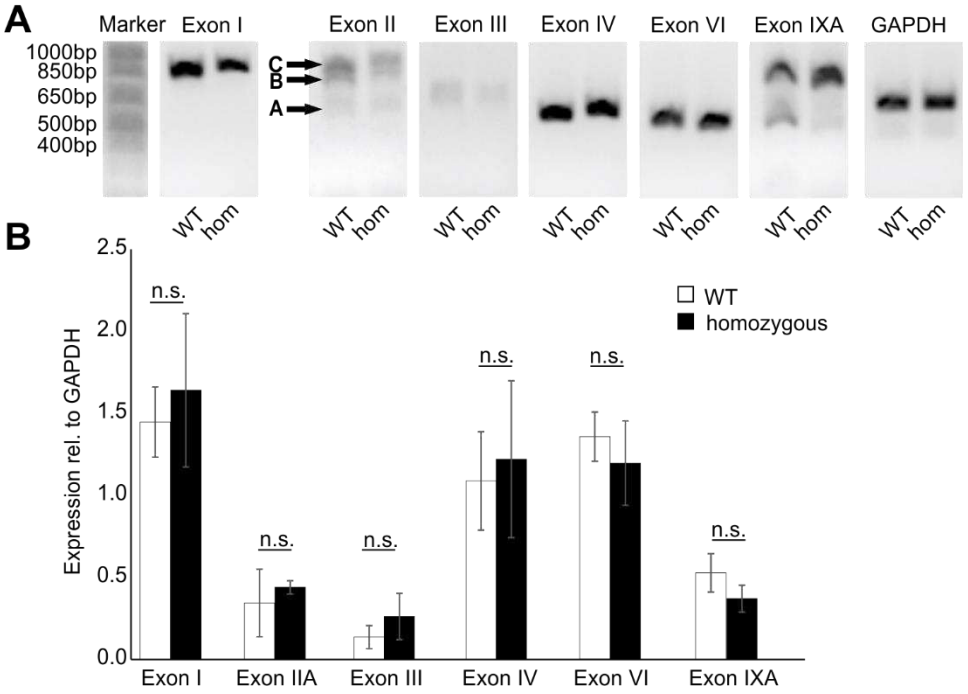

Supplementary Figure 3 Analysis of mRNA expression of the untranslated *Bdnf* exons I, II, III, IV, VI, IXA by RT-PCR in the hippocampus of BLEV mice for wildtype (WT) and homozygous (hom) animals. (**A**) Representative gel picture for *Bdnf* exon I, II, III, IV, VI and IXA. The previously described different transcript variants of *Bdnf* exon II (A, B, C) (Aid et al., 2007) are indicated by arrows. Due to the very similar size of the transcript variants B and C of exon II a separate quantification was not possible. Housekeeping gene: GAPDH. For original picture see Supplementary Figure 6D**.** (**B**) Quantitative analyses of the expression of *Bdnf* exon I, IIA, III, IV, VI, and IXA did not reveal any significant differences between WT and homozygous BLEV mice. Data represented as mean ± SEM (2-sided Student´s *t*-test with $\alpha = 0.05$, for details see Supplementary Table 2).

Supplementary Figure 4

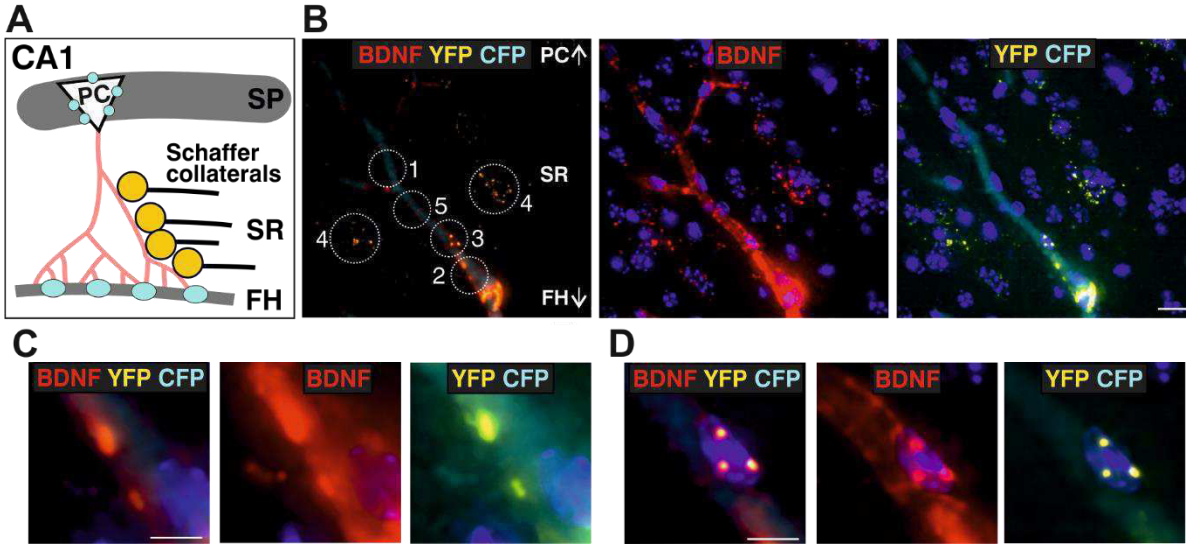

Supplementary Figure 4 Triple images of BDNF IR (red), YFP and CFP (**A**) Schematic overview of the CA1 region containing the stratum pyramidale (SP), the stratum radiatum (SR) and the fissura hippocampalis (FH). (**B**) Merged image of Figure 5B. Left picture: BDNF-IR in 5 different characteristic regions at the level of the SR co-localized with *Bdnf* exon-VI-YFP and *Bdnf* exon-IV-CFP. Middle picture: BDNF-IR (red). Right picture: Co-localization of *Bdnf* exon-VI-YFP and *Bdnf* exon-IV-CFP. Nuclei were stained with DAPI (blue). Scale bars: 100 µm. (**C**) Merged image of Figure 5E. Left picture: BDNF-IR co-localized with *Bdnf* exon-VI-YFP close to a *Bdnf* exon-IV-CFP positive capillary in the FH. Middle picture: BDNF-IR (red). Right picture: Co-localization of *Bdnf* exon-VI-YFP and *Bdnf* exon-IV-CFP. Nuclei were stained with DAPI (blue). Scale bar: 10 µm (**D**) Merged image of Figure 5H. Left picture: BDNF-IR co-localized with *Bdnf* exon-VI-YFP-positive puncta on *Bdnf* exon-IV-CFP-positive capillaries. Middle picture: BDNF-IR (red). Right picture: Co-localization of *Bdnf* exon-VI-YFP and *Bdnf* exon-IV-CFP. Nuclei were stained with DAPI (blue). Scale bar: 10 µm.

Supplementary Figure 5

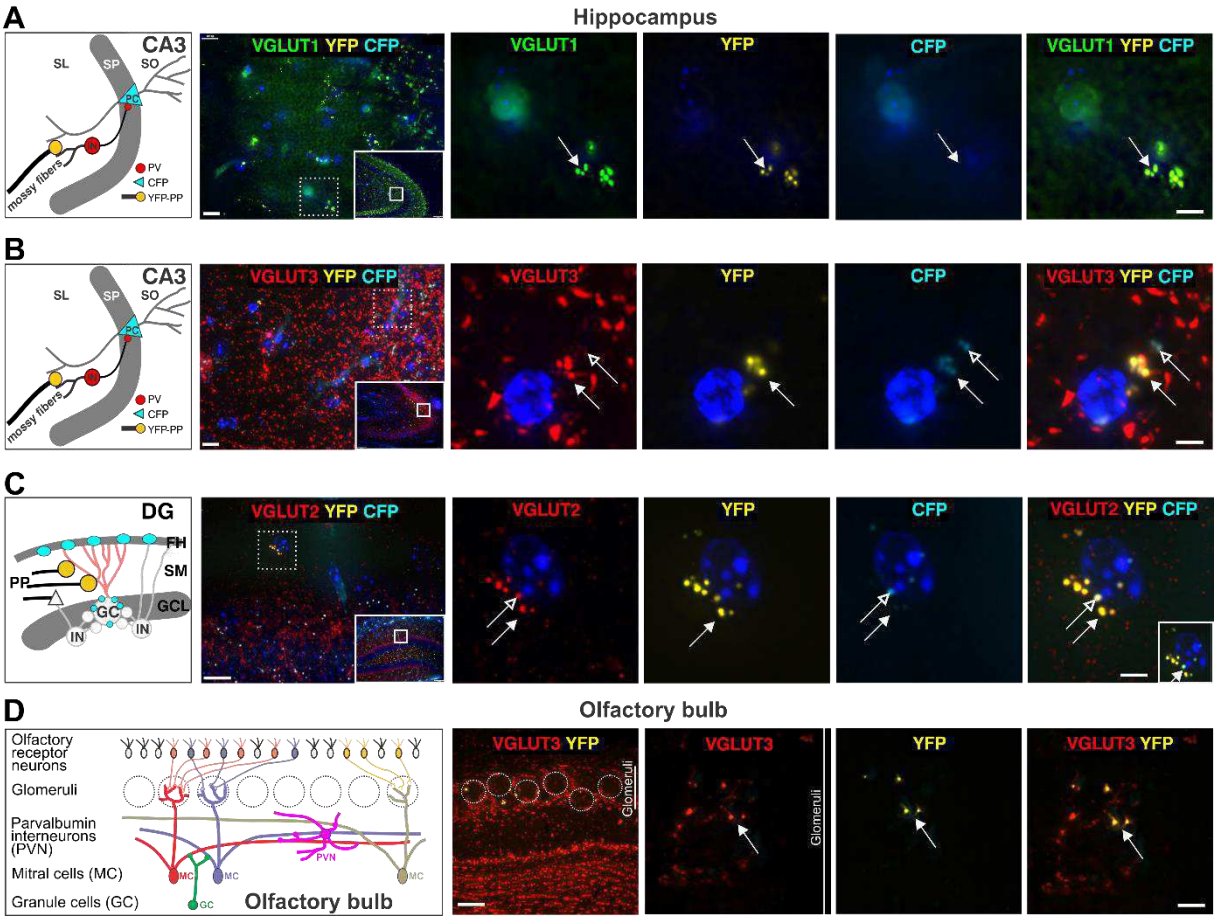

Supplementary Figure 5 Immunostaining of the presynaptic marker proteins VGLUT1, VGLUT2 and VGLUT3. (**A**) Schematic overview of the CA3 region containing the stratum lucidum (SL), stratum pyramidale (SP), the stratum oriens (SO), parvalbumin (PV) positive interneurons (IN) and pyramidal cells (PC). Second panel: VGLUT1 IR in green co-localized with *Bdnf* exon-VI-YFP and *Bdnf* exon-IV-CFP within the CA3 region. Inset: lower magnification of the same area (solid frame). Scale bar: 100 µm. Right panels: higher magnification depicting single channels of VGLUT1 (green), YFP and CFP demonstrate co-localized VGLUT1 and YFP positive dots (arrows). Scale bar: 10 µm. Nuclei were stained with DAPI (blue) (**B**) Schematic overview of the CA3 region. Second panel: VGLUT3 IR in red co-localized with *Bdnf* exon-VI-YFP and *Bdnf* exon-IV-CFP. Inset lower magnification of the area (solid frame). Scale bar: 100 µm. Right panels: higher magnification depicting single channels of VGLUT3 (red), YFP and CFP show co-localization of VGLUT3 and YFP (arrows). Some few dots show a co-localization of VGLUT3 (red) and CFP (open arrows). Scale bar: 10 µm.. Nuclei were stained with DAPI (blue) (**C**) Schematic overview of the dentate gyrus (DG) region containing the fissura hippocampalis (FH), stratum moleculare (SM), the granular cell layer (GCL), granular cells (GC), interneurons (IN) and the perforant path (PP). Second panel: VGLUT2 IR (red) co-localized with *Bdnf* exon-VI-YFP and *Bdnf* exon-IV-CFP. Inset: lower magnification of the same area (solid frame). Scale bar: 100 µm. Right panels: higher magnification depicting single channels of VGLUT2, YFP and CFP, which demonstrate a co-localization of VGLUT2 (red) and YFP (arrows). Some few dots show a co-localization of VGLUT2 (red), YFP and CFP (open arrows). Inset in the right panel shows Scale bar: 10 µm. Nuclei were stained with DAPI (blue). (**D**) Olfactory bulb. Left panel: Schematic overview of the olfactory bulb containing the olfactory receptor neurons, the glomeruli, parvalbumin–positive interneurons (PVN), the mitral cells (MC), and the granule cells (GC). Second panel:

VGLUT3 IR (red) in the olfactory bulb co-localized with *Bdnf* exon-VI-YFP. Scale bar: 100 μm. Right panels: higher magnification of the glomeruli. A clear co-localization of VGLUT3 IR (red) and *Bdnf* exon-VI-YFP was observed within the glomeruli. Scale bar: 10 μm.

Supplementary Figure 6

A *Bdnf* exon-IX mRNA hippocampus

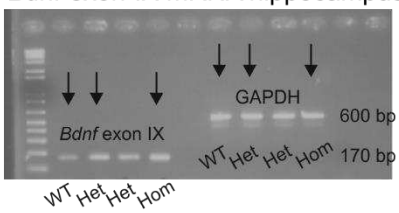

B BDNF protein hippocampus

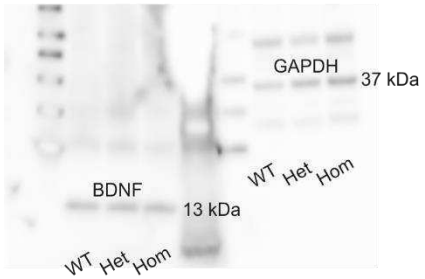

C CFP and YFP protein hippocampus

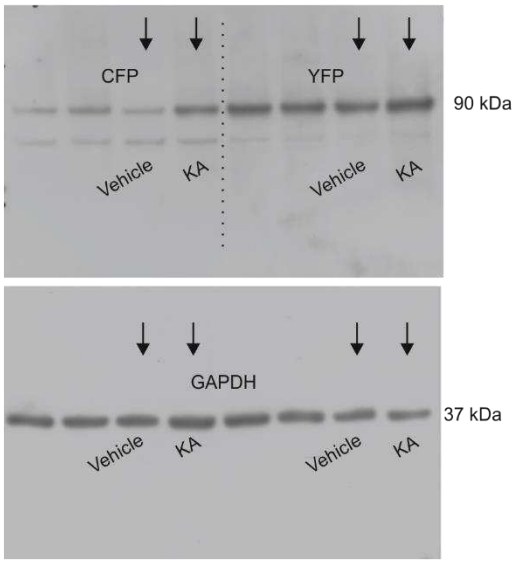

D RT-PCR untranslated *Bdnf* exons

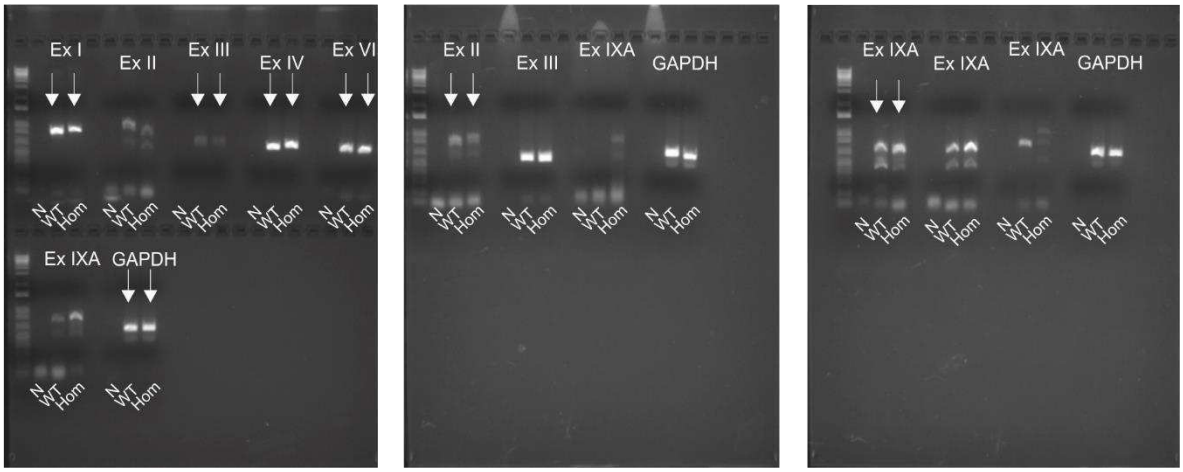

Supplementary Figure 6 Original PCR and Western Blots for Figures 4C/D and 7A. (**A**) Picture from the original PCR gel used for Figure 4C. Black arrows indicate bands used for the figure. As two heterozygous animals were used for PCR, one is left out. (**B**) Original Western blot used for Figure 4D. Contrast was increased for better visibility. For quantification the unmodified image was used. (**C**) Original Western blot used for Figure 7A. Black arrows indicate bands used for the figure. As other probes were run on the same blot relevant bands were cut. Contrast was increased for better visibility. For quantification the unmodified image was used. (**D**) Original PCR gel used for Supplementary Figure 2. Arrows indicate the used lanes. For quantification the unmodified images were used.

Supplementary Table 1 Antibody information for immunohistochemistry and Western blot

Primary Antibodies						
Immunohistochemistry	Antibody	Protein name	Product number	Source	Dilution	Protein size
Brain sections	Mouse anti-BDNF	Brain-derived neurotrophic factor	BDNF #9-b	Developmental Studies Hybridoma Bank University of Iowa	1:50	
	Rabbit anti-parvalbumin	Parvalbumin	ab11427	Abcam	1:2,000	
	Mouse anti-desmin	Desmin	ab8976	Abcam	1:100	
	Rabbit anti-Arc	Activity regulated cytoskeletal protein	156 003	Synaptic Systems	1:500	
	Rabbit anti-IBA-1	Ionized calcium-binding adaptor molecule 1	016-20001	Wako Chemicals	1:500	
	Rabbit anti-GFAP	Glial fibrillary acidic protein	Z 0334	Dako	1:2,000	
	Rabbit anti-p75NGFR	p75 neurotrophin receptor	AB1554	Millipore	1:100	
	Rabbit anti-b1-GC	b1-subunit of the nitric oxide-sensitive guanylate cyclase		Müllerhausen et al. 2004	1:200	
	Guinea pig anti-vGLUT1	Vesicular glutamate transporter 1	135304	Synaptic System	1:1,500	
	Rabbit anti-vGLUT2	Vesicular glutamate transporter 2	135403	Synaptic System	1:500	
	Rabbit anti-vGLUT1	Vesicular glutamate transporter 3	135203	Synaptic System	1:1,000	
Cell culture	Mouse anti-Myc	Myc-tagged protein	2276	Cell Signaling	1:500	
	Rabbit Anti-HA	HA-tagged protein	AB9110	Abcam	1:500	

Western blot	Rabbit anti-RCFP	Reef coral fluorescent protein pan antibody	632475	Clontech	1:1,000	30-35 kDa
	Rabbit anti-BDNF	Brain-derived neurotrophic factor	sc-546	Santa Cruz Biotechnology Inc.	1:400	15 kDa
	Mouse anti-GAPDH	Glyceraldehyde 3-phosphate dehydrogenase	ab8245	Abcam	1:10,000	40 kDa
Secondary antibodies						
Immunohistochemistry						
Brain sections						
	Antibody	Protein name	Product number	Source	Dilution	Protein size
	Cy3-conjugated goat anti-mouse antibody		115-1665-062	Jackson ImmunoResearch Laboratories	1:3,000	
	AlexaFluor 488 goat anti-guinea pig		A-11073	Molecular Probes	1:500	
Cell culture	AlexaFluor 568 conjugated goat anti-rabbit		A-11011	Invitrogen	1:500	
	AlexaFluor 647 conjugated goat anti-mouse		A-21235	Invitrogen	1:500	
Western blot	Cy3-conjugated goat anti-rabbit antibody		111-166-003	Jackson ImmunoResearch Laboratories	1:1,500	
	Alexa488-conjugated anti-mouse antibody		A11001	Molecular Probes, MoBiTec	1:500	
	Alexa488-conjugate		A11073	Molecular Probes, MoBiTec	1:500	

	d anti-guinea pig antibody					
	ECL anti-mouse IgG HRP linked		NA 931-100µl	GE Healthcare UK Limited	1:2,500	
	ECL anti-rabbit IgG HRP linked		NA 934-100µl	GE Healthcare UK Limited	1:2,500	

Supplementary Table 2 Statistical information

		Statistical test	**Test value**	**Degrees of freedom**	***p*-value**	**Post-hoc test with *p*-value**		**n-number**
Fig. 1E		1-way ANOVA			p = 0.0002	post-test 2-sided Student´s t-test		done in duplicate for 4 independent experiments
			F (3, 36) = 8.35			CFP	p = 0.008	
						YFP	p = 0.003	
Fig. 4B								WT n = 9 Het n = 11 Hom n = 11 animals
Fig. 4C	PCR (mRNA)	1-way ANOVA	F(2,9) = 0.15		p = 0.86			n = 3 animals / genotype
Fig. 4D	Westen blot (Protein)	1-way ANOVA	F(2,12) = 0.20		p = 0.82			n = 4 animals / genotype
Fig. 4E	click-ABR	1-way ANOVA	F(2, 26) = 1.988		p = 0.16			WT n = 20/10 ears/animals het n = 30/15 ears/ animals hom n = 10/5 ears/animals
	f-ABR	2-way ANOVA	F(18, 2665) = 0.50		p = 0.96			
Fig. 7A	Western blot (CFP)	1-sided Student's *t*-test	t = 6.25	DF = 4	p = 0.002			n = 3 animals / group
	Western blot (YFP)	1-sided Student's *t*-test	t = 1.99	DF = 6	p = 0.04			n = 4 animals / group
Fig. 7D	Integrated density (YFP)	1-sided Student's *t*-test	t = 4.14	DF = 3	p = 0.0128			n = 3 animals / group
Fig. 7F	Integrated density (CFP)	1-sided Student's *t*-test	t = 2.32	DF = 4	p = 0.0405			n = 2-3 animals / group
Supp. Fig. 2B	PCR (mRNA)	2-sided Student's *t*-test	Exon I t = 0.7327 Exon IIA t = 0.3913 Exon III t = 1.007 Exon IV t = 0.3009 Exon VI t = 0.5474	DF = 6 DF = 6 DF = 6 DF = 6 DF = 6 DF = 6	p = 0.4914 p = 0.7091 p = 0.3526 p = 0.7737 p = 0.6132 p = 0.3560			n = 3 animals / genotype; 4-5 replicates / animal

			Exon IXA t = 0.9908					

frontiers in Molecular Neuroscience

ORIGINAL RESEARCH
published: 31 July 2018
doi: 10.3389/fnmol.2018.00260

Visualizing BDNF Transcript Usage During Sound-Induced Memory Linked Plasticity

Lucas Matt[1†], Philipp Eckert[2†], Rama Panford-Walsh[2], Hyun-Soon Geisler[2], Anne E. Bausch[1], Marie Manthey[2], Nicolas I. C. Müller[3], Csaba Harasztosi[4], Karin Rohbock[2], Peter Ruth[1], Eckhard Friauf[3], Thomas Ott[5], Ulrike Zimmermann[2], Lukas Rüttiger[2], Thomas Schimmang[6], Marlies Knipper[2] and Wibke Singer[2]*

[1] Department of Pharmacology, Institute of Pharmacy, Toxicology, and Clinical Pharmacy, University of Tübingen, Tübingen, Germany, [2] Department of Otolaryngology, Tübingen Hearing Research Centre, Molecular Physiology of Hearing, University of Tübingen, Tübingen, Germany, [3] Animal Physiology Group, Department of Biology, University of Kaiserslautern, Kaiserslautern, Germany, [4] Section of Physiological Acoustics and Communication, Department of Otolaryngology, Tübingen Hearing Research Center, University of Tübingen, Tübingen, Germany, [5] Transgenic Facility Tübingen, University of Tübingen, Tübingen, Germany, [6] Instituto de Biologíay Genética Molecular, Universidad de Valladolid, Consejo Superior de Investigaciones Científicas (CSIC), Valladolid, Spain

OPEN ACCESS

Edited by:
Isabel Varela-Nieto, Consejo Superior de Investigaciones Científicas (CSIC), Spain

Reviewed by:
José María Frade, Instituto Cajal (IC), Spain
Anthony John Hannan, Florey Institute of Neuroscience and Mental Health, Australia

***Correspondence:**
Marlies Knipper
marlies.knipper@uni-tuebingen.de

[†]*These authors have contributed equally to this work.*

Received: *18 April 2018*
Accepted: *12 July 2018*
Published: *31 July 2018*

Citation:
Matt L, Eckert P, Panford-Walsh R, Geisler H-S, Bausch AE, Manthey M, Müller NIC, Harasztosi C, Rohbock K, Ruth P, Friauf E, Ott T, Zimmermann U, Rüttiger L, Schimmang T, Knipper M and Singer W (2018) Visualizing BDNF Transcript Usage During Sound-Induced Memory Linked Plasticity. Front. Mol. Neurosci. 11:260. doi: 10.3389/fnmol.2018.00260

Activity-dependent BDNF (brain-derived neurotrophic factor) expression is hypothesized to be a cue for the context-specificity of memory formation. So far, activity-dependent BDNF cannot be explicitly monitored independently of basal BDNF levels. We used the BLEV (***B***DNF-***l***ive-***e***xon-***v***isualization) reporter mouse to specifically detect activity-dependent usage of *Bdnf* exon-IV and -VI promoters through bi-cistronic co-expression of CFP and YFP, respectively. Enriching acoustic stimuli led to improved peripheral and central auditory brainstem responses, increased Schaffer collateral LTP, and enhanced performance in the Morris water maze. Within the brainstem, neuronal activity was increased and accompanied by a trend for higher expression levels of *Bdnf* exon-IV-CFP and exon-VI-YFP transcripts. In the hippocampus BDNF transcripts were clearly increased parallel to changes in parvalbumin expression and were localized to specific neurons and capillaries. Severe acoustic trauma, in contrast, elevated neither *Bdnf* transcript levels, nor auditory responses, parvalbumin or LTP. Together, this suggests that critical sensory input is essential for recruitment of activity-dependent auditory-specific BDNF expression that may shape network adaptation.

Keywords: *Bdnf* exon-IV, *Bdnf* exon-VI, LTP, memory acquisition, feed-forward inhibition, parvalbumin, vasculature, sound-accentuation

INTRODUCTION

Brain-derived neurotrophic factor (BDNF), identified in 1982 (Barde et al., 1982), is recognized as key modulator of synaptic plasticity during homeostatic readjustment processes and a master regulator of energy homeostasis (for review see: Bramham and Messaoudi, 2005; Rauskolb et al., 2010; Park and Poo, 2013; Marosi and Mattson, 2014; Nahmani and Turrigiano, 2014; Jeanneteau and Arango-Lievano, 2016; Mitre et al., 2017). BDNF is well-known for its involvement in Schaffer collateral long-term potentiation (LTP) (Minichiello, 2009) as well as in inhibition (Huang and Reichardt, 2001; Wardle and Poo, 2003; Lu et al., 2009; Waterhouse and Xu, 2009; Duguid et al., 2012; Park and Poo, 2013; Parkhurst et al., 2013; Nahmani and Turrigiano, 2014). Nevertheless,

we do not yet understand BDNF's influence on circuit stabilization in the adult system or its function in platelets (Chacón-Fernández et al., 2016), capillary endothelial cells (Donovan et al., 2000), microglia, and astrocytes (Ferrini and De Koninck, 2013; Parkhurst et al., 2013) during homeostatic readjustment processes (Nahmani and Turrigiano, 2014). Among other reasons, this is due to the difficulty of detecting the very low (Dieni et al., 2012) endogenous expression of BDNF in the mature central nervous system (CNS) (Dieni et al., 2012). Furthermore, many BDNF mutant mouse lines present severe phenotypes that complicate analysis of BDNF under normal physiological conditions (Ernfors et al., 1994; Rios et al., 2001; Postigo et al., 2002; Chourbaji et al., 2008; Hong et al., 2008; Sakata et al., 2009; Rauskolb et al., 2010; Lyons and West, 2011; Zuccotti et al., 2012; Vanevski and Xu, 2013; Mallei et al., 2015; Hill et al., 2016; Maynard et al., 2016).

Part of the multifaceted functions of BDNF might be obfuscated by the complex structure of the *Bdnf* gene, which is comprised of eight independently transcribed non-coding exons (I-VIII), each of which is spliced to a common protein encoding exon (IX) (Timmusk et al., 1993; Aid et al., 2007), resulting in multiple transcripts that display different stability, targeting, and translatability (Vaghi et al., 2014). BDNF expression from each of these eight different promoters is independently regulated (Vaghi et al., 2014). Of particular interest are exon-IV and exon-VI, both containing promoters directly or indirectly regulated by neuronal activity (Hong et al., 2008; West et al., 2014; Tuvikene et al., 2016). Dysfunction of these two *Bdnf* transcripts is associated with deficits in sleep, fear, and memory (Hill et al., 2016), as well as depression (Sakata et al., 2010), cortical inhibition deficiency (Hong et al., 2008), and cognitive decline (Vaghi et al., 2014; Mallei et al., 2015). Moreover, downregulation of activity-dependent BDNF was observed in stress-related neuropsychiatric disorders (Pariante, 2009; Castrén and Rantamäki, 2010) or in states of increased glucocorticoid resistance, for example during chronic stress (Bath et al., 2013; Gray et al., 2013; Jeanneteau and Arango-Lievano, 2016). Any stress reaction that may result in behavioral changes related to external cues requires an activity-dependent signal to provide context specificity to the otherwise ubiquitous glucocorticoid receptor (GR)-mediated stress response (de Kloet, 2014). For example, metabolic support for behaviorally relevant motor learning can only be provided through activity-dependent reallocation of GR effects (Liston et al., 2013; Arango-Lievano et al., 2015; Jeanneteau and Arango-Lievano, 2016). In this context, BDNF was previously hypothesized to provide the corresponding signal (Jeanneteau and Arango-Lievano, 2016).

So far, however, it was technically impossible to detect increased activity-dependent BDNF expression above the background of basal BDNF levels. We have generated ***B***DNF-***l***ive-***e***xon-***v***isualization (BLEV) knock-in reporter mice to specifically detect BDNF in response to *Bdnf* exon-IV and -VI promoter usage (Singer et al., submitted). The generation and validation of this new reporter mouse line is described in detail in Singer et al. (submitted). In BLEV mice, *Bdnf* exon-IV and -VI mRNA translation sites are tagged by bi-cistronic co-expression of cyan- and yellow-fluorescent-protein (CFP and YFP), respectively (Singer et al., submitted). BLEV reporter mice are viable without any BDNF-related mutant phenotype (Singer et al., submitted). Importantly, they allow the detection of *Bdnf* exon-IV-CFP and *Bdnf* exon-VI-YFP at sites of BDNF protein expression in neurons, microglia, astrocytes, and capillaries (Singer et al., submitted), cell types previously shown to express BDNF (Edelmann et al., 2014; Serra-Millàs, 2016). Furthermore, in BLEV mice it is possible to observe activity-dependent hippocampal BDNF expression in response to glutamate receptor activation through either CFP and YFP fluorescence or quantification of protein tags by Western blot (Singer et al., submitted). To test if BLEV mice also allow monitoring of activity-dependent BDNF during behaviorally relevant long-term adaptive processes in response to external cues, we monitored *Bdnf*-transcript changes in BLEV reporter mice following different sound exposure conditions. Previous experiments demonstrated that exposures to defined enriching, mild traumatic, or severe traumatic sound pressure levels (SPL) caused long-lasting alterations to sound-sensitivity and differentially induced hippocampal plasticity (Singer et al., 2013). Likewise, acoustically induced differences in central sound sensitivity correlated with sensitivity to stress as shown through a social stress paradigm or pharmacological inhibition of stress receptors (Singer et al., 2018).

In the present study we observed persistent sound sensitivity changes after these sound exposure paradigms in BLEV mice. In the auditory brainstem, these changes were accompanied by increased expression of VGLUT1, an established marker of excitation in auditory fibers, and a tendency to upregulate *Bdnf* exon-IV and exon-VI. These observations were specific for the auditory system and could not be detected in the olfactory bulb. Furthermore, different exposure levels correlated with altered *Bdnf* exon-IV and exon-VI expression in specific hippocampal neurons and vascular cells. In the hippocampus, this was paralleled by altered levels of GluA2 and parvalbumin expression and associated with a changed balance between excitatory vs. inhibitory inputs to CA1 pyramidal cells, underlined by altered Schaffer collateral LTP and spatial memory performance. These findings can only be explained by a critical sensory input that drives activity-dependent BDNF expression toward long-term adaptive responses.

METHODS

Animals

Animal care and use and experimental protocols correspond to national and institutional guidelines and were reviewed and approved by the animal welfare commissioner and the regional board for animal experimentation. All experiments were performed according to the European Union Directive 2010/63/EU for the protection of animals used for experimental and other scientific purposes. Mice were kept according to national guidelines for animal care in an SPF animal facility at 25°C on a 12/12 h light/dark cycle with average noise levels of around 50–60 dB.

Vector Construct for a Transgenic BDNF Mouse

For a detailed description of the generation of the new mouse model please see Singer et al., (submitted). In brief, the *Bdnf* exon-IV and -VI sequence, both including the corresponding promoter sequences, were extended by CFP or YFP, respectively, both containing a stop codon. A HA-tag was added to *Bdnf* exon-IV-CFP and a cMyc-tag to *Bdnf* exon-VI-YFP. The translation of the protein-coding *Bdnf* exon-IX is enabled by an IRES sequence, which keeps the mRNA at the ribosome, despite the presence of a stop codon. Additionally, the growth-associated protein 43 (GAP43), is added to anchor the fluorescent proteins at the site of translation. This allows differential monitoring of the non-coding *Bdnf* exon-IV and *Bdnf* exon-VI by the fluorescent proteins CFP and YFP without interfering with *Bdnf* exon-IX.

Hearing Measurements and Noise Exposure

The hearing function of 2–3 months old BLEV reporter mice of both sexes was studied by measuring auditory brainstem responses (ABRs), as previously described (Zuccotti et al., 2012; Rüttiger et al., 2013). For noise exposure, animals were exposed to 10 kHz for 40 min at 80, 100, or 120 dB SPL while under anesthesia. For ABR recordings and noise exposure, we anesthetized the animals with an intraperitoneal injection of a mixture of ketamine-hydrochloride (75 mg/kg body weight, Ketavet, Pharmacia, Erlangen, Germany) and xylazine hydrochloride (5 mg/kg body weight, Rompun, Bayer, Leverkusen, Germany). Additional doses of anesthetics were administered if needed. Sham-exposed animals were anesthetized and placed in the reverberating chamber but not exposed to acoustic stimulus (i.e., the speaker remained turned off). Mice were randomly allocated to the different treatment groups.

Tissue Preparation

For protein isolation, brains were dissected with small forceps and immediately frozen in liquid nitrogen and stored at −80°C before use. Brain and cochlear tissue for immunohistochemistry was prepared as previously described (Singer et al., 2016).

Protein Isolation and Western Blot

For isolation of cMyc-tagged proteins and HA-tagged proteins, the Mild Purification kit and the HA-tagged Protein Purification kit were used, respectively (BiozolDiagnostica). In brief, tissues were dissolved in a lysis buffer (CelLytic M, Sigma-Aldrich) and incubated for 1 h with anti-cMyc or anti-HA tag beads suspension. The suspension was then centrifuged and washed; cMyc- and HA-tagged proteins were eluted with Elution Peptide Solution from the kit. All samples underwent the same procedures. The flow-through of the IP after extraction of the HA- and cMyc-tagged proteins was loaded on the gel to detect GAPDH (see Supplementary Table 1) and all other antibodies (expect of RCFP). Equal amounts of proteins are loaded for each lane.

Proteins were separated by electrophoresis and placed on a transfer membrane; non-specific epitopes of the membrane were blocked with 5% milk powder solution and incubated overnight at 4°C with the primary antibody, see Supplementary Table 1. Membranes for one approach were incubated with several primary antibodies at the same time, see originals in Supplementary Figures 2, 3. On the second day, the membrane was washed three times with Tris buffer/0.1% Tween 20; the secondary antibody (see Supplementary Table 1) was incubated for 1 h at room temperature in a sealed envelope. The membrane was washed again three times with Tris buffer/0.1% Tween 20. Proteins were visualized with ECL Prime WB Detection Reagent (GE Healthcare) using the Proxima 2700 (Isogen Life Science). For protein sizes, see Supplementary Table 1.

Immunohistochemistry and Ribbon Counting

Cochleae were isolated, fixed, cryosectioned, and stained as described (Tan et al., 2007; Singer et al., 2016). Image acquisition and CtBP2/RIBEYE-immunopositive spot counting were carried out as previously described (Zuccotti et al., 2012; Singer et al., 2016).

Immunohistochemistry on brain sections was carried out as previously described (Singer et al., 2016). Antibodies are described in Supplementary Table 1.

Field Excitatory Postsynaptic Potential (fEPSP) Recordings in Hippocampal Slices

Extracellular fEPSP recordings were performed according to standard methods as previously described (Matt et al., 2011; Chenaux et al., 2016).

In brief: 400 µm thick slices were cut on a vibratome (Leica VT 1000S) while submerged in ice-cold dissection buffer (composition in mM) 127 NaCl, 1.9 KCl, 1.2 KH_2PO_4, 26 $NaHCO_3$, 10 D-glucose, 23 $MgSO_4$, and 1.1 $CaCl_2$, saturated with 5% CO_2 and 95% O_2 (pH 7.4). Slices were incubated in oxygenated artificial cerebrospinal fluid (ACSF, in mM: 127 NaCl, 26 $NaHCO_3$, 1.2 KH_2PO_4, 1.9 KCl, 2.2 $CaCl_2$, 1 $MgSO_4$ and 10 D-glucose; pH 7.4) for 1 h at 30°C and then stored at room temperature. Recordings were performed in a submerged-type recording chamber (Warner Instruments). Stimulation (TM53CCINS, WPI) and recording electrodes (ACSF-filled glass pipettes, 2–3 MΩ) were positioned in the stratum radiatum to record Schaffer collateral fEPSPs. Signals were amplified with an Axopatch 200B (Molecular Devices), digitized at 5 kHz with an ITC-16 (HEKA) and recorded using WinWCP from the Strathclyde Electrophysiology Suite. Stimuli (100 µs) were delivered through a stimulus isolator (WPI). The same stimulus intensity was used during baseline recording (0.067 Hz) and induction of long-term potentiation (LTP) using 100 stimuli given at 100 Hz (1 s). The baseline was determined by the average of fEPSP initial slopes from the period before the tetanus. The level of LTP was determined by the average of fEPSP initial slopes from the period between 50 and 60 min after the tetanus. For wash-in experiments with 50 µM picrotoxin (Sigma), the level of potentiation was determined by the average of fEPSP initial slopes from the period between 15 and 20 min after the beginning of wash-in. Before tetanic stimulation or wash-in, each

slice was used to record input-output relation (IOR) and paired-pulse facilitation (PPF) at the same stimulation strength as LTP recordings. Four traces were averaged for each data point.

Morris Water Maze (MWM)

The Morris water maze test was performed as previously described (Bausch et al., 2015) using 3.4–4.5 and 1.7–2.7-month-old homozygous and heterozygous female BLEV reporter mice 10 days after exposure to sham or 80 dB SPL. We included as control group 11 homozygous and seven heterozygous mice (four males, 14 females) and as 80 dB SPL exposure group 10 homozygous and seven heterozygous mice (two males, 15 females). Age and sex was equally distributed among the groups. In mice, no significant difference is observed in MWM performance between males and females (Jonasson, 2005). Furthermore, the chosen age ranges are well below the age in which declining memory performance is to be expected (see e.g., de Fiebre et al., 2006). Therefore, we expected either sex or age differences to significantly influence variability.

The learning paradigm was specifically designed to demonstrate improved learning performance. We therefore opted for a very challenging task consisting of only two learning trials per day, as the acquisition of the MWM task with less than four trials per day is very challenging for mice (Vorhees and Williams, 2006). A previous study demonstrated improved learning performance in the MWM after environmental enrichment, which was only detected by a 2-trial a day, but not a 4-trial a day paradigm (van Praag et al., 1999). The difficulty of the task was additionally exacerbated by the presence of only very sparse visual cues.

The circular pool, 112 cm in diameter, (Stoelting) was located in a room surrounded by extra-maze (distal) cues. Water was made opaque by addition of powdered milk and water temperature was maintained at 21 ± 1°C. A cylindrical escape platform, 12 cm in diameter, made of clear plastic, was submerged 0.5 cm beneath the water surface. The maze was virtually divided by two axes (N to S and W to E) into four quadrants (NE, SE, SW, NW). The hidden platform was positioned in the middle of the SW quadrant. During six acquisition trainings mice, starting from different, pseudo-random locations around the perimeter of the tank, received two swim trials a day (max. 60 s) with an inter-trial-interval of 15 s. A probe trial (60 s) without platform was performed 24 h after the last acquisition training day. Latencies of the two daily trials are averaged.

Data Analyses

Statistics and Numbers

All statistical information and n numbers can be found in the results part and in Supplementary Tables 2, 3. In figures, significance is indicated by asterisks ($^{*}p < 0.05$, $^{**}p < 0.01$, $^{***}p < 0.001$). n.s. denotes non-significant results ($p > 0.05$).

Western Blot

The intensity of the bands was analyzed using the TotalLab Quant software. Band intensities of the genes of interest were normalized to housekeeping gene GAPDH. The analyses were performed on original blots. For original blots see Supplementary Figures 2, 3.

Values for single animals and mean per treatment group are shown. Additionally the 95% confidence interval of the control group is marked as dotted lines.

Hearing Measurements

Click- and noise-ABR measurements were analyzed by 1-way ANOVA with $\alpha = 0.05$, post-test: Bonferroni-Holms. F-ABR measurements were group analyzed by 2-way ANOVA with $\alpha = 0.05$, post-test: Bonferroni-Holms (GraphPad Prism). Data are shown as mean ± SD.

ABR Analysis

For each individual ear, the peak input-output function (*peak I/O*) of the noise-ABR measurements was analyzed as previously described (Chumak et al., 2016).

Two peak classes were selected: (1) early peaks (at 1.2–1.8 ms, wave I) interpreted as the sum of the first stimulus-related action potential within the auditory nerve, and (2) delayed peaks (at 4.1–4.9 ms, wave IV), the response from the auditory midbrain. Data were analyzed by 2-way ANOVA with $\alpha = 0.05$ (GraphPad Prism).

Additionally a waveform correlation analysis was performed as described in (Rüttiger et al., 2013; Singer et al., 2013). Data were analyzed by 1-way ANOVA with $\alpha = 0.05$ (GraphPad Prism).

Electrophysiology

Data were analyzed and processed using Clampfit 10 (Molecular Devices) and Microsoft Excel. Statistics and visualization were performed with GraphPad Prism. Results between conditions were statistically compared using 1-way ANOVA and Bonferroni's Multiple Comparison Test to compare baseline vs. LTP or wash-in for both genotypes as well as LTP or wash-in between genotypes.

Morris Water Maze

Data were analyzed using Smart tracking software (Panlab) and Microsoft Excel by an experimenter unaware to the treatment of each mouse. Statistics were performed with IBM SPSS with $\alpha = 0.05$. One-way repeated measures ANOVA was used to test for effect of training over time within the two treatment groups, separately. Pairwise comparisons were further performed to test for significant differences between the first training day and the following days within the two treatment groups. Two mice that did not enter the platform at least once during acquisition phase were excluded from analysis.

Ribbon Counting

Ribbons are shown as average ribbon number per IHC (±SD). Statistical analysis was performed using 2-way ANOVA followed by a 1-tailed Student's *t*-test with $\alpha = 0.05$.

Fluorescence Analysis of Brain Immunohistochemistry

Pictures acquired from brain sections stained for parvalbumin (PV), were analyzed using the free software Image J. (NIH,

Bethesda, MD; USA). For each section, three pictures for each single channel (YFP, CFP, PV) were saved and analyzed independently. For the 10× magnified pictures, after conversion to an 8-bit image, background was reduced using the rolling ball algorithm (included in Image J) with standard parameters and a region of interest (ROI) of 300 × 100 µm was created and placed on the CA3 region in each single channel picture. Afterwards the average fluorescence intensity within the ROI was calculated as single pixel intensity (0–255)/no. of pixel. Data are shown as mean pixel intensity (±SEM). Data were analyzed by 1-way ANOVA with $\alpha = 0.05$, post-test: Bonferroni-Holms (GraphPad Prism).

To generate representative fluorescence profile plots, a ROI of 390 × 100 µm was created and the specific Image J built-in function was used. For the 60× magnified pictures, the same procedure was applied as for the 10× magnified pictures within a ROI of 300 × 650 µm. To generate representative fluorescence profile plots, a ROI of 350 × 100 µm was created and the specific Image J built-in function was used.

In pictures acquired from brain sections stained for $\delta GABA_A$-R, or $\alpha 1GABA_A$-R fluorescence puncta numbers were counted using ImageJ. A 300 × 300 µm ROI was cropped, individual channels were separated and binary masks created using an appropriate thresholding algorithm for each channel. Binary particles were counted using the inbuilt Analyze Particles function.

In monochannel pictures of brain sections stained for VGLUT1 in the VCN with 100× magnification, the mean fluorescence light intensity was measured in a frame of 85 × 60 µm (total picture) using build-in function in ImageJ.

Data Availability

The datasets generated during and/or analyzed during the current study are available from the corresponding author upon request.

RESULTS

Different Sound Exposure Conditions Indicate Changes in *Bdnf* Exon-IV and -VI Transcription That Reflect Sound Sensitivity in the Brainstem

BLEV reporter mice (described in detail in Singer et al., submitted), in which translation of *Bdnf* exon-IV and -VI can be monitored by co-expression of CFP and YFP, were exposed to different sound pressure levels (SPL) inducing acoustic enrichment (80 dB SPL) and mild (100 dB SPL) or severe (120 dB SPL) acoustic trauma (Knipper et al., 2013; Singer et al., 2013). 2 weeks after exposure we observed no (80, 100 dB SPL) or moderate (120 dB SPL) loss of hearing thresholds in click-, noise-burst and frequency-specific auditory brainstem responses (ABR, **Figures 1A–C**). Animals exposed to 80, 100, and 120 dB SPL show a temporary threshold shift in click-ABR [TTS; **Figure 1A** middle panel; TTS: 1-way ANOVA: $F_{(3, 129)} = 92.67$, $p < 0.0001$, post-hoc test Bonferroni's est: con vs. 80 dB SPL $p < 0.0001$, con vs. 100 dB SPL $p < 0.0001$; con vs. 120 dB SPL $p < 0.0001$] directly after exposure, but only animals subjected to 120 dB SPL developed a permanent threshold shift [PTS; **Figures 1A–C** right panel; PTS: 1-way ANOVA: $F_{(3, 144)} = 54.72$, $p < 0.0001$, post-hoc test Bonferroni's test: con vs. 120 dB SPL $p < 0.0001$; noise-ABR: 1-way ANOVA: $F_{(3, 142)} = 75.45$, $p < 0.0001$, post-hoc test Bonferroni's test: con vs. 120 dB SPL $p < 0.0001$; f-ABR: 2-way ANOVA: $F_{(3, 597)} = 79.9$, $p < 0.0001$, post-hoc test Bonferroni's test: con vs. 120 dB SPL $p < 0.05$]. As observed before in rats (Singer et al., 2013), the different sound exposure paradigms manifested as long-lasting adaptations along the ascending auditory pathway (**Figure 1D**). These included (i) elevated (80 dB SPL, middle turn), moderately reduced (100 dB SPL, midbasal turn), or considerably reduced (120 dB SPL) numbers of CtBP2/RIBEYE-positive active release sites in the first inner hair cell (IHC) synapse [**Figure 1E**; 2-way ANOVA: $F_{(3, 60)} = 11.08$, $p < 0.0001$, post-hoc test 1-tailed unpaired Student's *t*-tests: middle turn: control/80 dB SPL $p < 0.05$; control/120 dB SPL $p < 0.01$; midbasal turn: control/100 dB SPL $p < 0.05$; control/120 dB SPL $p < 0.01$; $n = 6$ ears from four animals per group, 1–3 repetitions each, 8–24 IHCs per turn and group]. (ii) that the overall ABR waves' fine structure showed a loss of ABR waveform with increasing exposure levels before and 2 weeks after exposure [**Figure 1F**; 1-way ANOVA: $F_{(3, 131)} = 17.51$, $p < 0.0001$, post-hoc test Tukey's Multiple Comparison test: control/120 dB SPL $p < 0.001$, 80/120 dB SPL $p < 0.001$, 100/120 dB SPL $p < 0.01$; $n = 8$ animals, 15 ears (control), $n = 9$ animals, 18 ears (80 dB SPL), $n = 5$ animals, 10 ears (100 dB SPL), $n = 9$ animals, 17 ears (120 dB SPL)], which could be confirmed by detailed analyses of supra-threshold ABR waves. The amplitudes of the early supra-threshold ABR wave I [**Figure 1G**; ABR wave I: 2-way ANOVA; con: $F_{(1, 1031)} = 0.003$, $p = 0.955$; 80 dB SPL: $F_{(1, 890)} = 6.02$, $p = 0.0143$; 100 dB SPL: $F_{(1, 836)} = 28.59$, $p < 0.0001$; 120 dB SPL: $F_{(1, 396)} = 185.8$, $p < 0.0001$] and late ABR wave IV [**Figure 1H**; ABR wave IV: 2-way ANOVA, con: $F_{(1, 1034)} = 1.296$, $p = 0.2551$; 80 dB SPL $F_{(1, 951)} = 0.89$, $p = 0.3446$; 100 dB SPL: $F_{(1, 743)} = 0.09$, $p = 0.7706$; 120 dB SPL: $F_{(1, 452)} = 82.88$, $p < 0.0001$] were elevated after enriching 80 dB SPL exposure, reduced but centrally compensated after mildly traumatic 100 dB SPL exposure, and reduced for both early and late ABR waves after severely traumatic 120 dB SPL exposure (**Figures 1G,H**).

This indicates that sound sensitivity is persistently increased after acoustic enrichment (80 dB SPL), preserved despite reduced auditory input after mild trauma (100 dB SPL), or decreased after severe acoustic trauma (120 dB SPL). In particular the elevated IHC ribbon number and ABR wave I and IV in response to 80 dB SPL or the compensated ABR wave IV despite a reduced ABR wave I in response to 100 dB SPL exposure, can only be explained through an adaptive response that permanently alters neuronal activity in auditory pathways. Following severe auditory trauma, this adaptive response consistently failed to occur (120 dB SPL) (**Figures 1G,H**) as seen before in the rat model (Singer et al., 2013; Knipper et al., 2015).

In case activity-dependent *Bdnf* transcription may alter sound responsiveness by strengthening synapses via BDNF-TrkB receptor signaling, as shown in different brain regions (Kellner et al., 2014), we might expect changes in sound sensitivity to

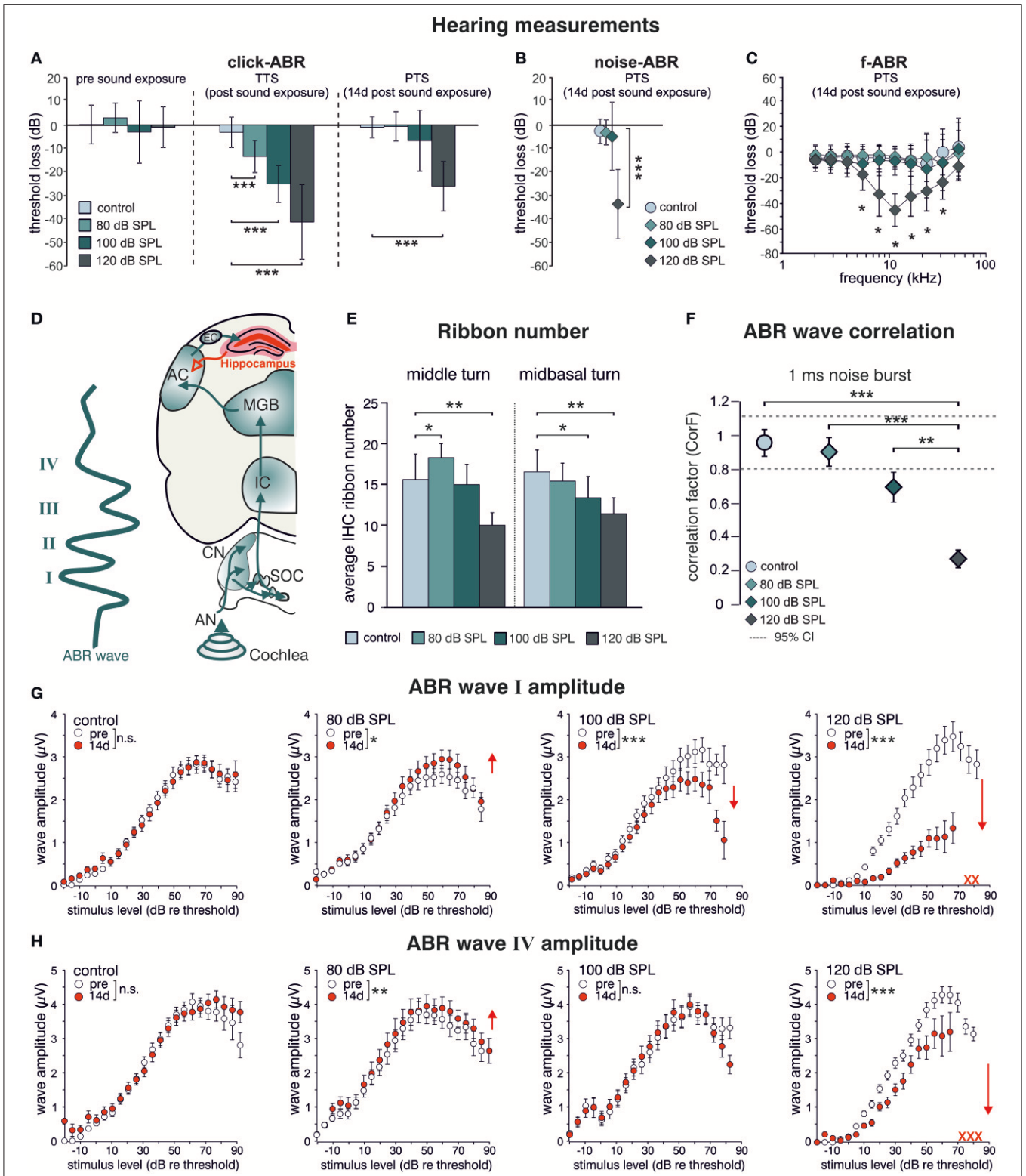

FIGURE 1 | Acoustic enrichment increases hearing acuity through central adaptation while acoustic trauma leads to uncompensated hearing loss. Homozygous BLEV reporter mice were sham exposed (control) or exposed to a 10 kHz tone of 80, 100, or 120 dB SPL for 40 min. Mean ABR thresholds ± SD for click stimuli (**A**, click-ABR) before (pre sound exposure), directly after (TTS) and 14 d after sound exposure (PTS), for noise burst stimuli (**B**, noise-ABR) and for frequency-specific stimuli (**C**, f-ABR) 14 d after exposure demonstrate a significant temporary threshold shift (TTS) for all paradigms directly after exposure becoming permanent (PTS)

(Continued)

FIGURE 1 | only after 120 dB SPL sound exposure. **A–C**; con $n = 19$ animals; 80 dB SPL; $n = 19$ animals; 100 dB SPL, $n = 16$ animals; 120 dB SPL, $n = 19$ animals. **(D)** Schematic drawing of an ABR waveform in relation to the corresponding auditory nuclei in the ascending auditory pathway (green arrows) starting at the auditory nerve (AN), cochlear nucleus (CN), superior olivary complex (SOC), inferior colliculus (IC), medial geniculate body (MGB), auditory cortex (AC), and entorhinal cortex (EC) to the hippocampus as well as hippocampal projections to cortical areas (red). **(E)** IHC ribbon numbers of BLEV reporter mice for the middle and midbasal cochlear turn, representing higher frequency areas, show an increase (80 dB SPL) or decline (100 and 120 dB SPL) 14 days after sound exposure. Data represented as mean ± SD. **(F)** Analyses of ABR waveform of control animals or mice exposed to 80, 100, or 120 dB SPL 14 days after exposure. The changes in waveforms and signals were calculated as correlation factor (CorF) (Rüttiger et al., 2013). Dashed lines indicate the 95% confidence interval for the controls. ABR waveform after 120 dB SPL exposure is significantly reduced. Data represented as mean ± SEM. **(G,H)** Mean peak growth input/output function of noise burst stimulus for early peaks (**G**, ABR wave I) and late peaks (**H**, ABR wave IV) before (open circles) and 14 days after exposure (red circles) were significantly increased after 80 dB SPL exposure, significantly decreased for early peaks, but non-significantly different for late peaks after 100 dB SPL, and massively decreased after 120 dB SPL. Red crosses: early and late peaks in mice exposed to 120 dB SPL (ABR wave IV) that could not be recorded anymore. Data represented as mean ± S.E.M.

correlate with *Bdnf* transcript levels and neuronal activity. We chose vesicular glutamate transporter-1 (VGLUT1) as a marker for activity levels, as it is the predominant glutamate transporter in auditory brainstem synapses (Zhou et al., 2007).

Western blot (WB) analysis of *Bdnf* exon-IV-CFP and exon-VI-YFP expression levels, following immunoprecipitation with HA and cMyc tags, respectively, indicated a qualitative increase of CFP and YFP levels after acoustic enrichment (80 dB SPL), but not after acoustic trauma in the auditory brainstem (120 dB SPL; **Figure 2A,** left panel, see Supplementary Figure 1A for a representative selection of WBs). Consistent with elevated neuronal activity, VGLUT1 levels were qualitatively increased 2 weeks after acoustic enrichment (80 dB SPL) but not after severe acoustic trauma (120 dB SPL, **Figure 2A,** 2nd panel). This suggests that pathological reduction of relevant auditory input persistently prevents activity-dependent elevation of BDNF and VGLUT1. We observed a trend for mobilization of *Bdnf* exon-IV-CFP and exon-VI-YFP and VGLUT1 not only in the auditory brainstem, but also in the inferior colliculus (**Figure 2A,** 3rd panel, see Supplementary Figure 1B for a representative selection of WBs). However, due to the highly variable immunoprecipitation yield, quantification of WB analyses did not reach statistical significance (**Figure 2B**). Importantly, following enriched sound no indications for mobilization of transcript-specific BDNF in the olfactory bulb was observed, as shown for *Bdnf* exon-IV-CFP and *Bdnf* exon-VI-YFP (**Figure 2A,** right panel). To quantitatively verify long-lasting changes of neuronal activity in the target cells of the auditory nerve, we additionally analyzed VGLUT1 immunoreactivity (IR) in bushy cells of the cochlear nucleus (CN) within the auditory brainstem 2 weeks after acoustic enrichment [80 dB SPL; **Figures 2C,D**; two-tailed Student's *t*-test: $t = 3.63$ $df = 10$ $p = 0.0046$; $n = 6$ mice/group 2–3 repetitions]. A significantly elevated punctate VGLUT1 IR at the level of CN bushy cells, exemplarily shown in **Figure 2C** and quantified in **Figure 2D**, was observed in comparison to sham (control) exposure. This suggested that 2 weeks following 80 dB SPL exposure, auditory nerve synapses may exhibit larger numbers of active release sites or greater spike fidelity, considered as a functional correlate of elevated VGLUT1 following sound exposure (Ngodup et al., 2015).

In summary, we observed increased expression of VGLUT1 together with a trend for upregulation of *Bdnf* exon-IV-CFP and exon-VI-YFP in the auditory brainstem in animals with elevated early (auditory nerve) or late (brainstem) supra-threshold auditory responses, but not in animals with critically reduced supra-threshold auditory nerve responses that failed to be centrally restored. This is consistent with the idea that a relevant auditory input drives *Bdnf* transcription and subsequently elevates levels of BDNF in the brainstem, which might alter VGLUT1 levels, as previously suggested for hippocampal neurons. This could strengthen synapses which depend on the activity of BDNF (Kellner et al., 2014). Comparable changes in *Bdnf* transcription were not detected in other sensory regions like the olfactory bulb, indicating specificity of activity-dependent BDNF transcription following auditory inputs.

Enriching Sound Exposure Indicates Changes in Hippocampal *Bdnf* Transcription Correlating With Increased Synaptic Plasticity and Improved Memory Acquisition

We previously observed altered levels of Arc (activity-regulated cytoskeletal protein) in the hippocampal CA1 region after acoustic enrichment, as well as after mild and severe acoustic trauma in rats (Singer et al., 2013). Arc plays a key role in determining synaptic strength through facilitation of AMPA receptor (AMPAR) endocytosis in response to BDNF signaling (Bramham et al., 2008; Wall and Corrêa, 2017). Similarly, as previously reported for Arc (Singer et al., 2013), we observed a trend for an increase in the hippocampal expression of another excitability marker, the GluA2 subunit of the AMPAR (Tanaka et al., 2000; Singer et al., 2013) 2 weeks after acoustic enrichment, but not after severe acoustic trauma in BLEV reporter mice (Singer et al., 2013). This elevation of hippocampal excitability was paralleled by a trend for higher levels of *Bdnf* exon-IV-CFP and exon-VI-YFP (**Figure 3A,** first panel**,** Supplementary Figure 1C for a representative selection of WBs) which was likewise only observed after acoustic enrichment, but not after severe acoustic trauma. These findings are in line with different sound exposure conditions driving adaptations of *Bdnf* transcript levels and glutamatergic neuronal activity not only in the brainstem but also in the hippocampus.

Modulation of BDNF-dependent Arc expression was previously associated with increased hippocampal synaptic plasticity (Kuipers et al., 2016), particularly with formation of long-term potentiation (LTP) (Messaoudi et al., 2007). Therefore, we went on to test if the altered hippocampal BDNF expression levels and neuronal excitability changes

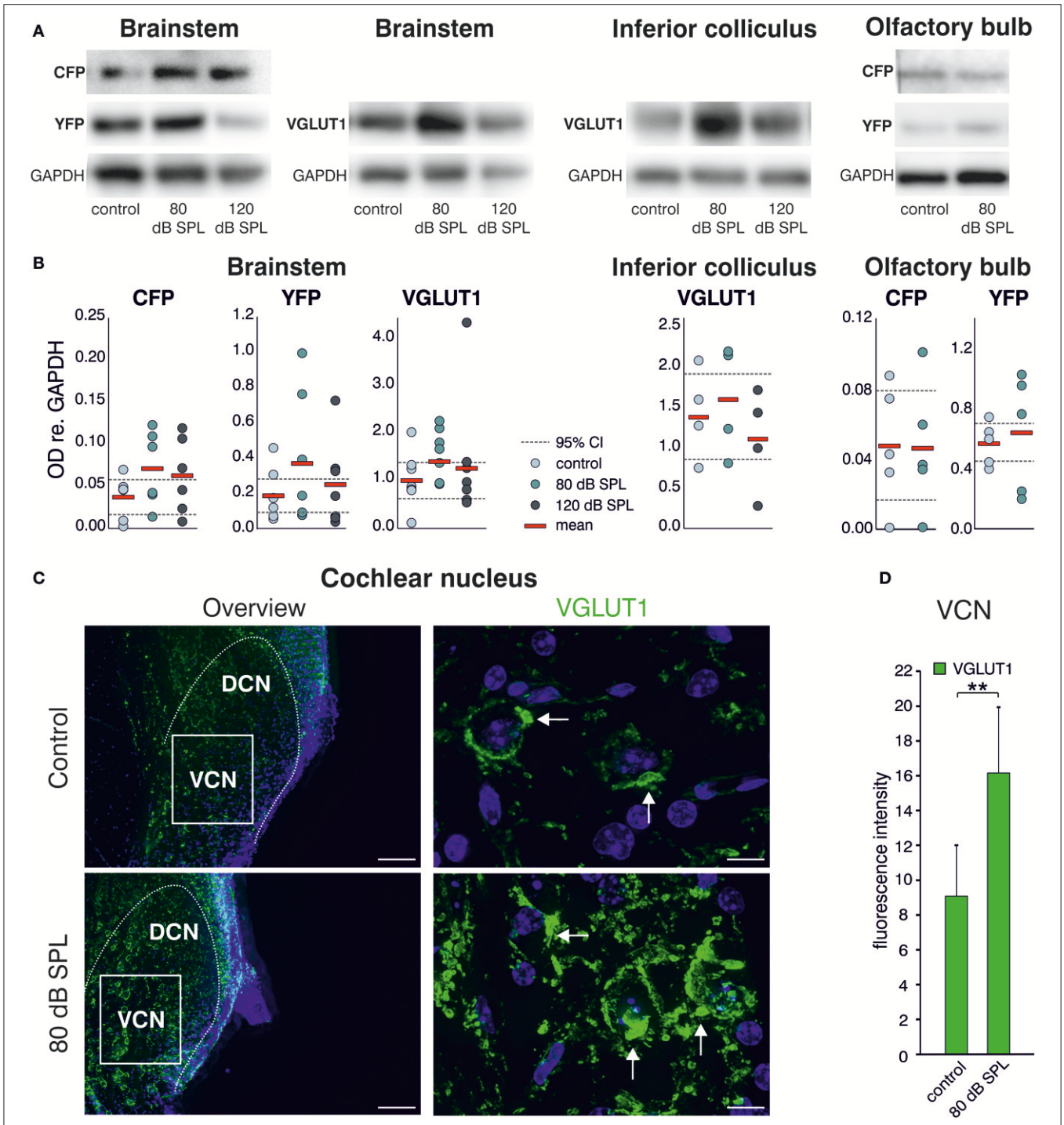

FIGURE 2 | Acoustic enrichment leads to a trend for higher expression of VGLUT1 in the brainstem and inferior colliculus together with *Bdnf* exon-IV-CFP and exon-VI-YFP. **(A)** Western blot analysis of CFP and YFP in the brainstem and olfactory bulb as well as VGLUT1 in the brainstem and inferior colliculus in homozygous BLEV reporter mice 2 weeks after exposure to either sham, 80, or 120 dB SPL. The housekeeping gene GAPDH is used for normalization between conditions. For originals see Supplementary Figures 2A–C. **(B)** Densitometric analyses of Western blots (dots: averaged results per animal, bars: means, dashed lines: 95% confidence interval for the controls; $n = 5$–6 mice/group 2–10 Western blots each). **(C)** VGLUT1 immunostaining (green) in cochlear nucleus mouse slices 2 weeks after exposure to sham or 80 dB SPL. After exposure to 80 dB SPL immunoreactivity (IR) for VGLUT1 is increased in the dorsal and ventral cochlear nucleus (DCN, VCN). Nuclei stained with DAPI (blue). Arrows indicate VGLUT1 localization. Scale bars: 100 μm; 5 μm. **(D)** Quantification of VGLUT1 IR in an 85 × 60 μm frame in the VCN following sham and 80 dB SPL exposure. Data represented as mean ± SD.

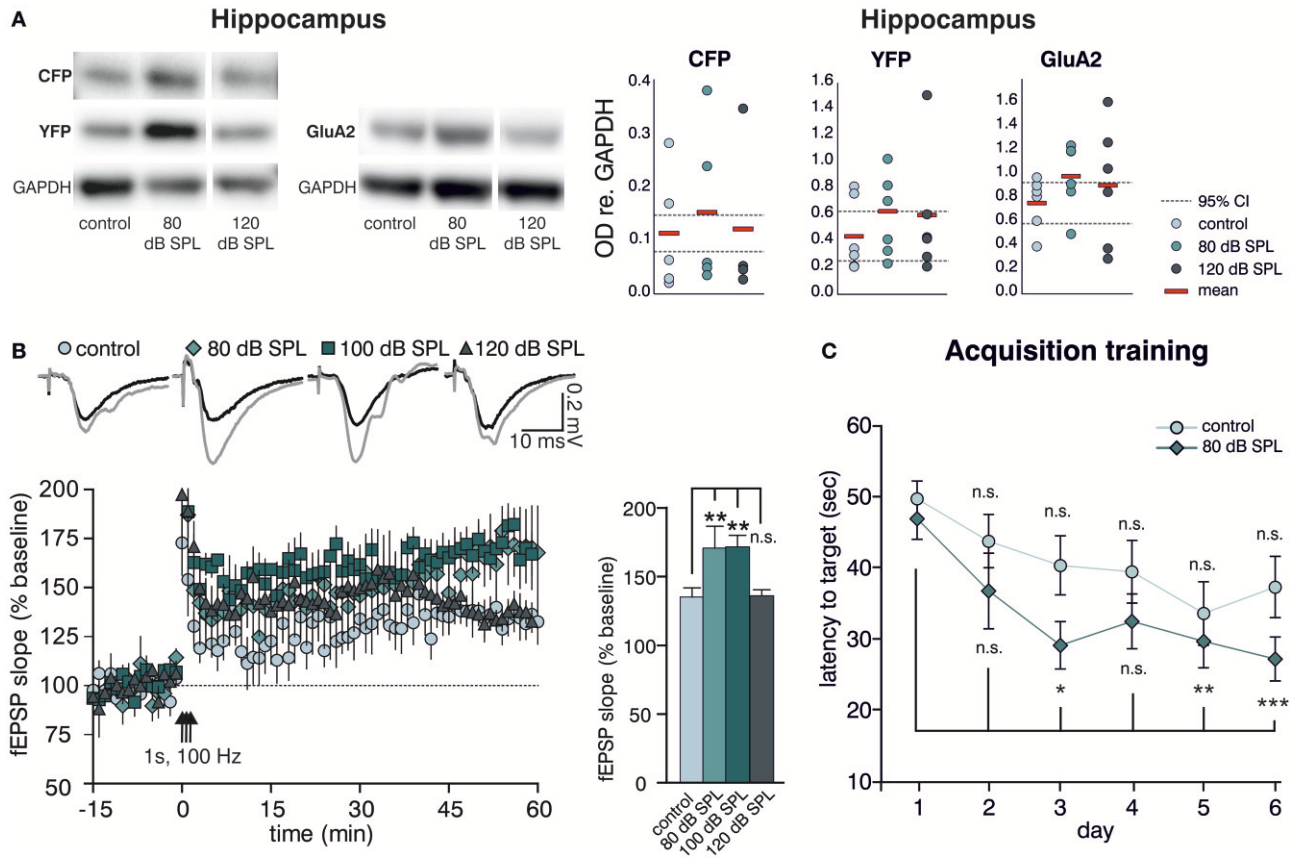

FIGURE 3 | Acoustic enrichment enhances hippocampal BDNF expression and LTP as well as memory acquisition in the Morris water maze (MWM). **(A)** Left panel: Western blot analysis of *Bdnf* exon-IV-CFP and exon-VI-YFP (left blot) as well as GluA2 (right blot) in the hippocampus of BLEV reporter mice exposed to sham, 80, or 120 dB SPL. Right panel: Densitometric analyses of Western blots (dots: averaged results per animal, bars: means, dashed lines: 95% confidence interval for the controls; $n = 5$ mice/group 2–10 Western blots each). For originals see Supplementary Figure 2D. **(B)** Left Panel: Averaged time courses of fEPSP slopes in acute brain slices from BLEV reporter mice 2 weeks after exposure to sham, 80, 100, or 120 dB SPL. Representative traces before (black) and after (gray) induction of LTP are shown on top. Animals from all conditions readily show significant SC LTP. Right panel: Significantly increased LTP was observed for 80 (171 ± 16% of baseline) and 100 (172 ± 8% of baseline) but not 120 dB SPL (136 ± 4% of baseline) compared to controls (135 ± 7% of baseline). Data are represented as mean ± SEM. **(C)** Latency to target during acquisition learning. After 3 days mice exposed to 80 dB SPL need less time to find the platform in comparison to the first experimental day than mice in the control group. Data are expressed as mean ± SEM.

observed after acoustic enrichment or acoustic trauma also influenced hippocampal synaptic plasticity in the BLEV reporter mouse. To this end, we recorded field excitatory postsynaptic potentials (fEPSP) in the CA3 to CA1 Schaffer collateral (SC) synapses in the stratum radiatum (SR) from acute forebrain slices of BLEV reporter mice 2 weeks after sham (control) treatment, acoustic enrichment, as well as mild and severe acoustic trauma [**Figure 3B**, Supplementary Figure 4; 1-way ANOVA: $F_{(3, 19)} = 4.99$, $p = 0.01$, post-hoc test Bonferroni's test baseline/tetanized (b/t) $n = 4$ animals/group con: 7 slices, 80 dB SPL: 7 slices, 100 dB SPL: 6 slices, 120 dB SPL: 5 slices, control $p < 0.01$, 80 dB SPL $p < 0.001$, 100 dB SPL $p < 0.001$, 120 dB SPL $p < 0.01$; tetanized/tetanized (t/t) con vs. 80 dB SPL $p < 0.01$ con vs. 100 dB SPL $p < 0.01$ con vs. 120 dB SPL n.s.]. None of the sound exposure paradigms led to changes in basal synaptic transmission, as all four conditions displayed similar fEPSP amplitudes in response to a range of input strengths (Supplementary Figure 4A). Additionally, similar levels of paired-pulse facilitation in all four conditions indicated no changes in presynaptic function (Supplementary Figure 4B). We were able to observe significant LTP in acute brain slices from mice under all four conditions in response to tetanic stimulation (1 s, 100 Hz). This potentiation, however, was significantly stronger in animals exposed to acoustic enrichment or mild acoustic trauma as compared to animals exposed to sham or severe acoustic trauma (**Figure 3B**). This finding suggests that persistently improved (after acoustic enrichment) or restored (after mild acoustic trauma) sound responses leads to altered *Bdnf* exon-IV-CFP and exon-VI-YFP expression as well as synaptic excitability and plasticity in the brainstem and hippocampus. Reduced sound responses after severe acoustic trauma, on the other hand, forestall activity-dependent BDNF expression, improved excitability, and synaptic plasticity.

We wanted to know next if elevated hippocampal BDNF expression not only correlates with increased GluA2 levels and SC LTP, but also with performance in hippocampus-dependent learning. To test this, starting 10 days after sound exposure, we subjected mice exposed to sham treatment (control) or acoustic enrichment (80 dB SPL) to a Morris water maze (MWM) task, which is a hippocampus-dependent learning paradigm. In order to identify increased learning performance (van Praag et al., 1999), we opted for a very challenging paradigm that included only two trials per day (for details, see Methods).

While control mice improved slightly but not significantly over time performing the task, acoustically enriched mice significantly improved their performance upon training. This was evidenced by reduced latencies in finding the platform as compared to the first day [**Figure 3C**; repeated measure ANOVA: con: $F = 2.56$ DF $= 5$ $p = 0.033$; post-hoc test Bonferroni's test: day 1 vs. 2 n.s., day 1 vs. 3 n.s., day 1 vs. 4 n.s., day 1 vs. 5 n.s., day 1 vs. 6 n.s.; 80 dB SPL: $F = 5.85$ $DF = 5$ $p < 0.001$; Bonferroni's test: day 1 vs. 2 n.s., day 1 vs. 3 $p = 0.013$, day 1 vs. 4 $p = 0.054$, day 1 vs. 5 $p = 0.006$, day 1 vs. 6 $p < 0.001$; con $n = 18$ animals 80 dB SPL $n = 17$]. We could not detect any correlation between MWM performance and gender or age.

So far, the presented data indicate that acoustic enrichment leads to elevated expression of *Bdnf* exon-IV-CFP and exon-VI-YFP together with excitatory markers in the auditory brainstem and the hippocampus, paralleled by increased hippocampal LTP and improved performance in a hippocampus-dependent learning paradigm. Neither sound-induced improval of auditory performance nor increased hippocampal LTP are observed in animals exposed to severe acoustic trauma, in which activity-dependent *Bdnf* transcript levels are not elevated in response to auditory sound exposure.

Acoustic Enrichment and Mild, but Not Severe Trauma, Synchronously Alter Hippocampal *Bdnf* Exon-IV and Exon-VI Transcription in Neuronal and Vascular Cells in Parallel to Parvalbumin Expression

We subsequently took advantage of the unique utility of the BLEV reporter mouse to identify the cell types where activity-dependent *Bdnf* transcription occurs in response to sound exposure. As inhibitory transmission is a major regulator of hippocampal synaptic plasticity (Matt et al., 2011) and BDNF is known to influence the function of parvalbumin (PV)-positive inhibitory interneurons (Marty, 2000; Yamada and Nabeshima, 2003; Messaoudi et al., 2007; Hong et al., 2008; Minichiello, 2009; Waterhouse et al., 2012; Park and Poo, 2013), we asked if changes in activity-dependent *Bdnf* transcript usage might be observed in neurons or cells known to target PV-positive interneurons. For example, mossy fibers express BDNF and are suggested to target PV-positive interneurons (Danzer et al., 2008; Dieni et al., 2012). We first examined *Bdnf* exon-IV-CFP, exon-VI-YFP, and PV expression in deconvoluted high-resolution fluorescence stacks of low-magnification (**Figure 4**) in the CA1 region (**Figure 4A**; Supplementary Video 1), the CA3 region (**Figure 4B**; Supplementary Video 1), and the dentate gyrus (**Figure 4C**) of the hippocampus. Compared to sham exposed animals (control), we observed a general upregulation of CFP, YFP, and PV (red) in all regions of the hippocampus after acoustic enrichment and mild acoustic trauma, the two conditions associated with increased hippocampal synaptic plasticity (**Figure 3B**, Supplementary Figure 4). In control animals, CFP fluorescence is mostly seen in capillary vessels of the highly vascularized fissura hippocampalis (FH) (**Figure 4A**). These CFP levels in the FH were significantly higher after acoustic enrichment and mild acoustic trauma but not after severe acoustic trauma [**Figure 4D**; 1-way ANOVA: $F_{(3,\ 19)} = 10.5$, $p < 0.0003$, post-hoc test Bonferroni's test: con vs. 80 dB SPL, $p = 0.0013$, con vs. 100 dB SPL n.s. con vs. 120 dB SPL n.s., 80 dB SPL vs. 120 dB SPL $p < 0.0001$, 100 dB SPL vs. 120 dB SPL $p = 0.0072$; con: $n = 6$ animals, 1–4 repetitions; 80 dB SPL $n = 6$ animals, 1–6 repetitions; 100 dB SPL $n = 5$ animals, 2–5 repetitions; 120 dB SPL $n = 6$ animals, 1–3 repetitions]. In the CA1 region of animals exposed to acoustic enrichment or mild acoustic trauma, we observed increased PV labeling in the CA1 pyramidal layer (**Figure 4A**, SP). In the CA3, we found strongly amplified signals of both PV and *Bdnf* exon-VI-YFP in the area where mossy fibers are predicted to target CA3 dendrites (**Figures 4B,E**). PV labeling was also increased in the supra-pyramidal blade of the DG (**Figure 4C**). This generalized pattern of up-regulation was not observed in animals exposed to 120 dB SPL (**Figures 4A–E**). Particularly within the stratum lucidum (SL) of the CA3 region (**Figure 4B**), the increase in *Bdnf* exon-VI-YFP expression, together with PV, was either robust (80 dB SPL), moderate (100 dB SPL), or absent [120 dB SPL, **Figure 4E**; YFP: 1-way ANOVA: $F_{(3,\ 11)} = 6.96$, $p = 0.0068$, post-hoc test Bonferroni's test con vs. 80 dB SPL $p < 0.01$, 80 dB SPL vs. 120 dB SPL $p < 0.01$; CFP: 1-way ANOVA $F_{(3,\ 11)} = 2.37$, $p = 0.13$; PV: 1-way ANOVA $F_{(3,\ 11)} = 10.07$, $p = 0.0017$, post-hoc test Bonferroni's test con vs. 80 dB SPL $p < 0.01$, 80 dB SPL vs. 120 dB SPL $p < 0.01$; con: $n = 4$ animals; 80 dB SPL $n = 3$ animals; 100 dB SPL $n = 3$ animals; 120 dB SPL $n = 5$ animals, 3 repetitions each]. Fluorescence intensity profiles taken through the SL and SP of CA3 of a control mouse revealed that YFP fluorescence was predominantly found in the SL, while CFP and PV fluorescence was restricted to the SP (representative profile plot in **Figure 4F**).

Consistent with our previous observations in terms of ABR wave amplitudes, the expression of excitatory markers in the auditory brainstem, the inferior colliculus, and the hippocampus, as well as hippocampal LTP and learning, we thus also confirmed a correlation between PV expression patterns and changes of *Bdnf* exon-IV-CFP and exon-VI-YFP levels in the tri-synaptic pathway.

This finding led us to perform a more detailed analysis of CFP, YFP, and PV expression in the hippocampal CA3 region at a high-magnification. CFP fluorescence was mainly restricted to blood vessels in the SL (**Figure 5A,** lower panels, open arrows) and to perisomatic regions in the SP (**Figure 5B,** open arrows). YFP fluorescence was predominantly found in the SL of the CA3 region (**Figure 5A,** lower panels; **Figure 5B,** closed arrows). In all these areas, fluorescence intensity was increased after acoustic enrichment and mild acoustic trauma, but not after severe acoustic trauma. Many of the YFP-positive puncta in the SL

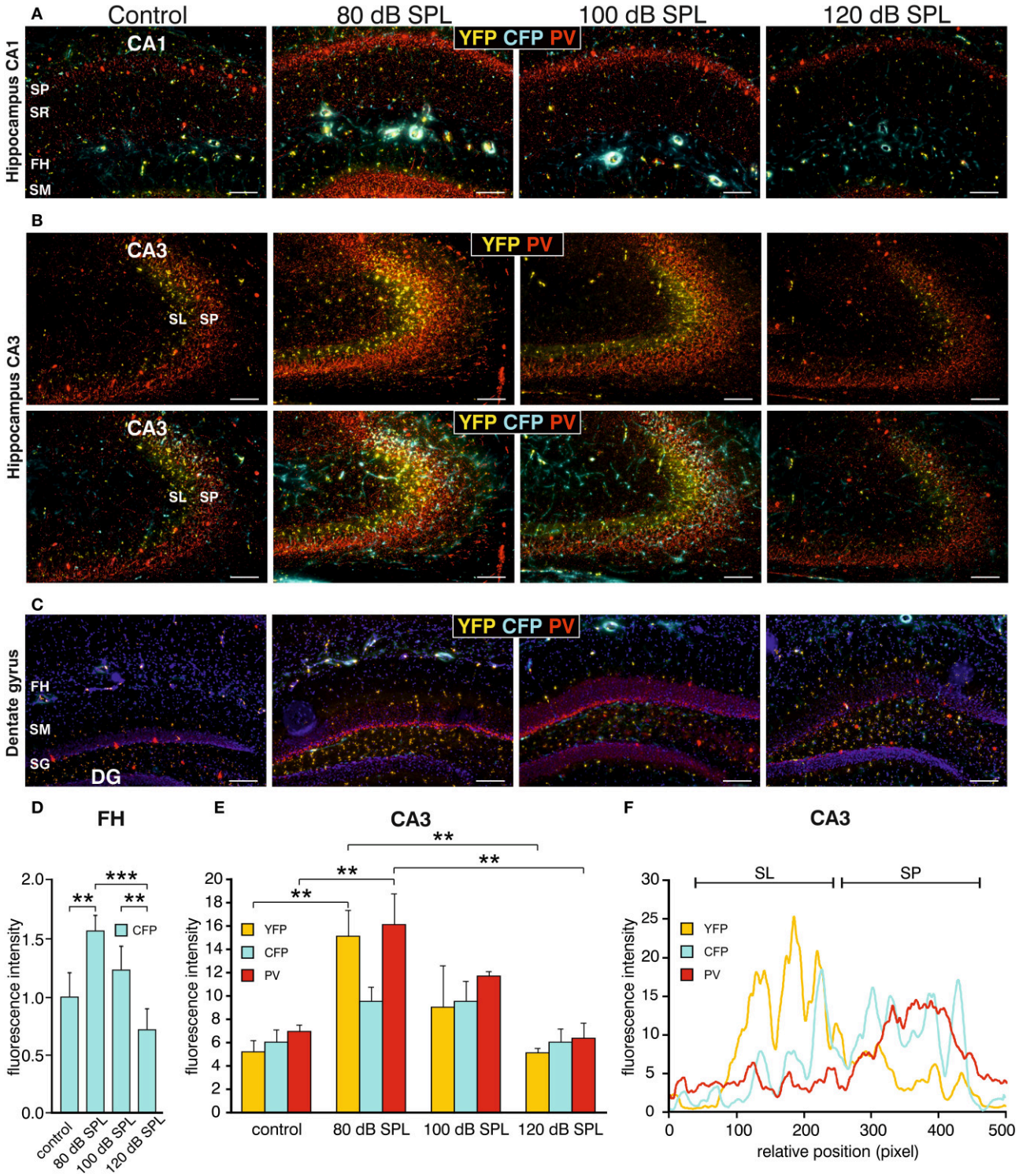

FIGURE 4 | Dynamic changes of *Bdnf* exon-IV and -VI transcripts and parvalbumin upon sound exposure in hippocampal circuits (Supplementary Video 1). **(A–C)** CFP/YFP fluorescence and parvalbumin immunostaining (PV, red) in dorsal hippocampal mouse slices 2 weeks after exposure to sham, 80, 100, or 120 dB SPL. Note a prominent dynamic change of PV (red) expression in the stratum pyramidale (SP) of the CA1 region **(A)**, in the stratum lucidum (SL) of the CA3 region ($n = 6$ animals/group) **(B)**, and stratum granulosum (SG) of the dentate gyrus (DG) **(C)** concomitant to distinct changes in YFP and CFP. SM, stratum moleculare; SR, stratum radiatum; FH, fissura hippocampalis. Scale bars, 100 μm. **(D)** Quantification of *Bdnf* exon-IV-CFP in capillary outlines at the level of the FH revealed a peak of fluorescence in 80 dB SPL exposed animals that declined below control levels in 120 dB SPL exposed animals. Data represented as mean ± SD. **(E)** Quantification of YFP, CFP, and PV intensities in the CA3 region in an area of 300 × 100 μm following different sound exposure paradigms. Data represented as mean ± SEM. **(F)** Intensity profile of CFP, YFP, and PV along a line through the CA3 of a control mouse, perpendicular to the SP (length: approximately 390 μm). Representative for four experiments.

overlapped with PV IR (**Figure 5C**), indicating that YFP positive terminals not only contact dendrites of pyramidal cells (PCs) but also those of PV-positive interneurons (**Figure 5E**). This suggests that *Bdnf* exon-IV translation in mossy fiber terminals (Danzer et al., 2008; Zheng et al., 2011; Dieni et al., 2012) in response to enriched or mild traumatic sound is linked to elevated levels of PV in the perisomatic area of CA3 pyramidal neurons (**Figure 5B,** red). Similarly as observed above, PV IR was strongly increased after acoustic enrichment and mild acoustic trauma, but not after severe acoustic trauma (**Figure 5B**). Quantification of fluorescence intensity in the SP revealed an increase of CFP fluorescence after acoustic enrichment in comparison to controls and a reduction between enriching and severe acoustic trauma. For YFP intensity, a significant reduction between enriching and severe acoustic trauma was observed [**Figure 5D**; CFP: 1-way ANOVA: $F_{(3, 25)} = 22.44$, $p < 0.0001$, post-hoc test Bonferroni's test con vs. 80 dB SPL $p < 0.001$ 80 dB SPL vs. 120 dB SPL $p < 0.0001$; YFP: 1-way ANOVA: $F_{(3, 25)} = 3.32$, $p = 0.036$ post-hoc test Bonferroni's test 80 dB SPL vs. 120 dB SPL $p < 0.05$ $n = 6$ animals/group; 4–6 repetition each]. These findings suggest that BLEV mice can be used to identify mossy fiber terminals and CA3 projection neurons that respond to defined behaviorally relevant sensory stimuli.

Acoustic Enrichment but Not Severe Acoustic Trauma Decreases Dendritic Inhibition of CA1 Pyramidal Cells

We next examined high-magnification images of the CA1 area. Following acoustic enrichment and mild trauma, CFP fluorescence increased in the FH (**Figure 6A,** open arrows), in perisomatic areas of the SP (**Figure 6B,** open arrows), and in blood vessels of the SR (**Figure 6C,** open arrows). YFP fluorescence on the other hand was increased in the FH and the SR after acoustic enrichment and mild acoustic trauma close to capillaries (**Figures 6A,C,** arrowheads) (Marosi and Mattson, 2014; Miyamoto et al., 2014). Similar to CA3, perisomatic PV IR (red) in the SP of CA1 was significantly increased after acoustic enrichment and mild acoustic trauma [**Figure 6A**; **Figure 6B,** closed arrows; **Figure 6D,** quantification; 1-way ANOVA: $F_{(3, 19)} = 5.96$, $p = 0.0049$, post-hoc test Bonferroni's test: con vs. 80 dB SPL n.s.; con vs. 100 dB SPL, $p = 0.0301$; con vs. 120 dB SPL n.s; 100 vs. 120 dB SPL $p = 0.01$; con $n = 6$ animals, 80 dB SPL $n = 6$ animals, 100 dB SPL $n = 5$ animals, 120 dB SPL $n = 6$ animals; 4–6 repetitions]. In the SR, however, we found a significant decrease of PV IR after acoustic enrichment and mild acoustic trauma [**Figure 6C,** red IR; **Figure 6E,** quantification; 1-way ANOVA: $F_{(3, 19)} = 4.61$, $p = 0.0138$, post-hoc test Bonferroni's test: con vs. 80 dB SPL $p < 0.05$, con vs. 100 dB SPL $p < 0.05$, con $n = 6$ animals 80 dB SPL $n = 5$ animals, 100 dB SPL $n = 6$ animals, 120 dB SPL, $n = 6$ animals; 2 repetitions each]. After severe acoustic trauma, we once more could not detect any differences in CFP and YFP fluorescence as well as PV IR in comparison to controls (**Figures 6A–E**).

These observations point to an increased perisomatic inhibitory connection in the SP derived from PV-positive interneurons and a simultaneous decrease of such connections in the SR. PV-positive interneurons target CA1 PC through perisomatic δ subunit containing $GABA_A$-receptors and its dendrites through α1 subunit containing $GABA_A$-receptors (Klausberger et al., 2003; Glykys et al., 2008) (**Figure 6F**). Indeed, we found that puncta of PV IR in the CA1 SP often co-localized with IR for the δ subunit containing $GABA_A$-receptor (Supplementary Figures 5A,B) and that α1 subunit containing $GABA_A$-receptor IR was localized in the CA1 SR (Supplementary Figure 5D). After acoustic enrichment and mild acoustic trauma, however, no significant changes of $\delta GABA_A$ receptor-immunopositive dots (Supplementary Figures 5C,E) or of $\alpha 1 GABA_A$-receptor IR in the CA1 SR (Supplementary Figures 5D,F) were detected.

As α1 subunit containing $GABA_A$-receptors in the CA1 SR are suggested to regulate excitability and action potential thresholds of PC dendrites (Willadt et al., 2013) a functional test of dendritic inhibition in the CA1 SR was performed [**Figure 6G;** 1-way ANOVA: $F_{(3, 19)} = 5.24$, $p = 0.005$, post-hoc test Bonferroni's test: con $p < 0.001$, 80 dB SPL n.s., 100 dB SPL n.s., 120 dB SPL $p < 0.001$; con vs. 120 dB SPL $p < 0.01$, con vs. 80 dB SPL $p < 0.01$, con vs. 100 dB SPL n.s.; baseline/wash-in $n = 4$ animals/group; 9 slices/group]. We observed SC fEPSP during wash-in of the $GABA_A$ receptor antagonist picrotoxin. The ensuing disinhibition was significantly decreased in mice exposed to acoustic enrichment and mild acoustic trauma (**Figure 6G**), which is consistent with the downregulation of PV-positive terminals (**Figures 6C,E**) and a slight decrease in α1 subunit containing $GABA_A$-receptor expression in the CA1 SR (Supplementary Figure 5D, green), compared to animals exposed to sham treatment or severe acoustic trauma. Additionally, this decrease in dendritic inhibition may serve as an explanation for increased LTP and learning capability observed after acoustic enrichment and mild acoustic trauma but not after severe acoustic trauma (**Figures 3B,C**, **6F**).

Taken together, the present findings suggest that exposure to acoustic enrichment (80 dB SPL) and mild acoustic trauma (100 dB SPL), conditions that increase sound sensitivity, hippocampal LTP, and learning appears to correlate with an elevation of *Bdnf* exon-IV-CFP and *Bdnf* exon-VI-YFP in the brainstem and hippocampus. In the hippocampus, sound-driven increase of *Bdnf* exon-VI-YFP levels reaches mossy fiber terminals and hippocampal capillaries where an elevation of *Bdnf* exon-IV-CFP is observed. In addition, *Bdnf* exon-IV-CFP in the pyramidal layer is activated in response to sound and within CA1 PC that receive more perisomatic, but a reduced number of dendritic PV-positive contacts (**Figures 7A–C**). In contrast, a reduction of auditory input after severe acoustic trauma (**Figures 7D–F**, discontinuous red lined arrow) showed no apparent mobilization of *Bdnf* exon-VI-YFP and *Bdnf* exon-IV-CFP transcripts, neither in the brainstem, nor in neuronal or capillary hippocampal cells. Under these conditions, we could not observe compensatory adaptation of sound sensitivity, nor increased hippocampal LTP (**Figures 7D–F**). These findings suggest that a crucial level of auditory input drives activity-dependent transcription of BDNF restricted to the ascending auditory pathway and the hippocampus to establish persistent adaptation of the auditory

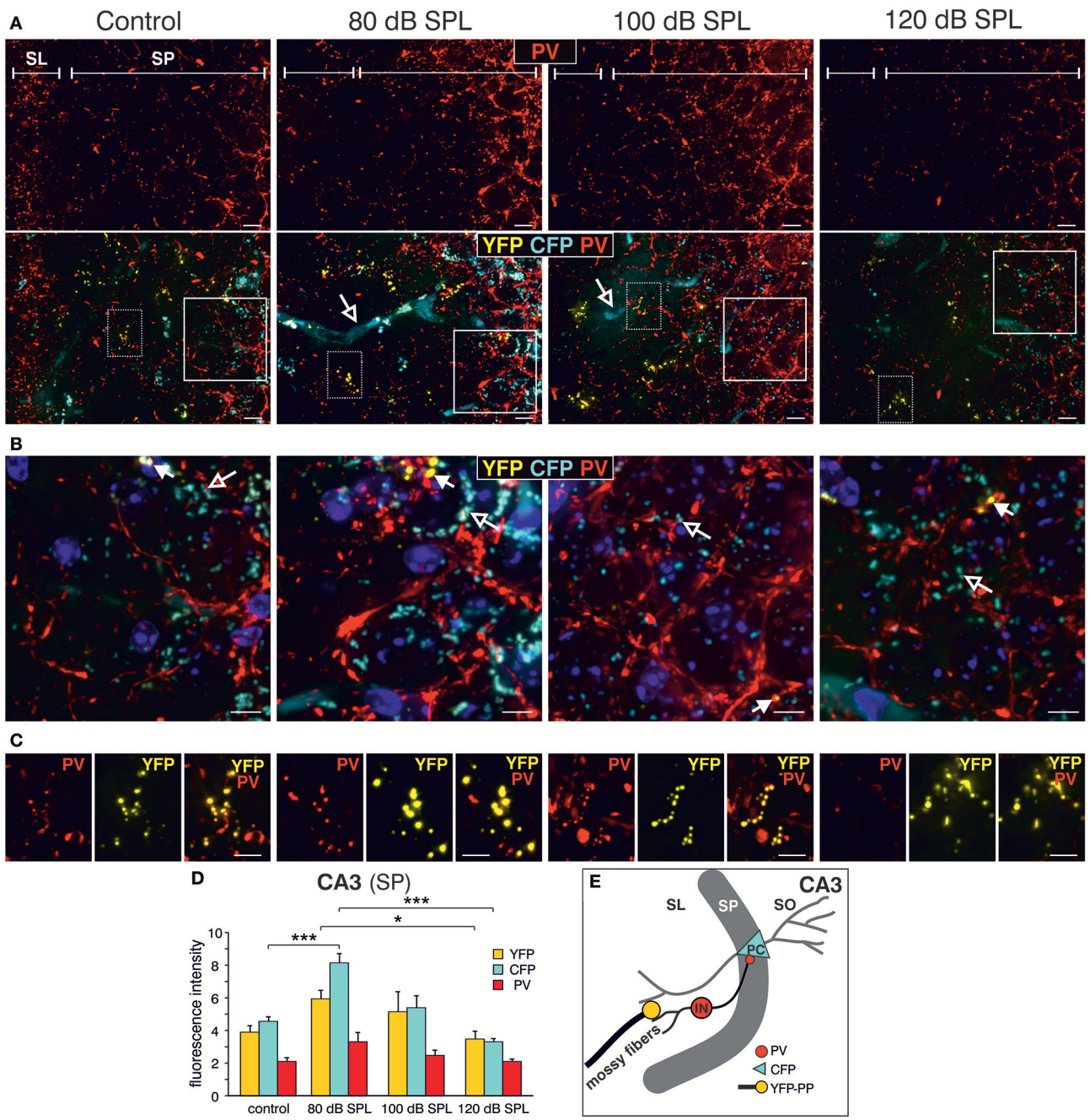

FIGURE 5 | Dynamic changes of *Bdnf* exon-IV and -VI transcripts and parvalbumin expression in the CA3 region following sound exposure. **(A,B)** Hippocampal CA3 region with magnification of the stratum lucidum (SL) and stratum pyramidale (SP). **(A)** Immunostaining of parvalbumin (PV, red). Note the difference in PV expression in the SP in dependence of the applied sound exposure. Scale bars: 10 μm. Lower panel: Triple staining of the same CA3 region. Open arrows indicate *Bdnf* exon-IV-CFP in blood vessels. Scale bars: 10 μm. **(B)** Magnified view from solid frame in **(A)**. CFP (open arrows) and PV (red) expression at the level of the SP. Closed arrows indicate *Bdnf* exon-VI-YFP. Nuclei stained with DAPI (blues). Scale bars: 5 μm. **(C)** Magnified view from dashed frame in **(A)**. *Bdnf* exon-VI-positive-YFP expression in mossy fiber terminals contacts overlaps with PV-positive (red) interneurons in the SL region of the CA3 and increases (80 dB SPL) or declines (120 dB SPL) with sound. Scale bars: 5 μm. **(A–C)** $n = 6$ animals/group. **(D)** Quantification of CFP, YFP, and PV fluorescence averaged over the SL and SP region of the CA3 region. *Bdnf* exon-IV-CFP fluorescence intensity peaks in animals subjected to 80 dB SPL. *Bdnf* exon-VI-YFP and *Bdnf* exon-IV-CFP after 80 dB SPL sound exposure were also significantly elevated when compared to 120 dB SPL-exposed animals. Data represented as mean ± SD. **(E)** Model depicting assumed locations of altered CFP, YFP, and PV expression after 80 dB SPL sound exposure. Mossy fiber terminals (yellow) terminate on dendrites of excitatory CA3 pyramidal cells (PC) and PV-positive inhibitory interneuron (IN, red). CFP is found in the perisomatic areas of CA3 PCs (blue). SO, stratum oriens.

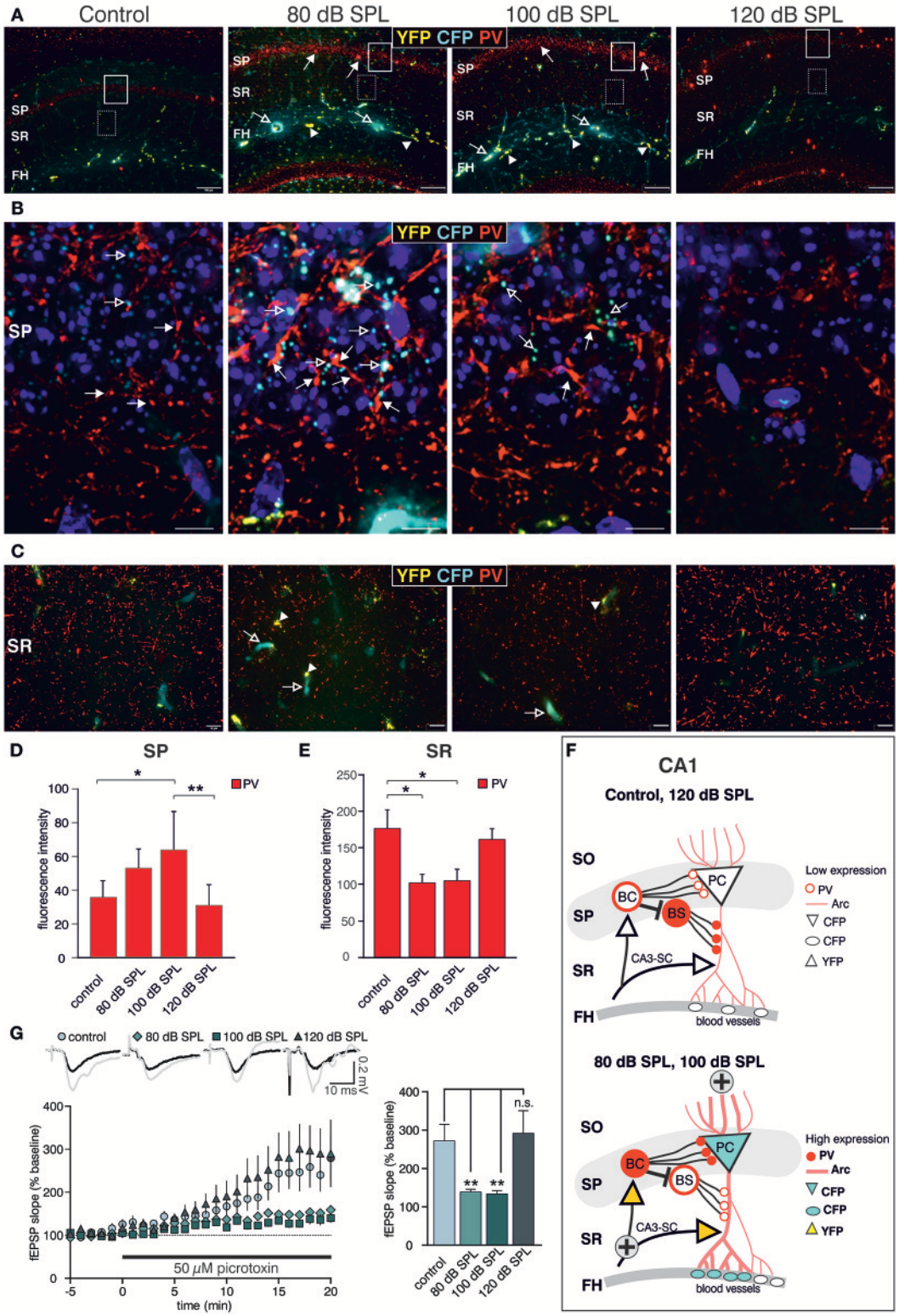

FIGURE 6 | Dynamic changes of *Bdnf* exon-IV and -VI transcripts and parvalbumin after sound exposure in the hippocampal CA1 region. **(A)** Low-magnification of parvalbumin (PV) IR in BLEV reporter mice 2 weeks after exposure to control, 80, 100, or 120 dB SPL. Note the up-regulation of PV IR (arrows) in the SP region

(Continued)

FIGURE 6 | parallel to *Bdnf* exon-IV-CFP (open arrows) in the vascularized FH region. Scale bars. 100 μm. **(B)** High-power magnification of PV IR in regions framed exemplarily in **(A)** unravels an increase in PV-immunopositive perisomatic contacts (closed arrows) concomitant to *Bdnf* exon-IV-CFP expression (open arrows) in a somatic localization at the SP level. Scale bars: 20 μm. **(C)** PV IR in the SR, see frames in exemplarily region in **(A)**, indicating reduced PV-immunopositive puncta in BLEV reporter mice 2 weeks after exposure to 80 and 100 dB SPL in comparison to control or 120 dB SPL. Scale bars: 100 μm. **(A–C)** $n = 6$ animals/group. **(D)** Quantification of PV-immunopositive puncta at the SP level are elevated for 80 and 100 dB SPL exposed animals. Data are represented as mean ± SD. **(E)** The quantification of PV-immunopositive puncta within the SR revealed a significant decline of PV-immunopositive dots for 80 and 100 dB SPL- and unchanged levels in 120 dB SPL-exposed animals. Data are represented as mean ± SEM. **(F)** Abstract figure of the CA1 region indicating the expression pattern of Arc, PV, CFP, and YFP. ⊕ Indicates increased activity. FH, Fissura hippocampalis; SO, Stratum oriens; SP, Stratum pyramidale; SR, Stratum radiatum; PC, pyramidal cell; BC, basket cell; BS, bistratified cell, SC, Schaffer collaterals. **(G)** Averaged time courses of picrotoxin wash-in experiments. Representative traces before (black) and after (gray) wash-in of 50 μM picrotoxin are shown on top. Wash-in of picrotoxin leads to an increase in fEPSP amplitude. This disinhibition is significantly stronger in controls (272 ± 43% of baseline) and 120 dB SPL (292 ± 59% of baseline) compared to 80 dB SPL (139 ± 7% of baseline) and 100 dB SPL (134 ± 8% of baseline). Data are represented as mean ± SEM.

sensory system. Using the BLEV reporter mouse, we will now be able to identify the neuronal and non-neuronal cell populations within the brainstem and hippocampus that guide this behaviorally relevant adaptation process.

DISCUSSION

We here provide evidence that BLEV mice allow specific identification of neurons and capillaries that respond to a critical behaviorally relevant sensory input by elevation of exon-IV and -VI derived *Bdnf* expression. Our data indicate that a sound-induced and memory-dependent improvement or restoration of sound sensitivity may take place in the auditory pathway and hippocampus. In contrast, an impairment of the critical auditory input after severe auditory trauma apparently leads to a failure to elevate *Bdnf* transcripts and to adapt to sound sensitivity. Therapeutic concepts for maladaptive diseases therefore need to reconsider BDNF replacement strategies in view of the present findings.

Acoustic Enrichment Persistently Increases Responsiveness of the Auditory System Coinciding With Increased Excitability and Translation of *Bdnf* Exon-IV and exon-VI

In the present study, different levels of acoustic exposure induced persisting changes in sound-sensitivity that apparently correlated with changes of *Bdnf* exon-IV-CFP and VI-YFP levels in the brainstem and hippocampus. Considering the driving force for these transcript-specific BDNF changes we have to take into account that these external sound exposure conditions, here presented by (novel) experience of enriching, mild traumatic, or severe traumatic sound for 40 min, will not only activate the auditory path but will also drive an immediate glucocorticoid (GC)-mediated stress response associated to arousal or fear (De Kloet et al., 2005; de Kloet, 2014; Hermans et al., 2014; Myers et al., 2014). In line with this assumption, the cortisol level is elevated 30 min after sound exposure onwards (Campeau and Watson, 1997). Likewise, elevated cortisol levels influence IHC synapses contacting postsynaptic auditory fibers as well as sound responses of afferent auditory fibers (Singer et al., 2013). Additionally, an acute behavioral stress paradigm and glucocorticoid receptor antagonists influence sound-induced suprathreshold auditory nerve responses, indicating that circulating cortisol reaches the cochlea via the bloodstream (Singer et al., 2013, 2018). Moreover, the same behavioral stress paradigm triggered sound-enrichment driven elevated levels of the LTP-associated activity-regulated cytoskeletal protein (Arc) in the hippocampus (Singer et al., 2013). On the other hand, stress paradigms that lead to high corticosterone blood levels, elevate the risk to reduce central auditory responses after acoustic trauma and reduced Arc levels (Singer et al., 2013). Overall, these previous studies support the hypothesis that various kinds of sound exposures influence long-lasting sensitivity-changes of responses through stress effects on the auditory nerve level. We additionally have to consider that immediate GC-mediated activities operate within minutes to hours after exposure (de Kloet, 2014) preceding BDNF-mediated actions. Accordingly, dependence of BDNF on Arc adaptation processes is documented only for late but not early activities (Chowdhury et al., 2006; Nakayama et al., 2015; Carmichael and Henley, 2018; Epstein and Finkbeiner, 2018). Consequently, the activation of glutamate-receptors by injection of kainaic acid into BLEV mice increased activity-dependent *Bdnf* transcription within hours (Singer et al., submitted). As both effects occur during a similar timeframe, it is likely that sound exposure may promote the activation of *Bdnf* promoters IV and VI in the brainstem (**Figure 2**) following immediate corticosterone-induced accentuation of auditory fiber responses. The failure of *Bdnf* exon-IV-CFP and VI-YFP upregulation in the olfactory bulb after acoustic enrichment indicates that BDNF transcripts are not elevated ubiquitously but in an auditory-specific manner. While it is well established that activation of the *Bdnf* exon-IV promoter occurs in response to elevated calcium (Ca^{2+}) levels subsequently to neuronal activity changes (West et al., 2014), it is only modestly activated by neuronal activity (Timmusk et al., 1993; Aid et al., 2007). It may, however, be activated indirectly in response to the same stimulus, through the involvement of the cAMP response element binding-protein (CREB) (Bambah-Mukku et al., 2014). Moreover, as previously proposed, *Bdnf* exon-IV in platelets may respond to the activity of store-operated calcium channels (Chacón-Fernández et al., 2016) and may thus be influenced by neuronal activity, which is known to tightly regulate blood flow (Hillman, 2014). Accordingly, a sound exposure-induced modification of auditory nerve activity may correspond to the driving force of altered activation of BDNF

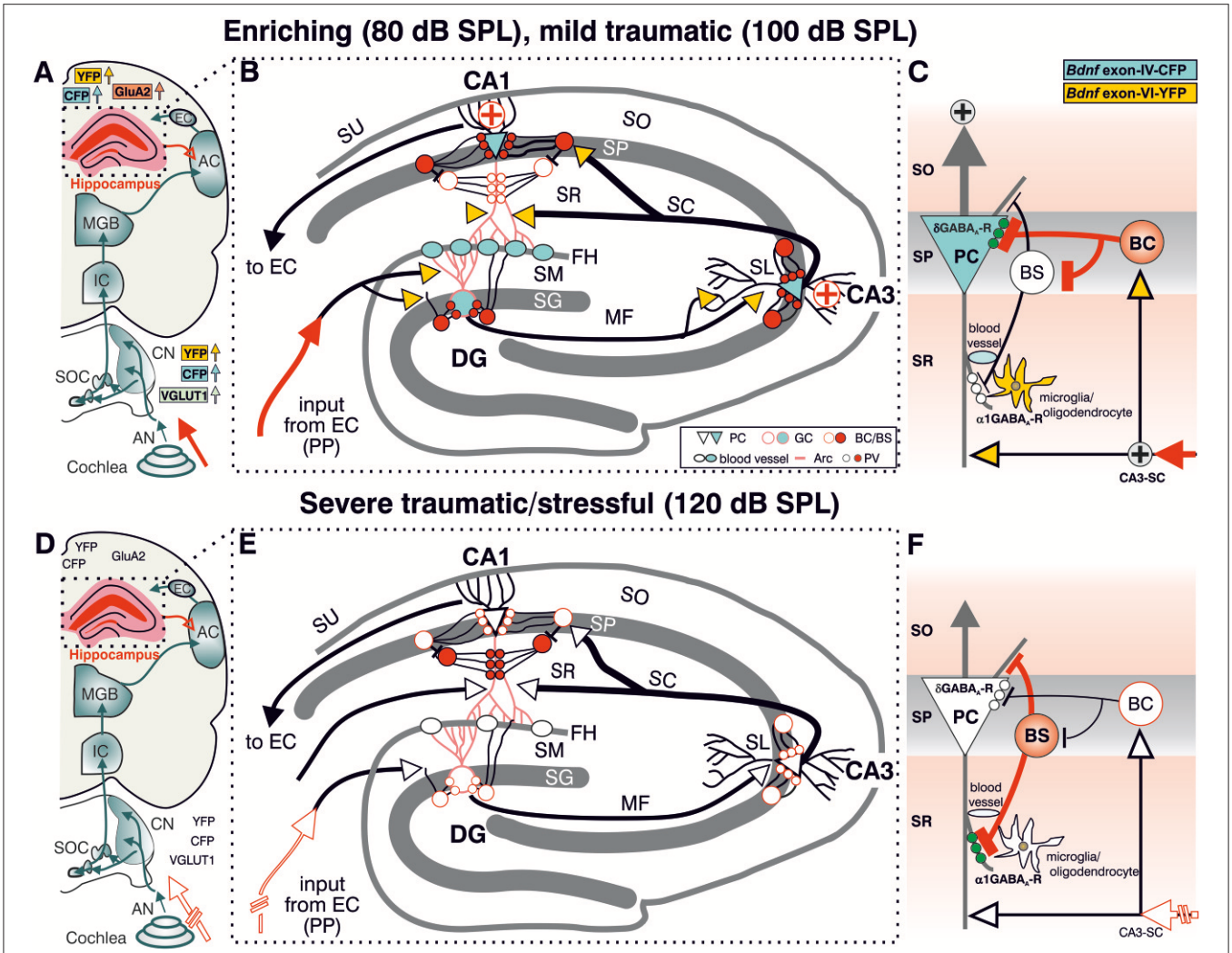

FIGURE 7 | Summary of the location pattern of CFP (blue), YFP (yellow), neuronal (PV) and activity markers (Arc) in the hippocampus. Depicted is the situation in response to enriching or mild traumatic events (80/100 dB SPL) **(A–C)** or to severe traumatic/stressful events (120 dB SPL) **(D–F)**. **(A,D)** Schematic drawing of the auditory pathway including hippocampal connections (red open arrow). **(B,E)** Schematic drawing of hippocampus with perforant path (PP). **(C,D)** Schematic drawing of dendritic (BS) and somatic (BC) inhibitory inputs onto a pyramidal cell (PC). CFP, YFP, VGLUT1 (**A**, light green), GluA2 (**A**, light orange), Arc (**B** red dendrites), PV (**B** red filled circles), and the δ subunit containing $GABA_A$ receptors in PCs (green dots in **C**) were shown to be mobilized after exposure to 80 or 100 dB SPL **(A–C)** but not to 120 dB SPL **(D–F). (C,F)** The cooperative transcript-specific BDNF release may drive a long-lasting reduction of dendritic (**C**, α1 subunit containing $GABA_A$ receptors, white small dots) and increase of perisomatic inhibition (**C**, δ subunit containing $GABA_A$ receptors, green small dots) of CA1 PC by PV expressing inhibitory interneurons (BS, BC) and in parallel possibly improve the recruitment of vascularization (**B,E**, blood vessels). This central facilitating or adaptive responsiveness (**A–C**, solid red arrow indicating increased input activity) is severely hampered when a critical damage of peripheral auditory input occurs (**D–F** discontinuous red lined arrow). ⊕ symbol indicates increased output activity in 80 or 100 dB SPL exposed animals **(C)**. Green dots in **(C)** represent δ subunit containing $GABA_A$ receptors in SP, green dots in **(F)** represent α1 subunit containing $GABA_A$ receptors in SR. AC, auditory cortex; AN, Auditory nerve; BC, basket cell; BS, bistratified cell; CA3-SC, excitatory input from CA3 Schaffer collaterals; CN, cochlear nucleus; DG, dentate gyrus; EC, entorhinal cortex; FH, fissura hippocampalis; GC, granule cell; IC, inferior colliculus; MF, mossy fibers; SC, Schaffer collaterale; SG, stratum granulare; SL, stratum lucidum; SM, stratum moleculare; SO, stratum oriens; SOC, superior olivary complex; SP, stratum pyramidale; SR, stratum radiatum; SU, subiculum.

promoters in brainstem neurons, targeted by auditory nerves. In line with this, adaptations of *Bdnf* exon-IV-CFP and VI-YFP levels in the brainstem appear to correlate with increased expression of VGLUT1 (**Figure 2**), a specific presynaptic marker for auditory-specific synapses in the brainstem (Zhou et al., 2007). This indicates elevated numbers of active release sites, which were previously associated with greater spike fidelity of auditory specific synapses (Ngodup et al., 2015). Interestingly, BDNF regulates VGLUT1 expression during development and hippocampal LTP (Melo et al., 2013), and is able to prevent VGLUT1 reduction in cognitive diseases (Anglada-Huguet et al., 2016). This suggests that *Bdnf* exon-IV-CFP and VI-YFP levels in the brainstem following enriched or severe acoustic trauma may directly drive increased or reduced expression of VGLUT1, respectively. This process needs to be regarded in the context of activity-dependent BDNF which induces strengthening of

synapses (Kellner et al., 2014) and acts as trans-synaptic messenger to control auditory-specific excitability.

Increased Activity in the Auditory System Enhances Hippocampal BDNF Transcription and Synaptic Plasticity

We also observed a trend for increased usage of *Bdnf* exon-IV and -VI in the hippocampus similar to the brainstem and accompanied by elevated levels of the AMPAR subunit GluA2, a marker for synaptic activity in the hippocampus (Tanaka et al., 2000), after acoustic enrichment, but not after severe acoustic trauma (**Figure 3**). Thus, we may assume that BDNF-modified auditory-specific excitability changes after enriching or traumatic sound exposure reach the hippocampus. Indeed, neuronal activity of the auditory pathway after sound exposure can propagate from auditory association cortices through the entorhinal cortex (EC) and via the performant path (PP) into the dorsal hippocampus (Munoz-Lopez et al., 2010). Activation of the dorsal hippocampus was shown after stress (Fanselow and Dong, 2010; Kirby et al., 2013) and environmental enrichment (Tanti et al., 2012), processes that also led to increased LTP (Korz and Frey, 2005) or to improved memory (Hullinger et al., 2015). Furthermore, like environmental enrichment (Weinberger, 2003; Chavez et al., 2009), acoustic enrichment improves frequency discrimination in the auditory cortex as well as the sensitivity to quiet sounds (Engineer et al., 2004; Cai et al., 2009; Bose et al., 2010; Centanni et al., 2013) by a mechanism that most likely involves projection pathways of the medial geniculate body (MGB) (Malmierca and Merchan, 2004). Fittingly, the present study shows acoustic enrichment to coincide with elevated LTP and improved performance in a hippocampus-dependent memory task (**Figure 3**). Moreover, these processes led to *Bdnf* exon-VI-YFP fluorescence that was most prominently increased in the hippocampal CA3 region, while B*dnf* exon-IV-CFP expression was highest in capillaries of the FH and in PC soma (**Figure 4**). Mossy fiber terminals in the CA3 area drive rapid generation and contextualization of episodic memories through elevated neurogenesis and feed-forward inhibition (Donato et al., 2013), for example in response to environmental enrichment. This process fails in post-traumatic stress disorders (Kheirbek et al., 2012; Zaletel et al., 2017). We thus may assume that unlike severe acoustic trauma, acoustic enrichment and mild acoustic trauma improve the generation and contextualization of memory traces because the exposure conditions modify auditory input in such a way that it activates *Bdnf* transcripts in the brainstem and alters auditory-specific ascending glutamatergic excitability. This constitutes an auditory-specific information flow that conveys to the hippocampus through the ascending auditory pathway. This assumption is supported by the failure to recruit *Bdnf* transcript activation in the brainstem and hippocampus following severe acoustic trauma that is also associated with a failure to restore sound sensitivity (ABR wave I and IV reduction, **Figure 1**).

In summary, the changes in *Bdnf* exon-IV usage in hippocampal projecting neurons and *Bdnf* exon-VI in mossy fibers may be interpreted as a result of a sound-induced alteration of the driving force that spreads along the auditory path from the cochlea in an auditory-specific manner. This model could explain the simultaneous changes in the expression of the excitatory marker GluA2 and BDNF in the hippocampus that interestingly coincided with the expression of PV, a marker for a wide array of inhibitory interneurons (Kepecs and Fishell, 2014). Particularly fast-spiking PV-positive interneurons serve a crucial function for microcircuit formation (Hu et al., 2014) and feed-forward inhibition (Donato et al., 2013) under control of BDNF (Waterhouse et al., 2012). PV-positive interneurons are also targeted by BDNF-expressing mossy-fibers and there is evidence that PV expressing basket-cell (BC) interneurons are activated by BDNF (Danzer and Mcnamara, 2004; Danzer et al., 2008). The changes in PV expression observed here could therefore be the direct result of excitability changes arising from the auditory input side. This would perfectly explain the all-encompassing correlation of events that differed between sound-exposure paradigms. In addition, altered PV and BDNF expression patterns observed after sound exposure share characteristics of feed-forward inhibition. First, there is a correlation of *Bdnf* exon-VI-YFP levels in mossy fibers and PV-positive neurons in the CA1 that are likely to correspond to BCs (**Figure 6**). BCs contact neighboring PCs through perisomatic δ subunit containing $GABA_A$-receptor positive synapses (Klausberger et al., 2003; Glykys et al., 2008). Here we observed *Bdnf* exon-IV-CFP expressing PCs and PV-positive BCs that express δ subunit containing $GABA_A$-receptors located nearby the PC soma (**Figures 7C,F**). Future studies might demonstrate recruitment of δ subunit containing $GABA_A$ receptors to *Bdnf* exon-VI-YFP positive synapses in the CA1 pyramidal layer as previously observed (Glykys et al., 2008). Furthermore, we found a reduction of PV and α1 subunit containing $GABA_A$-receptor IR in the SR of animals exposed to acoustic enrichment (80 dB SPL) or mild acoustic trauma (100 dB SPL, **Figures 6C,E**; Supplementary Figures 5D,F). This may represent BC-mediated inhibition of PV-positive bistratified (BS) interneurons that target CA1 dendrites through α1 subunit containing $GABA_A$-receptor expressing synapses (Klausberger and Somogyi, 2008; Willadt et al., 2013). The present findings in BLEV mice do not support a causal link of BDNF levels with PV-mediated feed-forward inhibition. The absence of *Bdnf* transcript mobilization in the tri-synaptic path together with unaltered PV expression and LTP after the reduction of auditory input by severe acoustic trauma (120 dB SPL, **Figures 7D–F**), however, indicates that activity-dependent BDNF expression in the hippocampal tri-synaptic path is a consequence of task-specific BDNF activities in lower auditory brainstem regions. This might be the initial cue to adapt the processing of auditory information within the circuits. It is challenging to consider that during memory-linked adaptation processes the previously shown mossy cell-mediated BDNF-dependent enhancement of dentate granule cell output to the CA3 region (Hashimotodani et al., 2017) might also be activated. The monitoring of these processes is now empowered in BLEV mice.

Our findings thus provide a model for a general mechanism through which sound stimulation is linked to behaviorally relevant alterations in activity of neural networks. Furthermore, our data suggest that the precise nature of auditory experience

may sculpt synaptic traffic in the auditory brain and its connections, including regions such as the hippocampus that are critical for navigating the environment and mapping memories. We propose that a mechanism of this kind may be relevant to establish critical auditory periods in different species including humans (Chen and Yuan, 2015) and may also play an important role in the pathophysiology of human neurodegenerative diseases. Hearing loss has been shown to be associated with an increased risk of dementia in epidemiological studies (Lin et al., 2017), however the nature of this linkage has not been defined. Loss of a critical driving force for recruitment of activity-dependent BDNF expression in neuronal, glial and vascular cells is a plausible mechanism that could contribute to a non-adapting metabolic supply. This may cause accelerated regional brain (in particular, parahippocampal) atrophy (Lin et al., 2014) followed by chronic peripheral hearing impairment such as in older people developing Alzheimer's disease. The findings suggest that possible neurodegenerative proteinopathies (Hardy et al., 2016) may not necessarily be overcome by systemic BDNF therapies. In contrast, sustained patterns of neural network activity may promote the spread of specific proteinopathies ("molecular nexopathies") (Warren et al., 2013), and BDNF expression might be one mediator of such activity-dependent network degenerations in the setting of proteinopathies, as recently also demonstrated in Alzheimer's disease (Hardy et al., 2017). From the finding in the present study it is challenging to speculate that "auditory enrichment" (for example, via regular music listening) might also engage a BDNF-dependent mechanism, with intriguing implications for neuroprotective strategies.

In conclusion, here we demonstrate for the first time that translation of exon-IV and -VI derived BDNF is elevated after sound exposure conditions that induce long-lasting changes in sound-sensitivity correlating with increased hippocampal LTP. We verify the BLEV reporter mouse as a model to identify and examine those neurons, non-neuronal glial and capillary cells that in a task-specific and orchestrated way respond to those environmental changes that induce behavioral relevant adaptation processes. BLEV mice may thus be used to demonstrate that the synchronized activation of BDNF in neurons, glia, and capillaries provides the specific cues for GC-mediated metabolic support (de Kloet, 2014; Jeanneteau and Arango-Lievano, 2016) in the context of a specific sensory organ, a hypothesis that needs to be tested in more detail in future studies. To sum up, BLEV mice allow monitoring of which networks and which of their parts are activated and altered to accentuate behaviorally important auditory input (Berlau and Weinberger, 2008; Munoz-Lopez et al., 2010; Kraus and White-Schwoch, 2015). Our findings suggest a candidate mechanism whereby auditory experience may sculpt neural networks in the ascending auditory pathway and beyond. This in turn has potentially wide-reaching implications for understanding the role of auditory stimulation in promoting normal development of the human auditory brain and the contribution of auditory dysfunction to disease states, notably the neurodegenerative proteinopathies.

AUTHOR CONTRIBUTIONS

WS, PE, LM, RP-W, H-SG, TO, and MK: Conceptualization. WS, LM, AB, PE, MM, CH, EF, LR, and MK: Analysis. WS, LM, H-SG, AB, PE, MM, NM, and KR: Investigation. WS, RP-W, LM, PE, UZ, LR, TS, and MK: Writing. WS, PR, EF, TO, LR, and MK: Supervision. LM, WS, PR, UZ, LR, and MK: Review and Editing.

FUNDING

This work was supported by the Deutsche Forschung sgemeinschaft DFG-Kni-316-10-1 (RP-M, WS, H-SG, MK, and TO); FOR 2060 project RU 713/3-2 (LR and CH); SPP 1608 RU 316/12-1 (PE, KR, H-SG); KN 316/12-1 (MM, UZ, and MK); SPP 1608 FR 1784/17-1 (EF and NM); the Brain and Behavior Research Foundation NARSAD Young Investigator Grant 20748 (LM), BFU2013-40944 (TS); DFG KFO134 (PR and AB). We acknowledge support by Deutsche Forschungsgemeinschaft and Open Access Publishing Fund of University of Tübingen.

ACKNOWLEDGMENTS

Thank you to Michael Paolillo for reading the manuscript.

SUPPLEMENTARY MATERIAL

The Supplementary Material for this article can be found online at: https://www.frontiersin.org/articles/10.3389/fnmol.2018.00260/full#supplementary-material

REFERENCES

Aid, T., Kazantseva, A., Piirsoo, M., Palm, K., and Timmusk, T. (2007). Mouse and rat BDNF gene structure and expression revisited. *J. Neurosci. Res.* 85, 525–535. doi: 10.1002/jnr.21139

Anglada-Huguet, M., Vidal-Sancho, L., Giralt, A., Garcia-Diaz Barriga, G., Xifro, X., and Alberch, J. (2016). Prostaglandin E2 EP2 activation reduces memory decline in R6/1 mouse model of Huntington's disease by the induction of BDNF-dependent synaptic plasticity. *Neurobiol. Dis.* 95, 22–34. doi: 10.1016/j.nbd.2015.09.001

Arango-Lievano, M., Lambert, W. M., Bath, K. G., Garabedian, M. J., Chao, M. V., and Jeanneteau, F. (2015). Neurotrophic-priming of glucocorticoid receptor signaling is essential for neuronal plasticity to stress and antidepressant treatment. *Proc. Natl. Acad. Sci. U.S.A.* 112, 15737–15742. doi: 10.1073/pnas.1509045112

Bambah-Mukku, D., Travaglia, A., Chen, D. Y., Pollonini, G., and Alberini, C. M. (2014). A positive autoregulatory BDNF feedback loop via C/EBPb mediates hippocampal memory consolidation. *J. Neurosci.* 34, 12547–12559. doi: 10.1523/JNEUROSCI.0324-14.2014

Barde, Y. A., Edgar, D., and Thoenen, H. (1982). Purification of a new neurotrophic factor from mammalian brain. *EMBO J.* 1, 549–553.

Bath, K. G., Schilit, A., and Lee, F. S. (2013). Stress effects on BDNF expression: effects of age, sex, and form of stress. *Neuroscience* 239, 149–156. doi: 10.1016/j.neuroscience.2013.01.074

Bausch, A. E., Dieter, R., Nann, Y., Hausmann, M., Meyerdierks, N., Kaczmarek, L. K., et al. (2015). The sodium-activated potassium channel Slack is required for optimal cognitive flexibility in mice. *Learn. Mem.* 22, 323–335. doi: 10.1101/lm.037820.114

Berlau, K. M., and Weinberger, N. M. (2008). Learning strategy determines auditory cortical plasticity. *Neurobiol. Learn. Mem.* 89, 153–166. doi: 10.1016/j.nlm.2007.07.004

Bose, M., Muñoz-Llancao, P., Roychowdhury, S., Nichols, J. A., Jakkamsetti, V., Porter, B., et al. (2010). Effect of the environment on the dendritic morphology of the rat auditory cortex. *Synapse* 64, 97–110. doi: 10.1002/syn.20710

Bramham, C. R., and Messaoudi, E. (2005). BDNF function in adult synaptic plasticity: the synaptic consolidation hypothesis. *Prog. Neurobiol.* 76, 99–125. doi: 10.1016/j.pneurobio.2005.06.003

Bramham, C. R., Worley, P. F., Moore, M. J., and Guzowski, J. F. (2008). The immediate early gene arc/arg3.1: regulation, mechanisms, and function. *J. Neurosci.* 28, 11760–11767. doi: 10.1523/JNEUROSCI.3864-08.2008

Cai, R., Guo, F., Zhang, J., Xu, J., Cui, Y., and Sun, X. (2009). Environmental enrichment improves behavioral performance and auditory spatial representation of primary auditory cortical neurons in rat. *Neurobiol. Learn. Mem.* 91, 366–376. doi: 10.1016/j.nlm.2009.01.005

Campeau, S., and Watson, S. J. (1997). Neuroendocrine and behavioral responses and brain pattern of c-fos induction associated with audiogenic stress. *J. Neuroendocrinol.* 9, 577–588.

Carmichael, R. E., and Henley, J. M. (2018). Transcriptional and post-translational regulation of Arc in synaptic plasticity. *Semin. Cell. Dev. Biol.* 77, 3–9. doi: 10.1016/j.semcdb.2017.09.007

Castrén, E., and Rantamäki, T. (2010). The role of BDNF and its receptors in depression and antidepressant drug action: reactivation of developmental plasticity. *Dev. Neurobiol.* 70, 289–297. doi: 10.1002/dneu.20758

Centanni, T. M., Engineer, C. T., and Kilgard, M. P. (2013). Cortical speech-evoked response patterns in multiple auditory fields are correlated with behavioral discrimination ability. *J. Neurophysiol.* 110, 177–189. doi: 10.1152/jn.00092.2013

Chacón-Fernández, P., Säuberli, K., Colzani, M., Moreau, T., Ghevaert, C., and Barde, Y. A. (2016). Brain-derived neurotrophic factor in megakaryocytes. *J. Biol. Chem.* 291, 9872–9881. doi: 10.1074/jbc.M116.720029

Chavez, C. M., Mcgaugh, J. L., and Weinberger, N. M. (2009). The basolateral amygdala modulates specific sensory memory representations in the cerebral cortex. *Neurobiol. Learn. Mem.* 91, 382–392. doi: 10.1016/j.nlm.2008.10.010

Chen, Z., and Yuan, W. (2015). Central plasticity and dysfunction elicited by aural deprivation in the critical period. *Front. Neural. Circuits* 9, 26. doi: 10.3389/fncir.2015.00026

Chenaux, G., Matt, L., Hill, T. C., Kaur, I., Liu, X.-B., Kirk, L. M., et al. (2016). Loss of SynDIG1 reduces excitatory synapse maturation but not formation *in vivo*. *eNeuro* 3, ENEURO.0130-16.2016. doi: 10.1523/ENEURO.0130-16.2016

Chourbaji, S., Brandwein, C., Vogt, M. A., Dormann, C., Hellweg, R., and Gass, P. (2008). Nature vs. nurture: can enrichment rescue the behavioural phenotype of BDNF heterozygous mice? *Behav. Brain Res.* 192, 254–258. doi: 10.1016/j.bbr.2008.04.015

Chowdhury, S., Shepherd, J. D., Okuno, H., Lyford, G., Petralia, R. S., Plath, N., et al. (2006). Arc/Arg3.1 interacts with the endocytic machinery to regulate AMPA receptor trafficking. *Neuron* 52, 445–459. doi: 10.1016/j.neuron.2006.08.033

Chumak, T., Rüttiger, L., Lee, S. C., Campanelli, D., Zuccotti, A., Singer, W., et al. (2016). BDNF in lower brain parts modifies auditory fiber activity to gain fidelity but increases the risk for generation of central noise after injury. *Mol. Neurobiol.* 53, 5607–5627. doi: 10.1007/s12035-015-9474-x

Danzer, S. C., Kotloski, R. J., Walter, C., Hughes, M., and Mcnamara, J. O. (2008). Altered morphology of hippocampal dentate granule cell presynaptic and postsynaptic terminals following conditional deletion of TrkB. *Hippocampus* 18, 668–678. doi: 10.1002/hipo.20426

Danzer, S. C., and Mcnamara, J. O. (2004). Localization of brain-derived neurotrophic factor to distinct terminals of mossy fiber axons implies regulation of both excitation and feedforward inhibition of CA3 pyramidal cells. *J. Neurosci.* 24, 11346–11355. doi: 10.1523/JNEUROSCI.3846-04.2004

de Fiebre, N. C., Sumien, N., Forster, M. J., and De Fiebre, C. M. (2006). Spatial learning and psychomotor performance of C57BL/6 mice: age sensitivity and reliability of individual differences. *Age (Dordr).* 28, 235–253. doi: 10.1007/s11357-006-9027-3

de Kloet, E. R. (2014). From receptor balance to rational glucocorticoid therapy. *Endocrinology* 155, 2754–2769. doi: 10.1210/en.2014-1048

De Kloet, E. R., Joëls M., and Holsboer, F. (2005). Stress and the brain: from adaptation to disease. *Nat. Rev. Neurosci.* 6, 463–475. doi: 10.1038/nrn1683

Dieni, S., Matsumoto, T., Dekkers, M., Rauskolb, S., Ionescu, M. S., Deogracias, R., et al. (2012). BDNF and its pro-peptide are stored in presynaptic dense core vesicles in brain neurons. *J. Cell Biol.* 196, 775–788. doi: 10.1083/jcb.201201038

Donato, F., Rompani, S. B., and Caroni, P. (2013). Parvalbumin-expressing basket-cell network plasticity induced by experience regulates adult learning. *Nature* 504, 272–276. doi: 10.1038/nature12866

Donovan, M. J., Lin, M. I., Wiegn, P., Ringstedt, T., Kraemer, R., Hahn, R., et al. (2000). Brain derived neurotrophic factor is an endothelial cell survival factor required for intramyocardial vessel stabilization. *Development* 127, 4531–4540.

Duguid, I., Branco, T., London, M., Chadderton, P., and Hausser, M. (2012). Tonic inhibition enhances fidelity of sensory information transmission in the cerebellar cortex. *J. Neurosci.* 32, 11132–11143. doi: 10.1523/JNEUROSCI.0460-12.2012

Edelmann, E., Lessmann, V., and Brigadski, T. (2014). Pre- and postsynaptic twists in BDNF secretion and action in synaptic plasticity. *Neuropharmacology* 76, 610–627. doi: 10.1016/j.neuropharm.2013.05.043

Engineer, N. D., Percaccio, C. R., Pandya, P. K., Moucha, R., Rathbun, D. L., and Kilgard, M. P. (2004). Environmental enrichment improves response strength, threshold, selectivity, and latency of auditory cortex neurons. *J. Neurophysiol.* 92, 73–82. doi: 10.1152/jn.00059.2004

Epstein, I., and Finkbeiner, S. (2018). The arc of cognition: Signaling cascades regulating arc and implications for cognitive function and disease. *Semin. Cell Dev. Biol.* 77, 63–72. doi: 10.1016/j.semcdb.2017.09.023

Ernfors, P., Lee, K. F., and Jaenisch, R. (1994). Mice lacking brain-derived neurotrophic factor develop with sensory deficits. *Nature* 368, 147–150. doi: 10.1038/368147a0

Fanselow, M. S., and Dong, H. W. (2010). Are the dorsal and ventral hippocampus functionally distinct structures? *Neuron* 65, 7–19. doi: 10.1016/j.neuron.2009.11.031

Ferrini, F., and De Koninck, Y. (2013). Microglia control neuronal network excitability via BDNF signalling. *Neural Plast.* 2013, 429815. doi: 10.1155/2013/429815

Glykys, J., Mann, E. O., and Mody, I. (2008). Which $GABA_A$ receptor subunits are necessary for tonic inhibition in the hippocampus? *J. Neurosci.* 28, 1421–1426. doi: 10.1523/JNEUROSCI.4751-07.2008

Gray, J. D., Milner, T. A., and Mcewen, B. S. (2013). Dynamic plasticity: the role of glucocorticoids, brain-derived neurotrophic factor and other trophic factors. *Neuroscience* 239, 214–227. doi: 10.1016/j.neuroscience.2012.08.034

Hardy, C. J. D., Hwang, Y. T., Bond, R. L., Marshall, C. R., Ridha, B. H., Crutch, S. J., et al. (2017). Donepezil enhances understanding of degraded speech in Alzheimer's disease. *Ann. Clin. Transl. Neurol.* 4, 835–840. doi: 10.1002/acn3.471

Hardy, C. J., Marshall, C. R., Golden, H. L., Clark, C. N., Mummery, C. J., Griffiths, T. D., et al. (2016). Hearing and dementia. *J. Neurol.* 263, 2339–2354. doi: 10.1007/s00415-016-8208-y

Hashimotodani, Y., Nasrallah, K., Jensen, K. R., Chávez, AE., Carrera, D., and Castillo, P. E. (2017). LTP at Hilar Mossy cell-dentate granule cell synapses modulates dentate gyrus output by increasing excitation/inhibition balance. *Neuron 95*, 928–943.e923. doi: 10.1016/j.neuron.2017.07.028

Hermans, E. J., Henckens, M. J., Joëls M., and Fernandez, G. (2014). Dynamic adaptation of large-scale brain networks in response to acute stressors. *Trends Neurosci.* 37, 304–314. doi: 10.1016/j.tins.2014.03.006

Hill, J. L., Hardy, N. F., Jimenez, D. V., Maynard, K. R., Kardian, A. S., Pollock, C. J., et al. (2016). Loss of promoter IV-driven BDNF expression impacts oscillatory activity during sleep, sensory information processing and fear regulation. *Transl. Psychiatry* 6, e873. doi: 10.1038/tp.2016.153

Hillman, E. M. (2014). Coupling mechanism and significance of the BOLD signal: a status report. *Annu. Rev. Neurosci.* 37, 161–181. doi: 10.1146/annurev-neuro-071013-014111

Hong, E. J., Mccord, A. E., and Greenberg, M. E. (2008). A biological function for the neuronal activity-dependent component of Bdnf transcription in the development of cortical inhibition. *Neuron* 60, 610–624. doi: 10.1016/j.neuron.2008.09.024

Hu, H., Gan, J., and Jonas, P. (2014). Interneurons. Fast-spiking, parvalbumin(+) GABAergic interneurons: from cellular design to microcircuit function. *Science* 345:1255263. doi: 10.1126/science.1255263

Huang, E. J., and Reichardt, L. F. (2001). Neurotrophins: roles in neuronal development and function. *Annu. Rev. Neurosci.* 24, 677–736. doi: 10.1146/annurev.neuro.24.1.677

Hullinger, R., O'riordan, K., and Burger, C. (2015). Environmental enrichment improves learning and memory and long-term potentiation in young adult rats through a mechanism requiring mGluR5 signaling and sustained activation of p70s6k. *Neurobiol. Learn. Mem.* 125, 126–134. doi: 10.1016/j.nlm.2015.08.006

Jeanneteau, F., and Arango-Lievano, M. (2016). Linking mitochondria to synapses: new insights for stress-related neuropsychiatric disorders. *Neural Plast.* 2016:3985063. doi: 10.1155/2016/3985063

Jonasson, Z. (2005). Meta-analysis of sex differences in rodent models of learning and memory: a review of behavioral and biological data. *Neurosci. Biobehav. Rev.* 28, 811–825. doi: 10.1016/j.neubiorev.2004.10.006

Kellner, Y., Gödecke N., Dierkes, T., Thieme, N., Zagrebelsky, M., and Korte, M. (2014). The BDNF effects on dendritic spines of mature hippocampal neurons depend on neuronal activity. *Front. Synaptic Neurosci.* 6:5. doi: 10.3389/fnsyn.2014.00005

Kepecs, A., and Fishell, G. (2014). Interneuron cell types are fit to function. *Nature* 505, 318–326. doi: 10.1038/nature12983

Kheirbek, M. A., Klemenhagen, K. C., Sahay, A., and Hen, R. (2012). Neurogenesis and generalization: a new approach to stratify and treat anxiety disorders. *Nat. Neurosci.* 15, 1613–1620. doi: 10.1038/nn.3262

Kirby, E. D., Muroy, S. E., Sun, W. G., Covarrubias, D., Leong, M. J., Barchas, L. A., et al. (2013). Acute stress enhances adult rat hippocampal neurogenesis and activation of newborn neurons via secreted astrocytic FGF2. *Elife* 2, e00362. doi: 10.7554/eLife.00362

Klausberger, T., Magill, P. J., Marton, L. F., Roberts, J. D., Cobden, P. M., Buzsaki, G., et al. (2003). Brain-state- and cell-type-specific firing of hippocampal interneurons *in vivo*. *Nature* 421, 844–848. doi: 10.1038/nature01374

Klausberger, T., and Somogyi, P. (2008). Neuronal diversity and temporal dynamics: the unity of hippocampal circuit operations. *Science* 321, 53–57. doi: 10.1126/science.1149381

Knipper, M., Panford-Walsh, R., Singer, W., Rüttiger, L., and Zimmermann, U. (2015). Specific synaptopathies diversify brain responses and hearing disorders: you lose the gain from early life. *Cell Tissue Res.* 361, 77–93. doi: 10.1007/s00441-015-2168-x

Knipper, M., Van Dijk, P., Nunes, I., Rüttiger, L., and Zimmermann, U. (2013). Advances in the neurobiology of hearing disorders: recent developments regarding the basis of tinnitus and hyperacusis. *Prog. Neurobiol.* 111, 17–33. doi: 10.1016/j.pneurobio.2013.08.002

Korz, V., and Frey, J. U. (2005). Bidirectional modulation of hippocampal long-term potentiation under stress and no-stress conditions in basolateral amygdala-lesioned and intact rats. *J. Neurosci.* 25, 7393–7400. doi: 10.1523/JNEUROSCI.0910-05.2005

Kraus, N., and White-Schwoch, T. (2015). Unraveling the biology of auditory learning: a cognitive-sensorimotor-reward framework. *Trends Cogn. Sci.* 19, 642–654. doi: 10.1016/j.tics.2015.08.017

Kuipers, S. D., Trentani, A., Tiron, A., Mao, X., Kuhl, D., and Bramham, C. R. (2016). BDNF-induced LTP is associated with rapid Arc/Arg3.1-dependent enhancement in adult hippocampal neurogenesis. *Sci. Rep.* 6:21222. doi: 10.1038/srep21222

Lin, F. R., Ferrucci, L., An, Y., Goh, J. O., Doshi, J., Metter, E. J., et al. (2014). Association of hearing impairment with brain volume changes in older adults. *Neuroimage* 90, 84–92. doi: 10.1016/j.neuroimage.2013.12.059

Lin, V. Y., Chung, J., Callahan, B. L., Smith, L., Gritters, N., Chen, J. M., et al. (2017). Development of cognitive screening test for the severely hearing impaired: Hearing-impaired MoCA. *Laryngoscope* 127, S4–S11. doi: 10.1002/lary.26590

Liston, C., Cichon, J. M., Jeanneteau, F., Jia, Z., Chao, M. V., and Gan, W. B. (2013). Circadian glucocorticoid oscillations promote learning-dependent synapse formation and maintenance. *Nat. Neurosci.* 16, 698–705. doi: 10.1038/nn.3387

Lu, B., Wang, K. H., and Nose, A. (2009). Molecular mechanisms underlying neural circuit formation. *Curr. Opin. Neurobiol.* 19, 162–167. doi: 10.1016/j.conb.2009.04.004

Lyons, M. R., and West, A. E. (2011). Mechanisms of specificity in neuronal activity-regulated gene transcription. *Prog. Neurobiol.* 94, 259–295. doi: 10.1016/j.pneurobio.2011.05.003

Mallei, A., Baj, G., Ieraci, A., Corna, S., Musazzi, L., Lee, F. S., et al. (2015). Expression and dendritic trafficking of BDNF-6 splice variant are impaired in knock-in mice carrying human BDNF Val66Met polymorphism. *Int. J. Neuropsychopharmacol.* 18, pyv069. doi: 10.1093/ijnp/pyv069

Malmierca, M., and Merchan, M. (2004). "The auditory system," in *The Rat Nervous System*, ed G. Paxinos (San Diego, CA: Academic Press), 997–1082.

Marosi, K., and Mattson, M. P. (2014). BDNF mediates adaptive brain and body responses to energetic challenges. *Trends Endocrinol. Metab.* 25, 89–98. doi: 10.1016/j.tem.2013.10.006

Marty, S. (2000). Differences in the regulation of neuropeptide Y, somatostatin and parvalbumin levels in hippocampal interneurons by neuronal activity and BDNF. *Prog. Brain Res.* 128, 193–202. doi: 10.1016/S0079-6123(00)28017-5

Matt, L., Michalakis, S., Hofmann, F., Hammelmann, V., Ludwig, A., Biel, M., et al. (2011). HCN2 channels in local inhibitory interneurons constrain LTP in the hippocampal direct perforant path. *Cell. Mol. Life Sci.* 68, 125–137. doi: 10.1007/s00018-010-0446-z

Maynard, K. R., Hill, J. L., Calcaterra, N. E., Palko, M. E., Kardian, A., Paredes, D., et al. (2016). Functional role of BDNF production from unique promoters in aggression and serotonin signaling. *Neuropsychopharmacology* 41, 1943–1955. doi: 10.1038/npp.2015.349

Melo, C. V., Mele, M., Curcio, M., Comprido, D., Silva, C. G., and Duarte, C. B. (2013). BDNF regulates the expression and distribution of vesicular glutamate transporters in cultured hippocampal neurons. *PLoS ONE* 8:e53793. doi: 10.1371/journal.pone.0053793

Messaoudi, E., Kanhema, T., Soule, J., Tiron, A., Dagyte, G., Da Silva, B., et al. (2007). Sustained Arc/Arg3.1 synthesis controls long-term potentiation consolidation through regulation of local actin polymerization in the dentate gyrus *in vivo*. *J. Neurosci.* 27, 10445–10455. doi: 10.1523/JNEUROSCI.2883-07.2007

Minichiello, L. (2009). TrkB signalling pathways in LTP and learning. *Nat. Rev. Neurosci.* 10, 850–860. doi: 10.1038/nrn2738

Mitre, M., Mariga, A., and Chao, M. V. (2017). Neurotrophin signalling: novel insights into mechanisms and pathophysiology. *Clin. Sci. (Lond).* 131, 13–23. doi: 10.1042/CS20160044

Miyamoto, N., Pham, L. D., Seo, J. H., Kim, K. W., Lo, E. H., and Arai, K. (2014). Crosstalk between cerebral endothelium and oligodendrocyte. *Cell. Mol. Life Sci.* 71, 1055–1066. doi: 10.1007/s00018-013-1488-9

Munoz-Lopez, M. M., Mohedano-Moriano, A., and Insausti, R. (2010). Anatomical pathways for auditory memory in primates. *Front. Neuroanat.* 4:129. doi: 10.3389/fnana.2010.00129

Myers, B., Mcklveen, J. M., and Herman, J. P. (2014). Glucocorticoid actions on synapses, circuits, and behavior: implications for the energetics of stress. *Front. Neuroendocrinol.* 35, 180–196. doi: 10.1016/j.yfrne.2013.12.003

Nahmani, M., and Turrigiano, G. G. (2014). Adult cortical plasticity following injury: recapitulation of critical period mechanisms? *Neuroscience* 283, 4–16. doi: 10.1016/j.neuroscience.2014.04.029

Nakayama, D., Iwata, H., Teshirogi, C., Ikegaya, Y., Matsuki, N., and Nomura, H. (2015). Long-delayed expression of the immediate early gene Arc/Arg3.1 refines neuronal circuits to perpetuate fear memory. *J. Neurosci.* 35, 819–830. doi: 10.1523/JNEUROSCI.2525-14.2015

Ngodup, T., Goetz, J. A., Mcguire, B. C., Sun, W., Lauer, A. M., and Xu-Friedman, M. A. (2015). Activity-dependent, homeostatic regulation of neurotransmitter release from auditory nerve fibers. *Proc. Natl. Acad. Sci. U.S.A.* 112, 6479–6484. doi: 10.1073/pnas.1420885112

Pariante, C. M. (2009). Risk factors for development of depression and psychosis. Glucocorticoid receptors and pituitary implications for treatment with antidepressant and glucocorticoids. *Ann. N. Y. Acad. Sci.* 1179, 144–152. doi: 10.1111/j.1749-6632.2009.04978.x

Park, H., and Poo, M. M. (2013). Neurotrophin regulation of neural circuit development and function. *Nat. Rev. Neurosci.* 14, 7–23. doi: 10.1038/nrn3379

Parkhurst, C. N., Yang, G., Ninan, I., Savas, J. N., Yates, J. R. III, et al. (2013). Microglia promote learning-dependent synapse formation through brain-derived neurotrophic factor. *Cell* 155, 1596–1609. doi: 10.1016/j.cell.2013.11.030

Postigo, A., Calella, A. M., Fritzsch, B., Knipper, M., Katz, D., Eilers, A., et al. (2002). Distinct requirements for TrkB and TrkC signaling in target innervation by sensory neurons. *Genes Dev.* 16, 633–645. doi: 10.1101/gad.217902

Rauskolb, S., Zagrebelsky, M., Dreznjak, A., Deogracias, R., Matsumoto, T., Wiese, S., et al. (2010). Global deprivation of brain-derived neurotrophic factor in the CNS reveals an area-specific requirement for dendritic growth. *J. Neurosci.* 30, 1739–1749. doi: 10.1523/JNEUROSCI.5100-09.2010

Rios, M., Fan, G., Fekete, C., Kelly, J., Bates, B., Kuehn, R., et al. (2001). Conditional deletion of brain-derived neurotrophic factor in the postnatal brain leads to obesity and hyperactivity. *Mol. Endocrinol.* 15, 1748–1757. doi: 10.1210/mend.15.10.0706

Rüttiger, L., Singer, W., Panford-Walsh, R., Matsumoto, M., Lee, S. C., Zuccotti, A., et al. (2013). The reduced cochlear output and the failure to adapt the central auditory response causes tinnitus in noise exposed rats. *PLoS ONE* 8:e57247. doi: 10.1371/journal.pone.0057247

Sakata, K., Jin, L., and Jha, S. (2010). Lack of promoter IV-driven BDNF transcription results in depression-like behavior. *Genes Brain Behav.* 9, 712–721. doi: 10.1111/j.1601-183X.2010.00605.x

Sakata, K., Woo, N. H., Martinowich, K., Greene, J. S., Schloesser, R. J., Shen, L., et al. (2009). Critical role of promoter IV-driven BDNF transcription in GABAergic transmission and synaptic plasticity in the prefrontal cortex. *Proc. Natl. Acad. Sci. U.S.A.* 106, 5942–5947. doi: 10.1073/pnas.0811431106

Serra-Millàs, M. (2016). Are the changes in the peripheral brain-derived neurotrophic factor levels due to platelet activation? *World J. Psychiatry* 6, 84–101. doi: 10.5498/wjp.v6.i1.84

Singer, W., Geisler, H. S., Panford-Walsh, R., and Knipper, M. (2016). Detection of excitatory and inhibitory synapses in the auditory system using fluorescence immunohistochemistry and high-resolution fluorescence microscopy. *Methods Mol. Biol.* 1427, 263–276. doi: 10.1007/978-1-4939-3615-1_15

Singer, W., Kasini, K., Manthey, M., Eckert, P., Armbruster, P., Vogt, M. A., et al. (2018). The glucocorticoid antagonist mifepristone attenuates sound-induced long-term deficits in auditory nerve response and central auditory processing in female rats. *FASEB J.* 32, 3005–3019. doi: 10.1096/fj.201701041RRR

Singer, W., Zuccotti, A., Jaumann, M., Lee, S. C., Panford-Walsh, R., Xiong, H., et al. (2013). Noise-induced inner hair cell ribbon loss disturbs central arc mobilization: a novel molecular paradigm for understanding tinnitus. *Mol. Neurobiol.* 47, 261–279. doi: 10.1007/s12035-012-8372-8

Tan, J., Rüttiger, L., Panford-Walsh, R., Singer, W., Schulze, H., Kilian, S. B., et al. (2007). Tinnitus behavior and hearing function correlate with the reciprocal expression patterns of BDNF and Arg3.1/arc in auditory neurons following acoustic trauma. *Neuroscience* 145, 715–726. doi: 10.1016/j.neuroscience.2006.11.067

Tanaka, H., Grooms, S. Y., Bennett, M. V., and Zukin, R. S., (2000). The AMPAR subunit GluR2: still front and center-stage. *Brain Res.* 886, 190–207. doi: 10.1016/S0006-8993(00)02951-6

Tanti, A., Rainer, Q., Minier, F., Surget, A., and Belzung, C. (2012). Differential environmental regulation of neurogenesis along the septo-temporal axis of the hippocampus. *Neuropharmacology* 63, 374–384. doi: 10.1016/j.neuropharm.2012.04.022

Timmusk, T., Palm, K., Metsis, M., Reintam, T., Paalme, V., Saarma, M., et al. (1993). Multiple promoters direct tissue-specific expression of the rat BDNF gene. *Neuron* 10, 475–489. doi: 10.1016/0896-6273(93)90335-O

Tuvikene, J., Pruunsild, P., Orav, E., Esvald, E. E., and Timmusk, T. (2016). AP-1 transcription factors mediate BDNF-positive feedback loop in cortical neurons. *J. Neurosci.* 36, 1290–1305. doi: 10.1523/JNEUROSCI.3360-15.2016

Vaghi, V., Polacchini, A., Baj, G., Pinheiro, V. L., Vicario, A., and Tongiorgi, E. (2014). Pharmacological profile of brain-derived neurotrophic factor (BDNF) splice variant translation using a novel drug screening assay: a "quantitative code." *J. Biol. Chem.* 289, 27702–27713. doi: 10.1074/jbc.M114.586719

Vanevski, F., and Xu, B. (2013). Molecular and neural bases underlying roles of BDNF in the control of body weight. *Front. Neurosci.* 7:37. doi: 10.3389/fnins.2013.00037

van Praag, H., Christie, B. R., Sejnowski, T. J., and Gage, F. H. (1999). Running enhances neurogenesis, learning, and long-term potentiation in mice. *Proc. Natl. Acad. Sci. U.S.A.* 96, 13427–13431. doi: 10.1073/pnas.96.23.13427

Vorhees, C. V., and Williams, M. T. (2006). Morris water maze: procedures for assessing spatial and related forms of learning and memory. *Nat. Protoc.* 1, 848–858. doi: 10.1038/nprot.2006.116

Wall, M. J., and Corrêa, SAL. (2017). The mechanistic link between Arc/Arg3.1 expression and AMPA receptor endocytosis. *Semin. Cell Dev. Biol.* 77, 17–24. doi: 10.1016/j.semcdb.2017.09.005

Wardle, R. A., and Poo, M. M. (2003). Brain-derived neurotrophic factor modulation of GABAergic synapses by postsynaptic regulation of chloride transport. *J. Neurosci.* 23, 8722–8732. doi: 10.1523/JNEUROSCI.23-25-08722.2003

Warren, J. D., Rohrer, J. D., Schott, J. M., Fox, N. C., Hardy, J., and Rossor, M. N. (2013). Molecular nexopathies: a new paradigm of neurodegenerative disease. *Trends Neurosci.* 36, 561–569. doi: 10.1016/j.tins.2013.06.007

Waterhouse, E. G., An, J. J., Orefice, L. L., Baydyuk, M., Liao, G. Y., Zheng, K., et al. (2012). BDNF promotes differentiation and maturation of adult-born neurons through GABAergic transmission. *J. Neurosci.* 32, 14318–14330. doi: 10.1523/JNEUROSCI.0709-12.2012

Waterhouse, E. G., and Xu, B. (2009). New insights into the role of brain-derived neurotrophic factor in synaptic plasticity. *Mol. Cell. Neurosci.* 42, 81–89. doi: 10.1016/j.mcn.2009.06.009

Weinberger, N. M. (2003). The nucleus basalis and memory codes: auditory cortical plasticity and the induction of specific, associative behavioral memory. *Neurobiol. Learn. Mem.* 80, 268–284. doi: 10.1016/S1074-7427(03)00072-8

West, A. E., Pruunsild, P., and Timmusk, T. (2014). Neurotrophins: transcription and translation. *Handb. Exp. Pharmacol.* 220, 67–100. doi: 10.1007/978-3-642-45106-5_4

Willadt, S., Nenniger, M., and Vogt, K. E. (2013). Hippocampal feedforward inhibition focuses excitatory synaptic signals into distinct dendritic compartments. *PLoS ONE* 8:e80984. doi: 10.1371/journal.pone.0080984

Yamada, K., and Nabeshima, T. (2003). Brain-derived neurotrophic factor/TrkB signaling in memory processes. *J. Pharmacol. Sci.* 91, 267–270. doi: 10.1254/jphs.91.267

Zaletel, I., Filipović, D, Puškaš, N. (2017). Hippocampal BDNF in physiological conditions and social isolation. *Rev. Neurosci.* 28, 675–692. doi: 10.1515/revneuro-2016-0072

Zheng, K., An, J. J., Yang, F., Xu, W., Xu, Z. Q., Wu, J., et al. (2011). TrkB signaling in parvalbumin-positive interneurons is critical for gamma-band network synchronization in hippocampus. *Proc. Natl. Acad. Sci. U.S.A.* 108, 17201–17206. doi: 10.1073/pnas.1114241108

Zhou, J., Nannapaneni, N., and Shore, S. (2007). Vessicular glutamate transporters 1 and 2 are differentially associated with auditory nerve and spinal trigeminal inputs to the cochlear nucleus. *J. Comp. Neurol.* 500, 777–787. doi: 10.1002/cne.21208

Zuccotti, A., Kuhn, S., Johnson, S. L., Franz, C., Singer, W., Hecker, D., et al. (2012). Lack of brain-derived neurotrophic factor hampers inner hair cell synapse physiology, but protects against noise-induced hearing loss. *J. Neurosci.* 32, 8545–8553. doi: 10.1523/JNEUROSCI.1247-12.2012

Conflict of Interest Statement: The authors declare that the research was conducted in the absence of any commercial or financial relationships that could be construed as a potential conflict of interest.

Supplementary Figure 1

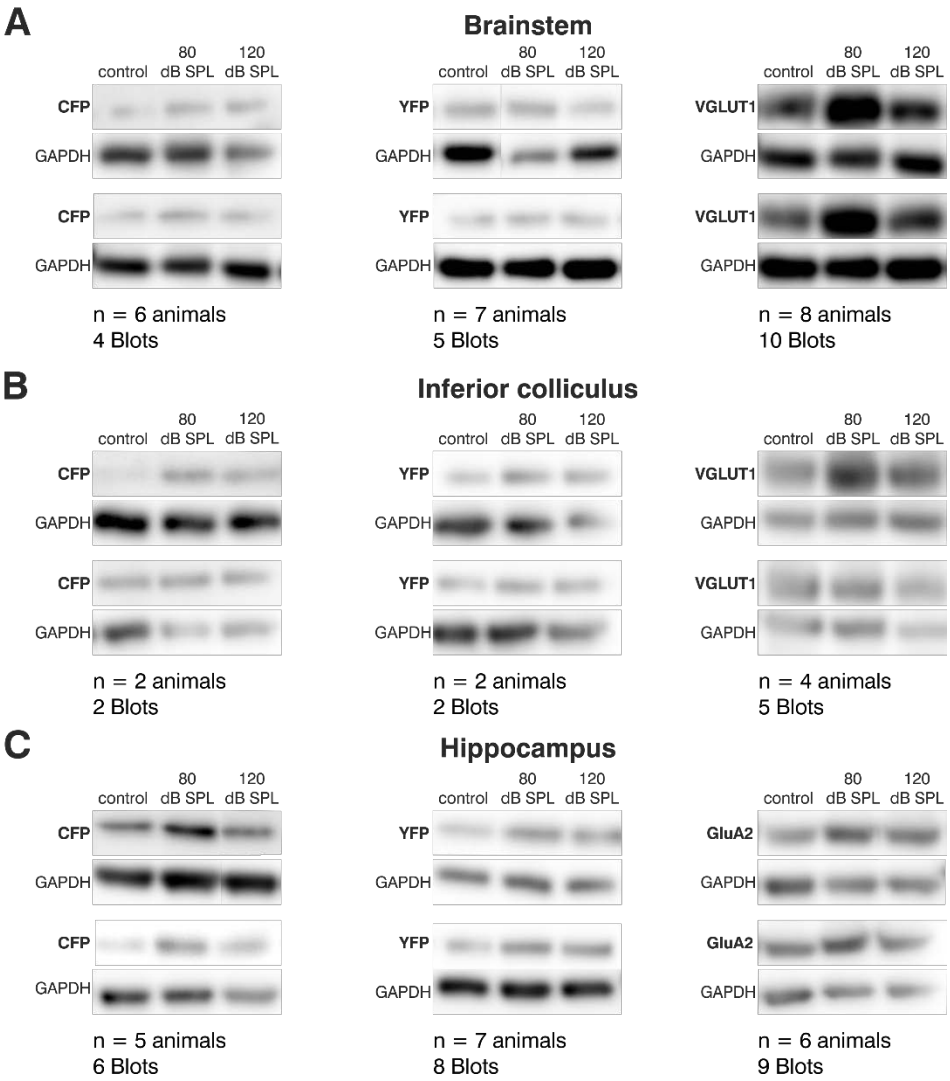

Supplementary Figure 1. Western blot analyses of CFP and YFP for (**A**) brainstem, (**B**) inferior colliculus and (**C**) hippocampus in control mice and mice exposed to 80 or 120 dB SPL. For brainstem and inferior colliculus, VGLUT1 was additionally analyzed, and for the hippocampus, GluA2 was additionally analyzed. Two examples are shown for each tissue and antibody. GAPDH is used as house-keeping gene. Note an increase of CFP, YFP, VGLUT1 and GluA2 in all tissues of mice exposed to 80 dB SPL. For originals see **Supplementary Figure 3**.

Supplementary Figure 2

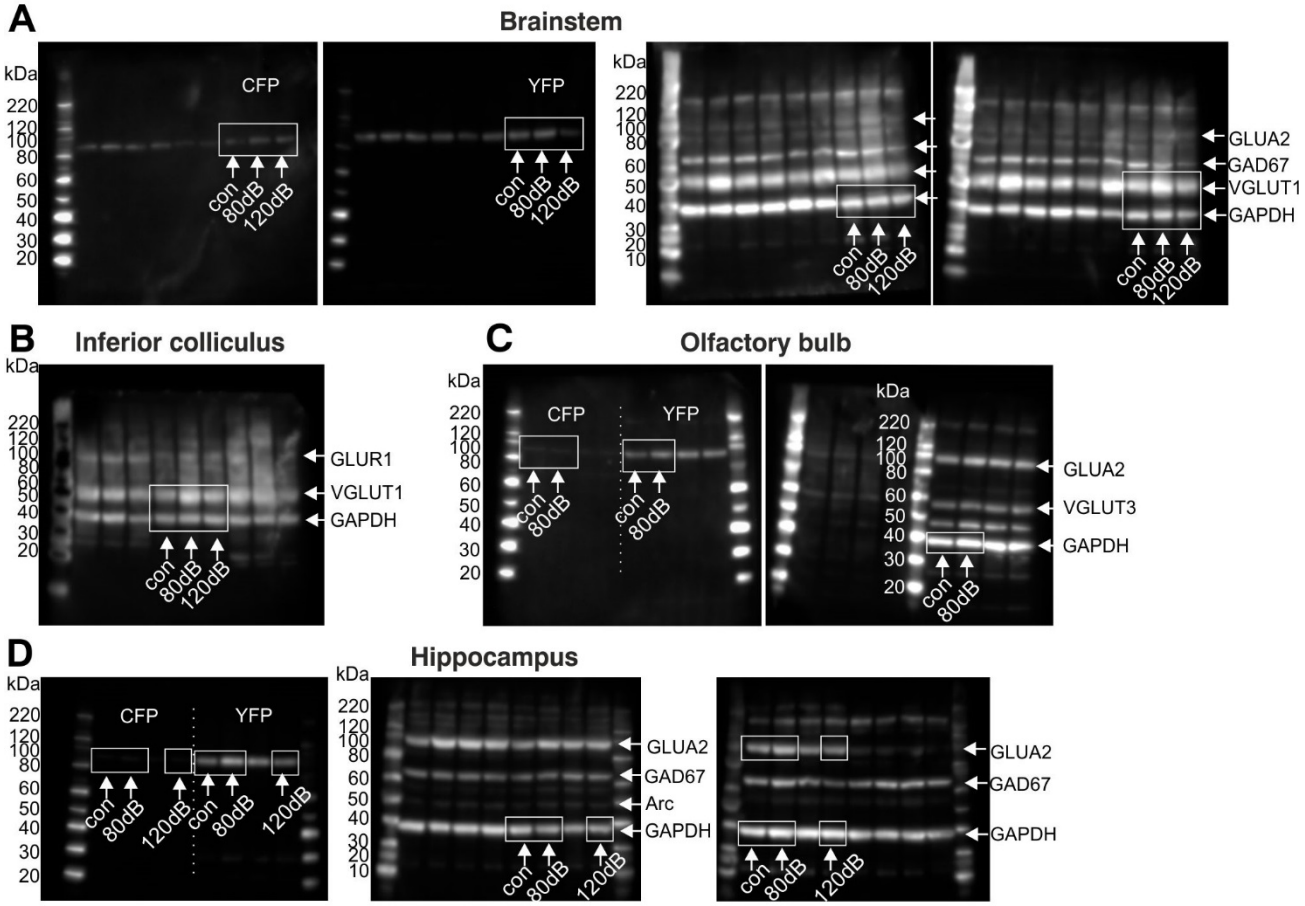

Supplementary Figure 2. Original Western blots for Figure 2 A (**A-C**) and Figure 3 A (**D**). (**A**) – (**D**) Arrows indicate bands used in Figures. Images were inverted and for better visibility the contrast was adjusted. All quantitative analyses were performed on original images (**A**) Original Western blots for CFP, YFP, vGlut1 and GAPDH in the brainstem. (**B**) Original Western blots for vGlut1 and GAPDH in the inferior colliculus. (**C**) Original Western bolts for CFP, YFP and GAPDH in the olfactory bulb. (**D**) Original Western blots for CFP, YFP, GluA2 and GAPDH in the hippocampus.

Supplementary Figure 3

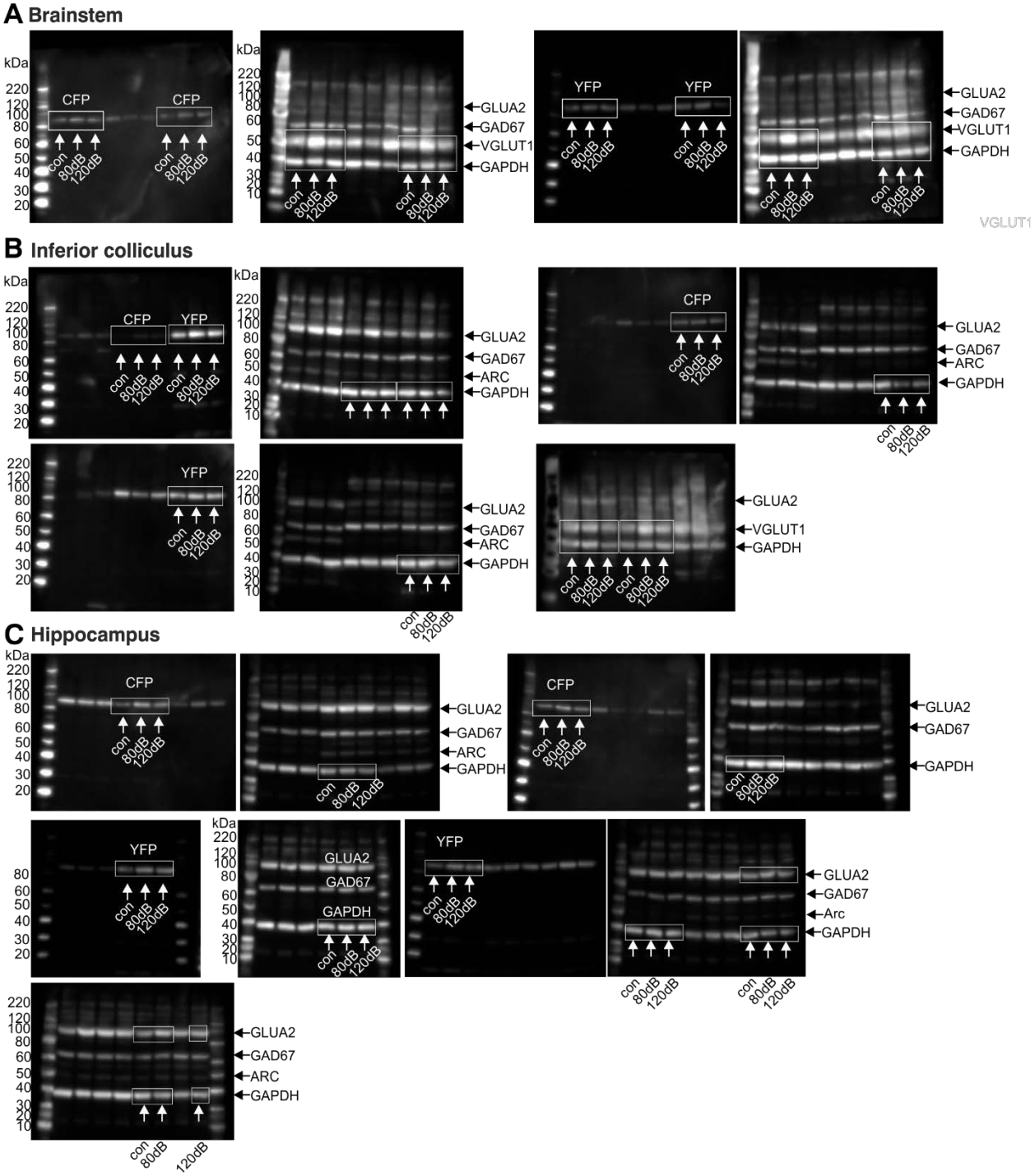

Supplementary Figure 3. Original Western blots for Supplementary Figure 1. Arrows indicate bands used in Supplementary Figure 1. Images were inverted and for better visibility the contrast was adjusted. All quantitative analyses were performed on original images (**A**) Original Western blots for CFP, YFP, vGlut1 and GAPDH in the brainstem. (**B**) Original Western blots for CFP, YFP, vGlut1 and GAPDH in the inferior colliculus. (**C**) Original Western blots for CFP, YFP, GluA2 and GAPDH in the hippocampus.

Supplementary Figure 4

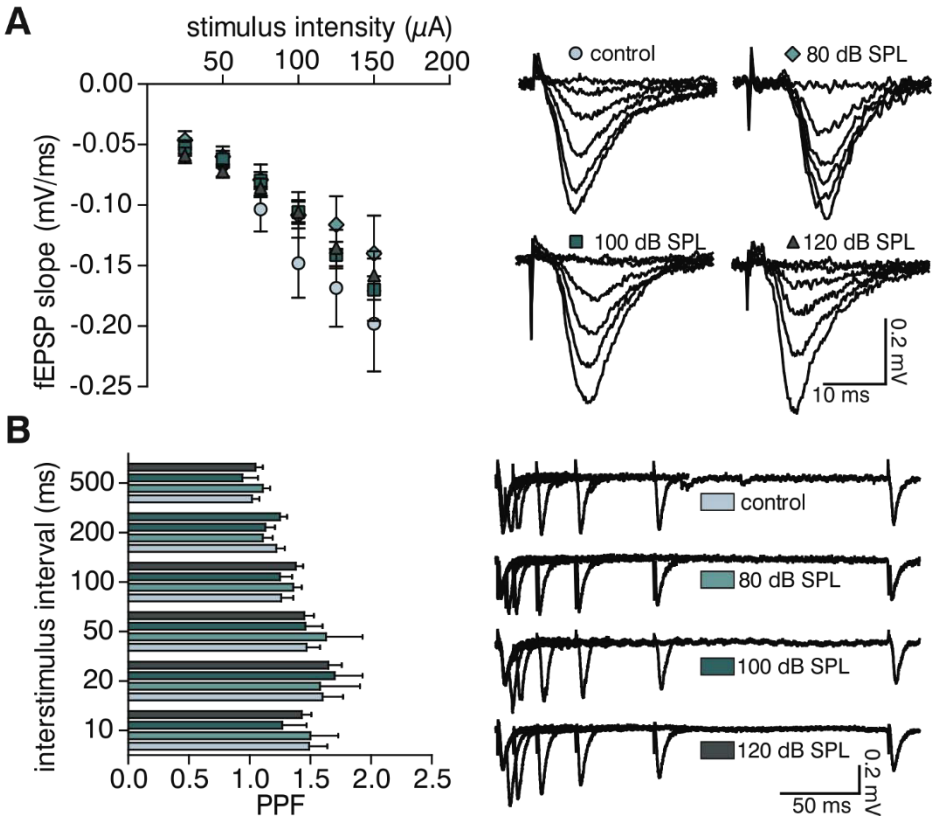

Supplementary Figure 4. (**A, B**) Schaffer collateral fEPSPs were recorded from acute forebrain slices of 8-12-week-old mice. (**A**) Average fEPSP slope was plotted against stimulus intensity. No difference was observed between slices from controls or animals exposed to 80 dB SPL, 100 dB SPL, and 120 dB SPL. Traces from representative recordings are shown on the right. Data represented as mean ± SEM (con $n = 11$ slices, 80 dB SPL $n = 14$ slices, 100 dB SPL $n = 11$ slices, 120 dB SPL $n = 14$ slices.) (**B**) Paired-pulse facilitation (PPF) was not different between slices from controls or animals exposed to 80 dB SPL, 100 dB SPL, and 120 dB SPL for all inter-stimulus intervals (I.S.I.). Traces from representative recordings are shown on the right. Data represented as mean ± SEM (con $n = 10$ slices, 80 dB SPL $n = 13$ slices, 100 dB SPL $n = 11$ slices, 120 dB SPL $n = 15$ slices).

Supplementary Figure 5

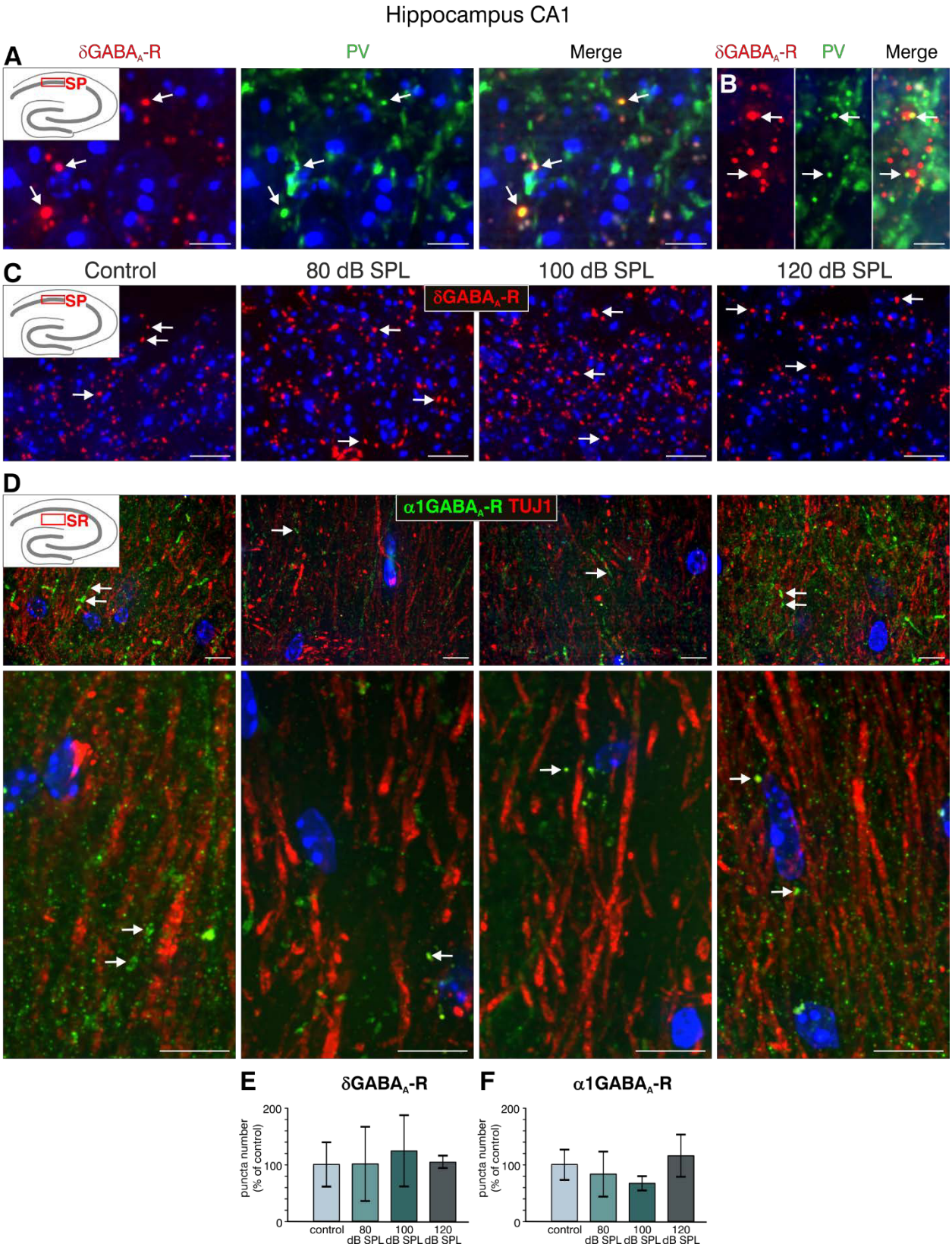

Supplementary Figure 5. Expression of δ subunit containing $GABA_A$ receptors ($\delta GABA_A$-R) and α subunit containing $GABA_A$ receptor ($\alpha 1GABA_A$-R) in the hippocampal CA1 region. (**A-C**) Hippocampal CA1 region with magnification of the stratum pyramidale (SP) stained for $\delta GABA_A$-R (red) and parvalbumin (PV, green). (**A**) Note the co-localization of PV with $\delta GABA_A$-R-positive dots (arrows). Scale bars: 5 µm. (**B**) $\delta GABA_A$-R-positive dots are contacted by PV-positive dendrites (arrows) of CA1 interneurons. Scale bars: 2.5 µm. (**C**) No obvious changes are observed in $\delta GABA_A$-R expression (red, arrows) between the different treatment groups. Scale bars: 10 µm. (**D**) Hippocampal CA1 region with magnification of the stratum radiatum (SR)

stained for αGABA$_A$-R (green, arrows) and TUJ1 (red). Note the dynamic change in αGABA$_A$-R expression dependent on sound exposure (green, arrows). Bottom panel: High-power examination of the SR. Changes in αGABA$_A$-R expression around TUJ1-positive neurons can be observed. Scale bars: 10 µm. (n = 4-5 animals /group). (**E**) Quantification of δGABA$_A$-R (1-way ANOVA: $F(3, 14) = 0.22$ $p = 0.88$; con, 80 dB SPL $n = 5$ animals; 100 dB SPL, 120 dB SPL $n = 4$ animals) and (**F**) αGABA$_A$-R fluorescence in the CA1 region. Data represented as mean ± SD (1-way ANOVA: $F(3, 16) = 2.08$ $p = 0.14$; $n = 5$ animals / group 2-3 repetitions).

Supplementary Table 1 Antibody information for immunohistochemistry and Western blot

Primary Antibodies						
Immunohistochemistry	Antibody	Protein name	Product number	Source	Dilution	Protein size
Cochlea / Brain sections	rabbit anti-CtBP2/ RIBEYE	CtBP2/RIBEYE	10-P1554	American research Products, Inc.,	1:1,000	
	rabbit anti-parvalbumin	Parvalbumin	ab11427	Abcam	1:2,000	
	mouse anti-parvalbumin	Parvalbumin	P3088	Sigma-Aldrich	1:500	
	guinea pig anti-α1GABA$_A$-receptor	Gamma-aminobutyric acid type A receptor α subunit	224204	Synaptic Systems	1:500	
	rabbit anti-δGABA$_A$-receptor	Gamma-aminobutyric acid type A receptor δ subunit	AB9752	Millipore	1:1,500	
	guinea pig anti-VGLUT1	Vesicular glutamate transporter 1	135304	Synaptic Systems	1:1,500	
Western blot	rabbit anti-RCFP	Reef coral fluorescent protein pan antibody	632475	Clontech	1:1,000	30-35 kDa
	guinea pig anti-VGLUT1	Vesicular glutamate transporter 1	135304	Synaptic Systems	1:5,000	50 kDa
	rabbit anti-GluA2	Glutamate receptor AMPA 2	182103	Synaptic Systems	1:1,500	100 kDa
	mouse anti-GAPDH	Glyceraldehyde 3-phosphate dehydrogenase	ab8245	Abcam	1:10,000	40 kDa
Secondary antibodies						
Immunohistochemistry	Antibody	Protein name	Product number	Source	Dilution	Protein size
Cochlea / Brain sections	Cy3-conjugated goat anti-rabbit antibody		111-166-003	Jackson ImmunoResearch Laboratories	1:1,500	
	Alexa488-conjugated anti-mouse antibody		A11001	Molecular Probes, MoBiTec	1:500	
	Alexa488-conjugated anti-guinea pig antibody		A11073	Molecular Probes, MoBiTec	1:500	
Western blot	ECL anti-mouse IgG HRP linked		NA 931-100µl	GE Healthcar	1:2,500	

				e UK Limited		
	ECL anti-rabbit IgG HRP linked		NA 934-100µl	GE Healthcare UK Limited	1:2,500	
	Goat anti-gionea pig IgG-HRP		Sc-2438	Santa Cruz Biotechnology Inc.	1:7,000	

Supplementary Table 2 Statistical information of the results

		Statistical test	**Test value**	**Degrees of freedom**	***p*-value**	**Post-hoc test with *p*-value**		**n-number**
Fig. 1A	Click-ABR TTS post AT	1-way ANOVA	F(3, 129) = 92.67		p < 0.0001	Bonferroni's test con vs. 80 dB SPL con vs. 100 dB SPL con vs. 120 dB SPL	 p<0.0001	con n = 19 animals 80 dB SPL n= 19 animals 100 dB SPL n = 16 animals 120 dB SPL n = 19 animals
	Click-ABR 14d post AT	1-way ANOVA	F(3, 144) = 54.72		p < 0.0001	con vs. 120 dB SPL	p <0.0001	
Fig. 1B	noise-ABR 14d post AT	1-way ANOVA	F(3, 142) = 75.45		p < 0.0001	con vs. 120 dB SPL	p < 0.0001	
Fig. 1C	f-ABR	2-way ANOVA	F(3, 597) = 79.9		p < 0.0001	con vs. 120 dB SPL	p < 0.05	
Fig. 1E	ribbon number	2-way ANOVA	F(3, 60) = 11.08		p < 0.0001	1-sided unpaired Student's t-tests middle turn: con vs. 80 dB SPL con vs. 120 dB SPL midbasal turn: con vs. 100 dB SPL con vs. 120 dB SPL	 p < 0.05 p < 0.01 p < 0.05 p < 0.01	n = 6 ears from 4 animals per group, 1-3 repetitions each, 8-24 IHCs per turn and group
Fig. 1F	CorF	1-way ANOVA	F(3, 131) = 17.51		p < 0.0001	Tukey's Multiple Comparison test: con vs. 120 dB SPL 80 dB SPL vs. 120 dB SPL 100 dB SPL vs. 120 dB SPL	 p < 0.001 p < 0.001 p < 0.01	con n = 8 animals, 15 ears; 80 dB SPL n = 9 animals, 18 ears 100 dB SPL n = 5 animals, 10 ears; 120 dB SPL n = 9 animals, 17 ears
Fig. 1G	wave I control	2-way ANOVA	F(1, 1031) = 0.003		p = 0.955			n = 18 mice/group
	wave I 80 dB SPL	2-way ANOVA	F(1, 890) = 6.02		p = 0.0143			n = 16 mice/group
	wave I 100 dB SPL	2-way ANOVA	F(1, 836) = 28.59		p < 0.0001			n = 15 mice/group

Fig. 1H	wave I 120 dB SPL	2-way ANOVA	F(1, 396) = 185.8		p < 0.0001		n = 18 mice/group
	wave I V control	2-way ANOVA	F(1, 1034) = 1.296		p = 0.2551		n = 18 mice/group
	wave I V 80 dB SPL	2-way ANOVA	F(1, 951) = 0.89		p = 0.3446		n = 16 mice/group
	wave I V 100 dB SPL	2-way ANOVA	F(1, 743) = 0.09		p = 0.7706		n = 15 mice/group
	wave I V 120 dB SPL	2-way ANOVA	F(1, 452) = 82.88		p < 0.0001		n = 18 mice/group
Fig. 2A/B							n = 5 - 6 mice/group 2 - 10 Western blots each
Fig. 2C/D	VGLUT1	two-tailed student's t-test	t = 3.63 df = 10		p = 0.0046		n = 6 mice/group 2 - 3 repetitions
Fig. 3A							n = 5 mice/group 2 - 10 Western blots each
Fig. 3B	fEPSP	1-way ANOVA	F(3, 19) = 4.99		p = 0.01	Bonferroni's test baseline/tetanized (b/t) control 80 dB SPL 100 dB SPL 120 dB SPL tetanized/tetanized (t/t) con vs. 80 dB SPL con vs. 100 dB SPL con vs. 120 dB SPL	 p < 0.01 p < 0.001 p < 0.001 p < 0.01 p < 0.01 p< 0.01 n.s.	n = 4 animals /group con 7 slices 80 dB SPL 7 slices 100 dB SPL 6 slices 120 dB SPL 5 slices
Fig. 3C	con	repteaed measure ANOVA	F = 2.56	DF = 5	p = 0.033	Bonferroni's test day 1 vs. day 2 day 1 vs. day 3 day 1 vs. day 4 day 1 vs. day 5 day 1 vs. day 6	 n.s. 	con n= 18 animals 80 dB SPL n = 17 animals
	80dB SPL		F = 5.85	DF = 5	p < 0.001	day 1 vs. day 2 day 1 vs. day 3 day 1 vs. day 4 day 1 vs. day 5 day 1 vs. day 6	n.s. p = 0.013 p = 0.054 p = 0.006 p < 0.001	

Fig. 4A-C							n = 6 animals/group
Fig. 4D	CFP	1-way ANOVA	F(3, 19) = 10.5	p < 0.0003	Bonferroni's test con vs. 80 dB SPL con vs. 100 dB SPL con vs. 120 dB SPL 80 dB SPL vs. 120 dB SPL 100 dB SPL vs. 120 dB SPL	 p = 0.0013 n.s. n.s. p < 0.0001 p = 0.0072	con n= 6 animals; 1-4 repetitions 80 dB SPL n = 6 animals; 1-6 repetitions 100 dB SPL n = 5 animals; 2-5 repetitions 120 dB SPL n = 6 animals; 1-3 repetitions
Fig. 4E	YFP	1-way ANOVA	F(3, 11) = 6.96	p = 0.0068	Bonferroni's test con vs. 80 dB SPL 80 dB SPL vs. 120 dB SPL	 p < 0.01 p < 0.01	con n = 4 animals 80 dB SPL n = 3 animals 100 dB SPL n = 3 animals 120 dB SPL n = 5 animals; 3 repetitions each
	CFP	1-way ANOVA	F(3, 11) = 2.37	p = 0.13			
	PV	1-way ANOVA	F(3, 11) = 10.07	p = 0.0017	con vs. 80 dB SPL 80 dB SPL vs. 120 dB SPL	p < 0.01 p < 0.01	
Fig. 5A-C							n = 6 animals/group
Fig. 5D	CFP	1-way ANOVA	F(3,25) = 22.44	p < 0.0001	Bonferroni's test con vs. 80 dB SPL 80dB SPL vs. 120 dB SPL	 p < 0.001 p < 0.0001	n=6 animals / group 4-6 repetition each
	YFP	1-way ANOVA	F(3, 25) = 3.32	p = 0.036	80 dB SPL vs. 120 dB SPL	p < 0.05	
Fig. 6A-C							n = 6 animals/group
Fig. 6D		1-way ANOVA	F(3, 19) = 5.96	p = 0.0049	Bonferroni's test con vs. 80 dB SPL con vs. 100 dB SPL con vs. 120 dB SPL 100 vs. 120 dB SPL	 n.s. p = 0.0301 n.s. p = 0.01	con n= 6 animals 80 dB SPL n = 6 animals 100 dB SPL n = 5 animals 120 dB SPL n = 6 animals; 4-6 repetitions
Fig. 6E		1-way ANOVA	F(3, 19) = 4.61	p = 0.0138	Bonferroni's test con vs. 80 dB SPL con vs. 100 dB SPL	 p < 0.05 p < 0.05	con n = 6 animals 80 dB SPL n = 5 animals 100 dB SPL n = 6 animals 120 dB SPL n= 6 animals 2 repetitions each
Fig. 6G		1-way ANOVA	F(3, 19) = 5.24	p = 0.005	Bonferroni's test baseline/wash-in con 80 dB SPL 100 dB SPL	 p < 0.001 n.s. n.s.	n = 4 animals / group; 9 slices / group

120 dB SPL	p < 0.001
con vs. 120 dB SPL	p < 0.01
con vs. 80 dB SPL	p < 0.01
con vs. 100 dB SPL	n.s.

Supplementary Table 3 Statistical information of the supplementray information

		Statistical test	**Test value**	**Degrees of freedom**	***p*-value**	**Post-hoc test with *p*-value**	**n-number**
S Fig. 4B							con n = 10 slices 80 dB SPL n = 13 slices 100 dB SPL n = 11 slices 120 dB SPL n = 15 slices
SFig. 5A-D							n = 4-5 animals /group
S Fig. 5E	δGABAA-R	1-way ANOVA	F(3, 14) = 0.22		p = 0.88		con; 80 dB SPL n = 5 animals 100 dB SPL; 120 dB SPL n = 4 animals
S Fig. 5F	α1GABAA-R	1-way ANOVA	F(3, 16) = 2.08		p = 0.14		n = 5 animals / group 2-3 repetitions